REGIONAL VOLCANOGENIC MASSIVE SULPHIDE METALLOGENY OF THE NEOARCHEAN GREENSTONE BELT ASSEMBLAGES ON THE NORTHWEST MARGIN OF THE WAWA SUBPROVINCE, SUPERIOR PROVINCE

by

Robert Wilfred David Lodge

A thesis submitted in partial
requirement for the degree of
Doctor of Philosophy
In
Mineral Deposits and Precambrian Geology

School of Graduate Studies
Laurentian University
Sudbury, Ontario, Canada

THESIS DEFENCE COMMITTEE/COMITÉ DE SOUTENANCE DE THÈSE

Laurentian Université/Université Laurentienne
School of Graduate Studies/École des études supérieures

Title of Thesis Titre de la thèse	REGIONAL VOLCANOGENIC MASSIVE SULPHIDE METALLOGENY OF THE NEOARCHEAN GREENSTONE BELT ASSEMBLAGES ON THE NORTHWEST MARGIN OF THE WAWA SUBPROVINCE, SUPERIOR PROVINCE
Name of Candidate Nom du candidat	Lodge, Robert Wilfred David
Degree Diplôme	Doctor of Philosophy
Department/Program Département/Programme	Mineral Deposits and Precambrian Geology
Date of Defence Date de la soutenance	September 27, 2013

APPROVED/APPROUVÉ

Thesis Examiners/Examinateurs de thèse:

Dr. Harold Gibson
(Co-supervisor/Codirecteur de thèse)

Dr. Greg Stott
(Co-supervisor/Codirecteur de thèse)

Dr. Doug Tinkham
(Committee member/Membre du comité)

Dr. James Franklin
(Committee member/Membre du comité)

Dr. Ali Polat
(External Examiner/Examinateur externe)

Dr. Nelson Belzile
(Internal Examiner/Examinateur interne)

Approved for the School of Graduate Studies
Approuvé pour l'École des études supérieures
Dr. David Lesbarrères
M. David Lesbarrères
Director, School of Graduate Studies
Directeur, École des études supérieures

ACCESSIBILITY CLAUSE AND PERMISSION TO USE

ABSTRACT

The ca. 2720 Ma Vermilion, Shebandowan, Winston Lake, and Manitouwadge greenstone belts (VGB, SGB, WGB, and MGB, respectively) are located along the northern margin of the Wawa subprovince. They are interpreted to have formed in broadly similar rifted arc to back-arc environments, but their base and precious endowment and, in particular, their endowment in VMS deposits, differ markedly. These difference is metal endowment reflect differences in their metallogenic history that were examined by comparing their regional, belt-scale lithostratigraphy, chemostratigraphy, petrogenesis and tectonic history constrained by new U-Pb zircon geochronology.

The MGB is the most VMS-endowed and isotopically juvenile (Pb and Nd) greenstone belt. It has a trace element chemostratigraphy that is consistent with a rifted arc to back-arc environment. The trace element chemostratigraphy of the WGB is also consistent with a rifted-arc to back arc geodynamic setting. The Winston Lake VMS deposits formed during early rifting of the arc and their timing is tightly constrained at ca. 2720 Ma by U-Pb ages of the host felsic strata and post-VMS Zenith gabbro. The Zn-dominated VMS mineralization formed from hydrothermal fluids that were <300 ° and were possibly boiling in relatively shallow water.

The trace element chemostratigraphy of the VGB, SGB, and WGB indicates a plume-driven rifted arc to back-arc geodynamic settings. The composition of VMS mineralization, lithofacies, and alteration in these belts are consistent with a relatively shallower-water environment, which may have compromised VMS formation. The high-Mg andesites that are typical of, but restricted to, the SGB formed during compressional “hot” subduction, which resulted in the development of a thicker arc crust. This thicker crust may have inhibited VMS formation, but favoured the formation of magmatic sulphide and gold mineralization.

New detrital and magmatic zircon U-Pb geochronology allowed comparison and correlation of lithostratigraphy and metallogeny between the greenstone belts. U-Pb ages within the VGB also defined younger, Timiskaming-type volcanic and sedimentary strata that are coeval with similar deposits in the SGB. These strata are spatially and temporally associated with gold mineralization in both belts and are coeval with similar deformation and magmatic events in the WGB and along the northern margin of the Wawa-Abitibi terrane. This indicates that the formation of Timiskaming-type pull apart basins in the northern part of the Wawa-Abitibi terrane were synchronous, and earlier than in the southern part, which is consistent with oblique convergence of the Wawa-Abitibi terrane onto the Superior Province. Detrital zircon geochronology also revealed the presence of a >2720 Ma

zircon population within the Timiskaming-type sedimentary strata of the SGB. This is consistent with their derivation from the Wabigoon subprovince and suggests trans-terrane transport of detritus in a foreland –type basin resulting from uplift of the Wabigoon subprovince during accretion of the Wawa subprovince.

KEYWORDS

Archean, Superior Province, Wawa Subprovince, Greenstone Belts, Volcanogenic Massive Sulphides, U-Pb Geochronology, Metallogeny, Geochemistry

ACKNOWLEDGEMENTS

First of all, I thank Dr. Harold Gibson and Dr. Greg Stott for co-supervising this project and for opening the door to a very successful Laurentian University-Ontario Geological Survey mapping school project. Their guidance, wisdom, enthusiasm, and insightful discussions have made me a better geologist and have set up my future career in the field of volcanology and economic geology for big successes. They always asked the right question to stimulate and motivate me and their critical (and sometimes a little harsh) reviews of my work has vastly improved the quality of my research. I am very much looking forward to evolving our relationships from student/supervisor to colleagues.

I thank the other members of my thesis committee, Doug Tinkham and Jim Franklin, for their time and knowledge throughout these past 4 years. I hope to continue collaboration with both of you beyond my days here at Laurentian University. I'd like to thank my external examiner, Dr. Ali Polat from the University of Windsor, for reviewing this thesis.

This project would not have been as successful if it wasn't for the generous financial and logistic support of the Ontario Geological Survey. I would like to thank managers Jack Parker and Tom Brown for their support throughout my summer employments with the OGS. Their professionalism and commitment to safety made me a much better supervisor and mapper. Numerous technical and administrative staff assisted in field preparation including Jon Webb, Sara McIlraith, Steve Josey, and Sue Peelow. I've also enjoyed many insightful conversations with the skilled geoscientists employed with the OGS, including Gary Beakhouse, Ben Berger, Mark Smyk, John Scott, and Dorothy Campbell. My field assistants, Peter Cecutti and Karin Ostler, deserve a lot of credit for hanging in there through all the sun, sweat, bugs, and rough terrane.

Additional funding was received from the National Science and Engineering Research Council of Canada and the Society of Economic Geologists to support research outside of Ontario in Minnesota. I'm thankful for this opportunity, not only because of the research potential of the area, but for introducing me to George Hudak. In addition to showing me around the area, we have developed a strong collaborative relationship that will result in several publications beyond my thesis. I'd also like to thank Dean Peterson and Mark Jirsa for sharing their time and expertise in the geology of Minnesota.

I feel extremely lucky to have been a member of the Department of Earth Science at Laurentian University and a citizen of the city of Greater Sudbury. I am very appreciative of the conversations and guidance received from faculty members Phil Thurston, Mike Lesher, Steve Piercey (Adjunct, Memorial University), Bruno Lafrance, Darrel Long, and Dan Kontak. The administrative staff in the department, Roxane Mehes and Edda Bozzato, made life within the department a little easier by handing general inquires and providing home-made goodies almost every day. I'm also very grateful for the friends and colleagues that I've gained from my fellow graduate students: Geoff, Taus, Joe, Joshua, Craig, Mike (x2), Kate, Kurt, Lindsey...to name a few.

I'd like to thank my parents, Wilson and Marie, for their support throughout this degree and for not showing me too much grief when I moved away from Newfoundland. They have raised me to become a person with intelligence, independence, and integrity through their strong morals, principles, and guidance. Even during those crazy teenage years, their unwavering love and sense of pride in their son kept me on the right path.

Most importantly, I would not be where I am today without the love and support I get every day at home from my beautiful wife, Cassie. She has shown great patience and has said so many words of encouragement throughout the entire process of completing this thesis. No matter how each day went, I was able to come home to a warm smile and unmatched enthusiasm for every milestone completed or accomplishment. In addition to becoming a better geologist, I am also becoming a better husband for Cassie and better father for my newborn baby, Hillary. Thank you for everything and I love you both!

TABLE OF CONTENTS

LIST OF FIGURES

LIST OF TABLES

LIST OF APPENDICES

CHAPTER 1

INTRODUCTION TO THESIS

1.1. Geology and Metallogeny of the Wawa Subprovince

The Wawa subprovince comprises the western half of the Wawa-Abitibi terrane, which is the youngest granite-greenstone terrane in the Superior Province (**Figure 1.1**). It is bound to the north by metasedimentary and intrusive rocks of the Quetico subprovince, and is separated from the Abitibi subprovince to the east by the Kapuskasing structural zone (Williams et al., 1991; Stott et al., 2010; Stott, 2011). The southern part of the Wawa subprovince is unconformably overlain by Proterozoic rocks.

Neodymium, hafnium, and lead isotopic data suggest that the Wawa subprovince formed via rifting of a Mesoarchean protocontinent (Ketchum et al., 2008), which is preserved as the 2.9 Ga Hawk assemblage in the Wawa region of Ontario (Ayer et al., 2010). Rocks in the southernmost parts of the Wawa and Abitbi subprovinces have isotopic abundances that suggest the presence of an older ca. 2.8-2.9 Ga crust (Ketchum et al., 2008). Greenstone belt assemblages along the northern margin of the Wawa subprovince and distal to the older Mesoarchean protocontinental core have juvenile isotopic abundances suggesting that they are the products of rifting and were derived from an uncontaminated depleted mantle source (Vervoort et al., 1994; Ketchum et al., 2008). Numerous volcanic and geodynamic settings have been interpreted for the greenstone belts indicating that protocontinental rifting was followed by a period of microplate-like tectonics that developed a complex array of arcs, back arcs, and oceanic plateaus (Polat and Kerrich, 2006; Kerrich et al., 2008; Polat, 2009). The timing of accretion of the Wawa subprovince onto the rest of the Superior Province is relatively well constrained at ca. 2690 Ma by syn-deformation magmatism along the northern margin of the Wawa-Abitibi terrane (Corfu and Stott, 1998; Zaleski et al., 1999; David et al., 2007; Lodge et al., 2013).

The greenstone belts along the northern margin of the Wawa subprovince are dominated by ca. 2720 Ma supracrustal assemblages and are the focus of this study (**Figure 1.2**). These greenstone belts are interpreted have formed in broadly similar geodynamic settings (e.g., Ketchum et al., 2008; Ayer et al., 2010), but their known base and precious metal endowment are significantly different. The Manitouwadge and Winston Lake greenstone belts are the only two

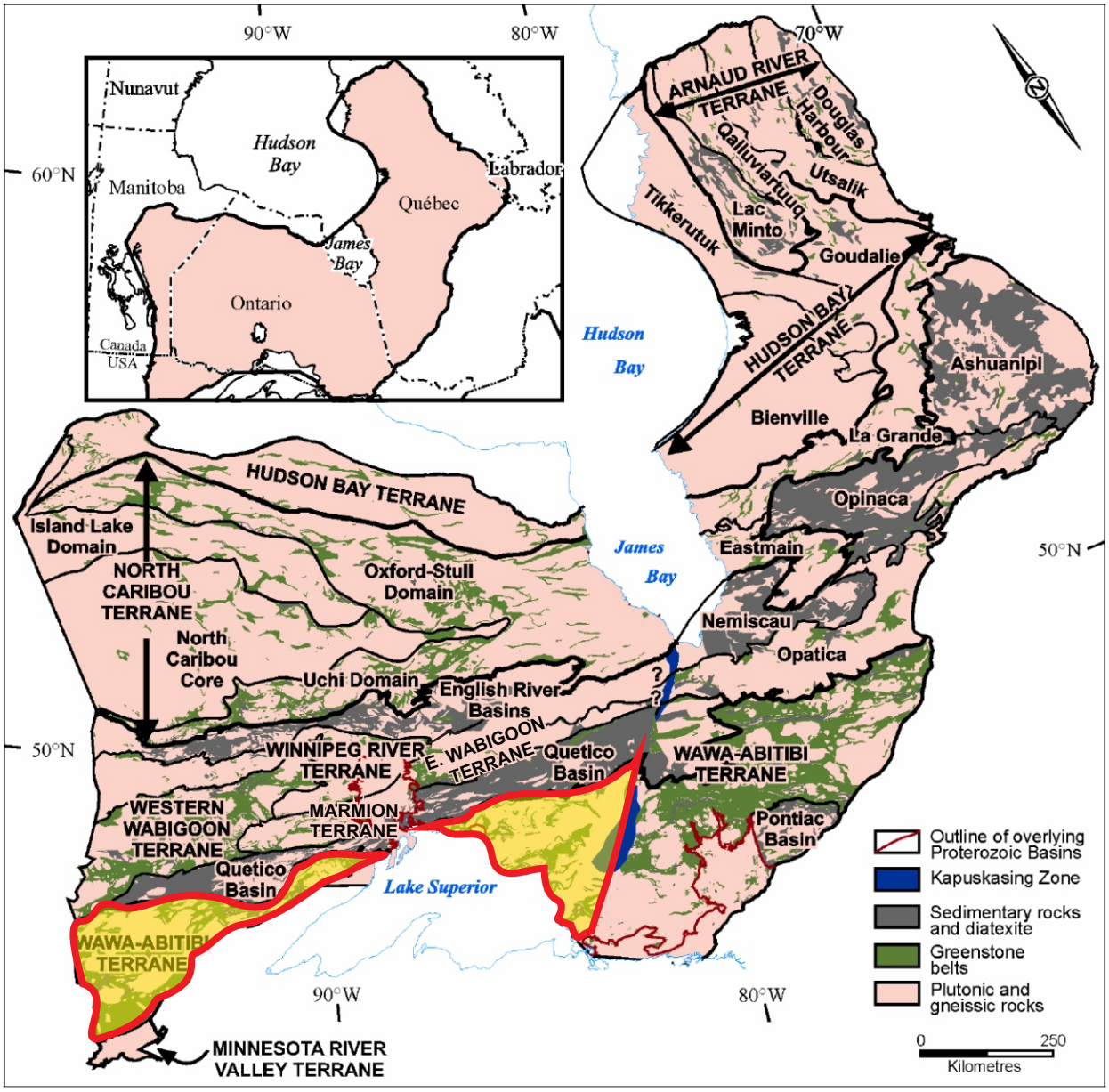

Figure 1.1: Terrane map of the Archean Superior Province highlighting the Wawa subprovince of the Wawa-Abitibi terrane. Figure modified from Stott et al. (2010) and Stott (2011).

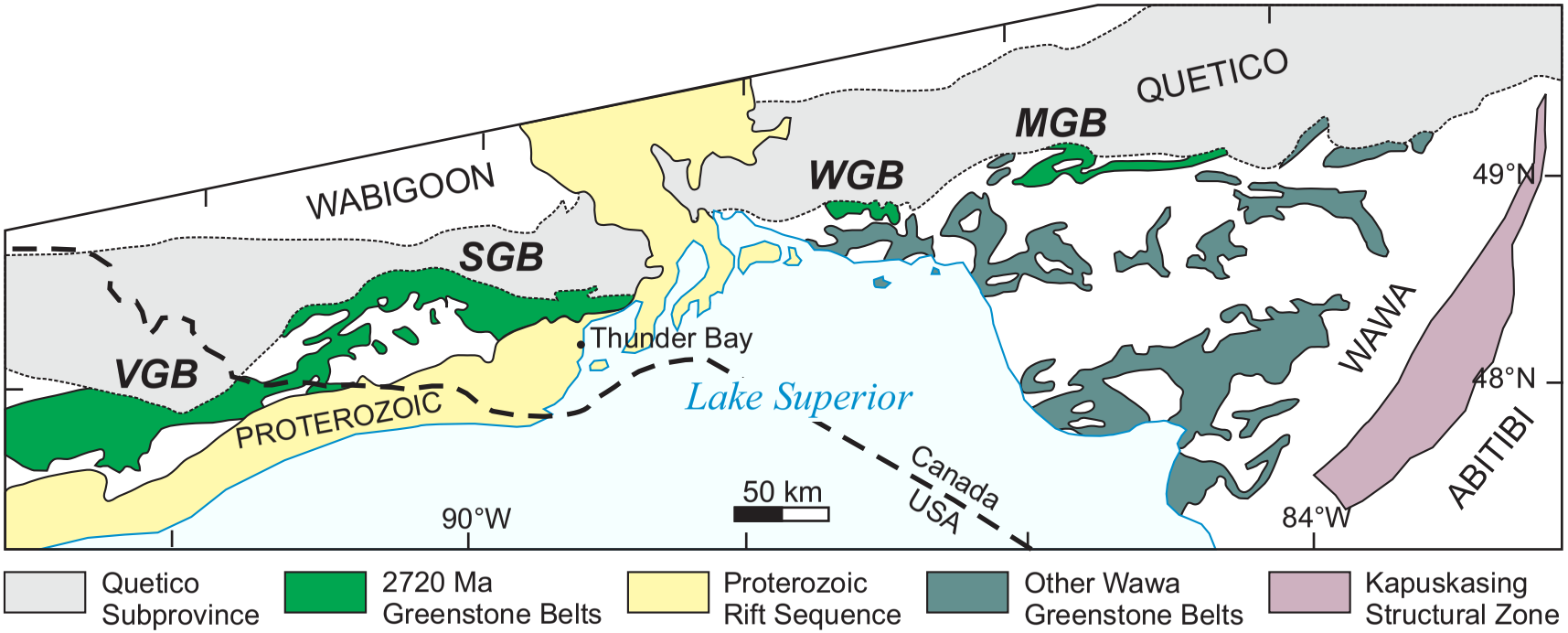

Figure 1.2: Regional geology of the Wawa subprovince showing the location of the Vermilion (VGB), Shebandowan (SGB), Winston Lake (WGB), and Manitouwadge (MGB) greenstone belts. Figure from Lodge (2011).

greenstone belts known to host economic volcanogenic massive sulphide (VMS) mineralization in the Wawa subprovince. There are numerous VMS showings in the Shebandowan and Vermilion greenstone belts, but they are small in size and are not economic. However, the Shebandowan greenstone belt is unique amongst these belts in that it contains past-producing magmatic Ni-Cu sulphide and gold mines. These metallogenic differences suggest that there may be fundamental differences in the petrogenesis and crustal architecture controlling the metallogeny of these belts, even though they are all were interpreted to have formed in broadly similar geodynamic settings.

1.2. Purpose of Study

The metallogenic significance of ca. 2720 Ma volcanism and greenstone belt construction in the Wawa-Abitibi terrane has been recognized in previous research (e.g., Davis et al., 1994; Corfu and Stott, 1998). There are many past-producing Cu-Zn-Pb VMS mines whose ore deposits are hosted ca. 2720 strata (Davis et al., 1994; Zaleski et al., 1999; Ayer et al., 2010) including the Geco, Winston Lake, and Estrades mines. There is also a past-producing magmatic Ni-Cu mine (Shebandowan Mine) associated with the ca. 2720 Ma greenstone belt construction event. The ca. 2720 Ma Vermilion, Shebandowan, Winston Lake, and Manitouwadge greenstone belts lie along the northern margin of the Wawa subprovince and all were interpreted to have formed in rifted arc to backarc geodynamic settings (Davis et al., 1994; Corfu and Stott, 1998; Zaleski et al., 1999; Peterson et al., 2001). These geodynamic settings are ideal VMS-forming environments (Franklin et al., 2005; Galley et al., 2007), but this is not reflected in a similar endowment of VMS deposits. The largest two belts, the Vermilion and Shebandowan, have yet to yield an economic VMS deposit. However, the Shebandowan greenstone belt is unique amongst these belts in that it is host to a past-producing magmatic Ni-Cu sulphide (North Coldstream, Shebandowan) and gold (Moss) mines. Therefore, a better understanding of their petrogenesis and crustal architecture is needed to provide insight into the variations in the metallogeny of these greenstone belts. These four tectono- and chrono-stratigraphic equivalent belts are an ideal location to study variations in greenstone belt construction and metallogeny. However, research in greenstone belt- and terrane-scale petrogenesis and metallogeny in this region has been hindered by the lack of comparable datasets and varying scales of understanding.

For example, numerous geological problems or dataset deficiencies in each belt impair regional-scale interpretations and comparisons between the greenstone belts. Prior to this study, only the Shebandowan and Manitouwadge greenstone belts had adequate U-Pb geochronological data that made interpretations of the geological history of these belts possible (Corfu and Stott, 1986, 1998; Zaleski et al., 1999). The Vermilion and Winston Lake greenstone belts each had only one U-Pb age indicating the presence of ca. 2720 Ma strata (Davis et al., 1994; Peterson et al., 2001). Therefore, an improved geochronological dataset was required to correlate magmatic events between belts and to improve the understanding of the geological and deformational history.

Previous research in these greenstone belts provided a framework for this study, but lacked the systematic detail, coverage, trace and isotopic geochemistry, and geochronological constrains required for belt-scale metallogenic and petrogenetic comparisons. For example, research in the Winston Lake greenstone belt established an initial lithostratigraphy for the VMS deposits (Osterberg, 1993; Gorton and Schandl, 1995) and Au prospects (Ritcey, 1992). However, previous geochemical data in these studies lacked geospatial control and critical immobile trace elements that are useful for determining petrogenetic processes. The regional geological maps of the Winston Lake greenstone belt did not recognize amphibolite facies VMS alteration assemblages (e.g., Pye, 1964) and although the Vermilion greenstone has been recently mapped by the Minnesota Geological Survey (Peterson and Jirsa, 1999), the collection of systematic geochemical data was restricted to VMS properties (Hudak et al., 2002). Despite a comprehensive study of the Manitouwadge greenstone belt (Zaleski and Peterson, 1995; Peterson and Zaleski, 1999; Zaleski et al., 1999; Zaleski and Peterson, 2001), the geochemical datasets were not published impairing chemostratigraphic correlations and interpretations. The Shebandowan greenstone belt was mapped recently by the Ontario Geological Survey (e.g., Brown and Fogal, 1995; Rogers, 1995; Osmani, 1997; Hart and Metsaranta, 2009); however, chemostratigraphic variation on a belt-wide scale were not examined.

Specific objectives of this research include:

- Reconstruct the regional volcanotectonic evolution and geodynamic setting of the Vermilion, Shebandowan, Winston Lake, and Manitouwadge greenstone belts through strategic belt-scale mapping as well as systematic lithogeochemical and isotopic sampling of representative strata.

- Determine the petrogenesis and crustal architecture of each greenstone belt in areas of VMS, magmatic sulphide, and gold mineralization.
- Determine the volcanic architecture, depositional history, and geodynamic setting of VMS mineralization in the under-studied Winston Lake greenstone belt.
- Use magmatic and detrital zircon U-Pb geochronology to improve the understanding and regional correlations of strata in the Vermilion and Winston Lake greenstone belts to other magmatic and depositional events in the Wawa subprovince and to place these events into the context of the Neoarchean assembly of the Superior Province.
- Interpret the metallogeny of the *circa* 2720 Ma greenstone belt construction event in light of the reconstructed geodynamic settings and depositional histories for each belt.

1.3. Field and Analytical Methods

The tectonostratigraphic- and chronostratigraphic-equivalent greenstone belts along the northern margin of the Wawa subprovince provide a coeval setting to establish how the variations in crustal architecture and petrogenesis of Archean greenstone belt assemblages can result in differences in their metallogeny despite their formation in broadly similar geodynamic environment. Existing or past-producing mineral deposits are well documented in each greenstone belt by the Ontario and Minnesota geological surveys and have had long histories of exploration and mining. In addition, each of these belts has a lot of easily accessed outcrop exposure, which is typical of or better than many other greenstone belts in the region.

Mapping traverses along semi-linear transects at a scale of 1:20,000 were completed in each greenstone belt, proximal to strata hosting VMS, magmatic sulphide, or gold mineralization. The mapping strategy was aimed at describing and sampling the belt-scale supracrustal stratigraphy, and reconstructing the depositional and geodynamic history of the ca. 2720 Ma assemblages in each belt. This approach was aided by the geological context provided by maps from the Ontario and Minnesota geological surveys. Mapping and field descriptions of lithofacies including primary textures and facies variations, primary and secondary mineralogy, stratigraphic relationships, and tectonic structures were used to: (1) define and describe lithofacies and stratigraphy; (2) reconstruct the volcanotectonic history of the greenstone belts; and (3) provide well constrained samples for petrographic, geochemical, and isotopic analyses that are essential for establishing the genetic relationships between each greenstone belt.

Due to the variable intensities of hydrothermal alteration, metamorphism, and preservation of primary textures in the volcanic assemblages, regional-scale interpretations relied largely on geochemical variation rather than primary petrographic observations. Major and trace earth element lithogeochemical data were analyzed at the Ontario Geoscience Laboratories and were used to characterize major lithostratigraphic units within each belt and to construct a chemostratigraphy to establish the petrogenetic variation across each greenstone belt. Radiogenic isotope data (whole rock $^{147}Sm/^{143}Nd$, and $^{206}Pb/^{204}Pb$) of rocks and sulphide mineralization from each belt was analyzed at the Radiogenic Isotope Facility at the University of Alberta. These data were used to determine the crustal architecture and amount of crustal contamination within volcanic rocks in each greenstone belt assemblage, and to link these to the metallogenic variation between the belts.

New U-Pb geochronology better constrained the emplacement history of the greenstone belts, the timing of volcanism and deformation, and allowed the correlation of lithostratigraphic units between adjacent greenstone belts that previously had poorly constrained ages (mainly the Vermilion and Winston Lake greenstone belts). Geochronology of magmatic zircons, analyzed at the Jack Satterly Geochronology Laboratory at the University of Toronto, and detrital zircons, analyzed at the Mineral Exploration Research Centre at Laurentian University, significantly improved our understanding of the depositional histories of the greenstone belts and aided in identifying the ca. 2720 Ma strata of the Wawa subprovince.

1.4. Structure of Thesis

This dissertation is presented in four chapters. Chapters 2, 3, and 4 have been written as manuscripts for submission to refereed scientific journals. Due to their stand-alone manuscript format, the “Introduction” and “Regional Geology” sections may overlap in their content so that they can exist as individual papers.

A number of collaborators provided supervision and scientific guidance throughout the preparation of these manuscripts. These collaborators stimulated scientific discussions of the various geological problems that were addressed in this thesis and provided editorial comments in the final stages of manuscript preparation. The editorial staff and geological assistants at the Ontario Geological Survey provided technical assistance in preparing government publications found in Appendices F to J. However, as first author, I completed all of the mapping and

gathering of field data, interpretations of petrographic and geochemical data, drafted all of the figures, wrote the first drafts of each manuscript, and communicated with the journal editors.

Chapter 1 introduces the purpose and objectives of the dissertation, the methods and procedures used to achieve those objectives, the structure of the thesis, and information concerning co-authorship on the manuscripts.

Chapter 2 is written as a manuscript entitled "**New U-Pb geochronology from Timiskaming-type assemblages in the Shebandowan and Vermilion Greenstone Belts, Wawa Subprovince, Superior Province: Implications for the Neoarchean development of the southwestern Superior Province**" (*Precambrian Research, vol. 235, pages 264-277*). This manuscript describes magmatic and detrital zircon geochronology collected in the Shebandowan and Vermilion greenstone belts and the correlation of supracrustal assemblages between the adjacent greenstone belts. The field observations and U-Pb geochronology collected in the Vermilion belt confirmed the presence of a previously unknown Timiskaming-type assemblage and correlated syn-deformation depositional and magmatic events along the nothern margin of the Wawa-Abitibi terrane.

The co-authors on this publication are: Gibson, H.L., Mineral Exploration Research Centre, Department of Earth Sciences, Laurentian University, Sudbury, Ontario, Canada P3E 2C6; Stott, G.M., Ontario Geological Survey (Retired), Stott Geoconsulting Ltd, 92 Crater Crescent, Sudbury, Ontario, Canada P3E 5Y6; Hudak, G.J., Precambrian Research Center, Natural Resources Research Institute, University of Minnesota Duluth, 5013 Miller Trunk Highway, Duluth, Minnesota, USA 55804; Jirsa, M.A., Minnesota Geological Survey, 2642 University Avenue W., St. Paul, MN, USA 55114-1032; and Hamilton, M.A. Jack Satterly Geochronology Lab, Department of Earth Sciences, University of Toronto, Toronto, Ontario, Canada M5S 3B1.

Chapter 3 is written as a manuscript entitled **"Geodynamic reconstruction of the Winston Lake greenstone belt and VMS deposits: New trace element geochemistry and U-Pb geochronology"** (*Economic Geology, In press*). This manuscript describes a comprehensive belt-scale geochemical, geochronological, and Nd- isotopic study of the Winston Lake greenstone belt. This is the first study to present geospatially- and stratigraphically-controlled analytical data for the Winston Lake greenstone belt. The manuscript describes the geodynamic evolution of the belt and the spatial and temporal development of VMS mineralization.

The co-authors on this publication are: Gibson, H.L., Mineral Exploration Research Centre, Department of Earth Sciences, Laurentian University, Sudbury, Ontario, Canada P3E 2C6; Stott, G.M., Ontario Geological Survey (Retired), Stott Geoconsulting Ltd, 92 Crater Crescent, Sudbury, Ontario, Canada P3E 5Y6; Franklin, J.M., Franklin Geosciences Ltd, 24 Commanche Drive, Ottawa, Ontario, Canada K2E 6E9; and Hamilton, M.A. Jack Satterly Geochronology Lab, Department of Earth Sciences, University of Toronto, Toronto, Ontario, Canada M5S 3B1.

Chapter 4 is written as a manuscript entitled **"The geodynamic setting, crustal architecture, and VMS metallogeny of ca. 2720 Ma greenstone belt assemblages of the northern Wawa subprovince, Superior Province"** (to be submitted to *Precambrian Research*). This manuscript illustrates how regional-scale geochemical and Nd/Pb isotopic data, collected from the Vermilion, Shebandowan, Winston Lake, and Manitouwadge greenstone belts can be used to highlight that differences in the metallogeny of each greenstone belt are reflected in the differences in petrogenesis and geodynamic setting for each belt. This chapter also serves as a concluding chapter as it summarizes the main objective of the dissertation based on knowledge gained from the greenstone belt-scale studies presented in the manuscripts from Chapters 2 and 3. This chapter also describes recommendations for future research based on the knowledge gained from the regional VMS synthesis.

The co-authors on this publication are: Gibson, H.L., Mineral Exploration Research Centre, Department of Earth Sciences, Laurentian University, Sudbury, Ontario, Canada P3E 2C6; Stott, G.M., Ontario Geological Survey (Retired), Stott Geoconsulting Ltd, 92 Crater Crescent, Sudbury, Ontario, Canada P3E 5Y6; Franklin, J.M., Franklin Geosciences Ltd, 24 Commanche Drive, Ottawa, Ontario, Canada K2E 6E9; and Hudak, G.J., Precambrian Research Center, Natural Resources Research Institute, University of Minnesota Duluth, 5013 Miller Trunk Highway, Duluth, Minnesota, USA 55804.

Appendix A contains quality assurance/quality control analyses for lithogeochemical data collected from the Ontario Geoscience Laboratories from 2010 to 2011.

Appendices B through E contain raw lithogeochemical, Nd and Pb isotopic, and U-Pb geochronological data that was collected in Minnesota or funded by sources other than the Ontario Geological Survey.

Appendix F contains Miscellaneous Release – Data 306 published by the Ontario Geological Survey. This contains all field and analytical data that was collected within Ontario that was funded by the Ontario Geological Survey. These data are presented geospatially in ArcGIS© format. The co-author for this publication is Chartrand, J.E., Ontario Geological Survey, 933 Ramsey Lake Road, Sudbury, Ontario, Canada, P3E 6B5.

Appendices G through F contain self-authored reports and field trip guidebooks that were published by the Ontario Geological Survey.

1.5. Statement of Original Contributions

The following points outline the original contributions presented by the author in this dissertation:

1. This study added a new magmatic zircon U-Pb age to the Vermilion greenstone belt in an area that previously had very few dates. The results indicated that the Gafvert Lake sequence is a younger, Timiskaming-type volcanic assemblage and is co-depositional with similar assemblages in the Shebandowan greenstone belt.
2. This study documented two types of syn-deformational sedimentary basins that developed in the Shebandowan and Vermilion greenstone belts. Detrital zircon analyses from these belts suggest that there was co-deposition of locally-derived detritus in transpressional pull-apart basins and detritus derived from the Wabigoon subprovince that was deposited in a foreland-type basin.
3. This study compiled trace element geochemistry from government and peer-reviewed publications and demonstrated that the volcanic rocks from the Timiskaming-type assemblages from the Shebandowan and Vermilion greenstone belts are notably less alkalic and enriched in incompatible elements compared to those from the Timiskaming assemblage in the Abitibi subprovince. Magmatic fluids from alkalic intrusions are better at mobilizing gold, and this may be partially responsible for the discrepancy in economic gold mineralization between the two regions despite being deposited in similar geodynamic settings.
4. This study is intended to provide the first detailed lithostratigraphic and ore body descriptions of the VMS-hosting Winston Lake greenstone belt in peer-reviewed literature (pending the acceptance of the manuscript for publication).

5. This study resulted in geospatially and lithostratigraphically controlled geochemical, Nd isotopic and U-Pb geochronological data for the Winston Lake greenstone belt that provides the first complete belt-scale description of the geological, petrogenetic, and metallogenic history of the belt.
6. This project describes variations in the petrogenesis, crustal-architecture, and metallogeny between the Vermilion, Shebandowan, Winston Lake, and Manitouwadge greenstone belts, based on geochemical and isotopic data (Pb/Nd) collected from representative strata from each belt. The isotopically juvenile Manitouwadge greenstone belt was deposited in an extensional back-arc setting and is the most enriched in VMS mineralization. Plume-driven arc rifting in the Winston Lake greenstone belt formed Zn-rich VMS mineralization in a shallow water environment during the early stages of rifting. Similar rifted-arc geodynamic settings are present in the Vermilion greenstone belt, but the ideal VMS-forming geodynamic setting appears to be hindered by a shallow water environment. Finally, the Shebandowan greenstone belt was dominated by crustal thickening and compression during "hot" subduction and VMS-forming events are localized to plume-driven rifting. However, the crustal thickening may have been a key factor in relative enrichment of magmatic sulphides and gold prospectivity in comparison to compare to the other belts.

1.6. References

Ayer, J.A., Goutier, J., Thurston, P.C., Dubé, B., Kamber, B.S., 2010. Tectonic and metallogenic evolution of the Abitibi and Wawa Subprovinces; *in* Summary of Field Work and Other Activities, Open File Report 6260. Ontario Geological Survey, pp. 3-1 to 3-6.

Brown, G.H., Fogal, R.I., 1995. Precambrian geology, Oliver Township. Ontario Geological Survey, Map 2615, 1:20,000.

Corfu, F., Stott, G.M., 1986. U-Pb ages for late magmatism and regional deformation in the Shebandowan Belt, Superior Province, Canada. Can. J. Earth Sci. 23, 1075-1082.

Corfu, F., Stott, G.M., 1998. Shebandowan greenstone belt, western Superior Province: U-Pb ages, tectonic implications, and correlations. GSA Bulletin 110, 1467-1484.

David, J., Davis, D.W., Dion, C., Goutier, J., Legault, M., Roy, P., 2007. U–Pb age dating in the Abitibi Subprovince in 2005–2006. Ministère des Ressources naturelles et de la Faune du Québec, RP 2007-01(a), 2 p.

Davis, D.W., Schandl, E.S., Wasteneys, H.A., 1994. U-Pb dating of minerals in alteration halos of Superior Province massive sulfide deposits; syngenesis versus metamorphism. Contributions to Mineralogy and Petrology 115, 427-437.

Franklin, J.M., Gibson, H.L., Jonasson, I.R., Galley, A.G., 2005. Volcanogenic massive sulphide deposits; *in* Hedenquist, J.F.H., Goldfarb, R.J., Richards, J.P. (Eds.), Economic Geology, 100th Anniversary Volume, pp. 523-560.

Galley, A.G., Hannington, M.D., Jonasson, I.R., 2007. Volcanogenic massive sulphide deposits; *in* Goodfellow, W.D. (Ed.) Mineral Deposits of Canada: A Synthesis of Major Deposit-Types, District Metallogeny, the Evolution of Geological Provinces, and Exploration Methods: Geological Association of Canada, Mineral Deposits Division, Special Publication No. 5, pp. 141-161.

Gorton, M.P., Schandl, E.S., 1995. An unusual sink for rare earth elements: the rhyolite-basalt contact of the Archean Winston Lake volcanogenic massive sulphide deposit, Superior Province, Canada. Economic Geology 90, 2065-2072.

Hart, T.R., Metsaranta, D.-A., 2009. Precambrian geology of the Wye and Hamlin Lakes area. Ontario Geological Survey, Preliminary Map P.2511, 1:20,000.

Hudak, G.J., Heine, J., Newkirk, T., Odette, J.D., Huack, S., 2002. Comparative geology, stratigraphy, and lithogeochemistry of the Fivemile Lake, Quartz Hill, and Skeleton Lake VMS occurrences, Vermilion district, NE Minnesota. State of Minnesota: Natural Resources Research Institute Technical Report NRII/TR-2002/03, 390 p.

Kerrich, R., Polat, A., Xie, Q., 2008. Geochemical systematics of a 2.7 Ga Kinojevis Group (Abitibi), and Manitouwadge and Winston Lake (Wawa) Fe-rich basalt-rhyolite associations: Backarc rift oceanic crust? Lithos 101, 1-23.

Ketchum, J.W.F., Ayer, J.A., Van Breemen, O., Pearson, N.J., Becker, J.K., 2008. Pericontinental crustal growth of the southwestern Abitibi subprovince, Canada - U-Pb, Hf, and Nd isotope evidence. Economic Geology 103, 1151-1184.

Lodge, R.W.D., 2011. A progress report on the volcanology, stratigraphy and geodynamic setting of greenstone belts of age 2720 Ma near the Wawa– Quetico Subprovincial boundary; *in* Summary of Field Work and Other Activities, Open File Report 6270. Ontario Geological Survey, pp. 11-11 to 11-13.

Lodge, R.W.D., Gibson, H.L., Stott, G.M., Hudak, G.J., Jirsa, M., 2013. New U-Pb geochronology from Timiskaming-type assemblages in the Shebandowan and Vermilion greenstone belts, Wawa Subprovince, Superior Craton: Implications for the Neoarchean development of the southwestern Superior Province. Precambrian Research 235, 264-277.

Osmani, I.A., 1997. Precambrian geology, Moss Township. Ontario Geological Survey, Map 2624, 1:20,000.

Osterberg, S.A., 1993. Stratigraphy, physical volcanology, and hydrothermal alteration of the footwall rocks to the Winston Lake massive sulfide deposits, northwestern Ontario. Ph.D. Thesis, University of Minnesota at Minneapolis, 351 p.

Peterson, D., Gallup, C., Jirsa, M., Davis, D.W., 2001. Correlation of the Archean assemblages across the U.S.-Canadian border: Phase I geochronology; *in* 47th Annual Meeting, Institute on Lake Superior Geology, Proceedings Volume 47, Part 1 - Program and Abstracts, pp. 77-78.

Peterson, D., Jirsa, M., 1999. Bedrock geologic map and mineral exploration data, western Vermilion district, St. Louis and Lake Counties, northeastern Minnesota. Minnesota Geological Survey, Miscellaneous Map M-98, 1:48,000.

Peterson, V.L., Zaleski, E., 1999. Structural history of the Manitouwadge greenstone belt and its volcanogenic Cu-Zn massive sulphide deposits, Wawa Subprovince, south-central Superior Province. Can. J. Earth Sci. 36, 605-625.

Polat, A., 2009. The geochemistry of Neoarchean (ca. 2700 Ma) tholeiitic basalts, transitional to alkaline basalts, and gabbros, Wawa Subprovince, Canada: Implications for petrogenetic and geodynamic processes. Precambrian Research 168, 83-105.

Polat, A., Kerrich, R., 2006. Reading the geochemical fingerprints of Archean hot subduction volcanic rocks: Evidence for accretion and crustal recycling in a mobile tectonic regime. Geophysical Monograph Series 164, 189-213.

Pye, E.G., 1964. Mineral deposits of the Big Duck Lake area, district of Thunder Bay. Ontario Department of Mines Geological Report 27, 58 p.

Ritcey, D.J., 1992. Geology and mineralization in the vicinity of Big Duck Lake, Ontario. M.Sc. Thesis, University of Ottawa, 235 p.

Rogers, M.C., 1995. Precambrian geology, Duckworth Township. Ontario Geological Survey, Map 2621, 1:20,000.

Stott, G.M., 2011. A revised terrane subdivision of the Superior Province of Ontario. Ontario Geological Survey, Miscellaneous Release - Data 278, p.

Stott, G.M., Corkery, M.T., Percival, J.A., Simard, M., Goutier, J., 2010. A revised terrane subdivision of the Superior Province; *in* Summary of Field Work and Other Activities, Open File Report 6260. Ontario Geological Survey, pp. 20-21 to 20-10.

Vervoort, J.D., White, W.M., Thorpe, R.I., 1994. Nd and Pb isotope ratios of the Abitibi greenstone belt: new evidence for very early differentiation of the Earth. Earth and Planetary Science Letters 128, 215-229.

Williams, H.R., Stott, G.M., Heather, K.B., Muir, T.L., Sage, R.P., 1991. Wawa Subprovince; *in* Thurston, P.C., Williams, H.R., Sutcliffe, R.H., Stott, G.M. (Eds.), Geology of Ontario, Ontario Geological Survey, Special Volume 4, Part 1, pp. 485-541.

Zaleski, E., Peterson, V.L., 1995. Depositional setting and deformation of massive sulfide deposits, iron formation, and associated alteration in the Manitouwadge greenstone belt, Superior Province, Ontario. Economic Geology 90, 2244-2261.

Zaleski, E., Peterson, V.L., 2001. Geology of the Manitouwadge greenstone belt and the Wawa-Quetico subprovince boundary, Ontario. Geological Survey of Canada, Map 1917A, 1:25,000.

Zaleski, E., van Breemen, O., Peterson, V.L., 1999. Geological evolution of the Manitouwadge greenstone belt and Wawa-Quetico subprovince boundary, Superior Province, Ontario, constrained by U-Pb zircon dates of supracrustal and plutonic rocks. Can. J. Earth Sci. 36, 945-966.

CHAPTER 2

NEW U-PB GEOCHRONOLOGY FROM TIMISKAMING-TYPE ASSEMBLAGES IN THE SHEBANDOWAN AND VERMILION GREENSTONE BELTS, WAWA SUBPROVINCE, SUPERIOR PROVINCE: IMPLICATIONS FOR THE NEOARCHEAN DEVELOPMENT OF THE SOUTHWESTERN SUPERIOR PROVINCE

2.1. Abstract

Timiskaming-type assemblages in the Wawa-Abitibi terrane of the Superior Province and other Archean cratons worldwide are economically important because of their spatial and temporal association with world-class orogenic gold mineralization, especially in the Kirkland Lake area of Ontario. These mainly locally-derived sedimentary assemblages were deposited in transtensional, pull-apart basins that developed during the final stages of terrane accretion, and are commonly associated with calc-alkalic to alkalic volcanic and plutonic rocks. The Shebandowan and Vermilion greenstone belts (SGB, VGB) in the Wawa subprovince have significantly less economic base and precious metal mineralization than the greenstone belts of the Abitibi subprovince and the timing of deformation and magmatism in the SGB and VGB is less well constrained. This study presents new U-Pb geochronology from the SGB and VGB that demonstrates that sedimentary and volcanic rocks of the Lake Vermilion Formation in the VGB are coeval with similar rocks in the SGB, and that their interpreted depositional environments are consistent with these units being Timiskaming-type assemblages. Analyses of magmatic zircons in a dacitic tuff breccia from the Gafvert Lake sequence, the volcanic member of the Lake Vermilion Formation, provided a high precision U-Pb age of 2689.7 ± 0.8 Ma using thermal ionization mass spectrometry. Detrital zircon geochronology using LA-ICP-MS confirms that the source of the detritus in the Lake Vermilion Formation was locally derived from the Gafvert Lake metavolcanic lithofacies. A similar temporal pattern was observed in many of the Timiskaming-type sedimentary rocks that were sampled in the SGB. The locally-derived, alluvial-fluvial to shallow marine depositional environment of long, narrow basins with rapid lateral facies changes described in the SGB and VGB are consistent with deposition in structurally-controlled, pull-apart basins. However, one sample from the SGB had detrital zircons with ages that were more akin to the age range found to the north in the Wabigoon

subprovince, which suggests trans-terrane transport of detritus in a foreland-type basin. Geochemically, the Timiskaming-type volcanic rocks in the VGB and SGB are less enriched in incompatible elements and are comparatively less alkalic than volcanic rocks in the Timiskaming assemblage of Kirkland Lake. This may indicate that the structures that formed the basins within the SGB and VGB in the Wawa subprovince were not as deeply penetrating as those of the Abitibi, which may explain the paucity of economic gold mineralization associated with the former. The Timiskaming-type deposits of the northern Wawa-Abitibi terrane are 20 Ma older than the Timiskaming assemblage in the Abitibi subprovince, and co-depositional with the flysch-like deposits of the Porcupine assemblage in the southern part of that terrane.

2.2. Introduction

The Wawa-Abitibi terrane (Stott et al., 2010) is the southernmost and youngest granite-greenstone terrane of the Superior Province and is divided into two subprovinces: The Wawa subprovince to the west of the Kapuskasing structural zone, and the Abitibi subprovince to the east (**Figure 2.1, inset)**. It is host to many world-class synvolcanic hydrothermal and magmatic base-metal as well as orogenic gold mineral deposits. In the Wawa subprovince, geochronological studies in the Shebandowan (Corfu and Stott, 1986, 1998; Hart, 2007), Manitouwadge (Zaleski et al., 1999), Vermilion (Peterson et al., 2001), and Winston Lake (Davis et al., 1994) greenstone belts have shown that the volcanic assemblages of these greenstone belts are coeval. Most of the pre-D_1 volcanic construction along the margin of the Wawa subprovince occurred between 2722-2718 Ma (**Figure 2.1, inset**). During this time, large volcanogenic Cu-Zn-Pb±Au±Ag deposits (Winston Lake/Geco Mines; Davis et al., 1994) and magmatic Ni-Cu deposits (Shebandowan Mine; Morton, 1982) formed. Subsequent deformation and accretion of the Wawa to the Superior Province between 2695-2680 Ma (Corfu and Stott, 1998) culminated in the deposition of Timiskaming-type, calc-alkalic to alkalic metavolcanic and metasedimentary rocks (Shegelski, 1980; Borradaile and Brown, 1987; Jirsa, 2000) **(Figure 2.1)**. The shear zones and calc-alkalic to alkalic magmatism of the Timiskaming-type deposits in the Wawa subprovince are commonly temporally associated with gold mineralization (Stott and Schnieders, 1983; Osmani, 1997; Peterson and Jirsa, 1999; Jobin-Bevans et al., 2006). In the Abitibi subprovince, the Timiskaming assemblage is associated with the world-class gold deposits in the Timmins and Kirkland Lake areas of Ontario (Dubé and Gosselin, 2007; Bateman et al., 2008).

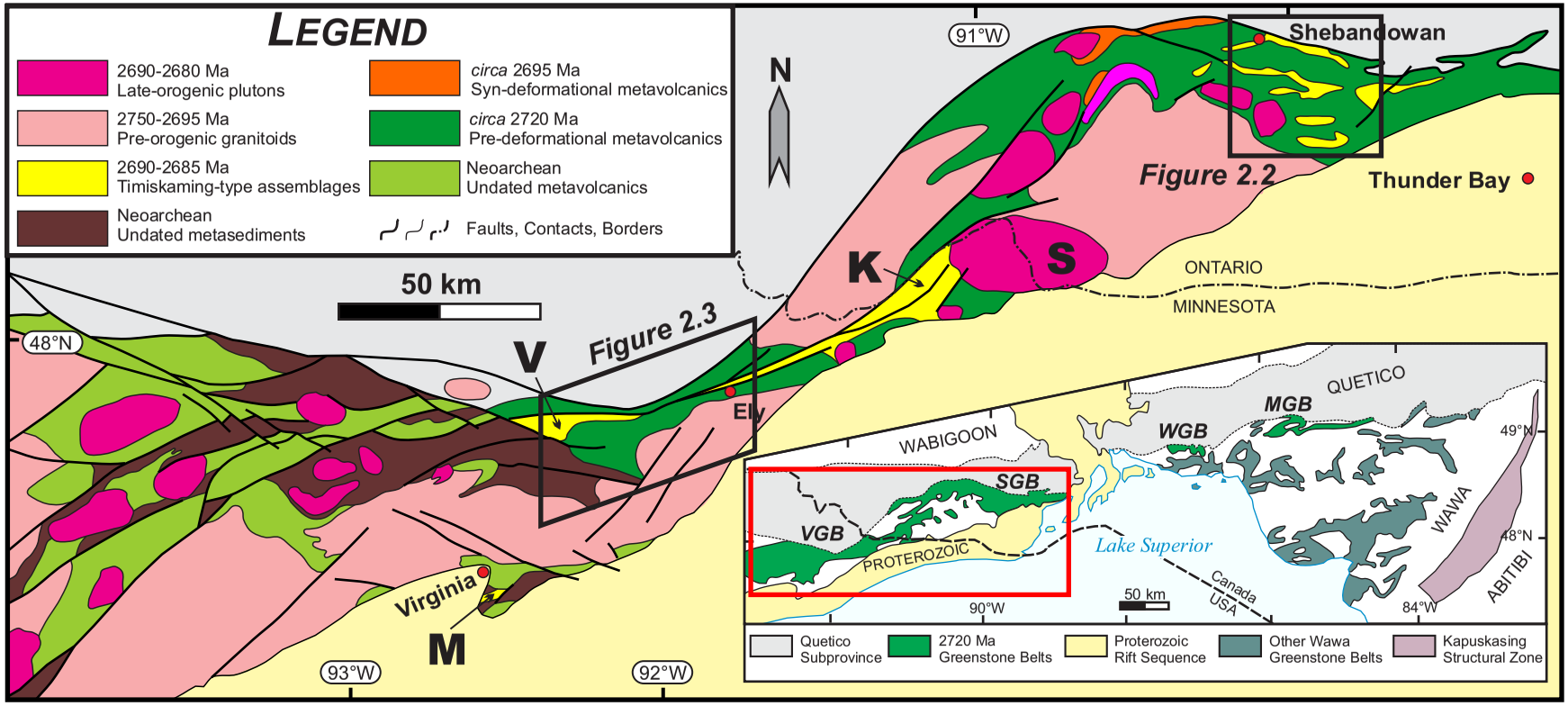

Figure 2.1 - Regional geochronology for the Shebandowan and Vermilion greenstone belts at the Ontario-Minnesota border. Figure modified from Peterson et al. (2001) to include geochronology from Corfu and Stott (1998), Hart (2007), Peterson et al. (2001), Lodge (2012), and this study. Saganaga Tonalite is labeled as "S". Knife Lake Group is labeled "K". Lake Vermilion Formation is labeled "V". Midway sequence is labeled as "M". Inset map is of the Wawa subprovince. VGB = Vermilion greenstone belt. SGB = Shebandowan greenstone belt. WGB = Winston Lake greenstone belt. MGB = Manitouwadge greenstone belt. Inset map modified from Lodge (2011).

The classic lithologic character and relative timing of Timiskaming-type assemblages are based on the Timiskaming assemblage at Kirkland Lake in the Abitibi subprovince where the structures and alkalic magmatism/volcanism in this group are associated with some of the largest orogenic gold deposits in the world (e.g., Bateman et al., 2008; Ispolatov et al., 2008). Timiskaming-type assemblages comprise Neoarchean syn-orogenic sedimentary and volcanic lithofacies in greenstone belts that are deposited in localized, fault- and unconformity-bounded pull-apart basins developed by extensional transtensional shearing during terrane accretion or orogenic collapse (Christie-Blick and Biddle, 1985; Corcoran and Mueller, 2007). These pull-apart basins are elongate, narrow basins that are in close spatial association with strike-slip faulting where offsets or bends in strike-slip faults result in localized extension (Gürbüz, 2010). They represent some of the youngest supracrustal assemblages in greenstone belts and are deposited unconformably on older, pre-deformed volcanic arc successions (e.g., Shegelski, 1980; Corcoran and Mueller, 2007; Driese et al., 2011). Sedimentary facies of Timiskaming-type deposits resemble terrestrial to shallow marine molasse-like successions (Hyde, 1980; Mueller and Corcoran, 1998). Conglomerate-sandstone lithofacies were deposited in alluvial fans and braided streams and contain locally-derived detritus from the greenstone belt in which they are deposited within, as well as younger magmatic rocks that are temporally and spatially associated with transtensional deformation. Sandstone-argillite lithofacies represent fluvial, fluvial-deltaic, floodplain, and local lacustrine and shallow marine deposition. Rapid lateral changes, stacking of the sedimentary lithofacies, and proximity to major basin-bounding faults support a tectonically induced sedimentary basin model (Mueller and Corcoran, 1998). Volcanic deposits are not found in every Timiskaming-type deposit in the Superior Province, but where present they are calc-alkalic to alkalic in composition (Othman et al., 1990; Carter, 1993). Gold mineralization in Timiskaming-type assemblages is commonly temporally associated with this magmatism, which may have contributed to the fluids that mobilize and deposit gold in coeval faults and shear zones.

Timiskaming-type metasedimentary and metavolcanic successions in the Shebandowan greenstone belt, westernmost Wawa subprovince, have been well constrained in Ontario by field observations (Shegelski, 1980; Borradaile and Brown, 1987; Rogers and Berger, 1995) and geochronological research (Corfu and Stott, 1986, 1998). Understanding the distribution, composition, and relative age of comparable assemblages in Minnesota may identify

assemblages having higher gold potential in a region that has seen little exploration for precious metals (Peterson and Patelke, 2004). Sparse geochronological data in the Vermilion greenstone belt, Minnesota, has inhibited adequate correlation of assemblages and deformation events with the Shebandowan greenstone belt, as well as the identification of Timiskaming-type deposits. This study presents the results of new U-Pb zircon geochronology of the metasedimentary and metavolcanic rocks of the Lake Vermilion Formation in the VGB of Minnesota that confirm that at least some portion of the strata assigned to the Lake Vermilion Formation, including felsic volcanic lithofacies of the informally named Gafvert Lake sequence, represents a Timiskaming-type assemblage. The geochemistry of metavolcanic rocks from the Timiskaming-type deposits of the VGB and SGB is compared to the Timiskaming assemblage metavolcanic rocks in the Kirkland Lake area of the Abitibi subprovince to investigate the relationship between the composition and petrogenesis of magmas and economic gold mineralization. Lastly, the provenance of the newly-defined Timiskaming-type deposits of Minnesota is interpreted in light of new detrital zircon geochronology obtained from the Shebandowan assemblage in Ontario to determine variations in the source of detritus for these basins and implications for the assembly of the Superior Province.

2.3. Regional Geology

2.3.1. Shebandowan Greenstone Belt (SGB)

The Shebandowan Greenstone Belt (SGB) is 150 km long and extends west from Thunder Bay to the Ontario-Minnesota border near the Saganaga Tonalite (**Figure 2.1**). The SGB is locally in fault contact with the Quetico subprovince to the north and is bounded on the south by younger granitic intrusions, slivers of older 2750 Ma tonalitic gneiss, and Proterozoic rift deposits (Williams et al., 1991a; Corfu and Stott, 1998). The SGB is mostly composed of pre-D_1 rifted-arc and/or plume-generated calc-alkaline to tholeiitic volcanic suites of *circa* 2720 Ma age (Corfu and Stott, 1998; Hart, 2007). These deposits were initially divided into the Burchell and Greenwater assemblages based primarily on opposing younging directions (Williams et al., 1991a), but have since been shown to be the same age and likely represent a fold-thrust repetition of a single (Greenwater) assemblage (Corfu and Stott, 1998). The 2720 Ma volcanics are tectonically interleaved with syn-D_1 (*circa* 2695 Ma) calc-alkalic diorite sills and related intermediate volcanic rocks of the Kashabowie assemblage (Corfu and Stott, 1998) and

the 2696 ± 2 Shebandowan Lake Pluton (Corfu and Stott, 1986). Timiskaming-type lithofacies in the SGB (known as the Shebandowan assemblage) were deposited prior to D_2 transpression (Corfu and Stott, 1998) and are composed of wacke, sandstone, and conglomerate with minor calc-alkalic to alkalic intermediate volcanic rocks and intrusions. Hornblende trachyandesite flows and volcaniclastic rocks, the syenitic to dioritic Tower Stock, and the Saganaga Tonalite have U-Pb radiometric ages *circa* 2690 Ma (Corfu and Stott, 1998). Detrital zircon geochronology has confirmed that the metasedimentary rocks in the Finmark and the southern part of Adrian Township area are younger than the Greenwater assemblage, but the data were insufficient to establish a relationship to the Shebandowan assemblage (Corfu and Stott, 1998). The youngest assemblage in the SGB is the Auto Road assemblage located east of the study area. Conglomerate from this unit contains clasts of late-tectonic granites that have a U-Pb age of 2682 ± 3 Ma and is affected by D_2 lineations (Corfu and Stott, 1998). D_2 lineations are overprinted by localized deformation associated with the emplacement of post-D_2 intrusions (2683 ± 3 Ma Kekekuab pluton; Corfu and Stott, 1998). Taking into account the errors, the timing of D_2 deformation can be constrained to 2680-2685 Ma. The focus of this study is in the eastern part of the SGB where the largest concentration of Timiskaming-type deposits is found **(Figure 2.2**).

The Timiskaming-type successions of the SGB are interpreted to have been deposited in subaerial to shallow marine environments (Shegelski, 1980). The characteristics of poorly-sorted, matrix-supported alluvial fan-like conglomerate and green- to purple-colored trachyandesite tuff breccia are similar to those of Timiskaming-type deposits elsewhere in the Wawa-Abitibi terrane (Corcoran and Mueller, 2007). Well-preserved mud-draped wacke and herring-bone cross-laminated sandstone in the Finmark area west of Thunder Bay are interpreted to be deposition in an intertidal environment (Koebernick and Fralick, 1995). In Adrian Township, exposures of subaerially weathered hornblende-phyric felsic to intermediate lava flows are capped by a poorly-sorted heterolithic conglomerate in close spatial association with wacke and sandstone with erosional features such as channel and rip-up structures (Lodge, 2011). These are suggestive of alluvial fan and fluvial depositional environments, similar to those interpreted to characterize the Knife Lake Group (Driese et al., 2011). Turbiditic deposits described in Adrian Township are interpreted to be indicative of a deeper-water environment of deposition (Rogers and Berger, 1995). Prior to the results of this study, data from a few detrital

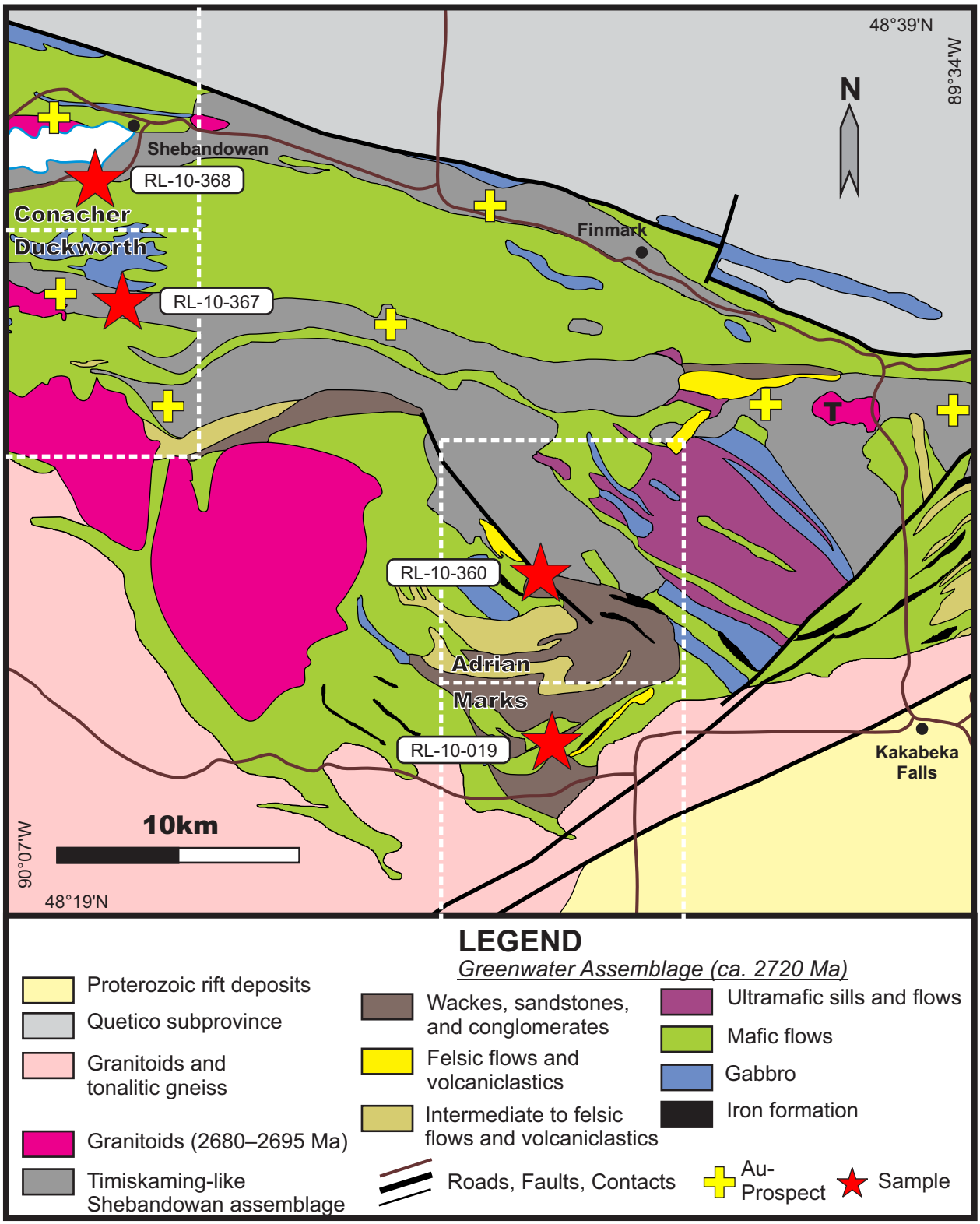

Figure 2.2 - Regional geology of the eastern part of the Shebandowan greenstone gelt showing location of samples. Geology modified from Santaguida (2001). Tower Stock, referred to throughout the text, is labeled "T". Townships discussed in text are outlined by dashed white line.

zircon grains were not conclusive in determining if the Adrian Township sedimentary strata are part of the Shebandowan assemblage or another post-Greenwater sedimentary basin (Corfu and Stott, 1998).

2.3.2. Vermilion Greenstone Belt (VGB)

The Vermilion Greenstone Belt (VGB) in Minnesota is near-continuous with the SGB, separated only by the Saganaga Tonalite **(Figure 2.1)**. The VGB has historically been subdivided into the Soudan and Newton belts on the basis of stratigraphic and structural settings, and the boundary between the belts is marked by the Mud Creek shear zone and the Knife Lake Group (Jirsa et al., 1992; Southwick et al., 1998) **(Figure 2.3)**. The Newton belt contains locally abundant ultramafic flows and sills and has been inferred to be continuous with the Greenwater assemblage of the SGB (Southwick et al., 1998; Peterson et al., 2001). The Soudan belt, the focus of this study, is a broadly folded assemblage of calc-alkalic to tholeiitic volcanic strata containing the Soudan Iron Formation and associated siliciclastic rocks. A quartz-phyric rhyolite dome at the Fivemile Lake Cu-Zn prospect, stratigraphically beneath the Soudan Iron Formation (Hudak et al., 2002), has a U-Pb zircon age of 2722 ± 0.9 Ma (Peterson et al., 2001) and is coeval with the Greenwater assemblage in the SGB. Lithologically, the Soudan belt is similar to, and has been correlated with, the Saganagons assemblage (Southwick et al., 1998). Timiskaming-type successions have been identified by petrological and geochronological data in the Virginia area (Jirsa, 2000; Jirsa and Boerboom, 2003) and Knife Lake Group (Jirsa et al., 2012). They typically occur as isolated linear belts of conglomerate-bearing strata that lie in fault and unconformable contact with subjacent volcanic and intrusive rocks. The Knife Lake Group consists of basal trachyandesite strata and derived volcaniclastic rocks that are locally cut by synvolcanic intrusions with a U-Pb age of 2690.7 ± 0.6 Ma (Jirsa et al., 2012). The upper Knife Lake Group contains conglomerate and sandstone sourced from the Saganaga Tonalite (2690.83 ± 0.26 Ma; Driese et al., 2011). D_2 deformation produced a regional penetrative metamorphic fabric in nearly all rocks of the VGB. One exception is a feldspar porphyry intrusion in the Newton Belt that lacks foliation and is 2683 +1/-1.4 Ma (Peterson et al., 2001), which provides a minimum age for the regional D_2 deformation event.

A prominent feature of the Soudan belt is the Tower-Soudan anticline that is delineated by three members of the VGB designated stratigraphically upward as the Lower Ely, Soudan, and Upper Ely members. Strata within the Soudan belt are largely intact and young outward from

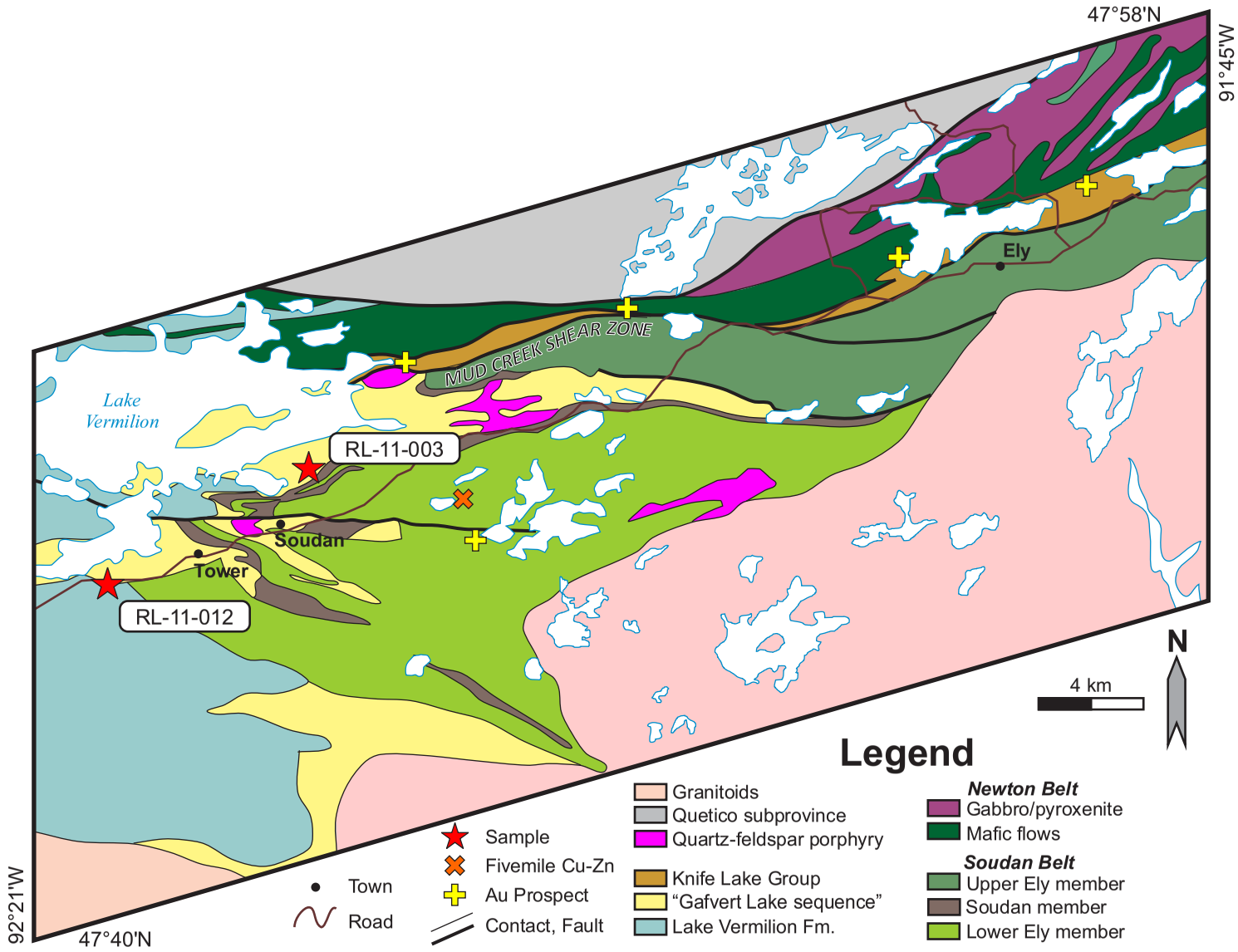

Figure 2.3 - Regional geology of the Soudan-Ely region of the Vermilion greenstone belt showing location of samples. Geology modified from Peterson (2004) and Peterson and Jirsa (1999).

the core of the anticline. The Lower Ely member is composed of calc-alkalic and tholeiitic mafic to intermediate flows and volcaniclastic rocks and minor felsic metavolcanic rocks (Hudak et al., 2002; Hudak et al., 2012). The Soudan member is an Algoma-type, cherty iron formation with minor interlayered mafic flows, felsic tuffs, and intermediate to mafic sills (Peterson and Patelke, 2003). The Upper Ely member is composed of predominantly massive to sparsely amygdaloidal tholeiitic mafic flows with local lenses of intercalated iron formation (Southwick et al., 1998; Hudak et al., 2012). The Gafvert Lake sequence of the Lake Vermilion Formation directly overlies parts of the Soudan member. The contact between the Soudan member and Gafvert Lake sequence is not exposed. However, the Gafvert Lake sequence within 2-3 metres of the contact contains angular intraclasts of cherty iron formation derived from the underlying Soudan Iron Formation (Hoffman, 2007; Radakovich et al., 2010; Heim et al., 2012). The presence of angular iron formation intraclasts, the similarity in bedding attitudes, and the absence of a pronounced foliation or mylonitic fabric in the rocks immediately adjacent to the contact suggests the contact is a disconformity. The Lake Vermilion Formation (which includes the Gafvert Lake sequence) is composed of wacke, arenite, mudstone, and conglomerate, and has been interpreted to have been derived, in part, from detritus sourced from the Gafvert felsic volcanic rocks (Ojakangas, 1972; Southwick et al., 1998). Prior to this study, geochronological data were lacking to confirm the source or age of detritus that comprises Lake Vermilion Formation.

Prior to this study, known Timiskaming-type assemblages in the VGB were limited to two sequences: the Knife Lake Group and the Midway sequence (Jirsa, 1998). The Knife Lake Group is a fault- and unconformity-bounded pre-D_2 succession of conglomerate, sandstone, wacke, and mudstone locally associated with trachyandesite (Arth and Hanson, 1975; Shirey and Hanson, 1984; Driese et al., 2011). Based on macroscopic and petrographic observations, sedimentary detritus comprising the Knife Lake Group was derived from older (ca. 2720 Ma) volcanic and intrusive rocks, younger (ca. 2690 Ma) trachyandesite volcanic strata, and the ca. 2690 Ma Saganaga Tonalite (Goldich et al., 1972; Ojakangas, 1972; Driese et al., 2011). The depositional environments of this group range over the duration of deposition from subaerial, to alluvial-fan and fluvial, to lacustrine and shallow marine. Subaerial weathering is apparent from a paleosaprolitic zone in the uppermost Saganaga Tonalite that is overlain by conglomerate containing weathered and fresh tonalite fragments (Driese et al., 2011). The hornblende- and augite-bearing trachyandesite flows and breccia in the lower Knife Lake Group are

petrographically similar to the Shebandowan assemblage in the SGB (Vinje, 1978), and are the same age, *circa* 2690 Ma (Corfu and Stott, 1998; Driese et al., 2011). The Midway sequence occurs in the Virginia area of Minnesota **(Figure 2.1)**. The Archean rocks of the Midway sequence are not continuous with the adjacent VGB or SGB and no geochronologic data exist to confirm their absolute age relationship to the Neoarchean rocks in the Soudan-Ely region. Precise stratigraphic correlation is not known, but the Midway sequence has been included within the Soudan belt on regional geological maps (e.g., Peterson et al., 2001) based on lithological similarities (Jirsa, 1998). The Midway sequence is composed of a subaerially-deposited alluvial-fluvial conglomerate coeval with hornblende-phyric trachyandesite flows and breccia (Jirsa, 2000). Clasts within the conglomerate are locally derived from the alkalic volcanic strata within the basin and from surrounding greenstone belt lithofacies (Jirsa and Boerboom, 2003). Trachyandesite shares the same sea-green to purplish-red coloration as the hornblende-phyric volcanic units in the Timiskaming-type Shebandowan assemblage of the SGB (Shegelski, 1980).

2.4 Detrital Zircon Geochronology

Five samples from sedimentary lithofacies in the VGB and SGB were collected to determine the approximate age and sedimentary provenance of the detritus. Regional compilation maps by the Ontario Geological Survey (Santaguida, 2001) have highlighted sedimentary units designated as part of the Greenwater assemblage (**Figure 2.2).** The best exposures of these presumed older metasedimentary rocks occur in Marks and Adrian Townships west of Thunder Bay. These rocks are typically dark-colored turbiditic wacke to fluvial siltstone and sandstone with erosional features such as channel structures (**Figure 2.4D**) and rip-up clasts. Elsewhere in the SGB, Timiskaming-type wacke, siltstone, and sandstone are generally similar to those in Marks Township. The primary structures and types of sedimentary rocks indicate an alluvial-fluvial depositional environment for both units. Therefore, the pre- and post Timiskaming-type units cannot be distinguished on the basis of their interpreted environment of deposition alone. East-plunging mineral lineations indicate that the sedimentary rocks in Marks Township were affected by D_2, which has been preferentially confined to the Timiskaming-type Shebandowan assemblage in the southeastern part of the SGB (Stott and Schnieders, 1983). Conglomeratic units are more common in the Timiskaming-type assemblages in Conacher (**Figure 2.4C**) and

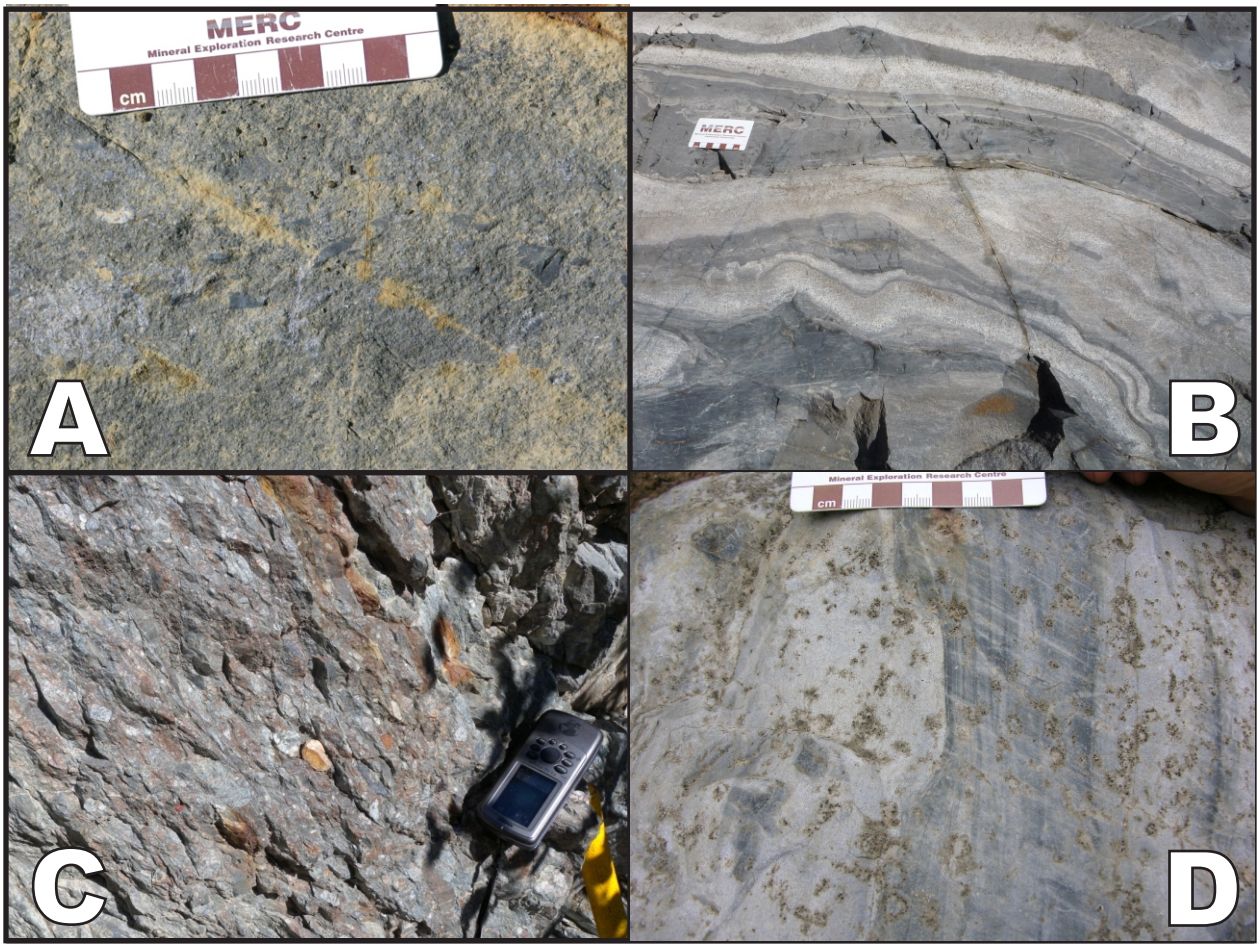

Figure 2.4 – Timiskaming-type metasedimentary rocks in the Vermilion and Shebandowan greenstone belts. A) Coarse sandstone to matrix-supported heterolithic pebble conglomerate near sample RL-10-360 in Adrian Township, Ontario. B) Folded slate and graded wacke of the Lake Vermilion Formation near Tower, Minnesota, near sample RL-11-012. C) Clast-supported heterolithic conglomerate near sample RL-11-368 in Conacher Township, Ontario. D) Wacke and sandstone with channel structures near sample RL-10-019 in Marks Township, Ontario.

Adrian Townships (**Figure 2.4A**). Finer-grained clastic sedimentary strata are common in the SGB. In the VGB, the complexly-folded turbiditic metasedimentary rocks of the Lake Vermilion Formation (**Figure 2.4B**) near Tower, Minnesota, were sampled to: 1) compare the age of detritus to the Timiskaming-type assemblages in the SGB and to the magmatic age for the Gafvert Lake sequence; 2) to determine if the Lake Vermilion Formation is also a Timiskaming-type assemblage; and 3) if the Gavfert Lake felsic volcanic strata are the dominant source of detritus for the Lake Vermilion Formation.

The U-Pb ages of detrital zircons were analyzed using laser ablation inductively coupled plasma mass spectrometry (LA-ICP-MS) at the Mineral Exploration Research Centre at Laurentian University, Sudbury, Ontario. Samples were crushed, milled, and passed over a Wilfley Table to obtain a pre-concentrate of heavy minerals. The pre-concentrate was split into magnetic fractions before the least magnetic fraction was passed through heavy liquids to separate zircons and other heavy minerals (pyrite, apatite, etc). Zircons were then picked and mounted in epoxy for analysis. All grains were analyzed using a 193 nm ArF excimer laser to vaporize material from each grain with a spot size of 17 μm. The ablated material was carried via a stream of He (600 ml/min), Ar (740 ml/min), and N_2 (6 ml/min) to a Thermo X Series II quadrupole ICP-MS where it was then analyzed for U, Th, and Pb isotopic content. Additional elements were analyzed to confirm composition (Zr) and to qualitatively assess alteration or common Pb-contamination (Bi, Sr) of each grain, but were not calibrated to determine their absolute content. U-Th-Pb data were calibrated using the 91500 geostandards zircon (Wiedenbeck et al., 1995), and quality control was completed with analysis of the Plešovice (Sláma et al., 2008) and Temora-2 (Black et al., 2003) geostandards. The Plešovice and Temora-2 standards were analyzed regularly throughout each sample run and the calculated $^{207}Pb/^{206}Pb$ ages were within error of their accepted age of (337.13 ± 0.37 Ma and 416.8 ± 1.1 Ma, respectively) before proceeding with age determinations for the detrital zircons. Each individual zircon analysis was inspected in terms of signal intensity as a function of time so as to distinguish distinct zones of different Th/U, $^{207}Pb/^{206}Pb$, ^{204}Pb, ^{88}Sr, and/or ^{209}Bi. Zones of signal showing evidence for alteration (high ^{88}Sr) or common Pb-contamination (high ^{204}Pb, ^{209}Bi, erratic $^{207}Pb/^{206}Pb$ ages) were not selected for integration in the final age determination of the zircon. U-Pb concordia diagrams were constructed using Iolite (Paton et al., 2011) and VizualAge (Petrus and Kamber, 2012). Error ellipses of data points (**Figure 2.5**) represent the

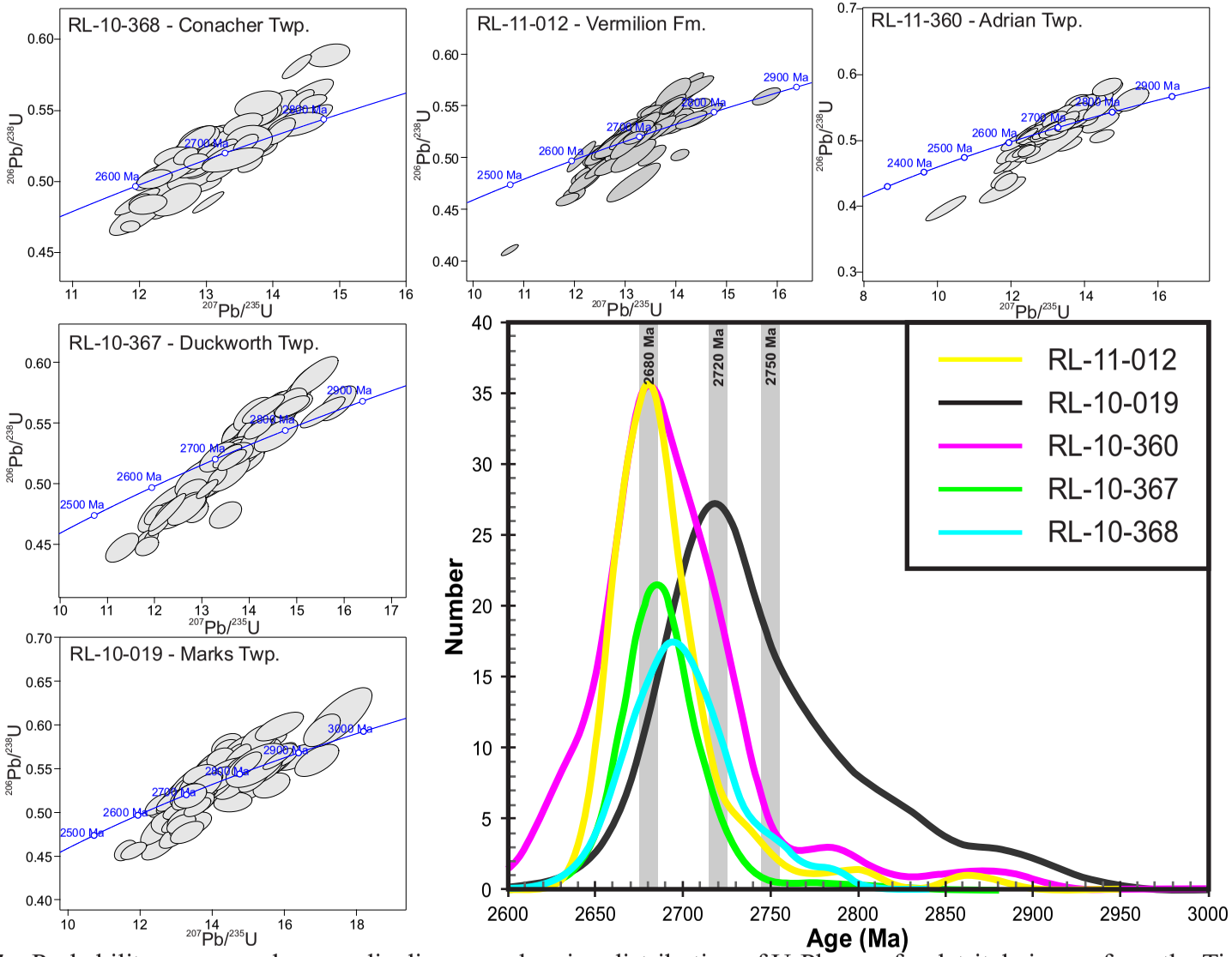

Figure 2.5 – Probability curves and concordia diagrams showing distribution of U-Pb ages for detrital zircons from the Timiskaming-type assemblages from the Vermilion (RL-11-012) and Shebandowan (RL-10-019, 360, 367, 368) greenstone belts. Grey bars represent a range of magmatic ages previously described by Corfu and Stott (1998). Post-2680 Ma ages are likely skewed by analysis of metamorphic overprints.

reproducibility of the ratio measurements within an ablation profile and are 2x the standard error. Histograms and probability curves for each sample were generated using Isoplot for Microsoft Excel (Ludwig, 2012).

The tables presenting the data collected by LA-ICP-MS (which includes U-Pb and Pb-Pb ages, errors, error correlations, and estimated U and Th concentrations, and Th/U ratios) from the VGB are available in a digital data repository accompanying this manuscript. The data collected from samples from the SGB are available in a publication from the Ontario Geological Survey (Lodge and Chartrand, 2013). By using VizualAge to calculate and display U-Pb ages (Petrus and Kamber, 2012), most of the data points are are nearly concordant and only a few were rejected. Rejected compositions were not plotted on the histogram if more than 10% discordant. The 2-times standard error for the $^{207}Pb/^{206}Pb$ ages for individual grains averaged 20-40 Ma, but is as low as 10 Ma in some cases, representing approximately 0.5% to 2.0% of the reported age. Therefore, trends in the age of the population are more relevant for interpreting the data rather than the age of individual grains. Samples from designated Timiskaming-type basins in the SGB from Adrian (RL-10-360), Conacher (RL-10-368), and Duckworth (RL-10-367) Townships had the majority of their detrital zircons with ages between 2680-2695 Ma (**Figure 2.5**). These samples also had detrital grains that were of Greenwater Assemblage age (2720 Ma). A similar distribution of detrital ages was observed in the sample from the Lake Vermilion Formation (RL-11-012) in Minnesota. The sample from Marks Township (RL-10-019) in the SGB is unlike the other samples in that the majority of detrital zircon ages are around 2720 Ma and there is a significant proportion of detrital zircons that are older than 2750 Ma, the oldest dated material in this part of the Wawa Subprovince (Corfu and Stott, 1998). Thus, there must be a different source of detritus for this basin, which suggests that it may not represent a Timiskaming-type assemblage with locally-sourced detritus deposited in a pull-apart basin.

2.5. Magmatic Zircon Geochronology

A sample from the Gafvert Lake sequence was used to determine the age of volcanism and its relationship to the 2722 Ma Lower Ely and Soudan members. Sample RL-11-003 is from a quartz- and feldspar-phyric dacite tuff breccia (**Figure 2.6A**) from the basal part of the Gafvert Lake sequence, approximately 2 meters from the contact with the underlying Soudan member. The lowermost tuff breccias of the Gafvert Lake sequence have intraclasts of chert and there

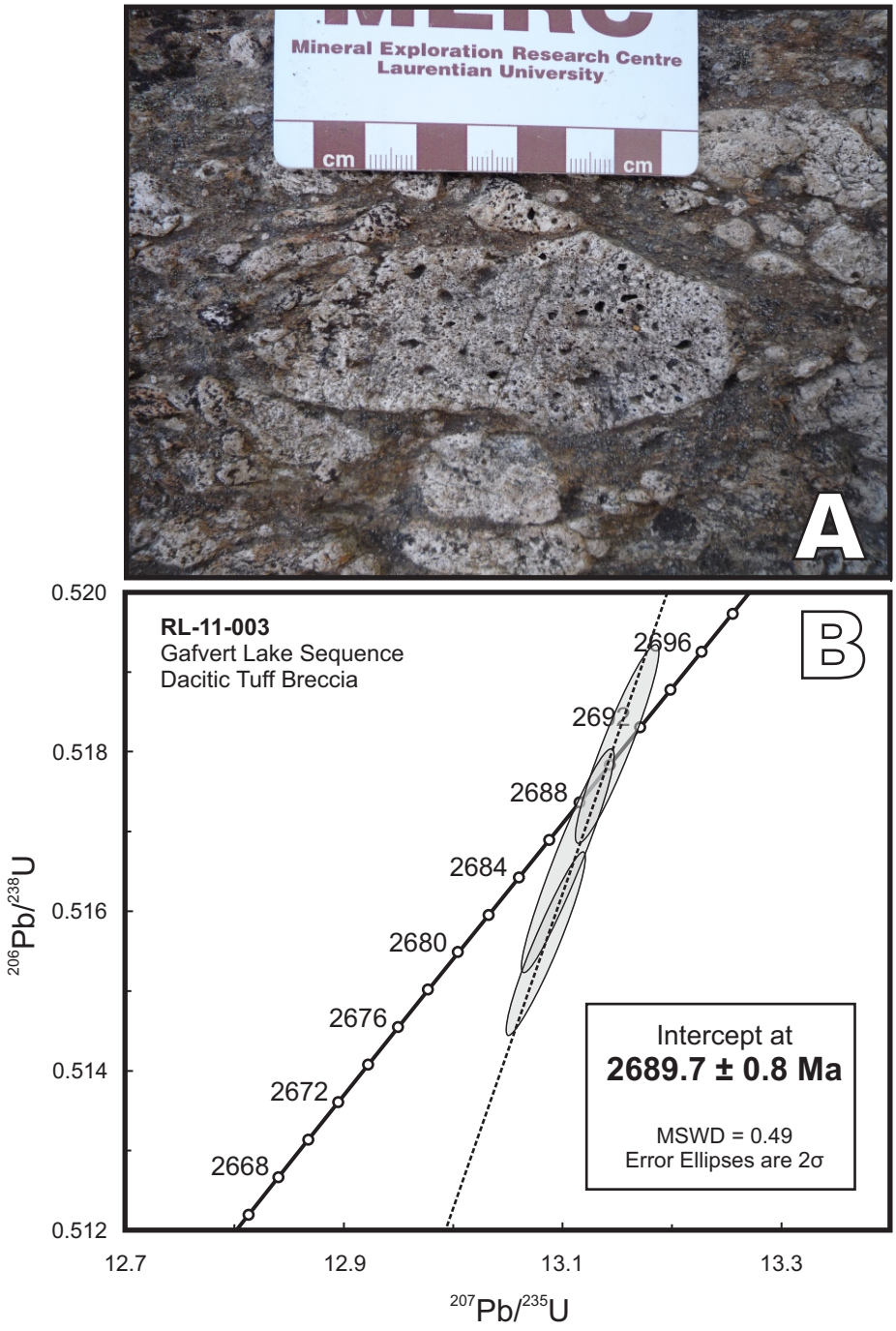

Figure 2.6 – A) Dacitic tuff breccia of the Gafvert Lake sequence from which sample RL-11-003 was obtained. B) The concordia diagram for zircons analyzed from sample RL-11-003 from the Gafvert Lake sequence showing an upper intercept $^{207}Pb/^{206}Pb$ age of 2689.7 ± 0.8 Ma.

appears to be no obvious structural discordance such as schist or mylonite at the contact. Therefore, the contact between the Soudan and the Gafvert is most likely a disconformity. Previously, the nature of the contact was poorly understood because of a lack of geochronologic data.

Zircons in the sample from the Gafvert Lake Sequence were analyzed using thermal ion mass spectrometry (TIMS) at the Jack Satterly Geochronology Laboratory, University of Toronto. After a procedure to separate zircons similar to that at Laurentian University, zircons were thermally annealed and chemically etched using the methodologies outlined by Mattinson (2005) for improved precision of calculated ages for analyzed zircon grains. Following treatment of the grains, zircons were dissolved in accordance to the procedures outlined by Krogh (1973). U and Pb were separated using anion exchange columns before analysis (Krogh, 1973). U-Pb age determinations and plotting of Concordia diagrams were completed using Isoplot for Microsoft Excel (Ludwig, 2012) and decay constants from Jaffey et al. (1971). The composition and U-Pb isotopic values of three analyzed zircon grains are summarized in **Table 2.1**. Analysis of the grains resulted in a tight grouping of near concordant ages that gave an anchored (at 0 Ma) intercept $^{207}Pb/^{206}Pb$ age of 2689.7 ± 0.8 Ma (**Figure 2.6B**).

2.6. Discussion

2.6.1 Timiskaming-Type Basins of the Western Wawa Subprovince

The high-precision U-Pb age of the Gafvert Lake sequence of *circa* 2690 Ma has important implications for both the evolution of the VGB and the western Wawa subprovince. Based on similar ages for Timiskaming-type assemblages in the SGB (Corfu and Stott, 1998) , close spatial association of the Gafvert Lake sequence with the Mud Creek shear zone (**Figure 2.3**), and rapid lateral facies changes within a relatively narrow basin, it is geochronologically and lithologically consistent with the Gafvert Lake sequence and the sampled portion of the Lake Vermilion Formation being Timiskaming-type assemblages. These assemblages are essentially coeval with other Timiskaming-type deposits in the region, including the Shebandowan assemblage in the SGB (Corfu and Stott, 1986, 1998) and Knife Lake Group in the VGB (Jirsa et al., 2012). The dominance of 2680-2690 Ma detrital zircon ages from the Lake Vermilion Formation is within error of the age of the dacitic Gafvert Lake sequence, which supports previous interpretations that a significant source of detritus for the Lake Vermilion Formation in

Table 1: U-Pb CA-ID-TIMS data for magmatic zircons in sample RL-11-003 from the Gafvert Lake sequence.

Analysis No.	Fraction	Weight (µg)	U (ppm)	Th/U	Pb_{tot} (pg)	Pb_{com} (pg)	$^{206}Pb/^{204}Pb$ measured	$^{206}Pb/^{238}U$	2σ	$^{207}Pb/^{235}U$	2σ	$^{206}Pb/^{238}U$ Age (Ma)	2σ	$^{207}Pb/^{235}U$ Age (Ma)	2σ	$^{207}Pb/^{206}Pb$ Age (Ma)	2σ	% Disc	Rho
RL-11-03	**Dacite Tuff Breccia**																		
Z1	1 cls, clr, el, 3:1 sq, euh pr	2.3	270	0.350	153.5	0.55	16208	0.515581	0.000944	13.08526	0.02957	2680.4	4.0	2685.8	2.1	2689.9	1.3	0.4	0.942
Z2	1 cls, clr, short broken pr	0.9	78	0.355	44.5	0.33	7861	0.516631	0.001150	13.10584	0.03436	2684.9	4.9	2687.3	2.5	2689.1	1.4	0.2	0.948
Z3	1 cls, clr, assym pr	2.1	224	0.302	126.7	0.47	15890	0.518087	0.001021	13.15032	0.03100	2691.1	4.3	2690.5	2.2	2690.1	1.4	0.0	0.935

Key: cls = colourless; clr = clear; euh = euhedral; pr = prism; assym = assymetric; sq = square x-section
Pbtot - total Pb, corrected for fractionation, blank and spike; **Pbcom** - common Pb assuming the isotopic composition of laboratory blank: 206/204 - 18.221; 207/204 - 15.612; 208/204 - 39.360 (errors of 2%).
Th/U calculated from radiogenic 208Pb/206Pb ratio and 207Pb/206Pb age assuming concordance.
Disc - per cent discordance for the given 207Pb/206Pb age. **Rho** - Error correlation coefficient.

this region is from the Gafvert Lake sequence (Ojakangas, 1972; Southwick et al., 1998). In the SGB, clasts of late-tectonic plutons *circa* 2680-2685 Ma are present in the Auto Road assemblage (Corfu and Stott, 1998). It is likely that detrital zircons with *circa* 2680 ages in the VGB and SGB Timiskaming-type assemblages are derived from these late-tectonic plutons, and their presence indicates that these basins continued to evolve throughout the duration of D_2 transpression. It should be noted that since the Lake Vermilion Formation is a laterally extensive unit that has a wide variety of sedimentary lithofacies and is exposed to the west of the VGB in contact with other greenstone assemblages, the interpretations are limited to the studied portion of the formation.

The overall similarity between the magmatic and detrital zircon ages of Timiskaming-type assemblages in the SGB and VGB indicates widespread, structurally controlled deposition of calc-alkalic to alkalic volcanic and plutonic rocks (Carter, 1993) and associated rift-type sedimentary successions deposited in subaqueous to subaerial environments. Transtensional pull-apart basins and coeval volcanism occurred along strike for over 200 km between the SGB and VGB in several narrow basins in close spatial association with regional structures, which is comparable in character and extent to the Timiskaming assemblage of the Abitibi subprovince (Ayer and Chartrand, 2011) that was deposited approximately 20 million years later. The dominance of <2720 Ma detrital zircons suggests that the source of detritus was largely local and likely from within the basin with a lesser contribution from the greenstone belt strata upon which the basins formed. The abundance of locally-derived material in the pull-apart basins of the sampled portions of the VGB and SGB is compatible with interpretations of the depositional models for other pull-apart basins in the Wawa subprovince including the Knife Lake Group (Driese et al., 2011), Midway sequence, (Jirsa, 2000), Timiskaming assemblage of the Abitibi subprovince (Mueller and Corcoran, 1998), as well as in modern-day collisional domains (e.g., New Zealand; Ballance, 1980).

The analysis of a large number of detrital grains has revealed a more complex distribution of ages than previously known in the western Wawa subprovince. The youngest rocks in the study region that may have contributed detrital grains are 2680-2685 Ma (Corfu and Stott, 1998). Granitic clasts within the Auto Road assemblage of the SGB are 2682 ± 3 Ma and are overprinted by D_2 fabric (Corfu and Stott, 1998). Therefore, the timing of basin development and Timiskaming-type sedimentation in the VGB and SGB can be constrained between the age of

Timiskaming-type volcanic rocks (ca. 2690 Ma) and the timing of D_2 deformation (ca. 2685-2680 Ma). This 10-15 My period of basin development and sedimentary deposition is similar to the duration of deposition for the Timiskaming assemblage in the Abitibi subprovince (e.g., Ayer et al., 2002).

Detrital zircons that have ages that are definitely younger than 2680 Ma most likely represent metamorphic zircons, zircons that have metamorphic overgrowths, or zircons that have experience a loss of Pb. Thermal (metamorphic) events in the Wawa subprovince during D_2 deformation and post-tectonic plutonism at *circa* 2680-2685 Ma (Corfu and Stott, 1998; Peterson et al., 2005), *circa* 2660-2675 Ma (Davis et al., 1994), and *circa* 2650 Ma, producing high-grade metamorphism and partial melting in the Quetico subprovince (Pan et al., 1998; Valli et al., 2004), are most likely partially responsible for these younger zircons ages. Metamorphic zircons typically have a low Th/U ratio compared to igneous zircons (Th/U < 0.1) (Hoskin and Schaltegger, 2003). The Th/U ratios of the detrital zircons in this study are mostly within typical magmatic-derived ranges (average Th/U ~0.4-1.4) and lower Th/U ratios (Th/U < 0.2) are not consistently correlated with post-2680 Ma ages (see tables in digital appendix and in Lodge and Chartrand, 2013). Therefore, metamorphic overgrowths cannot exclusively account for the anomalously young detrital zircon ages. Lead loss early in a zircon grain's history can also result in an anomalously young age (Anderson, 2002; Petrus and Kamber, 2012). Detrital grains were not thermally annealed or chemically etched to remove any potential metamorphic overgrowths or damaged crystal edges prior to analysis. Therefore, the younger ages may reflect analysis of these metamorphic overgrowths or loss of lead early in the grain's history. Future work should utilize cathodoluminescent imaging to detect metamorphic rims (e.g., Hanchar and Miller, 1993) and/or follow procedures for grain abrasion to minimize analysis of damaged parts of the crystals susceptible to Pb-loss (e.g., Mattinson, 2005).

The oldest known magmatic age in the western part of the Wawa subprovince is 2750 Ma (Corfu and Stott, 1998). With the exception of the sample from Marks Township, there are only a few older zircons most likely derived or inherited from undated older magmatic sources within the Wawa subprovince. Alternatively, these older zircons may have been transported southward from the Wabigoon subprovince where older magmatism is well documented (Tomlinson et al., 2004). The concept of sediment transport southward from the Wabigoon has been discussed in other parts of the Wawa (Fralick et al., 2006) and Quetico subprovinces (Davis et al., 1990;

Zaleski et al., 1999). The relative abundance of pre-2750 Ma ages for detrital grains in sample RL-11-019 from Marks Township compared to other samples in the SGB support trans-terrane sediment transport.

2.6.2. Geochemistry of Timiskaming-Type Metavolcanic Rocks

Despite developing in similar geodynamic environments, the compositions of magmas vary significantly among the Timiskaming-type volcanic rocks in the Wawa-Abitibi terrane. There are numerous descriptions of hornblende-phyric trachyandesite in both the SGB and VGB (Shegelski, 1980; Brown, 1995) and they are commonly compared to alkalic magmatism described at Kirkland Lake (e.g., Corfu and Stott, 1998). However, metavolcanic rocks from the Timiskaming-type assemblages in the SGB differ somewhat in being mostly calc-alkalic, with alkalic compositions only rarely reported. They have normalized LREE values up to 100 times chondrite (Brown, 1995; Rogers and Berger, 1995; Osmani, 1997) **(Figure 2.7C)**. The Tower Stock and associated metavolcanic rocks have normalized LREE as high as 400x (Carter, 1993) but the Saganaga Tonalite has lower LREE, up to 40x chondrite (Evans and Hanson, 1993). Compared to the metavolcanic rocks from the Timiskaming assemblage at Kirkland Lake (Othman et al., 1990; Ayer et al., 2005; Ayer and Chartrand, 2011), the Timiskaming-type volcanic rocks from the SGB and VGB have lower abundances of rare earth, high field strength, and other incompatible trace elements **(Figure 2.7A)**, including elements such as Cu, which is associated with some gold-bearing syenite intrusions in the Abitibi (Robert, 2001).

In contrast, the dominant type of magmatism at Kirkland Lake during transtensional deformation was alkalic (Othman et al., 1990; Ayer et al., 2005), and magmatic fluid derived from the alkalic magmatism is interpreted to have contributed to gold-mineralization within the shears and veins associated with deformation (Robert, 2001; Ispolatov et al., 2008). The alkalinity of the magmas at Kirkland Lake and relative enrichment of incompatible elements (**Figure 2.7A**), when compared to the SGB and VGB Timiskaming-type metavolcanic rocks, is consistent with their derivation from a deep, enriched metasomatized mantle source (e.g., Edgar, 1987; Corfu et al., 1991) potentially during slab detachment and upwelling of enriched asthenospheric mantle (e.g., Kadıoğlu et al., 2006). Therefore, the high-angle, reverse-oblique strike-slip structures that developed during transpression in the Abitibi (Sibson et al., 1988) appear to have been capable of tapping deeper mantle sources than the largely strike-slip structures associated with transpression and calc-alkaline volcanism in the SGB and VGB. This

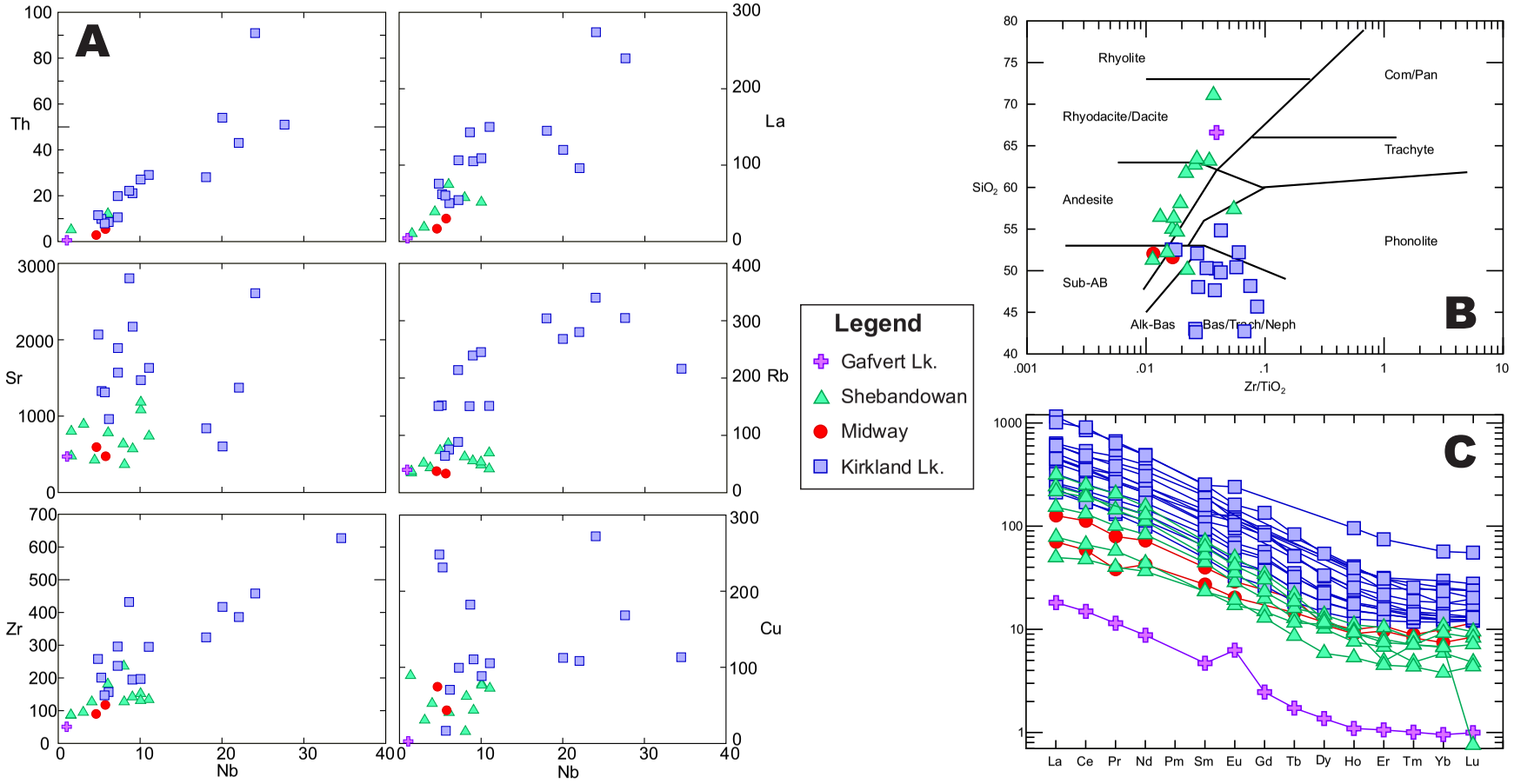

Figure 2.7 – Comparison of trace element geochemistry of volcanic rocks associated with Timiskaming-type deposits in the Wawa-Abitibi Terrane. A) Binary diagrams showing enrichment of trace elements in Kirkland Lake relative to the VGB and SGB. B) Rock classification from Winchester and Floyd (1977). C) Chondrite-normalized rare earth element diagram. Normalization values from Sun and McDonough (1989). Kirkland Lake geochemistry (squares) compiled from Othman et al. (1990) and the Ontario Geological Survey (Ayer and Chartrand, 2011; Ayer et al, 2005). Shebandowan geochemistry (triangles) compiled from the Ontario Geological Survey (Brown, 1995; Carter, 1993; Osmani, 1997; Rogers and Berger, 1995). Vermilion geochemistry (circles) compiled from the Minnesota Geological Survey (Jirsa and Boerboom, 2003). Gafvert Lake sequence geochemistry (crosses) is from the sample dated by TIMS in this study.

variability in the depth of structural penetration during transpression is supported by the different geometries of the basins in the SGB versus those in the Kirkland Lake area. As was noted by Corfu and Stott (1998), the Timiskaming-type assemblages of the SGB appear to be relatively thin layers on top of the older Greenwater assemblage, whereas the Timiskaming assemblage at Kirkland Lake appears to have been deposited in deep tectonic wedges. As a result, transpression, and extensional basin development, within the SGB and VGB were not associated with gold-related alkaline magmatism and volcanism as in the Abitibi.

Alkalic magmatism in the SGB and VGB consists of late to post-tectonic intrusions (Corfu and Stott, 1998). Coincidently, the most explored gold prospects in the SGB are associated with or are in close proximity to these more alkalic late-tectonic plutons, such as at the Moss Lake (Risto and Breede, 2010) and Tower Mountain (Jobin-Bevans et al., 2006) properties. In the VGB, small gold prospects occur adjacent to Timiskaming-type assemblages and are associated with D_2 structures (Peterson and Jirsa, 1999) (**Figure 2.3**), rather than alkalic magmatism. These showings and prospects are small and economic mineralization has yet to be found.

2.6.3 Timiskaming-type Basins versus Foreland Basins

The ages of detrital zircons in sample RL-10-019 from Marks Township are significantly different from all the other detrital samples analyzed in this study. Some ages are younger than the 2720 Ma Greenwater assemblage, but there is also a significant proportion of detrital grains that are older than the oldest rocks dated within the SGB by Corfu and Stott (1998). Detrital zircon ages presented in this study show two main sources of detritus: locally-derived from Timiskaming-type metavolcanics and intrusions, and a second source that is dominated by >2720 Ma zircons. Previous geochronological studies in the SGB have identified igneous rocks as old as 2750 Ma, but have detrital zircons as old as 2830 Ma (Corfu and Stott, 1998) in a sample from Adrian Township. This was the only sample that contained these older detrital grains, and is also within the same “older” sedimentary unit on compilation maps as RL-10-019 (Santaguida, 2001). The discrepancy between the ages found within this wacke and the known magmatic ages of the western Wawa subprovince suggests that the detritus has a provenance other than the immediate region surrounding the SGB and VGB. There are several possible sources of this older detritus found in the SGB. Old supracrustal assemblages (ca. 2.9 Ga) and Hf isotopic data suggests the presence of older ca. 2.8-2.9 Ga crustal material in the southeastern part of the Wawa

subprovince (Ketchum et al., 2008; Ayer et al., 2010). Alternatively, and a more likely sedimentary source, is the Wabigoon subprovince to the north. The age distribution of detrital grains in this sample is characteristic of the range of U-Pb ages found in the Western Wabigoon and Marmion terranes of the Wabigoon subprovince (Tomlinson et al., 2004) and is consistent with other Wabigoon-derived sedimentary rocks within the Wawa and Quetico subprovinces (Davis et al., 1990; Zaleski et al., 1999; Fralick et al., 2006). The older assemblages from within the Wawa subprovince are comparatively small in volume and evidence for a more substantial protocratonic root is based on the presence of inherited zircons and isotopic signatures. Based on the relatively large proportion of older zircons in sample RL-10-019, it is more likely that the detritus was derived from a readily exposed source, such as the Wabigoon subprovince, as opposed to a source that is largely based on inheritance and small supracrustal slivers, like the older crust of the southeastern Wawa subprovince. Trans-terrane sedimentation has been demonstrated in the northeastern part of the SGB in the Wawa subprovince (Fralick et al., 2006) and has been interpreted to have formed during accretion of the Wawa subprovince to the Wabigoon subprovince. Subduction of the Wawa underneath the Wabigoon, as suggested by Lithoprobe research (Percival et al., 2006), would have caused uplift and rapid erosion of the Wabigoon, resulting in a foreland-type sedimentary environment. The Quetico subprovince appears as a thin wedge-shaped terrane atop Wabigoon-Wawa boundary in Lithoprobe surveys (Percival et al., 2006) suggesting the Quetico is likely an accretionary-like foreland basin composed of detritus derived from the uplifting suprasubduction terrane (Williams et al., 1991a; 1991b). The Quetico basin would have eventually been either filled or cut-off by continuous uplift during collision, and eroding sediments from the Wabigoon could have spilled over the Quetico foreland basin and into the evolving Wawa volcanic arc terrane located to the south.

Structural analysis in the eastern part of SGB and VGB has shown two distinct zones of deformation: westerly plunging mineral lineations characteristic of the southern two thirds of the older Greenwater assemblage rocks, and easterly plunging mineral lineations localized in the northern one third of the Greenwater assemblage and pervasively characterize the Timiskaming-type assemblages (Stott and Schwerdtner, 1981; Stott and Schnieders, 1983; Hudleston et al., 1988). Easterly plunging lineations proximal to sample RL-10-019 in Marks Township suggest that foreland-type sedimentary rocks were deformed along with Timiskaming-type deposits in the SGB, if not co-depositional with them. The overlap of the younger ca. 2680 Ma detrital

grains in all samples suggests that they have a similar maximum depositional age, but because of the inferred transport over the Quetico, younger grains may have come from the Quetico rather than from Timiskaming-type igneous material within the SGB. However, because these basins are deformed by the same deformation event that was localized along D_2 shear zones with the Timiskaming-type deposits, the sediments transported from the Wabigoon into the Wawa subprovince may have been deposited in or near a pull-apart basin (**Figure 2.8**). There is insufficient evidence to determine if the Timiskaming-type basins preserve later infilling by trans-terrane molasses or if they are separate linear basins that are now structurally interleaved. Another alternative is the possibility of significant terrane transport along strike-slip faults and the source of detritus is no longer adjacent to the deposits. More detailed mapping and geochronology would be required to properly address these alternative depositional settings. These are important distinctions that would have implications for Archean terrane accretion and it deserves more attention in future research.

The dominance of locally-derived detritus in the extensional setting of a Timiskaming-type basin of the SGB and VGB appears to be contrary to the distribution of detrital zircon ages in Phanerozoic extensional tectonic settings where rift basins are dominated by old zircons derived from the basement (Cawood et al., 2012). Zircons that are significantly older than the Timiskaming-type pull-apart basins of the VGB and SGB are not present because the volcanic strata that the basins formed in were predominately mafic in composition. Therefore, the contribution of detrital zircons from these older strata would have been limited. The deposition of syn- to late-deformation volcanic and intrusive rocks spatially associated with these basin-forming structures would have been a major contributor of detritus. Finally, the 2750-2680 Ma magmatic history of the western Wawa subprovince was comparatively short in comparison to the magmatic history (~3.5 Ga) available for sources of detritus for the Phanerozoic rift basins described by Cawood et al. (2012). Therefore, the relationship between tectonic setting, distribution of detrital zircon ages, and age of sedimentation proposed by Cawood et al. (2012) for the Phanerozoic may not be applicable to this part of the Superior Province.

2.6.4 Implications for evolution of Wawa-Abitibi Terrane

The coeval deposition of Timiskaming-type assemblages in the SGB and VGB indicates that similar transtensional pull-apart basins were forming synchronously across the westernmost Wawa subprovince (**Figure 2.8**). This unifies the deformation event that caused transtensional

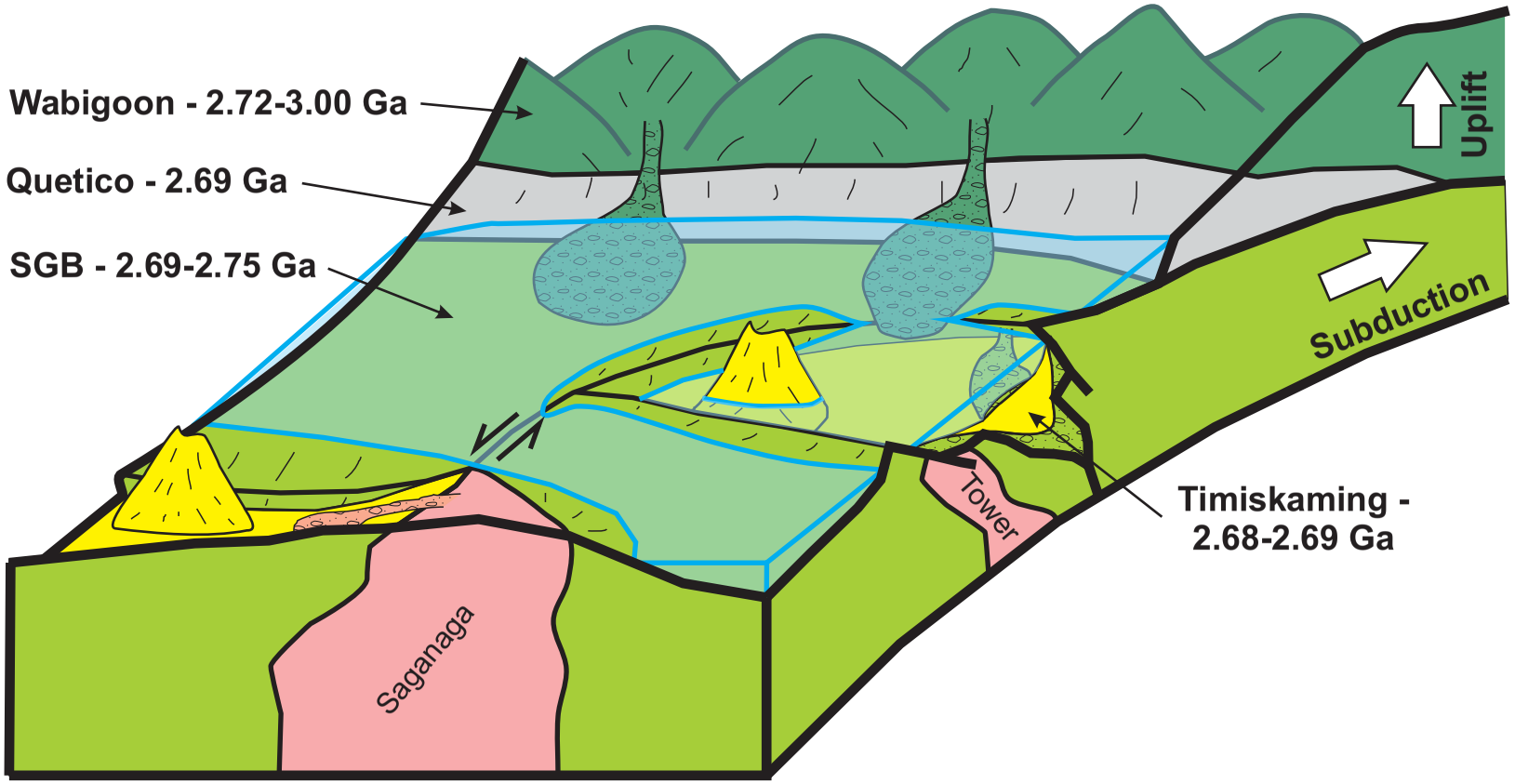

Figure 2.8 – Schematic block diagram showing inferred geodynamic environment of deposition for the Timiskaming-type and foreland-type basins of the western Wawa subprovince. Subduction of the Wawa under the Wabigoon subprovince may have caused significant uplift and rapid erosion of the Wabigoon transporting detritus southward to lower land. Uplift and localized filling of the Quetico basin may have allowed for sediment transport across the filled basin and into the actively-deforming Wawa Subprovince, similar to processes interpreted by Fralick et al. (2006). Calc-alkalic to alkalic magmas (Saganaga and Tower intrusions) are intruded into pull-apart basins and contribute to concurrent volcanism. In the SGB and VGB, the pull-apart basins are dominated by detritus from the Timiskaming-type metavolcanic rocks. Uplift and unroofing of the Saganaga Tonalite resulted in subaerial weathering and erosion of the Saganaga Tonalite, contributing detritus to the Knife Lake Group (Driese et al. 2011). Sea level as drawn schematic and would have been variable reflecting changes in subsidence and uplift. Sketch is not to scale.

shearing and the formation of pull-apart basins in the region. The earliest deformation event, D_1, produced regional-scale folding observed at the Tower-Soudan anticline in the VGB (**Figure 2.3**) and fold-thrust imbrication of the Newton belt of the VGB (Peterson et al., 2005) and Greenwater assemblage in the SGB *circa* 2695 Ma (Stott and Schnieders, 1983; Corfu and Stott, 1998). The next regional deformation event, D_2, was synchronous with regional metamorphism and production of metamorphic fabric in the VGB (Peterson et al., 2005). Regional strain during this deformation event appears to have become increasingly partitioned, eventually producing crustal-scale shear zones that separate the Soudan and Newton belts, that bracket the Knife Lake Group in the VGB (Jirsa et al., 1992) and that formed the structures that pervasively deform the Shebandowan Assemblage in the SGB (Corfu and Stott, 1998). The D_2 event is constrained to 2685-2680 Ma (Corfu and Stott, 1998; Peterson et al., 2001). The correlation of regional-scale deformation events suggests that the western Wawa subprovince was undergoing the same tectonic processes, and that the SGB and VGB were accreted onto the Superior Province at the same time. This scale of deformation and development of transtensional basins is common in modern-day collisional orogens (e.g., Gürbüz, 2010).

The formation of Timiskaming-type pull-apart basins during transtensional deformation in the VGB and SGB represents one of the last deformation phases during the accretion of the Wawa subprovince to the evolving Superior Province. In the southern Abitibi subprovince away from the Wawa-Quetico boundary, the Timiskaming assemblage in the Kirkland Lake area was deposited *circa* 2670 Ma (Ayer and Chartrand, 2011), about 20 million years later than the Timiskaming-type assemblages hosted on the northern margin of the Wawa subprovince. Transtensional shearing, sedimentation, and volcanism in the Wawa subprovince is co-depositional with the Porcupine assemblage in the Abitibi, a sequence of flysch-like, deep water turbidites associated with uplift and erosion of older Abitibi lithofacies (Bateman et al., 2008). In the Chibougamau region of the northern Abitibi subprovince, the 2725-2730 Ma metavolcanic Roy Group (Leclerc et al., 2011) is unconformably overlain by the shear-bounded Opémisca Group that is interpreted to have had a similar molasse-like depositional environment as the Timiskaming assemblage (Hyde, 1980; Mueller and Donaldson, 1992; Mueller and Corcoran, 1998). Within the Opémisca Group, trachyte breccias of the Häuy Formation have been dated at 2691.7 ± 2.9 Ma (David et al., 2007). Even though the pre-tectonic volcanic lithofacies are older, the products of transcurrent shearing near the northern margin of the Wawa-Abitibi terrane are

the same age. This indicates that the accretion and formation of pull-apart basins in the northern part of the Wawa-Abitibi terrane were synchronous, and were much earlier than in the southern part. This supports oblique convergence of the Wawa-Abitibi terrane onto the Superior, with the northern parts docking while the southern parts were still being assembled, uplifted, and eroded. Deformation and magmatism in the northern parts of the terrane appear to be over before the southern parts of the terrane began to experience transcurrent deformation and the deposition of the Timiskaming assemblage in the Kirkland Lake area.

2.7. Conclusions

New U-Pb age determinations in the VGB from the Lake Vermilion Formation, including the Gafvert Lake dacitic breccia, indicate that these deposits are *circa* 2690 Ma, and are unconformably deposited on the *circa* 2720 Ma Lower Ely and Soudan members. The position of these deposits in close proximity with the shear zones and faults that separate the Soudan and Newton belts, as well as being coeval with the fault-bounded Knife Lake Group and Shebandowan assemblage of the SGB, indicate that the Lake Vermilion Formation is a newly defined Timiskaming-type assemblage that formed during transtensional shearing and accretion of the Wawa subprovince to the Superior Province. The recognition of coeval Timiskaming-type assemblages in the SGB and VGB indicates that this part of the Wawa was accreted to the Superior Province as one terrane and that it docked significantly earlier (~20 Ma) than the southern Abitibi subprovince.

A comparison of the ages of detrital zircons from the Shebandowan assemblage of the SGB and the Lake Vermilion Formation in the VGB indicate that most of the detritus is locally derived from the volcanic and plutonic rocks that are associated with the Timiskaming-type basins. Locally derived detritus is common for tectonically-controlled basins (e.g., Corcoran and Mueller, 2007), consistent with Lake Vermilion Formation and Shebandowan assemblage as Timiskaming-type deposits.

The age distribution of detrital zircons from the sample in Marks Township in the SGB is notably different from that of detritus in the other samples from Timiskaming-type basins. The age distribution is more akin to the older Wabigoon subprovince to the north rather than the relatively young volcanic and plutonic rocks in the Wawa subprovince. This implies that these sedimentary rocks represent a foreland-type depositional environment with sediments being

eroded from the uplifted Wabigoon subprovince during accretion of the Wawa to the rest of the Superior Province. Sediments would have been transported across the Quetico subprovince and deposited into or near D_2 structures developing in the SGB. Detailed mapping and geochronological sampling of the sedimentary rocks in this area are insufficient to distinguish if the foreland-type detritus was deposited in a pre-existing Timiskaming-type basin or were deposited in a separate basin. This type of trans-subprovince sedimentation in the Wawa has also been observed in the Schreiber area of Ontario (Davis et al., 1990; Fralick et al., 2006).

The volcanic rocks from the Timiskaming-type deposits in the SGB and VGB are mostly calc-alkaline to transitionally alkalic, whereas the volcanic rocks in the Kirkland Lake area are more enriched in trace elements and are much more alkalic in composition. The relative alkalinity and enrichment of incompatible elements at Kirkland Lake indicates that transtensional structures penetrated to deeper levels of the crust facilitating the generation of mantle-derived melts and influx of ore-forming fluids. In addition, alkaline magmatism at Kirkland Lake was syn-transtensional deformation, whereas most of the alkalic magmatism was late- to post-tectonic in the Wawa subprovince. The relatively low alkalinity, timing of magmatism and penetration depth of structures may explain why the Timiskaming-type deposits in the Wawa subprovince have less economic gold-mineralization than the Timiskaming-type deposits of the Kirkland Lake area.

2.8. Acknowledgements

The authors of this paper thank the generous financial and logistic support of the Ontario Geological Survey for all of the geochronological and geochemical data from samples collected within Ontario, including most of the compiled geochemical data. Support for geochronologic data collected in Minnesota is provided by NSERC (Discovery Grant) and the Society of Economic Geologists (Student Research Grant). The authors acknowledge the Minnesota Department of Natural Resources and the management at the Soudan Underground Mine State Park and Lake Vermilion State Park in Soudan, MN, for permission to access parts of their property for sample collection. This paper benefited from discussions from Balz Kamber, Dean Peterson, and Darrel Long. Field work in Ontario was assisted by Peter Cecutti from Laurentian University. The readability of this manuscript and clarity of arguments were greatly improved by reviews from P. Thurston, D. Davis, and J. Franklin.

2.9 References

Anderson, T., 2002. Correction of common lead in U-Pb analyses that do not report ^{204}Pb. Chemical Geology 192, 59-79.

Arth, J.G., Hanson, G.N., 1975. Geochemistry and origin of the early Precambrian crust of northeastern Minnesota. Geochimica et Cosmochimica Acta 39, 325-362.

Ayer, J.A., Amelin, Y., Corfu, F., Kamo, S.L., Ketchum, J., Kwok, K., Trowell, N., 2002. Evolution of the southern Abitibi greenstone belt based on U–Pb geochronology: autochthonous volcanic construction followed by plutonism, regional deformation and sedimentation. Precambrian Research 115, 63-95.

Ayer, J.A., Chartrand, J.E., 2011. Geological compilation of the Abitibi greenstone belt. Ontario Geological Survey, Miscellaneous Release - Data 282, p.

Ayer, J.A., Goutier, J., Thurston, P.C., Dubé, B., Kamber, B.S., 2010. Tectonic and metallogenic evolution of the Abitibi and Wawa Subprovinces; *in* Summary of Field Work and Other Activities, Open File Report 6260. Ontario Geological Survey, pp. 3-1 to 3-6.

Ayer, J.A., Thurston, P.C., Bateman, R., Gibson, H.L., Hamilton, M.A., Hathaway, B., Hocker, S., Hudak, G.J., Lefrance, B., Ispolatov, V., MacDonald, P.J., Peloquin, A.S., Piercey, S.J., Reed, L.E., Thompson, P.H., Izumi, H., 2005. Digital compilation of maps and data from the Greenstone Architecture Project in the Timmins-Kirkland Lake Region: Discover Abitibi Initiative. Ontario Geological Survey, Miscellaneous Release - Data 155, p.

Ballance, P.F., 1980. Models of sediment distribution in non-marine and shallow marine environments in oblique-slip fault zones.; *in* Ballance, P.F., Heading, H.G. (Eds.), Sedimentation in Oblique-Slip Mobile Zones:. International Association of Sedimentologists Special Publication 4, pp. 229-236.

Bateman, R., Ayer, J.A., Dubé, B., 2008. The Timmins-Porcupine gold camp, Ontario: Anatomy of an Archean greenstone belt and ontogeny of gold mineralization. Economic Geology 103, 1285-1308.

Black, L.P., Kamo, S.L., Allen, C.M., Aleinikoff, J.N., Davis, D.W., Korsch, R.J., Foudoulis, C., 2003. TEMORA 1: a new zircon standard for Phanerozoic U-Pb geochronology. Chemical Geology 200, 155-170.

Borradaile, G.J., Brown, H., 1987. The Shebandowan group: "Timiskaming-like" Archean rocks in northwestern Ontario. Can. J. Earth Sci. 24, 185-188.

Brown, G.H., 1995. Precambrian geology, Oliver and Ware townships. Ontario Geological Survey, Report 294, 48 p.

Carter, M.W., 1993. The geochemical characteristics of Neoarchean alkalic magmatism in central Superior Province. Ontario Geological Survey Miscellaneous Paper 162, 13-19.

Cawood, P.A., Hawkesworth, C.J., Dhuime, B., 2012. Detrital zircon record and tectonic setting. Geology 40, 875-878.

Christie-Blick, N., Biddle, K.T., 1985. Deformation and basin formation along strike-slip faults; *in* Biddle, K.T., Christie-Blick, N. (Eds.), Strike-Slip Deformation, Basin Formation, and Sedimentation. The Society of Economic Paleontologists and Mineralogists Special Publication No. 37, pp. 1-34.

Corcoran, P.L., Mueller, W.U., 2007. Time-transgressive Archean unconformities underlying molasse basin-fill successions of dissected oceanic arcs, Superior Province, Canada. The Journal of Geology 115, 655-674.

Corfu, F., Jackson, S.L., Sutcliffe, R.H., 1991. U-Pb ages and tectonic significance of late Archean alkalic magmatism and nonmarine sedimentation: Timiskaming Group, southern Abitibi belt, Ontario. Can. J. Earth Sci. 28, 489-503.

Corfu, F., Stott, G.M., 1986. U-Pb ages for late magmatism and regional deformation in the Shebandowan Belt, Superior Province, Canada. Can. J. Earth Sci. 23, 1075-1082.

Corfu, F., Stott, G.M., 1998. Shebandowan greenstone belt, western Superior Province: U-Pb ages, tectonic implications, and correlations. GSA Bulletin 110, 1467-1484.

David, J., Davis, D.W., Dion, C., Goutier, J., Legault, M., Roy, P., 2007. U–Pb age dating in the Abitibi Subprovince in 2005–2006. Ministère des Ressources naturelles et de la Faune du Québec, RP 2007-01(a), 2 p.

Davis, D.W., Pezzutto, F., Ojakangas, R.W., 1990. The age and provenance of metasedimentary rocks in the Quetico subprovince, Ontario, from single zircon analyses: Implications for Archean sedimentation and tectonics in the Superior Province. Earth and Planetary Science Letters 99, 195-205.

Davis, D.W., Schandl, E.S., Wasteneys, H.A., 1994. U-Pb dating of minerals in alteration halos of Superior Province massive sulfide deposits; syngenesis versus metamorphism. Contributions to Mineralogy and Petrology 115, 427-437.

Driese, S.G., Jirsa, M.A., Ren, M., Brantley, S.L., Sheldon, N.D., Parker, D., Schmitz, M.D., 2011. Neoarchean paleoweathering of tonalite and metabasalt: Implications for reconstructions of 2.69 Ga early terrestrial ecosystems and paleoatmospheric chemistry. Precambrian Research 189, 1-17.

Dubé, B., Gosselin, P., 2007. Greenstone-hosted quartz-carbonate vein deposits; *in* Goodfellow, W.D. (Ed.) Mineral Deposits of Canada: A Synthesis of Major Deposit-Types, District Metallogeny, the Evolution of Geological Provinces, and Exploration Methods: Geological Association of Canada, Mineral Deposits Division, Special Publication No. 5, pp. 49-73.

Edgar, A.D., 1987. The genesis of alkaline magmas with emphasis on their source regions:: inferences from experimental studies. Geological Society, London, Special Publications 30, 29-52.

Evans, O.C., Hanson, G.N., 1993. Accessory-mineral fractionation of rare-earth element (REE) abundances in granitoid rocks. Chemical Geology 110, 69-93.

Fralick, P., Purdon, R.H., Davis, D.W., 2006. Neoarchean trans-subprovince sediment transport in southwestern Superior Province: sedimentological, geochemical, and geochronological evidence. Can. J. Earth Sci. 43, 1055-1070.

Goldich, S.S., Hanson, G.N., Hallford, C.R., Mudrey, M.G., 1972. Early Precambrian rocks in the Saganaga Lake-Northern Light Lake area, Minnesota-Ontario. Part 1: Petrology and structure; *in* Doe, B.R., Smith, D.K. (Eds.), Studies in Mineralogy and Precambrian Geology: Geological Society of America Memoir 135, pp. 151-178.

Gürbüz, A., 2010. Geometric characteristics of pull-apart basins. Lithosphere 2, 199-206.

Hanchar, J.M., Miller, C.F., 1993. Zircon zonation patterns as revealed by cathodoluminescence and backscattered electron images: Implications for interpretation of complex crustal histories. Chemical Geology 110, 1-13.

Hart, T.R., 2007. Geochronology of the Hamlin and Wye Lakes Area, Shebandowan Greenstone Belt, Thunder Bay District; *in* Summary of Field Work and Other Activities, Open File Report 6213. Ontario Geological Survey, pp. 9-1 to 9-8.

Heim, N., Scott, H., Kilduff, R., Rahtz, C., Vial, A., Young, S., Mahr, C., Hudak, G.J., 2012. Preliminary bedrock geological map of the eastern part of Lake Vermilion State Park, St. Louis County, NE Minnesota.; *in* 57th Annual Meeting, Institute on Lake Superior Geology, Proceedings Volume 57, Part 1 - Program and Abstracts, pp. 39-40.

Hoffman, A.T., 2007. Lithostratigraphy, hydrothermal alteration, and lithogeochemistry of the Neoarchean rocks in the Lower and Soudan Members of the Ely Greenstone Formation, Vermilion District, NE Minnesota: Implications for volcanogenic massive sulphide deposits. M.Sc. Thesis, University of Minnesota - Duluth, 295 p.

Hoskin, P.W.O., Schaltegger, U., 2003. The composition of zircon and igneous and metamorphic petrogenesis; *in* Hanchar, J.M., Hoskin, P.W.O. (Eds.), Zircon. Reviews in Mineralogy and Geochemistry, vol. 53. Mineralogical Society of America, pp. 27-62.

Hudak, G.J., Heine, J., Lodge, R.W.D., Jansen, A., 2012. Recent developments understanding the volcanic, magmatic, tectonic, and metallogenic evolution of the Ely Greenstone Formation, Vermilion District, NE Minnesota. Geological Association of Canada - Mineralogical Association of Canada, Abstracts and Program 35, 59.

Hudak, G.J., Heine, J., Newkirk, T., Odette, J.D., Huack, S., 2002. Comparative geology, stratigraphy, and lithogeochemistry of the Fivemile Lake, Quartz Hill, and Skeleton Lake VMS occurrences, Vermilion district, NE Minnesota. State of Minnesota: Natural Resources Research Institute Technical Report NRII/TR-2002/03, 390 p.

Hudleston, P.J., Schultz-Ela, D., Southwick, D.L., 1988. Transpression in an Archean greenstone belt, northern Minnesota. Can. J. Earth Sci. 25, 1060-1068.

Hyde, R.S., 1980. Sedimentary facies in the Archean Timiskaming Group and their tectonic implications, Abitibi greenstone belt, northeastern Ontario, Canada. Precambrian Research 12, 161-195.

Ispolatov, V., Lefrance, B., Dube, B., Creaser, R.A., Hamilton, M.A., 2008. Geologic and structural setting of gold mineralization in the Kirkland Lake-Larder Lake gold belt, Ontario. Economic Geology 103, 1309-1340.

Jaffey, A.H., Flynn, K.F., Glendenin, L.E., Bentley, W.C., Essling, A.M., 1971. Precision measurement of half-lives and specific activities of ^{235}U and ^{238}U. Physical Review 4, 1889-1906.

Jirsa, M., 1998. Timiskaming-type pull-apart basin sequences in the western Superior Province of Minnesota. Geological Society of America, Abstracts with Program 30, A-291.

Jirsa, M., 2000. The Midway sequence: a Timiskaming-type, pull-apart basin deposit in the western Wawa subprovince, Minnesota. Can. J. Earth Sci. 37, 1-15.

Jirsa, M.A., Boerboom, T.J., 2003. Geology and mineralization of Archean bedrock in the Virginia horn.; *in* Jirsa, M., Morey, G.B. (Eds.), Contributions to the geology of the Virginia horn area, St. Louis County, Minnesota. Minnesota Geological Survey Report of Investigations 53, pp. 10-73.

Jirsa, M.A., Southwick, D.L., Boerboom, T.J., 1992. Structural evolution of Archean rocks in the western Wawa subprovince, Minnesota: refolding of precleavage nappes during D_2 transpression. Can. J. Earth Sci. 29, 2146-2155.

Jirsa, M.A., Starns, E.C., Schmitz, M.D., 2012. Bedrock geologic map of the 2006 Cavity Lake forest fire area, Boundary Waters Canoe Area Wilderness, northeastern Minnesota. Minnesota Geological Survey, Miscellaneous Map M-193, 1:24,000.

Jobin-Bevans, S., Kelso, I., Cullen, D., 2006. NI 43-101 Technical Report on the Tower Mountain Gold Deposit, Conmee Township, northwestern Ontario, Canada. ValGold Resources Ltd., 95 p.

Kadıoğlu, Y.K., Dilek, Y., Foland, K.A., 2006. Slab break-off and syncollisional origin of the Late Cretaceous magmatism in the Central Anatolian crystalline complex, Turkey. Geological Society of America Special Papers 409, 381-415.

Ketchum, J.W.F., Ayer, J.A., Van Breemen, O., Pearson, N.J., Becker, J.K., 2008. Pericontinental crustal growth of the southwestern Abitibi subprovince, Canada - U-Pb, Hf, and Nd isotope evidence. Economic Geology 103, 1151-1184.

Koebernick, C.F., Fralick, P., 1995. Neoarchean coastal sedimentation in the Shebandowan Group, northeastern Ontario; *in* 41st Annual Meeting, Institute on Lake Superior Geology, Proceedings Volume 47, Part 1 - Program and Abstracts, pp. 31-32.

Krogh, T.E., 1973. A low contamination method for hydrothermal decomposition of zircon and extraction of U and Pb for isotopic age determinations. Geochimica et Cosmochimica Acta 37, 485-494.

Leclerc, F., Bédard, J.H., Harris, L.B., McNicoll, V.J., Goulet, N., Roy, P., Houle, P., 2011. Tholeiitic to calc-alkaline cyclic volcanism in the Roy Group, Chibougamau area, Abitibi Greenstone Belt — revised stratigraphy and implications for VHMS exploration. Can. J. Earth Sci. 48, 661-694.

Lodge, R.W.D., 2011. A progress report on the volcanology, stratigraphy and geodynamic setting of greenstone belts of age 2720 Ma near the Wawa– Quetico Subprovincial boundary; *in* Summary of Field Work and Other Activities, Open File Report 6270. Ontario Geological Survey, pp. 11-11 to 11-13.

Lodge, R.W.D., 2012. Preliminary results of uranium–lead geochronology from the Shebandowan Greenstone Belt, Wawa Subprovince; *in* Summary of Field Work and Other Activities, Open File Report 6280. Ontario Geological Survey, pp. 10-11 to 10-10.

Lodge, R.W.D., Chartrand, J.E., 2013. Establishing regional geodynamic settings and the metallogeny of volcanogenic massive sulphide mineralization of greenstone belt assemblages (circa 2720 Ma) of the Wawa Subprovince via geochemical comparisons, Ontario Geological Survey, Miscellaneous Release - Data 306.

Ludwig, K.R., 2012. User's manual for Isoplot 3.75: A geochronological toolkit for Microsoft Excel. Berkeley Geochronology Center, Special Publication No. 4, 75 p.

Mattinson, J.M., 2005. Zircon U-Pb chemical abrasion ("CA-TIMS") method: Combined annealing and multi-step partial dissolution analysis for improved precision and accuracy of zircon ages. Chemical Geology 220, 47-66.

Morton, P., 1982. Archean volcanic stratigraphy, and petrology and chemistry of mafic and ultramafic rocks, chromite, and the Shebandowan Ni-Cu Mine, Shebandowan, northwestern Ontario. Ph.D. Thesis, Carleton University, 346 p.

Mueller, W.U., Corcoran, P.L., 1998. Late-orogenic basins in the Archean Superior Province, Canada: Characteristics and inferences. Sedimentary Geology 120, 177-203.

Mueller, W.U., Donaldson, J.A., 1992. Development of sedimentary basins in the Archean Abitibi belt, Canada: an overview. Can. J. Earth Sci. 29, 2249-2265.

Ojakangas, R.W., 1972. Archean volcanogenic graywackes of the Vermilion District, northweastern Minnesota. Geological Society of America Bulletin 83, 429-442.

Osmani, I.A., 1997. Geology and mineral potential: Greenwater Lake area, West-Central Shebandowan Greenstone Belt. Ontario Geological Survey, Report 296, 135 p.

Othman, D.B., Arndt, N.T., White, W.M., Jochum, K.P., 1990. Geochemistry and age of Timiskaming alkali volcanics and the Otto syenite stock, Abitibi, Ontario. Can. J. Earth Sci. 27, 1304-1311.

Pan, Y., Fleet, M.E., Heaman, L., 1998. Thermo-tectonic evolution of an Archean accretionary complex: U-Pn geochronological constraints on granulites from the Quetico Subprovince, Ontario, Canada. Precambrian Research 92, 117-128.

Paton, C., Hellstrom, J., Paul, B., Woodhead, J., Hergt, J., 2011. Iolite: freeware for the visualization and processing of mass spectrometer data. Journal of Analytical Atomic Spectrometry 26, 2508-2518.

Percival, J.A., Sanborn-Barrie, M., Skulski, T., Stott, G.M., Helmstaedt, H., White, D.J., 2006. Tectonic evolution of the western Superior Province from NATMAP and Lithoprobe studies. Can. J. Earth Sci. 43, 1085-1117.

Peterson, D., 2004. Bedrock geological and volcanogenic massive deposit mineral potential map of the Lower Ely Greenstone and Adjacent Areas: Soudan, Eagles Nest, and Bear Island 7.5 Quadrangles, St. Louis County, Northeastern Minnesota. Institute on Lake Superior Geology 50th Annual Meeting, Map for Field Trip 7., 1:20,000.

Peterson, D., Gallup, C., Jirsa, M., Davis, D.W., 2001. Correlation of the Archean assemblages across the U.S.-Canadian border: Phase I geochronology; *in* 47th Annual Meeting, Institute on Lake Superior Geology, Proceedings Volume 47, Part 1 - Program and Abstracts, pp. 77-78.

Peterson, D., Jirsa, M., 1999. Bedrock geologic map and mineral exploration data, western Vermilion district, St. Louis and Lake Counties, northeastern Minnesota. Minnesota Geological Survey, Miscellaneous Map M-98, 1:48,000.

Peterson, D., Jirsa, M., Hudak, G.J., 2005. Architecture of an Archean greenstone belt: Stratigraphy, structure, and mineralization; *in* Robinson, L. (Ed.) Field Trip Guidebook for Selected Geology in Minnesota and Wisconsin. Minnesota Geological Survey Guidebook 21, pp. 154-180.

Peterson, D.M., Patelke, R.D., 2003. National Underground Science and Engineering Laboratory (NUSEL): Geological site investigation for the Soudan Mine, northeastern Minnesota.

State of Minnesota: Natural Resources Research Institute, Technical Report NRRI/TR-2003/29, 88 p.

Peterson, D.M., Patelke, R.D., 2004. Economic geology of Archean gold occurrences in the Vermilion District, northeast of Soudan, Minnesota.; *in* Severson, M.J., Heinz, J. (Eds.), 50th Annual Meeting, Institute on Lake Superior Geology, Field Trip Guidebook, pp. 200-226.

Petrus, J.A., Kamber, B.S., 2012. VizualAge: A novel approach to laser ablation ICP-MS U-Pb geochronology data reduction. Geostandards and Geoanalytical Research, DOI: 10.1111/j.1751-1908X.2012.00158.x.

Radakovich, A., Parent, C., Partridge, M., Ritts, A., Pierce, R., Hudak, G.J., 2010. Reconnaissance bedrock geological map of the northern part of Soudan Underground Mine State Park and the northwestern part of Lake Vermilion State Park, St. Louis County, MN; *in* 56th Annual Meeting, Institute on Lake Superior Geology, Proceedings Volume 56, Part 1 - Program and Abstracts, pp. 67-68.

Risto, R.W., Breede, K., 2010. NI 43-101 Technical Report on the Moss Lake Gold Property, including an updated mineral resource estimate, Moss Township, northwestern Ontario. Moss Lake Gold Mines Ltd., 106 p.

Robert, F., 2001. Syenite-associated disseminated gold deposits in the Abitibi greenstone belt, Canada. Mineralium Deposita 36, 503-516.

Rogers, M.C., Berger, B.R., 1995. Precambrian Geology, Adrian, Marks, Sackville, Aldina and Duckworth townships. Ontario Geological Survey, Report 295, 66 p.

Santaguida, F., 2001. Precambrian geology compilation series - Thunder Bay sheet. Ontario Geological Survey, Map 2664, 1:250,000.

Shegelski, R.J., 1980. Archean cratonization, emergence and red bed development, Lake Shebandowan area, Canada. Precambrian Research 12, 331-347.

Shirey, S.B., Hanson, G.N., 1984. Mantle derived Archean monzodiorites and trachyandesites. Nature 310, 222-224.

Sibson, R.H., Robert, F., Poulsen, K.H., 1988. High-angle reverse faults, fluid-pressure cycling, and mesothermal gold-quartz deposits. Geology 16, 551-555.

Sláma, J., Košler, J., Condon, D.J., Crowley, J.L., Gerdes, A., Hanchar, J.M., Horstwood, M.S.A., Morris, G.A., Nasdala, L., Noberg, N., Schaltegger, U., Schoene, B., Turbrett, M., Whitehouse, M.J., 2008. Plešovice zircon - a new natural reference material for U-Pb and Hf isotopic microanalysis. Chemical Geology 249, 1-35.

Southwick, D.L., Boerboom, T.J., Jirsa, M., 1998. Geologic setting and descriptive geochemistry of Archean supracrustal and hypabyssal rocks, Soudan-Bigfork area, northern Minnesota: Implications for metallic mineral exploration. Minnesota Geological Survey, Report of Investigations 51, 69 p.

Stott, G.M., Corkery, M.T., Percival, J.A., Simard, M., Goutier, J., 2010. A revised terrane subdivision of the Superior Province; *in* Summary of Field Work and Other Activities, Open File Report 6260. Ontario Geological Survey, pp. 20-21 to 20-10.

Stott, G.M., Schnieders, B.R., 1983. Gold mineralization in the Shebandowan Belt and its relation deformation patterns; *in* The Geology of Gold in Ontario, Miscellaneous Paper 110. Ontario Geological Survey, pp. 181-193.

Stott, G.M., Schwerdtner, W.M., 1981. A structural analysis of the central part of the Shebandowan metavolcanic-metasedimentary belt. Ontario Geoscience Research Grant Program, Final Research Reports, 1980. Ontario Geological Survey, Open File Report 5349, 44 p.

Sun, S., McDonough, W.F., 1989. Chemical and isotopic systematics of oceanic basalts: implications for mantle composition and processes; *in* Saunders, A.D., Norry, M.J. (Eds.), Magmatism in the Ocean Basins. Geological Society Special Publication 42, pp. 313-345.

Tomlinson, K.Y., Stone, D., Stott, G.M., Percival, J.A., 2004. Basement terranes and crustal recycling in the western Superior Province: Nd isotopic character of granitoid and felsic volcanic rocks in the Wabigoon subprovince, N. Ontario, Canada. Precambrian Research 132, 245-274.

Valli, F., Guillot, S., Hattori, K.H., 2004. Source and tectono-metamorphic evolution of mafic and pelitic metasedimentary rocks from the central Quetico metasedimentary belt, Archean Superior Province of Canada. Precambrian Research 132, 155-177.

Vinje, S.P., 1978. Archean geology of an area between Knife Lake and Kekekabic Lake, eastern Vermilion District, northeastern Minnesota. M.Sc. Thesis, University of Minnesota at Minneapolis, 176 p.

Wiedenbeck, M., Allé, P., Corfu, F., Griffen, W.L., Meier, M., Oberli, F., Von Quadt, A., Roddick, J.C., Spiegel, W., 1995. Three natural zircon standards for U-Th-Pb, Lu-Hf, trace element and REE analyses. Geostandards Newsletter 19, 1-23.

Williams, H.R., Stott, G.M., Heather, K.B., Muir, T.L., Sage, R.P., 1991a. Wawa Subprovince; *in* Thurston, P.C., Williams, H.R., Sutcliffe, R.H., Stott, G.M. (Eds.), Geology of Ontario, Ontario Geological Survey, Special Volume 4, Part 1, pp. 485-541.

Williams, H.R., Stott, G.M., Thurston, P.C., Sutcliffe, R.H., Bennett, G., Easton, R.M., Armstrong, D.K., 1991b. Tectonic Evolution of Ontario: Summary and Synthesis; *in* Thurston, P.C., Williams, H.R., Sutcliffe, R.H., Stott, G.M. (Eds.), Geology of Ontario, Ontario Geological Survey, Special Volume 4, Part 2, pp. 1255-1332.

Winchester, J.A., Floyd, P.A., 1977. Geochemical discrimination of different magma series and their differentiation products using immobile elements. Chemical Geology 20, 325-343.

Zaleski, E., van Breemen, O., Peterson, V.L., 1999. Geological evolution of the Manitouwadge greenstone belt and Wawa-Quetico subprovince boundary, Superior Province, Ontario, constrained by U-Pb zircon dates of supracrustal and plutonic rocks. Can. J. Earth Sci. 36, 945-966.

CHAPTER 3

GEODYNAMIC RECONSTRUCTION OF THE WINSTON LAKE GREENSTONE BELT AND VMS DEPOSITS: NEW TRACE ELEMENT GEOCHEMISTRY AND U-PB GEOCHRONOLOGY

3.1. Abstract

The 2720 Ma Winston Lake greenstone belt of the Wawa-Abitibi terrane, Superior Province, is located on the northern margin of the Wawa subprovince and has important regional tectonostratigraphic implications for the Neoarchean development of the Superior Province. The metallogenic importance of the belt is evident from the presence of the Winston Lake, Pick Lake, and Zenith volcanogenic massive sulfide (VMS) deposits. However, neither the tectonostratigraphic history or metallogeny of the belt has been fully examined at the greenstone belt-scale, nor have the VMS deposits been examined from the perspective of the belt-scale petrogenesis and volcanic reconstruction. This study (1) reviews the geology and VMS mineralization in the Winston Lake greenstone belt; and (2) reconstructs its geodynamic setting, and its magmatic and metallogenetic history using new geological, trace element, and Nd-isotopic data constrained by new U-Pb geochronology.

The belt is subdivided into two main lithotectonic assemblages: the Winston Lake assemblage (WLA) composed of tholeiitic to calc-alkalic bimodal volcanic lithofacies, and the Big Duck Lake assemblage (BDLA) composed of alkalic to tholeiitic mafic flows and sills. The WLA-BDLA contact is intruded by the differentiated Zenith gabbro, which hosts the 0.16 Mt Zenith VMS orebody as a series of xenoliths. The variably altered felsic lithofacies of the WLA host the 3.1 Mt Winston Lake Main and 1.3 Mt Pick Lake Zn-rich VMS deposits. The felsic volcanic lithofacies of the WLA are FIII-type rhyolites and have a bimodal distribution of Zr/Ti indicating two distinct magmas formed by different temperatures of partial melting. Mafic lithofacies of the WLA are typically calc-alkalic to transitional in composition. They have arc- to back-arc-like trace element contents with negative Nb and Ti anomalies, enrichment in the LREE, and higher Th/Nb ratios. Mafic lithofacies from the BDLA have trace element characteristics similar to mature back-arc tholeiitic basalts and OIB-like or oceanic plateau alkalic basalts with high Nb/Th and Ti/V ratios.

The chemostratigraphy of the Winston Lake greenstone belt is consistent with a geodynamic model where arc rifting is followed by back arc development. Nd-isotopic data indicate that strata from the WLA and BDLA are juvenile and show no evidence for contamination by significantly older crust during petrogenesis. Therefore, crustal contamination signatures in the mafic flows from the WLA would have been of similar age and consistent with a co-magmatic relationship between the mafic and felsic strata. The mafic lithofacies of the BDLA represent a mature back-arc setting with evidence for enriched plume-generated basalts in the upper mafic unit. The Winston VMS deposit formed during the early rifting of the arc and the timing is tightly constrained by the hydrothermally altered ca. 2720 Ma VMS-hosting felsic strata and younger, post-mineralization, Zenith gabbro. The Zn-dominated VMS mineralization suggests that temperature of the hydrothermal fluid during discharge was relatively cool (<300 °C) and did maintain sufficiently high temperatures to precipitate large amounts of copper relative to zinc. This is likely due to adiabatic cooling of the fluid because of a shallow water environment and/or permeable volcaniclastic strata.

A U-Pb age of emplacement of 2692.1 ± 0.7 Ma from the syn-deformation quartz-feldspar porphyry in the BDLA indicate it is coeval with syn-deformation felsic intrusions found in other greenstone belts along the northern margin of the Wawa-Abitibi terrane. This event is interpreted to correspond with the timing of terrane accretion of the Wawa-Abitibi terrane to the Superior Province.

3.2. Introduction

The Winston Lake greenstone belt (also known as the Big Duck Lake greenstone belt) is located on the northern margin of the Wawa-Abitibi terrane (Stott et al., 2010) at the boundary between the Wawa and Quetico subprovinces (Pye, 1964; Williams et al., 1991) (**Figure 3.1)**. This relatively small greenstone belt is host to the Winston Lake (3.1 Mt at 16% Zn, 1% Cu), Pick Lake (1.3 Mt at 16.5% Zn, 0.9% Cu), and Zenith (0.16 Mt at 16.5% Zn) Zn-rich volcanogenic massive sulfide (VMS) ore bodies (e.g., Severin et al., 1991) and several Au prospects in the Big Duck Lake area (e.g., MacDonald, 2003). Exploration and mining activities prompted and facilitated academic research (e.g., Ritcey, 1992; Osterberg, 1993; Gorton and Schandl, 1995) and field trips (e.g., Severin et al., 1991), but these activities essentially ceased when the mine closed in 1998. Since mine closure, research involved regional-scale geochemical

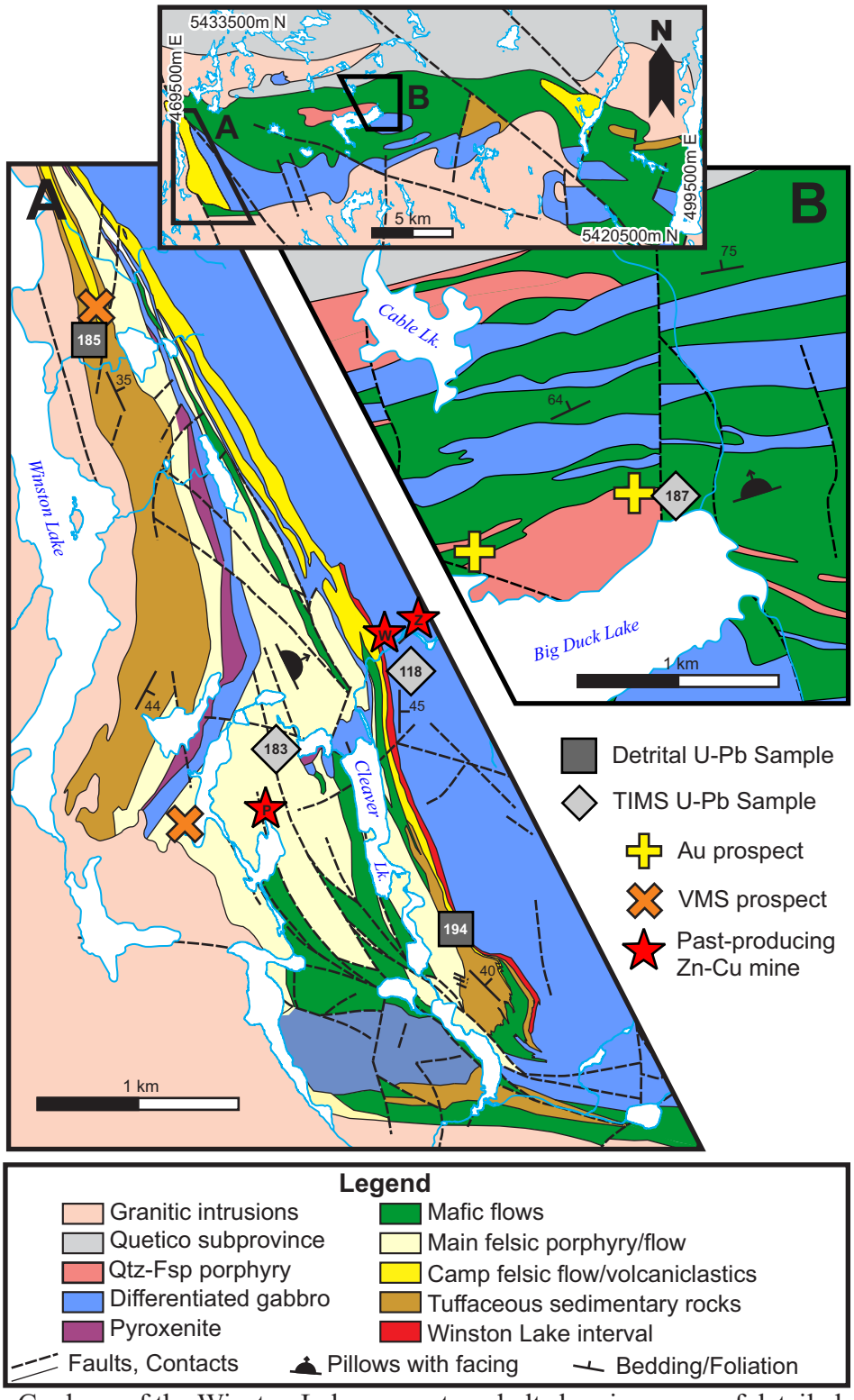

Figure 3.1: Geology of the Winston Lake greenstone belt showing areas of detailed study. Geology modified from the Ontario Geological Survey (Bartley, 1940; Pye, 1964). A) Geology of the Winston Lake assemblage. Past-producing mines are: Z = Zenith, W = Winston Lake, P = Pick Lake. Geology modified from Osterberg (1993). B) Geology of a portion of the Big Duck Lake assemblage modified from Ritcey (1992).

sampling directed at determining terrane-scale magmatic and tectonic processes in the Wawa-Abitibi terrane (e.g., Polat et al., 1999; Polat and Kerrich, 2000; Kerrich et al., 2008). Previous research focused on the deposit-scale VMS- and gold-mineralization (e.g., Ritcey, 1992; Osterberg, 1993), but the metallogenic and tectonostratigraphic importance of this belt has not been fully addressed at the greenstone-belt scale (e.g., Corfu and Stott, 1998; Kerrich et al., 2008).

The 2723 ± 3 Ma (Davis et al., 1994) age of volcanism for the Winston Lake greenstone belt corresponds to a period of extensive and voluminous volcanism and magmatism, which constructed a significant portion of the greenstone belts that now constitute the Wawa-Abitibi terrane. These belts include the Shebandowan (Corfu and Stott, 1998), Manitouwadge (Zaleski et al., 1999) and Vermilion (Peterson et al., 2001) greenstone belts, located along the northern margin of the Wawa subprovince, and the chronostratigraphically equivalent 2723-2720 Ma Stoughton-Roquemaure assemblage of the northern Abitibi subprovince (Ayer et al., 2002). These 2723-2720 Ma greenstone belts are host to the Geco-Willroy deposits in the Manitouwadge greenstone belt (Zaleski and Peterson, 1995), the Winston Lake deposits, and the Au-rich Estrades deposit in the Stoughton-Roquemaure assemblage in the Abitibi greeonstone belt (Goutier et al., 2010). Despite the known tectonic and metallogenic significance of the *circa* 2720 Ma greenstone belt constructional event, the lack of modern research in the Winston Lake greenstone belt has hindered comparisons with other, more extensively studied greenstone belts in the Wawa-Abitibi terrane. In addition, there is no formal description of the Winston Lake VMS deposit in peer-reviewed literature.

We present new geological and trace element geochemical data and U-Pb zircon ages, at the scale of the Winston Lake VMS deposits and at the greenstone belt-scale. Using this data we establish the regional geodynamic setting for the VMS-mineralization, its geological history and magmatic evolution. We also present a more detailed terrane-scale evaluation of the Winston Lake greenstone belt with respect to other Wawa-Abitibi greenstone belts of similar age. The geochemical, isotopic, and geochronological data presented in this paper are contained within a Miscellaneous Release – Data from the Ontario Geological Survey (Lodge and Chartrand, 2013).

3.3. Winston Lake Greenstone Belt Geology

The Winston Lake greenstone belt is a bimodal mafic–felsic volcanic succession with only a few intermediate volcanic rocks (**Figure 3.7**). The lithostratigraphic subdivision of the Winston Lake greenstone belt has evolved over several decades of mapping and research. It is subdivided into two main lithotectonic assemblages: the Winston Lake assemblage (**Figure 3.1A**) and the Big Duck Lake assemblage (**Figure 3.1B**) (Severin et al., 1991; Polat et al., 1999). A summary of the historical lithostratigraphic terminology used in this study is presented in **Table 3.1**. Unit names are modified from previous classifications (e.g., Severin et al., 1991; Ritcey, 1992; Osterberg, 1993) in order to preserve their historical context.

The Winston Lake assemblage (WLA), host to the Zenith, Winston and Pick Lake VMS deposits, consists of calc-alkaline to tholeiitic, bimodal volcanic and tuffaceous siliciclastic metasedimentary lithofacies (Osterberg, 1993; Gorton and Schandl, 1995). The WLA is a moderately dipping homoclinal sequence striking north-northwest (**Figures 3.1 and 3.2**). Preserved pillow facings in mafic flows (**Figure 3.3A**) and cross-bedded volcaniclastic rocks indicate strata consistently young to the northeast. There is no evidence for repetition of units by folding and/or faulting in the nothern part of the WLA and the units are laterally extensive. Several faults and changes in strike are interpreted in the southern part of the WLA and are possibly responsible for thickening of the supracrustal units southward (**Figure 3.1**) (Osterberg, 1993).

The Big Duck Lake assemblage (BDLA) is composed of Mg- to Fe-tholeiitic basalt, and quartz-feldspar porphyry dykes and sills and their brecciated equivalents (Ritcey, 1992; Polat et al., 1999). Anomalous gold values are spatially associated with a quartz-feldspar porphyry and shear zones in the Big Duck Lake area (e.g., MacDonald, 2003). The strata of the BDLA consist of westerly striking massive and pillowed mafic flows (**Figure 3.3E**) and gabbroic sills. Preserved pillows throughout the Big Duck Lake area indicate strata consistently young northward.

The contact between WLA and BDLA is poorly documented and the Zenith gabbro was emplaced along much of the contact. Pye (1964) mapped the contact as conformable, but provides no description of the contact and transitional lithofacies.

Two main structural events are recognized in the Winston Lake greenstone belt. D_1 is defined by a foliation that, in the WLA, is generally north-northwest striking (Severin et al.,

Table 3.1 – Summary of current and historical stratigraphic subdivisions and names. Some units that are described in previous literature have limited exposure on surface.

This Study		*Polat et al. (1999)*	*Pye (1964)*	*Osterberg (1993)*	*Unpublished Industry Terminology*
Assemblage	**Unit**				
Winston Lake Assemblage	**Lower clastic succession**	*Winston Lake Assemblage*	*Lower Metasedimentary Unit*	*Lower Clastic Succession*	*Pick Lake Sediments*
				Ciglen Clotted Rhyolite	*Ciglen Clotted Rhyolite*
	"Main" felsic unit			*Main QFP*	*Main QFP*
	"Ladder" mafic unit			*Ladder Flow*	*Ladder Flow*
	"Camp" felsic unit			*Camp Flow Rhyolite*	*Camp Flow*
				Clotted Rhyolite	*Clotted Rhyolite*
	"Middle" mafic unit			*Middle Mafic Flow*	*Middle Mafic Flow*
	Winston Lake interval			*Winston Lake Horizon*	*Footwall Mafic Flow*
				Footwall Flow	*Winston Lake Horizon*
Zenith Gabbro					
Big Duck Lake Assemblage	**Lower mafic unit**	*Big Duck Lake Assemblage*	*Metavolcanic Unit*	*Big Duck Lake Sequence*	*Big Duck Lake Sequence*
	Upper mafic unit				

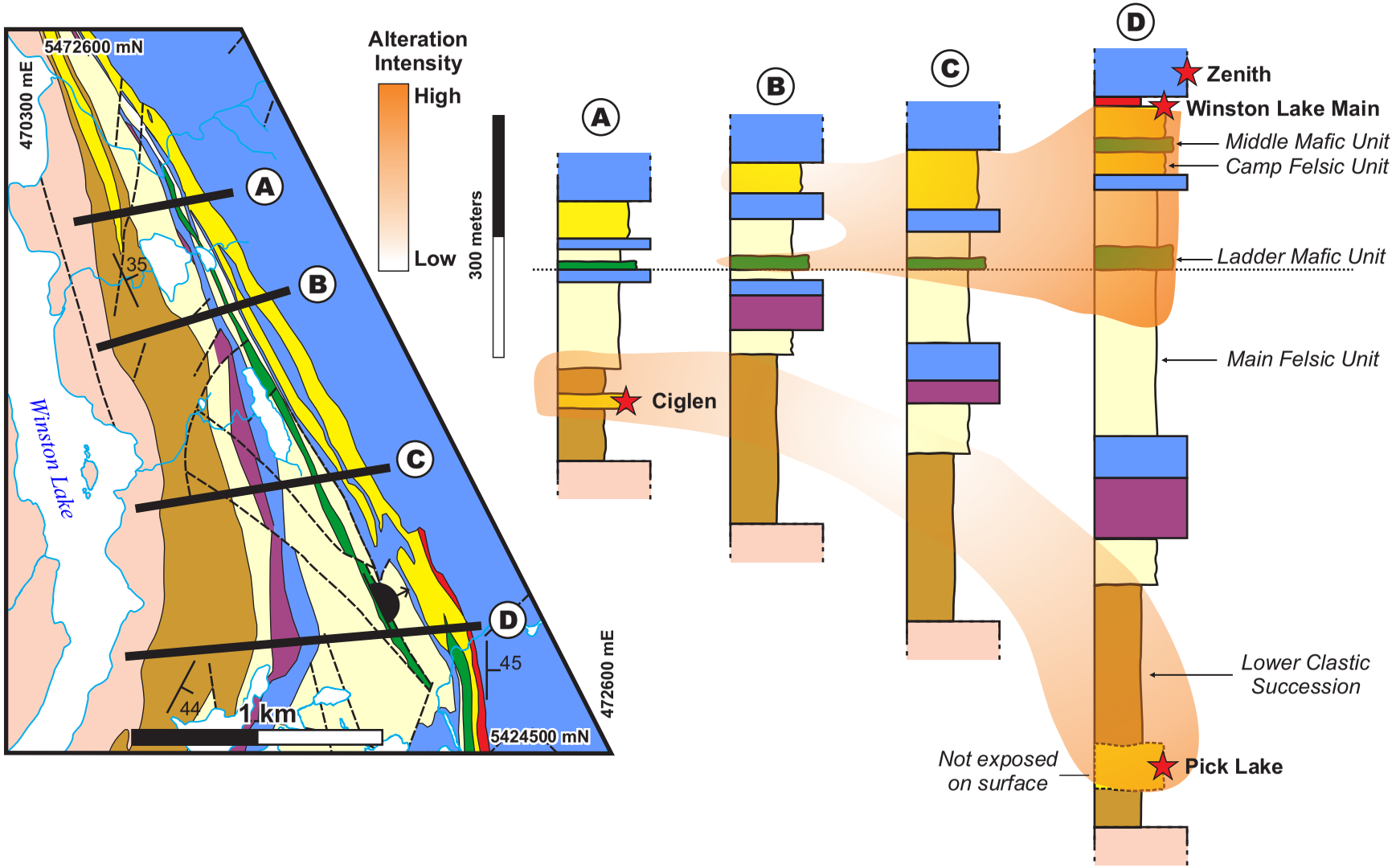

Figure 3.2 - Stratigraphic representation of the Winston Lake assemblage. Inset map shows location of sections. Distance between columns is not to scale. Strata are hung and stacked from the bottom of the Ladder mafic unit as this is the most continuously exposed marker interval and it is assumed to approximate the paleo-horizontal. Geology and alteration intensity are modified from Osterberg (1993) and Thomas (1991) based on mapping and geochemical data in this study.

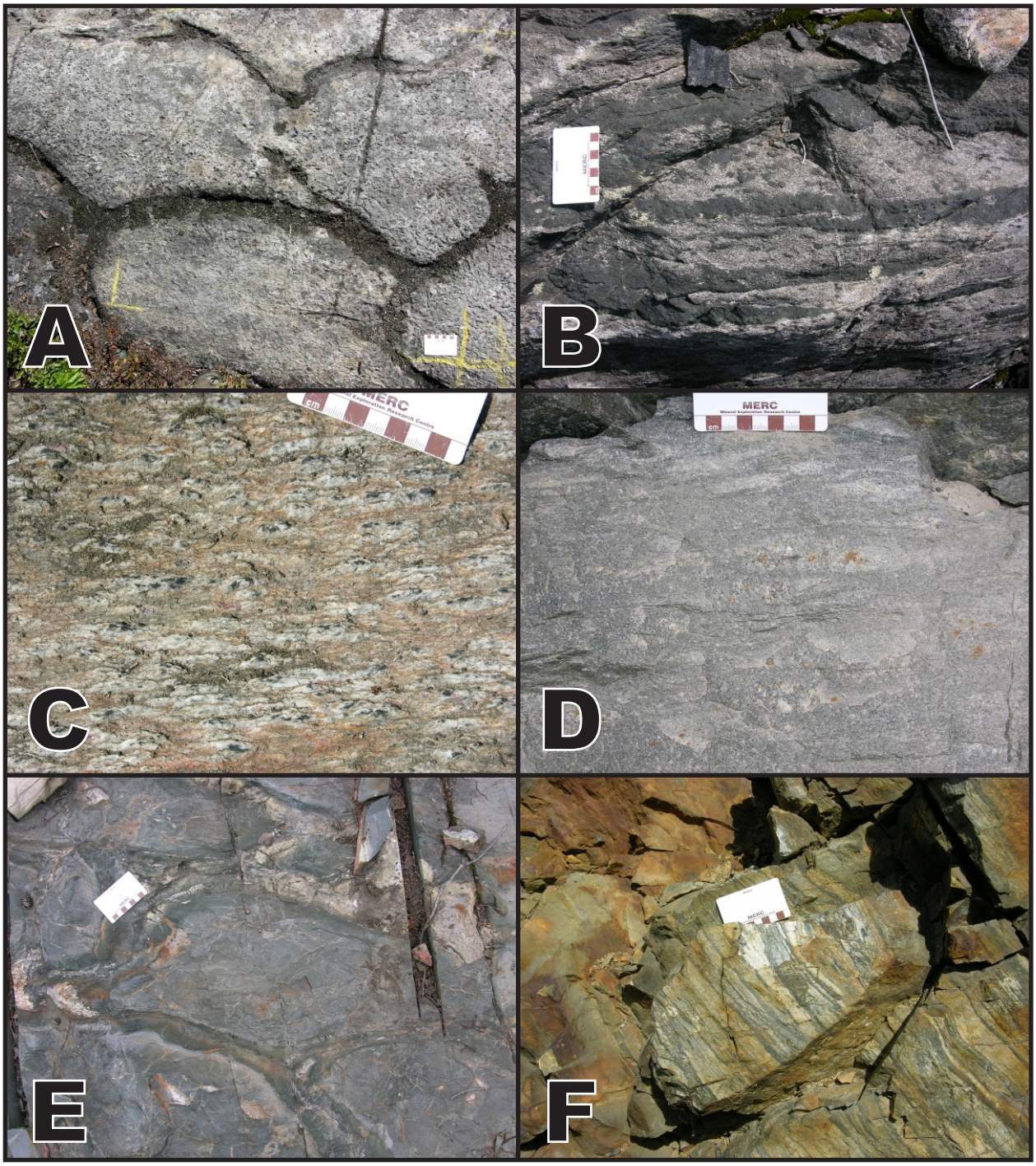

Figure 3.3: Photographs from various lithostratigraphic units in the Winston Lake greenstone belt. A) Orthoamphibole-cordierite altered pillow flows from the Ladder flow. B) Interlayered leucocratic and melanocratic phases of the Zenith gabbro. C) Muscovite-biotite-sillimanite altered Main felsic unit. D) Silicified quartz-phyric volcaniclastic breccia from the Camp felsic unit. E) Pillow structures in amphibolitic flows from the lower Big Duck Lake assemblage. F) Planar bedded felsic volcaniclastic unit from the Winston Lake interval.

1991; Osterberg, 1993). In the BDLA, the D_1 foliation has a westerly strike (Pye, 1964; Ritcey, 1992). The change in the strike of D_1 foliation has been interpreted to be either an apex of a northeast plunging regional syncline, or deflection of the foliation due to the emplacement of the granitoid complex on the western and southern margin of the belt (Figure 1) (Pye, 1964). D_2 is represented by localized shearing subparallel to foliation and minor folding (Ritcey, 1992; Osterberg, 1993) that are associated with orogenic gold-type alteration and mineralization in the Big Duck Lake area (Ritcey, 1992). D_2 structures are interpreted to have formed as a consequence of strike-slip movement during terrane accretion of the Wawa subprovince onto the Wabigoon and Quetico subprovinces to the north (Ritcey, 1992). The quartz-feldspar porphyry in the Big Duck Lake area has D_1 foliation overprinting its margin, but D_2 shearing is penetrative and present throughout the intrusion suggesting that it was emplaced syn-D_1 to D_2 (Ritcey, 1992). A late D_3 event is responsible for belt-scale north to northeast trending brittle faults that offset contacts at the map scale (Ritcey, 1992; Osterberg, 1993).

U-Pb geochronology of monazite within the WLA has estimated the timing of peak metamorphism at 2676 Ma, which is consistent with the timing of regional metamorphism in the southern part of the Superior Province (Davis et al., 1994). Mineral assemblages containing sillimanite, cordierite, staurolite, and gahnite in metamorphosed alteration assemblages in the WLA, and epidote-hornblende mineral assemblages in altered mafic rocks of the BDLA constrain regional metamorphic grade to amphibolite facies (e.g., Blatt and Tracy, 2000). Unaltered mafic lithofacies are now metamorphosed to hornblende-plagioclase-quartz mineral assemblages. Unaltered felsic lithofacies are metamorphosed to quartz-feldspar-biotite assemblages.

3.3.1. Winston Lake Assemblage

The general stratigraphy of the WLA and stratigraphic position of known VMS deposits are illustrated in **Figure 3.2**. Detailed mapping in the WLA interpreted the strata to be intact and homoclinal (Osterberg, 1993). The oldest and lowermost unit of the WLA is the “lower clastic succession” and hosts the Ciglen and Pick Lake VMS deposits (Osterberg, 1993) (**Figure 3.2**). The majority of the rocks within this unit have poorly preserved primary textures due to a combination of hydrothermal alteration and metamorphic recrystallization (Lodge and Chartrand, 2013) (**Figure 3.3C**). The lithologies are now quartz-feldspar-biotite schists and gneisses with variable amounts of garnet, hornblende, and/or muscovite depending on the amount of

hydrothermal alteration (Osterberg, 1993). In the vicinity of the Ciglen deposit, planar sedimentary layering is more obvious (**Figure 3.3A**) with cm-scale bedding distinguished by variations in mineral abundance and grain size. These layered rocks are interpreted to represent variably reworked, felsic-derived volcaniclastic lithofacies based on trace element geochemistry that is similar to other felsic units in the WLA. VMS-deposits are associated with the intercalated felsic volcanic lithofacies, which include flows, tuffs, and breccias (Osterberg, 1993). These felsic lithofacies are not exposed on surface near the Pick Lake VMS deposit (**Figure 3.2**) (Osterberg, 1993).

Massive felsic volcanic lithofacies are the most voluminous in the WLA and are divisible into two geochemically-distinct units. The largest of the felsic units is the "main" felsic unit, which is composed of variably altered massive quartz- and feldspar-phyric flows and minor volcaniclastic breccias. In general, the intensity of VMS-type alteration increases stratigraphically upward in this unit and toward the Winston Lake VMS deposit (**Figure 3.2**). Metamorphosed hydrothermal alteration assemblages include "knotted" quartz-sillimanite-biotite schists (**Figure 3.3C**), quartz-feldspar-biotite ± garnet ± staurolite schists, and quartz-cordierite-orthoamphibole±garnet gneiss that are broadly similar to other VMS alteration assemblages that have been metamorphosed to amphibolite facies (e.g., Snow Lake, Manitoba; Galley et al., 1993). The "main" felsic unit contains 5-10% quartz and feldspar crystals in the coherent massive and volcaniclastic lithofacies unless it is strongly altered.

Stratigraphically above the "main" felsic unit is the "camp" felsic unit, which contains more volcaniclastic than coherent lithofacies. The volcaniclastic lithofacies include tuff breccia and thinly bedded tuff. Some volcaniclastic facies contain hornblende-rich "clots" that are interpreted to be altered glassy fragments or mafic-intermediate accidental fragments (Osterberg, 1993) (**Figure 3.3D**). Quartz and/or feldspar crystals are present, but are generally in lower abundance and are smaller in size than those in the "main" felsic unit. Flow lithofacies are typically aphyric and massive and sometimes preserve convoluted flow banding. Alteration assemblages in the "camp" felsic unit are similar to those of the "main" felsic unit, but differ with the inclusion of zones of silicification recognized by layers of massive, coarse-grained volcaniclastic rocks that have bleached coloration and anomalously low mica content (**Figure 3.3D**).

Minor units of mafic strata are interlayered with the felsic strata of the WLA, and constitute important marker units that are laterally continuous and easily identified. The lowermost mafic unit in the WLA is the "ladder" mafic unit and it is interlayered with the "main" felsic unit. The "ladder" mafic unit is generally strongly altered but locally has well preserved primary volcanic features ranging from massive flows, pillows, and flow-top breccias (Osterberg, 1993; Lodge, 2012b) (**Figure 3.3A**). Least altered facies of the "ladder" flow are typically plagioclase-phyric amphibolite with plagioclase phenocrysts up to 3-4 mm in size composing 5-10% of the rock. Metamorphic assemblages of the altered mafic lithofacies include orthoamphibole-cordierite and orthoamphibole-biotite-cordierite-garnet. Garnet porphyroblasts range up to 8 cm in size and are sometimes concentrated into cm-wide bands that define features reminiscent of altered pillows and breccia textures (Osterberg, 1993; Lodge, 2012b). In the immediate footwall to the Winston Lake VMS deposit is the "middle" mafic unit, which is interlayered within the "camp" felsic unit. The unit is mostly a massive aphyric to sparsely plagioclase-phyric amphibolite with metamorphosed alteration assemblages including cordierite-orthoamphibole-hornblende±biotite±garnet gneiss. Pillowed mafic flows within this unit have been described as small, tightly packed pillows with thin selvages and minimal inter-pillow material (Osterberg, 1993).

The Winston Lake interval is a plane-bedded volcaniclastic unit ranging in thickness from 10 to 100 m southward along strike from the Winston Lake main ore body (Osterberg, 1993) (**Figure 3.3F**). Layering in this unit is defined by layers rich in hornblende alternating with layers rich in fine, microcrystalline quartz, interpreted to be a mixture of tuff and exhalative chemical sediment (Osterberg, 1993). Not surprisingly this unit has an intermediate composition reflecting mixed mafic and felsic compositions (Lodge and Chartrand, 2013). South of the Winston Lake ore body, the Winston Lake interval consists of intercalated mafic flows, gabbroic intrusions, and mixed-provenance volcaniclastic units (Osterberg, 1993). The intercalated flows and intrusions are compositionally similar to the "middle" mafic unit (Osterberg, 1993). The flows and intrusions are exposed at surface southward along strike of the VMS deposits, but are observed in drill core and mine workings in close proximity to the main ore body (referred to as the "footwall flows" in previous work; **Table 3.1**)

The mixed volcaniclastic sedimentary lithofacies are volcanic wackes that contain sparse mafic lithic fragments. In some areas, well-preserved cross-bedding and symmetrical ripple

laminations are present in thinly bedded wackes (**Figure 3.4A)**. Bedding in these rocks is manifest by variations in biotite, quartz, and feldspar abundance.

3.3.2. Zenith Gabbro

The Zenith gabbro is a thick, differentiated mafic to ultramafic sill that was emplaced at the contact between the WLA and BDLA, and along the southern margin of the Winston Lake greenstone belt (**Figure 3.1**). Thinner sills of the Zenith gabbro occur in the "main" felsic unit of the WLA. Differentiation is defined by layers of variable amphibole and plagioclase content that are interpreted to represent primary gabbroic and pyroxenitic layers (**Figure 3.3B**). Cumulate textures are locally preserved and pegmatitic phases occur as metre-scale lenses (**Figure 3.5A**). The Zenith gabbro was emplaced along the contact between the WLA and BDLA and along its lower contact entrained portions of the Winston lake VMS deposit that now occurs as a series of larger massive sulfide xenoliths that constitute the former Zenith ore body (Severin et al., 1991).

3.3.3. Big Duck Lake Assemblage

The BDLA is the "metavolcanic" unit of Pye (1964) and is the most voluminous assemblage within the Winston Lake greenstone belt. Two geochemically-distinct mafic flow units were recognized by Ritcey (1992), but their petrogenesis were not fully understood. They are indistinguishable on the outcrop and petrographic scales. Variably preserved pillows are recognized and locally display epidote-altered cores and selvages and quartz- and carbonate-filled amygdules. Gabbroic sills are geochemically identical to the mafic flows they intrude and are interpreted to be synvolcanic (Ritcey, 1992). Thinly layered mafic volcaniclastic units are sparse.

A felsic quartz-feldspar porphyry intrusion (**Figure 3.5C**) and associated irregular sill-like bodies occur within the mafic flows of the BDLA (Pye, 1964; Ritcey, 1992). The intrusions contain phenocrysts of quartz and feldspar up to 1 cm in size and that constitute up to 10% of the intrusion. The intrusion is weakly to moderately foliated along its margin and becomes increasingly massive in its interior. It is interpreted to be emplaced during late-D_1 to syn-D_2 deformation (Ritcey, 1992). Brecciated felsic lithofacies located proximal to this porphyry are interpreted to be the tectonically brecciated marginal facies to the intrusion, and not a felsic volcaniclastic lithofacies (Ritcey, 1992).

3.4. Geology of the Winston Lake VMS Deposits

The economic VMS ore bodies in the Winston Lake greenstone belt totalled approximately 4.6 million tonnes of Zn-rich ore (unpublished Inmet Mining Corporation records). Early mapping described massive sphalerite mineralization that is now known as the Zenith ore body, as being hosted in gabbroic rocks (Bartley, 1940; Pye, 1964; Williams et al., 1991). The 0.16 million tonnes (Mt) Zenith ore bodies contained 16.5% Zn and trace amounts of Cu. The exploration activity that followed exploitation of the Zenith ore body discovered the Winston Lake Main ore body. This is the largest known ore body in the belt and it contained 3.1 Mt of ore at 16% Zn, 1% Cu, 30.1 g/t Ag, and 1.0 g/t Au. The Pick Lake deposit, discovered after mining started at Winston Lake Main ore body contained 1.3 Mt of ore at 16.5% Zn and 0.9% Cu (unpublished Inmet Mining Corporation records).

The gabbro-hosted Zenith orebody has been interpreted to comprise xenoliths that were entrained from the main Winston Lake Main ore body during the intrusion of the Zenith gabbro (e.g., Severin et al., 1991). The ore bodies have lenticular shapes that range in thickness from <1 to 13.4 m and are dominated by massive to locally disseminated coarse-grained sphalerite with rims of pyrrhotite, pyrite, and chalcopyrite (Pye, 1964). The footwall strata to the Winston Lake Main ore body is composed of altered mafic flows from the Winston Lake interval (the footwall flows) and “clotted” rhyolites from the “camp” felsic unit and are in sharp contact with the ore noted by the presence of a 1-3 cm thick chloritic seam (Severin et al., 1991). The hanging wall is composed of the cherty, bimodal tuff of the Winston Lake interval and is partially intruded by the Zenith gabbro (Severin et al., 1991). The ore zone ranges in thickness from 2-20 m and consists of two main ore types: “low grade” (7-14% Zn) massive and banded fine- to medium-grained sphalerite, pyrrhotite, pyrite, and chalcopyrite, and “high grade” (up to 54% Zn) coarse-grained sphalerite locally banded with chalcopyrite and pyrrhotite (Severin et al., 1991). The ore zones contain 10-20% amphibolitic fragments that presumably represent pre-metamorphic gangue assemblages (Severin et al., 1991). The Pick Lake deposit is a 1.5-14 m thick, sheet-like body that has sharp contacts with altered felsic rocks within the lower clastic sequence (unpublished Inmet Mining Corporation Reports). The ore body shows evidence for remobilization (unpublished Silvore Fox Minerals Corporation Records) along structures present in the southern part of the WLA. It is composed of fine- to medium-grained sphalerite and pyrrhotite with minor amounts of chalcopyrite and pyrite.

The VMS-associated alteration assemblages have been metamorphosed to amphibolite facies with mineral assemblages that are atypical for metamorphosed felsic and mafic volcanic strata that have not been chemically altered. About 50% of the WLA strata have been hydrothermally altered (Thomas, 1991; Osterberg, 1993) and are characterized by losses of Na and Ca, and gains in Mg, Fe, and K; compositional changes that are consistent with a pre-metamorphic chlorite alteration that is typical of bimodal mafic and bimodal felsic VMS deposits (e.g., Franklin et al., 2005). In general, alteration intensity increases toward the main VMS deposits both along strike and up section. In the mafic lithofacies, least altered rocks show preserved plagioclase phenocrysts and are dominated by an assemblage of hornblende, plagioclase, and quartz. The most intensely altered mafic lithofacies are characterized by orthoamphibole-cordierite-quartz and orthoamphibole-cordierite-garnet±biotite±chlorite mineral assemblages (Thomas, 1991). The presence of micaceous minerals indicates the K-addition during alteration. These mineral assemblages are typical of strongly chloritized mafic rocks metamorphosed to amphibolite facies (Galley et al., 1993; Zaleski et al., 1995). Anthophyllite porphyroblasts range from 1 to 20 cm in length in the strongly altered "ladder" mafic unit (e.g., Lodge, 2012b). Unaltered felsic volcanic lithofacies are weakly to moderately foliated and have well preserved quartz and feldspar phenocrysts. Weakly altered samples are characterized by an increase in biotite (25-40%) and contain trace amounts of garnet in a quartzofeldspathic matrix; consistent with a pre-metamorphic sericite±chlorite alteration (Galley et al., 1993; Galley et al., 2007). With increasing alteration the most common alteration mineral assemblage in felsic lithofacies is quartz-sillimanite-biotite±garnet±staurolite; consistent with a pre-metamorphic transitional sericite to chlorite alteration (Galley et al., 1993). These rocks commonly have sillimanite "clots" that give the rock a knobby-like texture (**Figure 3.3C**). The most intensely altered felsic rocks are closest to the VMS deposits and have an orthoamphibole-cordierite-quartz±garnet mineral assemblage, consistent with a pre-metamorphic chloritic alteration (Galley et al., 1993; Zaleski et al., 1995; Galley et al., 2007), and can only be distinguished from similar assemblages in the most strongly altered mafic lithofacies on the basis of differences in their trace element geochemistry.

The original porosity and permeability of the volcanic rocks appear to have been an important physical control on the distribution of hydrothermal alteration in the WLA (Osterberg, 1993). Alteration is laterally extensive and semi-conformable in morphology in lithofacies that

are interpreted to be volcaniclastic as these had higher primary permeability; this applies to most of the “camp” felsic unit, lower clastic sequence, and the uppermost part of the “main” felsic unit. Massive coherent lithofacies of the “main” felsic unit are generally least altered to weakly-altered, where the latter is manifest by an increased abundance of biotite. Mafic lithofacies are most strongly altered within pillowed or brecciated facies and adjacent to contacts with felsic rocks. The “main” felsic unit is most strongly altered near its upper contact with the “ladder” mafic unit. The extensive alteration of the “ladder” mafic unit may indicate that the relatively reduced permeability of this unit, in contrast to the underlying breccias and volcaniclastic lithofacies of the “main” felsic unit, resulted in less permeable “cap” or aquiclude that restricted ascending hydrothermal fluids and promoted lateral fluid flow (e.g., Franklin et al., 2005). The semiconformable to obliquely crosscutting morphology of the VMS alteration in **Figure 3.2**, may reflect primary lateral fluid movement within permeable footwall strata and, in part, subsequent transposition into bedding during D_1 deformation.

3.5. U-Pb Geochronology Results

Prior to this study, only a single age of 2723 ± 3 Ma (Davis et al., 1994) existed for the Winston Lake greenstone belt and it was from the “camp” felsic unit associated with the Winston Lake VMS-deposit. For this study, a total of five samples were analyzed for U-Pb zircon geochronology as summarized in **Table 3.2**. The samples were located to constrain the magmatic/volcanic history, the provenance of volcaniclastic units of the VMS-hosting WLA, and to determine the temporal relationship of these rocks to the Zenith gabbro and BDLA. Their locations are shown in **Figure 3.1.** Data for all analyses are available in a Miscellaneous Release – Data published by the Ontario Geological Survey (Lodge and Chartrand, 2013).

3.5.1. Detrital Zircon Geochronology

Detrital zircon U-Pb geochronology was determined using laser ablation inductively coupled plasma mass spectrometry (LA-ICP-MS) at the Mineral Exploration Research Centre, Laurentian University. LA-ICP-MS was utilized for detrital zircon geochronology because of the cost-effectiveness and ability to analyze a larger number and spectrum of grains. Details of the analytical procedure and calibrations are summarized in Lodge (2012a). U-Pb concordia diagrams were constructed using Iolite (Paton et al., 2011) and VizualAge (Petrus and Kamber, 2012). Histograms and probability curves for each sample were generated using Isoplot 4.1 for

Table 3.2 – Summary of the location of samples for geochronology from the Winston Lake greenstone belt and the analytical methods. UTM co-ordinates are reported in meters in Zone 16 using NAD83.

Sample	*Rock Type*	*Unit*	*Easting*	*Northing*	*Method*	*Age Type*
RL-11-118	Pegmatitic Gabbro	Zenith gabbro	472351	5425030	TIMS	Magmatic
RL-11-183	Felsic Porphyry	"Main" felsic unit	471626	5424624	TIMS	Volcanic
RL-11-185	Felsic Volcaniclastic	Lower clastic succession	470731	5426771	LA-ICP-MS	Detrital
RL-11-187	Big Duck Lake QFP	Big Duck Lake Assemblage	480557	5428178	TIMS	Magmatic
RL-11-194	Intermediate Volcaniclastic	Winston Lake interval	472693	5423107	LA-ICP-MS	Detrital

Microsoft Excel (Ludwig, 2012). VizualAge allowed for careful selection of the most concordant part of the signal (Petrus and Kamber, 2012). The average error for the $^{207}Pb/^{206}Pb$ ages for individual grains averaged 15-25 Ma, but were frequently as low as 10 Ma. Because of this relatively large error, trends in the age of the population are more relevant for interpreting the data rather than the age of individual grains.

Sample RL-11-185 is from a planar bedded, biotite- and muscovite-rich felsic volcaniclastic unit (**Figure 3.4A**) from the lowermost clastic unit. Zircons from this sample are largely euhedral with well-formed crystal faces. Most grains are stubby to moderately prismatic with a minor amount of elongated narrow crystals. The $^{207}Pb/^{206}Pb$ ages of the sampled zircons formed a relatively tight group of ages between ~2685-2740 Ma with a single central population peak at ~2714 Ma (**Figure 3.4C**). The youngest single zircon analyzed is 2672 ± 25 Ma, but it is possible that metamorphic rims were analyzed due to insufficient polishing or analysis of metamorphic rims on the bottom side of the crystal, resulting in a mixed, slightly younger age. Lead loss early in the grain's history may also result in an erroneously young age (e.g., Anderson, 2002) The oldest zircon present in this sample is 2757 ± 24 Ma.

Sample RL-11-194 is from a cross-bedded volcaniclastic rock with an intermediate composition (**Figure 3.4B**) that is located within the immediate footwall 2 km along strike from the Winston Lake ore body (**Figure 3.1A**). Zircon grains are stubby to slightly prismatic, euhedral crystals that are weakly to strongly colored and have a high to moderate opacity. The zircons yielded a range of concordant ages with a distribution of ages that formed a broad peak from ~2685-2740 Ma with a single population peak at 2717 Ma (**Figure 3.4C)**. The youngest grain analyzed has a $^{207}Pb/^{206}Pb$ age of 2665 ± 12 Ma, which is anomalously younger than known magmatic events in the Wawa subprovince (Corfu and Stott, 1998; Zaleski et al., 1999; Muir, 2003) and, therefore, may represent a metamorphic age or Pb-loss early in the grains history resulting in an erroneously young age (e.g., Anderson, 2002). The oldest zircon is 2781 ± 14 Ma.

3.5.2. Magmatic Zircon Geochronology

For magmatic zircons the U-Pb geochronology was determined using thermal ionization mass spectrometry (TIMS) at the Jack Satterly Geochronology Laboratory, University of Toronto. Zircons were thermally annealed and chemically etched using the methodologies outlined by Mattinson (2005) prior to being dissolved according to procedures outlined by Krogh

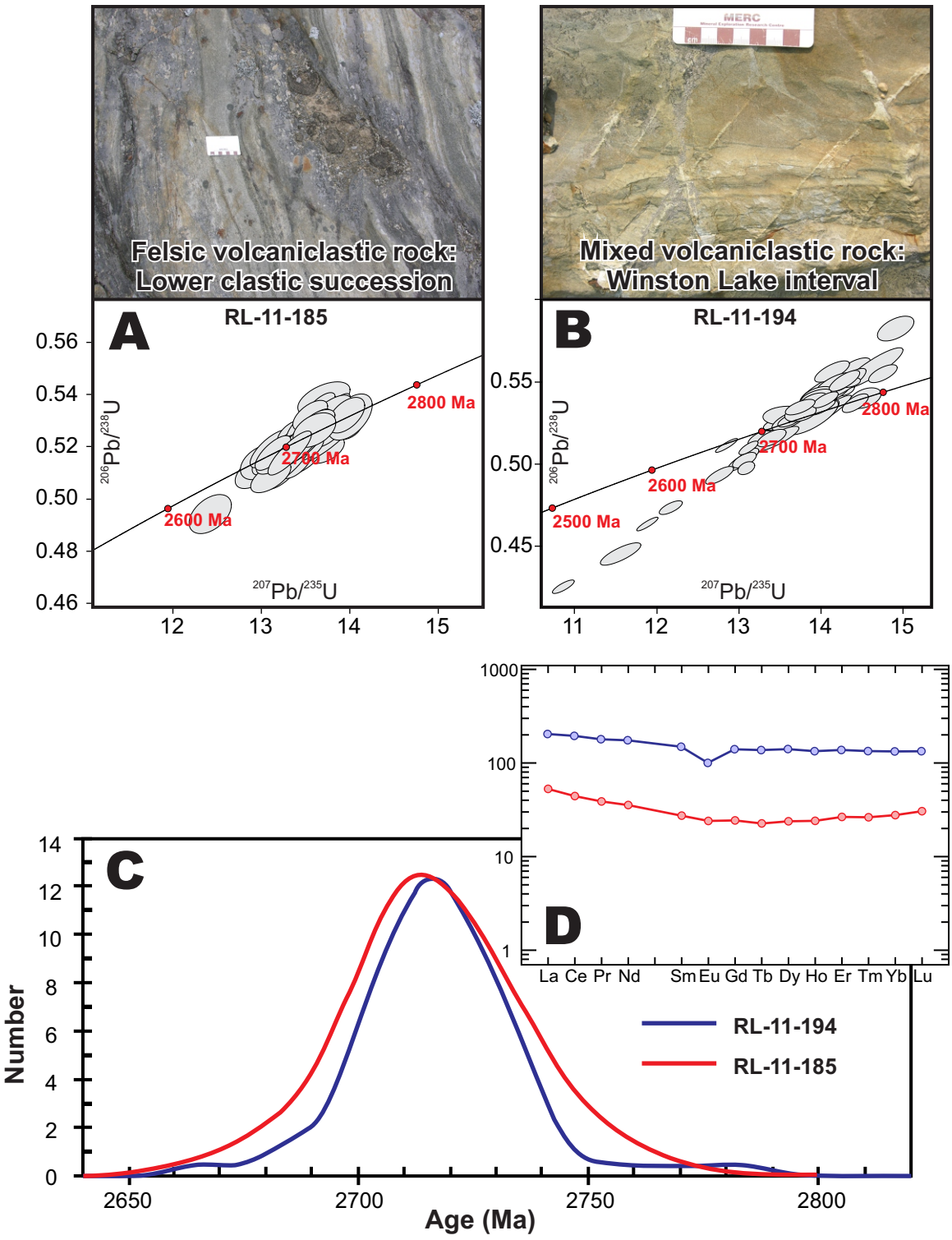

Figure 3.4 - A and B) Photographs of samples RL-11-185 and RL-11-194 with concordia diagrams showing U-Pb ages from detrital zircons. C) Frequency distribution of U-Pb ages collected from these samples showing broad peak centered at 2710-2720 Ma. D) Chondrite-normailzed REE spider diagram of each sample.

(1973). U and Pb were separated using anion exchange columns (Gerstenberger and Haase, 1997). U-Pb age determinations were carried out using Isoplot for Microsoft Excel (Ludwig, 2012) relying on decay constants from Jaffey et al. (1971). Concordia diagrams were generated using Isoplot.

Sample RL-11-118 is from a pegmatitic phase of the Zenith gabbro that intrudes the Winston Lake ore body and is host to the Zenith ore body. The analyzed zircons from this sample have magmatic morphologies and their low U abundances and high Th/U ratios are typical of mafic magmas (e.g., Wang et al., 2011), and are distinctly different than the Th/U ratios from zircons of the "camp" (Davis et al., 1994) and "main" felsic units. Data for four fractions are all collinear, have identical $^{207}Pb/^{206}Pb$ ratios, and have an upper intercept $^{207}Pb/^{206}Pb$ age of 2719 ± 4 Ma (**Figure 3.5A**). This age is within error or slightly younger than the felsic volcanic rocks that the gabbro intrudes.

Sample RL-11-183 is representative of a weakly altered phase of a massive quartz-feldspar phyric felsic flow from the "main" felsic unit of the WLA. This felsic flow is located stratigraphically between the Pick Lake and Winston Lake VMS ore bodies (**Figure 3.2**) and comprises the most voluminous phase of the felsic lithofacies within the WLA. Zircons from this sample constitute a homogeneous population of sharp, clear, and prismatic crystals. Three single grain fractions, though variably discordant even following chemical abrasion, are collinear and give an upper intercept age of 2721.2 ± 0.9 Ma (**Figure 3.5B**). This age is the same age as the sample from the "camp" felsic unit (Davis et al., 1994) indicating that the felsic rocks are all the same age, even though the felsic units are geochemically distinct from each other (see Felsic Geochemistry section below).

Sample RL-11-187 is the only sample from the BDLA, and it is from an unfoliated, felsic quartz-feldspar porphyry that intrudes mafic flows in the vicinity of Big Duck Lake. This porphyry yielded a variable population of zircon morphologies that include large, flat, clear euhedral crystals, long slender needle-like grains, shorter prisms, and some irregular grains. A total of eight single grains were analyzed from the sharpest, most pristine and prismatic forms. However, each analysis yielded a different $^{207}Pb/^{206}Pb$ age and so it remains unclear what the true magmatic age of this unit. A weighted average of the three youngest fractions yields a mean $^{207}Pb/^{206}Pb$ age of 2692 ± 0.7 Ma (**Figure 3.5C**) with a probability of fit of only 8%. The remaining analyses scatter from 2700 to 2716 Ma and represent xenocrystic zircons. Given the

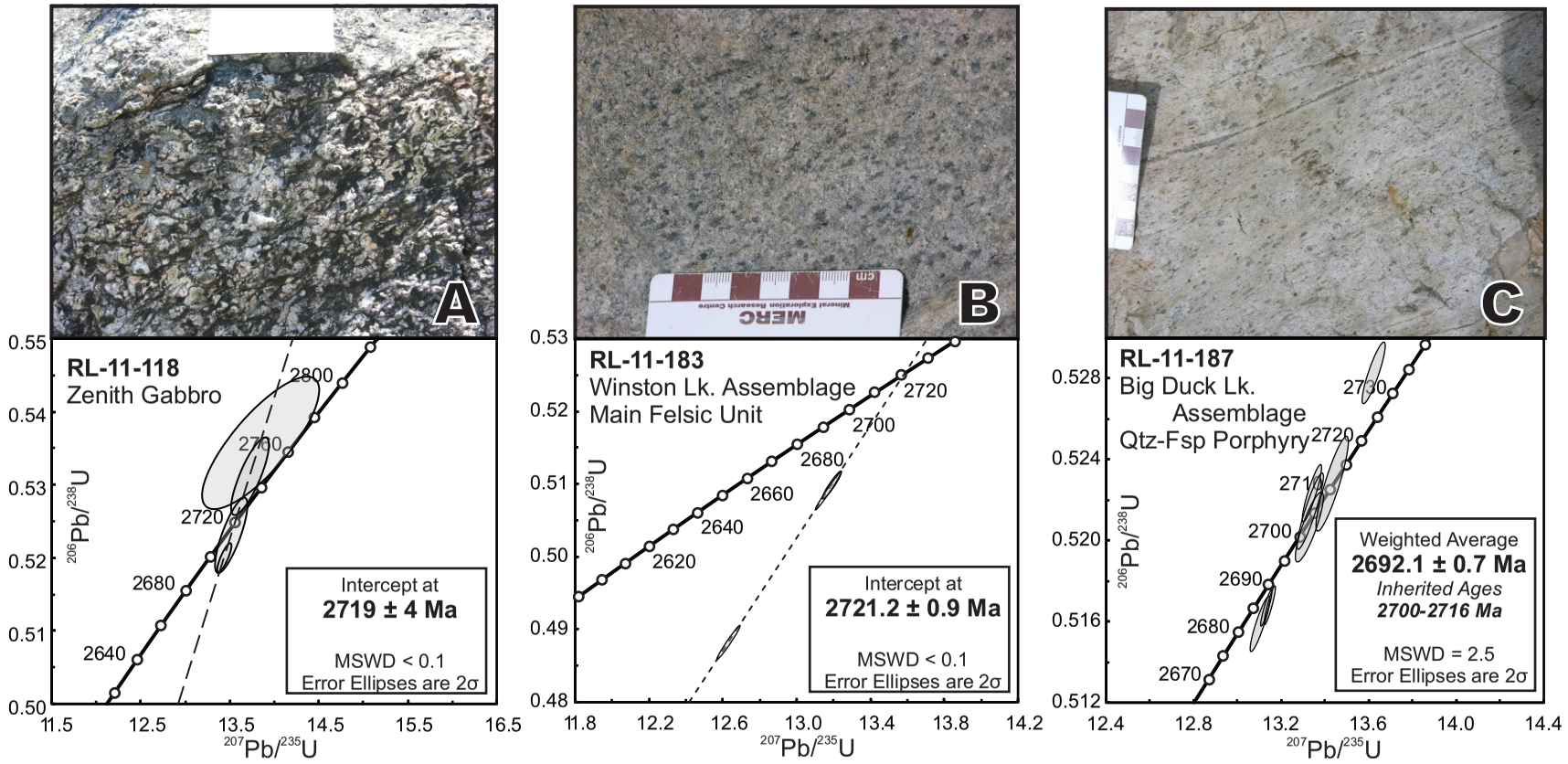

Figure 3.5 – A) Pegmatitic phase of the Zenith gabbro that hosts the Zenith ore body and intrudes the Winston Lake ore body. Low-U zircons analyzed in sample RL-11-118 from this intrusion provide an upper intercept $^{207}Pb/^{206}Pb$ age of 2719 ± 4 Ma. B) Biotite-altered, high Zr/Ti felsic quartz-feldspar porphyry from the Winston Lake assemblage. Zircons analyzed in sample RL-11-183 have an upper intercept $^{207}Pb/^{206}Pb$ age of 2721.2 ± 0.9 Ma. C) Quartz-feldspar porphyry from the Big Duck Lake sequence. The youngest zircons in sample RL-11-187 have a weighted average $^{207}Pb/^{206}Pb$ age of 2692.1 ± 0.7 Ma. This sample also contains inherited zircons that range in age from 2716 Ma to 2700 Ma.

scatter of zircon ages, it is possible that all zircons from this sample are xenocrystic. Therefore, the 2692 ± 0.7 Ma age for the youngest zircon fractions from the porphyry is interpreted to be the maximum age of emplacement for the intrusion and constrains the timing of deformation since the intrusion was emplaced post-D_1 and syn- to late-D_2 (Ritcey, 1992).

3.6. Geochemical Results

3.6.1 Analytical Procedures

Samples were crushed using a steel jaw crusher prior to pulverization in an agate mill. Major, trace, and rare earth elements were analyzed at the Ontario Geoscience Laboratories (Sudbury, Ontario). Major elements were analyzed with X-ray fluorescence (XRF) using a fused disk with a borate flux. Trace and rare earth elements were analyzed using inductively coupled plasma mass spectrometry (ICP-MS). Samples underwent closed beaker four acid digestion. Any sample that had residue after digestion was not included in the data set presented. All sample preparation methods, analytical procedures, instrumental calibrations, and quality assurance standards at the Ontario Geoscience Laboratories are outlined in several publications by the Ontario Geological Survey (Burnham, 2008; Keating and Burnham, 2012).

Neodymium isotopic geochemistry was completed at the Radiogenic Isotope Facility at the University of Alberta (Edmonton, Alberta) using static mode by multi-collector inductively coupled plasma mass spectrometry (MC-ICP-MS) (Schmidberger et al., 2007) following the procedures outlined in Creaser et al. (1997) and Unterschutz et al. (2002). All isotope ratios are normalized for variable mass fractionation to a value of $^{146}Nd/^{144}Nd = 0.7219$ using the exponential fractionation law. The $^{143}Nd/^{144}Nd$ ratio of samples is presented here relative to a value of 0.511844 for the La Jolla Nd isotopic standard, monitored by use of an in-house Alfa Nd isotopic standard for each analytical session. Analysis of the Geological Survey of Japan Nd isotope standard "Shin Etsu: J-Ndi-1" (Tanaka et al., 2000), which has an accepted value of $^{143}Nd/^{144}Nd$ at 0.512107 ± 0.000007, had an average value of $^{143}Nd/^{144}Nd$ of 0.512091 ± 0.000011 (1σ, n = 35) during the reported analysis. Initial εNd values were calculated using Uniform Chondritic Reservoir (CHUR) $^{147}Sm/^{144}Nd$ (0.1967) and $^{143}Nd/^{144}Nd$ (0.512638) values and the U-Pb zircon age (2720 Ma) of the volcanic assemblages.

3.6.2. Effects of Hydrothermal alteration

The effects of hydrothermal alteration are profound within the WLA, and post-alteration metamorphism of VMS discordant alteration zones resulted in distinctive mineral assemblages comprising aluminosilicate minerals (sillimanite, staurolite, cordierite), micas (biotite, chlorite, muscovite), Fe-Mg orthoamphibole, and porphyroblastic garnets. The occurrence of metapelite-like mineral assemblages with the altered volcanic rocks explains why earlier researchers classified rocks of the WLA as metasediments (e.g., Pye, 1964). Hydrothermal alteration followed by metamorphic recrystallization resulted in significant mobility of most major elements as well as some typically immobile elements such as the light rare earth elements (LREE) (Gorton and Schandl, 1995). REE mobility has been determined to be restricted to the contact between mafic and felsic lithofacies that are strongly altered and is attributed to metamorphic recrystallization of REE-bearing minerals such as monazite (Gorton and Schandl, 1995). Simple elemental binary diagrams reveal the nature of this element mobility (relative to Zr) (**Figure 3.6**). Major elements show major mobility in most units, especially within the WLA. LREE (Ce) exchange between mafic and felsic lithofacies is evident by the paired enrichment of LREE in WLA mafic units and depletion of LREE in WLA felsic units. Enrichment of Th is also evident in the most strongly altered samples of the "main" felsic unit. VMS-type discordant hydrothermal alteration is limited in the mapped portions of BDLA with the exception of local epidote-altered pillowed mafic flows. Most of the alteration in the BDLA is syn-deformation and is limited to lithofacies that are proximal to shear zones and is not VMS-related (e.g., Ritcey, 1992).

Several geochemical filters were applied to the data set to select least altered samples that could be used for petrogenetic interpretations. Altered samples were identified by significant enrichment in L.O.I. (> 4.5 wt.%), depletion in Na_2O to values < 2 wt.%, and/or Al_2O_3/Na_2O ratios greater than 10 (Spitz and Darling, 1978). In general, this major element was able to discriminate altered and least altered lithofacies. Some tholeiitic basalts from the lower mafic unit had low Na_2O contents without any field or petrographic evidence for significant alteration. In this case, these rocks were not considered altered despite being filtered by the geochemical criteria. REE mobility during alteration was assessed using Ce anomalies, and samples with Ce/Ce* values that significantly deviate from 1 (0.9-1.1 were acceptable as unaltered) were marked (Polat and Hoffman, 2003). A limitation of these geochemical filters is that it is unable to

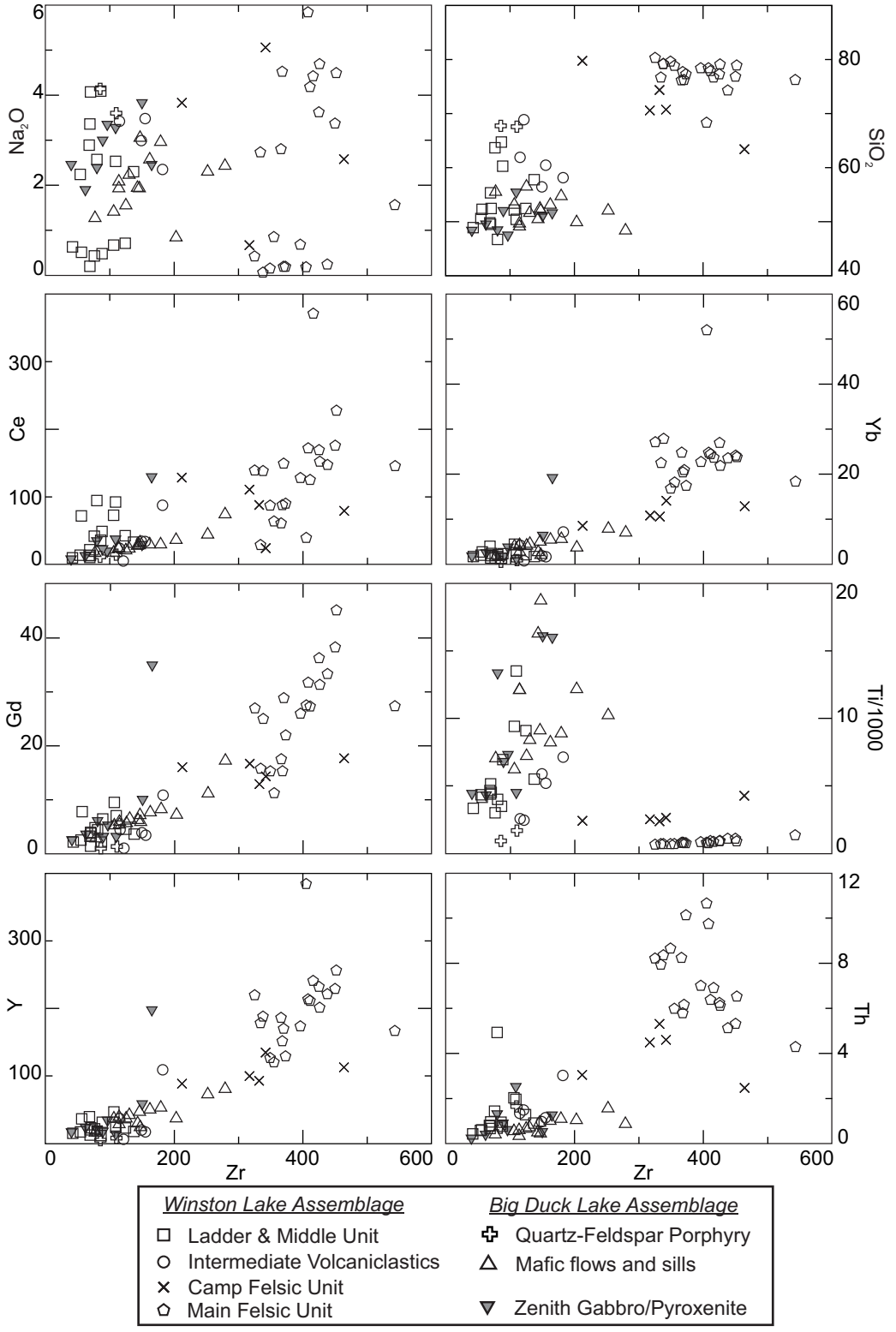

Figure 3.6 – Binary diagrams showing element immobility and mobility relative to Zr. Most major elements, with the exception of Ti, show considerable of mobility across all units. LREE show some mobility with enrichment in mafic lithofacies and depletion in felsic lithofacies. Th shows moderate mobility in the felsic lithofacies.

discriminate multiple generations of overprinting alteration and a sodium-enrichment alteration event overprinting an alteration characterized by sodium-depletion would not be properly identified as an altered sample. Regardless of the limitations, samples that were identified as being altered were assigned a separate symbol in discrimination and trace element diagrams, but are not the primary source of any significant geochemical variation. Strongly altered samples and samples with large porphyroblasts were plotted on REE and extend trace element diagrams because of their irregular trace and rare earth elemental patterns (Lodge and Chartrand, 2013).

3.6.3. Trace Element Geochemistry of Mafic Rocks

The mafic rocks of the Winston Lake greenstone belt assemblages have Zr/Ti and Nb/Y ratios that are consistent with sub-alkaline basalt to basaltic andesite (**Figure 3.7**). However, several of the samples from the WLA and upper mafic unit of the BDLA plot within the basaltic andesite field and have elevated abundances of compatible elements Cr and Ni, which is more consistent with basaltic rocks (Pearce, 1996). Only samples that are classified as basalt are discussed further in this section.

Basaltic rocks in the "ladder" and "middle" mafic units of the WLA are similar in their trace element geochemistry. These mafic units have Ti/V ratios consistent with an island arc to backarc tectonic affinity (Ti/V ≈ 18 to 40) (**Figure 3.8A**) (Shervais, 1982), and have Th/Yb and Zr/Y ratios consistent with a calc-alkalic to tholeiitic magmatic affinity (**Figure 3.8B**) (Ross and Bédard, 2009). Their chondrite-normalized REE patterns have a gentle to moderate slope due to LREE enrichment, up to 100 times chondrite (**Figure 3.9**). Altered samples from the WLA have variable Eu anomalies. Primitive mantle-normalized trace element spider diagrams show pronounced negative Nb, Ti, and Zr anomalies (**Figure 3.9**). The mafic rocks of the WLA have relatively enriched Th/Nb ratios (Nb/Th > 0.15) compared to those from the BDLA (**Figure 3.8C**). Primitive mantle normalized Nb/Th ratios are low (<1) (**Figure 3.8D**).

Basaltic rocks of the BDLA are geochemically distinct from those of the WLA. Flows from the lower mafic unit of the BDLA have generally higher Ti/V ratios than the WLA flows and are indicative of a back-arc affinity (Ti/V ≈ 25 to 40) (Shervais, 1982). The Ti/V ratios of flows from the upper mafic unit indicate a more alkalic affinity (Ti/V ≈ 50 to 195) (**Figure 3.8A**) (Shervais, 1982). Th/Yb and Zr/Y ratios from the BDLA are consistent with transitional to tholeiitic magmatic affinities, and flows with a calc-alkalic affinity are absent (**Figure 3.8B**) (Ross and Bédard, 2009). Chondrite-normalized REE diagrams indicate that the upper mafic unit

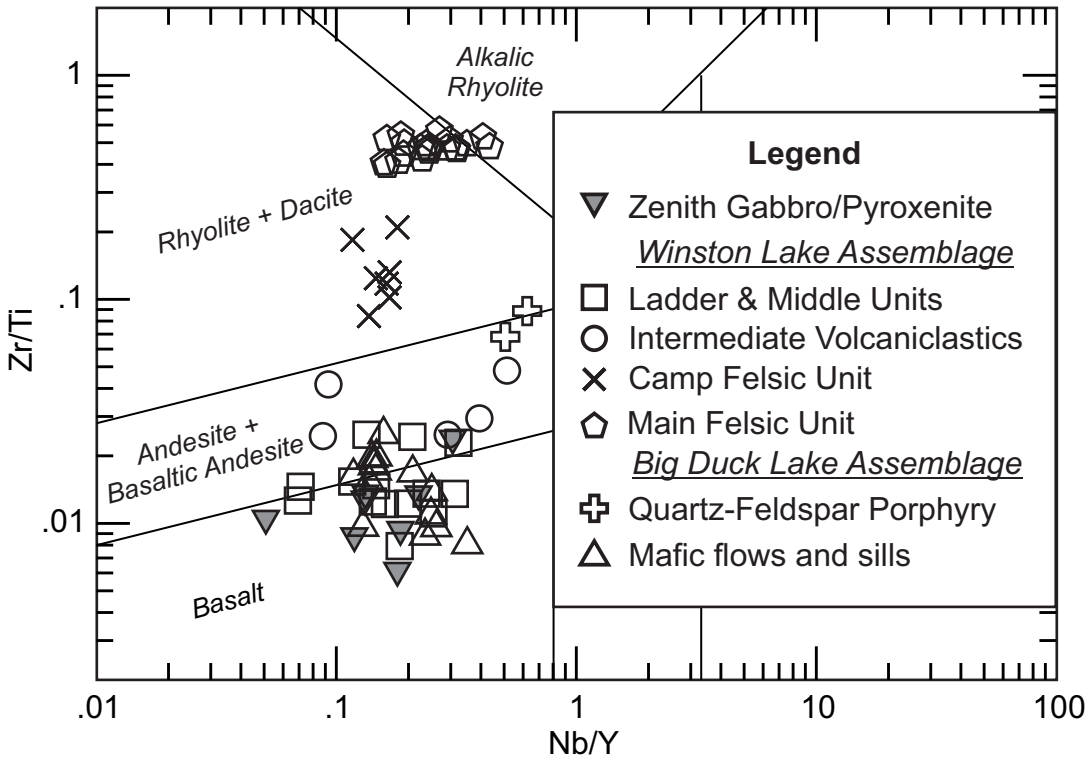

Figure 3.7 - Trace element rock classification diagram showing the bimodal composition of volcanic rocks in the Winston Lake greenstone belt. Figure is from Pearce (1996) and is modified from Winchester and Floyd (1977).

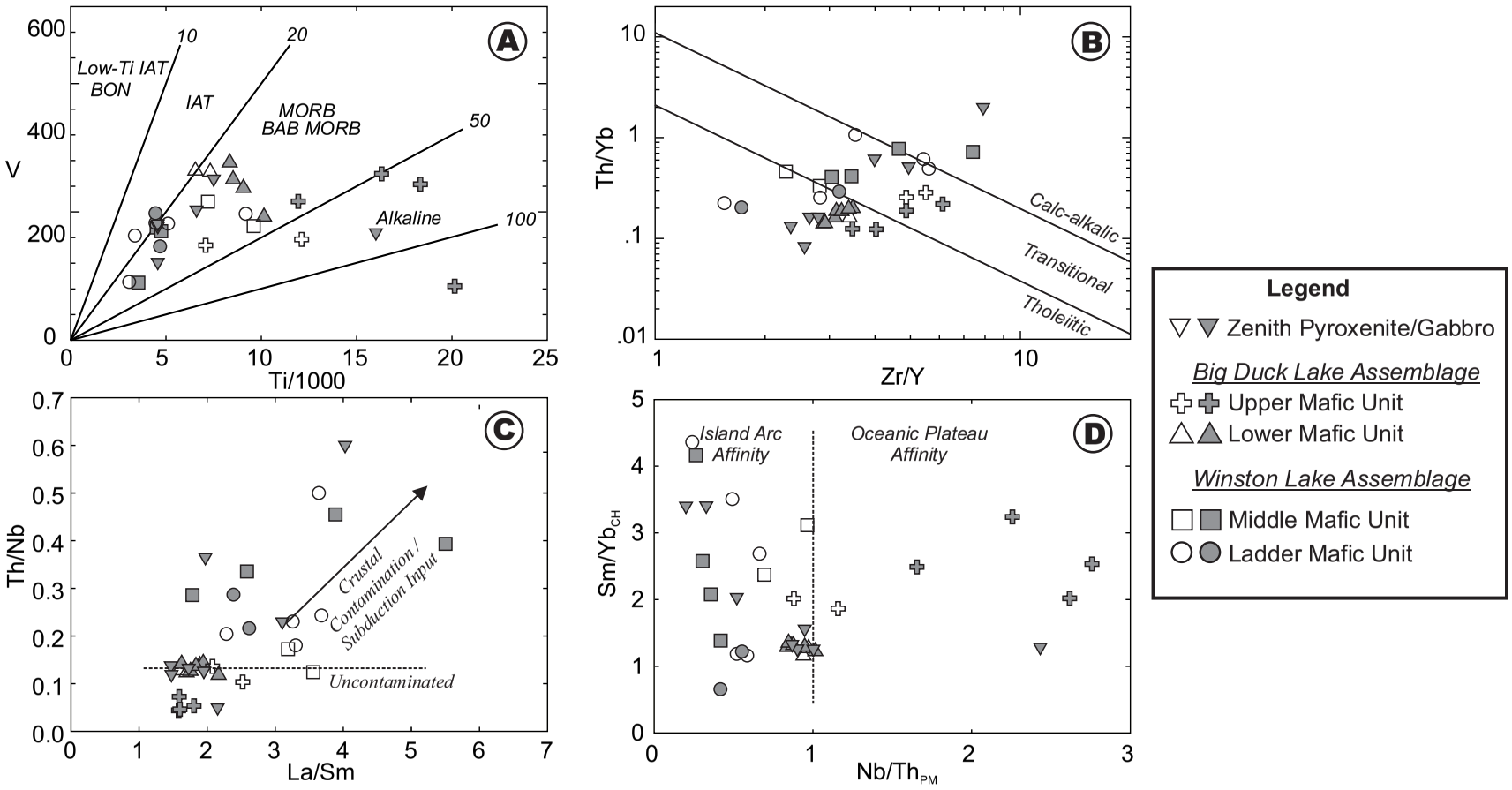

Figure 3.8 - Trace element binary diagrams showing the tectonic affinity and degree of crustal contamination for fresh (closed symbols) and altered (open symbols) basalts, as well as pyroxenite (open triangles) and gabbro (closed triangles) in the Winston Lake greenstone belt. In general, the Winston Lake assemblage (WLA) basalts have more arc-like affinities and have a higher degree of crustal contamination than the Big Duck Lake assemblage (BDLA) basalts. (A) Ti-V discrimination diagram (Shervais, 1982). (B) Zr/Y-Th/Yb discrimination diagram (Ross & Bedard, 2009). (C) La/Sm-Th/Nb diagram showing higher degree of crustal contamination or subduction input in WLA basalts (from Piercey et al. 2002). (D) Nb/Th_{PM}-Sm/Yb_{CH} diagram showing arc-like signatures independent of REE fractionation (modified from Polat, 2009).

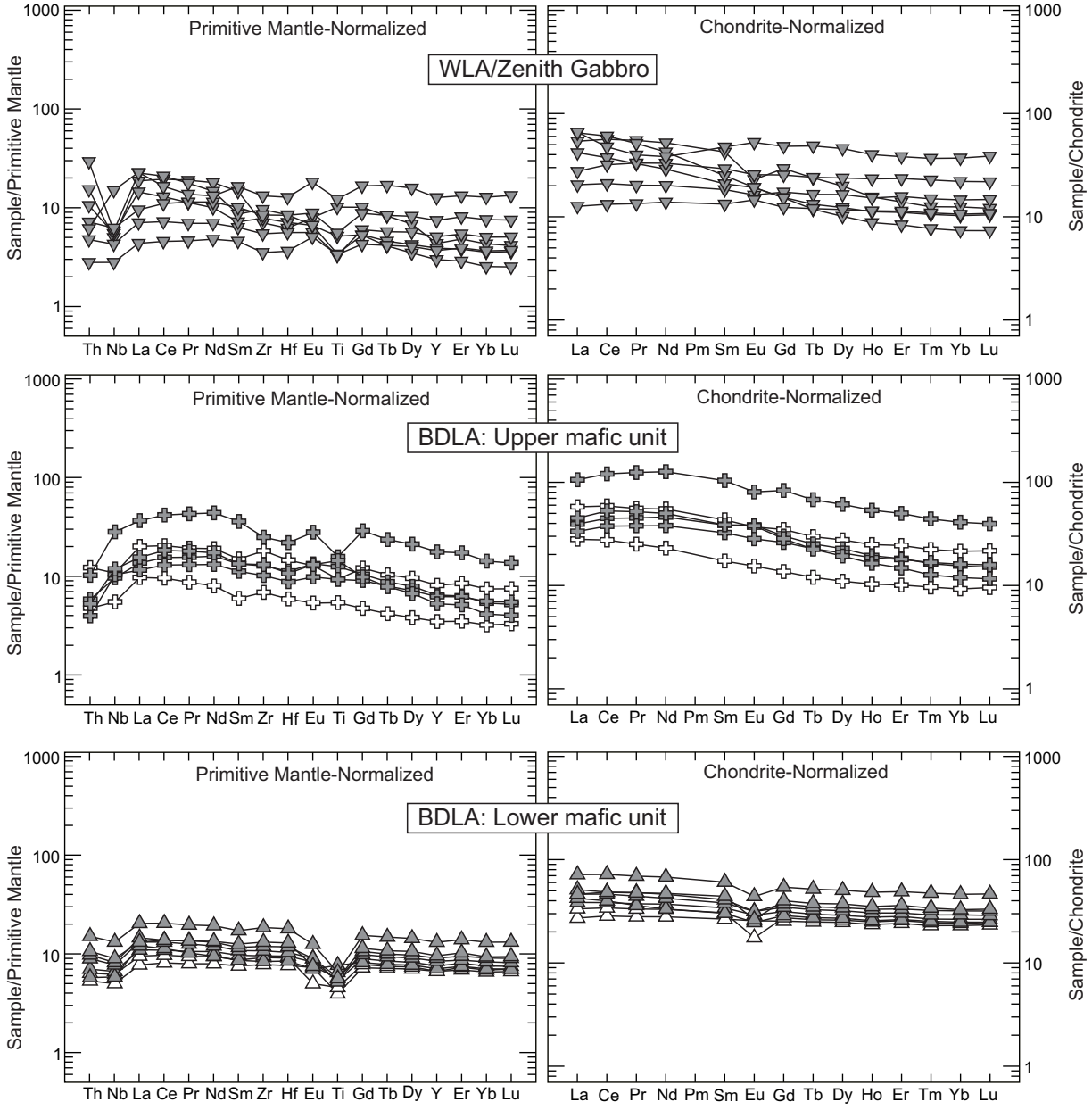

Figure 3.9 - Chondrite-nomalized rare earth element diagrams and primitive mantle-normalized trace element diagrams for mafic and gabbroic rocks from the Winston Lake greenstone belt. Normalizing values from Sun & McDonough (1989). Symbol legend is same as in Figure 3.8.

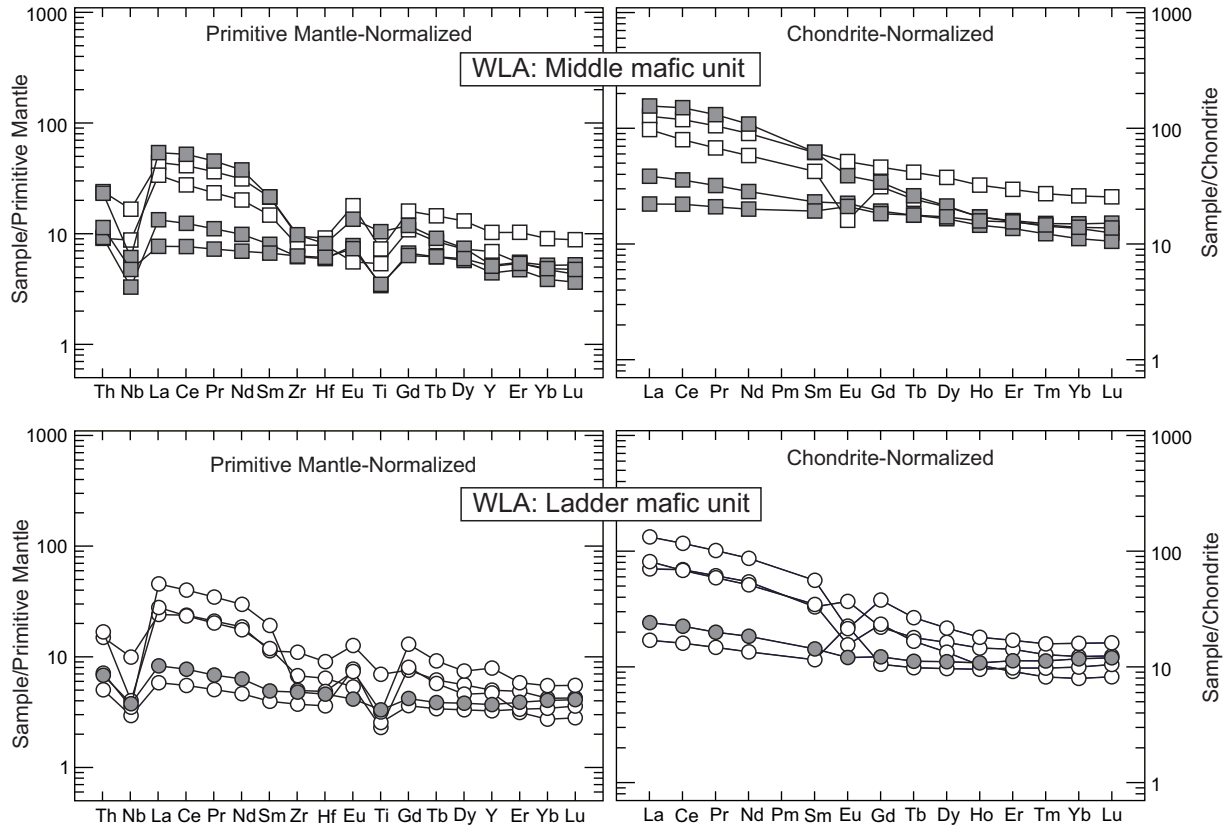

Figure 3.9 - Continued.

is significantly more enriched in the LREE relative to HREE, than flows from the lower mafic unit (**Figure 3.9**). Primitive mantle-normalized trace element diagrams show that the flows from the upper mafic unit are depleted in Th relative to Nb (**Figure 3.9**). Normalized Nb/Th ratios are higher in the upper mafic unit (normalized Nb/Th > 1) (**Figure 3.8D**). Both the upper and lower mafic units have low Th/Nb and La/Sm ratios (**Figure 3.8C**).

The Zenith gabbro and associated gabbroic sills in the WLA have similar geochemical patterns to flows of the WLA and BDLA. Thicker differentiated gabbro bodies that are interlayered with pyroxenite have trace element characteristics similar to flows of the BDLA. They are characterized by flat to gently sloping chondrite-normalized REE patterns and depleted Th relative to Nb on primitive mantle-normalized trace element spider diagrams (**Figure 3.9**). They have uncontaminated to weakly contaminated signatures (**Figure 3.8C**) and have tholeiitic to transitional magmatic affinities (**Figure 3.8B**). Thin, massive gabbroic sills that are interlayered with the WLA display trace element characteristics that are similar to flows of the "middle" and "ladder" mafic units of the WLA and have pronounced negative Nb and Ti anomalies on primitive mantle-normalized trace element diagrams (**Figure 3.9**).

3.6.4. Trace Element Geochemistry of Felsic Rocks

Supracrustal felsic lithofacies in the WLA occur in the "main" and "camp" felsic units. The BDLA contains very few felsic supracrustal units (Pye, 1964; Ritcey, 1992) and only geochemical data from a younger syndeformational quartz-feldspar porphyry in the vicinity of Big Duck Lake is presented.

Felsic volcanic rocks in the WLA have distinct bimodal Zr/Ti ratios (**Figures 3.7 and 3.10C**) that clearly distinguish the higher Zr/Ti (Zr/Ti ≈ 0.4 to 0.5) "main" felsic unit from the lower Zr/Ti (Zr/Ti ≈ 0.1 to 0.2) "camp" felsic unit. The higher Zr/Ti "main" felsic unit has a relatively larger range in Ti/Sc ratios (**Figure 3.10C**). Otherwise, the trace element contents of the main felsic and camp units are similar, and are characterized by flat to gently sloping REE patterns that are 100-500 times chondrite and have pronounced negative Eu anomalies (**Figure 3.11**). Primitive mantle-normalized trace element diagrams show strong negative Nb and Ti anomalies, with the "main" felsic unit having slight negative Zr anomalies (**Figure 3.11**). Both units are classified as FIIIb-type rhyolites based on their Zr/Y ratios versus Y abundance (Lesher et al., 1986) (**Figure 3.10A**) and their enriched, flat chondrite-normalized REE patterns (Hart et al., 2004) (**Figure 3.11**). The degree of alteration does not appear to correlate with any

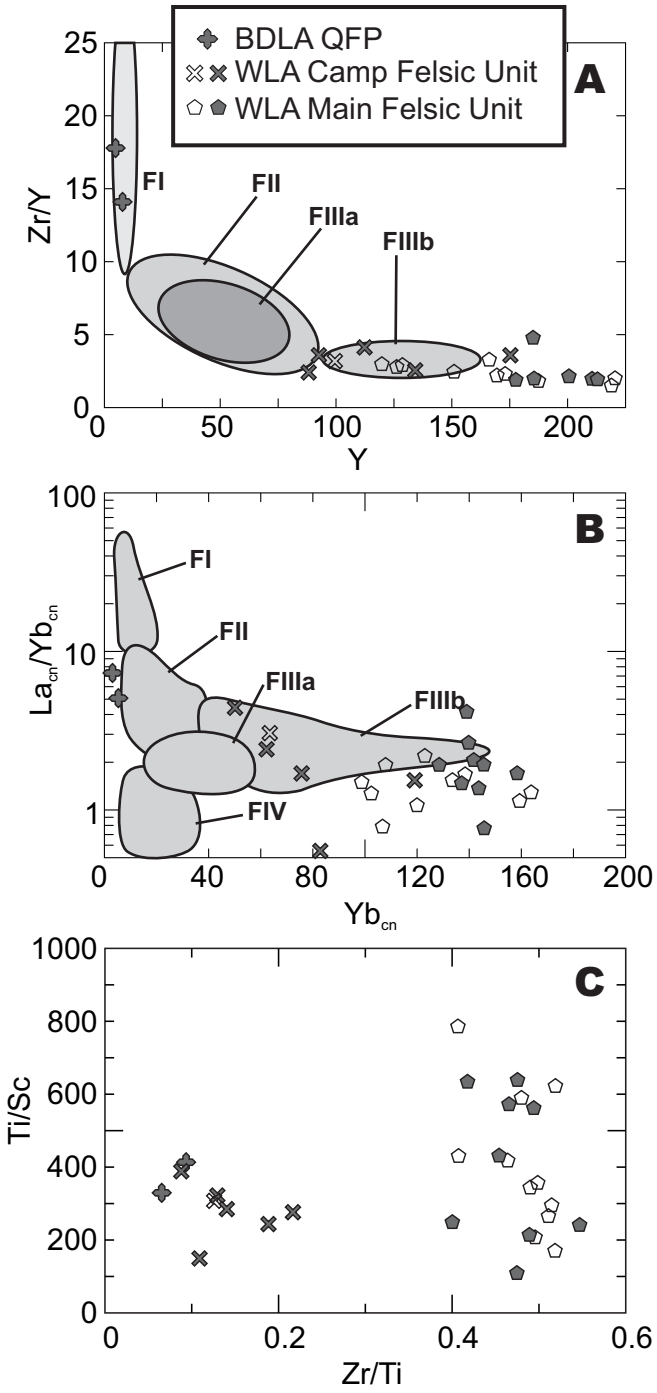

Figure 3.10 – Trace element discrimination diagrams for fresh (closed symbols) and altered (open symbols) felsic rocks from the Winston Lake greenstone belt. A) F-type discrimination diagram modified from Lesher et al. (1986) showing F-III type affinities in the Winston Lake assemblage and F-I type affinities for the quartz-feldspar porphyry (QFP) in the Big Duck Lake assemblage. B) F-Type discrimination diagram from Hart et al. (2004) showing F-III type volcanic rocks for the Winston Lake assemblage and F-I to F-II type affinity for the QFP in the Big Duck Lake assemblage. C) Ti/Sc versus Zr/Ti plot showing bimodal Zr/Ti distribution. The "main" felsic unit has a larger range in Ti/Sc ratios relative to the "camp" felsic unit.

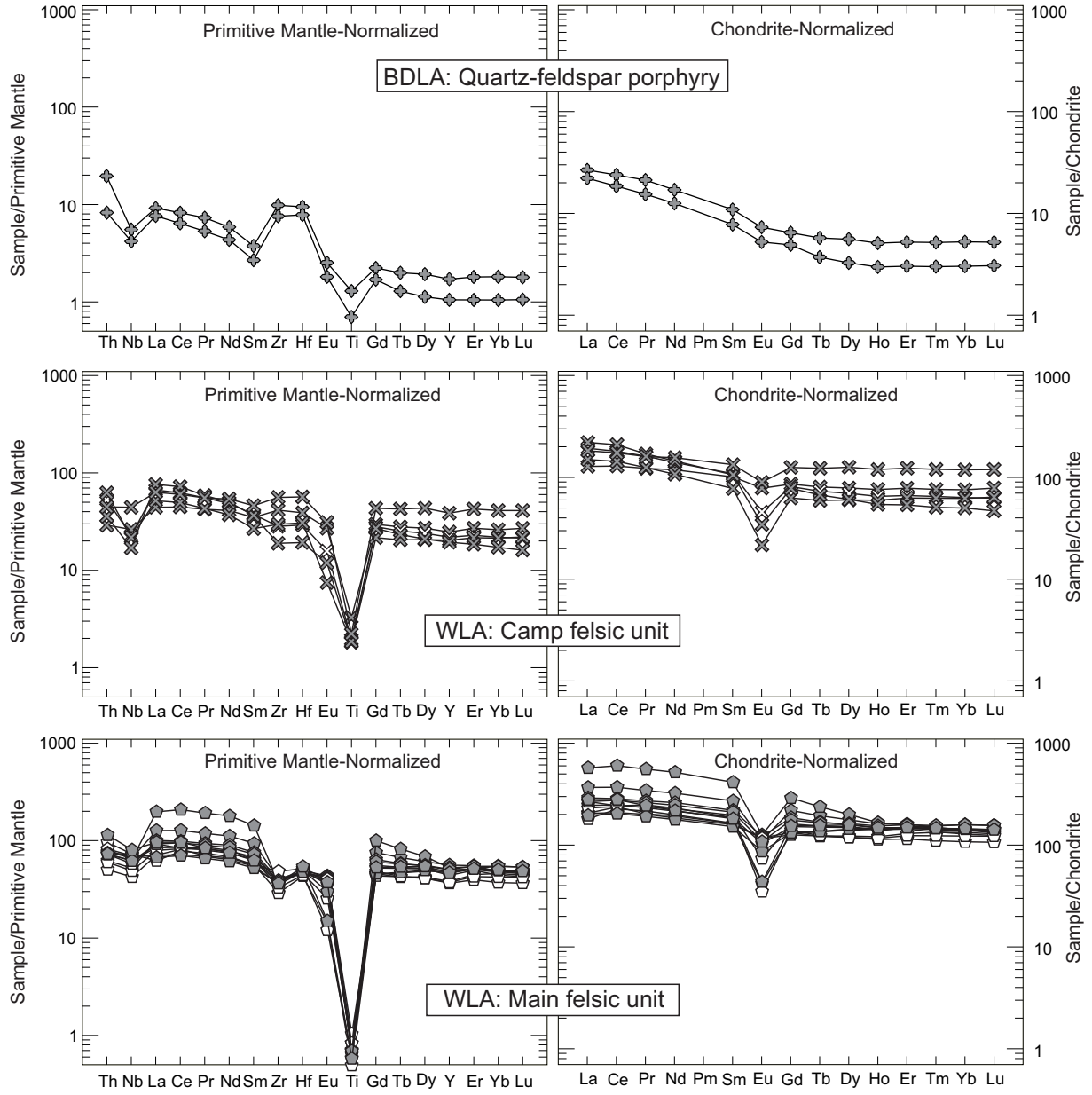

Figure 3.11 – Chondrite-normalized rare earth element diagrams and primitive mantle-normalized trace element diagrams for felsic rocks from the Winston Lake greenstone belt. Normalizing values from Sun & McDonough (1989). Symbol legend is same as that in Figure 3.10.

variability in the above geochemical signatures, but there is some degree of mobility of REE, Th, and Y as evidenced by binary diagrams versus Zr (**Figure 3.6**). On Zr versus Th binary diagrams (**Figure 3.6**), Th mobility is apparent in the "main" felsic unit. There is a moderate correlation of enriched Th with increasing alteration intensity and the strongest altered samples produced irregular REE and trace element patterns (Lodge and Chartrand, 2013) and were not included in petrogenetic interpretations.

The younger quartz-feldspar porphyry in the BDLA is different from the felsic rocks of the WLA. The chondrite-normalized REE are significantly less enriched with LREE up to 20 times chondrite and have smooth, moderately sloped patterns (**Figure 3.11**). The primitive mantle-normalized trace element spider diagrams show enrichment in Th and Zr relative to REE abundances, and negative Nb and Ti anomalies (**Figure 3.11**). The porphyry has FI- (Lesher et al., 1986) (**Figure 3.10A**) to FII-type (Hart et al., 2004) (**Figure 3.10B**) felsic affinity.

3.6.4. Nd-Isotopic Geochemistry

Only least altered samples were selected for isotopic analysis as outlined in Section 5.2. Their chondrite-normalized REE plots are smooth and do not have any irregular anomalies. Due to the demonstrated mobility of LREE in the Winston Lake VMS camp (Campbell et al., 1984; Gorton and Schandl, 1995), these precautions were necessary to ensure the reliability of the Nd isotopic data.

Neodymium isotopic signatures from the mafic and felsic rocks are similar and they have similar overlapping ranges of low positive juvenile εNd values (+0.2 to +2.8) (**Figure 3.12**) that are consistent with values expected for the depleted mantle at 2720 Ma (Goldstein et al., 1984).

3.7. Discussion

Previous terrane-scale geochemical studies have speculated that the spatial association of arc-like volcanic lithofacies in the Winston Lake VMS camp and transitional to tholeiitic basalts elsewhere in the greenstone belt were emplaced during arc rifting and opening of a back-arc basin (Kerrich et al., 2008; Polat, 2009). However, in the absence of geochronological and lithological constraints, these interpretations were largely based on geochemistry. Results of the geological, geochemical and geochronological studies presented herein, where geochemistry and geochronology are tied to detailed stratigraphy, support the earlier interpretation of a

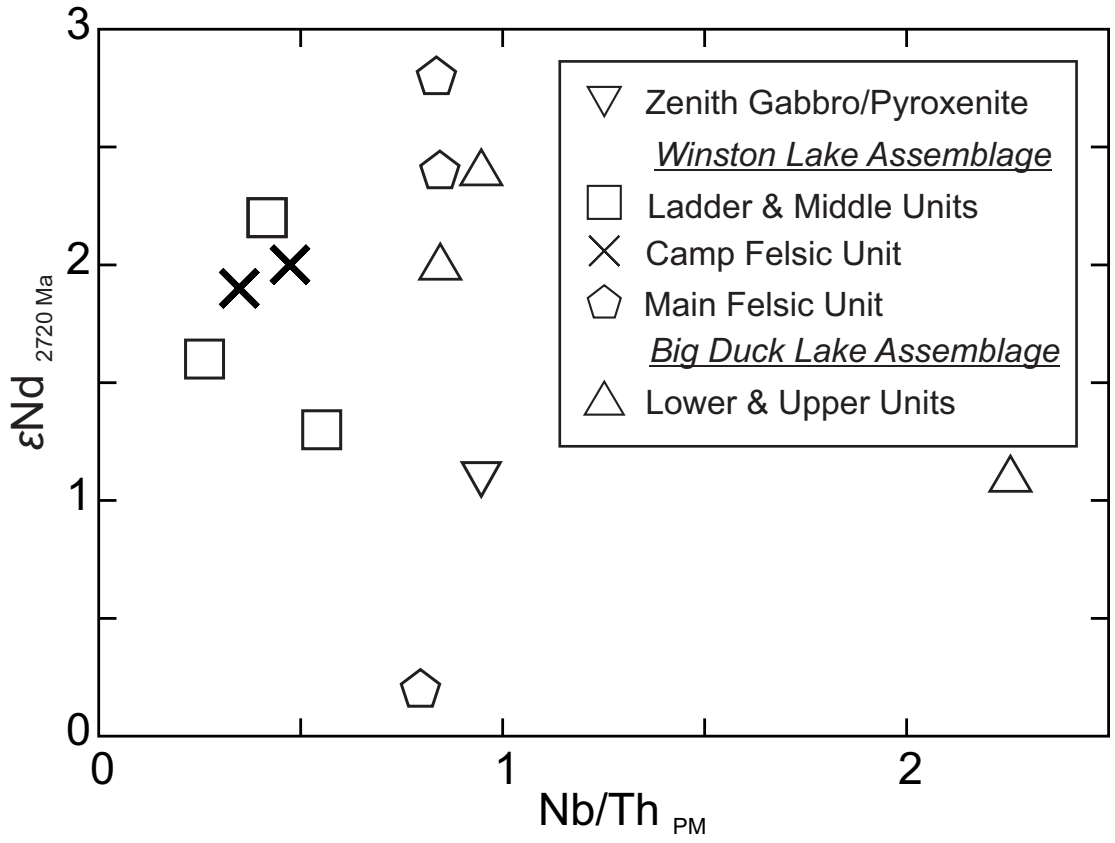

Figure 3.12 – Plot of $\varepsilon Nd_{2720\ Ma}$ versus primitive mantle-normalized Nb/Th ratio for mafic and felsic rocks from the Winston Lake greenstone belt. In general, low positive εNd values for all rock types indicate a juvenile petrogenetic source.

geodynamic setting characterized by arc rifting and back-arc development, and provide a more detailed view of the magmatic and metallogenic evolution of the belt.

In the discussion which follows, it is assumed that the strata of the Winston Lake greenstone belt represent a relatively intact homoclinal sequence. This assumption is based on the overall lack of repetition of lithofacies or geochemical patterns and consistent eastward younging directions in both mafic flow and felsic volcaniclastics in the WLA and to north younging directions in the BDLA. This assumption is consistent with the interpretations of previous mapping in the Winston Lake greenstone belt (Pye, 1964; Ritcey, 1992; Osterberg, 1993).

3.7.1. Chemostratigraphy and Petrogenesis of the Winston Lake Greenstone Belt

The systematic stratigraphic variation in the trace element geochemistry of the Winston Lake greenstone belt constrains the petrogenesis of its volcanic and intrusive facies. The general arrangement of strata and variation in trace element characteristics are summarized in **Figure 3.13**.

The dominance of FIII-type rhyolitic (**Figure 3.10A and 3.10B**) volcaniclastics and flow lithofacies within the camp and main rhyolitic units is consistent with a high temperature, low pressure petrogenesis through partial melting at shallow crustal levels such that HREE- and HFSE- bearing minerals such as garnet and hornblende are stable (Hart et al., 2004). Such conditions are favoured in thinner, rifted crust where deep structures that formed during extension allowed ascent of mafic magmas into more shallower-levels of the crust to induce partial melting and the formation of FII- and FIII-type magmas (Hart et al., 2004). However, there are subtle but important variations in the normalized REE and HFSE values of felsic lithofacies within the WLA that suggest slightly different petrogenetic histories. The felsic lithofacies in the lower volcaniclastic succession and the “camp” felsic unit have slightly lower normalized abundances of REE and HFSE (**Figure 3.11**) and have distinctly lower Zr/Ti values than the “main” felsic unit regardless of the degree of alteration (**Figure 3.10C**). These differences are most likely attributed to primary variations in the temperatures of partial melting. Elevated REE and HFSE in felsic rocks have been attributed to higher temperature melting in the source region (Creaser and White, 1991; Bea, 1996; Hanchar and Watson, 2003; Piercey et al., 2008). Higher temperature melting resulted in more effective incorporation of REE- and HFSE-bearing minerals, such as zircon. Alternatively, the differences in Zr/Ti ratios may be attributed

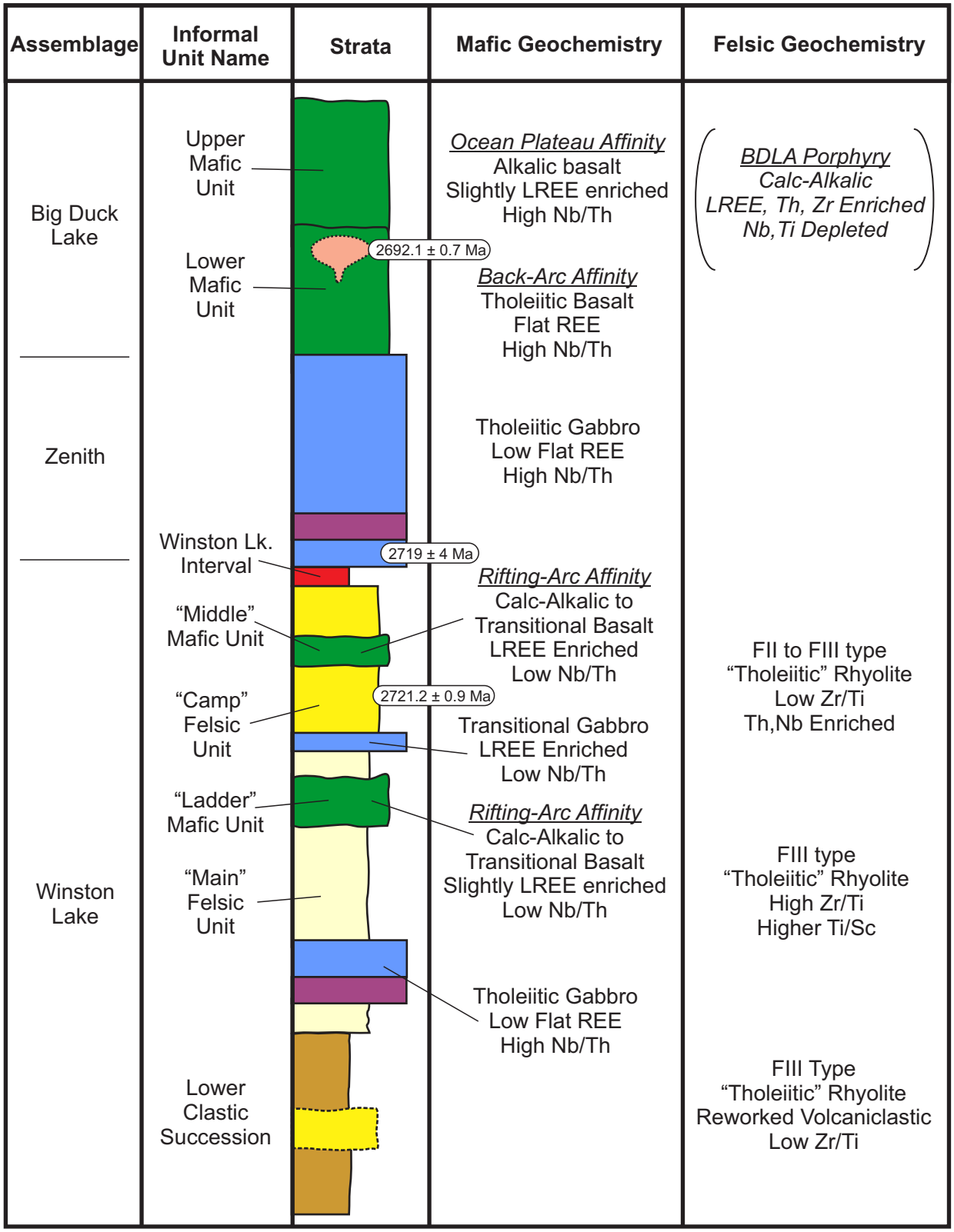

Figure 3.13 – Summary of geochemical characteristics and U-Pb geochronology of the Winston Lake greenstone belt from this study. Note stratigraphic thickness of units is not to scale but sequence of strata is representative.

to fractional crystallization of a single parental magma resulting in HFSE enrichment. However, fractional crystallization would result in an enrichment of Zr relative to Ti over time (e.g., Barrett and MacLean, 1994), which is the opposite trend observed within the felsic rocks of the WLA. The considerable range in Ti/Sc ratios for the "camp" (Ti/Sc ≈ 150-400) and "main" felsic units may be explained by variable interaction between "crustal" (high Ti/Sc) and "mantle" (low Ti/Sc) magmas indicating that there was some amount of mixing between mafic, mantle-derived magmas emplaced during rifting and crust-derived felsic magmas (Piercey et al., 2008). This interpretation is supported by the interlayering of mafic and felsic units in the WLA (**Figures 3.3 & 3.13**), and the co-magmatic relationship of the WLA felsic rocks and the Zenith gabbro, as determined by U-Pb geochronology (**Figure 3.5**).

Mafic lithofacies also have stratigraphic variations in their trace element geochemistry. The oldest mafic flows from the WLA are calc-alkalic to transitional and have pronounced normalized negative Nb and Ti anomalies. LREE values are also relatively enriched (up to 100 times chondrite) and there is evidence for some amount of "crustal" contamination based on enriched LREE and Th/Nb ratios (Piercey et al., 2002). The overall low normalized abundance of Th relative to LREE in the mafic volcanic lithofacies indicate that they are not subduction-generated magmas, which are typically characterized by a high absolute abundance of Th (e.g., Hawkesworth et al., 1997; Polat and Kerrich, 2006). These geochemical patterns are consistent with contemporaneous, bimodal mafic and felsic magmatism in a rifted, back-arc setting that has trace element signatures from the depleted mantle in the back-arc rift and the subduction-enriched mantle below a juvenile arc (Pearce and Stern, 2006; Polat, 2009). Thinner, synvolcanic gabbroic sills within the WLA are the remnants of the subvolcanic intrusive architecture.

The geochemical signature of the BDLA is notably more tholeiitic to transitional than the mafic lithofacies in the WLA. Geochemical signatures of crustal contamination are absent (**Figure 3.8D**) and normalized trace element plots are weakly to moderately depleted in Th relative to Nb in the upper mafic unit (**Figure 3.9**), atypical of supra-subduction environments. The subtle geochemical differences between the lower and upper mafic units of the BDLA suggest the presence of an enriched-mantle plume. The lower mafic unit has flat to slightly dipping normalized REE patterns with depleted Nb and Ti, characteristic of mature back-arc magmas (e.g., Pearce and Stern, 2006; Piercey, 2007) with minimal enrichment from subduction (Martinez and Taylor, 2006). The upper mafic unit has Ti/V ratios and enrichment in K_2O and

P_2O_5 (Lodge and Chartrand, 2013) that suggest an alkalic affinity (**Figure 3.8A**), which shows more LREE-enrichment on normalized trace element diagrams. The upper mafic unit is notably more depleted in Th relative to Nb on normalized trace element diagrams, and the Nb/Th ratio is generally greater than in the lower mafic unit. These enriched trace element patterns, without negative Nb and Ti anomalies or Th enrichment are characteristic of an oceanic plateau or ocean island basalt (OIB) geodynamic environment (Sun and McDonough, 1989; Piercey, 2007; Polat, 2009).

The basaltic rocks of the WLA and BDLA have similar overlapping εNd values despite having significantly different primitive mantle-normalized Nb/Th ratios (**Figure 3.12)** suggesting an equally juvenile petrogenesis for the calc-alkalic island arc basaltic rocks and the tholeiitic ocean plateau basaltic rocks (**Figure 3.8A-D**). Crustal contamination as indicated by increased La/Sm and Th/Nb ratios (**Figure 3.8C**) must have been by "crust" that was of similar age to the mafic lithofacies in order to preserve a juvenile εNd signature. Older xenocrystic detrital zircons provide some evidence for the presence of older crustal material (**Figure 3.4**), but this older crustal signature is not obvious in the Nd-isotopic data. The range of εNd values of the Winston Lake greenstone belt is similar to the εNd values reported for assemblages of similar age in the Abitibi subprovince (Vervoort et al., 1994; Ketchum et al., 2008) indicating widespread production of juvenile crust at this time.

The younger, quartz-feldspar porphyry that intrudes the central portion of the BDLA is calc-alkalic in composition and was emplaced during deformation (Ritcey, 1992) accompanying terrane accretion to the Superior Province. Its FI-type affinity (**Figure 3.10A**) suggest that its source was deeper in the crust (Hart et al., 2004) than the felsic volcanics of the WLA, and it may have been formed by partial melting of a mafic source at high pressures (Lesher et al., 1986). On normalized trace element plots, the quartz-feldspar porphyry displays moderately enriched LREE (~10x), positive Th and Zr anomalies, and negative Nb and Ti anomalies (**Figure 3.11**). The geochemical patterns of this porphyry are very similar to other syntectonic plutons in the Abitibi subprovince (e.g., Beakhouse, 2011).

3.7.2. Geodynamic Evolution of the Winston Lake Greenstone Belt

The lithofacies and chemostratigraphic variations in the trace and REE geochemistry of the Winston Lake greenstone belt are consistent with the evolution of a rifted arc to back-arc basin model and a variable mingling of subduction-derived (arc), crustal-derived felsic and rift-

derived (back-arc) magmas (e.g., Martinez and Taylor, 2006; Pearce and Stern, 2006). The youngest volcanic strata in the belt have an enriched mantle plume petrogenetic source. Arc-like geochemical signatures in the oldest supracrustal rocks and pervasive juvenile εNd values throughout the strata suggest that the original volcanic edifice was a juvenile arc formed in a suprasubduction setting. There is some evidence for the presence of older 2780-2750 Ma crust based on the older detrital zircons, but low positive, juvenile εNd values indicate that it was not a significant source of crustal contamination during petrogenesis. A schematic model for the geodynamic evolution of the Winston Lake greenstone belt is illustrated in **Figure 3.14**.

Siliciclastic and felsic volcaniclastic lithofacies of the lower clastic succession have FIII-type geochemistry (**Figure 3.4D**) and a single ca. 2720 Ma source of detritus. This is consistent with a primary derivation via explosive pyroclastic eruptions; however, poor preservation due to deformation and metamorphism inhibit distinguishing between primary pyroclastic deposition and a syn-eruptive origin through resedimentation of unconsolidated primary pyroclastic deposits. Regardless, these felsic volcaniclastic rocks and/or their sedimentary equivalents were likely formed and deposited during the early stages of arc rifting (**Figure 3.14A**). The Zr/Ti ratios of these rocks are lower than the overlying "main" felsic unit suggesting they are from the same, relatively low temperature parent magma or magma formed by similar petrogenetic processes to that of the "camp" felsic unit. The "main" felsic unit is the thickest and most massive of the felsic units in the WLA. Eruption and emplacement of the "ladder" mafic unit interrupted felsic volcanism associated with the "main" felsic unit since it both overlies and is overlain by the felsic unit (Osterberg, 1993; Lodge, 2012b). The occurrence of mafic volcanism associated with the main felsic volcanism suggests higher heat flow and the generation of higher temperature FIII felsic magmas characterized by high Zr/Ti ratios, perhaps related to more extensive underplating of the crust by mantle derived melts during rifting (**Figure 3.14B**). The deposition of the volcaniclastic-dominated "camp" felsic unit and massive "middle" mafic unit are some of the last supracrustal units in the WLA prior to the deposition of the rift-dominated lower mafic unit of the BDLA (**Figure 3.14C**).

Continued rifting and a brief hiatus in volcanism resulted in the development of a high temperature convective hydrothermal system that was likely driven by the heat generated by unidentified subvolcanic intrusions feeding the felsic and mafic volcanic rocks of the WLA, or by a high geothermal gradient resulting from righting and proximal mafic and felsic volcanism.

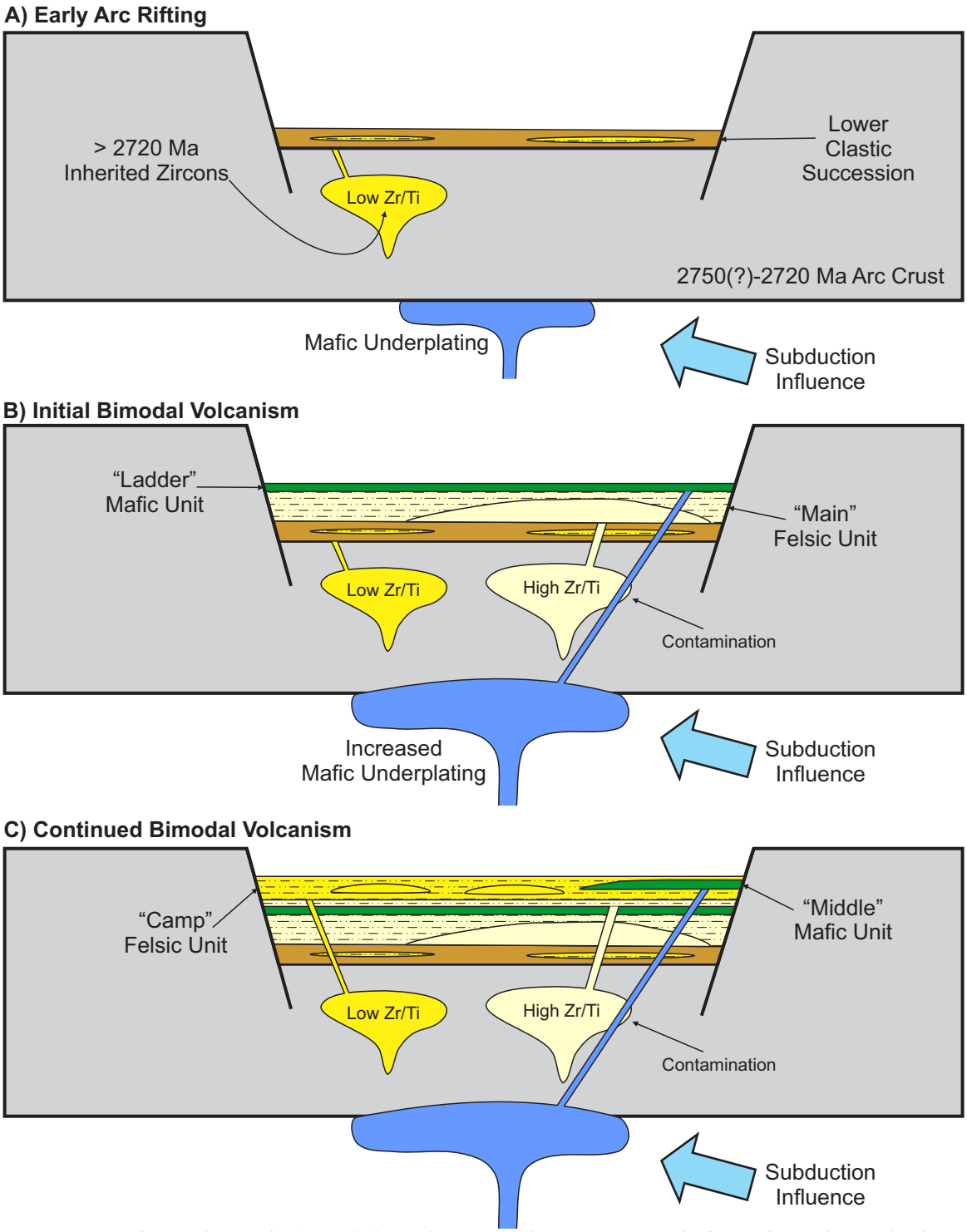

Figure 3.14 – Schematic evolution of the Winston Lake greenstone belt. Color scheme is the same as Figure 1. A) Initial rifting depositing felsic-dominated volcaniclastic and siliciclastic rocks. B) Increased mafic magma underplating increases the temperature of melting for the genesis of the "main" felsic unit. Emplacement of the "ladder" mafic unit. C) Continued bimodal volcanism depositing volcaniclastic-dominated "camp" felsic unit and "middle" mafic unit.
Continued:

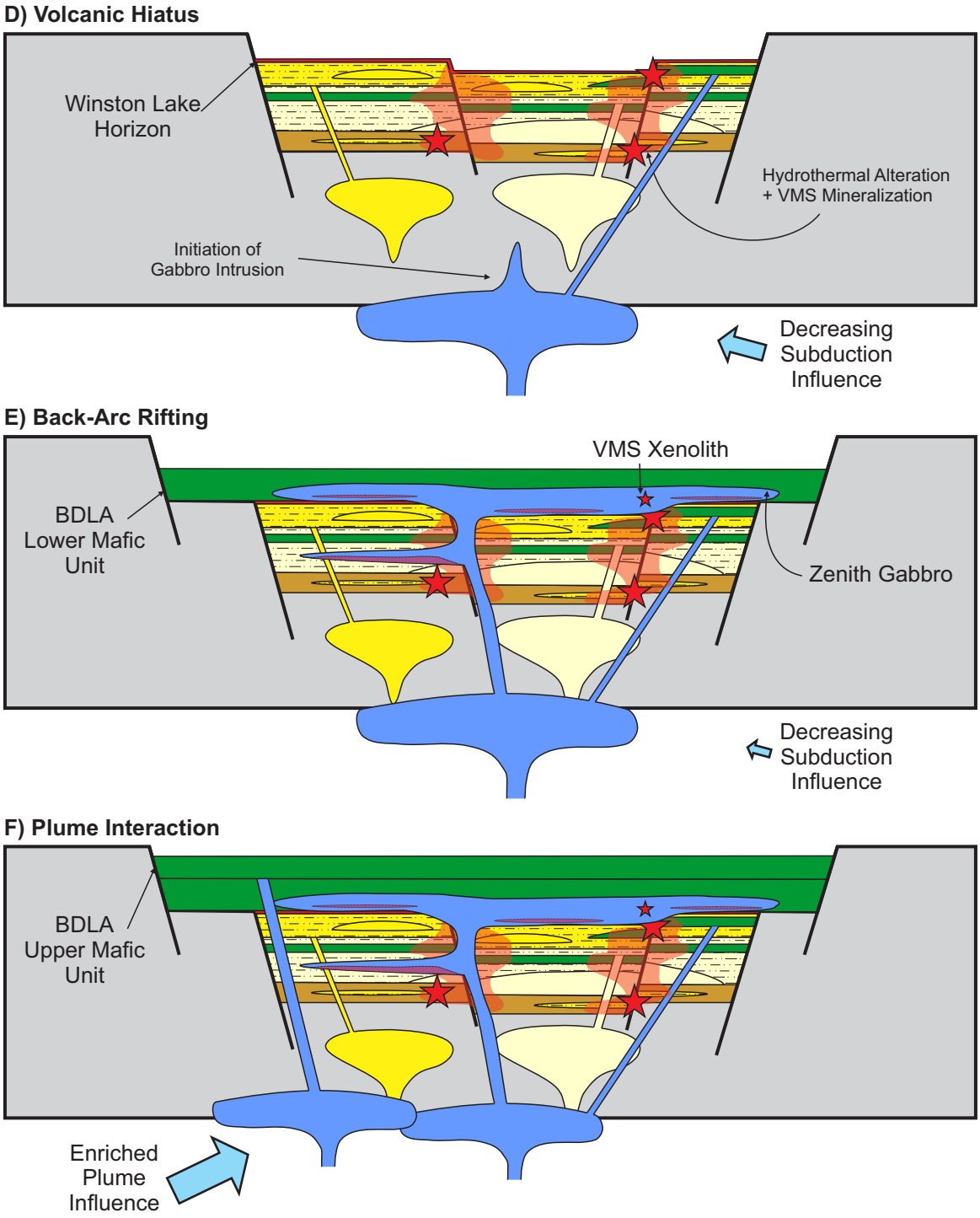

Figure 3.14 – Continued:
D) Hiatus in the volcanic activity developed the hydrothermal system and formation of VMS deposits. Mixed rift-like sedimentation and exhalative Winston Lake horizon were deposited. E) Continued back-arc rifting and emplacement of tholeiitic lower mafic unit of the BDLA and Zenith gabbro. F) Eruption and emplacement of the plume-generated upper mafic unit of the BDLA prior to terrane accretion and deformation.

VMS deposition occurred during a relative hiatus in voluminous eruptive episodes and was associated with the deposition of felsic volcaniclastic units (Severin et al., 1991; Osterberg, 1993). Exhalative activity, rift sedimentation, and potentially violent pyroclastic eruptions could have produced the fine, siliceous volcaniclastic lithofacies of the Winston Lake interval. "Intermediate" volcaniclastic rocks along strike from the Winston Lake deposits have a chondrite-normalized REE pattern that is consistent with a mixed mafic-felsic source (see patterns in **Figure 3.9 and 3.11**). This supports field and petrographic observations that suggests that the intermediate volcaniclastic rocks are bimodal as they are characterized by alternating quartzofeldspathic and amphibole-rich layers representative of a resedimented detritus derived from a bimodal volcanic provenance. Calc-alkalic mafic flows associated with the Winston Lake interval (Osterberg, 1993) are the final products of the WLA (**Figure 3.14D**).

The deposition of the lower mafic unit of the BDLA and emplacement of the Zenith gabbro represent a change from calc-alkalic, subduction-influenced petrogenesis to a tholeiitic rift-dominated petrogenesis. The lower mafic unit of the BDLA is dominated by massive lithofacies and represents a rapidly extruded and voluminous unit (e.g., Gibson et al., 1999). The differentiated Zenith gabbro, sharing a trace element geochemistry that is similar to the lower mafic unit of the BDLA, is likely a conduit for the magmas. During emplacement, the Zenith Gabbro entrained xenoliths of the felsic lithofacies, the Winston Lake interval, and the Winston Lake VMS deposit (Osterberg, 1993) (**Figure 3.14E**). While localized epidote-quartz alteration is present in the flows of the lower mafic unit, a vigorous, widespread hydrothermal system did not develop and it is unknown if there is significant metal depletion from these zones (Ritcey, 1992). The OIB-like geochemistry of the upper mafic unit indicates a change to plume-generated, alkalic volcanism. The relatively sharp contact between the lower and upper mafic units suggests that the upper mafic unit represents a separate volcanic edifice, possibly an ocean plateau (**Figure 3.14F**). The quartz-feldspar porphyry was emplaced during subsequent D_1-D_2 deformational events.

3.7.3. Implications for the Emplacement of VMS

Lithological relationships in combination with high-precision U-Pb ages constrain the timing of VMS formation in the WLA. The presence of hydrothermal alteration throughout most of the mafic and felsic strata and the location of VMS mineralization at multiple stratigraphic positions indicate that the VMS hydrothermal system spanned much of the WLA, and that the

largest deposit formed during waning WLA volcanism. Significantly, the high-precision U-Pb zircon ages are all *circa* 2720 Ma indicating that the volcanic units of the WLA and Zenith gabbro are essentially co-magmatic. Therefore, the formation of the VMS hydrothermal system, alteration of volcanic lithofacies, and mobilization/concentration of base metals is bracketed by the deposition of the "main" felsic unit and the emplacement of the Zenith gabbro: 2721.2 ± 0.9 Ma and 2719 ± 4 Ma, respectively.

The absence of a significant VMS prospect in the younger BDLA can be attributed to several volcanological factors. The dominance of massive mafic flows and synvolcanic gabbroic sills in the BDLA with minor pillowed flows and sparse inter-flow volcaniclastic deposits suggest that mafic lithofacies were deposited rapidly at a high effusive rate (e.g., Griffiths and Fink, 1992; Gibson et al., 1999). Secondly, supracrustal felsic lithofacies are very rare (Ritcey, 1992) suggesting that the extensional tectonic setting and/or presence of a heat source required to melt basaltic crust was too short-lived to generate bimodal volcanic suites (e.g., Franklin et al., 2005). Thirdly, evidence for prolonged hiatus in volcanic activity is also largely absent, which is important for development of stable high temperature hydrothermal systems as well as seafloor or near sea floor VMS deposits (e.g., Peter and Goodfellow, 1996; Franklin et al., 2005; Thurston et al., 2008).

The Zn-rich ores of the Winston Lake VMS camp suggest they are a product of relatively cool hydrothermal system that developed within a rifted arc or back arc. The dominance of Zn relative to Cu in the Zenith, Winston Lake, and Pick Lake ores (Zn:Cu = 15-30:1; unpublished Inmet Mining Corp. data) could indicate that the discharging hydrothermal fluids were relatively lower temperature (≤ 300 °C) and were unable to precipitate significant amounts of Cu (Hannington et al., 2005). Adiabatic cooling of an ascending, boiling, high temperature hydrothermal fluid that was discharging into a shallow water environment (low hydrostatic pressure) could result in preferential precipitation of Cu at depth and more Zn-rich fluid discharge at the seafloor (Franklin et al., 2005). A shallower marine depositional setting for VMS formation, although not unequivocal, is evident from the presence of reworked, cross-bedded, and ripple-laminated volcaniclastic rocks in the WLA along strike from the VMS deposits.

Alternatively, the lower Cu:Zn ratios could be explained by development of the hydrothermal system in felsic-dominated strata. The solubility and availability of base metals in

hydrothermal systems is dependent on several factors including the temperature and pH of the hydrothermal fluid, and the composition of the footwall rocks (Franklin et al., 2005). Evolved sea water fluids in VMS hydrothermal systems that developed in equilibrium with felsic lithofacies in the reservoir zone obtain a sufficiently low pH at lower temperatures and can solubilize zinc, but not copper (James et al., 2003) and this is consistent with the Zn-rich nature of the ores and a felsic-dominated WLA succession. However, most Archean VMS systems have mafic-dominated high-temperature reaction zones with extensively developed epidote-quartz and epidosite alteration assemblages characterized by base metal depletion and modest gains in Si, Ca, and Na (Galley, 1993; Franklin et al., 2005; Galley et al., 2007). These lower semi-conformable alteration zones or high-temperature reaction zones have not been recognized in the Winston Lake greenstone belt and the lowermost strata exposed in the WLA are characterized by Na and Ca depletion (Thomas, 1991; Osterberg, 1993). The juvenile isotopic signature of the rocks from the Winston Lake greenstone belt suggests that the deepest parts of the strata were most likely mafic-dominated but these rocks are not exposed, have been structurally displaced, or have been assimilated by the felsic plutons west of the greenstone belt. In addition, VMS deposits that have developed with a felsic-dominated reservoir zone usually have higher Pb contents (e.g., Bathurst Mining Camp; Franklin et al., 2005; Goodfellow, 2007).

3.7.4. Implications for the Assembly of the Wawa-Abitibi Terrane and Superior Province

The U-Pb geochronology refines the regional correlation of magmatic and deformation events within the Wawa subprovince as summarized in **Figure 3.15**. The tectonic and metallogenic significance of the *circa* 2720 Ma period of greenstone belt construction along the northern margin of the Wawa subprovince has been recognized (e.g., Corfu and Stott, 1998; Zaleski et al., 1999); however, only a single age of 2723 ± 3 Ma (Davis et al., 1994) linked the Winston Lake greenstone belt to the other *circa* 2720 Ma assemblages. In addition to establishing that the majority of the Winston Lake greenstone belt is also *circa* 2720 Ma, we have established an age for the emplacement of the syn-deformation quartz-feldspar porphyry in the BDLA. The age of this intrusion, *circa* 2690 Ma, is similar to the age of syn-deformation plutons in the Shebandowan, Vermilion, and Manitouwadge greenstone belts (Corfu and Stott, 1998; Zaleski et al., 1999; Lodge et al., 2013). These intrusions and the deformation events they are temporally associated with are important targets for gold mineralization in the Wawa subprovince (Stott and Schnieders, 1983; MacDonald, 2003; Jobin-Bevans et al., 2006; Leonard

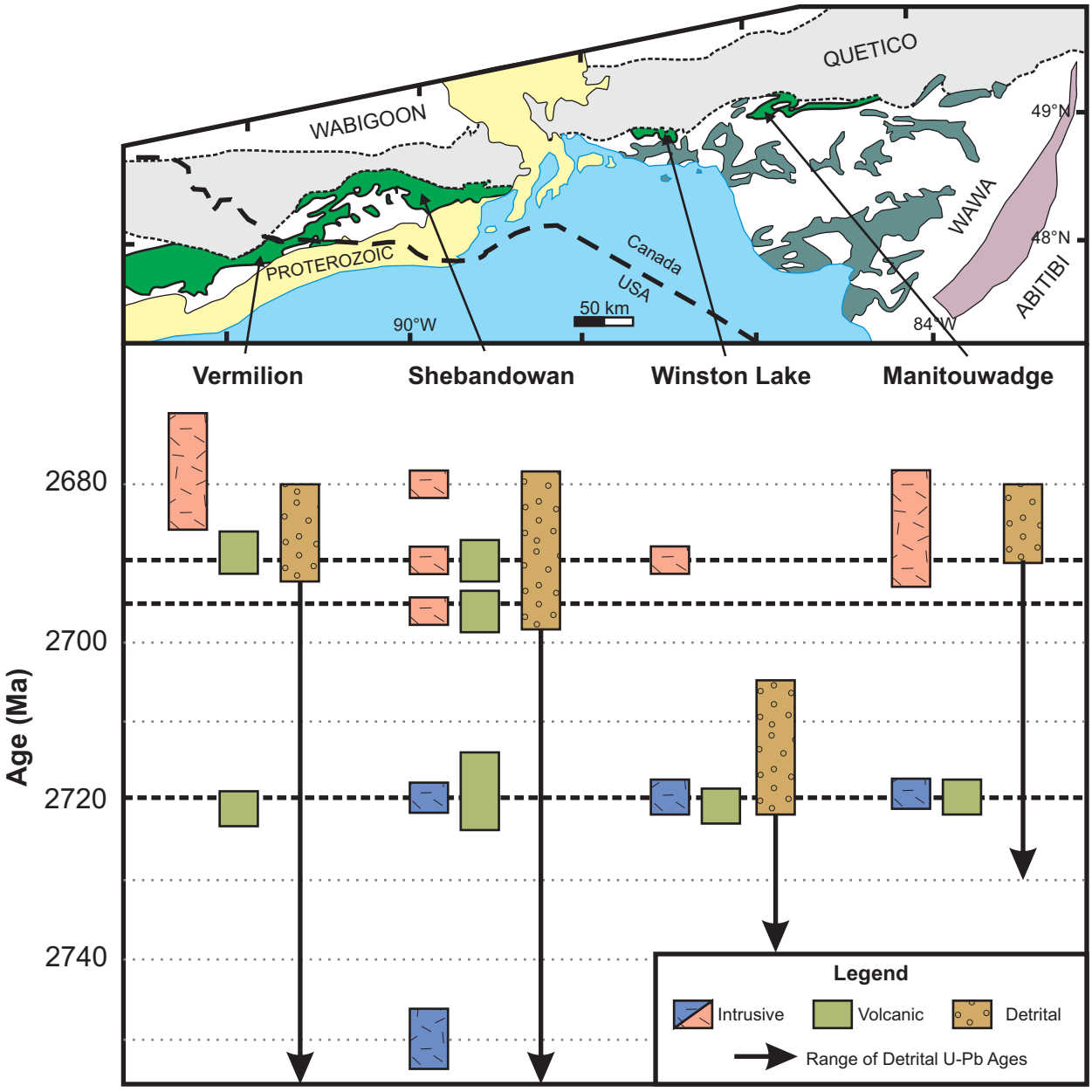

Figure 3.15 - Summary of U-Pb geochronology in the 2720 Ma greenstone belts of the northern Wawa Subprovince. Dashed lines represent major volcanic episodes, of which the 2720 Ma volcanic episode comprises the majority of the exposed greenstone belt lithofacies. Vermilion geochronology data compiled from Peterson et al. (2001) and Lodge et al. (2013). Shebandowan geochronology compiled from Corfu and Stott (1986, 1998), Hart (2007), and Lodge (2012). Manitouwadge geochronology compiled from Zaleski and Peterson (1999).

and Ilieva, 2008). The *circa* 2690 Ma deformation and magmatic event is consistent across the northern margin of the Wawa-Abitibi terrane and extends from the Vermilion greenstone belt at the western edge of the Wawa subprovince to the Chibougamau area in the northeastern Abitibi subprovince (~1500 km) and is associated with syn-deformation Timiskaming-type assemblages (Lodge et al., 2013). This event is interpreted to be a product of the accretion of the Wawa-Abitibi terrane onto the Superior Province (Corfu and Stott, 1998; Zaleski et al., 1999; Lodge et al., 2013).

3.8. Summary and Conclusions

1) The relatively intact strata of the Winston Lake greenstone belt allowed for a near complete sampling of major belt-scale lithostratigraphic units. Field observations of the mafic flows and volcaniclastic rocks in the belt indicate that strata are consistently younging to the north in the BDLA and to the northeast in the WLA. The stratigraphic units are laterally extensive and there is little evidence for significant fault or fold repetition of units at a regional-scale. High-precision U-Pb geochronology has shown that the dated pre-deformation strata has an age of *circa* 2720 Ma.

2) The geochemical results of this study have confirmed a juvenile rifted arc to back-arc geodynamic setting for the WLA and contained VMS deposits (Kerrich et al., 2008; Polat, 2009). The oldest mafic lithofacies in the WLA have transitional to calc-alkalic magmatic affinities and have back-arc to arc-like trace element characteristics. The younger mafic lithofacies of the lower mafic unit in the BDLA are tholeiitic and are more characteristic of a mature back-arc setting. Felsic lithofacies are FIII-type magmas, which are indicative of an origin through high temperature, low pressure partial melting of arc crust. The “camp” and “main” felsic units have distinctly different Zr/Ti ratios that were most likely caused by differences in temperature during melt formation. Alternatively, the differences in Zr/Ti ratio may be due to fractional crystallization but the expected temporal trend for fractionating Zr/Ti ratio is opposite to that observed. A large range of Ti/Sc ratios, overlapping U-Pb ages, and juvenile εNd values for both mafic and felsic lithofacies all indicate co-magmatic bimodal volcanism and the same parentage.

3) VMS mineralization is associated with the early stages of rifting (WLA) before the back-arc matured followed by the rapid emplacement of basalts and thick gabbroic sequences (BDLA). The timing of development and duration of the VMS-producing hydrothermal system in the

WLA is tightly constrained by U-Pb geochronology and lithostratigraphic relationships. The VMS system developed during the deposition of the footwall lithofacies in the WLA, but before the intrusion of the Zenith Gabbro. The dominance of Zn in all of the VMS deposits indicate that the temperature of the discharging hydrothermal fluid was relatively low (<300 °C) and likely underwent adiabatic cooling due to boiling in a shallow marine environment.

4) The U-Pb age of the quartz-feldspar porphyry in the BDLA provides an important constraint on the timing of deformation in the region. Of equal importance is the co-magmatic relationship of the *circa* 2690 Ma age of the BDLA porphyry with other syn-deformation magmatic events along the northern margin of the Wawa-Abitibi terrane (Corfu and Stott, 1998; Zaleski et al., 1999; Lodge et al., 2013). This event is interpreted to represent the timing of accretion for the Wawa-Abitibi terrane to the Superior Province and is temporally associated with several orogenic gold events.

3.9 References

Anderson, T., 2002, Correction of common lead in U-Pb analyses that do not report ^{204}Pb: Chemical Geology, v. 192, p. 59-79.

Ayer, J. A., Amelin, Y., Corfu, F., Kamo, S. L., Ketchum, J., Kwok, K., and Trowell, N., 2002, Evolution of the southern Abitibi greenstone belt based on U–Pb geochronology: autochthonous volcanic construction followed by plutonism, regional deformation and sedimentation: Precambrian Research, v. 115, p. 63-95.

Barrett, T. J., and MacLean, W. H., 1994, Mass changes in hydrothermal alteration zones associated with VHMS deposits in the Noranda area: Exploration and Mining Geology, v. 3, p. 131-160.

Bartley, M. W. 1940, Geology of the Big Duck-Aquasabon Lakes area, Ontario Geological Survey, Map 49k, 1:31,680.

Bea, F., 1996, Controls on the trace element composition of crustal melts: Transactions of the Royal Society of Edinburgh, Earth Sciences, v. 87, p. 33-41.

Beakhouse, G. P., 2011, The Abitibi subprovince plutonic record: Tectonic and metallogenic implications, Ontario Geological Survey, Open File Report 6268, p. 161.

Blatt, H., and Tracy, R. J., 2000, Petrology: Igneous, Sedimentary, and Metamorphic: New York, NY, W.H. Freeman and Company, 529 p.

Burnham, O. M., 2008, Trace element analysis of geological samples by inductively coupled plasma mass spectrometry (ICP-MS) at the Geoscience Laboratories: Revised capabilities due to method improvements, *in* Summary of Field Work and Other Activities, Open File Report 6226, Ontario Geological Survey, p. 38-1 to 38-10.

Campbell, I. H., Lesher, C. M., Coad, P., Franklin, J. M., Gorton, M. P., and Thurston, P. C., 1984, Rare-earth element mobility in alteration pipes below massive Cu-Zn-sulphide deposits: Chemical Geology, v. 45, p. 181-202.

Corfu, F., and Stott, G. M., 1998, Shebandowan greenstone belt, western Superior Province: U-Pb ages, tectonic implications, and correlations: GSA Bulletin, v. 110, p. 1467-1484.

Creaser, R. A., Erdmer, P., Stevens, R. A., and Grant, S. L., 1997, Tectonic affinity of Nusultin and Anvil assemblage strata from the Telsin tectonic zone, northern Canadian Cordillera: Constraints from neodymium isotope and geochemical evidence: Tectonics, v. 16, p. 107-121.

Creaser, R. A., and White, A. J. R., 1991, Yardea dacite - Large-volume, high-temperature felsic volcanism from the Middle Proterozoic of South Australia: Geology, v. 19, p. 48-51.

Davis, D. W., Schandl, E. S., and Wasteneys, H. A., 1994, U-Pb dating of minerals in alteration halos of Superior Province massive sulfide deposits; syngenesis versus metamorphism: Contributions to Mineralogy and Petrology, v. 115, p. 427-437.

Franklin, J. M., Gibson, H. L., Jonasson, I. R., and Galley, A. G., 2005, Volcanogenic massive sulphide deposits, *in* Hedenquist, J. F. H., Goldfarb, R. J., and Richards, J. P., eds., Economic Geology, 100th Anniversary Volume, p. 523-560.

Galley, A. G., 1993, Characteristics of semi-conformable alteration zones associated with volcanogenic massive sulfide districts: Journal of Geochemical Exploration, v. 49, p. 175-199.

Galley, A. G., Bailes, A. H., and Kitzler, G., 1993, Geological setting and hydrothermal evolution of the Chisel Lake and North Chisel Zn-Pb-Ag-Au massive sulphide deposit, Snow Lake, Manitoba: Exploration and Mining Geology, v. 2, p. 271-295.

Galley, A. G., Hannington, M. D., and Jonasson, I. R., 2007, Volcanogenic massive sulphide deposits, *in* Goodfellow, W. D., ed. Mineral Deposits of Canada: A Synthesis of Major Deposit-Types, District Metallogeny, the Evolution of Geological Provinces, and Exploration Methods: Geological Association of Canada, Mineral Deposits Division, Special Publication No. 5, p. 141-161.

Gerstenberger, H., and Haase, G., 1997, A highly effective emitter substance for mass spectrometric Pb isotope ratio determinations: Chemical Geology, v. 136, p. 309-312.

Gibson, H. L., Morton, R. L., and Hudak, G. J., 1999, Submarine volcanic processes, deposits, and environments favorable for the location of volcanic-associated massive sulphide deposits, *in* Barrie, C. T., and Hannington, M. D., eds., Volcanic-hosted massive sulfide deposits: Processes and examples in modern and ancient settings: Society of Economic Geologists Reviews in Economic Geology, 8, p. 13-51.

Goldstein, R. L., O'nions, R. K., and Hamilton, P. J., 1984, A Sm-Nd isotopic study of atmospheric dusts and particulates from major river systems: Earth and Planetary Science Letters, v. 70, p. 221-236.

Goodfellow, W. D., 2007, Metallogeny of the Bathurst Mining Camp, Northern New Brunswick, *in* Goodfellow, W. D., ed. Mineral Deposits of Canada: A Synthesis of Major Deposit-Types, District Metallogeny, the Evolution of Geological Provinces, and Exploration Methods: Geological Association of Canada, Mineral Deposits Division, Special Publication No. 5, p. 471-508.

Gorton, M. P., and Schandl, E. S., 1995, An unusual sink for rare earth elements: the rhyolite-basalt contact of the Archean Winston Lake volcanogenic massive sulphide deposit, Superior Province, Canada: Economic Geology, v. 90, p. 2065-2072.

Goutier, J., Mercier-Langevin, P., McNicoll, V. J., and Ayer, J. A., 2010, The Abitibi subprovince, its evolution and its VMS deposits - an overview, *in* Yilgarn-Superior Workshop - Abstracts, Fifth International Archean Symposium, 10 September 2010: Geological Survey of Western Australia, Record 2010/20, p. 51-56.

Griffiths, R. W., and Fink, J. H., 1992, Solidification and morphology of submarine lavas: A dependence on extrusion rate: Journal of Geophysical Research: Solid Earth, v. 97, p. 19729-19737.

Hanchar, J. M., and Watson, E. B., 2003, Zircon saturation thermometry: Reviews in Mineralogy and Geochemistry, v. 53, p. 59-112.

Hannington, M. D., de Ronde, C. E. J., and Petersen, S., 2005, Sea-floor tectonics and submarine hydrothermal systems, *in* Hedenquist, J. F. H., Goldfarb, R. J., and Richards, J. P., eds., Economic Geology, 100th Anniversary Volume, p. 111-141.

Hart, T. R., 2007, Geochronology of the Hamlin and Wye Lakes Area, Shebandowan Greenstone Belt, Thunder Bay District, *in* Summary of Field Work and Other Activities, Open File Report 6213, Ontario Geological Survey, p. 9-1 to 9-8.

Hart, T. R., Gibson, H. L., and Lesher, C. M., 2004, Trace element geochemistry and petrogenesis of felsic volcanic rocks associated with volcanogenic massive Cu-Zn-Pb sulfide deposits: Economic Geology, v. 99, p. 1003-1013.

Hawkesworth, C. J., Turner, S. P., McDermott, F., Peate, D. W., and van Calsteren, P., 1997, U-Th isotopes in arc magmas: implications for element transfer from the subducted crust: Science, v. 276, p. 551-555.

Jaffey, A. H., Flynn, K. F., Glendenin, L. E., Bentley, W. C., and Essling, A. M., 1971, Precision measurement of half-lives and specific activities of ^{235}U and ^{238}U: Physical Review, v. 4, p. 1889-1906.

James, R. H., Allen, D. E., and Seyfried, W. E., Jr., 2003, An experimental study of alteration of coeanic crust and terrigenous sediments at moderate temperatures (51°-350°C): Insights as to chemical processes in near-shore ridge-flank hydrothermal systems: Geochimica et Cosmochimica Acta, v. 67, p. 681-691.

Jobin-Bevans, S., Kelso, I., and Cullen, D., 2006, NI 43-101 Technical Report on the Tower Mountain Gold Deposit, Conmee Township, northwestern Ontario, Canada, ValGold Resources Ltd., p. 95.

Keating, G. L., and Burnham, O. M., 2012, Revision of the calibration for major element analysis of geological samples by wavelength dispersive X-ray fluorescence at the Geoscience Laboratories, *in* Summary of Field Work and Other Activities, Open File Report 6280, Ontario Geological Survey, p. 39-1 to 39-4.

Kerrich, R., Polat, A., and Xie, Q., 2008, Geochemical systematics of a 2.7 Ga Kinojevis Group (Abitibi), and Manitouwadge and Winston Lake (Wawa) Fe-rich basalt-rhyolite associations: Backarc rift oceanic crust?: Lithos, v. 101, p. 1-23.

Ketchum, J. W. F., Ayer, J. A., Van Breemen, O., Pearson, N. J., and Becker, J. K., 2008, Pericontinental crustal growth of the southwestern Abitibi subprovince, Canada - U-Pb, Hf, and Nd isotope evidence: Economic Geology, v. 103, p. 1151-1184.

Krogh, T. E., 1973, A low contamination method for hydrothermal decomposition of zircon and extraction of U and Pb for isotopic age determinations: Geochimica et Cosmochimica Acta, v. 37, p. 485-494.

Leonard, B., and Ilieva, T., 2008, NI 43-101 Technical Report on the Goldcreek Property, Shebandowan area, Ontario, Canada, Mengold Resources Inc. and Solomon Resources Ltd., p. 93.

Lesher, C. M., Goodwin, A. M., Campbell, I. H., and Gorton, M. P., 1986, Trace-element geochemistry of ore-associated and barren, felsic metavolcanic rocks in the Superior Province, Canada: Canadian Journal of Earth Sciences, v. 23, p. 222-237.

Lodge, R. W. D., 2012a, Preliminary results of uranium–lead geochronology from the Shebandowan Greenstone Belt, Wawa Subprovince, *in* Summary of Field Work and Other Activities, Open File Report 6280, Ontario Geological Survey, p. 10-1 to 10-10.

Lodge, R. W. D., 2012b, Winston Lake and Manitouwadge revisited: Modern views of two volcanogenic massive sulphide (VMS)-endowed greenstone belts. A field trip guidebook., Ontario Geological Survey Open File Report 6282, p. 37.

Lodge, R. W. D., and Chartrand, J. E., 2013, Establishing regional geodynamic settings and the metallogeny of volcanogenic massive sulphide mineralization of greenstone belt assemblages (circa 2720 Ma) of the Wawa Subprovince via geochemical comparisons, Ontario Geological Survey, Miscellaneous Release - Data 306.

Lodge, R. W. D., Gibson, H. L., Stott, G. M., Hudak, G. J., and Jirsa, M., 2013, New U-Pb geochronology from Timiskaming-type assemblages in the Shebandowan and Vermilion greenstone belts, Wawa Subprovince, Superior Craton: Implications for the Neoarchean development of the southwestern Superior Province: Precambrian Research, v. 235, p. 264-277.

Ludwig, K. R., 2012, User's manual for Isoplot 3.75: A geochronological toolkit for Microsoft Excel, Berkeley Geochronology Center, Special Publication No. 4, p. 75.

MacDonald, C. J. D., 2003, NI 43-101 Technical Report on the Big Duck Lake Project, Ontario, Tri-Alpha Investments Ltd., p. 46.

Martinez, F., and Taylor, B., 2006, Modes of crustal accretion in back-arc basins: Inferences from the Lau Basin: Geophysical Monograph Series, v. 166, p. 5-30.

Mattinson, J. M., 2005, Zircon U-Pb chemical abrasion ("CA-TIMS") method: Combined annealing and multi-step partial dissolution analysis for improved precision and accuracy of zircon ages: Chemical Geology, v. 220, p. 47-66.

Muir, T. L., 2003, Structural evolution of the Hemlo greenstone belt in the vacinity of the world-class Hemlo gold deposit: Canadian Journal of Earth Sciences, v. 40, p. 695-430.

Osterberg, S. A., 1993, Stratigraphy, physical volcanology, and hydrothermal alteration of the footwall rocks to the Winston Lake massive sulfide deposits, northwestern Ontario: Unpub. Ph.D. thesis, University of Minnesota at Minneapolis, 351 p.

Paton, C., Hellstrom, J., Paul, B., Woodhead, J., and Hergt, J., 2011, Iolite: freeware for the visualization and processing of mass spectrometer data.: Journal of Analytical Atomic Spectrometry, v. 26, p. 2508-2518.

Pearce, J. A., 1996, A users guide to basalt discrimination diagrams, Trace Element Geochemistry of Volcanic Rocks: Applications for Massive Sulphide Exploration. Geological Association of Canada, Short Course Notes 12, p. 79-133.

Pearce, J. A., and Stern, R. A., 2006, Origin of back-arc basin magmas: Trace element and isotope perspectives: Geophysical Monograph Series, v. 166, p. 63-86.

Peter, J. M., and Goodfellow, W. D., 1996, Mineralogy, bulk and rare earth element geochemistry of massive sulphide-associated hydrothermal sediments of the Brunswick horizon, Bathurst mining camp, New Brunswick: Canadian Journal of Earth Sciences, v. 33, p. 252-283.

Peterson, D., Gallup, C., Jirsa, M., and Davis, D. W., 2001, Correlation of the Archean assemblages across the U.S.-Canadian border: Phase I geochronology, *in* 47th Annual Meeting, Institute on Lake Superior Geology, Proceedings Volume 47, Part 1 - Program and Abstracts, p. 77-78.

Petrus, J. A., and Kamber, B. S., 2012, VizualAge: A novel approach to laser ablation ICP-MS U-Pb geochronology data reduction: Geostandards and Geoanalytical Research, p. DOI: 10.1111/j.1751-908X.2012.00158.x.

Piercey, S. J., 2007, An overview of the use of petrochemistry in regional exploration for volcanogenic massive sulfide (VMS) deposits, *in* Milkereit, B., ed. Proceedings of Exploration '07: Fifth Devennial International Conference on Mineral Exploration, p. 223-246.

Piercey, S. J., Mortensen, J. K., Murphy, D. C., Paradis, S., and Creaser, R. A., 2002, Geochemistry and tectonic significance of alkalic mafic magmatism in the Yukon-Tanana terrane, Finlayson Lake region, Yukon: Canadian Journal of Earth Sciences, v. 39, p. 1729-1744.

Piercey, S. J., Peter, J. M., Mortensen, J. K., Paradis, S., Murphy, D. C., and Tucker, T. L., 2008, Petrology and U-Pb geochronology of footwall porphyritic rhyolites from the Wolverine volcanogenic massive sulphide deposit, Yukon, Canada: Implications for the genesis of massive sulphide deposits in continental margin environments: Economic Geology, v. 103, p. 5-33.

Polat, A., 2009, The geochemistry of Neoarchean (ca. 2700 Ma) tholeiitic basalts, transitional to alkaline basalts, and gabbros, Wawa Subprovince, Canada: Implications for petrogenetic and geodynamic processes.: Precambrian Research, v. 168, p. 83-105.

Polat, A., and Hoffman, A. W., 2003, Alteration and geochemical patterns in the 3.7-3.8 Ga Isua greenstone belt, West Greenland: Precambrian Research, v. 126, p. 197-218.

Polat, A., and Kerrich, R., 2000, Archean greenstone belt magmatism and the continental growth-mantle evolution connection: constraints from Th-U-Nb_LREE systematics of the 2.7 Ga Wawa subprovince, Superior Province, Canada: Earth and Planetary Science Letters, v. 175, p. 41-54.

Polat, A., and Kerrich, R., 2006, Reading the geochemical fingerprints of Archean hot subduction volcanic rocks: Evidence for accretion and crustal recycling in a mobile tectonic regime: Geophysical Monograph Series, v. 164, p. 189-213.

Polat, A., Kerrich, R., and Wyman, D. A., 1999, Geochemical diversity in oceanic komatiites and basalts from the late Archean Wawa greenstone belts, Superior Province, Canada: trace element and Nd isotope evidence for a heterogeneous mantle: Precambrian Research, v. 94, p. 139-173.

Pye, E. G., 1964, Mineral deposits of the Big Duck Lake area, district of Thunder Bay, Ontario Department of Mines Geological Report 27, p. 58.

Ritcey, D. J., 1992, Geology and mineralization in the vicinity of Big Duck Lake, Ontario: Unpub. M.Sc. thesis, University of Ottawa, 235 p.

Ross, P.-S., and Bédard, J. H., 2009, Magmatic affinity of modern and ancient subalkaline volcanic rocks determined from trace-element discriminant diagrams.: Canadian Journal of Earth Sciences, v. 46, p. 823-839.

Schmidberger, S. S., Heaman, L. M., Simonetti, A., Creaser, R. A., and Whiteford, S., 2007, Lu-Hf, in-situ Sr and Pb isotope and trace element systematics for mantle eclogites from the Daivik diamond mine: Evidence for Paleoproterozoic subduction beneath the Slave craton, Canada: Earth and Planetary Science Letters, v. 254, p. 55-68.

Severin, P. W. A., Balint, F., and Sim, R., 1991, Geological setting of the Winston Lake massive sulphide deposit, Mineral Deposits in the Western Superior Province, Ontario, Geological Survey of Canada Open File 2164, p. 58-73.

Shervais, J. W., 1982, Ti-V plots and the petrogenesis of modern and ophiolitic lavas.: Earth and Planetary Science Letters, v. 59, p. 101-118.

Spitz, G., and Darling, R., 1978, Major and minor element lithogeochemical anomalies surrounding the Louvem copper deposit, Val d'Or, Quebec.: Canadian Journal of Earth Sciences, v. 15, p. 1161-1169.

Stott, G. M., Corkery, M. T., Percival, J. A., Simard, M., and Goutier, J., 2010, A revised terrane subdivision of the Superior Province, *in* Summary of Field Work and Other Activities, Open File Report 6260, Ontario Geological Survey, p. 20-1 to 20-10.

Stott, G. M., and Schnieders, B. R., 1983, Gold mineralization in the Shebandowan Belt and its relation deformation patterns, *in* The Geology of Gold in Ontario, Miscellaneous Paper 110, Ontario Geological Survey, p. 181-193.

Sun, S., and McDonough, W. F., 1989, Chemical and isotopic systematics of oceanic basalts: implications for mantle composition and processes, *in* Saunders, A. D., and Norry, M. J., eds., Magmatism in the Ocean Basins, Geological Society Special Publication 42, p. 313-345.

Tanaka, T., Togashi, S., Kamioka, H., Amakawa, H., Kagami, H., Hamamoto, T., Yuhara, M., Orihashi, Y., Yoneda, S., Shimizu, H., Kunimaru, T., Takahashi, K., Yanagi, T., Nakano, T., Fujimaki, H., Shinjo, R., Asahara, Y., Tanimizu, M., and Dragusanu, C., 2000, JNdi-1: A neodymium isotopic reference in consistency with La Jolla neodymium: Chemical Geology, v. 168, p. 279-281.

Thomas, D. A., 1991, The application of mineralogy, whole rock chemistry, and mineral chemistry to volcanogenic massive sulphide exploration at the Winston Lake Zn-Cu deposit, northwestern Ontario: Unpub. M.Sc. thesis, Queen's University, 331 p.

Thurston, P. C., Ayer, J. A., Goutier, J., and Hamilton, M. A., 2008, Depositional gaps in Abitibi greenstone belt stratigraphy: A key to exploration for syngenetic mineralization: Economic Geology, v. 103, p. 1097-1134.

Unterschutz, J. L. E., Creaser, R. A., Erdmer, P., Thompson, R. I., and Daughtry, K. L., 2002, North American margin origin of Quesnel terrane strata in the southern Canadian Cordillera: Inferences from geochemical and Nd isotopic characteristics of Triassic metasedimentary rocks: Geological Society of America Bulletin, v. 114, p. 462-475.

Vervoort, J. D., White, W. M., and Thorpe, R. I., 1994, Nd and Pb isotope ratios of the Abitibi greenstone belt: new evidence for very early differentiation of the Earth: Earth and Planetary Science Letters, v. 128, p. 215-229.

Wang, X., Griffin, W. L., Chen, J., Huang, P., and Li, X., 2011, U and Th contents and Th/U ratios of zircon in felsic and mafic magmatic rocks: Improved zircon-melt distribution coefficients: Acta Geologica Sinica - English Edition, v. 85, p. 164-174.

Williams, H. R., Stott, G. M., Heather, K. B., Muir, T. L., and Sage, R. P., 1991, Wawa Subprovince, *in* Thurston, P. C., Williams, H. R., Sutcliffe, R. H., and Stott, G. M., eds., Geology of Ontario, Ontario Geological Survey, Special Volume 4, Part 1, p. 485-541.

Winchester, J. A., and Floyd, P. A., 1977, Geochemical discrimination of different magma series and their differentiation products using immobile elements: Chemical Geology, v. 20, p. 325-343.

Zaleski, E., and Peterson, V. L., 1995, Depositional setting and deformation of massive sulfide deposits, iron formation, and associated alteration in the Manitouwadge greenstone belt, Superior Province, Ontario: Economic Geology, v. 90, p. 2244-2261.

Zaleski, E., Peterson, V. L., Lockwood, H. C., and van Breemen, O., 1995, Geology, structure and age relationships of the Manitouwadge greenstone belt and the Wawa subprovince boundary, northwestern Ontario, Field Trip Guidebook: Institute on Lake Superior Geology, 41st annual meeting, Proceedings volume 41, Part 2B, 41, Part 2b, p. 77.

Zaleski, E., van Breemen, O., and Peterson, V. L., 1999, Geological evolution of the Manitouwadge greenstone belt and Wawa-Quetico subprovince boundary, Superior Province, Ontario, constrained by U-Pb zircon dates of supracrustal and plutonic rocks: Canadian Journal of Earth Sciences, v. 36, p. 945-966.

CHAPTER 4

GEODYNAMIC SETTING, CRUSTAL ARCHITECTURE, AND VMS METALLOGENY OF CA. 2720 MA GREENSTONE BELT ASSEMBLAGES OF THE NORTHERN WAWA SUBPROVINCE, SUPERIOR PROVINCE.

4.1. Abstract

The greenstone belts along the northern margin of the Wawa subprovince of the Superior Province (Vermilion, Shebandowan, Winston Lake, Manitouwadge) formed at ca. 2720 Ma and have been interpreted to be representative of a rifted-arc to back-arc tectonic setting. Despite a common inferred tectonic setting and broad similarities, these greenstone belts have a significantly different metallogeny as evidenced by different endowments in volcanogenic massive sulphide, magmatic sulphide, and orogenic gold deposits. In this paper we examine differences in geodynamic setting and crustal architecture as they pertain to the volcanogenic massive sulphide (VMS) metallogeny of each region by characterizing the regional-scale trace element and isotopic (Nd and Pb) geochemistry of each belt.

The trace element geochemistry of the Vermilion greenstone belt (VGB) shows evidence for a transition from arc-like to back-arc mafic rocks in the Soudan belt, to plume-driven rifted arcs in the ultramafic-bearing Newton belt. The Shebandowan greenstone belt (SGB) has a significant proportion of calc-alkalic, arc-like basalts, intermediate volcanic rocks, and high-Mg andesites, which are characteristic of low-angle, “hot” subduction. Extensional settings within the SGB are plume-driven and associated with ultramafic rocks and MORB-like basalts. The Winston Lake greenstone belt (WGB) is characterized by a transition from calc-alkalic arc-like basalts to back-arc basalts upward in the strata and is capped by alkalic OIB-like basalts. This association commonly reflects plume-driven rifting of a mature arc setting. Each of the VGB, SGB, and WGB show some isotopic evidence for the interaction with a juvenile or slightly older evolved crust. The Manitouwadge greenstone belt is characterized by isotopically juvenile bimodal tholeiitic to transitional volcanic lithofacies in a back-arc setting.

The MGB is the most isotopically-juvenile belt of this study and is also the most productive in terms of VMS mineralization. The Zn-rich VMS mineralization within the WGB suggests a relatively lower-temperature hydrothermal system, possibly within a relatively

shallower water environment. Zn-dominated and locally Au-enriched VMS mineralization, as well as brecciated mafic lithofacies and argillic alteration assemblages are characteristic of relatively shallower water deposition in the VGB and SGB and indicate that the ideal VMS-forming tectonic condition may have been compromised by a shallower water depositonal environment. However, the thickened arc-crust and compressional tectonics of the SGB suprasubduction zone during "hot" subduction may have provided crustal settings more favourable for the magmatic Ni-Cu sulphide and gold endowment of this belt.

4.2. Introduction

The Wawa subprovince is part of the Wawa-Abitibi terrane, which is the youngest accreted granite-greenstone terrane of the Superior Province (Stott, 2011). The Neoarchean greenstone belts of the Wawa subprovince have a long history of mineral exploration (e.g., MacDonald, 2003; Leonard and Ilieva, 2008; Risto and Breede, 2010) and research, which has provided an understanding of the tectonic evolution and metallogeny of the southern part of the craton (e.g., Kerrich et al., 2008; Polat, 2009; Lodge and Chartrand, 2013; Lodge et al., 2013). The majority of pre-deformation and metamorphic volcanic and magmatic assemblages of the greenstone belts along the northern margin of the Wawa subprovince formed *circa* 2720 Ma. These ca. 2720 Ma greenstone belts are the Vermilion (Peterson et al., 2001), Shebandowan (Corfu and Stott, 1998; Hart, 2007; Lodge, 2012), Winston Lake (Davis et al., 1994; Lodge et al., in press), and Manitouwadge (Zaleski et al., 1999) greenstone belts (**Figure 4.1**).

Despite these belts being co-depositional and broadly interpreted to have formed within a similar volcanotectonic setting (e.g., Osmani, 1997a; Zaleski et al., 1999; Hudak et al., 2002), their endowment of volcanogenic massive sulphide (VMS) deposits is notably different. The Winston Lake and Manitouwadge belts have had a rich history of mining and exploration for Zn-Cu-Pb VMS deposits and have produced almost 70 million tonnes of Zn-Cu-Pb ore. In contrast, the larger Vermilion and Shebandowan greenstone belts do not share the same (discovered) VMS-endowment and no economic VMS deposits have been discovered to date. While lacking in VMS-type mineralization, the Shebandowan Greenstone Belt is host to magmatic Ni-Cu deposits, including the past-producing Shebandowan (Ni-Cu) mine (e.g., Morton, 1982) and North Coldstream (Cu) mine (e.g., Farrow, 1994), numerous orogenic Au prospects (e.g., Leonard and Ilieva, 2008; Risto and Breede, 2010), as well an iron oxide-copper-gold (IOCG)

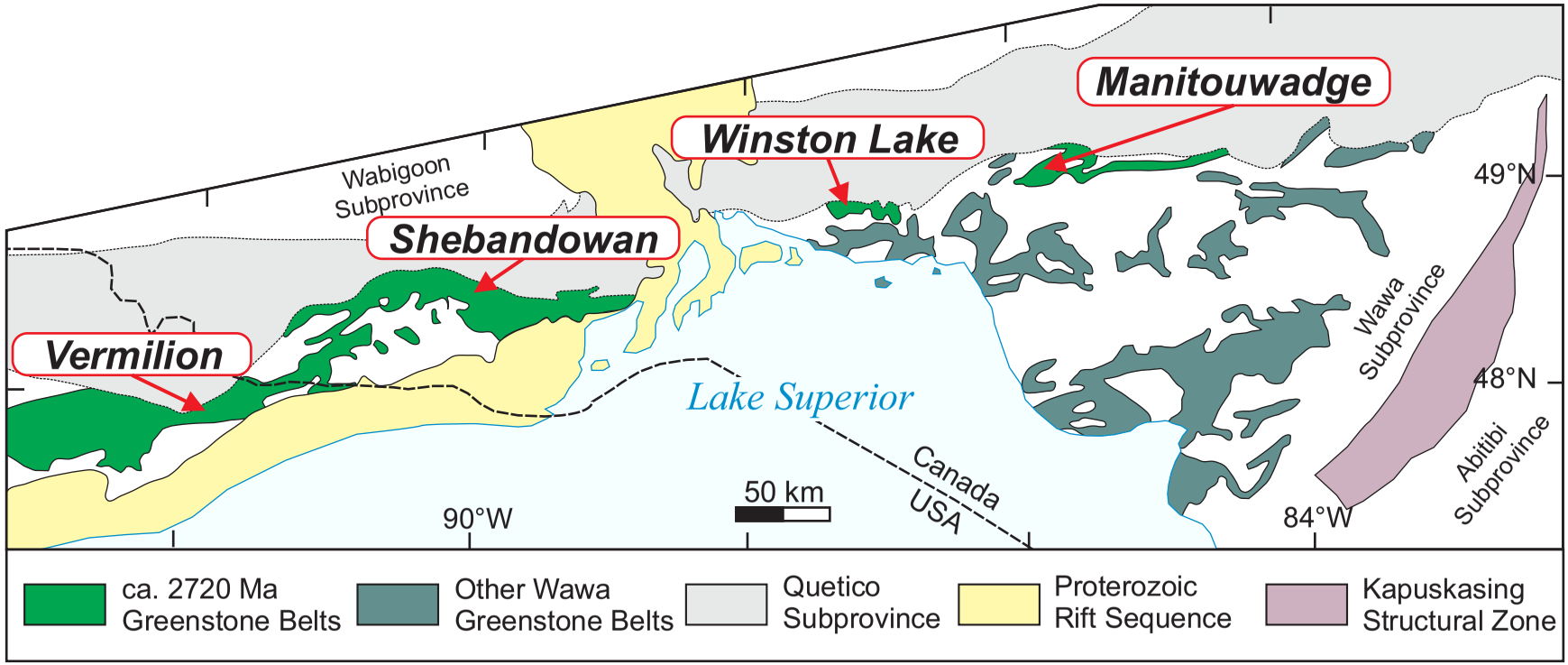

Figure 4.1: Regional geology of the Wawa subprovince highlighting the ca. 2720 Ma greenstone belts that were examined. Figure modified from Lodge (2011).

occurrence (e.g., Forslund, 2012). The reason for these metallogenic differences has not been fully investigated, but may have implications for the tectonic assembly and metallogeny of the Wawa subprovince and for granite-greenstone terranes in general.

In this manuscript we examine the trace element and isotopic geochemistry of the ca. 2720 Ma greenstone belts on a regional-scale to determine how the relation between their geodynamic settings and their VMS metallogeny. Regional-scale mapping and sampling transects were conducted throughout each greenstone belt to characterize the variation in trace element and isotopic geochemistry of the major lithostratigraphic units and to determine their petrogenetic variation. The geochemical and isotopic data collected within Ontario are available in a Miscellaneous Release – Data by the Ontario Geological Survey (Lodge and Chartrand, 2013). The data from Minnesota is available as a digital appendix to this manuscript.

4.3. Greenstone Belt Geology

The greenstone belts studied are diverse in their metamorphic and alteration attributes in addition to their major lithofacies. Metamorphism has locally obscured pre-metamorphic alteration histories, volcanological characteristics, and deformation histories. Metamorphic grade ranges from lower greenschist facies in the Shebandowan and Vermilion greenstone belts to upper amphibolite facies in the Manitouwadge greenstone belt. This section summarizes for each greenstone belt the major regional-scale lithostratigraphic units with an age of ca. 2720 Ma.

4.3.1 Vermilion Greenstone Belt

The Vermilion greenstone belt (VGB) in northeastern Minnesota is near-continuous with the Shebandowan greenstone belt, separated only by the Saganaga Tonalite **(Figure 4.1)**. The VGB has historically been subdivided into the Soudan and Newton belts on the basis of differences in stratigraphic and structural settings, and the boundary between the belts is marked by the Mud Creek shear zone and the Knife Lake Group (Jirsa et al., 1992; Southwick et al., 1998) **(Figure 4.2**). Both the Soudan and Newton belts are composed of predominantly calc-alkalic to tholeiitic mafic lithofacies. Despite their belt-scale differences, they are interpreted to be lithostratigraphically and chronostratigraphically equivalent to the ca. 2720 Ma Greenwater assemblage of the Shebandowan greenstone belt (Southwick et al., 1998; Peterson et al., 2001).

The Soudan belt is subdivided into the Lower Ely, Soudan, and Upper Ely members. The Lower Ely member is composed of highly amygdaloidal mafic to intermediate lithofacies and

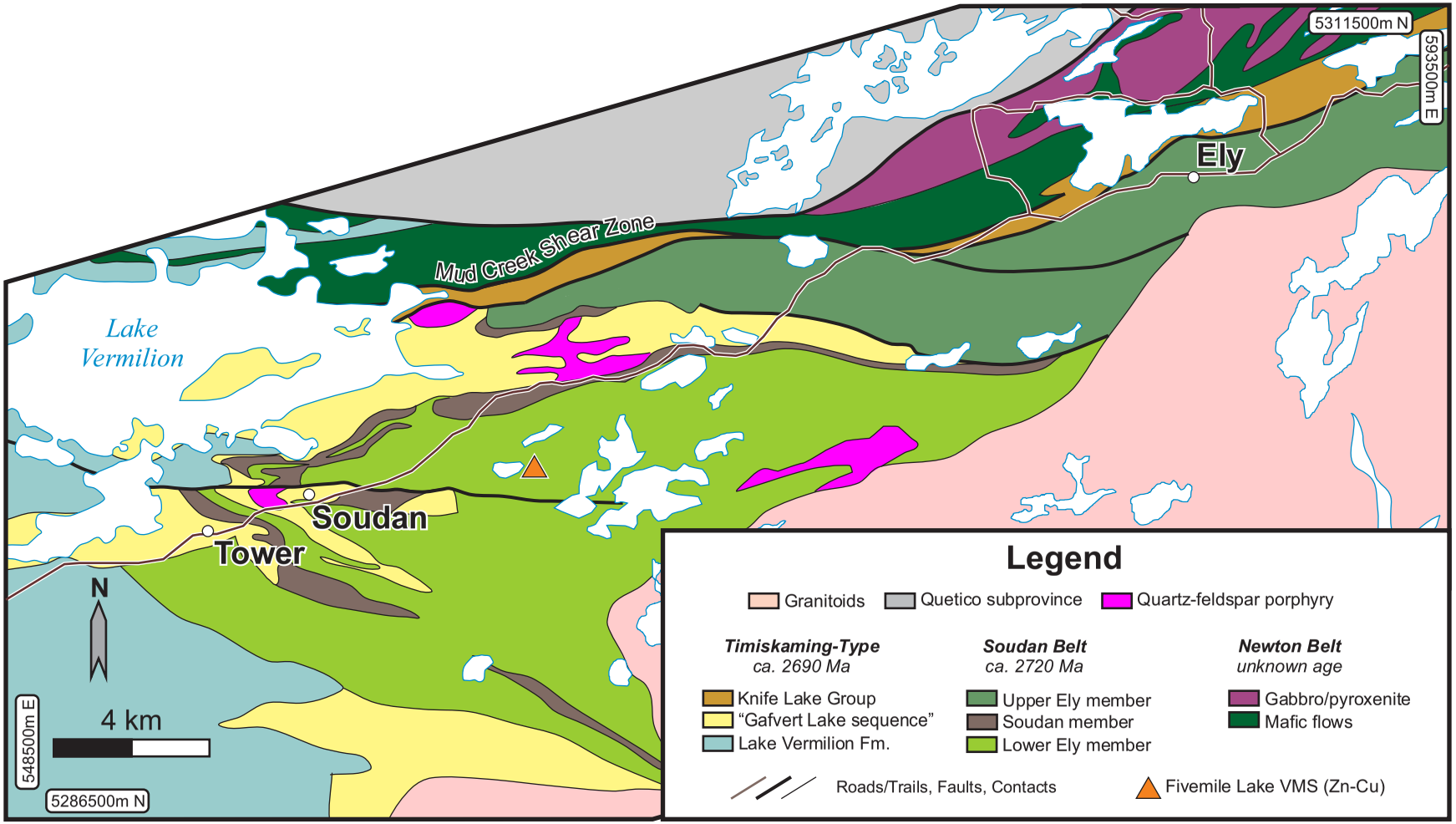

Figure 4.2: Geology of the Soudan-Ely region of the Vermilion greenstone belt modified from Peterson (2004), Peterson and Jirsa (1999), and Lodge et al. (2013).

minor felsic lithofacies that host the Fivemile Lake VMS occurrence (Hudak et al., 2002; Hudak et al., 2012) (see **Figure 4.2**). The Soudan member is an Algoma-type, cherty iron formation with minor interlayered mafic and felsic volcanic strata (Peterson and Patelke, 2003). The Upper Ely member is composed of predominantly massive to sparsely amygdaloidal mafic lithofacies with minor intercalated iron formation (Southwick et al., 1998; Hudak et al., 2012). The Newton belt consists of predominantly mafic to locally abundant ultramafic lithofacies (Southwick et al., 1998). Felsic lithofacies are not abundant in the Newton belt and were not present in the areas examined during this study. They are described as being lithologically similar to the dacitic lithofacies of the Lake Vermilion Formation (Southwick et al., 1998) but their age is unknown and therefore may not represent younger, Timiskaming-type units as is the case for the Gafvert Lake sequence (Lodge et al., 2013).

Magmatic and detrital U-Pb geochronology in the Tower-Soudan area has identified the sedimentary and volcanic rocks of the Lake Vermilion Formation, Gafvert Lake sequence, and Knife Lake Group as younger, Timiskaming-type assemblages that were deposited during terrane accretion at ca. 2690-2680 Ma (Driese et al., 2011; Jirsa et al., 2012; Lodge et al., 2013). These younger assemblages have important metallogenic implications for gold mineralization during post-2720 Ma deformation, but will not be discussed further in this manuscript.

4.3.2 Shebandowan Greenstone Belt

The Shebandowan greenstone belt (SGB) is a large, 150 km long greenstone belt that extends west from Thunder Bay to the Ontario-Minnesota border (**Figure 4.1**). The SGB is mostly composed of pre-D_1, calc-alkaline to tholeiitic volcanic suites of *circa* 2720 Ma age (Corfu and Stott, 1998; Hart, 2007; Lodge, 2012) (**Figure 4.3**). Historically, the strata of the SGB was divided into the Burchell and Greenwater assemblages based primarily on opposing younging directions (Williams et al., 1991). U-Pb geochronology has shown both the Burchell and Greenwater assemblage to be the same age (ca. 2720 Ma); they have been re-interpreted to be a fold-thrust repetition of a single (Greenwater) assemblage (Corfu and Stott, 1998). Accordingly, the Greenwater assemblage spans the breath of the greenstone belt and is dominated by massive to pillowed, variably amygdaloidal mafic lithofacies. The Greenwater assemblage also contains locally abundant intermediate lithofacies and minor felsic lithofacies that are hosts to all known VMS prospects in the SGB. The best documented VMS occurrences in the belt are the Vanguard, Wye Lake, Calvert-Stares, and Mud Lake prospects (see **Figure**

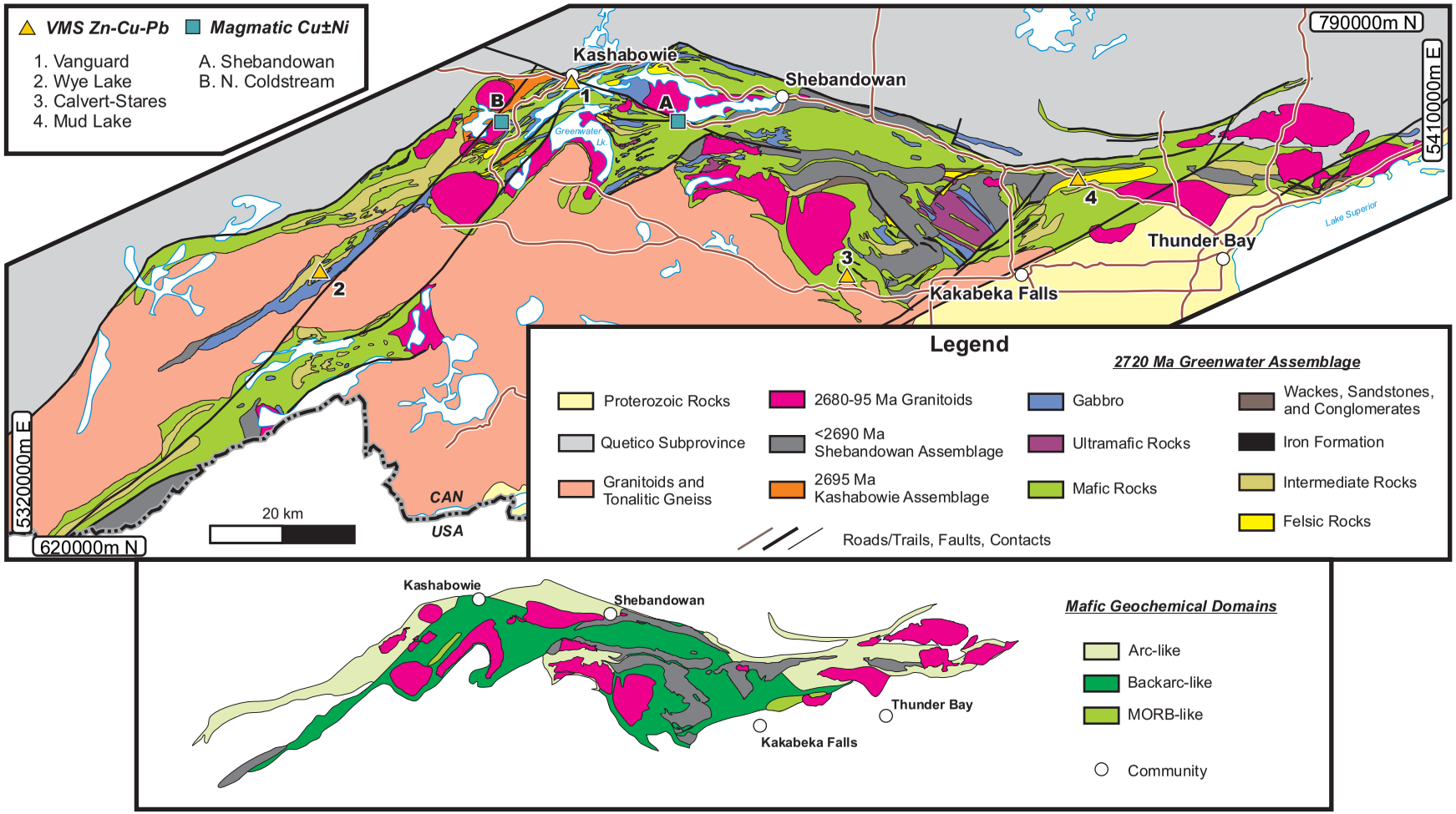

Figure 4.3: Regional geology and mafic geochemical domains of the Shebandowan greenstone belt. Geology modified from Santaguida (2001) based on mapping, geochemistry, and geochronology from the Ontario Geological Survey (Lodge, 2012; Lodge and Chartrand, 2013; Lodge et al. 2013).

4.3). In the region east of Greenwater Lake, abundant ultramafic flows and sills are associated with the past-producing Shebandowan Ni-Cu Mine (8.34 Mt at 2.00% Ni, 1.2% Cu, 3.96 g/t PGE) (Morton, 1982; Lavigne et al., 1990). A substantial, differentiated gabbroic complex has also been dated at ca. 2720 Ma (Corfu and Stott, 1998) and is associated with several base metal showings (e.g., Farrow, 1993) and the past-producing North Coldstream Cu mine (2.7 Mt at 2.0% Cu, 7 g/t Ag, 0.4 g/t Au) (Lavigne and Scott, 1993).

The Greenwater assemblage of the SGB has not been stratigraphically subdivided, but several lithological domains have been highlighted based on the dominant rock types and presence of major structures. Near the Wye Lake VMS prospect, the SGB is characterized by approximately equal amounts of variably amygdaloidal mafic to intermediate (andesite to dacite) volcanic rocks with localized felsic lithofacies (Osmani, 1997e; Hart and Metsaranta, 2009). The vicinity of the Mud Lake VMS prospect is also dominated by mafic and intermediate lithofacies (Brown and Fogal, 1995a, b; Lodge and Chartrand, 2013). In contrast, strata near the past-producing Shebandowan Ni-Cu Mine is dominated by massive to pillowed mafic flows, gabbros, and ultramafic rocks with only minor intermediate to felsic rocks (Osmani, 1997c, b). The strata south of the Vanguard prospect and North Coldstream mine are also dominated by mafic flows and gabbros, but the mafic lithofacies are generally more amygdaloidal and ultramafic rocks are very rare (Osmani, 1997d).

The 2720 Ma volcanic rocks are tectonically interleaved with syn-D_1 (*circa* 2695 Ma) calc-alkalic diorite sills and related intermediate volcanic rocks of the Kashabowie assemblage (Corfu and Stott, 1998) and the 2696 ± 2 Ma Shebandowan Lake Pluton (Corfu and Stott, 1986). Timiskaming-type assemblages in the SGB (known as the Shebandowan assemblage) were deposited prior to D_2 transpression (Corfu and Stott, 1998) and consist of wacke, sandstone, and conglomerate lithofacies with minor associated calc-alkalic to alkalic intermediate volcanic rocks and intrusions. Hornblende trachyandesitic flows and volcaniclastic rocks, the syenitic to dioritic Tower Stock, and the Saganaga Tonalite have been dated at *circa* 2690 Ma (Corfu and Stott, 1998). U-Pb detrital zircon geochronology and lithological comparisons by Corfu and Stott (1998) has allow to infer that the metasedimentary rocks in the Shebandowan and Kakabeka Falls regions are younger Timiskaming-type or foreland basin-type assemblages, as documented by Lodge et al. (2013). The younger Kashabowie and Shebandowan assemblages will not be discussed further herein.

4.3.3 Winston Lake Greenstone Belt

The Winston Lake greenstone belt (WGB) is a mafic-dominated belt (**Figure 4.4**) located directly north of, and almost connected to the Schreiber-Hemlo greenstone belt (Williams et al., 1991) (**Figure 4.1**); however, the contact relationship of these belts is poorly constrained (Carter, 1982b, a). The belt is bound to the north by the Quetico subprovince and granitic intrusions to the west, east and south (Pye, 1964; Severin et al., 1991). Regional metamorphic grade in the belt is lower amphibolite facies (Williams et al., 1991). The belt has been informally subdivided into two main lithotectonic assemblages, the Winston Lake and Big Duck Lake assemblages, which are separated by a thick, differentiated gabbro sill (Severin et al., 1991; Polat et al., 1999). The felsic strata of the Winston Lake assemblage and the differentiated gabbro sill have magmatic ages of ca. 2720 Ma (Davis et al., 1994; Lodge et al., in press).

The Winston Lake assemblage is a felsic-dominated, bimodal sequence of volcanic strata and siliciclastic rocks on the western margin of the WGB that hosts the past-producing Winston Lake (3.1 Mt at 16% Zn, 1% Cu, 30 g/t Ag, 1 g/t Au), Pick Lake (1.3 Mt at 16.5% Zn, 0.9% Cu), and Zenith (0.16 Mt at 16.5% Zn) VMS mines (unpublished Inmet Mining Corporation reports) as well as other VMS prospects (Gorton and Schandl, 1995; Lodge et al., in press) (**Figure 4.4**). Despite strong hydrothermal alteration and metamorphic recrystallization, well-preserved volcanic features, such as pillows in mafic flows and cross-bedded volcaniclastic rocks, suggest the strata consistently young to the northeast. Felsic units are predominantly massive to brecciated flow facies or bedded volcaniclastic facies. Mafic units are mostly massive to pillowed flows. The Big Duck Lake assemblage consists of predominantly massive and pillowed mafic flow lithofacies and lesser quartz-feldspar porphyry dykes and sills (Ritcey, 1992; Polat et al., 1999; Lodge et al., in press). Supracrustal felsic volcanic lithofacies are sparse in the Big Duck Lake assemblage, and felsic breccias in the Big Duck Lake area are interpreted to be brecciated facies of a quartz-feldspar porphyritic intrusion (Ritcey, 1992) which has a maximum age of emplacement of 2691 ± 0.7 Ma (Lodge et al., in press).

4.3.4 Manitouwadge Greenstone Belt

The Manitouwadge greenstone belt (MGB) is also located north of the Scheiber-Hemlo greenstone belt on the northern margin of the Wawa subprovince and adjacent to the Quetico subprovince (Williams et al., 1991). The belt is composed of bimodal volcanic, intrusive, and

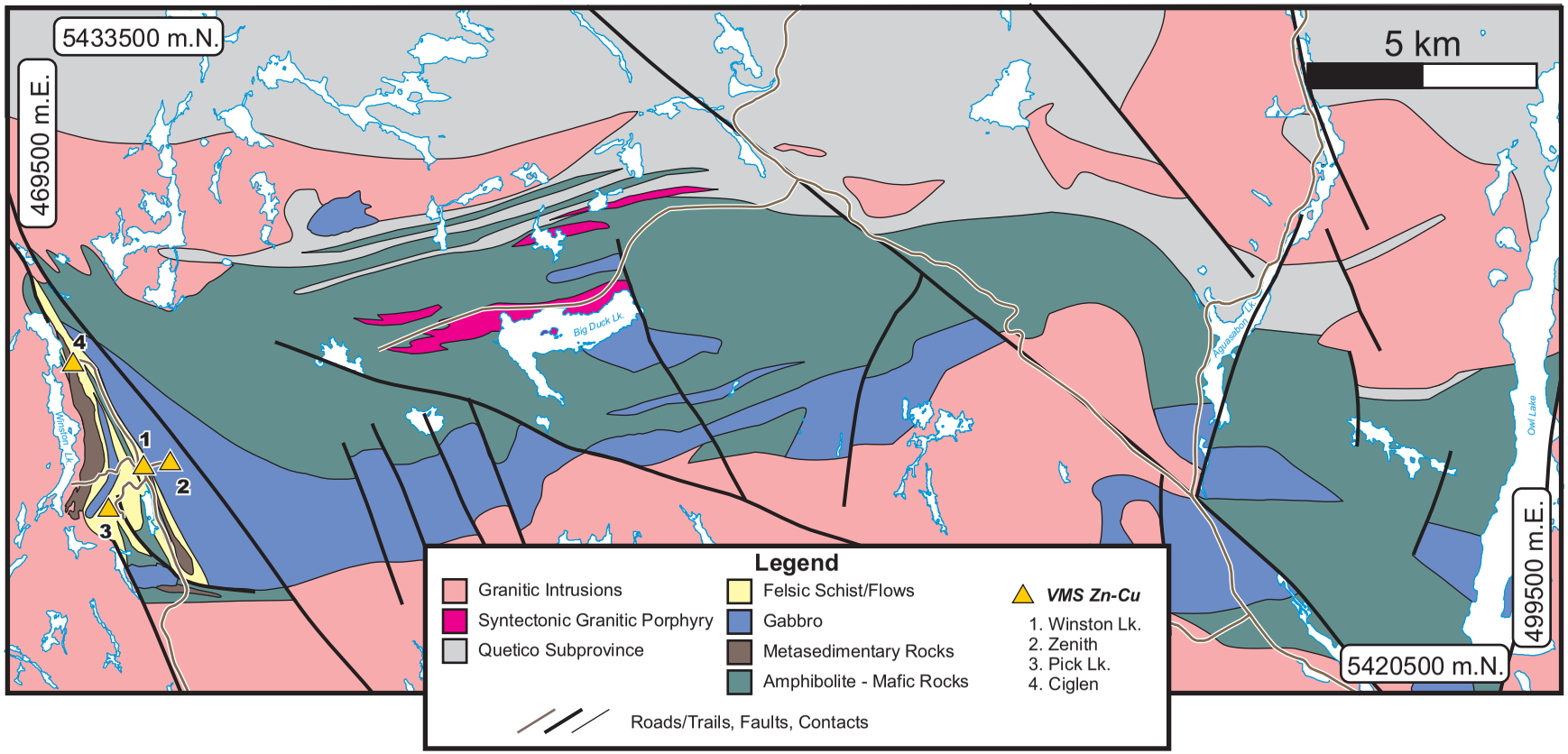

Figure 4.4: Geology of the Winston Lake greenstone belt compiled and modified from Osterberg (1993), Pye (1964), Ritcey (1992), and Carter (1982a,b).

sedimentary lithofacies that have been metamorphosed to upper amphibolite facies. The metamorphic grade increases to granulite facies at the northern margin of the belt and into the adjacent Quetico subprovince. The supracrustal volcanic assemblages and a synvolcanic trondhjemite intrusion yielded U-Pb zircon ages of ca. 2720 Ma (Zaleski et al., 1999). Most of the other granitic and alkalic intrusions in the belt are younger (<2690 Ma) and intruded during or subsequent to the regional, penetrative deformation. Terrigenous metasedimentary rocks in the southern part of the belt have a maximum depositional age of approximately 2693 Ma (Zaleski et al., 1999).

Intense deformation and metamorphism of hydrothermally altered volcanic strata have made geological interpretations of the original lithofacies and stratigraphic relationships very difficult (Peterson and Zaleski, 1999; Zaleski et al., 1999). The most prominent map-scale structural feature of the belt is the large Manitouwadge synform that formed during D_3 deformation with a synvolcanic trondhjemite (Zaleski et al., 1999) in the core of the synform (**Figure 4.5**). The supracrustal assemblages of the MGB mantle the synvolcanic trondhjemite. These supracrustal rocks are subdivided into inner and outer volcanic belts, separated by a band of terrigenous metasedimentary rocks along the southern limb of the Manitowadge synform. The inner volcanic belt hosts all of the past-producing VMS mines including the Geco (55 Mt at 2.3% Cu, 8.2% Zn, 74 g/t Ag), Willroy (4.6 Mt at 1.3% Cu, 5.7% Zn, 48 g/t Ag), Willecho (3.8 Mt at 0.6% Cu, 3.9% Zn, 53 g/t Ag), and Nama Creek (0.3 Mt at 0.8% Cu, 3.9% Zn, 28 g/t Ag) deposits (unpublished Noranda Incorporated reports; Zaleski and Peterson, 2001). The inner belt is composed of thin amphibolite (mafic) units, orthoamphibole-cordierite-garnet gneiss (altered volcanic facies), and interlayered felsic volcanic rocks, sillimanite-quartz-biotite-muscovite-garnet schists (altered felsic facies), and iron formation (Zaleski and Peterson, 1995). The outer volcanic belt is dominated by mafic lithofacies. These rocks are notably less altered than those of the inner volcanic belt and felsic and altered lithofacies are uncommon (Zaleski and Peterson, 1995).

4.4. Trace Element Geochemistry

Analysis and comparison of immobile trace element patterns and ratios reveals a high degree of variability of pre-deformation hydrothermal alteration, structural overprinting, and metamorphic recrystallization in the lithofacies between greenstone belts. Primary mineralogy

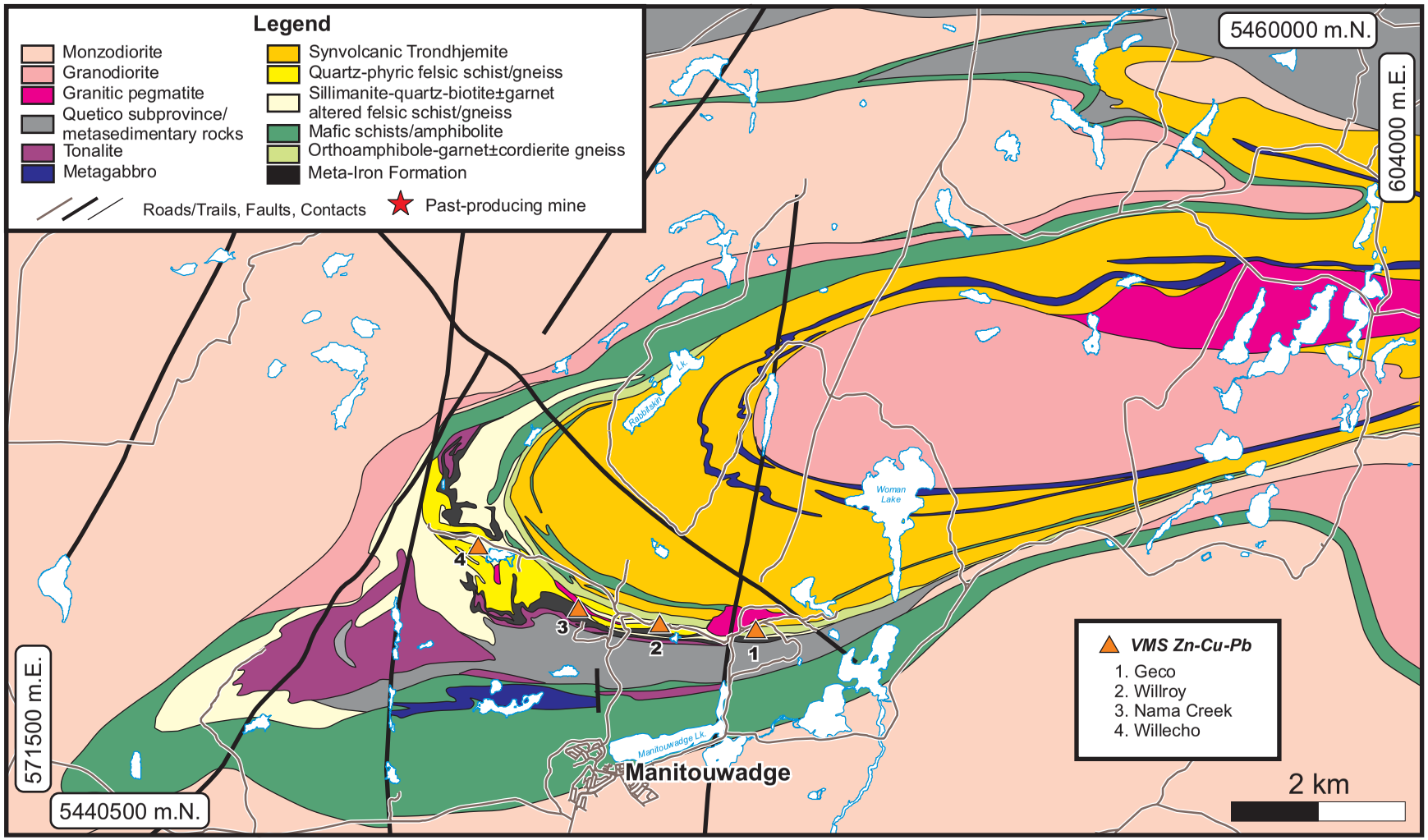

Figure 4.5: Geology of the Manitouwadge greenstone belt compiled and modified from Zaleski and Peterson (2001) and Lodge (2012b).

and volcanic textures were variably destroyed by post-depositional metamorphism and/or deformation and therefore even basic rock classifications were difficult to compare between belts. A simple trace element classification diagram using typically immobile trace elements (Pearce, 1996) shows the compositional variation of the samples analyzed (Lodge and Chartrand, 2013)in each greenstone belt (**Figure 4.6**). The sampling strategy in each greenstone belt was focused on characterizing representative belt-scale units or assemblages. The SGB has not been stratigraphically subdivided to the same detail as others, so the mafic rocks of the SGB are discussed more generally, based on differences in geochemistry. Local, deposit-scale variability in each greenstone belt may not be fully represented in these analyses.

The mobility of typically immobile trace elements has been documented in strongly altered rocks at amphibolite facies metamorphism in the WGB (Gorton and Schandl, 1995; Lodge et al., in press). Although it has not been formally documented in the other greenstone belts (e.g., Zaleski and Peterson, 1995), the possibility of trace element mobility has to be accounted for. Therefore, the trace element geochemistry presented in this section does not include analyses from strongly altered lithofacies that may have resulted in significant mobility of elements used for petrogenetic interpretations, such as Th and rare earth elements. Alteration intensity was assessed by petrography and by applying geochemical filters (see discussion in Section 4.5).

4.4.1 Analytical Procedures

Major, trace, and rare earth elements were analyzed at the Ontario Geoscience Laboratories (Sudbury, Ontario). Major elements were analyzed with X-ray fluorescence (XRF) using a fused disk with a borate flux. Trace and rare earth elements were analyzed using inductively coupled plasma mass spectrometry (ICP-MS). Samples were pulverized using an agate mill and underwent closed beaker digestion using a four acid digestion. Any sample that had a clearly visible residue after digestion was not included in the data set. These residues are typically composed of accessory minerals (such as zircon, rutile, spinel, or xenotime) that contain abundant trace elements, such as Th or Zr, that are important for petrogenetic interpretations. Incomplete digestion of these minerals can alter the resulting elemental abundances measured by the analytical equipment (Burnham et al., 2002). Unfortunately, logistical limitations imposed by the laboratory inhibit additional digestion to dissolve these residues. Analytical procedures, instrumental calibrations, and quality assurance standards at the

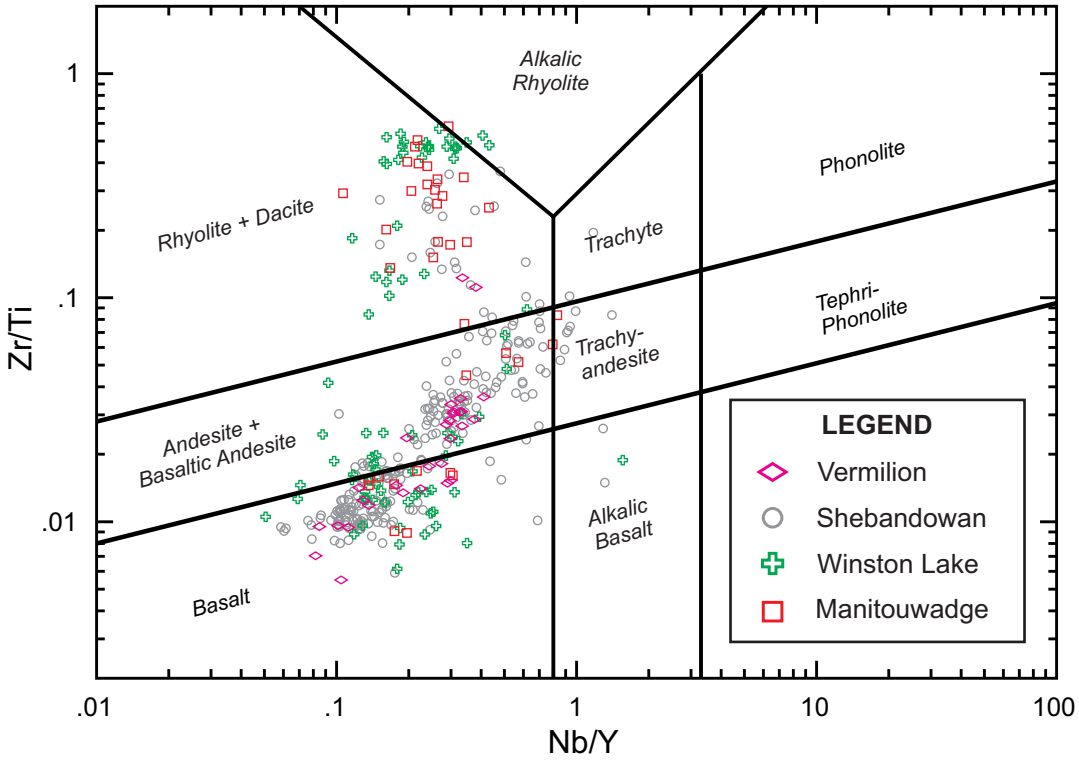

Figure 4.6: Rock classification from Pearce (1996) for samples collected from the Vermilion, Shebandowan, Winston Lake, and Manitouwadge greenstone belts in this study.

Ontario Geoscience Laboratories are outlined in reports by the Ontario Geological Survey (Burnham, 2008; Keating and Burnham, 2012).

4.4.2 Trace Element Geochemistry of Mafic Rocks

The mafic rocks of the VGB have been subdivided into their respective stratigraphic units: the Newton belt, and the Upper and Lower Ely members of the Soudan belt (**Figure 4.2**). Most of the samples from the Newton belt display weakly to moderately negative Nb and Ti anomalies and flat to gently sloping REE patterns on primitive mantle-normalized trace element plots (**Figure 4.7**). These rocks also have normalized Nb/Th ratios close to 1, indicating that Th is not significantly enriched relative to Nb. Th/Yb and Zr/Y ratios are characteristic of tholeiitic magmatic affinities on discrimination diagrams by Ross and Bédard (2009). One sample collected from the northernmost visited portion of the Newton belt had enriched Th, negative Nb anomaly (normalized Nb/Th = 0.3), and a relatively flat REE pattern on primitive mantle-normalized plots (**Figure 4.7**). The Upper Ely member of the Soudan belt is also dominated by rocks with flat to gently sloping REE patterns with slight negative Nb and Ti anomalies on primitive mantle-normalized plots (**Figure 4.7**). Normalized Nb/Th ratios are approximately equal to 1 (0.8 to 1.2) and Th/Yb and Zr/Y ratios are characteristic of tholeiitic magmas (Ross and Bédard, 2009; Hudak et al., 2012). Samples collected from the base of the Upper Ely member, have more pronounced Th enrichment (normalized Nb/Th = 0.1 to 0.4), negative Nb and Ti anomalies, and steeply sloping REE patterns (**Figure 4.7**). The Lower Ely member is characterized by predominately enriched Th relative to Nb (normalized Nb/Th < 0.5), negative Nb and Ti anomalies, and moderately to steeply sloping REE patterns on primitive mantle-normalized trace element plots (**Figure 4.7**). The Th/Yb and Zr/Y ratios are characteristic of calc-alkalic magmatic affinities (Ross and Bédard, 2009; Hudak et al., 2012). The uppermost parts of the Lower Ely member, near the base of the Soudan Iron Formation, have depleted Th, Nb, and LREE (**Figure 4.7**) and have a tholeiitic magmatic affinity based on their Th/Yb and Zr/Y ratios (Hudak et al., 2012).

The 2720 Ma mafic rocks of the SGB have not been stratigraphically subdivided but rather have been divided by their arc-like, back-arc, or MORB-like geochemical patterns (e.g., Piercey, 2007) into discrete spatial domains. This geochemical and spatial subdivision is relatively successful in subdividing the SGB into larger, belt-scale geochemical domains that are structurally separated (Lodge and Chartrand, 2013). Mafic lithofacies with a back-arc affinity

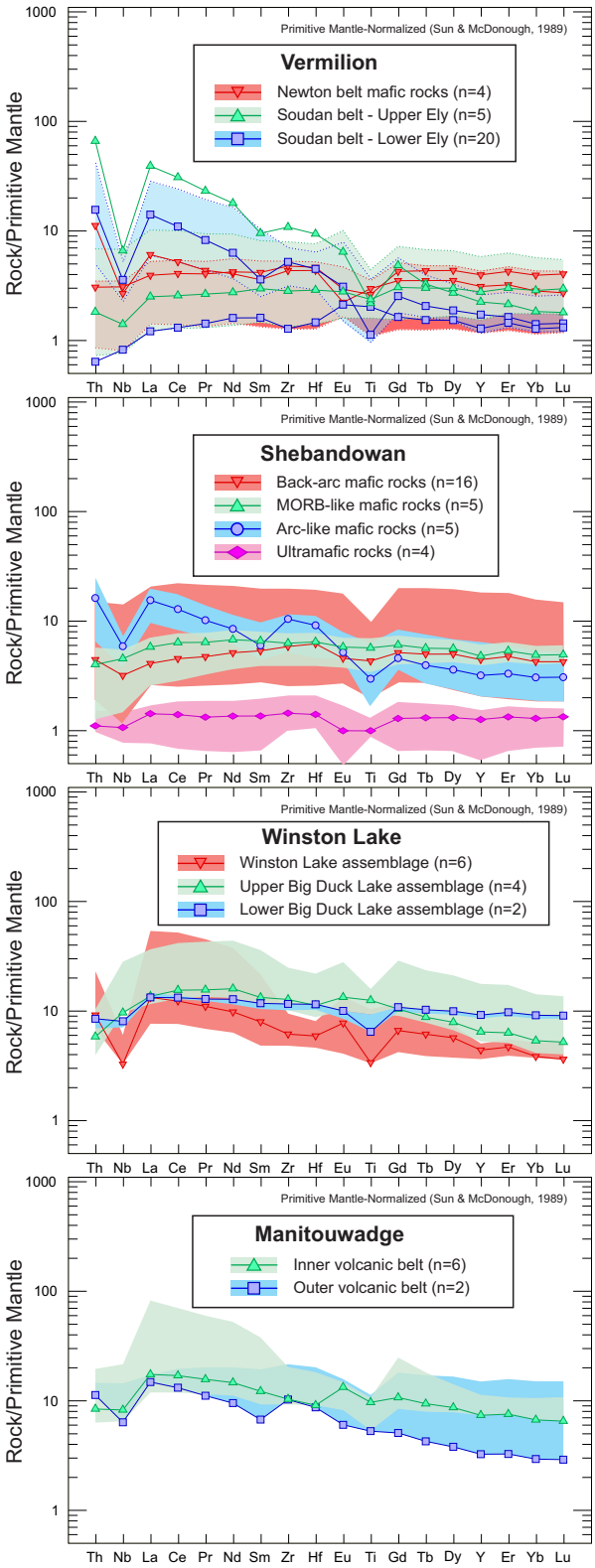

Figure 4.7 – Primitive mantle-normalized trace element diagrams for mafic to ultramafic rocks from the ca. 2720 Ma assemblages of the Wawa subprovince. Colored areas represent the typical range of the data. Lines and symbols are representative patterns for each assemblage. Normalizing values from Sun & McDonough (1989).

constitute the dominant rock type in the belt and are present both east and west of Greenwater Lake, south of the village of Shebandowan, and in the vicinity of the Calvert-Stares VMS prospect (**Figure 4.3**) (Lodge and Chartrand, 2013). These are characterized by relatively flat to gently sloping REE patterns, slightly negative Nb and Ti anomalies, and normalized Nb/Th ratios that are close to 1 (**Figure 4.7**). Their Th/Yb and Zr/Y ratios are characteristic of transitional to tholeiitic magmas (Ross and Bédard, 2009; Lodge and Chartrand, 2013). Arc-like magmas dominate the strata along the northern margin of the SGB and in the strata north of the Wye Lake VMS prospect (**Figure 4.3**) (Lodge and Chartrand, 2013). These rocks are characterized by higher Th (normalized Nb/Th < 0.5), pronounced negative Nb and Ti anomalies, and moderately to steeply sloping REE patterns on primitive-mantle normalized trace element plots (**Figure 4.7**). MORB-like rocks are relatively uncommon and occur as structurally-bound slivers north of the town of Kakabeka Falls and west of Greenwater Lake (**Figure 4.3**) (Lodge and Chartrand, 2013). These rocks are characterized by smooth trace element and REE patterns with slight Th, Nb, and LREE depletion on primitive mantle-normalized trace element plots (**Figure 4.7**). The SGB is unique among the belts in this study as it contains komatiitic flows and sills that host the past-producing Shebandowan Ni-Cu mine and also occur northwest of the town of Kakabeka Falls (**Figure 4.3**). Most of the primitive mantle-normalized trace element plots for ultramafic rocks show negative Nb and Ti anomalies and there is slight enrichment in Th and Zr relative to REE (**Figure 4.7**).

The compositional variation in the mafic rocks within the WGB is well-represented by the stratigraphic subdivisions of the belt (Lodge et al., in press). The mafic rocks of the Winston Lake assemblage on the western margin of the belt (**Figure 4.4**) have pronounced negative Nb and Ti anomalies, enriched Th relative to Nb (normalized Nb/Th < 0.5), and have gently to moderately dipping REE patterns on primitive mantle-normalized trace element plots (**Figure 4.7**). LREE enrichment is as high as 50 x primitive mantle. Th/Yb and Zr/Y ratios are characteristic of a calc-alkalic to transitional magma affinity (Ross and Bédard, 2009; Lodge et al., in press). In contrast, the mafic rocks of the lower mafic unit of the Big Duck Lake assemblage have flatter REE patterns, slightly negative Nb and Ti anomalies, and Nb/Th ratios that are closer to 1 (**Figure 4.7**). The Th/Yb and Zr/Y ratios are characteristic of a tholeiitic magmatic affinity (Ross and Bédard, 2009; Lodge et al., in press). The upper mafic unit of the Big Duck Lake assemblage has enriched LREE and is depleted in Th (normalized Nb/Th >> 1)

(**Figure 4.7**). Ti/V ratios of this unit are characteristic of an alkalic magmatic affinity (Shervais, 1982; Lodge et al., in press) and the high Nb/Th ratios are similar to oceanic plateau basalts elsewhere in the Wawa subprovince (e.g., Polat, 2009).

The mafic rocks of the MGB occur as thin units at the core of the Manitouwadge synform within the synvolcanic trondhjemite and compose most of the outer volcanic belt (**Figure 4.5**). Most of the rocks in both belts have gently to steeply sloping REE patterns, slightly negative Nb and Ti anomalies, and normalized Nb/Th ratios that are approximately equal to 1 (**Figure 4.7**). These rocks have Th/Yb and Zr/Y ratios that are characteristic of a transitional to tholeiitic magmatic affinity (Ross and Bédard, 2009; Lodge and Chartrand, 2013). One sample, collected north of Rabbitskin Lake in the outer volcanic belt, has a pronounced enrichment of Th relative to Nb (normalized Nb/Th = 0.6), a strong negative Nb anomaly, and a moderately sloping REE pattern. The Th/Yb and Zr/Y ratios for this sample are characteristic of a calc-alkalic magmatic affinity (Ross and Bédard, 2009; Lodge and Chartrand, 2013).

4.4.3 Trace Element Geochemistry of Felsic Rocks

Felsic rocks in the VGB are very limited and they are not generally present as regional map-scale units. The only regional-scale felsic map unit is the dacitic Gafvert Lake sequence with a U-Pb zircon age of 2695 Ma (**Figure 4.2**) (Lodge et al., 2013). Deposit-scale units of FII- to FIII-type felsic volcanic rocks with a U-Pb zircon age of ca. 2720 Ma are associated with the Fivemile VMS prospect within the Lower Ely member of the Soudan Belt (Peterson et al., 2001; Hudak et al., 2012). Their primitive mantle-normalized trace element plots are characterized by pronounced negative Nb and Ti anomalies, moderately sloping REE patterns, and positive Zr and Hf anomalies (**Figure 4.8**). LREE and HREE are enriched up to 40x and 5x primitive mantle, respectively.

Felsic rocks of the SGB are mostly present as large, regional-scale felsic units east of the village of Kashabowie and near the Mud Lake VMS prospect. There are several local-scale felsic units interlayered with mafic volcanic rocks near the VMS prospects shown on **Figure 4.3**. These felsic rocks have two distinct geochemical patterns. The large felsic unit associated with the Mud Lake VMS prospect and smaller felsic units associated with the Calvert-Stares and Wye Lake VMS prospects have an FI-type geochemistry (Lesher et al., 1986; Hart et al., 2004). These rocks are characterized by steeply sloping primitive mantle-normalized REE patterns, and pronounced negative Nb and Ti and positive Zr and Hf anomalies (**Figure 4.8**). LREE and

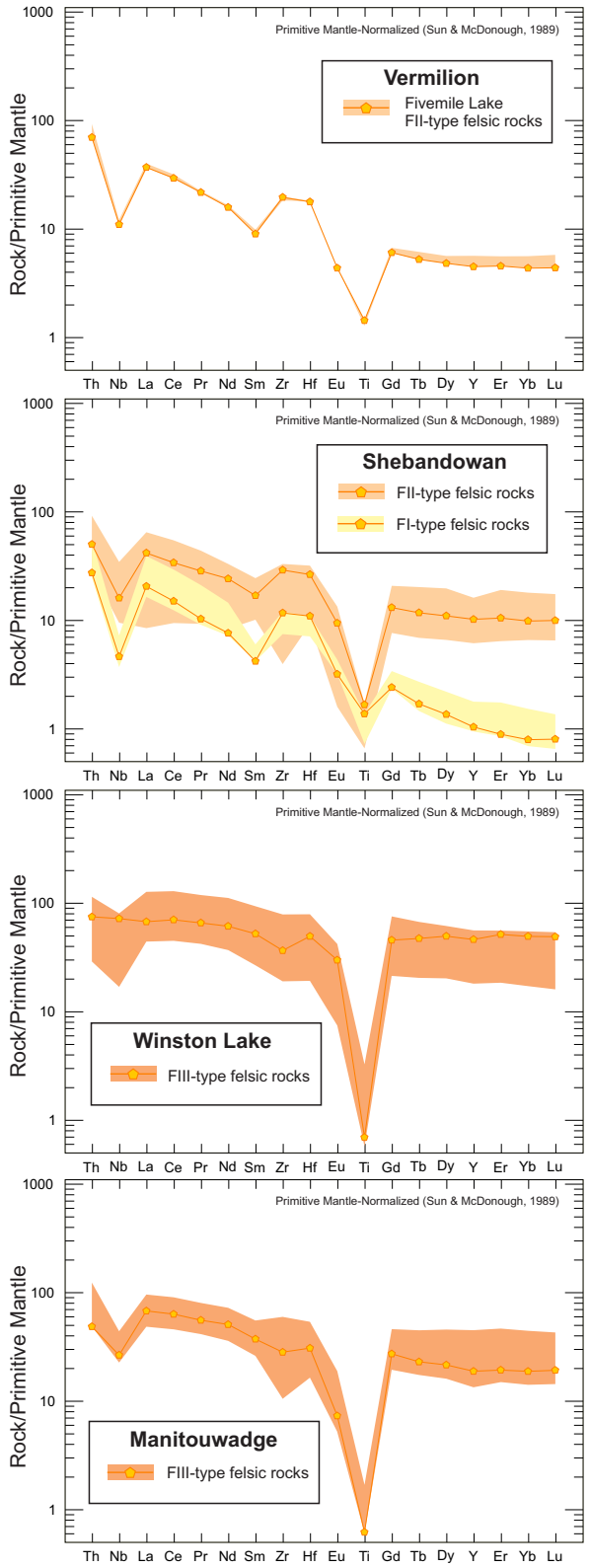

Figure 4.8 – Primitive mantle-normalized trace element diagrams for felsic rocks from ca. 2720 Ma assemblages of the Wawa subprovince. Colored areas represent the range of data. Line and symbols are representative for each type of rock. Normalizing values from Sun & McDonough (1989).

HREE abundances are 15-40x and 0.7-1.5x primitive mantle, respectively. The large felsic unit east of Kashabowie and several smaller felsic units near the Vanguard and Wye Lake VMS prospects have FII-type geochemistry (Lesher et al., 1986; Hart et al., 2004; Lodge and Chartrand, 2013). These rocks are characterized by moderately sloping primitive mantle-normalized REE patterns, negative Nb and Ti anomalies, and positive Zr and Hf anomalies (**Figure 4.8**). LREE and HREE abundances are 10-50x and 7-20x primitive mantle, respectively.

The Winston Lake assemblage of the WGB has two main felsic units that are associated with VMS mineralization and can be differentiated based on their Zr/Ti ratios (Lodge et al., in press) (**Figure 4.6**). However, their general trace element patterns are similar on primitive mantle-normalized plots and are classified as FIII-type rhyolites (Lesher et al., 1986; Hart et al., 2004; Lodge and Chartrand, 2013). These rocks have flat to gently sloping primitive mantle-normalized REE patterns, weak to moderate negative Nb and pronounced negative Ti anomalies (**Figure 4.8**). LREE and HREE are both enriched to 30-100x and 15-45x primitive mantle, respectively.

In the MGB, the high degree of synvolcanic hydrothermal alteration, deformation, and metamorphic recrystallization makes distinguishing individual felsic units difficult. There are several large quartz-phyric felsic units that are associated with the Willroy and Willecho deposits. Most of the sillimanite-quartz-biotite-garnet schist units and some of the cordierite-orthoamphibole-garnet gneiss units (**Figure 4.5**) are geochemically similar to the least-altered quartz-phyric felsic rocks in their trace element geochemistry (immobile elements) (Lodge and Chartrand, 2013). These felsic units are classified as FIII-type felsic volcanic rocks (Lodge and Chartrand, 2013) and are one of the type-localities for felsic rocks of this type (Lesher et al., 1986; Hart et al., 2004). These felsic rocks have gently sloping primitive mantle-normalized REE patterns, and strong negative Nb, Ti, and Eu anomalies (**Figure 4.8**). LREE and HREE enrichment are 40-100x and 15-30x primitive mantle, respectively.

4.5. Whole-Rock Isotopic Geochemistry

Only least altered samples from each belt were selected for isotopic analysis. Metamorphic recrystallization and structural overprinting can obscure primary assessment of the degree of alteration of a sample using mineralogy alone. Therefore, several geochemical filters were applied to the data set to select least altered samples prior to analyses. Hydrothermally-

altered samples were identified by significant enrichment in L.O.I. to values greater than 4.5 wt.%, depletion in Na_2O to values less than 2 wt.%, and/or Al_2O_3/Na_2O ratios greater than 10 (Spitz and Darling, 1978). In the WGB, light REE elements were documented to have a degree of mobility near the contact of altered mafic and felsic lithofacies (Campbell et al., 1984; Gorton and Schandl, 1995). REE mobility during hydrothermal alteration was assessed using the presence of Ce anomalies and samples with Ce/Ce* values that significantly deviate from 1 (0.9-1.1 was acceptable) (Polat and Hoffman, 2003).

Neodymium and lead isotopic analyses were performed at the Radiogenic Isotope Facility at the University of Alberta (Edmonton, Alberta) using multi-collector inductively coupled plasma mass spectrometry (MC-ICP-MS) (Schmidberger et al., 2007) following the procedures outlined in Creaser et al. (1997) and Unterschutz et al. (2002). Nd isotope ratios are relative to the La Jolla Nd isotopic standard and quality assurance was monitored by analysis of the Geological Survey of Japan Nd isotope standard "Shin Etsu: J-Ndi-1" (Tanaka et al., 2000). Initial εNd values were calculated using Uniform Chondritic Reservoir (CHUR) $^{147}Sm/^{144}Nd$ (0.1967) and $^{143}Nd/^{144}Nd$ (0.512638) values and the U-Pb zircon age (2720 Ma) of the volcanic assemblages. The measured lead isotope ratios were corrected for instrumental mass bias using the agreed value for $^{203}Tl/^{205}Tl$ ratio measured simultaneously with each Pb analysis (e.g., Belshaw et al., 1998). Quality assurance was monitored by the analyses of NIST Standard Reference Material SRM981 Pb isotope standard (Todt et al., 1996).

4.5.1 Nd Isotopes

εNd values for mafic rocks from all four greenstone belts have overlapping low positive juvenile values (+0.8 to +3.3) (**Figure 4.9**), which are similar to the values expected for the depleted mantle at 2720 Ma (Goldstein et al., 1984) and are similar to εNd values from other 2.7 Ga assemblages of the Wawa-Abitibi terrane (Vervoort et al., 1994; Ketchum et al., 2008; Polat, 2009). Felsic rocks show a similar range of εNd values (+0.2 to +2.8) (**Figure 4.10**). Therefore, it is likely that crustal contamination by significantly older crust was insignificant during their petrogenesis. The elevated La/Sm and Th/Nb ratios of basalts within the Winston Lake assemblage of the WGB suggest some degree of crustal contamination despite having juvenile εNd values (Lodge et al., in press). The lowest εNd values from the basalts of the 2720 Ma assemblages (εNd <1.5) occur in the VGB, SGB, and WGB and correlate with the lowest primitive mantle-normalized Nb/Th and chondrite-normalized La/Yb ratios (**Figure 4.9**). Despite

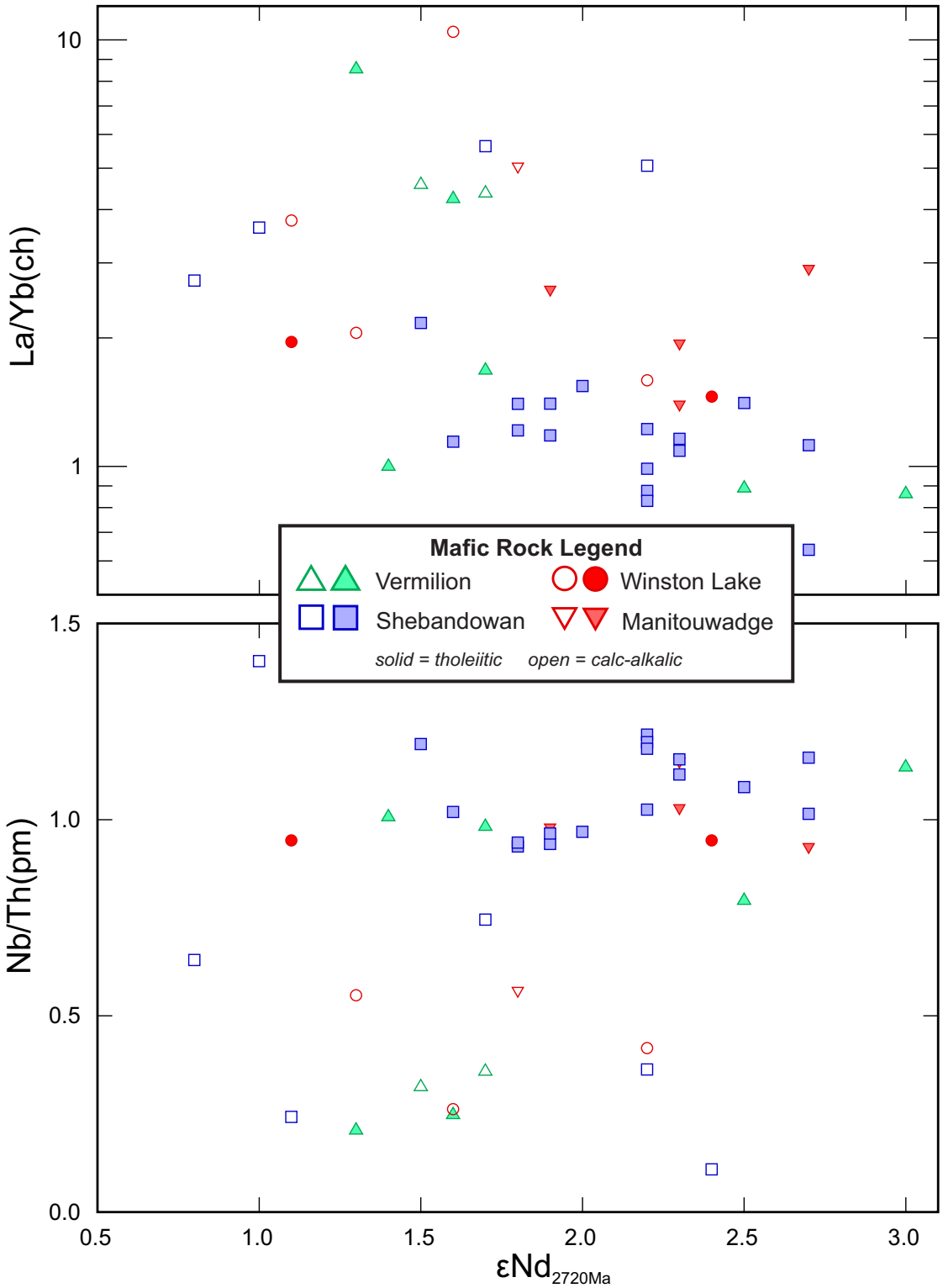

Figure 4.9 – Plot of εNd $_{2720\ Ma}$ versus primitive mantle-normalized Nb/Th ratio and chondrite-normalized La/Yb ratio for mafic rocks from the ca. 2720 Ma greenstone belt assemblages of the Wawa subprovince. Open symbols represent samples with calc-alkalic magmatic affinities whereas closed symbols represent samples with tholeiitic magmatic affinities.

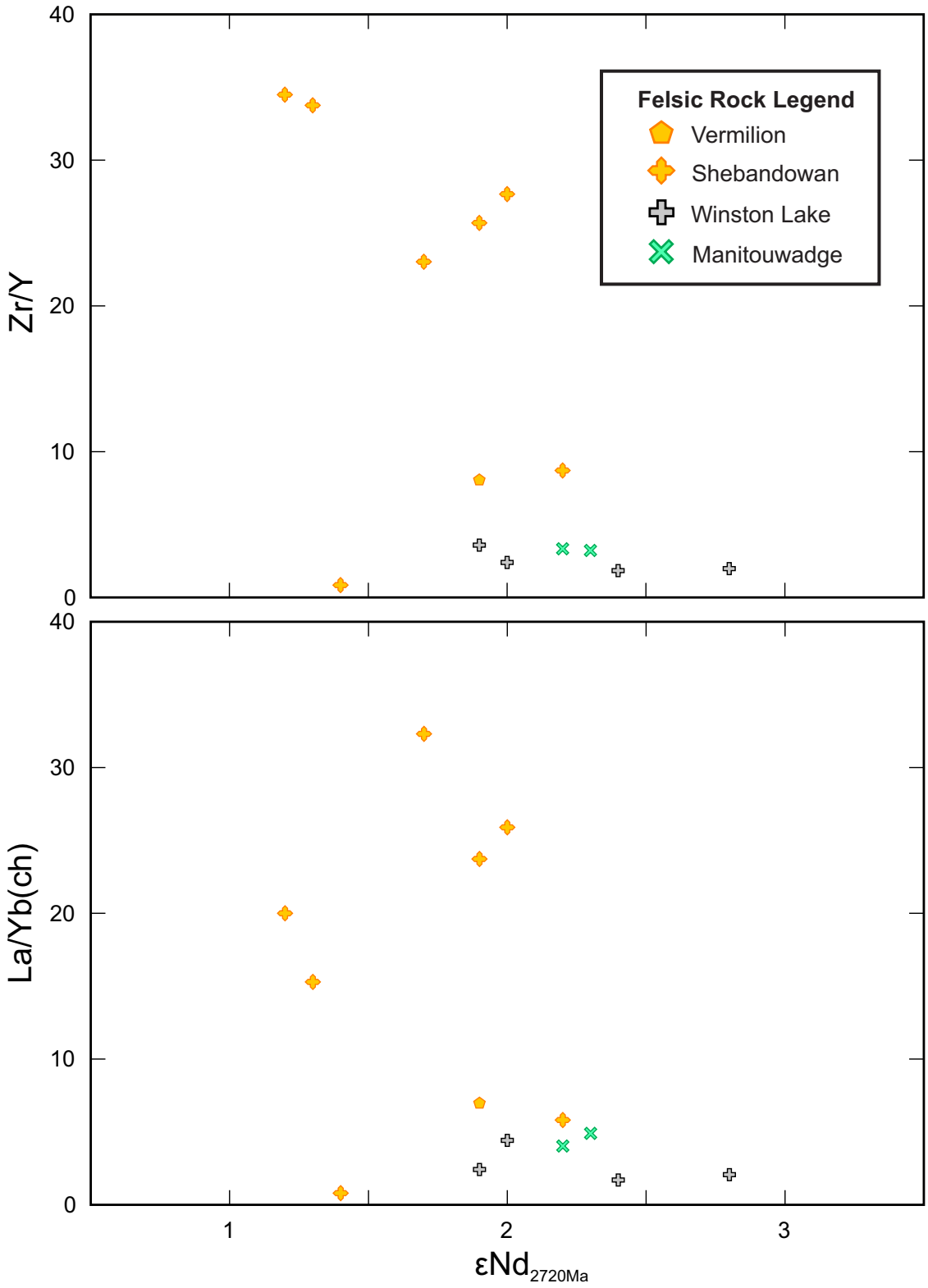

Figure 4.10 – Plot of εNd $_{2720\ Ma}$ versus Zr/Y ratio and chondrite-normalized La/Yb ratio for felsic rocks from the ca. 2720 Ma greenstone belt assemblages of the Wawa subprovince.

not having significantly low εNd values, the lowest εNd value from basalt in the MGB (+1.8) also has the highest normalized La/Yb and Nb/Th ratios from that belt (**Figure 4.9**). There is also a moderate correlation of calc-alkalic samples having lower εNd values than tholeiitic samples. Felsic rocks show weak to moderate correlations of higher Zr/Y and chondrite-normalized La/Yb ratios with the lowest εNd values for rhyolite (**Figure 4.10**). However, one sample from a felsic lithofacies in the WGB has an anomalous εNd value of +0.2 (Lodge and Chartrand, 2013), contradicts this correlation.

The lowest εNd value amongst the four greenstone belts was from an andesitic flow in the SGB (εNd = -0.2). This sample is atypical of other intermediate rocks collected in the SGB (+0.6 to +2.4) and other greenstone belts (+1.3 to +2.9) (Lodge and Chartrand, 2013).

4.5.2 Pb Isotopes

Lead isotopes are useful tracers of crustal source during petrogenesis based on the principal that U, and subsequently ^{206}Pb and ^{207}Pb, will be more enriched in the upper crust whereas Th, and subsequently ^{208}Pb, will be more enriched in the lower crust (Zartman and Doe, 1981; Tosdal et al., 1999). The mantle will be depleted in both Th and U and their daughter radiogenic isotopes. In general, the rocks from the four greenstone belts have $^{206}Pb/^{204}Pb$, $^{207}Pb/^{204}Pb$, and $^{208}Pb/^{204}Pb$ ratios that form a single errorchron (similar to pattern in **Figure 4.13**), likely representing a metamorphic errorchon, and have isotopic abundances that range from those typical of the depleted mantle to that of differentiated continental crust (Zartman and Doe, 1981; Tosdal et al., 1999). Alternatively, enrichment of radiogenic lead may be representative of melts derived from sublithospheric mantle enriched in U relative to Pb as a result of localized crustal assimilation (Hart, 1988). However, considering the variable Pb isotopic compositions within a particular greenstone belt assemblage (Lodge and Chartrand, 2013), it is more likely that radiogenic Pb is sourced from varying amounts of crustal contamination during emplacement.

Both calc-alkalic and tholeiitic basalts from each greenstone belt generally have $^{206}Pb/^{204}Pb$ ratios typical of mantle-derived melts (<18) (**Figure 4.11**). Mafic rocks that have $^{206}Pb/^{204}Pb$ ratios that are typical of crustal-derived melts also have lower primitive mantle-normalized Nb/Th ratios and higher chondrite-normalized La/Yb ratios (**Figure 4.11**). Pb-isotopic enrichment due to crustal contamination is most prevalent in the WGB, VGB, and SGB. Mafic rocks from the MGB do not show strong crustal enrichment (maximum $^{206}Pb/^{204}Pb$ ratio =

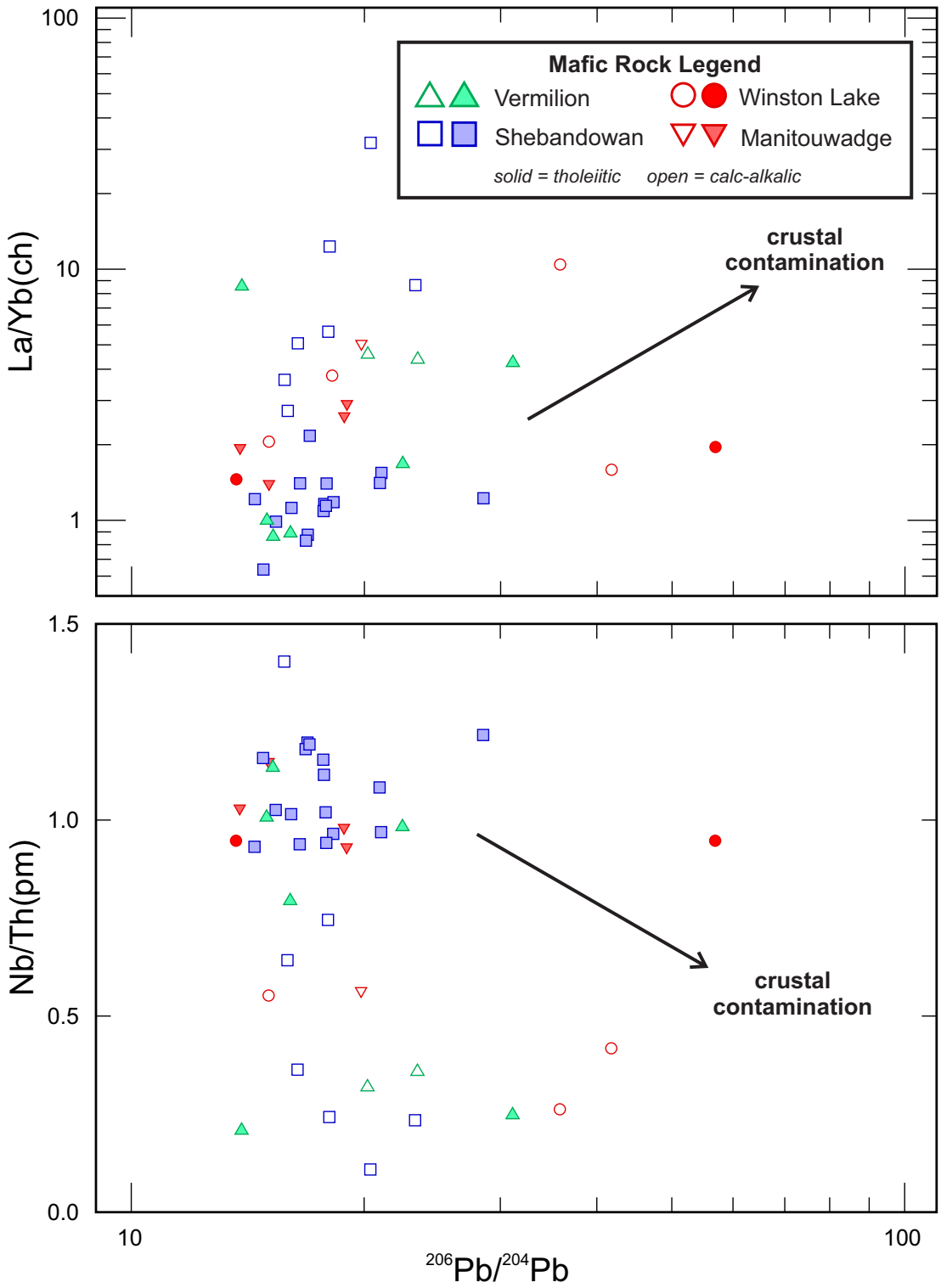

Figure 4.11 – Plot of $^{206}Pb/^{204}Pb$ ratio versus primitive mantle-normalized Nb/Th ratio and chondrite-normalized La/Yb ratio for mafic rocks from the ca. 2720 Ma greenstone belt assemblages of the Wawa subprovince. Open symbols represent samples with calc-alkalic magmatic affinities whereas closed symbols represent samples with tholeiitic magmatic affinities.

19.8) compared to the SGB (maximum $^{206}Pb/^{204}Pb$ ratio = 28.5), VGB (maximum $^{206}Pb/^{204}Pb$ ratio = 31.1), or WGB (maximum $^{206}Pb/^{204}Pb$ ratio = 56.9). The most isotopically primitive basaltic rocks from the SGB show relative crustal enrichment (minimum $^{206}Pb/^{204}Pb$ ratio = 14.1) compared to the VGB (minimum $^{206}Pb/^{204}Pb$ ratio = 13.9), WGB (minimum $^{206}Pb/^{204}Pb$ ratio = 13.7), and MGB (minimum $^{206}Pb/^{204}Pb$ ratio = 13.6). Andesites and other intermediate rocks show a similar Pb isotopic trend as the basalts from each belt.

The felsic rocks from the four greenstone belts show a moderate correlation of their $^{206}Pb/^{204}Pb$ ratio with Zr/Y and chondrite-normalized La/Yb ratios (**Figure 4.12**). Lower Zr/Y ratios and higher normalized La/Yb ratios approximate FII to FIII-type felsic rocks (Lesher et al., 1986; Hart et al., 2004). FII to FIII-type rocks from these greenstone belts have enriched crust-like $^{206}Pb/^{204}Pb$ ratios whereas FI to FII-type rocks have mantle-like $^{206}Pb/^{204}Pb$ ratios. Rhyolites from the WGB have the most enriched Pb isotopic signature ($^{206}Pb/^{204}Pb > 50$).

Whole-rock Pb isotopic analyses on massive to semi-massive sulphides from VMS and magmatic Ni-Cu sulphide deposits were analyzed to determine the variation in crustal source for the sulphides. In general, the ranges of $^{206}Pb/^{204}Pb$ and $^{207}Pb/^{204}Pb$ ratios for sulphides and hosting mafic assemblages formed a single isochron (or metachron) (**Figure 4.13**). Sulphide samples from the large, past-producing VMS mines (Winston Lake, Geco, Willroy) show mantle-like $^{206}Pb/^{204}Pb$ (13.2 to 13.8) and $^{207}Pb/^{204}Pb$ (14.4 to 14.6) ratios that are similar to sulphides from past-producing VMS deposits in the Abitibi subprovince (e.g., Vervoort et al., 1994). The VMS prospects from the VGB and SGB have higher $^{206}Pb/^{204}Pb$ (14.0 to 15.2) and $^{207}Pb/^{204}Pb$ (14.7 to 14.9) than the MGB and WGB sulphides. Past producing magmatic sulphide mines in the SGB also have an elevated Pb isotope ratio, with the North Coldstream deposit showing enriched radiogenic lead isotopic signatures. The isotopic composition of the North Coldstream deposit is significantly different than those collected from other ca. 2720 Ma sulphides and makes the interpreted magmatic origin of this deposit suspicious. It is possible that the isotopic composition of this sample is being influenced by radiogenic gangue minerals, like rutile, that are common in the North Coldstream host rocks (Lavigne and Scott, 1993).

Limited available data on the isotopic composition of galena from the VMS deposits in these belts (Thorpe, 2008) indicate that $^{206}Pb/^{204}Pb$ (13.2 to 13.4) and $^{207}Pb/^{204}Pb$ (14.4 to 14.6) ratios from each belt are very similar. Data collected from galena at the Calvert-Stares VMS occurrence in the SGB have the highest Pb isotopic values in this range. Whole-rock sulphide

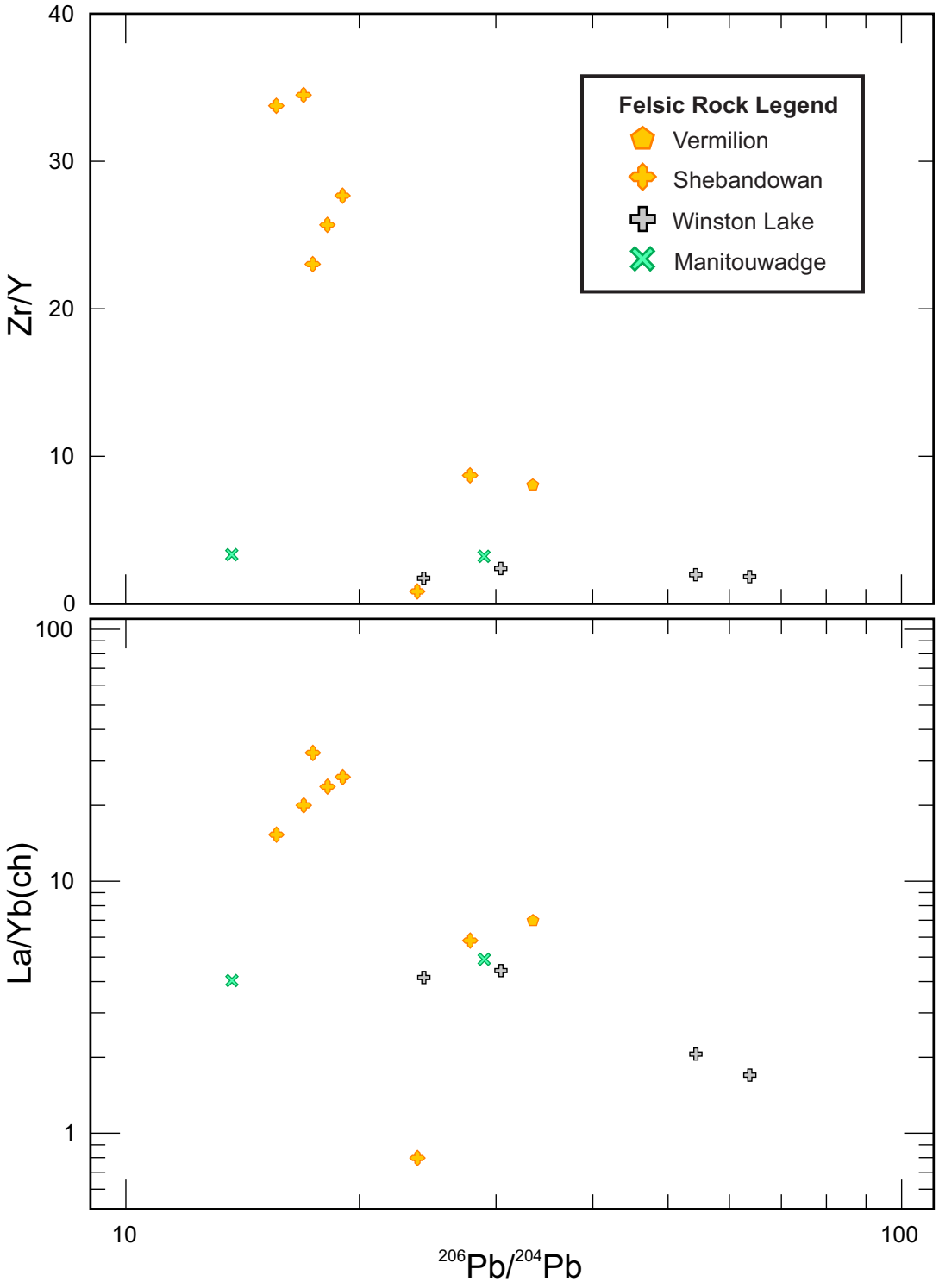

Figure 4.12 – Plot of $^{206}Pb/^{204}Pb$ versus Zr/Y ratio and chondrite-normalized La/Yb ratio for felsic rocks from the ca. 2720 Ma greenstone belt assemblages of the Wawa subprovince.

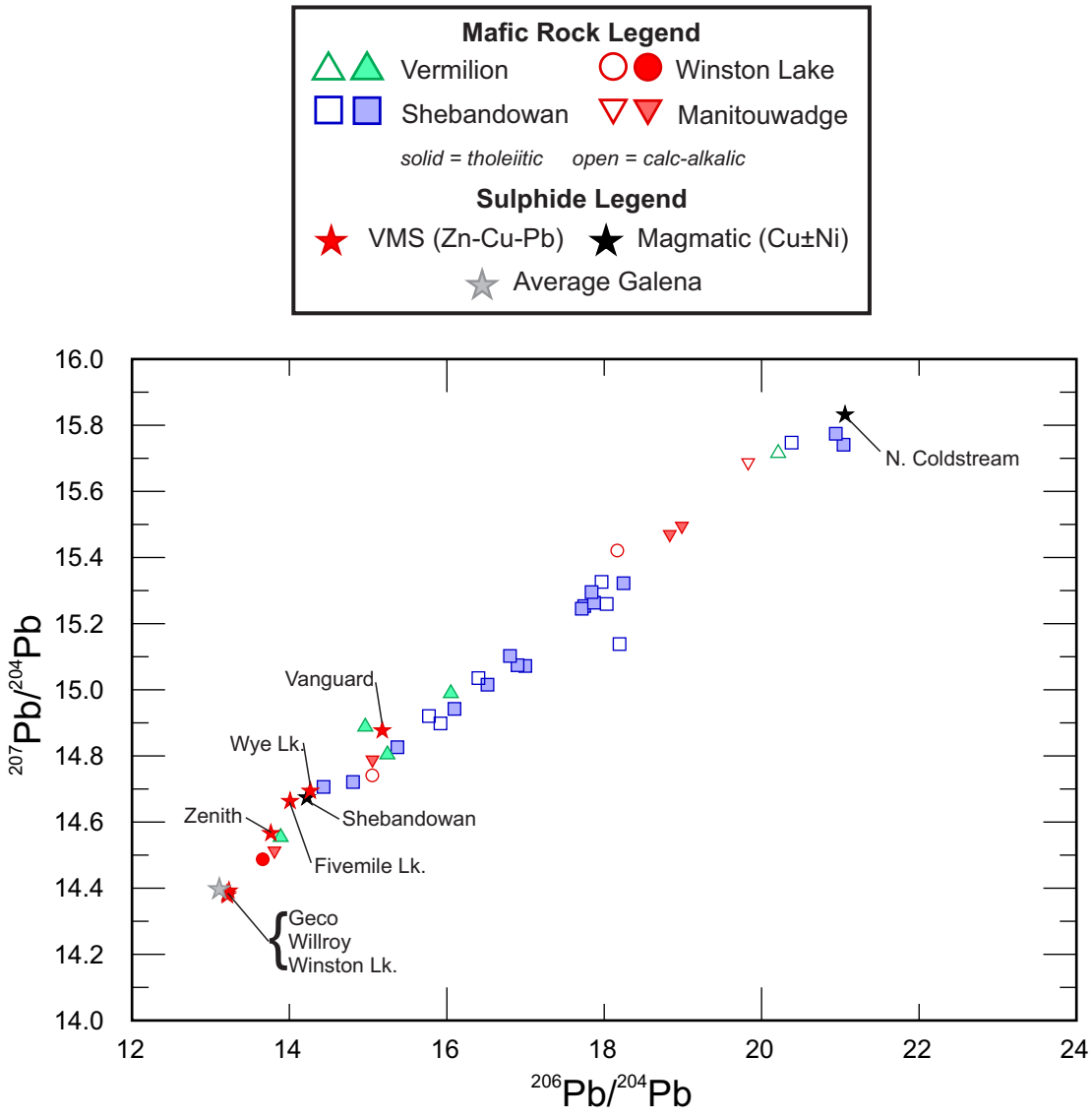

Figure 4.13 – Plot of $^{206}Pb/^{204}Pb$ versus $^{207}Pb/^{204}Pb$ for mafic rocks and sulphide mineralization (whole rock) from the ca. 2720 Ma greenstone belt assemblages of the Wawa subprovince. Open symbols represent samples with calc-alkalic magmatic affinity whereas closed symbols represent samples with tholeiitic magmatic affinities. Average galena isotopic composition is representative of galena compositions from VMS deposits from these belts (Thorpe, 2008).

analyses presented in this study show a larger range in Pb isotopic composition and may be a result of radiogenic Pb input from gangue silicate minerals. However, the massive sulphide sample from the Winston Lake main ore body contained up to 25% gangue minerals, but yet was one of the most isotopically juvenile samples analyzed.

4.6. Discussion

4.6.1 Petrogenesis of the ca. 2720 Ma Wawa Subprovince Greenstone Belts

There are several subtle differences in the trace element geochemistry and isotopic characteristics between each greenstone belt that suggest differences in their volcanic and geodynamic environments. The trimodal compositional variation of the rocks from these belts (**Figure 4.6**) indicate that the differences in composition cannot be explained by fractional crystallization and require a different petrogenesis. The regional-scale metallogenic differences may be linked to variations in petrogenesis and geodynamic setting of these greenstone belt assemblages.

The 2720 Ma assemblages of the VGB are dominated by mafic to intermediate lithofacies; felsic lithofacies are uncommon (**Figure 4.6**). Both the Lower and Upper Ely Members of the Soudan belt have a calc-alkalic, arc-like basalt to andesite base with pronounced negative Nb and Ti anomalies, lower normalized Nb/Th ratios, and enriched LREE (**Figure 4.7**). These sequences grade into volcanic lithofacies with a tholeiitic back-arc affinity that have weakly negative Nb and Ti anomalies, normalized Nb/Th ratios that are close to 1, and have flat to gently sloping REE patterns (**Figure 4.7**). MORB-like mafic lithofacies are present in the uppermost part of the Lower Ely member at the base of the Soudan Iron Formation (Hudak et al., 2012). The systematic variation of basalt geochemistry throughout the strata of the Soudan belt suggests that the volcanic strata and iron formations were emplaced during arc-rifting that evolved into a mature back arc as is documented in modern back-arc systems (e.g., Lau Basin; Taylor and Martinez, 2003). The deposition of the Soudan Iron Formation is associated with the development of mature back-arc. Lower positive εNd values (<1.8) and enriched $^{206}Pb/^{204}Pb$ (>20) ratios in association with higher La/Yb and lower Nb/Th ratios (**Figures 4.9 and 4.11**) suggest that arc-like magmas have interacted with an evolved upper crust that is of similar or slightly older age. The presence of FII-type felsic rocks and VMS mineralization (Fivemile Lake) in mafic-dominated strata is further evidence for an extensional rift-type setting and the

presence of these felsic rocks often records the onset of extensional tectonics (e.g., Hart et al., 2004; Franklin et al., 2005). The temporal change from arc-like to back-arc-like volcanism has been documented in other VMS-hosting sequences (Snow Lake, Galley et al., 1993; Flin Flon, DeWolfe et al., 2009). The Newton belt contains ultramafic lithofacies (Southwick et al., 1998) which require a high amount of partial melting of a mantle plume (Campbell and Griffiths, 1990) and thickened lithosphere where melting can occur at higher pressures (Begg et al., 2010). The presence of arc-like and back-arc basalts in the Newton belt suggests an arc-plume interaction where thicker arc crust was rifted via a mantle plume (Wyman and Kerrich, 2010) or rifting of thicker crust resulted in rapid upwelling of the asthenosphere. The ultramafic rocks likely represent the onset of this interaction before development of the back-arc rift. However, complex structural imbrication and transpressional shear zones limit our understanding of the original stratigraphic succession in the Newton belt (Jirsa et al., 1992).

The SGB contains a large proportion of intermediate volcanic rocks relative to mafic volcanic rocks in comparison to the other greenstone belts. These intermediate rocks are large, map-scale units and display a range in compositions from basaltic to andesitic on a trace element discrimination diagram (**Figure 4.7**). Virtually all of the intermediate rocks have a calc-alkalic affinity, have strongly negative Nb and Ti anomalies, and are enriched in Th with low primitive-mantle normalized Nb/Th ratios (0.1 to 1.0) (Lodge and Chartrand, 2013). Most of these andesites are classified as high Mg-andesite because of their high MgO (1.61 to 3.99 wt%), Cr (26-555 ppm), and Ni (18-188 ppm) (Kelemen, 1995; Polat and Kerrich, 2006; Manya et al., 2007). High-Mg andesitic rocks have been attributed to hybridization of subducted slab melts with melts derived from the peridotitic mantle wedge in “hot” subduction zones (Kelemen, 1995; Polat and Kerrich, 2006). Arc-like basalts with pronounced negative Nb and Ti anomalies and low normalized Nb/Th ratios (**Figure 4.7**) are also likely generated by melting of an enriched mantle wedge above a subduction zone (Polat and Kerrich, 2002). The locally abundant ultramafic rocks and differentiated gabbroic intrusions of the SGB indicate generation via melting of a mantle plume (Sproule et al., 2002; Begg et al., 2010). The rapid crustal thickening and compressional tectonics associated with “hot” subduction (Iwamori, 2000) may have provided sufficient lithospheric pressure to produce large-volume ultramafic melts during plume ascent (Herzberg and O'Hara, 2002) and maintain juvenile εNd signatures. The dominance of back-arc to MORB-like basalt in close spatial relationship with ultramafic rocks suggests that

plume interaction may have initiated arc-rifting resulting in the onset of rift-type magmatism. There is a crude spatial relationship between FI-type felsic volcanic rocks and large abundance of intermediate lithofacies in the SGB (e.g., Mud Lake prospect area; see **Figure 4.3**) supporting the hypothesis that the SGB had a thicker volcanic arc crust, whereas FII-type felsic rocks are generally associated with back-arc basalt-dominated regions (Lodge and Chartrand, 2013).

In the WGB, the change from a calc-alkalic to transitional arc-like to back-arc geochemistry (strong negative Nb and Ti anomalies, low normalized Nb/Th ratio) in the lowermost strata to a mature tholeiitic back-arc geochemistry (weak negative Nb and Ti anomalies, normalized Nb/Th ratio ~ 1) in the youngest strata (Lodge et al., in press) is interpreted to reflect arc-rifting and back-arc development. The predominately bimodal mafic-felsic composition of the Winston Lake assemblage is also characteristic of a rift-type setting (e.g., Franklin et al., 2005). FIII-type felsic lithofacies enriched in radiogenic Pb (**Figure 4.12**) indicate an upper crustal source that was dominated by mainly juvenile material based on relatively high εNd values (>1.8) (**Figure 4.10**). The uppermost strata of the WGB are dominated by alkalic OIB-like mafic flows and sills that have enriched incompatible elements (**Figure 4.7**) and high Ti/V ratios (Lodge et al., in press). The spatial association of alkalic OIB basalts and tholeiitic back-arc basalts are commonly linked to plume-driven rifting of an evolved volcanic environment (e.g., Piercey, 2007). Reworked felsic volcaniclastic rocks in the lowermost strata of the Winston Lake assemblage contains inherited 2780-2750 Ma zircons (Lodge et al., in press). The low positive εNd values for felsic volcanic rocks (+0.2) and the most enriched radiogenic Pb isotopes in this study (**Figure 4.11 and 4.12**) suggests a relatively evolved crust prior to the development of the strata currently exposed within the WGB. Felsic rocks from the Wawa greenstone belt have similarly high Pb isotopic compositions (Thorpe, 2008) where significantly older crustal material is exposed as narrow supracrustal slivers (Ayer et al., 2010) and is evident via the Hf-isotopic compositions of inherited zircons (Ketchum et al., 2008). Felsic rocks from classically juvenile greenstone belts, such as the southern Abitibi greenstone belt (e.g., Ketchum et al., 2008), have much lower abundances of radiogenic lead (Moritz et al., 1991; Thorpe, 2008).

The MGB was likely deposited in a juvenile back-arc setting because of the predominately bimodal mafic-felsic composition (**Figure 4.6**), dominance of tholeiitic, back-arc mafic rock geochemistry and FIII-type felsic lithofacies. Intense hydrothermal alteration,

deformation, and metamorphic recrystallization make interpretations of the original sequence of strata nearly impossible (Zaleski and Peterson, 1995; Peterson and Zaleski, 1999). However, the relatively high εNd values (>1.8) and insignificant enrichment of radiogenic Pb isotopes relative to the other belts suggests that the MGB is the most juvenile assemblage that was examined in this study. Geochronological studies did not find any inherited zircons to suggest the presence of older igneous material during petrogenesis (Zaleski et al., 1999). A juvenile back-arc setting for the MGB is consistent with previous regional interpretations (e.g., Kerrich et al., 2008; Polat, 2009).

4.6.2 Crustal Thickness/Maturity and VMS Metallogeny

The dominance of positive εNd values indicates that significantly older crust is largely absent from the western Wawa subprovince. The oldest dated igneous rock in the greenstone belts examined is from a tonalitic gneiss south of the SGB that has a U-Pb zircon age of 2750 Ma (Corfu and Stott, 1998). Although, detrital zircon analyses within Timiskaming-type syn-deformation basins in the VGB and SGB yielded U-Pb ages >2750 Ma, these older zircons may have been transported from adjacent subprovinces during terrane accretion in a foreland basin environment (Lodge et al., 2013). Detrital zircon analyses in the WGB have yielded 2780-2750 Ma inherited zircons in reworked volcaniclastic rocks that have a similar FIII-type felsic geochemistry and trace element ratios to felsic volcanic lithofacies in the belts (Lodge et al., in press). However, the nature and provenance of these clastic to volcaniclastic lithofacies in the WGB remain poorly constrained. In the southeastern part of the Wawa subprovince close to the Kapuskasing Structural Zone (**Figure 4.1**), slivers of 2.9 Ga supracrustal assemblages are present (Ayer et al., 2010) and may represent an older cratonic root of the Wawa subprovince that was rifted in the Neoarchean and formed the source of oldest inherited zircons and evolved Hf isotopic signatures in the region (Ketchum et al., 2008; Ayer et al., 2010). However, this old protocontinent does not appear to affect the isotopic signatures for most of the northern Wawa subprovince greenstone belt assemblages (e.g., Polat and Kerrich, 2002). Lower εNd values for the VGB, SGB, and MGB (-0.2 to 1.5) are suggestive, but not indicative of contamination with slightly older crust, especially because of moderate correlations with normalized La/Yb and Nb/Th ratios. Similar trace element correlations with $^{206}Pb/^{204}Pb$ also support the crustal contamination of the mantle-derived melts (Zartman and Doe, 1981). However, low positive εNd values with similar ranges documented elsewhere in the Wawa (Polat and Kerrich, 2002) and

Abitibi (Ketchum et al., 2008) subprovinces have been interpreted to be juvenile, and any variation in εNd values has been mostly attributed to a heterogeneous mantle source region (Vervoort et al., 1994). Whereas these studies have sampled across many different greenstone belts throughout the subprovinces, sampling in this study targeted volcanic rocks of the same age within the same tectonostratigraphic interval along the northern margin of the Wawa subprovince in an effort to minimize temporal and spatial variation in mantle composition. Hf isotopic studies in the western Wawa subprovince could help to resolve the nature of the crust in the northern Wawa subprovince greenstone belts since it is better at detecting older crust than the Nd isotopic system (e.g., Ketchum et al., 2008).

The formation of VMS deposits is favoured in extensional tectonic settings and deeper water depositional environments where volcanic edifices are undergoing subsidence (Franklin, 2005; Galley et al., 2007). In these environments VMS deposits are best developed during a hiatus in volcanism and development of a convective hydrothermal system. These hiatuses are often marked by the deposition of thin siliciclastic units and in some cases iron formation (e.g., Bathurst Mining Camp, Goodfellow, 2007). These conditions appear to have been fully satisfied in the MGB where significant VMS deposits are spatially associated with iron formation and bimodal volcanic rocks that have FIII-type geochemistry. The Nd and Pb isotopic compositions of the MGB volcanic rocks are the most juvenile of any within the greenstone belts examined in this study and show no evidence of isotopic enrichment or crustal contamination. The bimodal, rifted-arc setting for the WGB also contains the economic Winston Lake VMS deposit where a siliceous, mixed-provenance volcaniclastic unit defines the ore interval and marks a brief hiatus in volcanism (Lodge et al., in press). A rifted mature arc system, as evidenced by a more evolved Nd and Pb isotopic signature and the presence of older detrital zircons, may explain the composition of the ores in the WGB. The pre-rifting, mature arc may have been associated with a shallower water environment as suggested by the dominance of variably reworked volcaniclastic deposits in the lowermost parts of the WGB. A comparatively shallower water environment is also indicated by the presence of cross-bedded and ripple-laminated volcaniclastic deposits along strike from the Winston Lake Main ore body (Lodge et al., in press). However, in most instances, deformation, alteration, and metamorphism obscure or completely destroy any field evidence of shallower water. Nevertheless, the composition of the VMS ore bodies may provide independent evidence for the water depth during formation of the deposits. The dominance of Zn relative to

Cu in the VMS deposits of the WGB (Zn:Cu = 15-30:1; unpublished Inmet Mining Corporation data) suggests that the hydrothermal fluids were at a low temperature (≤ 300 °C) at the site of discharge and sulphide deposition (Hannington et al., 2005), possibly due to boiling and cooling of the hydrothermal fluid in shallow water conditions.

Despite having several VMS prospects, the SGB and VGB have yet to contain an economic VMS deposit. There are several potential reasons for the absence of economic VMS deposits in these belts. Although the VGB is interpreted to have formed in an extensional tectonic setting recorded as rifted arc cycles in the Soudan belt, the highly amygdaloidal mafic flows (>20%), the presence of large (>2 cm) oval amygdules, and the abundance of scoria-rich volcaniclastic lithofacies appear to indicate shallower water deposition (Hudak et al., 2004). Zn-mineralization at the Fivemile Lake VMS is generally iron-poor sphalerite and occurs as epithermal-like stringer mineralization that was likely deposited in a boiling hydrothermal system in relatively shallow water (Hudak et al., 2002; Hudak et al., 2012). Likewise, areas of extensional tectonics in the SGB (Lodge and Chartrand, 2013) appear to coincide with similar mafic lithofacies and volcanic textures as those in VGB and likely also indicate shallower water environments. Accretionary lapilli in intermediate volcaniclastic lithofacies of the SGB (Lodge et al., 2012) indicate the presence of a subaerial pyroclastic eruption column (Schumacher and Schmincke, 1995). A shallow water deposition is also suspected based on the mineralogy and composition of the VMS mineralization and alteration assemblages in the SGB. The dominance of siderite and chloritoid alteration associated with the Vanguard VMS prospect (Farrow, 1993; Lodge and Chartrand, 2013) is typical of Mattabi-type alteration systems. At the Mattabi VMS deposit, the siderite and chloritoid alteration is interpreted to form in relatively shallow water during effervescence of CO_2 that was derived from magmatic fluids (Morton et al., 1991; Franklin, 1997) or CO_2-enriched seawater. The Calvert-Stares VMS prospect is dominated by Zn-Au mineralization and muscovite and iron-carbonate alteration (Bottrill, 2003) and is typical of a boiling hydrothermal system that may have had input from magmatic fluids resulting in a volatile-rich hydrothermal fluid capable of mobilizing gold (Hannington et al., 1995; Dubé et al., 2007). However, it should be noted that the above evidence for relatively shallow water deposition only restricts the environment of deposition for the strata observed. It is not possible, based on the scale that data was collected, to completely exclude a deeper water depositional environment within the VGB and SGB because of the structural complexity and the sheer size of

these belts. Such deeper water environments may not have preserved environmental indicators in the volcanic lithofacies, or may not have been exposed and described during field work.

In terms of thickened crust, both the VGB and SGB have Pb-isotopic signatures that may indicate interaction with crustal material enriched in radiogenic lead. The SGB is interpreted to be a mature volcanic arc, and the occurrence of high Mg-andesites suggests more rapid thickening of the crust during a dominantly compressional tectonic regime (e.g., Southern Andes: Kay et al., 2005), which is an environment that is not commonly associated with the formation of VMS deposits (Franklin et al., 2005; Galley et al., 2007).

4.6.3 Comparison to Abitibi Greenstone Belt

The ca. 2720 Ma assemblages of the Wawa subprovince are similar in age to the Stoughton-Roquemaure assemblage (2723-2720 Ma) of the Abitibi subprovince (Ayer et al., 2002). The petrogenetic model of the Stoughton-Roquemaure assemblage is one of a mantle plume rising below an arc (the ca. 2730 Ma Deloro assemblage) causing rifting and emplacement of ultramafic rocks, tholeiitic basalts, and local felsic lithofacies (Dostal and Mueller, 1997). The Stoughton-Roquemaure assemblage is not VMS endowed, but does contain the Au-rich Estrades VMS deposit (Goutier et al., 2010). The ultramafic rocks of the Stoughton-Roquemaure assemblage typically do not show trace element evidence for crustal contamination (Sproule et al., 2002), nor do they host magmatic Ni-Cu-PGE deposits (Houlé and Lesher, 2011). εNd values for the Stoughton-Roquemaure assemblage have a similar range to the greeenstone belts examined in this study (Ayer et al., 2002; Ketchum et al., 2008).

A detailed systematic comparison of the Stoughton-Roquemaure assemblage has not been completed at a similar scale as for the 2720 Ma greenstone belts of the Wawa subprovince presented herein. The interpreted geodynamic setting of the Stoughton-Roquemaure assemblage is broadly similar to that of the Western Wawa subprovince greenstone belts. The VGB, SGB, and WGB are all interpreted to have some component of arc-rifting in their tectonic history associated with mantle plumes. The gold-rich Estrades VMS deposit in the Stoughton-Roquemaure assemblage and most of the VMS mineralization from the ca. 2720 Ma greenstone belt assemblages of Wawa subprovince belts may indicates that these VMS-forming events likely occurred in similar, relatively shallower water settings. The preservation and relative dominance of arc-like mafic lithofacies and high-Mg andesites indicate that the SGB is relatively unique among these belts in that there is preservation of a pre-rift arc assemblage. It is possible

that the thickened arc crust, a result of hot shallow subduction, and subsequent plume interaction could have created the right conditions for production of greater volumes of ultramafic magmas and the endowment of magmatic Ni-Cu sulphide deposits (Begg et al., 2010) relative to the Stoughton-Roquemaure assemblage.

The variation in geodynamic settings across the Wawa-Abitibi terrane at ca. 2720 Ma may be explained by an Archean microplate tectonic model where smaller, faster-moving plates result in a complex array of volcanic styles and tectonic stress regimes (Martin, 1986). Variation in geodynamic setting can also be explained by lateral changes in the nature of the overriding or subducting plate. The preservation of magmas generated in a low-angle, "hot" subduction setting in the SGB is consistent with this interpretation. Volcanic styles, stress regimes, and back-arc spreading are all influenced by the horizontal angle of plate collision and dip angle of subduction, which is variable in modern microplate settings, such as in the southwest Pacific Ocean (Taylor and Martinez, 2003; Martinez and Taylor, 2006). Interaction with one or more mantle plumes may explain synchronous plume-driven rifting and komatiitic volcanism in both the Wawa and Abitibi subprovinces and would further complicate the volcanic and tectonic styles.

4.7. Summary and Conclusions

Systematic geological, geochemical and isotopic analyses of the ca. 2720 Ma greenstone belt assemblages of the northern margin of the Wawa subprovince has successfully illustrated how subtle variations in the petrogenesis, crustal structure, and geodynamic setting may explain the metallogenic differences between these belts. Most of the variations in the geodynamic setting are easily explained by a microplate tectonic model, where variations in subduction/collision angles and degree of interaction with mantle plumes result in differences in petrogenesis and tectonic stress regimes. The genesis and VMS metallogeny of each belt is summarized as follows.

- The Vermilion greenstone belt (VGB) in the Soudan belt, which is characterized by calc-alkalic, and arc-like mafic rock geochemistry that transition to tholeiitic, back-arc to MORB-like mafic rock geochemistry upward in the strata, indicates progressive rifting of an arc. Nd and Pb isotopes indicate interaction with a juvenile, but differentiated crust that is of similar age. The VMS prospects in this region have epithermal-like stringer Zn

mineralization and are associated with FII-type rhyolites and mafic lithofacies that have relatively shallower-water features. The ultramafic-bearing Newton belt is not as well understood but the presence of arc-like basalts and ultramafic rocks suggests plume interaction in a rifted arc environment. There are no known magmatic Ni-Cu sulphide occurrences in the Newton belt.

- The Shebandowan greenstone belt (SGB) is the largest and most complex belt. The SGB has a significant proportion of andesite, high Mg-andesite, and calc-alkalic, arc-like basalts suggesting that a portion of the belt was generated via low-angle "hot" subduction. Ultramafic rocks in association with tholeiitic back-arc basalts and FII-type rhyolites indicate that rifting of this arc was plume-driven. VMS prospects have mineralization and alteration characteristics that are compatible with a relatively shallower-water environment. Nd and Pb isotopes hint at interaction with juvenile to slightly older, differentiated crust during petrogenesis. The predominately compressional stress regime during "hot" subduction is not as favourable for the formation of VMS, but may have contributed to rapid crustal thickening that is required to maintain relatively juvenile εNd values, allow for the production of higher volumes of ultramafic melts and formation of magmatic Ni-Cu sulphides, and may have produced favourable conditions for gold enrichment.
- The Winston Lake greenstone belt (WGB) is characterized by calc-alkalic to transitional arc-like to back-arc basaltic melts in the lowermost parts of the strata in association with FIII-type rhyolites. Basaltic rocks transition to a tholeiitic back-arc geochemistry above the VMS-hosting strata and are capped by alkalic, OIB-like basalts in the uppermost parts of the succession. The back-arc—OIB association is typical of rifting a mature arc system. Nd and Pb isotopic characteristics, like the SGB, are compatible with interaction with a juvenile to slightly older, differentiated crust during petrogenesis. VMS mineralization is Zn-dominated and likely developed in a relatively lower-temperature hydrothermal system and is spatially associated with a volcaniclastic lithofacies that indicates a hiatus in volcanism.
- The Manitouwadge greenstone belt (MGB) is characterized by a dominance of FIII-type felsic lithofacies and tholeiitic to transitional back-arc mafic lithofacies that were likely deposited in a back-arc setting. Nd and Pb isotopes indicate that the rocks were juvenile

and show no evidence for interaction with an older differentiated crust. Zn-Cu VMS mineralization is mostly associated with extensive iron formation and a hiatus in volcanism assisting the deposition and accumulation of sulphides from the hydrothermal fluids.

4.8. Considerations for Future Metallogenic Research

The regional comparison of crustal architecture and petrogenesis in these greenstone belts also highlighted several key differences that may have important implications for magmatic sulphide and gold metallogeny. In particular, the thickened crustal architecture and plume interaction interpreted at the SGB may explain the relative prosperity in Ni-Cu and Au mineralization relative to the other greenstone belts in this study. While the nature of this study cannot address the metallogeny of these deposit types fully, the results may have important implications for their genesis in the SGB and other greenstone belts in other Archean terranes.

The geochemistry of the komatiitic rocks in the SGB and their association with magmatic Ni-Cu sulphide deposits supports thickened crustal architecture of this part of the Wawa subprovince. Plume interaction associated with a thickened lithosphere or cratonic margin is generally the favoured environment for the formation for Ni-Cu-hosting ultramafic rocks (e.g., Begg et al., 2010). High temperature plumes are able to melt larger amounts of sublithospheric mantle under higher pressures without losing heat or magma to the crust. These large volume melts are then able to interact with large amounts of crust to assimilate more external sulphur required for deposit genesis (Herzberg and O'Hara, 2002). MORB-like geochemistry, massive sheet-like flows, and ultramafic rocks are locally associated with the rift-type assemblages in the SGB, suggesting that magma production and eruption rates were rapid (Griffiths and Fink, 1992; Gibson et al., 1999). These conditions are commonly found when a plume interacts with a cratonic margin or thickened crust. The negative Nb and Ti and positive Zr anomalies in the ultramafic rocks of the SGB indicate that there was some degree of crustal contamination during petrogenesis or emplacement of these magmas (Sproule et al., 2002).

The VGB and WGB also are interpreted to have plume interaction with isotopically differentiated crust resulting in the emplacement of ultramafic rocks and differentiated gabbroic intrusions. Was this pre-plume crust thick enough to generate large volumes of ultramafic rocks and would these melts be able to achieve sulphur saturation as they did in the SGB? The

geochemistry of the ultramafic assemblages in the Newton belt of the VGB is poorly constrained and significantly more research is needed to assess the Ni-Cu-PGE prospectivity of this area. However, it is conceivable that the Zenith gabbro in the WGB has assimilated sulphur because it is intruded into sulphide-rich, altered volcanic strata and has entrained VMS mineralization. The Zenith Gabbro has not been mapped in detail and is laterally extensive along the southern margin of the greenstone belt (**Figure 4.4**).

The SGB is the only greenstone belt in this study to have hosted a past-producing gold mine and is host to several advanced gold prospects (Jobin-Bevans et al., 2006; Leonard and Ilieva, 2008; Risto and Breede, 2010). Most of these deposits are associated with post-2720 Ma structures and magmatism associated with terrane accretion (Stott and Schnieders, 1983; Corfu and Stott, 1998; Lodge et al., 2013). Gold mining in the Hemlo greenstone belt of the Wawa subprovince is also younger (ca. 2700-2690 Ma: Muir, 2003), these post-magmatic gold deposits are not discussed in this manuscript. However, an important component of some recent models for the generation of gold mineralization in accretionary origins is an Au-enriched mantle source region that can be accessed during later accretionary events (Hronsky et al., 2012). The SGB is the only belt in this study that contains subduction-dominated petrogenetic assemblages and an abundance of high-Mg andesites. The interpreted “hot”, low-angle subduction setting for the SGB is ideal for upper mantle enrichment, where low-degrees of partial melting can enrich, and compressional tectonics can inhibit passage of some of these melts to the surface (e.g., Kay et al., 2005). This Au-enriched lithosphere is then tapped by melts produced during subsequent deformation during terrane accretion. Additional Au-enrichment may have occurred in the upper crust during the development of VMS-forming systems in shallow-water environments, as evidenced by the Zn-Au Calvert-Stares VMS occurrence (Bottrill, 2003). The combination of mantle and upper crustal Au-enrichment processes may be the main attributing factor for the relatively high gold prospectivity of the SGB compared to the other greenstone belts in this study. It would be interesting to compare gold occurrences in the SGB to determine the variation in gold sources, how the gold was initially deposited, and how this gold was subsequently transported during later deformation events.

4.9. References

Ayer, J.A., Amelin, Y., Corfu, F., Kamo, S.L., Ketchum, J., Kwok, K., Trowell, N., 2002. Evolution of the southern Abitibi greenstone belt based on U–Pb geochronology: autochthonous volcanic construction followed by plutonism, regional deformation and sedimentation. Precambrian Research 115, 63-95.

Ayer, J.A., Goutier, J., Thurston, P.C., Dubé, B., Kamber, B.S., 2010. Tectonic and metallogenic evolution of the Abitibi and Wawa Subprovinces; *in* Summary of Field Work and Other Activities, Open File Report 6260. Ontario Geological Survey, pp. 3-1 to 3-6.

Begg, G.C., Hronsky, J.A.M., Arndt, N.T., Griffin, W.L., O'Reilly, S.Y., Hayward, N., 2010. Lithospheric, cratonic, and geodynamic setting of Ni-Ci-PGE sulphide deposits. Economic Geology 105, 1057-1070.

Belshaw, N.S., Freedman, P.A., O'Nions, R.K., Frank, M., Guo, Y., 1998. A new variable dispersion double-focusing plasma mass spectrometer with performance illustrated for Pb isotopes. International Journal of Mass Spectrometry 181, 51-58.

Bottrill, T.J., 2003. NI 43-101 Technical Report on the Stares-Calvert Project, Adrian, Aldina, Marks, and Sackville Townships, Shebandowan Belt, Thunder Bay District, Ontario. RJK Explorations Ltd. and GLR Resources Inc., 52 p.

Brown, G.H., Fogal, R.I., 1995a. Precambrian geology, Oliver Township. Ontario Geological Survey, Map 2615, 1:20,000.

Brown, G.H., Fogal, R.I., 1995b. Precambrian geology, Ware Township. Ontario Geological Survey, Map 2616, 1:20,000.

Burnham, O.M., 2008. Trace element analysis of geological samples by inductively coupled plasma mass spectrometry (ICP-MS) at the Geoscience Laboratories: Revised capabilities due to method improvements; *in* Summary of Field Work and Other Activities, Open File Report 6226. Ontario Geological Survey, pp. 38-31 to 38-10.

Burnham, O.M., Hechler, J.H., Semenyna, L., Schweyer, J., 2002. Mineralogical controls on the determination of trace elements following mixed acid dissolution; *in* Summary of Field Work and Other Activities, Open File Report 6100. Ontario Geological Survey, pp. 36-31 to 36-12.

Campbell, I.H., Griffiths, R.W., 1990. Implications of mantle plume structure for the evolution of flood basalts. Earth and Planetary Science Letters 99, 79-93.

Campbell, I.H., Lesher, C.M., Coad, P., Franklin, J.M., Gorton, M.P., Thurston, P.C., 1984. Rare-earth element mobility in alteration pipes below massive Cu-Zn-sulphide deposits. Chemical Geology 45, 181-202.

Carter, M.W., 1982a. Precambrian geology of the Terrace Bay area, northeast sheet, Thunder Bay District. Ontario Geological Survey, Preliminary Map 2557, 1:15,840.

Carter, M.W., 1982b. Precambrian geology of the Terrace Bay area, northwest sheet, Thunder Bay District. Ontario Geological Survey, Preliminary Map 2556, 1:15,840.

Corfu, F., Stott, G.M., 1986. U-Pb ages for late magmatism and regional deformation in the Shebandowan Belt, Superior Province, Canada. Can. J. Earth Sci. 23, 1075-1082.

Corfu, F., Stott, G.M., 1998. Shebandowan greenstone belt, western Superior Province: U-Pb ages, tectonic implications, and correlations. GSA Bulletin 110, 1467-1484.

Creaser, R.A., Erdmer, P., Stevens, R.A., Grant, S.L., 1997. Tectonic affinity of Nusultin and Anvil assemblage strata from the Telsin tectonic zone, northern Canadian Cordillera: Constraints from neodymium isotope and geochemical evidence. Tectonics 16, 107-121.

Davis, D.W., Schandl, E.S., Wasteneys, H.A., 1994. U-Pb dating of minerals in alteration halos of Superior Province massive sulfide deposits; syngenesis versus metamorphism. Contributions to Mineralogy and Petrology 115, 427-437.

DeWolfe, Y.M., Gibson, H.L., Piercey, S.J., 2009. Petrogenesis of the 1.9 Ga mafic hanging wall sequence to the Flin Flon, Callinan, and Triple 7 massive sulphide deposits, Flin Flon, Manitoba, canada. Can. J. Earth Sci. 46, 509-527.

Dostal, J., Mueller, W.U., 1997. Komatiite flooding of a rifted Archean rhyolite arc complex: geochemical signature and tectonic significance of the Stoughton-Roquemaure Group, Abitibi greenstone belt. Can. J. Earth Sci. 105, 545-563.

Driese, S.G., Jirsa, M.A., Ren, M., Brantley, S.L., Sheldon, N.D., Parker, D., Schmitz, M.D., 2011. Neoarchean paleoweathering of tonalite and metabasalt: Implications for reconstructions of 2.69 Ga early terrestrial ecosystems and paleoatmospheric chemistry. Precambrian Research 189, 1-17.

Dubé, B., Gosselin, P., Hannington, M.D., Galley, A.G., 2007. Gold-rich volcanogenic massive sulphide deposits; *in* Goodfellow, W.D. (Ed.) Mineral Deposits of Canada: A Synthesis of Major Deposit-Types, District Metallogeny, the Evolution of Geological Provinces, and Exploration Methods: Geological Association of Canada, Mineral Deposits Division, Special Publication No. 5, pp. 75-94.

Farrow, C.E.G., 1993. Base Metal Sulphide Mineralization, Shebandowan Greenstone Belt. Summary of Field Work and Other Activities 1993, Ontario Geological Survey, Miscellaneous Paper 162, 4-8 p.

Farrow, C.E.G., 1994. Base metal mineralization, Shebandowan Greenstone Belt, District of Thundey Bay, Ontario; *in* Summary of Field Work and Other Activities, Miscellaneous Paper 163. Ontario Geological Survey, pp. 97-104.

Forslund, N., 2012. Alteration and fluid characterization of the Hamlin Lake IOCG occurence, northwestern Ontario, Canada. M.Sc. Thesis, Lakehead University, 284 p.

Franklin, J.M., 1997. Lithogeochemical and mineralogical methods for base metal and gold exploration; *in* Gubins, A.G. (Ed.) Proceedings of Exploration 97: Fourth Decennial International Conference on Mineral Exploration, pp. 191-208.

Franklin, J.M., 2005. Notes on the Sungold Property Kashabowie area, Ontario for Freewest Resources Canada Ltd. Franklin Geosciences Ltd. for Freewest Resources Canada Ltd.

Franklin, J.M., Gibson, H.L., Jonasson, I.R., Galley, A.G., 2005. Volcanogenic massive sulphide deposits; *in* Hedenquist, J.F.H., Goldfarb, R.J., Richards, J.P. (Eds.), Economic Geology, 100th Anniversary Volume, pp. 523-560.

Galley, A.G., Bailes, A.H., Kitzler, G., 1993. Geological setting and hydrothermal evolution of the Chisel Lake and North Chisel Zn-Pb-Ag-Au massive sulphide deposit, Snow Lake, Manitoba. Exploration and Mining Geology 2, 271-295.

Galley, A.G., Hannington, M.D., Jonasson, I.R., 2007. Volcanogenic massive sulphide deposits; *in* Goodfellow, W.D. (Ed.) Mineral Deposits of Canada: A Synthesis of Major Deposit-Types, District Metallogeny, the Evolution of Geological Provinces, and Exploration Methods: Geological Association of Canada, Mineral Deposits Division, Special Publication No. 5, pp. 141-161.

Gibson, H.L., Morton, R.L., Hudak, G.J., 1999. Submarine volcanic processes, deposits, and environments favorable for the location of volcanic-associated massive sulphide deposits; *in* Barrie, C.T., Hannington, M.D. (Eds.), Volcanic-hosted massive sulfide deposits: Processes and examples in modern and ancient settings: Society of Economic Geologists Reviews in Economic Geology, pp. 13-51.

Goldstein, R.L., O'nions, R.K., Hamilton, P.J., 1984. A Sm-Nd isotopic study of atmospheric dusts and particulates from major river systems. Earth and Planetary Science Letters 70, 221-236.

Goodfellow, W.D., 2007. Metallogeny of the Bathurst Mining Camp, Northern New Brunswick; *in* Goodfellow, W.D. (Ed.) Mineral Deposits of Canada: A Synthesis of Major Deposit-Types, District Metallogeny, the Evolution of Geological Provinces, and Exploration Methods: Geological Association of Canada, Mineral Deposits Division, Special Publication No. 5, pp. 471-508.

Gorton, M.P., Schandl, E.S., 1995. An unusual sink for rare earth elements: the rhyolite-basalt contact of the Archean Winston Lake volcanogenic massive sulphide deposit, Superior Province, Canada. Economic Geology 90, 2065-2072.

Goutier, J., Mercier-Langevin, P., McNicoll, V.J., Ayer, J.A., 2010. The Abitibi subprovince, its evolution and its VMS deposits - an overview; *in* Yilgarn-Superior Workshop - Abstracts, Fifth International Archean Symposium, 10 September 2010: Geological Survey of Western Australia, Record 2010/20, pp. 51-56.

Griffiths, R.W., Fink, J.H., 1992. Solidification and morphology of submarine lavas: A dependence on extrusion rate. Journal of Geophysical Research: Solid Earth 97, 19729-19737.

Hannington, M.D., de Ronde, C.E.J., Petersen, S., 2005. Sea-floor tectonics and submarine hydrothermal systems; *in* Hedenquist, J.F.H., Goldfarb, R.J., Richards, J.P. (Eds.), Economic Geology, 100th Anniversary Volume, pp. 111-141.

Hannington, M.D., Poulsen, K.H., Thompson, J.F.H., Sillitoe, R.H., 1995. Volcanogenic gold in the massive sulfide environment. Reviews in Economic Geology 8, 325-356.

Hart, S.R., 1988. Heterogeneous mantle domains: signatures, genesis and mixing chronologies. Earth and Planetary Science Letters 90, 273-296.

Hart, T.R., 2007. Geochronology of the Hamlin and Wye Lakes Area, Shebandowan Greenstone Belt, Thunder Bay District; *in* Summary of Field Work and Other Activities, Open File Report 6213. Ontario Geological Survey, pp. 9-1 to 9-8.

Hart, T.R., Gibson, H.L., Lesher, C.M., 2004. Trace element geochemistry and petrogenesis of felsic volcanic rocks associated with volcanogenic massive Cu-Zn-Pb sulfide deposits. Economic Geology 99, 1003-1013.

Hart, T.R., Metsaranta, D.-A., 2009. Precambrian geology of the Wye and Hamlin Lakes area. Ontario Geological Survey, Preliminary Map P.2511, 1:20,000.

Herzberg, C.T., O'Hara, M.J., 2002. Plume-associated ultramafic magmas of Phanerozoic age. Journal of Petrology 43, 1857-1883.

Houlé, M.G., Lesher, C.M., 2011. Komatiite-associated Ni-Cu-(PGE) mineralization in the Abitibi Greenstone Belt, Ontario. Reviews in Economic Geology 17, 89-121.

Hronsky, J.A.M., Groves, D.L., Loucks, R.R., Begg, G.C., 2012. A unified model for gold mineralization in accretionary orogens and implications for regional-scale exploration targeting methods. Mineralium Deposita 47, 339-358.

Hudak, G.J., Heine, J., Jirsa, M., Peterson, D., 2004. Volcanic stratigraphy, hydrothermal alteration, and VMS potential of the lower Ely Greenstone, Fivemile Lake to Sixmile Lake area; *in* Institute on Lake Superior Geology, 50th Annual Meeting, Thunder Bay, ON, v. 50, Part 2, pp. 1-44.

Hudak, G.J., Heine, J., Lodge, R.W.D., Jansen, A., 2012. Recent developments understanding the volcanic, magmatic, tectonic, and metallogenic evolution of the Ely Greenstone Formation, Vermilion District, NE Minnesota. Geological Association of Canada - Mineralogical Association of Canada, Abstracts and Program 35, 59.

Hudak, G.J., Heine, J., Newkirk, T., Odette, J.D., Huack, S., 2002. Comparative geology, stratigraphy, and lithogeochemistry of the Fivemile Lake, Quartz Hill, and Skeleton Lake VMS occurrences, Vermilion district, NE Minnesota. State of Minnesota: Natural Resources Research Institute Technical Report NRII/TR-2002/03, 390 p.

Iwamori, H., 2000. Thermal effects of ridge subduction and its implication for the origin of granitic batholith and paired metamorphic belts. Earth and Planetary Science Letters 181, 131-144.

Jirsa, M.A., Southwick, D.L., Boerboom, T.J., 1992. Structural evolution of Archean rocks in the western Wawa subprovince, Minnesota: refolding of precleavage nappes during D_2 transpression. Can. J. Earth Sci. 29, 2146-2155.

Jirsa, M.A., Starns, E.C., Schmitz, M.D., 2012. Bedrock geologic map of the 2006 Cavity Lake forest fire area, Boundary Waters Canoe Area Wilderness, northeastern Minnesota. Minnesota Geological Survey, Miscellaneous Map M-193, 1:24,000.

Jobin-Bevans, S., Kelso, I., Cullen, D., 2006. NI 43-101 Technical Report on the Tower Mountain Gold Deposit, Conmee Township, northwestern Ontario, Canada. ValGold Resources Ltd., 95 p.

Kay, S.M., Godoy, E., Kurtz, A., 2005. Episodic arc migration, crustal thickening, subduction erosion, and magmatism in the south-central Andes. Geological Society of America Bulletin 117, 67-88.

Keating, G.L., Burnham, O.M., 2012. Revision of the calibration for major element analysis of geological samples by wavelength dispersive X-ray fluorescence at the Geoscience Laboratories; *in* Summary of Field Work and Other Activities, Open File Report 6280. Ontario Geological Survey, pp. 39-31 to 39-34.

Kelemen, P.B., 1995. Genesis of high Mg# andesites and the continental crust. Contributions to Mineralogy and Petrology 120, 1-19.

Kerrich, R., Polat, A., Xie, Q., 2008. Geochemical systematics of a 2.7 Ga Kinojevis Group (Abitibi), and Manitouwadge and Winston Lake (Wawa) Fe-rich basalt-rhyolite associations: Backarc rift oceanic crust? Lithos 101, 1-23.

Ketchum, J.W.F., Ayer, J.A., Van Breemen, O., Pearson, N.J., Becker, J.K., 2008. Pericontinental crustal growth of the southwestern Abitibi subprovince, Canada - U-Pb, Hf, and Nd isotope evidence. Economic Geology 103, 1151-1184.

Lavigne, M.J., Aubut, A.J., Scott, J., 1990. Base metal mineralization in the Shebandowan Greenstone Belt; *in* Institute on Lake Superior Geology Proceedings, 35th Annual Meeting, v. 35, Part 2, Duluth, MN, pp. 67-97.

Lavigne, M.J., Scott, J.F., 1993. The North Coldstream mine, Burchell Lake, northwestern Ontario; *in* Institute on Lake Superior Geology Proceedings, 39th Annual Meeting, v. 39, Part 1, Eveleth, MN, p. 51.

Leonard, B., Ilieva, T., 2008. NI 43-101 Technical Report on the Goldcreek Property, Shebandowan area, Ontario, Canada. Mengold Resources Inc. and Solomon Resources Ltd., 93 p.

Lesher, C.M., Goodwin, A.M., Campbell, I.H., Gorton, M.P., 1986. Trace-element geochemistry of ore-associated and barren, felsic metavolcanic rocks in the Superior Province, Canada. Can. J. Earth Sci. 23, 222-237.

Lodge, R.W.D., 2011. A progress report on the volcanology, stratigraphy and geodynamic setting of greenstone belts of age 2720 Ma near the Wawa– Quetico Subprovincial boundary; *in* Summary of Field Work and Other Activities, Open File Report 6270. Ontario Geological Survey, pp. 11-11 to 11-13.

Lodge, R.W.D., 2012. Preliminary results of uranium–lead geochronology from the Shebandowan Greenstone Belt, Wawa Subprovince; *in* Summary of Field Work and Other Activities, Open File Report 6280. Ontario Geological Survey, pp. 10-11 to 10-10.

Lodge, R.W.D., Chartrand, J.E., 2013. Establishing regional geodynamic settings and the metallogeny of volcanogenic massive sulphide mineralization of greenstone belt assemblages (circa 2720 Ma) of the Wawa Subprovince via geochemical comparisons, Ontario Geological Survey, Miscellaneous Release - Data 306.

Lodge, R.W.D., Gibson, H.L., Stott, G.M., 2012. Trace element geochemistry and physical volcanology of the Shebandowan Greenstone Belt, Superior Craton, Canada; Implications for VMS mineralization and tectonic processes in the Neoarchean Geological Association of Canada - Mineralogical Association of Canada, Abstracts and Program 35, 80.

Lodge, R.W.D., Gibson, H.L., Stott, G.M., Franklin, J.M., Hamilton, M.A., in press. Geodynamic reconstruction of the VMS-hosting Winston Lake greenstone belt and VMS deposits: New trace element geochemistry and U-Pb geochronology. Economic Geology.

Lodge, R.W.D., Gibson, H.L., Stott, G.M., Hudak, G.J., Jirsa, M., 2013. New U-Pb geochronology from Timiskaming-type assemblages in the Shebandowan and Vermilion greenstone belts, Wawa Subprovince, Superior Craton: Implications for the Neoarchean development of the southwestern Superior Province. Precambrian Research 235, 264-277.

MacDonald, C.J.D., 2003. NI 43-101 Technical Report on the Big Duck Lake Project, Ontario. Tri-Alpha Investments Ltd., 46 p.

Manya, S., Maboko, M.A.H., Nakamura, E., 2007. The geochemistry of high-Mg andesite and associated adakitic rocks in the Musoma-Mara Greenstone Belt, northern Tanzania: Possible evidence for Neoarchean ridge subduction? Precambrian Research 159, 241-259.

Martin, H., 1986. Effect of steeper Archaean geothermal gradient on geochemistry of subduction zone magmas. Geology 14, 753-756.

Martinez, F., Taylor, B., 2006. Modes of crustal accretion in back-arc basins: Inferences from the Lau Basin. Geophysical Monograph Series 166, 5-30.

Moritz, R.P., Crocket, J.H., Dickin, A.P., 1991. Lead isotopic study of gold mineralization in the Dome mine quartz-fuchsite vein. Ontario Geological Survey, Open File Report 5743, 40 p.

Morton, P., 1982. Archean volcanic stratigraphy, and petrology and chemistry of mafic and ultramafic rocks, chromite, and the Shebandowan Ni-Cu Mine, Shebandowan, northwestern Ontario. Ph.D. Thesis, Carleton University, 346 p.

Morton, R.L., Walker, J.S., Hudak, G.J., Franklin, J.M., 1991. The early development of an Archean submarine caldera complex with emphasis on the Mattabi ash-flow tuff and its relationship to the Mattabi massive sulphide deposit. Economic Geology 86, 1002-1011.

Muir, T.L., 2003. Structural evolution of the Hemlo greenstone belt in the vacinity of the world-class Hemlo gold deposit. Can. J. Earth Sci. 40, 695-430.

Osmani, I.A., 1997a. Geology and mineral potential: Greenwater Lake area, West-Central Shebandowan Greenstone Belt. Ontario Geological Survey, Report 296, 135 p.

Osmani, I.A., 1997b. Precambrian geology, Begin, Lamport, and parts of Haines and Hagey townships, east half. Ontario Geological Survey, Map 2626, 1:20,000.

Osmani, I.A., 1997c. Precambrian geology, Begin, Lamport, and parts of Haines and Hagey townships, west half. Ontario Geological Survey, Map 2625, 1:20,000.

Osmani, I.A., 1997d. Precambrian geology, Burchell-Greenwater lakes area, west half. Ontario Geological Survey, Map 2622, 1:20,000.

Osmani, I.A., 1997e. Precambrian geology, Moss Township. Ontario Geological Survey, Map 2624, 1:20,000.

Pearce, J.A., 1996. A users guide to basalt discrimination diagrams. Trace Element Geochemistry of Volcanic Rocks: Applications for Massive Sulphide Exploration. Geological Association of Canada, Short Course Notes 12, 79-133 p.

Peterson, D., 2004. Bedrock geological and volcanogenic massive deposit mineral potential map of the Lower Ely Greenstone and Adjacent Areas: Soudan, Eagles Nest, and Bear Island 7.5 Quadrangles, St. Louis County, Northeastern Minnesota. Institute on Lake Superior Geology 50th Annual Meeting, Map for Field Trip 7., 1:20,000.

Peterson, D., Gallup, C., Jirsa, M., Davis, D.W., 2001. Correlation of the Archean assemblages across the U.S.-Canadian border: Phase I geochronology; *in* 47th Annual Meeting, Institute on Lake Superior Geology, Proceedings Volume 47, Part 1 - Program and Abstracts, pp. 77-78.

Peterson, D., Jirsa, M., 1999. Bedrock geologic map and mineral exploration data, western Vermilion district, St. Louis and Lake Counties, northeastern Minnesota. Minnesota Geological Survey, Miscellaneous Map M-98, 1:48,000.

Peterson, D.M., Patelke, R.D., 2003. National Underground Science and Engineering Laboratory (NUSEL): Geological site investigation for the Soudan Mine, northeastern Minnesota. State of Minnesota: Natural Resources Research Institute, Technical Report NRRI/TR-2003/29, 88 p.

Peterson, V.L., Zaleski, E., 1999. Structural history of the Manitouwadge greenstone belt and its volcanogenic Cu-Zn massive sulphide deposits, Wawa Subprovince, south-central Superior Province. Can. J. Earth Sci. 36, 605-625.

Piercey, S.J., 2007. An overview of the use of petrochemistry in regional exploration for volcanogenic massive sulfide (VMS) deposits; *in* Milkereit, B. (Ed.) Proceedings of

Exploration '07: Fifth Devennial International Conference on Mineral Exploration, pp. 223-246.

Polat, A., 2009. The geochemistry of Neoarchean (ca. 2700 Ma) tholeiitic basalts, transitional to alkaline basalts, and gabbros, Wawa Subprovince, Canada: Implications for petrogenetic and geodynamic processes. Precambrian Research 168, 83-105.

Polat, A., Hoffman, A.W., 2003. Alteration and geochemical patterns in the 3.7-3.8 Ga Isua greenstone belt, West Greenland. Precambrian Research 126, 197-218.

Polat, A., Kerrich, R., 2002. Nd-isotope systematics of ~2.7 Ga adakites, magnesian andesites, and arc basalts, Superior Province, Canada: Evidence for shallow crustal recycling at Archean subduction zones. Earth and Planetary Science Letters 202, 345-360.

Polat, A., Kerrich, R., 2006. Reading the geochemical fingerprints of Archean hot subduction volcanic rocks: Evidence for accretion and crustal recycling in a mobile tectonic regime. Geophysical Monograph Series 164, 189-213.

Polat, A., Kerrich, R., Wyman, D.A., 1999. Geochemical diversity in oceanic komatiites and basalts from the late Archean Wawa greenstone belts, Superior Province, Canada: trace element and Nd isotope evidence for a heterogeneous mantle. Precambrian Research 94, 139-173.

Pye, E.G., 1964. Mineral deposits of the Big Duck Lake area, district of Thunder Bay. Ontario Department of Mines Geological Report 27, 58 p.

Risto, R.W., Breede, K., 2010. NI 43-101 Technical Report on the Moss Lake Gold Property, including an updated mineral resource estimate, Moss Township, northwestern Ontario. Moss Lake Gold Mines Ltd., 106 p.

Ritcey, D.J., 1992. Geology and mineralization in the vicinity of Big Duck Lake, Ontario. M.Sc. Thesis, University of Ottawa, 235 p.

Ross, P.-S., Bédard, J.H., 2009. Magmatic affinity of modern and ancient subalkaline volcanic rocks determined from trace-element discriminant diagrams. Can. J. Earth Sci. 46, 823-839.

Santaguida, F., 2001. Precambrian geology compilation series - Thunder Bay sheet. Ontario Geological Survey, Map 2664, 1:250,000.

Schmidberger, S.S., Heaman, L.M., Simonetti, A., Creaser, R.A., Whiteford, S., 2007. Lu-Hf, in-situ Sr and Pb isotope and trace element systematics for mantle eclogites from the Daivik diamond mine: Evidence for Paleoproterozoic subduction beneath the Slave craton, Canada. Earth and Planetary Science Letters 254, 55-68.

Schumacher, R., Schmincke, H.-U., 1995. Models for the origin of accretionary lapilli. Bulletin of Volcanology 56, 626-639.

Severin, P.W.A., Balint, F., Sim, R., 1991. Geological setting of the Winston Lake massive sulphide deposit. Mineral Deposits in the Western Superior Province, Ontario, Geological Survey of Canada Open File 2164, 58-73 p.

Shervais, J.W., 1982. Ti-V plots and the petrogenesis of modern and ophiolitic lavas. Earth and Planetary Science Letters 59, 101-118.

Southwick, D.L., Boerboom, T.J., Jirsa, M., 1998. Geologic setting and descriptive geochemistry of Archean supracrustal and hypabyssal rocks, Soudan-Bigfork area, northern Minnesota: Implications for metallic mineral exploration. Minnesota Geological Survey, Report of Investigations 51, 69 p.

Spitz, G., Darling, R., 1978. Major and minor element lithogeochemical anomalies surrounding the Louvem copper deposit, Val d'Or, Quebec. Can. J. Earth Sci. 15, 1161-1169.

Sproule, R.A., Lesher, C.M., Ayer, J.A., Thurston, P.C., Herzberg, C.T., 2002. Spatial and temporal variations in the geochemistry of komatiites and komatiitic basalts in the Abitibi greenstone belt. Precambrian Research 115, 153-186.

Stott, G.M., 2011. A revised terrane subdivision of the Superior Province of Ontario. Ontario Geological Survey, Miscellaneous Release - Data 278, p.

Stott, G.M., Schnieders, B.R., 1983. Gold mineralization in the Shebandowan Belt and its relation deformation patterns; *in* The Geology of Gold in Ontario, Miscellaneous Paper 110. Ontario Geological Survey, pp. 181-193.

Sun, S., McDonough, W.F., 1989. Chemical and isotopic systematics of oceanic basalts: implications for mantle composition and processes; *in* Saunders, A.D., Norry, M.J. (Eds.), Magmatism in the Ocean Basins. Geological Society Special Publication 42, pp. 313-345.

Tanaka, T., Togashi, S., Kamioka, H., Amakawa, H., Kagami, H., Hamamoto, T., Yuhara, M., Orihashi, Y., Yoneda, S., Shimizu, H., Kunimaru, T., Takahashi, K., Yanagi, T., Nakano, T., Fujimaki, H., Shinjo, R., Asahara, Y., Tanimizu, M., Dragusanu, C., 2000. JNdi-1: A neodymium isotopic reference in consistency with La Jolla neodymium. Chemical Geology 168, 279-281.

Taylor, B., Martinez, F., 2003. Back-arc basin systematics. Earth and Planetary Science Letters 2003, 481-497.

Thorpe, R.I., 2008. Release of lead isotope data in 4 databases: Canadian, Western Superior, foreign, and whole rock and feldspar, Geological Survey of Canada, Open File 5664.

Todt, W., Cliff, R.A., Hanser, A., Hofmann, A.W., 1996. Evaluation of ^{202}Pb-^{205}Pb double spike for high-precision lead isotope analysis. Earth Process: Reading the Isotopic Code. Geophysical Monograph 95, 429-437.

Tosdal, R.M., Wooden, J.L., Bouse, R.M., 1999. Pb isotopes, ore deposits, and metallgenic terranes. Reviews in Economic Geology 12, 1-27.

Unterschutz, J.L.E., Creaser, R.A., Erdmer, P., Thompson, R.I., Daughtry, K.L., 2002. North American margin origin of Quesnel terrane strata in the southern Canadian Cordillera: Inferences from geochemical and Nd isotopic characteristics of Triassic metasedimentary rocks. Geological Society of America Bulletin 114, 462-475.

Vervoort, J.D., White, W.M., Thorpe, R.I., 1994. Nd and Pb isotope ratios of the Abitibi greenstone belt: new evidence for very early differentiation of the Earth. Earth and Planetary Science Letters 128, 215-229.

Williams, H.R., Stott, G.M., Heather, K.B., Muir, T.L., Sage, R.P., 1991. Wawa Subprovince; *in* Thurston, P.C., Williams, H.R., Sutcliffe, R.H., Stott, G.M. (Eds.), Geology of Ontario, Ontario Geological Survey, Special Volume 4, Part 1, pp. 485-541.

Wyman, D.A., Kerrich, R., 2010. Mantle plume - volcanic arc interaction: Consequences for magmatism, metallogeny, and cratonization in the Wawa and Abitibi Subprovinces, Canada. Can. J. Earth Sci. 47, 565-589.

Zaleski, E., Peterson, V.L., 1995. Depositional setting and deformation of massive sulfide deposits, iron formation, and associated alteration in the Manitouwadge greenstone belt, Superior Province, Ontario. Economic Geology 90, 2244-2261.

Zaleski, E., Peterson, V.L., 2001. Geology of the Manitouwadge greenstone belt and the Wawa-Quetico subprovince boundary, Ontario. Geological Survey of Canada, Map 1917A, 1:25,000.

Zaleski, E., van Breemen, O., Peterson, V.L., 1999. Geological evolution of the Manitouwadge greenstone belt and Wawa-Quetico subprovince boundary, Superior Province, Ontario, constrained by U-Pb zircon dates of supracrustal and plutonic rocks. Can. J. Earth Sci. 36, 945-966.

Zartman, L.E., Doe, B.R., 1981. Plumbotectonics - the model. Tectonophysics 75, 135-162.

SUMMARY OF APPENDICES

Appendix A:

Lithogeochemical QA/QC

Appendix B:

Lithogeochemistry from Minnesota (Digital)

Appendix C:

Whole-Rock Nd and Pb Isotopic data from Minnesota (Digital)

Appendix D:

Geochronologic data from Minnesota (Digital)

Appendix E:

Whole-Rock Pb Isotopic data from Sulphides (Digital)

Appendix F:

OGS Miscellaneous Release – Data 306 (2013) (DVD Sleeve)

Appendix G:

OGS Summary of Field Work and Other Activities – OFR 6280-10 (2012)

Appendix H:

OGS Summary of Field Work and Other Activities – OFR 6270-11 (2011)

Appendix I:

OGS Summary of Field Work and Other Activities – OFR 6260-16 (2010)

Appendix J:

OGS Open File Report 6282 (2012)

APPENDIX A: LITHOGEOCHEMICAL QUALITY ASSURANCE AND CONTROL

Samples for lithogeochemical analyses were over two summers of field work and they represent the most comprehensive, geospatially-controlled suites of samples for greenstone belt lithofacies along the northern margin of the Wawa subprovince. To ensure that the data presented in this thesis and published in government and peer-reviewed journals is of the highest quality and consistency, the precision and accuracy of analyses obtained from the Ontario Geoscience Laboratories (OGL) are presented herein.

Samples were crushed in a steel jaw crusher prior to pulverization in an agate mill. Major element abundances were determined by XRF analysis of a fused glass disk. High field strength element (HFSE) and rare earth element (REE) abundances were determined by ICP-MS analysis after a closed beaker four acid digestion. Diligent and thorough cleaning of the equipment between samples was completed to minimize the possibility of contamination during sample preparation. Details for procedures, calibrations, and internal quality assurance/quality control measures are described in OGS publications (Burnham, 2008; Keating and Burnham, 2012).

The precision of major elements, HFSE, and REE analyses were analyzed using scatter plots and Thompson-Howarth plots (**Figure A.1, A.2, and A.3**, respectively) (Thompson and Howarth, 1978). Measured abundances of commonly used major elements such as TiO_2 (N = 41; M = 1) and Na_2O (N = 41; M = 2) are precise to 5% at the 90^{th} percentile and the analyses that plot higher than 5% have a high percentage (>90 %) of being random occurrences. Measured abundances of Al_2O_3 (N = 41; M = 0) are precise to 3% at the 90^{th} percentile. Measured abundances of commonly used HFSE such as Nb (N = 46, M = 2) and Zr (N = 46, M = 2) are precise to 5% at the 90^{th} percentile. The analyses of Th (N = 46, M = 2) are precise to 7% at the 90^{th} percentile. Measured abundances of REE such as La (N = 46; M = 3), Y (N = 46; M = 2), and Yb (N = 46; M = 3) are precise to 5% at the 90^{th} percentile.

A large number of international and internal standards are used by the OGL to ensure their results are accurate. However, the diversity in standards used resulted in an incomplete series of reference materials to do a proper QA/QC analysis of the data presented in this study. This would require analyses from other jobs within the lab. For information on instrumental accuracy at the OGL, please refer to the publications available through the Ontario Geological Survey (Burnham, 2008; Keating and Burnham, 2012).

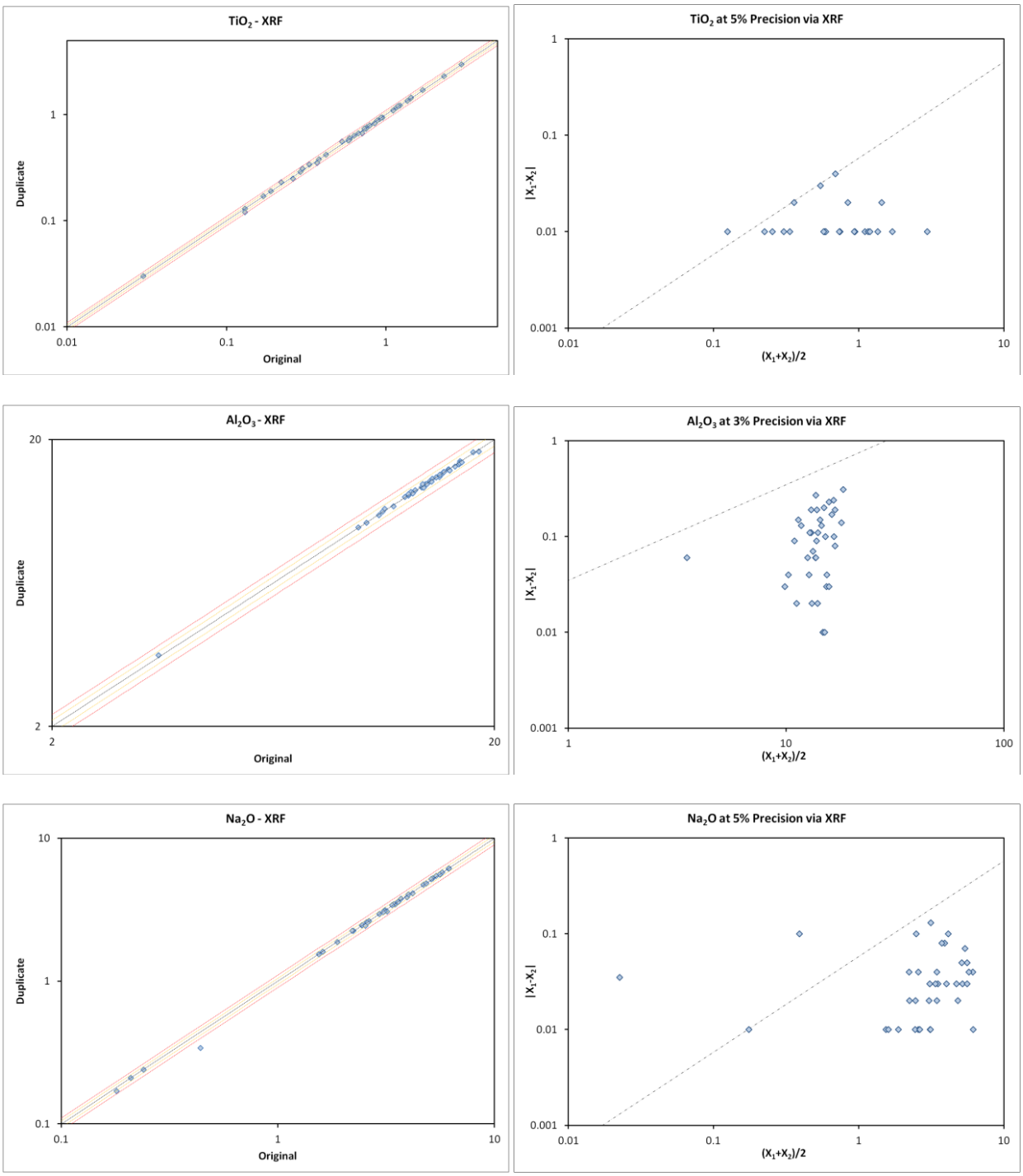

Figure A.1: Scatter plots (left) and Thompson-Howarth plots (right) illustrating precision for analyses of commonly used major element oxides. X1 and X2 correspond to original and duplicate analyses.

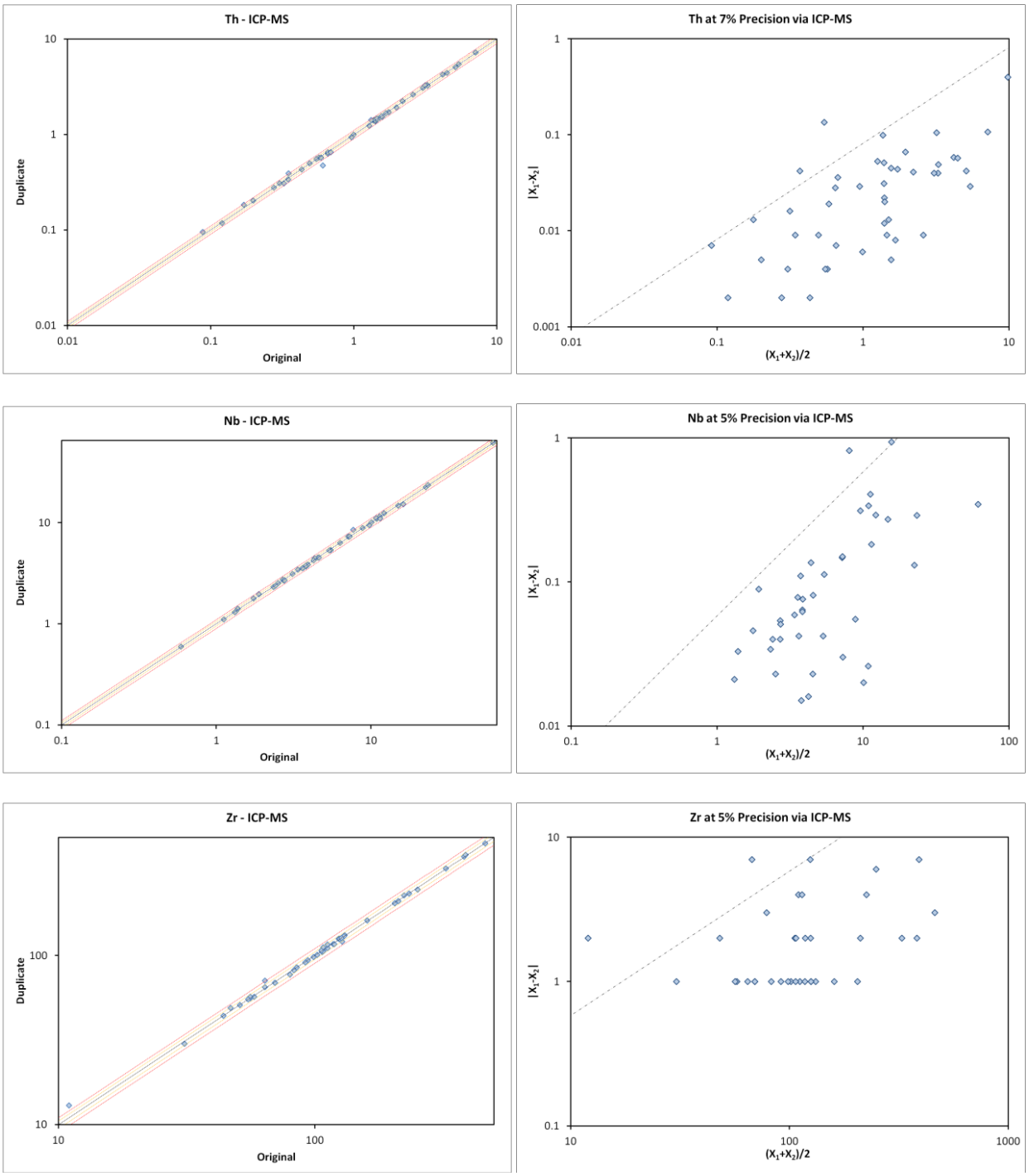

Figure A.2: Scatter plots (left) and Thompson-Howarth plots (right) illustrating precision for analyses of commonly used HFSE. X1 and X2 correspond to original and duplicate analyses.

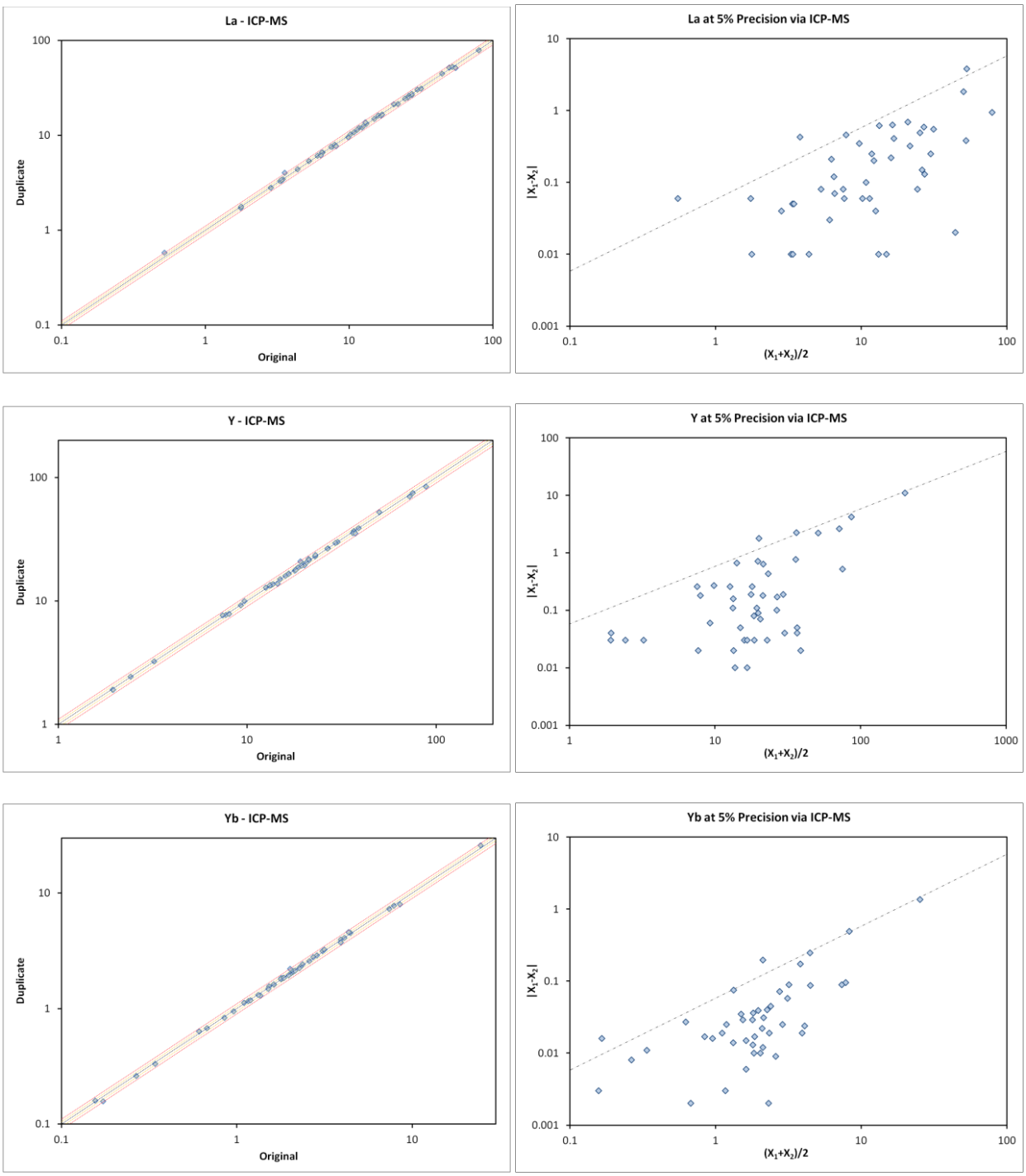

Figure A.3: Scatter plots (left) and Thompson-Howarth plots (right) illustrating precision for analyses of commonly used REE. X1 and X2 correspond to original and duplicate analyses.

References

Burnham, O.M., 2008. Trace element analysis of geological samples by inductively coupled plasma mass spectrometry (ICP-MS) at the Geoscience Laboratories: Revised capabilities due to method improvements, Summary of Field Work and Other Activities, Open File Report 6226. Ontario Geological Survey, pp. 38-31 to 38-10.

Keating, G.L., Burnham, O.M., 2012. Revision of the calibration for major element analysis of geological samples by wavelength dispersive X-ray fluorescence at the Geoscience Laboratories, Summary of Field Work and Other Activities, Open File Report 6280. Ontario Geological Survey, pp. 39-31 to 39-34.

Thompson, M., Howarth, R.J., 1978. A new approach to the estimation of analytical precision. Journal of Geochemical Exploration 9, 23-30.

APPENDIX B: LITHOGEOCHEMICAL DATA FROM MINNESOTA

This appendix consists of tables that list the lithogeochemical and geospatial data for samples collected or compiled from the Vermilion greenstone belt in Minnesota. All analyses were completed at the Ontario Geoscience Laboratories. Major elements were analyzed via X-ray fluorescence. Trace and rare earth elements were analyzed via inductively coupled plasma mass spectrometry.

The data from some of the samples is to be submitted to a refereed journal with the manuscript presented in Chapter 4.

Sample ID			FMH-00-123A	FMH-00-127A	FMH-00-206A	FMH-00-66	NBH-01-129B	NBH-01-80	NBJ-01-04	RL-11-001	RL-11-002
UTM Easting *(NAD83, Zone 15)*			564442	564364	563540	565373	564831	564011	565455	571808	567812
UTM Northing *(NAD83, Zone 15)*			5297158	5297055	5297247	5297120	5298342	5297952	5298401	5296797	5297810
	unit	detection limit									
SiO_2	*wt%*	*0.04*	75.24	58.06	58.79	54.06	71.95	57.58	47.31	60.56	59.47
TiO_2	*wt%*	*0.01*	0.28	0.49	0.51	0.59	0.33	0.39	1.29	0.46	0.72
Al2O3	*wt%*	*0.02*	13.20	15.73	17.29	16.67	12.94	17.14	20.01	14.42	15.24
FeO_T	*wt%*	*0.01*	1.93	6.02	5.38	7.54	3.45	6.52	8.67	5.13	4.50
Fe_2O_3	*wt%*		1.17	1.32	2.51	1.61	1.33	2.00	4.10	2.00	3.60
FeO	*wt%*	*0.06*	0.76	4.70	2.87	5.93	2.12	4.52	4.57	3.13	0.90
MnO	*wt%*	*0.002*	0.076	0.194	0.108	0.198	0.057	0.117	0.127	0.162	0.070
MgO	*wt%*	*0.01*	0.58	5.71	4.17	7.26	2.03	5.75	5.83	6.88	1.00
CaO	*wt%*	*0.006*	4.086	2.970	5.608	4.493	1.275	5.255	6.251	7.517	15.592
Na_2O	*wt%*	*0.02*	1.90	5.51	5.93	5.61	1.25	3.93	3.32	3.03	0.49
K_2O	*wt%*	*0.01*	1.66	0.17	0.59	0.52	2.84	0.30	1.88	1.45	0.11
P_2O_5	*wt%*	*0.002*	0.047	0.103	0.108	0.104	0.062	0.060	0.093	0.102	0.070
LOI	*wt%*	*0.05*	1.49	4.83	2.03	2.86	2.34	2.93	4.48	1.33	3.67
CO_2	*wt%*	*0.03*	0.14	1.72	0.24	0.23	0.02	0.02	0.52	0.06	2.13
S	*wt%*	*0.01*	0.04	<0.01	<0.01	<0.01	<0.01	<0.01	0.01	<0.01	0.01
Total	*wt%*		100.48	99.78	100.52	99.90	98.53	99.96	99.26	101.04	100.92
Ba	*ppm*	*0.8*	309.2	86.4	296.1	195.7	315.8	40.6	298.7	343.1	20.9
Be	*ppm*	*0.04*	0.80	0.42	0.69	0.46	0.80	0.56	0.59	0.80	0.48
Bi	*ppm*	*0.15*	0.17	0.17	<0.15	<0.15	0.18	<0.15	<0.15	<0.15	<0.15
Cd	*ppm*	*0.013*	0.087	0.834	0.150	0.102	0.056	0.036	0.040	0.085	0.094
Ce	*ppm*	*0.12*	55.04	31.42	28.74	18.07	52.28	15.14	18.02	28.37	14.43
Co	*ppm*	*0.13*	2.95	28.36	24.62	36.77	3.83	36.48	85.33	21.95	21.57
Cr	*ppm*	*3*	19	189	200	313	11	266	158	220	148
Cs	*ppm*	*0.013*	1.563	0.086	0.254	0.495	1.217	0.338	1.377	0.926	0.050
Cu	*ppm*	*1.4*	20.5	81.5	19.7	5.6	15.3	13.4	122.1	3.0	16.1
Dy	*ppm*	*0.009*	4.163	2.527	2.274	2.305	3.562	1.958	3.531	2.422	2.529
Er	*ppm*	*0.007*	2.672	1.418	1.323	1.395	2.192	1.136	2.187	1.393	1.579
Eu	*ppm*	*0.0031*	0.7404	0.8103	0.8009	0.5516	0.7352	0.4450	0.9642	0.8642	0.8787
Ga	*ppm*	*0.04*	13.45	14.08	15.62	12.45	13.92	12.74	24.66	14.63	18.76
Gd	*ppm*	*0.009*	4.003	2.775	2.447	2.423	3.617	1.855	3.261	2.567	2.308
Hf	*ppm*	*0.14*	5.59	2.55	2.28	2.04	5.51	1.79	3.02	2.22	1.48
Ho	*ppm*	*0.0025*	0.8896	0.4986	0.4629	0.4748	0.7310	0.3946	0.7350	0.4862	0.5290
In	*ppm*	*0.0018*	0.0195	0.0392	0.0364	0.0189	0.0249	0.0183	0.0407	0.0383	0.0429
La	*ppm*	*0.04*	26.92	15.61	13.64	7.49	25.47	6.30	7.18	13.76	6.36
Li	*ppm*	*0.4*	4.9	27.4	7.3	11.7	9.0	18.8	20.8	4.5	3.4
Lu	*ppm*	*0.002*	0.424	0.201	0.188	0.200	0.326	0.161	0.323	0.190	0.231

Sample ID			FMH-00-123A	FMH-00-127A	FMH-00-206A	FMH-00-66	NBH-01-129B	NBH-01-80	NBJ-01-04	RL-11-001	RL-11-002
UTM Easting *(NAD83, Zone 15)*			564442	564364	563540	565373	564831	564011	565455	571808	567812
UTM Northing *(NAD83, Zone 15)*			5297158	5297055	5297247	5297120	5298342	5297952	5298401	5296797	5297810
	unit	detection limit									
Mo	*ppm*	*0.08*	1.87	0.49	0.63	0.49	0.77	0.68	0.86	0.94	1.40
Nb	*ppm*	*0.028*	8.598	4.433	4.300	3.948	7.851	2.972	5.806	4.164	2.755
Nd	*ppm*	*0.06*	22.25	14.11	13.33	10.06	21.50	8.01	11.13	13.19	8.44
Ni	*ppm*	*1.6*	10.5	152.3	202.8	209.2	4.9	163.4	288.9	134.7	86.5
Pb	*ppm*	*0.6*	4.5	30.1	5.7	2.4	2.2	0.9	2.0	1.4	2.1
Pr	*ppm*	*0.014*	6.146	3.705	3.386	2.387	6.007	1.976	2.516	3.423	1.912
Rb	*ppm*	*0.23*	52.14	2.06	9.20	11.75	88.16	7.73	68.37	43.66	1.80
Sb	*ppm*	*0.04*	0.31	0.28	0.71	0.15	0.07	0.16	0.22	0.13	0.47
Sc	*ppm*	*1.1*	6.3	22.0	17.2	21.3	6.2	16.5	39.8	17.0	26.2
Sm	*ppm*	*0.012*	4.343	2.890	2.583	2.306	4.006	1.874	2.924	2.613	2.061
Sn	*ppm*	*0.16*	1.51	0.86	0.91	0.41	1.90	0.72	0.31	1.00	0.60
Sr	*ppm*	*0.6*	52.1	47.7	267.9	60.3	54.6	107.0	173.8	123.3	74.8
Ta	*ppm*	*0.023*	0.92	0.38	0.34	0.30	0.77	0.25	0.42	0.32	0.19
Tb	*ppm*	*0.0023*	0.6608	0.4208	0.3670	0.3796	0.5677	0.3072	0.5449	0.3857	0.3811
Th	*ppm*	*0.018*	7.841	2.541	1.897	1.451	5.957	1.431	1.256	1.865	0.660
Ti	*ppm*	*7*	1658	2793	3043	3530	1871	2313	7653	2698	4354
Tl	*ppm*	*0.005*	0.273	0.022	0.076	0.086	0.268	0.046	0.310	0.260	0.018
Tm	*ppm*	*0.0019*	0.4137	0.2015	0.1932	0.2022	0.3254	0.1644	0.3168	0.1944	0.2295
U	*ppm*	*0.011*	1.954	0.665	0.505	0.375	1.628	0.405	0.300	0.415	0.174
V	*ppm*	*0.8*	18.2	110.3	127.0	128.1	13.7	90.8	317.7	111.6	209.8
W	*ppm*	*0.05*	0.92	0.49	0.52	0.45	0.72	0.44	1.08	0.18	0.71
Y	*ppm*	*0.05*	25.58	13.42	12.96	13.18	20.50	9.63	19.31	13.81	14.47
Yb	*ppm*	*0.009*	2.772	1.312	1.260	1.325	2.151	1.067	2.097	1.251	1.514
Zn	*ppm*	*7*	43	355	70	261	30	42	59	42	19
Zr	*ppm*	*6*	206	104	95	83	220	71	118	92	58

Sample ID			RL-11-003	RL-11-004	RL-11-005	RL-11-006	RL-11-007	RL-11-008	RL-11-009	RL-11-010	RL-11-011	RL-11-014
UTM Easting *(NAD83, Zone 15)*			558989	574217	574328	574318	574283	574415	574243	574194	565510	578466
UTM Northing *(NAD83, Zone 15)*			5298210	5297739	5297893	5298071	5298242	5298677	5298963	5299199	5302210	5299557
	unit	detection limit										
SiO_2	*wt%*	*0.04*	66.59	53.10	59.06	55.04	57.77	55.81	51.55	57.01	51.28	47.66
TiO_2	*wt%*	*0.01*	0.13	0.63	0.58	0.79	0.62	0.81	0.67	0.52	0.82	0.79
Al2O3	*wt%*	*0.02*	16.57	16.66	15.47	16.02	19.15	17.80	17.21	16.19	14.20	16.73
FeO_T	*wt%*	*0.01*	1.12	7.84	6.92	9.21	4.69	4.31	9.18	7.25	8.52	11.43
Fe_2O_3	*wt%*		0.32	3.03	1.58	2.34	1.87	3.50	2.91	1.83	2.71	2.90
FeO	*wt%*	*0.06*	0.80	4.81	5.34	6.87	2.82	0.81	6.27	5.42	5.81	8.53
MnO	*wt%*	*0.002*	0.031	0.225	0.125	0.142	0.085	0.091	0.187	0.068	0.146	0.195
MgO	*wt%*	*0.01*	0.44	5.19	5.10	5.78	2.69	1.25	7.30	8.29	8.86	7.24
CaO	*wt%*	*0.006*	6.003	13.041	7.625	7.588	8.598	15.760	6.784	4.458	10.122	10.143
Na_2O	*wt%*	*0.02*	3.69	1.20	5.13	4.15	5.00	1.86	3.56	3.53	1.68	2.26
K_2O	*wt%*	*0.01*	1.50	0.32	0.26	0.58	0.34	0.13	0.70	0.43	1.15	1.02
P_2O_5	*wt%*	*0.002*	0.040	0.140	0.128	0.109	0.113	0.089	0.106	0.110	0.331	0.035
LOI	*wt%*	*0.05*	4.56	1.56	0.41	1.05	0.70	2.87	3.04	3.33	3.21	1.87
CO_2	*wt%*	*0.03*	2.95	0.04	0.01	0.21	0.07	2.11	0.07	0.04	0.10	0.14
S	*wt%*	*0.01*	<0.01	0.02	<0.01	0.18	0.05	0.27	0.01	<0.01	0.01	0.01
Total	*wt%*		100.67	99.91	100.81	100.46	99.76	100.77	100.30	101.18	100.31	99.38
Ba	*ppm*	*0.8*	329.4	17.3	75.1	175.5	85.7	32.8	138.7	99.2	485.2	130.6
Be	*ppm*	*0.04*	0.69	0.53	0.46	0.51	0.86	0.56	0.33	0.41	1.65	0.25
Bi	*ppm*	*0.15*	<0.15	0.16	<0.15	<0.15	0.15	0.19	<0.15	<0.15	<0.15	<0.15
Cd	*ppm*	*0.013*	0.034	0.060	0.073	0.088	0.096	0.138	0.065	0.101	0.100	0.097
Ce	*ppm*	*0.12*	9.09	26.57	19.66	18.90	24.17	15.10	16.56	21.43	71.76	4.21
Co	*ppm*	*0.13*	1.91	34.89	26.66	39.58	29.85	25.63	40.68	34.25	40.31	45.54
Cr	*ppm*	*3*	33	188	176	138	211	264	206	215	651	216
Cs	*ppm*	*0.013*	0.760	0.637	0.347	0.674	0.184	0.182	0.583	0.241	0.759	2.381
Cu	*ppm*	*1.4*	2.1	11.5	18.2	105.8	37.6	55.9	10.7	23.8	99.6	91.4
Dy	*ppm*	*0.009*	0.344	2.839	2.392	2.913	2.777	2.709	2.086	2.273	3.367	2.014
Er	*ppm*	*0.007*	0.174	1.699	1.394	1.743	1.673	1.720	1.268	1.434	1.769	1.248
Eu	*ppm*	*0.0031*	0.3619	0.8102	0.7548	0.9975	0.9113	0.9062	0.7079	0.6630	1.6634	0.6145
Ga	*ppm*	*0.04*	16.36	15.49	11.80	16.75	21.60	17.19	14.10	12.81	18.25	15.57
Gd	*ppm*	*0.009*	0.503	2.934	2.449	2.764	2.818	2.407	2.035	2.276	4.582	1.729
Hf	*ppm*	*0.14*	1.45	2.77	2.26	2.15	2.47	1.69	1.74	2.13	4.30	0.81
Ho	*ppm*	*0.0025*	0.0615	0.5792	0.4946	0.5911	0.5712	0.5725	0.4348	0.4716	0.6270	0.4298
In	*ppm*	*0.0018*	0.0055	0.0285	0.0340	0.0401	0.0466	0.0484	0.0325	0.0316	0.0458	0.0471
La	*ppm*	*0.04*	4.28	11.94	7.97	8.47	10.90	6.59	7.77	9.79	34.43	1.52
Li	*ppm*	*0.4*	10.6	8.8	2.8	8.6	3.1	1.0	11.4	20.5	18.1	12.5
Lu	*ppm*	*0.002*	0.025	0.240	0.206	0.249	0.237	0.256	0.191	0.208	0.234	0.176

Sample ID			RL-11-003	RL-11-004	RL-11-005	RL-11-006	RL-11-007	RL-11-008	RL-11-009	RL-11-010	RL-11-011	RL-11-014
UTM Easting *(NAD83, Zone 15)*			558989	574217	574328	574318	574283	574415	574243	574194	565510	578466
UTM Northing *(NAD83, Zone 15)*			5298210	5297739	5297893	5298071	5298242	5298677	5298963	5299199	5302210	5299557
	unit	detection limit										
Mo	*ppm*	*0.08*	1.03	1.13	0.79	0.84	1.99	4.61	0.38	0.63	0.66	0.32
Nb	*ppm*	*0.028*	0.980	5.261	4.347	4.425	4.632	3.453	2.869	3.873	7.231	1.115
Nd	*ppm*	*0.06*	4.07	13.78	10.44	10.42	12.58	8.68	8.48	11.17	33.64	3.86
Ni	*ppm*	*1.6*	4.0	186.0	99.9	148.3	149.5	83.5	137.4	118.5	199.6	68.8
Pb	*ppm*	*0.6*	2.0	1.3	1.6	2.0	2.5	5.2	1.2	1.2	9.3	0.9
Pr	*ppm*	*0.014*	1.082	3.367	2.505	2.486	3.083	1.973	2.048	2.702	8.638	0.707
Rb	*ppm*	*0.23*	39.37	9.24	6.01	14.06	6.34	3.65	20.32	8.88	16.94	37.74
Sb	*ppm*	*0.04*	0.07	0.14	0.09	0.04	0.11	0.26	0.09	0.11	0.78	0.14
Sc	*ppm*	*1.1*	2.5	21.0	19.1	25.7	21.3	32.0	28.6	21.7	22.3	42.0
Sm	*ppm*	*0.012*	0.714	2.980	2.516	2.604	2.797	2.151	1.943	2.350	6.256	1.269
Sn	*ppm*	*0.16*	0.32	0.53	0.82	0.97	1.18	0.71	0.45	0.56	1.59	0.20
Sr	*ppm*	*0.6*	467.4	57.1	181.2	185.8	105.1	98.0	168.4	99.2	358.2	181.7
Ta	*ppm*	*0.023*	0.08	0.37	0.31	0.33	0.34	0.24	0.23	0.29	0.50	0.08
Tb	*ppm*	*0.0023*	0.0641	0.4592	0.3876	0.4548	0.4303	0.4077	0.3289	0.3572	0.5841	0.2956
Th	*ppm*	*0.018*	0.419	1.571	1.190	1.151	1.592	0.955	1.074	1.438	6.818	0.106
Ti	*ppm*	*7*	664	3729	3371	4538	3718	4785	3951	3179	4883	4572
Tl	*ppm*	*0.005*	0.224	0.062	0.037	0.106	0.043	0.026	0.133	0.043	0.262	0.199
Tm	*ppm*	*0.0019*	0.0255	0.2483	0.2075	0.2540	0.2402	0.2544	0.1864	0.2076	0.2455	0.1762
U	*ppm*	*0.011*	0.222	0.393	0.305	0.309	0.405	0.246	0.275	0.365	1.763	0.029
V	*ppm*	*0.8*	13.0	124.0	114.1	192.4	163.2	223.2	167.9	121.8	164.8	258.3
W	*ppm*	*0.05*	0.32	0.39	0.11	0.23	0.21	0.31	0.21	0.17	0.91	0.56
Y	*ppm*	*0.05*	1.80	15.99	12.97	16.09	16.05	15.35	11.74	13.01	17.52	10.62
Yb	*ppm*	*0.009*	0.161	1.611	1.380	1.637	1.561	1.695	1.219	1.369	1.585	1.145
Zn	*ppm*	*7*	10	118	75	60	46	33	101	66	83	71
Zr	*ppm*	*6*	51	116	93	86	101	68	71	88	177	26

Sample ID			RL-11-015	RL-11-016	RL-11-017	RL-11-018	RL-11-019	RL-11-020	RL-11-021	RL-11-022	RL-11-023	RL-11-025
UTM Easting *(NAD83, Zone 15)*			578258	577979	577466	585777	585714	584069	585734	560280	560280	560102
UTM Northing *(NAD83, Zone 15)*			5299069	5298687	5298159	5309359	5309649	5311381	5310504	5299115	5299115	5298811
	unit	detection limit										
SiO_2	*wt%*	*0.04*	54.08	53.47	51.58	53.09	49.16	52.64	44.54	63.22	48.56	65.35
TiO_2	*wt%*	*0.01*	0.55	0.91	0.84	1.00	1.26	1.10	0.46	0.29	0.95	0.22
Al2O3	*wt%*	*0.02*	16.97	15.32	15.76	10.81	12.94	17.01	17.56	16.38	15.49	17.63
FeO_T	*wt%*	*0.01*	8.00	10.25	9.94	13.45	13.30	11.99	9.79	2.62	10.98	1.66
Fe_2O_3	*wt%*		1.67	2.90	3.91	2.69	3.63	2.45	2.64	0.88	2.34	0.41
FeO	*wt%*	*0.06*	6.33	7.35	6.03	10.76	9.67	9.54	7.15	1.74	8.64	1.25
MnO	*wt%*	*0.002*	0.166	0.147	0.179	0.210	0.202	0.137	0.150	0.042	0.074	0.025
MgO	*wt%*	*0.01*	7.28	6.34	6.40	6.69	7.08	5.30	10.54	1.95	8.53	1.33
CaO	*wt%*	*0.006*	6.292	9.941	9.794	9.674	11.564	3.659	11.439	3.838	5.637	3.888
Na_2O	*wt%*	*0.02*	2.41	3.12	3.76	3.18	1.07	4.68	0.85	4.77	2.73	5.32
K_2O	*wt%*	*0.01*	1.89	0.23	0.62	0.10	0.11	0.27	0.03	2.06	0.21	1.33
P_2O_5	*wt%*	*0.002*	0.117	0.155	0.434	0.110	0.153	0.096	0.035	0.123	0.143	0.121
LOI	*wt%*	*0.05*	2.82	0.62	1.10	1.52	2.89	3.00	4.59	4.61	7.66	3.64
CO_2	*wt%*	*0.03*	0.07	0.02	0.02	0.23	0.26	0.04	0.07	2.98	3.24	1.92
S	*wt%*	*0.01*	0.01	0.07	0.20	0.02	0.14	0.06	0.02	<0.01	0.01	0.06
Total	*wt%*		100.59	100.49	100.40	99.83	99.73	99.87	99.99	99.90	100.96	100.50
Ba	*ppm*	*0.8*	544.8	45.7	390.5	15.3	27.1	53.1	9.4	711.2	43.3	449.7
Be	*ppm*	*0.04*	0.51	0.50	1.65	0.34	0.49	0.45	0.20	1.18	0.47	1.08
Bi	*ppm*	*0.15*	<0.15	<0.15	<0.15	<0.15	<0.15	0.15	0.21	<0.15	<0.15	<0.15
Cd	*ppm*	*0.013*	0.143	0.151	0.107	0.110	0.184	0.069	0.123	0.041	0.092	0.055
Ce	*ppm*	*0.12*	20.58	22.74	56.95	11.70	15.11	14.63	4.50	24.05	16.61	22.25
Co	*ppm*	*0.13*	42.75	41.68	34.77	47.72	48.46	35.99	63.31	8.53	41.31	5.79
Cr	*ppm*	*3*	305	238	245	464	341	83	456	46	194	21
Cs	*ppm*	*0.013*	1.579	0.298	0.640	0.154	0.347	0.152	0.180	1.079	0.160	1.254
Cu	*ppm*	*1.4*	41.8	100.0	102.7	10.5	88.1	44.1	82.2	<1.4	73.8	8.4
Dy	*ppm*	*0.009*	2.553	2.895	3.939	5.150	5.667	4.259	1.720	1.481	2.645	0.519
Er	*ppm*	*0.007*	1.514	1.792	2.057	3.294	3.629	2.556	1.087	0.838	1.555	0.198
Eu	*ppm*	*0.0031*	0.5896	0.9327	1.9785	0.8228	1.2630	0.6435	0.4968	0.6293	0.8314	0.5649
Ga	*ppm*	*0.04*	12.88	14.86	16.56	11.85	15.62	16.15	13.18	17.23	14.39	16.32
Gd	*ppm*	*0.009*	2.518	2.841	5.228	4.088	4.851	3.433	1.372	1.879	2.658	1.114
Hf	*ppm*	*0.14*	2.44	1.97	3.02	2.29	2.56	2.16	0.72	2.56	1.94	2.03
Ho	*ppm*	*0.0025*	0.5301	0.6107	0.7428	1.1072	1.2116	0.8947	0.3645	0.2903	0.5455	0.0807
In	*ppm*	*0.0018*	0.0342	0.0485	0.0552	0.0781	0.0803	0.0386	0.0320	0.0220	0.0443	0.0122
La	*ppm*	*0.04*	9.15	9.60	25.57	4.38	5.74	6.47	1.76	11.02	6.67	10.36
Li	*ppm*	*0.4*	32.8	4.7	9.9	3.3	14.2	20.6	14.5	21.7	56.9	12.5
Lu	*ppm*	*0.002*	0.232	0.260	0.273	0.484	0.516	0.339	0.161	0.118	0.217	0.025

Sample ID			RL-11-015	RL-11-016	RL-11-017	RL-11-018	RL-11-019	RL-11-020	RL-11-021	RL-11-022	RL-11-023	RL-11-025
UTM Easting *(NAD83, Zone 15)*			578258	577979	577466	585777	585714	584069	585734	560280	560280	560102
UTM Northing *(NAD83, Zone 15)*			5299069	5298687	5298159	5309359	5309649	5311381	5310504	5299115	5299115	5298811
	unit	detection limit										
Mo	*ppm*	*0.08*	0.72	1.17	0.47	2.05	0.82	0.67	0.55	0.50	0.23	0.45
Nb	*ppm*	*0.028*	4.478	4.786	3.912	3.655	4.110	3.219	1.105	3.055	4.433	2.354
Nd	*ppm*	*0.06*	10.73	12.73	30.65	9.21	11.89	8.89	3.51	13.20	10.00	11.52
Ni	*ppm*	*1.6*	233.7	138.9	68.2	112.8	118.6	33.6	375.1	33.4	126.4	14.2
Pb	*ppm*	*0.6*	1.4	1.4	5.4	1.8	0.8	2.3	<0.6	3.8	0.8	6.5
Pr	*ppm*	*0.014*	2.599	2.981	7.248	1.807	2.305	1.932	0.678	3.091	2.276	2.844
Rb	*ppm*	*0.23*	52.32	4.10	15.98	0.69	2.76	4.36	0.45	52.34	3.95	31.63
Sb	*ppm*	*0.04*	<0.04	0.06	0.08	0.04	0.06	0.15	0.33	0.24	0.22	0.51
Sc	*ppm*	*1.1*	22.6	29.3	28.2	41.5	42.5	40.3	24.8	5.1	27.1	2.5
Sm	*ppm*	*0.012*	2.428	2.827	6.668	2.986	3.736	2.600	1.076	2.538	2.485	2.015
Sn	*ppm*	*0.16*	0.74	0.71	1.02	0.86	0.91	0.52	0.24	0.81	0.60	0.79
Sr	*ppm*	*0.6*	77.1	125.9	658.5	34.2	105.2	124.0	151.0	317.2	68.1	755.2
Ta	*ppm*	*0.023*	0.34	0.28	0.23	0.23	0.27	0.24	0.07	0.18	0.27	0.15
Tb	*ppm*	*0.0023*	0.3975	0.4500	0.6825	0.7500	0.8304	0.6228	0.2469	0.2552	0.4183	0.1149
Th	*ppm*	*0.018*	1.491	0.721	4.483	0.433	0.489	1.386	0.139	1.437	0.488	1.467
Ti	*ppm*	*7*	3249	5427	5126	5774	7607	6446	2638	1698	5441	1315
Tl	*ppm*	*0.005*	0.220	0.076	0.097	0.007	0.020	0.028	0.009	0.229	0.010	0.208
Tm	*ppm*	*0.0019*	0.2263	0.2589	0.2858	0.4870	0.5247	0.3688	0.1621	0.1191	0.2239	0.0275
U	*ppm*	*0.011*	0.397	0.187	1.177	0.110	0.126	0.433	0.041	0.536	0.122	0.548
V	*ppm*	*0.8*	125.0	180.5	216.0	245.1	257.2	287.4	148.7	36.8	181.1	23.1
W	*ppm*	*0.05*	0.66	0.16	0.58	0.13	0.06	0.32	0.26	0.27	<0.05	0.24
Y	*ppm*	*0.05*	14.46	16.42	19.85	29.25	31.66	23.50	9.83	7.90	14.63	2.27
Yb	*ppm*	*0.009*	1.503	1.724	1.859	3.148	3.440	2.338	1.044	0.781	1.471	0.163
Zn	*ppm*	*7*	69	77	126	102	97	120	72	43	77	31
Zr	*ppm*	*6*	102	81	119	85	94	78	26	88	79	69

Sample ID			RL-11-026	RL-11-027	RL-11-029	RL-11-030A	RL-11-031A
UTM Easting *(NAD83, Zone 15)*			560309	587871	583403	576397	576504
UTM Northing *(NAD83, Zone 15)*			5299705	5306979	5305706	5300939	5302293
	unit	detection limit					
SiO_2	*wt%*	*0.04*	52.22	46.29	49.73	51.78	49.17
TiO_2	*wt%*	*0.01*	1.54	0.64	0.80	0.67	0.93
Al2O3	*wt%*	*0.02*	15.37	17.35	13.82	16.89	13.80
FeO_T	*wt%*	*0.01*	10.92	9.86	12.60	8.71	13.28
Fe_2O_3	*wt%*		2.76	1.77	3.36	3.10	5.63
FeO	*wt%*	*0.06*	8.16	8.09	9.24	5.61	7.65
MnO	*wt%*	*0.002*	0.198	0.184	0.178	0.284	0.240
MgO	*wt%*	*0.01*	5.30	4.73	7.68	5.03	7.78
CaO	*wt%*	*0.006*	7.658	7.630	10.596	10.663	9.661
Na_2O	*wt%*	*0.02*	3.65	4.71	1.89	3.20	2.15
K_2O	*wt%*	*0.01*	0.83	0.23	0.10	1.36	1.28
P_2O_5	*wt%*	*0.002*	0.268	0.042	0.056	0.079	0.070
LOI	*wt%*	*0.05*	3.05	8.87	2.55	1.77	2.23
CO_2	*wt%*	*0.03*	0.63	5.03	0.06	0.51	0.09
S	*wt%*	*0.01*	<0.01	0.02	0.02	0.03	0.16
Total	*wt%*		100.99	100.54	100.00	100.43	100.06
Ba	*ppm*	*0.8*	140.6	41.6	20.1	218.5	156.2
Be	*ppm*	*0.04*	0.81	0.40	0.22	0.63	0.32
Bi	*ppm*	*0.15*	0.15	<0.15	<0.15	<0.15	<0.15
Cd	*ppm*	*0.013*	0.092	0.039	0.092	0.054	0.074
Ce	*ppm*	*0.12*	26.19	4.14	6.90	21.01	7.71
Co	*ppm*	*0.13*	32.66	57.72	50.95	33.94	53.70
Cr	*ppm*	*3*	168	344	314	234	203
Cs	*ppm*	*0.013*	1.395	0.597	0.084	1.612	2.042
Cu	*ppm*	*1.4*	1.6	83.4	96.0	11.2	85.7
Dy	*ppm*	*0.009*	7.455	2.180	3.235	2.237	3.679
Er	*ppm*	*0.007*	4.655	1.484	2.116	1.278	2.399
Eu	*ppm*	*0.0031*	2.4873	0.4765	0.7008	0.9110	0.7851
Ga	*ppm*	*0.04*	18.24	10.75	13.96	17.28	15.07
Gd	*ppm*	*0.009*	6.550	1.640	2.676	2.295	3.024
Hf	*ppm*	*0.14*	3.56	0.78	1.28	2.76	1.49
Ho	*ppm*	*0.0025*	1.5602	0.4840	0.7105	0.4570	0.7941
In	*ppm*	*0.0018*	0.0794	0.0361	0.0644	0.0288	0.0644
La	*ppm*	*0.04*	10.26	1.54	2.47	9.74	2.92
Li	*ppm*	*0.4*	14.5	33.7	10.1	12.6	16.5
Lu	*ppm*	*0.002*	0.632	0.230	0.311	0.192	0.366

Sample ID			RL-11-026	RL-11-027	RL-11-029	RL-11-030A	RL-11-031A
UTM Easting *(NAD83, Zone 15)*			560309	587871	583403	576397	576504
UTM Northing *(NAD83, Zone 15)*			5299705	5306979	5305706	5300939	5302293
	unit	detection limit					
Mo	*ppm*	*0.08*	0.75	0.29	0.44	1.35	0.83
Nb	*ppm*	*0.028*	7.333	1.034	1.892	4.706	1.804
Nd	*ppm*	*0.06*	18.78	3.35	5.75	10.61	6.24
Ni	*ppm*	*1.6*	37.9	162.0	70.4	142.4	126.7
Pb	*ppm*	*0.6*	0.8	<0.6	0.8	1.7	0.9
Pr	*ppm*	*0.014*	3.839	0.652	1.108	2.607	1.234
Rb	*ppm*	*0.23*	35.20	8.01	2.17	58.39	45.78
Sb	*ppm*	*0.04*	0.35	0.56	0.87	0.16	0.08
Sc	*ppm*	*1.1*	49.8	42.8	50.8	27.3	43.5
Sm	*ppm*	*0.012*	5.419	1.164	1.946	2.310	2.200
Sn	*ppm*	*0.16*	1.21	0.36	1.70	0.72	0.59
Sr	*ppm*	*0.6*	151.6	102.3	113.3	209.4	66.7
Ta	*ppm*	*0.023*	0.46	0.06	0.12	0.35	0.12
Tb	*ppm*	*0.0023*	1.1161	0.3102	0.4825	0.3488	0.5408
Th	*ppm*	*0.018*	0.890	0.119	0.199	1.519	0.271
Ti	*ppm*	*7*	9216	3694	4509	4409	5249
Tl	*ppm*	*0.005*	0.184	0.044	0.025	0.254	0.230
Tm	*ppm*	*0.0019*	0.6682	0.2226	0.3183	0.1881	0.3574
U	*ppm*	*0.011*	0.221	0.028	0.050	0.459	0.087
V	*ppm*	*0.8*	243.3	240.0	286.2	178.1	277.8
W	*ppm*	*0.05*	1.03	0.09	0.26	0.60	0.63
Y	*ppm*	*0.05*	41.19	12.59	18.55	12.49	21.15
Yb	*ppm*	*0.009*	4.384	1.522	2.057	1.272	2.359
Zn	*ppm*	*7*	60	73	81	53	73
Zr	*ppm*	*6*	134	27	46	115	53

APPENDIX C: WHOLE-ROCK ND AND PB ISOTOPIC DATA FROM MINNESOTA

This appendix contains tables that list the whole-rock neodymium and lead isotopic data for samples collected from within the Vermilion greenstone belt of Minnesota. All isotopic data were analyzed at the Radiogenic Isotope Facility at the University of Alberta via multi-collector inductively coupled plasma mass spectrometry. Some of the analyses were funded by a Society of Economic Geologists Canada Foundation Student Research Grant.

The data for some of these analyses is to be submitted to a refereed journal with the manuscript presented in Chapter 4.

Sample	Sm ppm	Nd ppm	$^{147}Sm/^{144}Nd$	$^{143}Nd/^{144}Nd_0$	2*SE	εNd_0	$^{143}Nd/^{144}Nd_T$	T_{DM} Ga	~TMa	CHUR @ TMa	εNd_T
RL-11-006	2.44	10.17	0.1452	0.511816	0.000008	-16.0	0.509210	N/A	2720	0.509108	2.0
RL-11-009	1.77	7.84	0.1366	0.511637	0.000010	-19.5	0.509185	3.00	2720	0.509108	1.5
RL-11-015	2.35	10.56	0.1347	0.511615	0.000008	-20.0	0.509196	2.97	2720	0.509108	1.7
RL-11-018	2.93	9.09	0.1950	0.512679	0.000012	0.8	0.509180	N/A	2720	0.509108	1.4
RL-11-031A	1.97	5.84	0.2038	0.512893	0.000011	5.0	0.509235	N/A	2720	0.509108	2.5
RL-11-029	1.53	4.69	0.1978	0.512813	0.000008	3.4	0.509262	N/A	2720	0.509108	3.0
RL-11-026	4.89	17.09	0.1731	0.512301	0.000009	-6.6	0.509194	N/A	2720	0.509108	1.7
FMH-00-123A	4.01	20.58	0.1178	0.511320	0.000009	-25.7	0.509206	2.91	2720	0.509108	1.9
FMH-00-127A	2.68	13.23	0.1225	0.511373	0.000007	-24.7	0.509173	2.97	2720	0.509108	1.3
NBH-01-80	1.98	8.51	0.1407	0.511714	0.000011	-18.0	0.509189	N/A	2720	0.509108	1.6

Notes:

T_{DM} not calculated for samples with $^{147}Sm/^{144}Nd > 0.14$

All samples relative to La Jolla $^{143}Nd/^{144}Nd = 0.511844$ (Tanaka et al. 2000)

Uncertainty is 2 x standard error (2*SE) on $^{143}Nd/^{144}Nd$

T_{DM} uses the linear model of Goldstein et al. (1984)

References:

Goldstein, R.L., O'Nions, R.K. and Hamilton, P.J. 1984. A Sm-Nd isotopic study of atmospheric dusts and particulates from major river systems; Earth and Planetary Science Letters, v.70, p.221-236.

Tanaka, T., Togashi, S., Kamioka, H., Amakawa, H., Kagami, H., Mamamoto, T., Yuhara, M., Orihashi, Y., Yoneda, S., Shimizu, H., Kunimaru, T., Takahashi, K., Yanagi, T., Nakano, T., Fujimaki, K., Shinjo, R., Asahara, Y., Tanimizu, M. and Dragusanu, C. 2000. JNdi-1: A neodymium isotopic reference in consistency with La Jolla neodymium; Chemical Geology, v.168, p.279-281.

Sample	$^{208}Pb/^{204}Pb$	±2 SE_8/4	$^{207}Pb/^{204}Pb$	±2 SE_7/4	$^{206}Pb/^{204}Pb$	±2 SE_6/4
RL-11-006	38.733	0.004	15.430	0.001	18.402	0.001
RL-11-009	40.194	0.004	15.715	0.002	20.211	0.002
RL-11-015	44.437	0.013	16.307	0.004	23.448	0.004
RL-11-018	34.942	0.003	14.888	0.002	14.965	0.001
RL-11-031A	35.405	0.005	14.989	0.004	16.052	0.001
RL-11-029	35.291	0.007	14.804	0.003	15.247	0.002
RL-11-026	43.120	0.005	16.071	0.002	22.427	0.002
FMH-00-123A	55.581	0.005	18.175	0.001	33.486	0.002
FMH-00-127A	33.787	0.002	14.554	0.001	13.889	0.001
NBH-01-80	50.715	0.010	17.703	0.004	31.126	0.006

Abbreviations:

±2 SE_8/4: 2 x Standard Error for $^{208}Pb/^{204}Pb$ ratio

±2 SE_7/4: 2 x Standard Error for $^{207}Pb/^{204}Pb$ ratio

±2 SE_6/4: 2 x Standard Error for $^{206}Pb/^{204}Pb$ ratio

APPENDIX D: GEOCHRONOLOGIC DATA FROM MINNESOTA

This appendix consists of tables that list the U-Pb geochronology data collected from samples within the Vermilion greenstone belt in Minnesota. Detrital zircon geochronology was analyzed via laser ablation inductively coupled plasma mass spectrometry at the Mineral Exploration Research Centre, Laurentian University. Magmatic geochronology was completed at the Jack Satterly Geochronology Laboratory at the University of Toronto and was funded by a Society of Economic Geologists Canada Foundation Student Research Grant.

Both of these tables are included with the manuscript presented in Chapter 2 and is published in the *Precambrian Research* (vol: 235, p. 264-277).

Analysis No.	Fraction	Weight (µg)	U (ppm)	Th/U	Pb_{tot} (pg)	Pb_{com} (pg)	$^{206}Pb/^{204}Pb$ measured	$^{206}Pb/^{238}U$	2σ	$^{207}Pb/^{235}U$	2s	$^{206}Pb/^{238}U$ Age (Ma)	2s	$^{207}Pb/^{235}U$ Age (Ma)	2s	$^{207}Pb/^{206}Pb$ Age (Ma)	2s	Disc %	Rho
RL-11-003	**Dacite Tuff Breccia**																		
Z1	1 cls, clr, el, 3:1 sq, euh pr	2.3	270	0.350	153.5	0.55	16208	0.515581	0.000944	13.08526	0.02957	2680.4	4.0	2685.8	2.1	2689.9	1.3	0.4	0.942
Z2	1 cls, clr, short broken pr	0.9	78	0.355	44.5	0.33	7861	0.516631	0.001150	13.10584	0.03436	2684.9	4.9	2687.3	2.5	2689.1	1.4	0.2	0.948
Z3	1 cls, clr, assym pr	2.1	224	0.302	126.7	0.47	15890	0.518087	0.001021	13.15032	0.03100	2691.1	4.3	2690.5	2.2	2690.1	1.4	0.0	0.935

Key: cls = colourless; clr = clear; euh = euhedral; pr = prism; assym = assymetric; sq = square x-section

Pb_{tot} - total Pb, corrected for fractionation, blank and spike

Pb_{com} - common Pb assuming the isotopic composition of laboratory blank: $^{206}Pb/^{204}Pb$ - 18.221; $^{207}Pb/^{204}Pb$ - 15.612; $^{208}Pb/^{204}Pb$ - 39.360 (errors of 2%).

Th/U calculated from radiogenic $^{208}Pb/^{206}Pb$ ratio and $^{207}Pb/^{206}Pb$ age assuming concordance.

Disc - per cent discordance for the given $^{207}Pb/^{206}Pb$ age. **Rho** - Error correlation coefficient.

RL-11-012 Grain ID	U (ppm)	Th (ppm)	Pb (ppm)	U/Th	$^{207}Pb/^{235}U$	2*SE	$^{206}Pb/^{238}U$	2*SE	Error Correlation
RL012-1	72.8	51.4	80.2	1.416	12.96	0.28	0.5148	0.0072	0.52565
RL012-2	97.9	72.5	101.7	1.359	13.71	0.26	0.5388	0.0084	0.67053
RL012-3	101.1	67.7	89.8	1.517	12.96	0.21	0.5095	0.0062	0.49709
RL012-4	90.3	61.9	80.8	1.537	13.23	0.23	0.5275	0.0081	0.62537
RL012-5	110.3	74.9	104.0	1.476	12.69	0.23	0.5078	0.0087	0.69959
RL012-6	117.9	93.2	120.3	1.266	12.95	0.22	0.5180	0.0069	0.62038
RL012-7	90.3	57.5	82.5	1.576	13.62	0.31	0.5410	0.0110	0.98506
RL012-8	165.0	164.0	228.0	0.997	14.04	0.33	0.5350	0.0120	0.56272
RL012-9	75.3	45.3	60.6	1.701	13.23	0.25	0.5208	0.0067	0.68323
RL012-10	67.0	59.7	84.9	1.199	13.15	0.34	0.5250	0.0130	0.79699
RL012-11	170.1	191.0	243.0	0.989	13.37	0.27	0.5272	0.0092	0.82372
RL012-12	49.8	26.7	31.6	1.890	13.21	0.33	0.5210	0.0110	0.62763
RL012-13	124.7	108.8	142.6	1.181	12.95	0.19	0.5227	0.0079	0.76752
RL012-14	107.7	57.1	70.8	2.070	12.87	0.20	0.5156	0.0064	0.60752
RL012-15	126.4	103.4	140.9	1.284	12.81	0.26	0.5160	0.0100	0.81802
RL012-16	176.0	147.0	167.3	1.204	12.88	0.23	0.5144	0.0060	0.60840
RL012-17	149.0	144.0	185.0	1.143	12.70	0.28	0.5076	0.0092	0.79548
RL012-18	70.0	75.0	138.0	0.975	13.17	0.53	0.4760	0.0190	0.87322
RL012-19	36.8	30.4	41.0	1.209	13.67	0.37	0.5380	0.0120	0.80310
RL012-20	108.5	73.7	91.6	1.478	12.49	0.28	0.5030	0.0110	0.75571
RL012-21	187.0	207.0	220.0	0.975	12.21	0.32	0.4780	0.0120	0.86159
RL012-22	144.0	116.0	142.0	1.511	12.73	0.26	0.5158	0.0099	0.89086
RL012-23	104.4	92.9	129.2	1.123	12.65	0.18	0.5030	0.0049	0.57393
RL012-24	68.0	55.6	86.7	1.256	13.75	0.20	0.5406	0.0060	0.56709
RL012-25	87.1	67.3	90.9	1.371	13.06	0.23	0.5248	0.0079	0.76658
RL012-26	226.0	246.0	287.0	0.920	12.16	0.15	0.4842	0.0058	0.74661
RL012-27	74.5	65.5	103.6	1.156	13.60	0.22	0.5265	0.0072	0.25807
RL012-28	111.9	97.3	145.0	1.262	13.64	0.33	0.5400	0.0120	0.85947
RL012-29	88.6	69.5	91.8	1.308	12.18	0.24	0.4803	0.0074	0.48680
RL012-30	83.6	57.3	82.0	1.526	13.52	0.22	0.5334	0.0063	0.56266
RL012-31	79.5	47.8	64.0	1.706	12.82	0.22	0.5131	0.0054	0.45990
RL012-32	204.3	124.0	161.0	1.840	12.47	0.21	0.4955	0.0069	0.56591
RL012-33	157.0	133.0	193.0	1.431	13.54	0.27	0.5020	0.0100	0.75080
RL012-34	108.9	91.6	151.0	1.207	14.05	0.27	0.5620	0.0100	0.70580
RL012-35	151.4	125.0	168.0	1.314	12.62	0.23	0.5076	0.0096	0.85241
RL012-36	182.5	167.5	270.0	1.115	14.55	0.38	0.5410	0.0120	0.87086
RL012-37	143.9	126.7	168.2	1.162	12.68	0.22	0.5069	0.0072	0.74494
RL012-38	86.9	59.3	76.4	1.575	13.07	0.21	0.5302	0.0071	0.68544
RL012-39	155.4	144.0	232.0	1.151	13.75	0.32	0.5500	0.0110	0.84545
RL012-40	132.0	108.2	136.0	1.331	12.91	0.20	0.5039	0.0075	0.84484
RL012-41	131.5	104.8	125.4	1.328	13.29	0.27	0.5150	0.0069	0.56319

RL-11-012 Grain ID	U (ppm)	Th (ppm)	Pb (ppm)	U/Th	$^{207}Pb/^{235}U$	2*SE	$^{206}Pb/^{238}U$	2*SE	Error Correlation
RL012-42	117.6	74.4	85.3	1.643	13.05	0.24	0.5183	0.0077	0.64188
RL012-43	106.7	81.1	97.3	1.357	12.98	0.24	0.5270	0.0100	0.87265
RL012-44	155.3	131.0	172.0	1.355	13.20	0.30	0.5240	0.0130	0.83985
RL012-45	115.7	75.0	100.2	1.573	12.76	0.21	0.5032	0.0086	0.72766
RL012-46	153.0	111.7	140.0	1.401	12.62	0.21	0.5055	0.0066	0.71102
RL012-47	153.0	135.0	175.0	1.155	13.32	0.21	0.5270	0.0070	0.45506
RL012-48	110.0	82.5	130.1	1.319	14.13	0.42	0.5660	0.0160	0.92239
RL012-49	90.1	60.4	75.3	1.660	12.88	0.19	0.5145	0.0050	0.49625
RL012-50	95.6	55.9	68.5	1.758	12.53	0.21	0.4965	0.0065	0.50419
RL012-51	104.3	67.7	97.0	1.525	13.71	0.36	0.5276	0.0098	0.74826
RL012-52	97.8	73.3	104.6	1.324	13.17	0.28	0.5190	0.0100	0.77183
RL012-53	148.2	99.8	119.0	1.558	12.60	0.23	0.4974	0.0080	0.72979
RL012-54	121.2	85.8	115.7	1.404	13.47	0.24	0.5305	0.0093	0.83977
RL012-55	240.0	304.0	388.0	0.949	13.44	0.27	0.5260	0.0097	0.87911
RL012-56	90.3	53.8	66.3	1.786	12.83	0.17	0.5122	0.0066	0.59967
RL012-57	105.4	65.7	81.9	1.723	12.49	0.24	0.4934	0.0072	0.55524
RL012-58	152.1	127.0	206.0	1.327	14.08	0.30	0.5477	0.0085	0.71413
RL012-59	163.1	127.6	166.0	1.306	12.76	0.21	0.5066	0.0068	0.80572
RL012-60	140.0	51.3	117.0	2.780	15.80	0.28	0.5591	0.0083	0.64452
RL012-61	138.0	129.0	162.0	1.201	12.98	0.35	0.5150	0.0130	0.87351
RL012-62	110.5	78.9	110.1	1.438	13.43	0.25	0.5227	0.0083	0.57079
RL012-63	152.8	100.6	122.7	1.509	11.99	0.22	0.4647	0.0075	0.45012
RL012-64	191.0	175.0	189.0	1.290	13.01	0.18	0.5173	0.0087	0.76064
RL012-65	270.0	323.0	381.0	0.869	12.29	0.23	0.4769	0.0089	0.85520
RL012-66	159.4	136.6	157.5	1.262	12.95	0.20	0.5148	0.0075	0.77000
RL012-67	134.8	101.6	128.2	1.311	12.70	0.31	0.5080	0.0120	0.87967
RL012-68	144.2	101.7	129.0	1.429	12.56	0.18	0.4991	0.0058	0.77642
RL012-69	169.3	149.0	194.0	1.135	12.48	0.15	0.4953	0.0067	0.75330
RL012-70	203.0	259.0	347.0	0.962	14.19	0.35	0.5600	0.0130	0.91171
RL012-71	218.0	123.0	155.0	2.040	12.39	0.16	0.4966	0.0070	0.73654
RL012-72	186.0	146.0	209.0	1.306	13.65	0.17	0.5511	0.0056	0.68003
RL012-73	91.1	72.9	95.6	1.255	13.41	0.16	0.5442	0.0055	0.59792
RL012-74	141.7	107.5	142.2	1.322	12.95	0.18	0.5189	0.0062	0.57916
RL012-75	225.0	216.0	252.0	1.050	13.17	0.18	0.5254	0.0060	0.70577
RL012-76	179.0	154.0	206.0	1.122	13.36	0.33	0.5230	0.0140	0.92362
RL012-77	184.0	194.0	246.0	1.037	12.67	0.17	0.4925	0.0059	0.21251
RL012-78	145.0	128.0	201.0	1.137	13.55	0.21	0.5247	0.0072	0.79281
RL012-79	171.6	192.0	210.0	0.887	13.37	0.22	0.5290	0.0110	0.43237
RL012-80	98.0	71.9	90.4	1.369	12.65	0.23	0.5077	0.0066	0.59212
RL012-81	212.0	155.2	174.5	1.363	10.72	0.17	0.4105	0.0054	0.83867
RL012-82	66.6	39.9	46.6	1.631	13.85	0.28	0.5467	0.0095	0.57565

RL-11-012 Grain ID	U (ppm)	Th (ppm)	Pb (ppm)	U/Th	$^{207}Pb/^{235}U$	2*SE	$^{206}Pb/^{238}U$	2*SE	Error Correlation
RL012-83	126.7	98.1	116.1	1.349	12.69	0.24	0.5071	0.0078	0.77950
RL012-84	85.1	43.9	55.8	1.975	13.07	0.20	0.5183	0.0052	0.46256
RL012-85	210.0	207.0	250.0	1.106	13.01	0.25	0.5160	0.0100	0.83738
RL012-86	139.1	89.8	116.0	1.587	13.26	0.28	0.5310	0.0120	0.76810
RL012-87	172.0	137.0	175.0	1.309	13.02	0.18	0.5217	0.0056	0.66871
RL012-88	143.6	144.5	186.4	1.083	12.70	0.14	0.5132	0.0054	0.61197
RL012-89	130.7	112.2	124.0	1.285	12.37	0.16	0.4937	0.0059	0.70600
RL012-90	116.5	82.2	112.9	1.518	13.36	0.21	0.5337	0.0089	0.74765
RL012-91	165.0	147.0	184.0	1.198	12.14	0.28	0.5010	0.0150	0.91630
RL012-92	101.9	59.5	78.5	1.799	12.94	0.22	0.5182	0.0087	0.72682
RL012-93	178.0	150.0	211.0	1.220	13.94	0.22	0.5503	0.0079	0.80076
RL012-94	141.6	124.3	172.0	1.145	13.18	0.22	0.5191	0.0062	0.55715
RL012-95	116.0	74.2	100.0	1.521	13.35	0.23	0.5298	0.0062	0.62551
RL012-96	138.0	120.6	155.0	1.113	13.09	0.38	0.5150	0.0170	0.84960
RL012-97	73.6	48.7	72.6	1.491	13.33	0.29	0.5210	0.0110	0.71724
RL012-98	102.7	79.9	113.5	1.307	13.88	0.20	0.5485	0.0068	0.64759
RL012-99	128.6	105.9	147.0	1.252	13.45	0.27	0.5234	0.0088	0.73662
RL012-100	120.1	105.7	167.8	1.157	14.31	0.31	0.5364	0.0087	0.72096
RL012-101	206.0	212.0	272.0	1.113	12.37	0.20	0.5016	0.0099	0.61356
RL012-102	163.2	145.2	195.0	1.132	12.93	0.24	0.5171	0.0095	0.80925
RL012-103	183.0	258.0	453.0	0.829	12.89	0.50	0.5150	0.0160	0.85447
RL012-104	89.9	57.5	80.4	1.576	13.07	0.23	0.5250	0.0079	0.78621
RL012-105	106.5	72.1	98.6	1.515	13.42	0.26	0.5330	0.0110	0.79558
RL012-106	141.0	121.0	140.0	1.272	13.17	0.44	0.5020	0.0160	0.81263
RL012-107	137.2	119.0	203.0	1.218	13.57	0.43	0.5240	0.0160	0.89893
RL012-108	121.2	116.0	157.0	1.174	12.71	0.31	0.4920	0.0094	0.75248
RL012-109	104.1	83.2	110.4	1.283	13.70	0.27	0.5418	0.0087	0.65610
RL012-110	145.0	142.7	191.6	1.011	13.30	0.25	0.5312	0.0078	0.81884
RL012-111	135.3	102.1	137.0	1.387	12.52	0.19	0.5050	0.0073	0.64423
RL012-112	94.9	70.3	97.9	1.483	12.84	0.26	0.5110	0.0067	0.56189
RL012-113	132.0	112.0	151.0	1.249	12.90	0.35	0.5130	0.0110	0.74835
RL012-114	105.8	109.4	143.6	0.988	12.94	0.23	0.5140	0.0062	0.58946
RL012-115	95.6	63.3	89.8	1.530	13.38	0.21	0.5346	0.0078	0.72810
RL012-116	91.1	59.6	80.3	1.562	13.03	0.27	0.5159	0.0076	0.76495
RL012-117	119.4	99.6	163.1	1.208	14.09	0.18	0.5024	0.0054	0.47982
RL012-118	476.0	733.0	672.0	0.660	9.27	0.39	0.3430	0.0160	0.95462
RL012-119	90.5	92.4	139.1	1.002	12.95	0.25	0.5160	0.0077	0.45209
RL012-120	151.0	161.0	243.0	0.982	13.29	0.28	0.5211	0.0089	0.72365
RL012-121	96.9	71.2	108.2	1.406	13.53	0.22	0.5444	0.0061	0.60544
RL012-122	152.9	142.0	207.0	1.166	12.82	0.22	0.5041	0.0075	0.76684
RL012-123	120.9	80.1	116.6	1.592	13.49	0.24	0.5288	0.0083	0.75949

RL-11-012 Grain ID	U (ppm)	Th (ppm)	Pb (ppm)	U/Th	$^{207}Pb/^{235}U$	2*SE	$^{206}Pb/^{238}U$	2*SE	Error Correlation
RL012-124	186.0	172.0	232.0	1.112	12.87	0.14	0.5151	0.0068	0.54006
RL012-125	114.9	90.7	130.1	1.328	13.42	0.21	0.5323	0.0076	0.75590
RL012-126	115.0	103.0	165.0	1.100	12.89	0.25	0.5138	0.0083	0.77288
RL012-127	195.0	186.0	236.0	1.077	12.50	0.30	0.4910	0.0110	0.91151
RL012-128	85.3	56.4	84.8	1.562	13.74	0.24	0.5396	0.0060	0.62163
RL012-129	117.8	93.8	156.0	1.257	13.85	0.36	0.5490	0.0120	0.88481
RL012-130	59.7	46.9	85.7	1.296	13.95	0.35	0.5620	0.0150	0.71343
RL012-131	165.0	148.0	195.0	1.206	12.86	0.29	0.5010	0.0091	0.75239
RL012-132	92.3	82.8	112.3	1.098	13.80	0.36	0.5430	0.0110	0.70254
RL012-133	87.0	58.4	83.1	1.559	13.58	0.19	0.5450	0.0060	0.53590
RL012-134	60.9	41.4	54.3	1.628	12.94	0.20	0.5206	0.0054	0.42087
RL012-135	138.6	135.0	163.0	1.033	12.99	0.24	0.5146	0.0064	0.66415
RL012-136	136.9	125.2	178.3	1.074	13.14	0.22	0.5214	0.0072	0.63006
RL012-137	120.7	101.3	138.7	1.236	13.22	0.21	0.5177	0.0063	0.59718
RL012-138	109.3	109.0	142.2	1.041	13.56	0.26	0.5406	0.0080	0.72575
RL012-139	92.7	95.5	64.3	1.130	11.86	0.23	0.4595	0.0061	0.60498
RL012-140	105.0	90.5	125.2	1.163	14.49	0.21	0.5522	0.0049	0.40131
RL012-141	111.4	33.4	49.5	3.290	13.07	0.25	0.5184	0.0097	0.82344
RL012-142	109.3	89.3	130.3	1.211	13.53	0.26	0.5380	0.0100	0.85644
RL012-143	104.2	93.7	136.0	1.109	14.28	0.48	0.5650	0.0140	0.88134
RL012-144	130.0	104.0	145.0	1.253	12.85	0.33	0.5150	0.0100	0.61176
RL012-145	157.0	141.0	176.0	1.402	13.10	0.32	0.5250	0.0120	0.83705
RL012-146	162.7	127.0	178.4	1.230	13.93	0.30	0.5310	0.0100	0.82008
RL012-147	91.7	67.0	117.0	1.510	13.23	0.55	0.5130	0.0220	0.92494
RL012-148	104.8	78.0	107.5	1.375	12.97	0.24	0.5159	0.0089	0.82945
RL012-149	153.0	121.0	181.0	1.291	12.97	0.23	0.5159	0.0081	0.63004
RL012-150	103.0	88.6	110.0	1.163	12.84	0.37	0.5120	0.0130	0.90265
RL012-151	86.4	51.3	64.0	1.707	12.71	0.30	0.5091	0.0093	0.65974
RL012-152	157.5	136.5	176.0	1.211	12.67	0.20	0.5105	0.0073	0.57327
RL012-153	120.5	115.9	166.1	1.065	13.19	0.30	0.5153	0.0080	0.70586
RL012-154	372.0	463.0	506.0	0.823	13.15	0.15	0.5248	0.0064	0.63157
RL012-155	101.0	81.0	100.0	1.500	13.13	0.41	0.5157	0.0095	0.61558
RL012-156	161.0	117.0	133.7	1.551	13.01	0.25	0.5197	0.0098	0.75566
RL012-157	125.8	86.6	118.8	1.548	13.00	0.18	0.5221	0.0059	0.60902

RL-11-012 Grain ID	$^{207}Pb/^{206}Pb$	2*SE	$^{238}U/^{206}Pb$	2*SE	Error Correlation	$^{206}Pb/^{238}U$ Age	2*SE	$^{207}Pb/^{235}U$ Age	2*SE
RL012-1	0.1835	0.0034	1.942502	0.02716786	0.16744	2677	31	2675	20
RL012-2	0.1860	0.0026	1.855976	0.02893504	0.20838	2785	35	2729	17
RL012-3	0.1858	0.0027	1.962709	0.02388379	0.29205	2653	26	2677	15
RL012-4	0.1817	0.0025	1.895735	0.02910986	0.37276	2733	35	2695	16
RL012-5	0.1806	0.0023	1.969279	0.03373913	0.30868	2650	38	2657	17
RL012-6	0.1830	0.0026	1.930502	0.02571518	0.10483	2690	29	2674	16
RL012-7	0.1832	0.0025	1.848429	0.03758358	0.70929	2786	48	2720	22
RL012-8	0.1909	0.0043	1.869159	0.04192506	0.41935	2761	51	2754	23
RL012-9	0.1824	0.0024	1.920123	0.02470204	0.04683	2706	29	2693	18
RL012-10	0.1826	0.0027	1.904762	0.04716553	0.06821	2727	56	2691	24
RL012-11	0.1827	0.0024	1.896813	0.03310069	0.36689	2728	39	2704	19
RL012-12	0.1852	0.0039	1.919386	0.04052446	0.23253	2700	47	2692	24
RL012-13	0.1799	0.0017	1.913143	0.02891493	0.36537	2709	33	2676	14
RL012-14	0.1839	0.0022	1.939488	0.02407433	0.16532	2680	27	2671	15
RL012-15	0.1790	0.0022	1.937984	0.03755784	0.19559	2683	43	2668	18
RL012-16	0.1820	0.0030	1.944012	0.02267511	0.03151	2675	25	2669	17
RL012-17	0.1820	0.0023	1.970055	0.03570628	0.15148	2644	39	2654	20
RL012-18	0.2042	0.0041	2.100840	0.08385707	0.29519	2520	79	2691	39
RL012-19	0.1844	0.0034	1.858736	0.04145880	0.13336	2772	48	2726	25
RL012-20	0.1823	0.0027	1.988072	0.04347671	0.15130	2630	46	2642	22
RL012-21	0.1860	0.0022	2.092050	0.05252009	0.27338	2516	53	2617	25
RL012-22	0.1815	0.0019	1.938736	0.03721110	0.41800	2679	42	2659	20
RL012-23	0.1837	0.0022	1.988072	0.01936690	0.15782	2626	21	2653	13
RL012-24	0.1833	0.0024	1.849797	0.02053048	0.19694	2785	25	2734	14
RL012-25	0.1827	0.0023	1.905488	0.02868398	0.13821	2718	33	2691	18
RL012-26	0.1831	0.0016	2.065262	0.02473879	0.36587	2545	25	2615	11
RL012-27	0.1854	0.0036	1.899335	0.02597382	0.61930	2726	31	2721	15
RL012-28	0.1843	0.0022	1.851852	0.04115226	0.11515	2779	50	2727	23
RL012-29	0.1833	0.0031	2.082032	0.03207795	0.33261	2528	32	2617	18
RL012-30	0.1833	0.0029	1.874766	0.02214290	0.16978	2755	26	2715	15
RL012-31	0.1819	0.0029	1.948938	0.02051114	0.22199	2669	23	2672	16
RL012-32	0.1831	0.0027	2.018163	0.02810359	0.20760	2593	30	2641	16
RL012-33	0.1958	0.0030	1.992032	0.03968191	0.26544	2620	43	2718	20
RL012-34	0.1833	0.0025	1.779359	0.03166120	0.43302	2871	41	2750	18
RL012-35	0.1813	0.0017	1.970055	0.03725873	0.17676	2644	41	2649	17
RL012-36	0.1972	0.0026	1.848429	0.04100027	-0.18453	2785	48	2783	25
RL012-37	0.1834	0.0025	1.972776	0.02802128	0.01902	2642	31	2654	17
RL012-38	0.1791	0.0018	1.886081	0.02525683	0.33729	2745	29	2685	15
RL012-39	0.1822	0.0021	1.818182	0.03636364	-0.05850	2822	46	2730	22
RL012-40	0.1861	0.0015	1.984521	0.02953742	0.20904	2634	31	2676	14
RL012-41	0.1881	0.0035	1.941748	0.02601565	0.20378	2677	30	2699	19

RL-11-012 Grain ID	$^{207}Pb/^{206}Pb$	2*SE	$^{238}U/^{206}Pb$	2*SE	Error Correlation	$^{206}Pb/^{238}U$ Age	2*SE	$^{207}Pb/^{235}U$ Age	2*SE
RL012-42	0.1831	0.0025	1.929385	0.02866344	0.05241	2691	33	2686	16
RL012-43	0.1809	0.0017	1.897533	0.03600632	0.27832	2725	42	2682	18
RL012-44	0.1835	0.0021	1.908397	0.04734573	0.39192	2711	56	2691	22
RL012-45	0.1842	0.0023	1.987281	0.03396387	0.35782	2635	36	2662	15
RL012-46	0.1812	0.0018	1.978239	0.02582864	0.19919	2636	28	2649	16
RL012-47	0.1838	0.0026	1.897533	0.02520443	0.35942	2732	30	2701	15
RL012-48	0.1824	0.0019	1.766784	0.04994444	0.08723	2892	68	2755	29
RL012-49	0.1835	0.0024	1.943635	0.01888858	0.18629	2675	21	2669	14
RL012-50	0.1816	0.0024	2.014099	0.02636786	0.44184	2598	28	2645	16
RL012-51	0.1895	0.0030	1.895375	0.03520599	-0.00051	2730	41	2730	24
RL012-52	0.1839	0.0022	1.926782	0.03712490	0.26393	2699	45	2689	20
RL012-53	0.1844	0.0025	2.010454	0.03233541	0.16786	2601	35	2648	17
RL012-54	0.1851	0.0020	1.885014	0.03304549	0.18488	2741	39	2713	17
RL012-55	0.1859	0.0016	1.901141	0.03505906	0.13052	2727	42	2708	18
RL012-56	0.1826	0.0021	1.952362	0.02515734	0.35924	2665	28	2666	13
RL012-57	0.1854	0.0031	2.026753	0.02957564	0.24655	2584	31	2640	18
RL012-58	0.1864	0.0028	1.825817	0.02833567	-0.01277	2814	35	2751	20
RL012-59	0.1838	0.0020	1.973944	0.02649589	0.02000	2641	29	2664	17
RL012-60	0.2066	0.0029	1.788589	0.02655211	0.30203	2862	34	2867	17
RL012-61	0.1828	0.0021	1.941748	0.04901499	0.15951	2676	55	2674	26
RL012-62	0.1867	0.0030	1.913143	0.03037897	0.34247	2709	35	2708	18
RL012-63	0.1863	0.0034	2.151926	0.03473089	0.59617	2460	33	2603	17
RL012-64	0.1844	0.0020	1.933114	0.03251130	0.51841	2686	37	2679	13
RL012-65	0.1862	0.0019	2.096876	0.03913230	0.30503	2519	40	2625	17
RL012-66	0.1841	0.0016	1.942502	0.02829985	0.27742	2676	32	2676	14
RL012-67	0.1805	0.0020	1.968504	0.04650009	0.30212	2647	51	2654	22
RL012-68	0.1828	0.0017	2.003606	0.02328375	0.23070	2609	25	2647	13
RL012-69	0.1840	0.0018	2.018978	0.02731103	0.37089	2592	29	2644	10
RL012-70	0.1844	0.0018	1.785714	0.04145408	-0.00216	2862	53	2761	23
RL012-71	0.1835	0.0018	2.013693	0.02838472	0.20415	2598	30	2633	12
RL012-72	0.1808	0.0017	1.814553	0.01843857	0.22492	2829	23	2725	12
RL012-73	0.1797	0.0020	1.837560	0.01857144	0.20121	2800	23	2711	12
RL012-74	0.1825	0.0021	1.927154	0.02302631	0.26135	2697	26	2676	13
RL012-75	0.1822	0.0018	1.903312	0.02173557	0.19179	2721	25	2690	13
RL012-76	0.1863	0.0020	1.912046	0.05118287	0.15601	2708	59	2704	23
RL012-77	0.1883	0.0029	2.030457	0.02432425	0.57885	2581	26	2657	13
RL012-78	0.1903	0.0021	1.905851	0.02615233	0.24631	2718	30	2722	16
RL012-79	0.1851	0.0030	1.890359	0.03930804	0.62732	2735	47	2705	16
RL012-80	0.1804	0.0024	1.969667	0.02560528	0.19389	2646	28	2655	17
RL012-81	0.1888	0.0018	2.436054	0.03204553	-0.04120	2217	24	2498	15
RL012-82	0.1836	0.0033	1.829157	0.03178524	0.25745	2810	40	2740	20

RL-11-012 Grain ID	$^{207}Pb/^{206}Pb$	2*SE	$^{238}U/^{206}Pb$	2*SE	Error Correlation	$^{206}Pb/^{238}U$ Age	2*SE	$^{207}Pb/^{235}U$ Age	2*SE
RL012-83	0.1823	0.0021	1.971998	0.03033244	0.05542	2643	33	2656	18
RL012-84	0.1828	0.0028	1.929385	0.01935713	0.22949	2691	22	2683	14
RL012-85	0.1829	0.0019	1.937984	0.03755784	0.25362	2679	43	2677	18
RL012-86	0.1808	0.0024	1.883239	0.04255908	0.47620	2744	49	2696	20
RL012-87	0.1825	0.0019	1.916810	0.02057531	0.18546	2709	23	2681	14
RL012-88	0.1809	0.0019	1.948558	0.02050314	0.33979	2670	23	2658	10
RL012-89	0.1809	0.0017	2.025522	0.02420615	0.24897	2586	26	2631	12
RL012-90	0.1823	0.0020	1.873712	0.03124608	0.33916	2755	38	2703	15
RL012-91	0.1805	0.0021	1.996008	0.05976072	0.31677	2613	63	2620	24
RL012-92	0.1811	0.0022	1.929757	0.03239847	0.40057	2690	37	2673	16
RL012-93	0.1831	0.0017	1.817191	0.02608724	0.19052	2825	33	2743	15
RL012-94	0.1834	0.0020	1.926411	0.02300857	0.29929	2695	26	2691	15
RL012-95	0.1824	0.0028	1.887505	0.02208858	0.07292	2740	26	2703	16
RL012-96	0.1845	0.0029	1.941748	0.06409652	0.46045	2674	70	2685	27
RL012-97	0.1880	0.0031	1.919386	0.04052446	0.25672	2699	46	2700	20
RL012-98	0.1837	0.0020	1.823154	0.02260246	0.27264	2821	28	2744	13
RL012-99	0.1882	0.0025	1.910585	0.03212294	0.07935	2712	37	2709	19
RL012-100	0.1935	0.0029	1.864280	0.03023721	0.08776	2767	36	2767	20
RL012-101	0.1813	0.0018	1.993620	0.03934777	0.57730	2611	40	2631	15
RL012-102	0.1811	0.0018	1.933862	0.03552831	0.27614	2685	40	2674	17
RL012-103	0.1803	0.0036	1.941748	0.06032614	0.03020	2673	66	2678	36
RL012-104	0.1814	0.0022	1.904762	0.02866213	0.09291	2719	33	2682	17
RL012-105	0.1834	0.0022	1.876173	0.03872026	0.33795	2752	45	2712	19
RL012-106	0.1947	0.0035	1.992032	0.06349106	0.15232	2618	68	2687	31
RL012-107	0.1861	0.0024	1.908397	0.05827166	-0.02008	2713	68	2715	31
RL012-108	0.1872	0.0028	2.032520	0.03883271	0.00798	2582	41	2656	22
RL012-109	0.1857	0.0028	1.845700	0.02963748	0.09500	2795	36	2729	19
RL012-110	0.1827	0.0021	1.882530	0.02764257	-0.12203	2745	33	2703	17
RL012-111	0.1815	0.0021	1.980198	0.02862464	0.32933	2634	31	2648	14
RL012-112	0.1828	0.0028	1.956947	0.02565860	0.07985	2660	29	2671	19
RL012-113	0.1819	0.0030	1.949318	0.04179824	0.01522	2672	48	2675	26
RL012-114	0.1833	0.0027	1.945525	0.02346743	0.15895	2673	26	2676	17
RL012-115	0.1824	0.0021	1.870557	0.02729208	0.26479	2759	33	2707	15
RL012-116	0.1837	0.0024	1.938360	0.02855502	-0.01256	2681	32	2679	20
RL012-117	0.2042	0.0023	1.990446	0.02139412	0.43001	2627	24	2754	12
RL012-118	0.1974	0.0026	2.915452	0.13599780	0.44263	1894	76	2360	38
RL012-119	0.1830	0.0035	1.937984	0.02891954	0.28270	2682	32	2675	18
RL012-120	0.1852	0.0025	1.919017	0.03277539	0.13506	2703	38	2698	20
RL012-121	0.1818	0.0025	1.836885	0.02058229	0.29847	2801	25	2719	15
RL012-122	0.1839	0.0022	1.983733	0.02951399	0.20569	2635	31	2667	16
RL012-123	0.1849	0.0020	1.891074	0.02968214	0.11125	2734	35	2715	16

RL-11-012 Grain ID	$^{207}Pb/^{206}Pb$	2*SE	$^{238}U/^{206}Pb$	2*SE	Error Correlation	$^{206}Pb/^{238}U$ Age	2*SE	$^{207}Pb/^{235}U$ Age	2*SE
RL012-124	0.1828	0.0022	1.941371	0.02562865	0.56896	2677	29	2669	11
RL012-125	0.1832	0.0021	1.878640	0.02682259	0.21583	2750	32	2710	15
RL012-126	0.1825	0.0023	1.946283	0.03144053	0.15608	2671	35	2668	18
RL012-127	0.1849	0.0016	2.036660	0.04562782	0.19870	2571	48	2641	22
RL012-128	0.1845	0.0023	1.853225	0.02060665	0.05251	2781	25	2730	16
RL012-129	0.1844	0.0022	1.821494	0.03981407	-0.02049	2818	50	2742	25
RL012-130	0.1825	0.0031	1.779359	0.04749180	0.38134	2872	61	2744	24
RL012-131	0.1883	0.0034	1.996008	0.03625484	-0.03106	2617	39	2667	21
RL012-132	0.1838	0.0028	1.841621	0.03730723	0.15964	2792	46	2734	23
RL012-133	0.1809	0.0024	1.834862	0.02020032	0.29335	2803	25	2723	13
RL012-134	0.1812	0.0026	1.920861	0.01992441	0.27639	2704	23	2675	15
RL012-135	0.1838	0.0027	1.943257	0.02416798	0.24097	2676	27	2683	17
RL012-136	0.1823	0.0025	1.917913	0.02648442	0.19871	2704	30	2688	16
RL012-137	0.1859	0.0024	1.931621	0.02350630	0.27639	2692	26	2693	15
RL012-138	0.1837	0.0024	1.849797	0.02737398	0.11796	2792	35	2719	18
RL012-139	0.1878	0.0026	2.176279	0.02889075	0.20366	2436	27	2591	18
RL012-140	0.1916	0.0026	1.810938	0.01606953	0.29695	2834	20	2784	13
RL012-141	0.1847	0.0021	1.929012	0.03609456	0.19495	2690	41	2684	18
RL012-142	0.1839	0.0020	1.858736	0.03454900	0.08269	2771	42	2714	18
RL012-143	0.1832	0.0030	1.769912	0.04385621	-0.29119	2885	56	2764	32
RL012-144	0.1843	0.0033	1.941748	0.03770384	0.16794	2675	43	2671	22
RL012-145	0.1826	0.0021	1.904762	0.04353741	0.13878	2722	50	2683	23
RL012-146	0.1900	0.0025	1.883239	0.03546590	0.05730	2751	45	2742	21
RL012-147	0.1894	0.0028	1.949318	0.08359647	-0.02751	2666	93	2700	42
RL012-148	0.1811	0.0019	1.938360	0.03343944	0.11671	2680	38	2675	18
RL012-149	0.1831	0.0026	1.938360	0.03043364	0.30640	2681	34	2678	16
RL012-150	0.1815	0.0023	1.953125	0.04959106	-0.08230	2667	58	2666	27
RL012-151	0.1811	0.0032	1.964251	0.03588201	0.26908	2651	40	2655	23
RL012-152	0.1812	0.0024	1.958864	0.02801118	0.34890	2658	31	2656	15
RL012-153	0.1863	0.0026	1.940617	0.03012796	-0.00937	2678	34	2691	22
RL012-154	0.1810	0.0015	1.905488	0.02323766	0.43236	2724	28	2690	11
RL012-155	0.1839	0.0046	1.939112	0.03572147	0.01068	2680	41	2685	30
RL012-156	0.1824	0.0025	1.924187	0.03628446	0.33014	2696	41	2679	18
RL012-157	0.1803	0.0018	1.915342	0.02164435	0.28551	2707	25	2678	13

RL-11-012 Grain ID	$^{208}Pb/^{232}Th$ Age	2*SE	$^{207}Pb/^{206}Pb$ Age	2*SE	Disc. (%)
RL012-1	2749	87	2680	30	3.44
RL012-2	2820	58	2703	23	5.33
RL012-3	2671	59	2698	24	4.75
RL012-4	2677	68	2667	23	5.01
RL012-5	2644	57	2654	22	5.3
RL012-6	2665	43	2676	23	3.84
RL012-7	2838	87	2681	21	6.52
RL012-8	3070	72	2743	38	5.8
RL012-9	2735	63	2671	22	4.1
RL012-10	2642	84	2679	25	5.46
RL012-11	2793	81	2666	21	4.6
RL012-12	2602	88	2695	34	5.4
RL012-13	2715	44	2647	16	4.59
RL012-14	2660	64	2683	20	3.43
RL012-15	2723	66	2639	20	5.67
RL012-16	2579	58	2665	27	3.19
RL012-17	2606	67	2667	21	4.5
RL012-18	3240	220	2858	31	10.4
RL012-19	2559	71	2683	30	6.4
RL012-20	2586	55	2669	25	5.23
RL012-21	2451	74	2700	20	6.9
RL012-22	2794	90	2659	17	5.56
RL012-23	2559	53	2679	20	2.8
RL012-24	2867	59	2677	22	3.73
RL012-25	2695	66	2668	20	4.54
RL012-26	2343	49	2678	15	4.77
RL012-27	2770	100	2696	33	3.4
RL012-28	2796	91	2684	20	6.45
RL012-29	2477	55	2686	31	5.3
RL012-30	2834	89	2674	26	4.32
RL012-31	2668	52	2661	27	4.05
RL012-32	2500	85	2678	23	3.88
RL012-33	2890	79	2782	25	7.3
RL012-34	3244	76	2675	23	7.1
RL012-35	2671	67	2661	16	4.75
RL012-36	3450	150	2795	22	3.87
RL012-37	2574	45	2676	23	3.8
RL012-38	2776	63	2644	18	4.69
RL012-39	3030	150	2668	19	5
RL012-40	2655	63	2703	13	4.39
RL012-41	2830	69	2725	29	3.77

RL-11-012 Grain ID	$^{208}Pb/^{232}Th$ Age	2*SE	$^{207}Pb/^{206}Pb$ Age	2*SE	Disc. (%)
RL012-42	2714	61	2676	23	3.86
RL012-43	2752	67	2662	15	4.79
RL012-44	2940	110	2680	19	6.1
RL012-45	2642	58	2689	21	4.97
RL012-46	2607	53	2658	17	4.06
RL012-47	2644	48	2682	23	4.76
RL012-48	3080	140	2668	17	8.6
RL012-49	2611	59	2680	21	3.24
RL012-50	2659	46	2659	22	4.49
RL012-51	3040	110	2728	27	4.7
RL012-52	2746	64	2683	20	5.66
RL012-53	2589	57	2688	22	4.5
RL012-54	2790	88	2694	17	4.68
RL012-55	2808	92	2699	14	4.59
RL012-56	2691	56	2669	19	4.09
RL012-57	2630	57	2700	30	4.43
RL012-58	3044	63	2705	24	4.76
RL012-59	2731	59	2689	18	4
RL012-60	4090	140	2877	23	2.85
RL012-61	2637	82	2674	19	5.45
RL012-62	2953	77	2707	26	5.34
RL012-63	2930	120	2717	33	7.8
RL012-64	2582	79	2686	18	5.25
RL012-65	2488	59	2701	17	7.2
RL012-66	2415	74	2684	14	3.86
RL012-67	2570	100	2650	18	5.4
RL012-68	2663	67	2670	15	3.74
RL012-69	2528	53	2682	16	4.76
RL012-70	3290	140	2688	16	6.6
RL012-71	2603	57	2681	16	4.48
RL012-72	3051	45	2653	16	5.37
RL012-73	2816	47	2648	18	4.85
RL012-74	2753	56	2675	18	3.89
RL012-75	2659	44	2671	17	3.52
RL012-76	2814	76	2702	18	6.27
RL012-77	2410	54	2719	25	5.1
RL012-78	3170	110	2737	18	3.88
RL012-79	2617	66	2694	27	4
RL012-80	2568	54	2651	22	4.06
RL012-81	2311	58	2723	16	16.32
RL012-82	2769	67	2682	30	5.6

RL-11-012 Grain ID	$^{208}Pb/^{232}Th$ Age	2*SE	$^{207}Pb/^{206}Pb$ Age	2*SE	Disc. (%)
RL012-83	2382	91	2671	19	4.4
RL012-84	2784	65	2672	25	4.32
RL012-85	2576	61	2671	17	5.18
RL012-86	2836	89	2653	21	5.4
RL012-87	2645	44	2668	17	3.51
RL012-88	2548	45	2657	17	3.1
RL012-89	2439	50	2660	16	3.86
RL012-90	2793	73	2671	18	4.57
RL012-91	2616	70	2651	20	7.7
RL012-92	2757	73	2663	20	4.96
RL012-93	3059	69	2680	16	5.45
RL012-94	2684	53	2680	18	2.89
RL012-95	2831	67	2674	24	4.46
RL012-96	2570	160	2687	26	7.6
RL012-97	2830	110	2717	27	6.5
RL012-98	2907	68	2682	18	5.39
RL012-99	2807	57	2726	22	4.3
RL012-100	3110	110	2769	23	4.39
RL012-101	2571	52	2657	17	5.42
RL012-102	2642	49	2661	16	4.75
RL012-103	2950	180	2653	34	5.9
RL012-104	2659	59	2669	19	4.12
RL012-105	2802	77	2681	20	5.54
RL012-106	2740	150	2777	29	7.5
RL012-107	3230	190	2703	22	6
RL012-108	2830	130	2717	25	6.5
RL012-109	2801	58	2702	25	4.76
RL012-110	2752	62	2674	19	4.13
RL012-111	2640	49	2661	19	4.47
RL012-112	2667	54	2672	26	3.81
RL012-113	2737	82	2672	27	5.45
RL012-114	2560	48	2680	23	3.62
RL012-115	2755	64	2669	19	4.97
RL012-116	2616	63	2680	21	3.9
RL012-117	3185	55	2855	19	7.5
RL012-118	1660	120	2801	22	29.7
RL012-119	2621	53	2677	32	3.32
RL012-120	2731	56	2697	23	3.6
RL012-121	2936	60	2664	23	5.31
RL012-122	2587	62	2688	20	4.48
RL012-123	2895	76	2691	17	4.57

RL-11-012 Grain ID	$^{208}Pb/^{232}Th$ Age	2*SE	$^{207}Pb/^{206}Pb$ Age	2*SE	Disc. (%)
RL012-124	2665	40	2672	20	3.82
RL012-125	2687	58	2679	19	4.9
RL012-126	2701	60	2673	20	4.97
RL012-127	2476	66	2696	14	6.98
RL012-128	2741	54	2687	20	3.69
RL012-129	2891	95	2689	19	5.87
RL012-130	3160	110	2676	26	7.4
RL012-131	2850	100	2721	29	4.6
RL012-132	2778	73	2681	26	6.4
RL012-133	2800	56	2658	22	4.96
RL012-134	2687	45	2661	24	4.38
RL012-135	2651	53	2682	24	3.18
RL012-136	2572	46	2667	23	3.68
RL012-137	2780	53	2700	21	3.46
RL012-138	2738	54	2687	21	5.2
RL012-139	1460	150	2719	22	8.4
RL012-140	2820	49	2750	22	3.96
RL012-141	2930	110	2693	18	5.47
RL012-142	2755	65	2683	18	5.21
RL012-143	3000	140	2681	27	6.8
RL012-144	2713	79	2682	30	4.4
RL012-145	2800	100	2671	20	5.6
RL012-146	2825	68	2739	22	4.49
RL012-147	3300	300	2733	25	6.7
RL012-148	2795	70	2658	17	4.17
RL012-149	2812	59	2680	23	4.01
RL012-150	2490	100	2662	21	5.4
RL012-151	2653	83	2660	30	4.49
RL012-152	2670	56	2664	23	4.44
RL012-153	2599	57	2704	23	3.36
RL012-154	2557	46	2664	16	2.89
RL012-155	2578	74	2687	43	4.11
RL012-156	2610	71	2665	23	4.35
RL012-157	2711	56	2647	16	3.85

APPENDIX E: WHOLE-ROCK PB ISOTOPIC DATA FROM SULPHIDES

This appendix contains a table with all whole-rock lead isotope analyses of volcanogenic and magmatic massive sulphide mineralization from several past-producing mines and prospects in the Vermilion, Shebandowan, Winston Lake, and Manitouwadge greenstone belt. The analyses were completed at the Radiogenic Isotope Facility at the University of Alberta via multi-collector inductively coupled plasma mass spectrometry.

The data within this appendix is to be submitted for publication in a refereed journal with the manuscript presented in Chapter 4.

Sample	$^{208}Pb/^{204}Pb$	±2 SE_8/4	$^{207}Pb/^{204}Pb$	±2 SE_7/4	$^{206}Pb/^{204}Pb$	±2 SE_6/4
FIVEMILE	33.880	0.003	14.663	0.001	14.011	0.001
GECO	33.064	0.005	14.392	0.002	13.233	0.002
WILLROY	33.038	0.004	14.383	0.002	13.206	0.001
WINSTON	33.050	0.003	14.378	0.001	13.214	0.001
ZENITH	33.811	0.008	14.566	0.004	13.764	0.002
WYE	34.312	0.002	14.694	0.001	14.267	0.001
VANGUARD	34.717	0.004	14.877	0.002	15.181	0.001
SHEBANDOWAN	34.464	0.008	14.674	0.003	14.223	0.003
N.COLDSTREAM	34.255	0.006	15.832	0.003	21.062	0.004

Abbreviations:

±2 SE_8/4: 2 x Standard Error for $^{208}Pb/^{204}Pb$ ratio

±2 SE_7/4: 2 x Standard Error for $^{207}Pb/^{204}Pb$ ratio

±2 SE_6/4: 2 x Standard Error for $^{206}Pb/^{204}Pb$ ratio

APPENDIX F: OGS MISCELLANEOUS RELEASE – DATA 306 (2013) (ONLINE/DVD)

This appendix is a digital product that is published by the Ontario Geological Survey and is the final deliverable required to satisfy the commitments of the Laurentian University-Ontario Geological Survey Mapping School Program. It is available for free download at the website address below or is available in hard copy in the DVD sleeve bound with this thesis. It is reproduced in this thesis with permission from the Publication Sales and Services of the Ontario Geological Survey.

This publication is a compilation of all field observations, sample information, and analytical results collected within Ontario and are geospatially presented in ESRI ArcGIS format. In addition to ArcGIS file formats, the analytical data is also included as Microsoft Excel files. The data contained in this release is referenced in each of the manuscripts presented in Chapters 2, 3, and 4.

Website:

http://www.geologyontario.mndmf.gov.on.ca/mndmaccess/mndm_dir.asp?type=pub&id=MRD306

APPENDIX G: OGS SUMMARY OF FIELD WORK AND OTHER ACTIVITIES – OFR 6280-10 (2012)

This appendix contains a report published by the Ontario Geological Survey summarizing U-Pb geochronological data collected within the Shebandowan greenstone belt. The raw data for this report is published within the publication included as Appendix F. This report is available for free download from the website address stated below and is reproduced in this thesis with the permission of the Publication Sales and Services section of the Ontario Geological Survey.

The data presented in this report was referenced in the manuscripts presented in Chapters 2 and 4.

Website

http://www.geologyontario.mndmf.gov.on.ca/mndmaccess/mndm_dir.asp?type=pub&id=OFR6280

10. Project Unit 10-010. Preliminary Results of Uranium–Lead Geochronology from the Shebandowan Greenstone Belt, Wawa Subprovince

R.W.D. Lodge[1,2]

[1]Mineral Exploration Research Centre, Department of Earth Sciences, Laurentian University, Sudbury, Ontario P3E 2C6
[2]Earth Resources and Geoscience Mapping Section, Ontario Geological Survey, Sudbury, Ontario P3E 6B5

INTRODUCTION

This article is the third report (*see* previous reports Lodge 2010, 2011) that summarizes some of the results of an ongoing four-year PhD thesis study designed to compare the geodynamic setting of volcanogenic massive sulphide (VMS) mineralization in the Shebandowan, Vermilion, Winston Lake and Manitouwadge greenstone belts along the northern boundary of the Wawa Subprovince adjacent to the Quetico Subprovince (Figure 10.1). This research is supported by the Ontario Geological Survey and the Department of Earth Sciences at Laurentian University through the Ontario Geological Survey–Laurentian University Graduate Mapping School Program.

Mapping during the summers of 2010 and 2011 focussed on investigating the volcanology and geodynamic setting of the Shebandowan, Vermilion, Winston Lake and Manitouwadge greenstone belts. Mapping and sampling were completed along semilinear, regional-scale transects through representative strata within each greenstone belt to determine geodynamic environment and petrogenetic processes of each belt as they relate to VMS-potential. During mapping, more than 800 rock samples were from these belts. Of these samples, 400 were chosen for full geochemical analyses, 70 for neodymium and lead isotopic analyses, 7 for magmatic zircon U/Pb geochronologic analysis, and 7 for detrital zircon U/Pb geochronologic analysis.

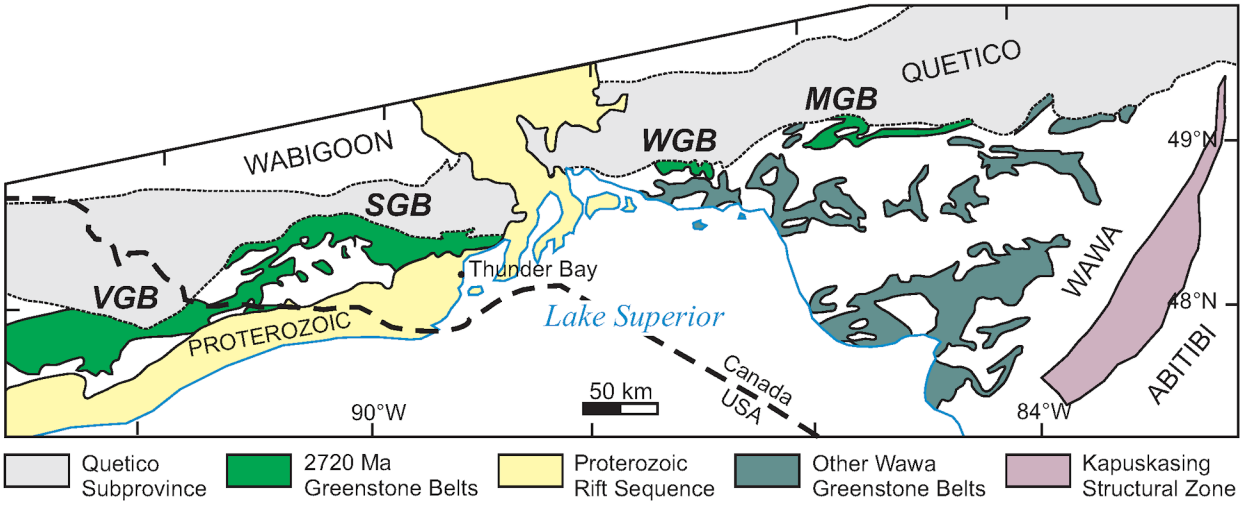

Figure 10.1. General geology of the Wawa Subprovince of the Superior Craton. Abbreviations: MGB, Manitouwadge greenstone belt; SGB, Shebandowan greenstone belt; VGB, Vermilion greenstone belt; WGB, Winston Lake greenstone belt. "Abitibi", "Quetico", "Wabigoon" and "Wawa" labels refer to subprovinces of the Archean Superior Province. Figure *from* Lodge (2011).

Summary of Field Work and Other Activities 2012,
Ontario Geological Survey, Open File Report 6280, p.10-1 to 10-10.

This report will discuss the preliminary results of the U/Pb geochronology of samples collected from the Shebandowan greenstone belt in 2010 and 2011.

ANALYTICAL METHODS

Three samples were submitted to the Jack Satterly Geochronology Laboratory at the University of Toronto for high-precision U/Pb age determinations by thermal ionization mass spectrometry (TIMS) analysis. One sample for lower-precision U/Pb ages and 5 samples for detrital zircon ages were sent to the laser ablation inductively coupled plasma mass spectrometry (LA-ICP–MS) lab at Laurentian University for analyses. The methodology for zircon separation was the same at both laboratories. Samples were crushed, milled, and passed over a Wilfley® table to obtain a pre-concentrate of heavy minerals. The pre-concentrate was then split into magnetic fractions before the least magnetic fraction was passed through heavy liquids to separate zircons and other heavy minerals (pyrite, apatite, etc). Zircons were then hand picked from the heavy minerals separates.

Thermal Ionization Mass Spectrometric Analysis at University of Toronto

The zircons from each sample were thermally annealed and chemically abraded with hydrofluoric (HF) acid using the methodologies outlined by Mattinson (2005) for improved precision of calculated ages for analyzed zircon grains. These processes chemically homogenize the grain and remove the outermost layer of the grains where lead-loss is most likely to occur. Following treatment of the grains, 3 to 5 "ideal" zircons were hand picked on the basis of crystal quality and clarity. These zircons were then dissolved in accordance to the procedures outlined by Krogh (1973). Uranium and lead were separated using anion exchange columns before analysis (Gerstenberger and Haase 1997). Uranium-lead age determinations and plotting of concordia diagrams were completed using Isoplot for Microsoft® Excel® (Ludwig 2012) and calculated using the U/Pb decay constants from Jaffey et al. (1971).

Laser Ablation Inductively Coupled Plasma Mass Spectrometric Analysis at Laurentian University

Untreated zircons were hand picked and mounted in epoxy for analysis by LA-ICP–MS. All grains were analyzed using a 193 nm ArF excimer laser to vaporize material from each grain with a spot size of 17 µm. The ablated material was carried via a gaseous stream of helium, argon and nitrogen to a Thermo X Series II quadrupole ICP–MS where it was then analyzed for uranium, thorium and lead content. Uranium-thorium-lead data were calibrated using the 91500 zircon geostandard (Wiedenbeck et al. 1995), and quality control was completed with analysis of 2 additional geostandards: the Plešovice (Plešovice quarry zircon, Blanský les granulite body, Bohemian Massif, Czech Republic: Sláma et al. 2008) and Temora-2 (Temora-2 zircon is from the Middledale gabbroic diorite, Temora, New South Wales, Australia: Black et al. 2003). Age determinations of each standard had to be within error from the published accepted age before proceeding with analysis and age determination of sample zircons. Each individual zircon analysis was inspected in terms of signal intensity as a function of time so as to distinguish distinct zones of different Th/U, $^{207}Pb/^{206}Pb$, ^{204}Pb, ^{88}Sr and/or ^{209}Bi. Zones of signal showing evidence of alteration (high ^{88}Sr) or common-lead contamination (high ^{204}Pb, ^{209}Bi, erratic $^{207}Pb/^{206}Pb$ ages) were not integrated for final age determination of the zircon. Uranium-lead concordia diagrams were constructed using Iolite (Paton et al. 2011) and VizualAge (Petrus and Kamber 2012) programs. Histograms were generated using Isoplot for Microsoft® Excel® (Ludwig 2012).

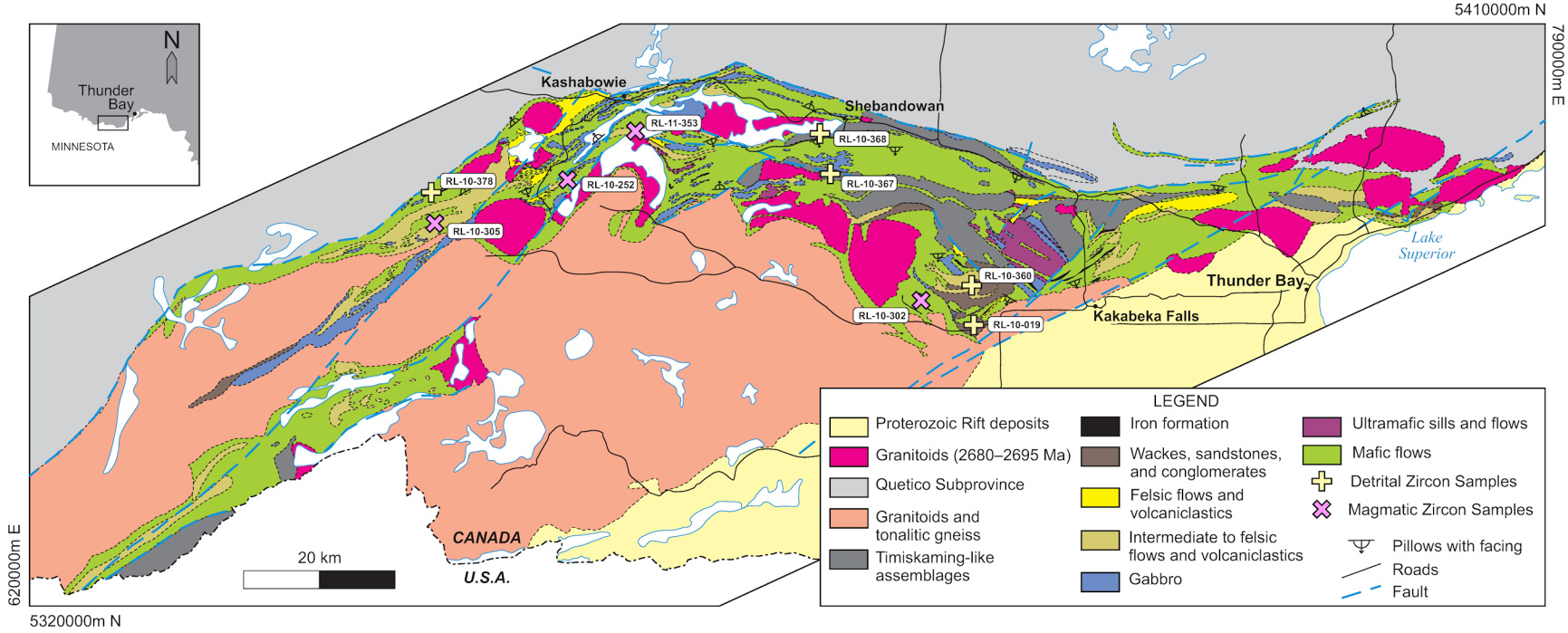

Figure 10.2. Regional geology of the Shebandowan greenstone belt showing locations of samples taken for U/Pb geochronological analysis. Figure *modified from* Lodge (2011) and compiled and *modified from* Santaguida (2001a, 2001b). Universal Transverse Mercator (UTM) co-ordinates are provided using North American Datum 1983 (NAD83), Zone 15.

Table 10.1. Details of samples collected from the Shebandowan greenstone belt.

Sample	Township or Area	UTM Zone	Easting (m)	Northing (m)	Method	Age Type
RL-10-019	Marks	16	291133	5364950	LA-ICP–MS	Detrital
RL-10-252	Burchell Lake Area	15	680320	5379603	TIMS	Volcanic
RL-10-302	Aldina	16	283069	5365089	TIMS	Volcanic
RL-10-360	Adrian	16	290767	5369539	LA-ICP–MS	Detrital
RL-10-367	Duckworth	15	715382	5387512	LA-ICP–MS	Detrital
RL-10-368	Conacher	15	715817	5383007	LA-ICP–MS	Detrital
RL-10-378	Moss	15	662733	5377895	LA-ICP–MS	Detrital
RL-11-305	Moss	15	664180	5375812	TIMS	Volcanic
RL-11-353	Greenwater Lake Area	15	688477	5387009	LA-ICP–MS	Volcanic

All UTM co-ordinates are reported in NAD83. Abbreviations: LA-ICP–MS, laser ablation inductively coupled plasma mass spectroscopy; TIMS, thermal ionization mass spectroscopy.

By using VizualAge to determine U/Pb ages (Petrus and Kamber 2012), most of the data points were near concordant and only a few samples that were more that 10% discordant were rejected from the final data set. Magmatic ages were determined in VizualAge by statistical analysis of clustered and overlapping data points. The average error for the $^{207}Pb/^{206}Pb$ ages for individual grains averaged 20 to 40 m.y., but was often as low as 10 to 15 m.y. Therefore, trends in the age of the population are more relevant for interpreting the data rather than the age of individual grains in detrital zircon analysis.

RESULTS AND DISCUSSION

Geochronologic sampling in the Shebandowan greenstone belt (*see* Figure 10.2 for sample locations) focussed on establishing the age of volcanism in VMS-prospective strata throughout the belt. Detrital zircon analysis was conducted on 5 samples from various metasedimentary basins to better understand the provenance of the detritus, tectonic evolution of the belt and metallogenic significance of the basins. Previous geochronological studies in the Shebandowan greenstone belt (Corfu and Stott 1986, 1998; Hart 2007) established 3 main assemblages: Greenwater (*circa* 2720 Ma), Kashabowie (*circa* 2695 Ma) and Shebandowan (*circa* 2680 to 2690 Ma). The details of each sample analyzed are summarized in Table 10.1.

Detrital zircon analyses for each of the samples produced ages that are significantly younger than 2680 Ma (Figure 10.3), which is the previous youngest age for a unit in the Shebandowan greenstone belt (Corfu and Stott 1998). These younger ages are interpreted to be the result of analyzing a metamorphic rim or overgrowth. Detrital grains were untreated before picking and mounting for analysis and, therefore, these younger zircon growths may have been preserved despite abrasion during polishing. Therefore, the youngest ages (post-2680 Ma) most likely reflect younger regional thermal events and not a younger sedimentary provenance.

Sample RL-10-019 Thinly Bedded Wacke

This sample is a dark, thinly bedded wacke to sandstone taken from a roadside outcrop on Adrian Lake Road in Marks Township. Bedding is planar and ranges in thickness from 1 to 3 cm in the sampled outcrop. Other outcrops in the immediate area are sandstones and heterolithic paraconglomerates that are interpreted to be deposited in a shallow marine to fluvial environment (Rogers and Berger 1995). Erosional features such as channel structures are present in nearby outcrops.

Detrital zircons from this sample (n = 143) are generally small, equant to slightly prismatic crystals. They are typically euhedral with slightly rounded crystal facies. Grains have a high to moderate level of

opacity and are colourless to weakly coloured. All analyzed grains fall within 10% discordance. The calculated $^{207}Pb/^{206}Pb$ ages for the detrital zircons are graphically summarized as a histogram in Figure 10.3. A preliminary version of this data is presented in Lodge (2010).

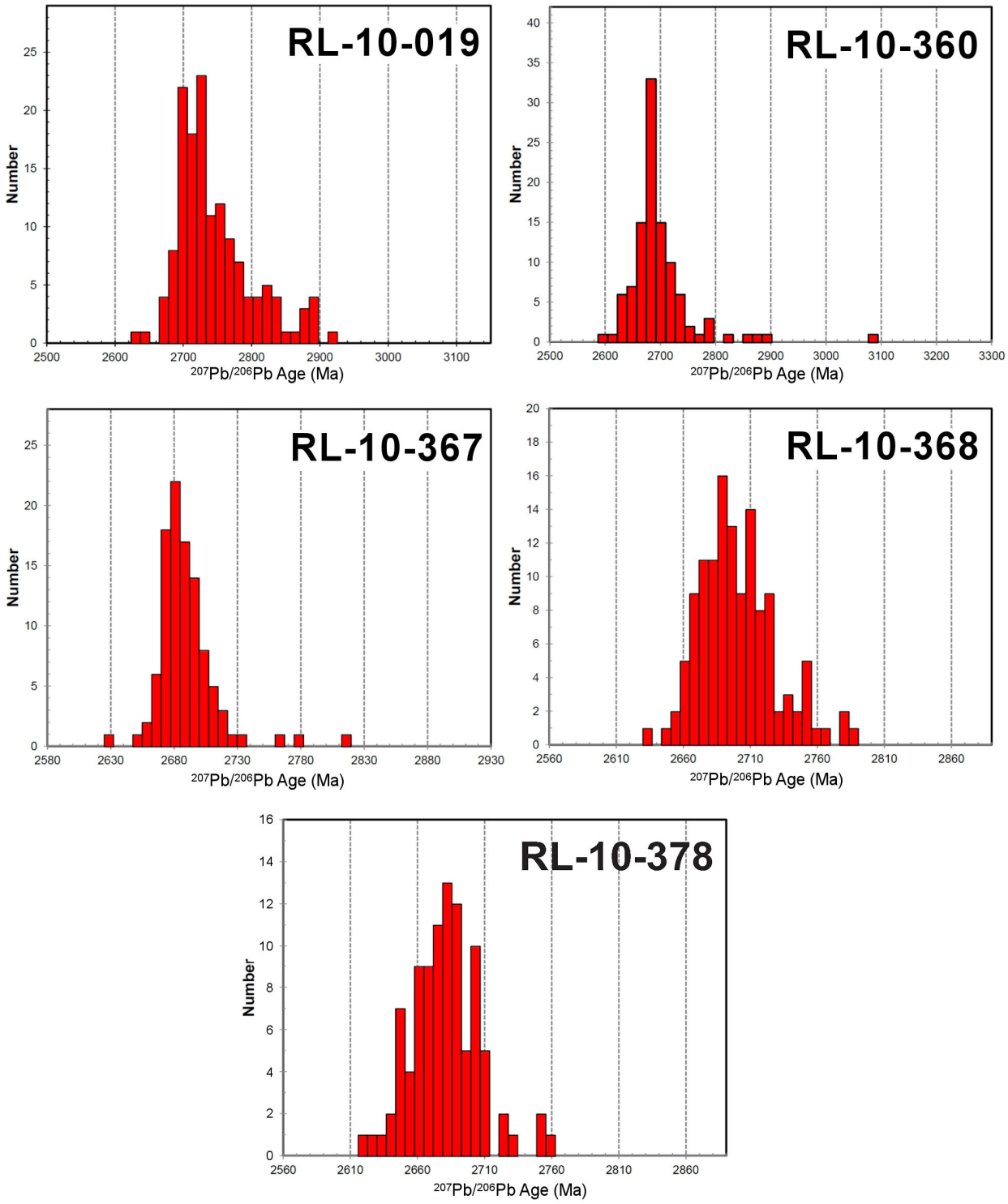

Figure 10.3. Histograms showing distribution of $^{207}Pb/^{206}Pb$ ages for detrital zircons for each sample analyzed in 2010 and 2011 from the Shebandowan and Winston Lake greenstone belts.

The ages define a broad peak centred at 2700 to 2720 Ma with zircons as young as 2620 Ma. A significant proportion of detrital zircon ages are older than 2750 Ma, which represents the oldest rocks for which ages have been determined in the Shebandowan greenstone belt (Corfu and Stott 1998). The higher proportion of older ages (>2750 Ma) suggests that the sedimentary provenance of this sample extends beyond this region of the Wawa Subprovince.

Sample RL-10-252 Bedded Felsic Tuff and Crystal Tuff

This sample is from a bedded felsic volcaniclastic unit located near the southern tip of Upper Shebandowan Lake. Bedding in this unit varied in thickness, ranging from centimetre-scale to massive metre-scale beds. The sample contained interbedded felsic crystal tuff and tuff. The crystal tuff was composed of 35 to 60% feldspar crystals. The tuff layers were composed of a silt- to sand-sized felsic ash and were locally graded. In the immediate area, this unit also had metre-scale beds of coarse monolithic tuff breccia and minor heterolithic tuff breccia. Localized chlorite-garnet-pyrite alteration resembling metamorphosed VMS-associated hydrothermal alteration was present within this volcaniclastic unit.

Four zircons were selected after treatment for analysis. These grains are generally equant to slightly prismatic, doubly terminated, euhedral, sharply facetted crystals. These single-grain analyses gave concordant and overlapping data that have a weighted mean $^{207}Pb/^{206}Pb$ age of 2693.82±0.87 Ma (Kamo 2011). This is interpreted to be the age of volcanism for this unit and this unit is assigned to the Kashabowie assemblage.

Sample RL-10-302 Massive Felsic Flow

This sample was from a massive siliceous, muscovite-bearing felsic metavolcanic flow. Faint feldspar phenocrysts are visible on a freshly sawed surface and compose 1 to 2% of the rock. This felsic metavolcanic flow is associated with the VMS prospect explored by RJK Exploration Ltd. and is taken from one of the trenched outcrop exposures. Felsic volcaniclastic rocks were intersected in diamond-drill core (Franklin 2001), but were not observed in surface exposures during the 2010 field investigation. There is very little outcrop in this area other than in the trenches, so regional variation in the unit is unknown.

Four zircons were selected after treatment for analysis. Three grains are long prismatic euhedral crystals and 1 grain was more equant. The single-grain analyses produced concordant and overlapping data that have a weighted mean $^{207}Pb/^{206}Pb$ age of 2719.7±1.0 Ma (Kamo 2011). This is interpreted to be the age of the felsic flow and this unit is assigned to the Greenwater assemblage.

Sample RL-10-360 Massive Pebbly Sandstone

This sample is from a dark pebbly sandstone located in Adrian Township. The heterolithic clasts are up to 1 cm in size and compose approximately 20 to 30% of the rock. The clasts are supported in a sandy feldspar-rich matrix. Clasts are subangular and are moderately sorted. Clast composition ranges from dominantly mafic volcanic to intermediate volcanic rocks. Variation in clast sizes and abundances define metre-scale bedding in this area. These sediments were interpreted to be deposited in a shallow marine to fluvial setting (Lodge 2011; Rogers and Berger 1995).

Detrital zircons from this sample (n = 128) range from equant to stubby to prismatic crystals. In general, the zircons are slightly rounded reflecting sedimentary transport. They are generally colourless to weakly coloured and have moderate to high opacity. Data from these zircons are mostly concordant, with some evidence for lead-loss resulting in a higher degree of discordance. Data obtained from 23 zircons were higher than 10% discordance and were not included when plotting the histogram in Figure 10.3.

Uranium–lead ages from this sample define a tight peak centred at 2685 to 2695 Ma. The dominance of detrital zircons with ages equivalent to the age of the Shebandowan assemblage suggest a localized provenance for the detritus that was likely sourced from Shebandowan assemblage metavolcanic rocks. There are some older zircons, younger than 2750 Ma, which were either inherited from basement strata (no age determined) or have a provenance outside this region of the Wawa Subprovince.

Sample RL-10-367 Weakly Bedded Wacke

This sample is from a dark wacke to sandstone located in the central part of Duckworth Township. There is faint planar bedding noted by slight, centimetre-scale colour changes. Most of the metasedimentary outcrops in the immediate area are similar to the sampled outcrop. Aside from the planar bedding, the sampled unit is featureless and exposure is generally poor because of lichen cover.

Detrital zircons from this sample (n = 113) range from equant to stubby to weakly prismatic crystals. In general, the degree of rounding in these grains is minimal. They are generally colourless to weakly coloured and have moderate to high opacity. Data from these zircons are mostly concordant, with some evidence for lead-loss resulting in a higher degree of discordance. Data obtained from 11 zircons exceed the 10% discordance limit and are not included in the histogram of Figure 10.3.

The sample shows a distribution of U/Pb ages that define a moderately tight peak centred at 2680 to 2695 Ma. The dominance of detrital zircons with ages equivalent to the age of the Shebandowan assemblage suggests a localized provenance for the detritus that was likely sourced from Shebandowan assemblage metavolcanic rocks. Older zircons, younger than 2750 Ma, were either inherited from basement strata (age not determined) or have a provenance outside this region of the Wawa Subprovince.

Sample RL-10-368 Heterolithic Paraconglomerate

This sample is from a foliated, heterolithic paraconglomerate located along the Shebandowan Mine road in Conacher Township. The clast composition is highly varied and includes mafic to felsic volcanic rocks, sulphide mineralization, jasper and minor mafic to intermediate intrusive rocks. The conglomerate is moderately sorted and bedding is defined by the abundance and size of clasts. The paraconglomerate has been interpreted to be deposited in a alluvial–fluvial environment (Shegelski 1980). This outcrop is in close association with a reddish green, hornblende-phyric andesite to trachyandesite tuff breccia that is the characteristic volcanic lithofacies of the Shebandowan assemblage (Carter 1993; Corfu and Stott 1998; Shegelski 1980).

Detrital zircons from this sample (n = 126) range from equant to stubby to prismatic crystals. In general, the zircons are euhedral and the degree of rounding in these grains was minimal. They are generally colourless to weakly coloured and have moderate to high opacity. Data from these zircons are all near concordant, with very little evidence for lead-loss. The age distribution of the detrital zircons is represented as a histogram in Figure 10.3.

The distribution of U/Pb ages form a broad peak centred at 2680 to 2695 Ma. The dominance of detrital zircons with ages equivalent to the age of the Shebandowan assemblage suggests a localized provenance for the detritus that was likely sourced from Shebandowan assemblage metavolcanic rocks. There is a significant population that have ages *circa* 2720 Ma, suggesting a provenance from the Greenwater assemblage. The few, older zircons younger than 2750 Ma were either inherited from basement strata (age not determined) or have a provenance outside this region of the Wawa Subprovince.

Sample RL-10-378 Heterolithic Paraconglomerate

This sample is from a roadside exposure of a massive heterolithic pebble paraconglomerate located in Moss Township. There is no obvious bedding in this exposure. The clasts are poorly to moderately size sorted and constitute 40 to 60% of the rock. Clasts are 1 to 2 cm in size and are composed of mafic and felsic volcanic rocks with minor felsic intrusion clasts. The clasts are supported in a sandy, green matrix. There are no other exposures of this conglomerate or any other metasedimentary rocks in the immediate area where the strata is dominated by mafic volcanic lithofacies.

Detrital zircons from this sample (n = 113) range from equant to weakly prismatic, euhedral crystals. In general, the degree of rounding in the zircons is minimal. They are generally colourless to weakly coloured and have moderate to high opacity. Data from these zircons are all near concordant, with evidence for minor lead-loss. Data obtained from 17 zircons were higher than the 10% discordance cut-off and were not included when plotting the histogram in Figure 10.3.

The U/Pb ages form a broad peak centred at 2660 to 2695 Ma. There are a larger proportion of younger ages (post-2680 Ma) in this sample compared to others, and this may reflect a stronger metamorphic overprint. This sample is in close proximity to the northern margin of the Shebandowan greenstone belt and may have been influenced by later thermal events in the Quetico Subprovince (e.g., Davis, Pezzutto and Ojakangas 1990). Additional work on the analyzed zircons would be required to establish whether or not the ablated material was from a metamorphic rim or if there is a younger magmatic rock contributing detritus to this basin. If the latter was the case, then this would represent one of the youngest basins, as well as youngest igneous detritus, in the Shebandowan greenstone belt. Other than the youngest zircons, the main provenance of detritus appears to be the Shebandowan and Greenwater assemblages.

Sample RL-11-305 Pumiceous Felsic Lapilli Tuff

This sample is a light-coloured felsic crystal-rich pumiceous lapilli tuff located in Moss Township. Feldspar crystals in the matrix are 1 to 3 mm in size and often show broken crystal shapes. The quartz-phyric pumice fragments are 1 to 6 cm in size and compose 20 to 40% of the rock. These volcaniclastic deposits are in close association with autobrecciated to massive felsic flows that are exposed nearby.

At the time of report writing, results have not been returned from the Jack Satterly Geochronology Laboratory. These results will be published in 2013 (*see* "Future Work Planned").

Sample RL-11-353 Pumiceous Felsic Lapilli Tuff

This sample is from a light coloured pumice-bearing, felsic lapilli tuff located on the northern shoreline of Greenwater Lake. The sample is notable for the exceptional preservation of pumice fragments and feldspar-rich siliceous matrix. Pumice ranges from 1 to 5 cm in size and composes 20 to 25% of the rock. The presence of a siliceous matrix and the high abundance of pumice is consistent with a primary volcaniclastic deposit. This felsic unit is located along strike from pyrite-chalcopyrite-bearing sericitic schist. The nature of this mineralization is uncertain, but appears to be shear hosted and the property is currently being explored by Benton Resources Ltd.

Zircons in this sample are largely subhedral and display moderately formed crystal faces. Most grains are stubby, equant, or moderately prismatic. This sample had a lower zircon yield and, therefore, only 18 grains were analyzed by LA-ICP–MS. All data obtained from this sample produced a tight group

of concordant ages. When the best analyses were isolated, they provided a concordant age of 2723.1±4.4 Ma. This is interpreted to be the age of volcanism for this unit and this felsic unit is assigned to the Greenwater assemblage.

FUTURE WORK PLANNED

A Miscellaneous Release—Data (MRD) of all geochemical (major, trace, REE), isotopic (Sm/Nd, $^{207}Pb/^{204}Pb$), and U/Pb geochronological data will be released in 2013 and will be available online at GeologyOntario (www.ontario.ca/geology). This MRD will be a geographic information system (GIS)–based product and all geochemical and isotopic data and interpretations will be spatially controlled by results of the 2010 and 2011 mapping programs conducted in the Shebandowan, Winston Lake and Manitouwadge greenstone belts. All data will be released in both shape (ESRI® ArcGIS®) and Microsoft® Excel® file formats. Tables of all zircon analyses discussed in this report will be included with the MRD.

ACKNOWLEDGMENTS

This is the third report of a four-year PhD thesis project supported by the Mineral Exploration Research Centre (MERC) at the Department of Earth Sciences, Laurentian University (LU) and the Ontario Geological Survey and is co-supervised by Dr. Harold Gibson (LU) and Dr. Greg Stott (Stott Geoconsulting Ltd. (formerly OGS)). Additional members of the thesis committee are Dr. Doug Tinkham (LU) and Dr. Jim Franklin (Consultant). Additional funding is provided by the Natural Sciences and Engineering Research Council of Canada (NSERC) and the Society of Economic Geologists (SEG) Student Research Grant. Joe Petrus assisted with LA-ICP–MS analysis at Laurentian University. Michael Hamilton and Sandra Kamo completed the TIMS analyses at the Jack Satterly Geochronology Laboratory, University of Toronto.

REFERENCES

Black, L.P., Kamo, S.L., Allen, C.M., Aleinikoff, J.N., Davis, D.W., Korsch, R.J. and Foudoulis, C. 2003. TEMORA 1: a new zircon standard for Phanerozoic U-Pb geochronology; Chemical Geology, v.200, p.155-170.

Carter, M.W. 1993. The geochemical characteristics of Neoarchean alkalic magmatism in central Superior Province; *in* Summary of Field Work and Other Activities 1993, Ontario Geological Survey, Miscellaneous Paper 162, p.13-19.

Corfu, F. and Stott, G.M. 1986. U–Pb ages for late magmatism and regional deformation in the Shebandowan Belt, Superior Province, Canada; Canadian Journal of Earth Sciences, v.23, p.1075-1082.

——— 1998. Shebandowan greenstone belt, western Superior Province: U-Pb ages, tectonic implications, and correlations; Geological Society of America Bulletin, v.110, p.1467-1484.

Davis, D.W., Pezzutto, F. and Ojakangas, R.W. 1990. The age and provenance of metasedimentary rocks in the Quetico Subprovince, Ontario, from single zircon analyses: implications for Archean sedimentation and tectonics in the Superior Province; Earth and Planetary Science Letters, v.99, p.195-205.

Franklin, J.M. 2001. Preliminary assessment of the lithogeochemistry of the Aldina township base metal-gold-silver property; unpublished report by Franklin Geosciences Ltd. for RJK Explorations–Greater Leonora Resource Corp.

Gerstenberger, H. and Haase, G. 1997. A highly effective emitter substance for mass spectrometric Pb isotope ratio determinations; Chemical Geology, v.136, p.309-312.

Hart, T.R. 2007. Geochronology of the Hamlin and Wye lakes area, Shebandowan greenstone belt, Thunder Bay District; *in* Summary of Field Work and Other Activities 2007, Ontario Geological Survey, Open File Report 6213, p.9-1 to 9-8.

Jaffey, A.H., Flynn, K.F., Glendenin, L.E., Bentley, W.C. and Essling, A.M. 1971. Precision measurement of half-lives and specific activities of 235U and 238U; Physical Reviews, v.4, p.1889-1906.

Kamo, S.L. 2011. Report on the U-Pb CA-ID-TIMS geochronology on volcanic and plutonic rocks, Grenville and Superior provinces, Ontario, for the Ontario Geological Survey; unpublished report, Jack Satterly Geochronology Laboratory, Department of Geology, University of Toronto, 22 Russell Street, Toronto, Ontario, 38p.

Krogh, T.E. 1973. A low contamination method for hydrothermal decomposition of zircon and extraction of U and Pb for isotopic age determinations; Geochimica et Cosmochimica Acta, v.37, p.485-494.

Lodge, R.W.D. 2010. Volcanology and lithofacies of the Shebandowan greenstone belt, Wawa Subprovince; *in* Summary of Field Work and Other Activities 2010, Ontario Geological Survey, Open File Report 6260, p.16-1 to 16-22.

——— 2011. A progress report on the volcanology, stratigraphy and geodynamic setting of greenstone belts of age 2720 Ma near the Wawa–Quetico subprovincial boundary; *in* Summary of Field Work and Other Activities 2011, Ontario Geological Survey, Open File Report 6270, p.11-1 to 11-13.

Ludwig, K.R. 2012. User's manual for Isoplot 3.75. A geochronological toolkit for Microsoft® Excel®; Berkley Geochronology Center, Special Publication No. 5, 75p.

Mattinson, J.M. 2005. Zircon U-Pb chemical abrasion ("CA-TIMS") method: combined annealing and multi-step partial dissolution analysis for improved precision and accuracy of zircon ages; Chemical Geology, v.220, p.47-66.

Paton, C., Hellstrom, J., Paul, B., Woodhead, J. and Hergt, J. 2011. Iolite: freeware for the visualization and processing of mass spectrometer data; Journal of Analytical Atomic Spectrometry, v.26, p.2508-2518.

Petrus, J.A. and Kamber, B.S. 2012. VizualAge: a novel approach to laser ablation ICP-MS U-Pb geochronology data reduction; Geostandards and Geoanalytical Research, v.36, p.247-270, DOI: 10.1111/j.1751-1908X.2012.00158.x.

Rogers, M.C. and Berger, B.R. 1995. Precambrian geology, Adrian, Marks, Sackville, Aldina and Duckworth townships; Ontario Geological Survey, Report 295, 66p.

Santaguida, F. 2001a. Precambrian geology compilation series–Quetico sheet; Ontario Geological Survey, Map 2663, scale 1:250 000.

——— 2001b. Precambrian geology compilation series–Thunder Bay sheet; Ontario Geological Survey, Map 2664, scale 1:250 000.

Shegelski, R.J. 1980. Archean cratonization, emergence and red bed development, Lake Shebandowan area, Canada; Precambrian Research, v.12, p.331-347.

Sláma, J., Košler, J., Condon, D.J., Crowley, J.L., Gerdes, A., Hanchar, J.M., Horstwood, M.S.A., Morris, G.A., Nasdala, L., Noberg, N., Schaltegger, U., Schoene, B., Turbrett, M. and Whitehouse, M.J. 2008. Plešovice zircon - a new natural reference material for U-Pb and Hf isotopic microanalysis; Chemical Geology, v.249, p.1-35.

Wiedenbeck, M., Allé, P., Corfu, F., Griffen, W.L., Meier, M., Oberli, F., Von Quadt, A., Roddick, J.C. and Spiegel, W. 1995. Three natural zircon standards for U-Th-Pb, Lu-Hf, trace element and REE analyses; Geostandards Newsletter, v.19, p.1-23.

APPENDIX H: OGS SUMMARY OF FIELD WORK AND OTHER ACTIVITIES – OFR 6270-11 (2011)

This appendix contains a report published by the Ontario Geological Survey summarizing observations made during field work completed in the summer of 2011. These include preliminary interpretations of transect mapping in the Vermilion, Shebandowan, Winston Lake, and Manitouwadge greenstone belts. This report is available for free download from the website address stated below and is reproduced in this thesis with the permission of the Publication Sales and Services section of the Ontario Geological Survey.

The figures generated for this report were modified and presented in the manuscripts presented in Chapters 2, 3, and 4.

Website

http://www.geologyontario.mndmf.gov.on.ca/mndmaccess/mndm_dir.asp?type=pub&id=OFR6270

11. Project Unit 10-010. A Progress Report on the Volcanology, Stratigraphy and Geodynamic Setting of Greenstone Belts of Age 2720 Ma near the Wawa–Quetico Subprovincial Boundary

R.W.D. Lodge[1]

[1]Mineral Exploration Research Centre, Department of Earth Sciences, Laurentian University, Sudbury, Ontario P3E 2C6

INTRODUCTION

This article represents the second progress report on a four-year PhD thesis study designed to determine why some greenstone belts of age 2720 Ma are productive in generating volcanogenic massive sulphide (VMS) whereas others are not. This will be achieved by comparing the volcanic and geodynamic setting of VMS mineralization in the Shebandowan, Vermilion, Winston Lake and Manitouwadge greenstone belts along the northern boundary of the Wawa Subprovince with the Quetico Subprovince (Figure 11.1). The main phase of construction and VMS-mineralization for each of these belts was *circa* 2720 Ma (Corfu and Stott 1998; Davis, Schandl and Wasteneys 1994; Peterson et al. 2001). This thesis work is supported through the Ontario Geological Survey–Laurentian University Graduate Mapping School Program (for work conducted in Ontario); and an NSERC Alexander Graham Bell Canada Graduate Scholarship (awarded to the author) and an NSERC Discovery Grant (Dr. H.L. Gibson, Laurentian University) (for work conducted in Minnesota).

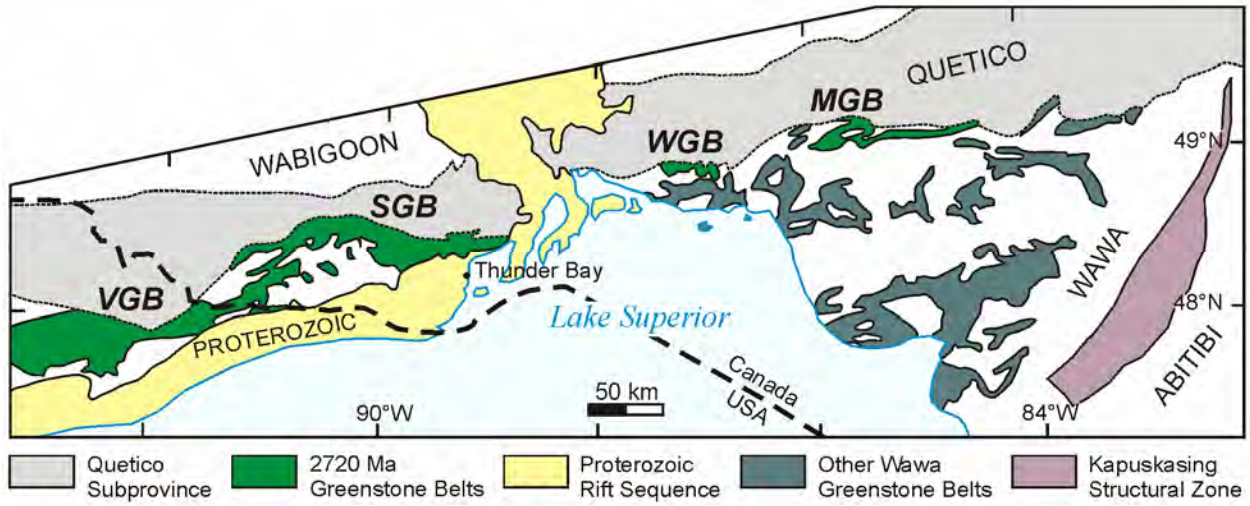

Figure 11.1. General geology of the Wawa Subprovince of the Superior Craton. Abbreviations: MGB, Manitouwadge greenstone belt; SGB, Shebandowan greenstone belt; VGB, Vermilion greenstone belt; WGB, Winston Lake greenstone belt. Abitibi, Quetico, Wabigoon and Wawa labels refer to subprovinces of the Archean Superior Province.

Summary of Field Work and Other Activities 2011,
Ontario Geological Survey, Open File Report 6270, p.11-1 to 11-13.

Bedrock mapping in the summer of 2010 (Lodge 2010) focussed on investigating the volcanology and geodynamic setting of the Shebandowan greenstone belt. In 2011, regional bedrock mapping was completed along semilinear transects though the representative strata in each of the Vermilion, Winston Lake and Manitouwadge greenstone belts. Additional mapping was completed in the Shebandowan greenstone belt to improve the regional coverage from the 2010 season. The goal of this phase of the field work is to compare the volcanology and geodynamic setting of the greenstone belts as they relate to the VMS-metallogeny. Despite the similar age and tectonostratigraphic setting of these greenstone belts, they are vastly different in their VMS endowment.

ACCESS AND PREVIOUS WORK

The Vermilion greenstone belt was accessed via logging and park roads off of US Route 1 near the towns of Ely, Soudan, and Tower in northeastern Minnesota (Figure 11.2). All of the mapped and sampled areas are within the bounds of recent regional maps from the Minnesota Geological Survey in the Soudan–Ely region (Peterson 2004; Peterson and Jirsa 1999). Property-scale mapping of VMS prospects has been completed by Hudak, Heine, Hocker and Huack (2002) and Hudak, Heine, Newkirk et al. (2002).

The Winston Lake greenstone belt (WGB) is more remote and access is limited. All-terrain vehicle (ATV) trails around the past-producing Winston Lake Mine property (Inmet Mining Corporation), north of the town of Schreiber on Highway 17, provided access to the western parts of the belt (Figure 11.3), whereas ATV trails and logging roads provide access to the eastern and central parts of the belt. There has been considerably less recent work completed in the WGB over the years. The most recent published research is a PhD thesis study that focussed on the Winston Lake Mine area (Osterberg 1993). Regional mapping was completed by the Ontario Geological Survey more than 40 years ago (Bartley 1940; Pye 1964).

The Manitouwadge greenstone belt (MGB) (Figure 11.4) is located north of Highway 17 near the town of Manitouwadge on Highway 614. Parts of the MGB that were mapped this summer were accessed via a logging road network centred on the town and through the mine road network on the past-producing Geco–Willroy Mine property (Xstrata Zinc). The belt was most recently mapped by the Geological Survey of Canada (Zaleski and Peterson 2001). The most recent published map from the Ontario Geological Survey is almost 40 years old (Milne 1974). The depositional setting (Zaleski and Peterson 1995) and structural history (Peterson and Zaleski 1999) of the MGB has been well documented and researched.

The Shebandowan greenstone belt (SGB) (Figure 11.5) extends west from Thunder Bay to the Quetico Provincial Park along Highway 102 and Highway 11 to the village of Kashabowie where the greenstone belt bends to the southwest and is then accessible via a logging road network. Field studies in the SGB have been regional- and township-scale mapping projects (e.g., Brown 1995; Hart and Trebilcock 2006; Osmani 1997; Rogers and Berger 1995) or property-scale maps and reports (e.g., Farrow 1994, 1995; Franklin 2003, 2005; Osmani 1996).

MAPPING RESULTS

Mapping in the Manitouwadge, Winston Lake and Vermilion greenstone belts focussed on establishing a regional litho- and chemostratigraphy for the respective belts. Detailed transect mapping and outcrop sketches were completed of strata hosting the past-producing Winston Lake Mine in the Winston Lake greenstone belt. Mapping in the Shebandowan greenstone belt focussed on completing the regional transects that were initiated in 2010 (Lodge 2010), describing the lithofacies and determining stratigraphic relationships. Data collected will provide the basis for regional comparisons of VMS-potential and geodynamic settings. Field photographs of relevant lithofacies from each greenstone belt are represented in Photo 11.1.

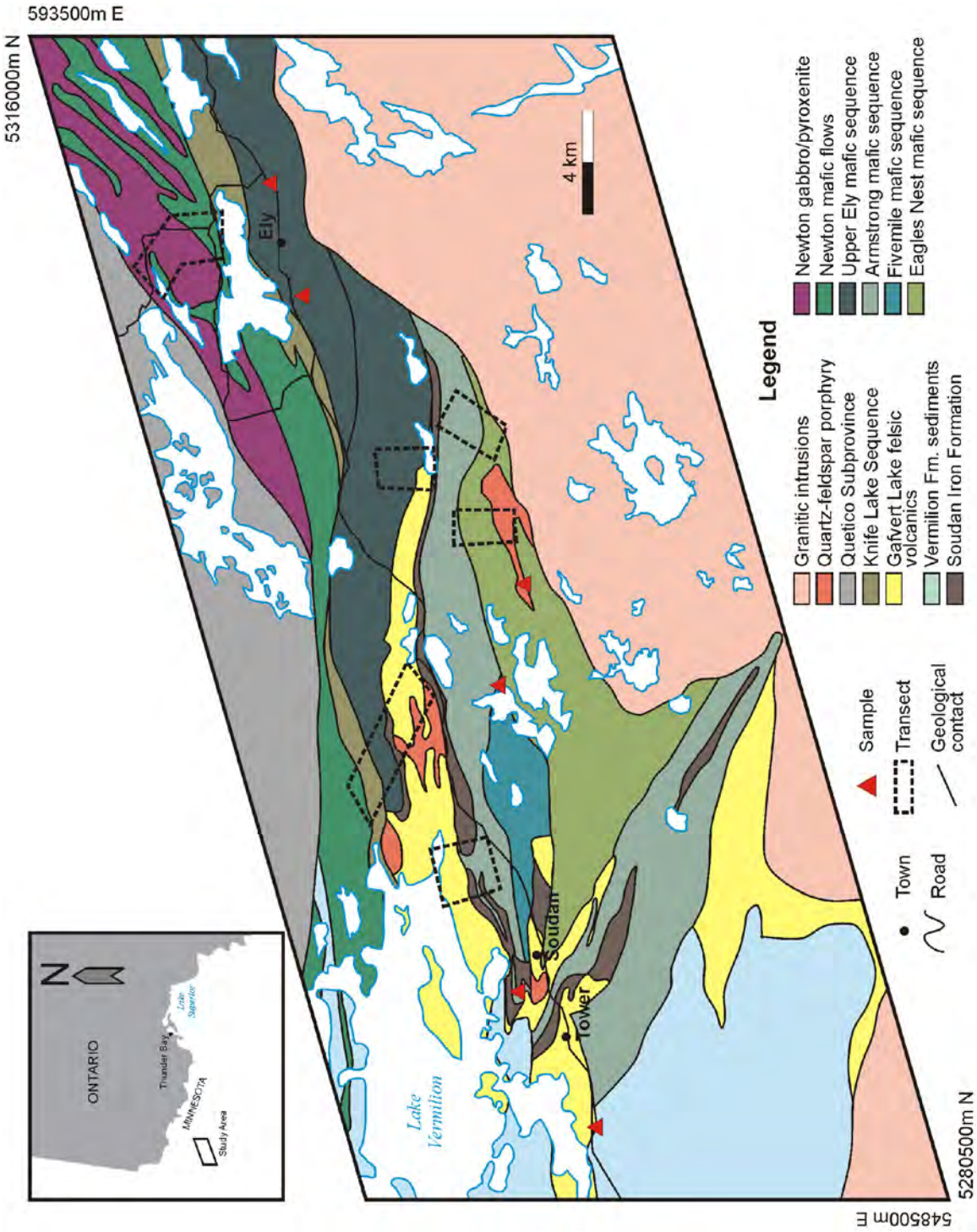

Figure 11.2. General geology of a portion of the Vermilion greenstone belt (geology *compiled from* Peterson (2004) and Peterson and Jirsa (1999)). Univeral Transverse Mercator (UTM) co-ordinates are provided using North American Datum 1983 (NAD83), Zone 15.

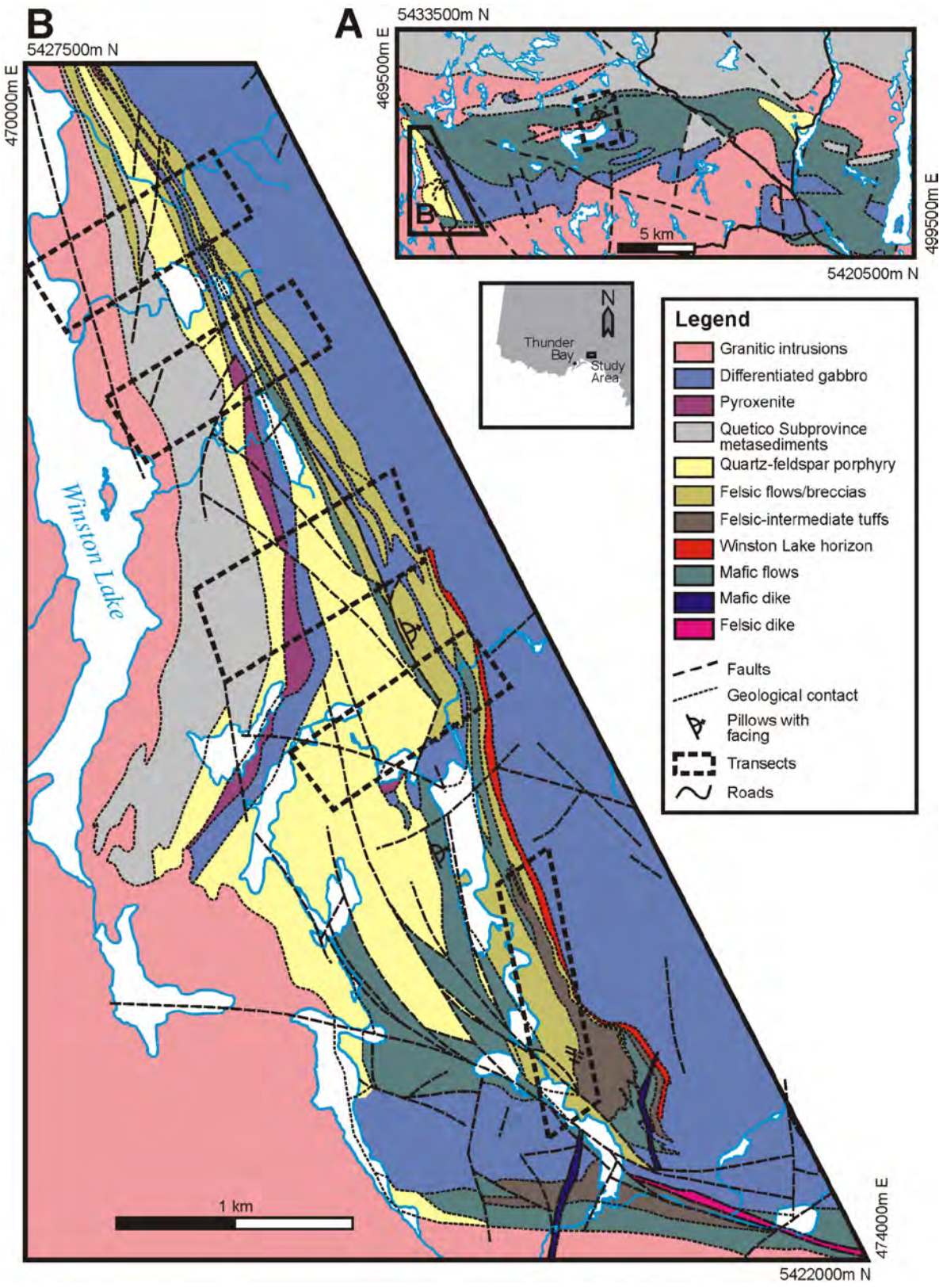

Figure 11.3. General geology of A) the Winston Lake greenstone belt and B) the Winston Lake Mine property (geology *compiled from* Osterberg (1993), Pye (1964) and Bartley (1940)). Univeral Transverse Mercator (UTM) co-ordinates are provided using NAD83, Zone 16.

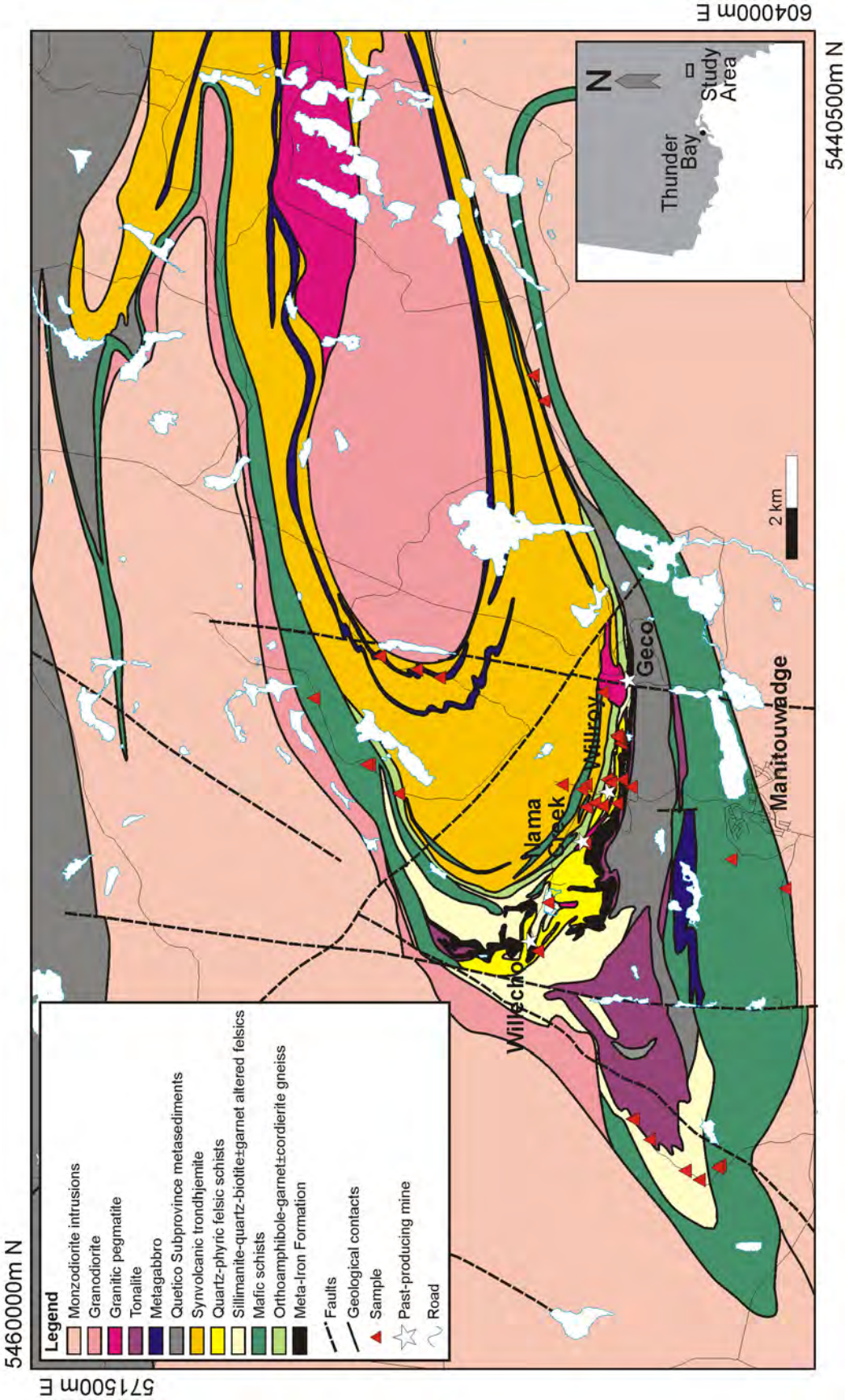

Figure 11.4. General geology of the Manitouwadge greenstone belt (geology *from* Zaleski and Peterson (2001)). Univeral Transverse Mercator (UTM) co-ordinates are provided using NAD83, Zone 16.

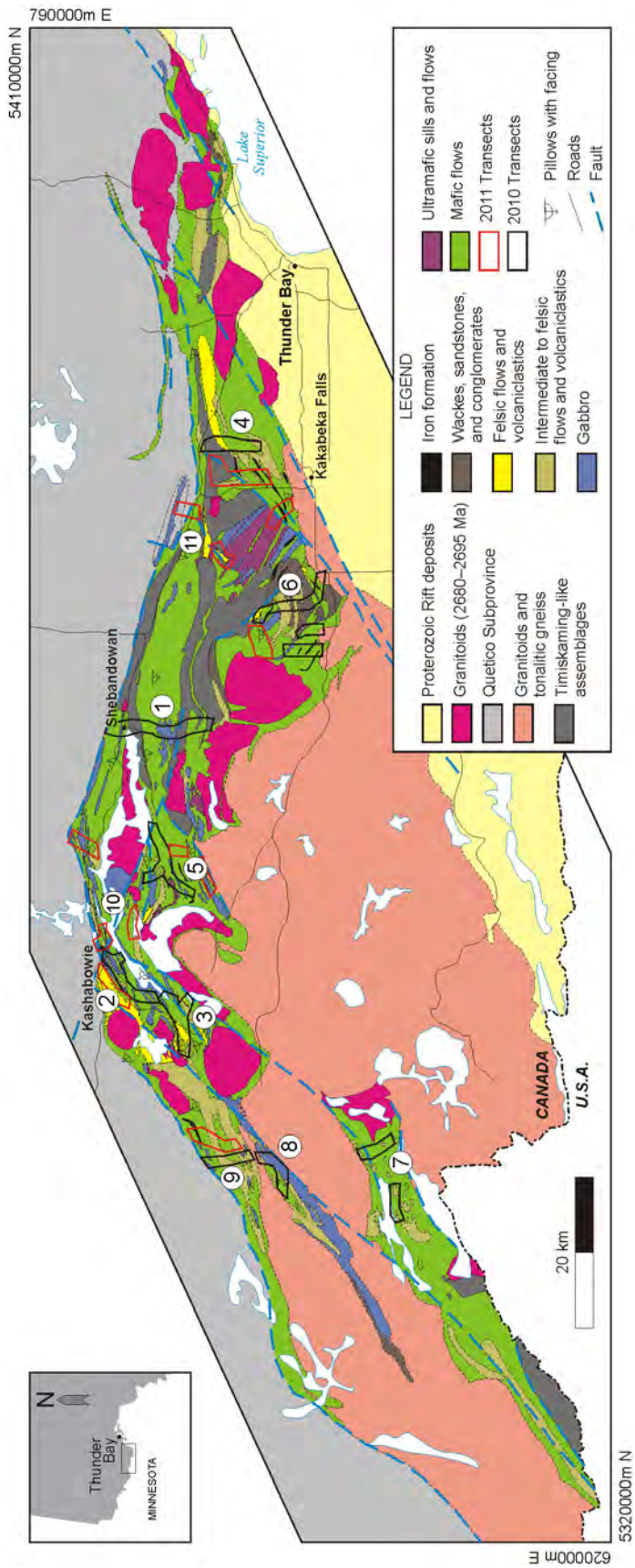

Figure 11.5. General geology of the Shebandowan greenstone belt showing 2010–2011 field work (geology compiled by Ontario Geological Survey). Transects: 1) Shebandowan–Duckworth, 2) Vanguard–Coldstream, 3) Grouse Lake–Hermia Road, 4) Mud Lake Road, 5) Shebandowan Mine–Greenwater Lake, 6) Adrian–Aldina, 7) Saganagons greenstone belt, 8) Wye Lake Area, 9) Hamlin Lake–Moss Lake area, 10) Kabaigon Lake–Amp Lake area and 11) Sunshine area (for details regarding the locations of transects 1 to 9 from 2010 (black outline), *see* Lodge (2010)). Univeral Transverse Mercator (UTM) co-ordinates are provided using NAD83, Zone 15.

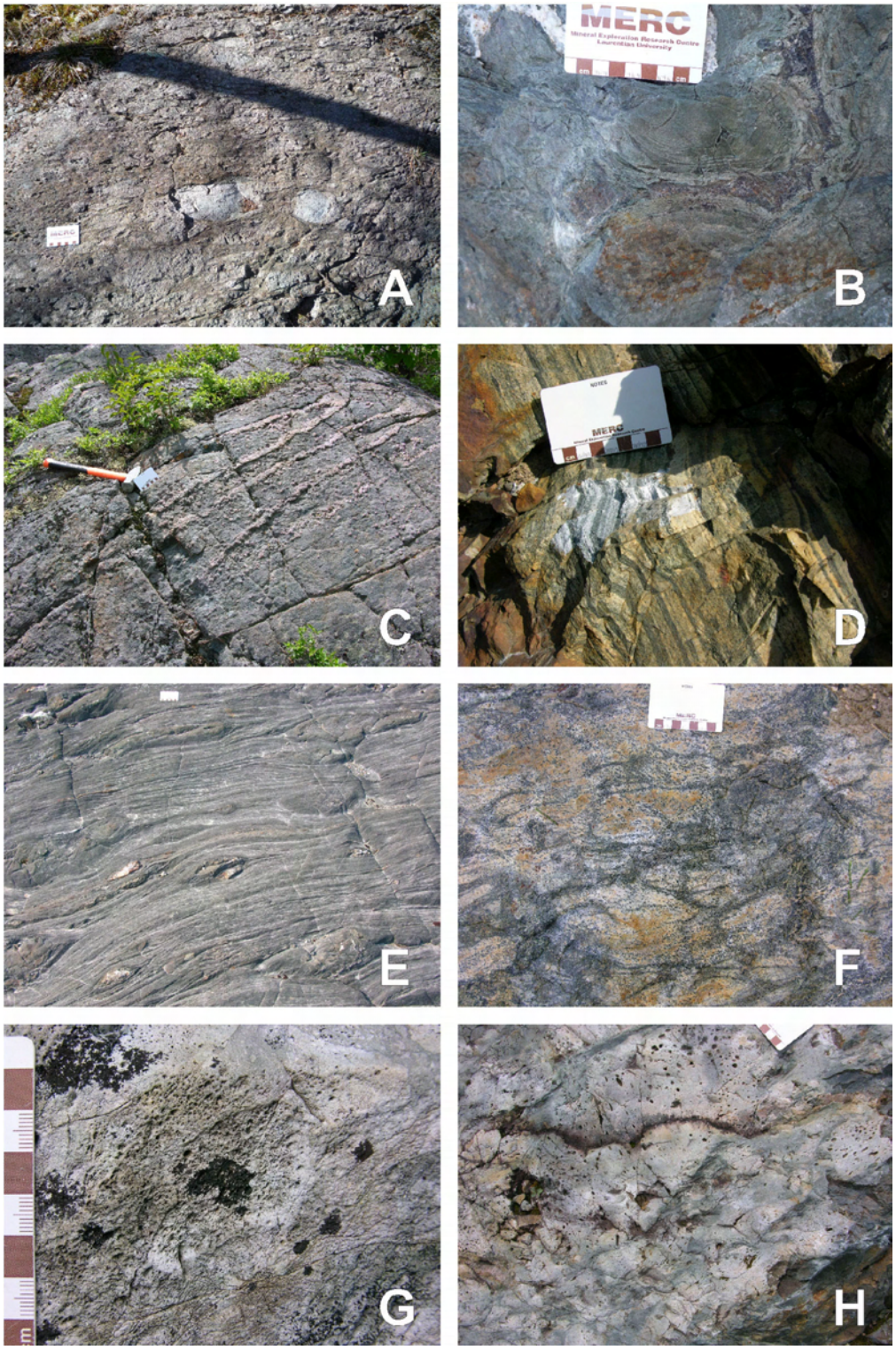

Photo 11.1. Field photographs from the Vermilion (A, B), Winston Lake (C, D), Manitouwadge (E, F) and Shebandowan (G, H) greenstone belts: A) felsic lapilli tuff to tuff breccia from the Gafvert Lake sequence; B) quenched and brecciated variolitic mafic pillow with hyaloclastite from the Newton belt; C) mineralized felsic tuff known as "Winston Lake horizon"; D) altered and flattened mafic pillows at the "ladder flow" with garnet-bearing selvages; E) dextrally sheared epidote-quartz altered (metamorphosed to clinopyroxene-quartz) mafic flow; F) quartz-phyric felsic flow breccia; G) felsic pumice lapilli tuff; H) silicified amygdaloidal mafic pillow flow.

Vermilion Greenstone Belt

The Vermilion greenstone belt is divided into 2 main belts: the Soudan and Newton belts. The Soudan belt to the north is composed of broadly folded calc-alkaline to tholeiitic volcanic strata and local turbiditic metasedimentary rocks. The Newton belt to the south contains komatiitic flows and peridotitic sills (Hudak et al. 2004). The focus of this portion of the study was to map 1:20 000 scale transects through the Soudan belt and complete reconnaissance sampling through accessible portions of the Newton belt. The depositional and structural history of the mapped area is well understood (Hudak et al. 2004; Peterson 2004); therefore, field work was designed as a sampling program within the context of previous interpretations of the geology.

Mafic metavolcanic rocks compose the majority of the Soudan belt and they have been subdivided into several sequences on the basis of field and geochemical characteristics (*see* Figure 11.2). The lower grade deformation and relatively intact stratigraphy of the region allowed for excellent preservation of primary volcanic textures. Many flows were highly amygdaloidal and pillowed with well-preserved hyaloclastite in pillow selvages. Moderate to intense epidote-quartz alteration is common in the Five Mile Lake and Armstrong Lake mafic metavolcanic sequences. The Ely mafic metavolcanic sequence is composed of variably altered, dark green pillowed mafic flows. Sampled outcrops of the Newton belt mafic flows were variolitic pillows with wispy and delicate hyaloclastite and quench-fractured pillow margins (Photo 11.1B). Medium- to coarse-grained gabbros and pyroxenites were also sampled in the Newton belt.

The Soudan iron formation is a significant component of the Soudan belt and appears to mark the transition between mafic-dominated and felsic-dominated volcanism of the Gafvert Lake sequence. The iron formation is largely deformed planar beds of jasper-hematite-magnetite. It is continuous for more than 30 km along strike and is up to 1 km thick.

Most of the felsic metavolcanic rocks in the Soudan belt occur in the Gafvert Lake sequence east of Lake Vermilion. The felsic metavolcanic rocks in this sequence are monolithic to heterolithic felsic lapilli tuff and tuff breccia. Fragments are mostly quartz-phyric felsic metavolcanic rocks with minor intraclasts of jasper and chert from the underlying Soudan iron formation (Photo 11.1A). The Gafvert Lake sequence is also intruded by a quartz-phyric granitic intrusion characterized by large, 5 to 10 mm euhedral quartz phenocrysts. There are also grey aphyric metavolcanic felsic flows associated with a VMS showing in the Five Mile Lake sequence.

Winston Lake Greenstone Belt

The Winston Lake greenstone belt (WGB) hosts the Winston Lake VMS deposit, which is located on the western margin of the belt. Detailed transect mapping at a scale of 1:5000 was completed through the VMS-hosting volcanic strata in order to establish a chemostratigraphy. In addition, 1:20 000 scale transect mapping was completed through the Big Duck Lake mafic metavolcanic flows to establish a chemostratigraphy for the central portion of the WGB. Lithofacies were continuous from the northern part of the Winston Lake Mine area to the Pick Lake area in the south-central part of the sequence (*see* Figure 11.3B) and it is assumed that this represents relatively intact stratigraphy. The WGB has undergone lower amphibolite-facies regional metamorphism.

Mafic metavolcanic rocks are metamorphosed to amphibolite with varying plagioclase content. Mafic metavolcanic flows are commonly pillowed with tops suggesting eastward-younging strata in the Winston Lake Mine area and northward-younging strata in the Big Duck Lake area. Volcanogenic massive sulphide-style alteration is a prominent characteristic in the Winston Lake Mine area. Amphibolitized, mafic metavolcanic flows were hydrothermally altered then metamorphosed and now have medium- to coarse-grained garnet + orthoamphibole ± biotite, orthoamphibole + cordierite ± biotite mineral assemblages. At

the “ladder flow”, altered intra-pillow material has been completely metamorphosed to garnet resulting in spectacular garnet “encrusted” pillow shapes (Photo 11.1D). Alteration was less common in the Big Duck Lake area, but, where present, it comprises bleaching of the rocks, silicification and epidote-quartz nodules. Medium- to coarse-grained amphibolitized metagabbro and metapyroxenite sills are found in both the Winston Lake Mine area and in the Big Duck Lake area.

Supracrustal felsic metavolcanic rocks were only observed in the Winston Lake Mine area. The “Winston Lake horizon” is a fine- to medium-grained pyrite-chalcopyrite-bearing quartzofeldspathic tuff with varying biotite ± orthoamphibole content defining thin layers (Photo 11.1C). More coherent quartz and feldspar-phyric felsic metavolcanic flows are present at the stratigraphic top and bottom of the transects. Most of the flows are altered and metamorphosed to a sillimanite+ biotite + muscovite ± garnet mineral assemblage that destroyed most primary volcanic textures. A thick and relatively homogeneous quartz-feldspar porphyry is exposed in the central part of the transects and may be a biotite + muscovite ± garnet altered synvolcanic intrusion. Where unaltered, this porphyry has an equigranular, intrusive-looking matrix.

In the Big Duck Lake area, a quartz-feldspar porphyry intrudes the mafic metavolcanic flows and has many sill-like protrusions around the margin of the porphyry. The intrusive margins of the porphyry are foliated with the mafic metavolcanic host rocks; however, the porphyry is more massive and equigranular in the interior suggesting it was emplaced during or prior to the deformation. There is active gold exploration along porphyry–mafic metavolcanic contact.

Metasedimentary rocks were observed in the western and northern margin of the WGB. These are metapsammites and metapelites that still retain their primary sedimentary bedding defined by varying mica content in a dominantly quartzofeldspathic matrix. Locally, at the west margin of the WGB, the metasedimentary rocks are composed of 50 to 80% porphyroblastic garnets up to 3 cm in size. Samples of the metasedimentary rocks at the west margin of the WGB are being analyzed for detrital zircon U/Pb geochronology.

Manitouwadge Greenstone Belt

The depositional and structural histories of the Manitouwadge greenstone belt (MGB) have already been described at a regional scale by Peterson and Zaleski (1999) and Zaleski and Peterson (1995). The main focus this summer was to map and sample along a transect through the relatively thick sequence of supracrustal strata that host the past-producing Willroy VMS deposits. These deposits have the best and most continuously exposed hanging-wall and footwall sequences of the MGB VMS deposits. Interpretation of the absolute stratigraphic relationships in the MGB is extremely difficult due to the complex structural history and high-grade metamorphism that affected the belt. In addition to this transect, representative samples from regional map units were obtained for geochemical comparisons within the MGB and for comparison to other greenstone belts. Regional metamorphic grade is upper amphibolite facies increasing to granulite facies northward toward the Quetico–Wawa subprovincial boundary.

Mafic metavolcanic rocks are metamorphosed to fine- to medium-grained hornblende amphibolite with the abundance of plagioclase ranging from 10 to 50%. Most primary volcanic textures are destroyed by intense shearing and deformation. Alteration is still evident as resistant clinopyroxene-quartz (originally epidote-quartz nodules) porphyroclasts in otherwise mylonitized amphibolite (Photo 11.1E). Stretched pillows with thin dark selvages are rare, but are locally preserved in the outer belt of mafic metavolcanic rocks. There are enclaves of mafic amphibolites and gneisses within the synvolcanic trondhjemite in the core of the Manitouwadge synform. Medium- to coarse-grained metagabbro sills are layered with the trondhjemite. Cordierite + orthoamphibole ± garnet gneisses are interpreted to be strongly altered mafic metavolcanic rocks in the footwall to the Willroy VMS mineralization.

Felsic metavolcanic rocks are generally noted by the presence of a quartzofeldspathic matrix as most of the felsic rocks were hydrothermally altered and metamorphosed to a sillimanite + biotite ± garnet ± muscovite mineral assemblage. Most primary volcanic textures are destroyed by alteration, deformation and metamorphism. In the immediate region of the Willroy deposits is a quartz-phyric felsic dome with associated flow breccias (Photo 11.1F) flanking a more massive and crystalline interior. There are other zones of apparent brecciation, but, due to the intense alteration and deformation, it is difficult to determine the nature and timing of the breccias. Coherent and equigranular felsic metavolcanic rocks in the sequence may be intrusions.

The Willroy, Nama Creek and Willecho VMS mineralization are associated with magnetite-chert-sulphide iron formation with folded and contorted laminations. Sulphide minerals in these iron formations are pyrite, sphalerite and chalcopyrite. Orthoamphibole + garnet ± cordierite gneisses are often found interlayered with the iron formations and are likely interbedded altered metavolcanic rocks.

Shebandowan Greenstone Belt

Bedrock mapping during the summer of 2011 was a continuation of the regional transect mapping initiated in 2010 (Lodge 2010). Transects 2, 4, 5, 6 and 9 (*see* Figure 11.5) were extended both parallel and perpendicular to regional strike. New transects (*see* Figure 11.5) were completed near the villages of Kashabowie and Sunshine, and near Kabaigon Lake and Amp Lake. Broader reconnaissance sampling targeting regional map units was completed in Conmee and McGregor townships. The SGB has 3 main phases of volcanism or magmatism grouped into the Greenwater (2720 Ma), Kashabowie (2695 Ma) and Shebandowan (2685 to 2690 Ma) assemblages (Corfu and Stott 1986, 1998). The Greenwater assemblage is associated with most of the VMS-style mineralization (e.g., Farrow 1993, 1994; Osmani 1997), although VMS-style alteration described in the Grouse Lake area (Lodge 2010) is Kashabowie assemblage in age (Kamo 2011).

Mafic metavolcanic rocks are extensive and vary in their textures and compositions. In the Greenwater Lake area, mafic metavolcanic rocks are massive to locally pillowed. They seem largely unaltered, aphyric or locally plagioclase phyric and do not contain amygdules or vesicles. There are pyroxene-phyric mafic to intermediate metavolcanic flows in the eastern transects located within Oliver Township. Mafic metavolcanic flows in the Kashabowie area and Moss Township are more varied in their flow textures. Flows are often highly amygdaloidal with amygdules composing up to 35% of the rock (Photos 11.1G and 11.1H). Pillows and pillow breccias are more common than massive flows. Alteration in the mafic metavolcanic flows includes local concentrations of epidote-quartz nodules and silicification that is not regionally developed. Variolitic mafic metavolcanic flows were observed in Conmee Township and in the Greenwater Lake area. Peridotite and gabbroic intrusions were common in the Greenwater Lake area and in Conmee Township. Ultramafic flows and/or sills were observed in the Greenwater Lake and past-producing Shebandowan Mine areas.

Intermediate to felsic metavolcanic rocks were described in Moss Township, and in the Greenwater and Kabaigon Lake areas. Felsic lapilli tuff and ignimbrite with pumice lapilli (*see* Photo 11.1G), broken feldspar crystals and quartz-phyric felsic volcanic fragments are exposed in the Greenwater Lake area and in Moss Township. Ignimbrites in Moss Township are closely associated with coherent and autobrecciated felsic flows. In the Burchell Lake and Kabaigon Lake areas, intermediate to felsic tuffs and/or flows are essentially aphanitic and siliceous and locally sericitic schists. In strongly deformed areas, rocks are fissile and foliations were kinked and folded resulting in the destruction of most primary volcanic textures. In the Mud Lake area, felsic metavolcanic flows are quartz and feldspar phyric with a fine-grained to aphanitic matrix. In all areas mapped this summer, the felsic rocks display weak to locally moderate VMS-style alteration.

Exposures of the Shebandowan assemblage were encountered on several transects in the eastern and central parts of the SGB. Most of these were turbiditic wackes, sandstones and conglomerates. A noteworthy outcrop of a subaerially weathered hornblende-phyric felsic metavolcanic flow capped by matrix-supported heterolithic conglomerates sits stratigraphically above turbiditic wackes and quartzofeldspathic tuffaceous metasedimentary rocks. This transition between styles of sedimentation may be evidence for gradual uplift of the SGB during D_2 deformation.

PRELIMINARY REGIONAL COMPARISIONS

Economic VMS mineralization is most favourable in hydrothermal systems developed in deep-water depositional settings in an extensional tectonic environment (e.g., Galley, Hannington and Jonasson 2007). This allows for the development of large and long-lived hydrothermal systems that have time to alter and remove metals from the footwall strata on a regional scale. Some factors that can inhibit the development of a long-lived, vigorous hydrothermal system include boiling of a hydrothermal system due to development in shallow water, compressional tectonic stresses during volcanic activity, or the presence or absence of juvenile magmas and/or continental crust.

The Vermilion, Manitouwadge and Winston Lake greenstone belts each have regionally extensive VMS-style alteration. The lack of regional-scale alteration in the Shebandowan greenstone belt compared to the other Wawa Subprovince greenstone belts suggests a regionally limited VMS-producing hydrothermal system. The western part of the SGB has many highly amygdaloidal mafic metavolcanic flows and appears broadly similar to those in the VGB. These flows, in combination with other evidence, were interpreted by Hudak, Heine, Newkirk et al. (2002) as shallow-water deposition in the VGB. Shallow-water hydrothermal systems have been proposed based on lithological and geochemical evidence at VMS-prospects in the Calvert–Stares showing in Aldina Township (Franklin 2001). There is detrital zircon evidence (Lodge 2010) and neodymium isotopic evidence (Shute 2008) for the presence of older crust that interacted with the SGB magmas. However, it is uncertain if this has played a role in limiting VMS mineralization until similar data are available from the other greenstone belts. Another interesting comparison is the common association of VMS-style alteration and iron formation in the Vermilion and Manitouwadge greenstone belts.

FUTURE WORK

Lithogeochemical data (Geoscience Laboratories, Ontario Geological Survey, Sudbury) will be used to characterize lithofacies and construct chemostratigraphic sections that will aid stratigraphic correlation between transects and greenstone belts. Radiogenic isotope data (Sm/Nd, $^{207}Pb/^{206}Pb$) will be used to characterize the petrogenesis, magmatic evolution and amount of crustal contamination in each of the greenstone belts. Uranium–lead (U/Pb) geochronology of single-grain zircons from igneous rocks (Jack Satterly Geochronology Laboratory, University of Toronto) and detrital zircons from metasedimentary rocks (ICP–MS Laboratory, Laurentian University) will be used to better constrain and compare the emplacement history of the different greenstone belts.

ACKNOWLEDGMENTS

This is the second report of a four-year PhD thesis project supported by the Mineral Exploration Research Centre (MERC) at the Department of Earth Sciences, Laurentian University (LU), and the Ontario Geological Survey and is co-supervised by Dr. Harold Gibson (LU) and Dr. Greg Stott (Stott Geoconsulting Ltd. (formerly OGS)). Additional members of the thesis committee are Dr. Doug Tinkham (LU) and Dr. Jim Franklin (Consultant). Additional funding is provided by the Natural Sciences and Engineering Research Council of Canada (NSERC) and the Society of Economic Geologists (SEG) Student Research Grant. Field work in Minnesota was assisted by Dr. George Hudak (University of Minnesota).

REFERENCES

Bartley, M.W. 1940. Geology of the Big Duck–Aquasabon lakes area; Ontario Geological Survey, Map 49k, scale 1:31 680.

Brown, G.H. 1995. Precambrian geology, Oliver and Ware townships; Ontario Geological Survey, Report 294, 48p.

Corfu, F. and Stott, G.M. 1986. U–Pb ages for late magmatism and regional deformation in the Shebandowan Belt, Superior Province, Canada; Canadian Journal of Earth Sciences, v.23, p.1075-1082.

——— 1998. Shebandowan greenstone belt, western Superior Province: U–Pb ages, tectonic implications, and correlations; Geological Society of America Bulletin, v.110, p.1467-1484.

Davis, D.W., Schandl, E.S. and Wasteneys, H.A. 1994. U-Pb dating of minerals in alteration halos of Superior Province massive sulfide deposits; syngenesis versus metamorphism; Contributions to Mineralogy and Petrology, v.115, p.427-437.

Farrow, C.E.G. 1993. Base metal sulphide mineralization, Shebandowan greenstone belt; *in* Summary of Field Work and Other Activities, 1993, Ontario Geological Survey, Miscellaneous Paper 162, p.4-8.

——— 1994. Base metal mineralization, Shebandowan greenstone belt, District of Thunder Bay, Ontario; *in* Summary of Field Work and Other Activities, 1994, Ontario Geological Survey, Miscellaneous Paper 163, p.97-104.

——— 1995. Alteration and sulphide mineralogy associated with base metal mineralization, Shebandowan greenstone belt, District of Thunder Bay, Ontario; *in* Summary of Field Work and Other Activities, 1995, Ontario Geological Survey, Miscellaneous Paper 164, p.82-86.

Franklin, J.M. 2001. Preliminary assessment of the lithogeochemistry of the Aldina Township base metal-gold-silver property, for RJK Explorations Ltd.–Greater Leonora Resources Corp. by Franklin Geosciences Ltd.; unpublished report, 38p.

——— 2003. Review of the Canadian Golden Dragon base metal exploration program, Shebandowan Belt, NW Ontario, for Canadian Golden Dragon Resources Ltd. by Franklin Geosciences Ltd., December 30, 2003; unpublished report, 18p.

——— 2005. Notes on the Sungold property, Kashabowie area, Ontario, for Freewest Resources Canada Ltd. by Franklin Geosciences Ltd.; unpublished report, 14p.

Galley, A.G., Hannington, M.D. and Jonasson, I.R. 2007. Volcanogenic massive sulphide deposits; *in* Mineral deposits of Canada: a synthesis of major deposit-types, district metallogeny, the evolution of geological provinces, and exploration methods, Geological Association of Canada, Mineral Deposits Division, Special Publication No. 5, p.141-161.

Hart, T.R. and Trebilcock, D.-A. 2006. Geology of the Hamlin and Wye lakes area, Shebandowan greenstone belt, Thunder Bay District; *in* Summary of Field Work and Other Activities, 2006, Ontario Geological Survey, Open File Report 6192, p.9-1 to 9-9.

Hudak, G.J., Heine, J., Hocker, S. and Huack, S. 2002. Geological mapping of the Needleboy Lake–Six Mile Lake area, northeastern Minnesota: a summary of volcanogenic massive sulphide potential; University of Minnesota–Duluth, Natural Resources Research Institute, Report of Investigations NRRI/RI-2002/14, 15p.

Hudak, G.J., Heine, J., Jirsa, M. and Peterson, D. 2004. Volcanic stratigraphy, hydrothermal alteration, and VMS potential of the lower Ely Greenstone, Fivemile Lake to Sixmile Lake area; 50th Institute on Lake Superior Geology, Annual Meeting, Duluth, Minnesota, v.50, pt.2 – Field Trip Guidebook, p.1-44.

Hudak, G.J., Heine, J., Newkirk, T., Odette, J.D. and Huack, S. 2002. Comparative geology, stratigraphy, and lithogeochemistry of the Five Mile Lake, Quartz Hill, and Skeleton Lake VMS occurrences, western Vermilion district, NE Minnesota; University of Minnesota–Duluth, Natural Resources Research Institute, Technical Report NRRI/TR-2002/03, 350p.

Kamo, S.L. 2011. Report on the U-Pb CA-ID-TIMS geochronology on volcanic and plutonic rocks, Grenville and Superior Provinces, Ontario; unpublished report for Precambrian Geoscience Section of the Ontario Geological Survey, Jack Satterly Geochronology Laboratory, University of Toronto, Toronto, Ontario, 26p.

Lodge, R.W.D. 2010. Volcanology and lithofacies of the Shebandowan greenstone belt, Wawa Subprovince; *in* Summary of Field Work and Other Activities, 2010, Ontario Geological Survey, Open File Report 6260, p.16-1 to 16-22.

Milne, V.G. 1974. Mapledoram–Gemmell, Thunder Bay District; Ontario Geological Survey, Map 2280, scale 1:12 000.

Osmani, I.A. 1996. Geology and mineral potential of the upper and middle Shebandowan Lakes area, west-central Shebandowan greenstone belt; Ontario Geological Survey, Open File Report 5938, 82p.

——— 1997. Geology and mineral potential: Greenwater Lake area, west-central Shebandowan greenstone belt; Ontario Geological Survey, Report 296, p.135.

Osterberg, S.A. 1993. Stratigraphy, physical volcanology, and hydrothermal alteration of the footwall rocks to the Winston Lake massive sulfide deposits, northwestern Ontario; unpublished PhD thesis, University of Minnesota at Minneapolis, Minneapolis, Minnesota, 351p.

Peterson, D. 2004. Bedrock geological and volcanogenic massive deposit mineral potential map of the Lower Ely greenstone and adjacent areas: Soudan, Eagles Nest, and Bear Island 7.5′ quadrangles, St. Louis County, northeastern Minnesota; *in* Economic geology of Archean gold occurrences in the Vermilion District, northeast of Soudan, Minnesota, 50th Institute on Lake Superior Geology, Annual Meeting, Duluth, Minnesota, v.50, pt.2 – Field Trip Guidebook, map for Field Trip 7, scale 1:20 000.

Peterson, D., Gallup, C., Jirsa, M. and Davis, D.W. 2001. Correlation of the Archean assemblages across the U.S.-Canadian border: Phase I geochronology; 47th Institute on Lake Superior Geology, Annual Meeting, Proceedings, Programs and Abstracts, v.47, pt.1, p.77-78.

Peterson, D. and Jirsa, M. 1999. Bedrock geologic map and mineral exploration data, western Vermilion district, St. Louis and Lake counties, northeastern Minnesota; Minnesota Geological Survey, Miscellaneous Map M-98, scale 1:48 000.

Peterson, V.L. and Zaleski, E. 1999. Structural history of the Manitouwadge greenstone belt and its volcanogenic Cu-Zn massive sulphide deposits, Wawa Subprovince, south-central Superior Province; Canadian Journal of Earth Sciences, v.36, p.605-625.

Pye, E.G. 1964. Mineral deposits of the Big Duck Lake area, District of Thunder Bay; Ontario Department of Mines, Geological Report 27, 58p.

Rogers, M.C. and Berger, B.R. 1995. Precambrian geology, Adrian, Marks, Sackville, Aldina and Duckworth townships; Ontario Geological Survey, Report 295, 66p.

Shute, A.L. 2008. Geology and alteration associated with the Hamlin Lake VMS system, Shebandowan greenstone belt, northwestern Ontario, Canada; unpublished MSc thesis, Lakehead University, Thunder Bay, Ontario, 225p.

Zaleski, E. and Peterson, V.L. 1995. Depositional setting and deformation of massive sulfide deposits, iron-formation, and associated alteration in the Manitouwadge greenstone belt, Superior Province, Ontario; Economic Geology, v.90, p.2244-2261.

——— 2001. Geology of the Manitouwadge greenstone belt and the Wawa–Quetico subprovince boundary, Ontario; Geological Survey of Canada, Map 1917A, scale 1:25 000.

APPENDIX I: OGS SUMMARY OF FIELD WORK AND OTHER ACTIVITIES – OFR 6260-16 (2010)

This appendix contains a report published by the Ontario Geological Survey summarizing observations and preliminary stratigraphic interpretations made during the 2010 summer field season in the Shebandowan greenstone belt. This report is available for free download from the website address stated below and is reproduced in this thesis with the permission of the Publication Sales and Services section of the Ontario Geological Survey.

Some of the field observations recorded in this report are referenced in the manuscript presented in Chapter 2.

Website

http://www.geologyontario.mndmf.gov.on.ca/mndmaccess/mndm_dir.asp?type=pub&id=OFR6260

16. Project Unit 10-010. Volcanology and Lithofacies of the Shebandowan Greenstone Belt, Wawa Subprovince

R.W.D. Lodge[1,2]

[1]Mineral Exploration Research Centre, Department of Earth Sciences, Laurentian University, Sudbury, Ontario P3E 2C6
[2]Precambrian Geoscience Section, Ontario Geological Survey, Sudbury, Ontario P3E 6B5

INTRODUCTION

This article represents the first report of a four-year PhD thesis study designed to study the geodynamic setting of volcanogenic massive sulphide (VMS) mineralization in the Shebandowan, Vermilion, Winston Lake and Manitouwadge greenstone belts, which are relatively the same age (Davis, Schandl and Wasteneys 1994; Peterson et al. 2001) and are found along the northern margin of the Wawa Subprovince. This thesis work is supported by the Ontario Geological Survey and the Department of Earth Science at Laurentian University through the OGS Graduate Mapping School Program.

Mapping this summer focussed on investigating the volcanology and geodynamic setting of the Shebandowan greenstone belt (SGB). Mapping was completed along semi-linear transects oriented perpendicular to regional stratigraphy throughout the SGB in areas of known VMS mineralization. Understanding the depositional history and setting of the Shebandowan and other time-stratigraphic equivalent (2720 Ma) greenstone belts is critical to understanding the assembly of the Superior Province during the Neoarchean.

The SGB of the western Wawa Subprovince in northwestern Ontario is an approximately 200 km long, arcuate greenstone belt located west of Thunder Bay, Ontario, which is bounded to the north by the Quetico metasedimentary subprovince and is unconformably overlain to the south by Proterozoic strata of the Animikie basin and Duluth intrusive complex (Figure 16.1). The SGB is a composite of the Shebandowan and Saganagons greenstone belts. It has been proposed that these 2 greenstone belts were once continuous (Williams et al. 1991) and have been interpreted to be of the same age (Corfu and Stott 1988). Williams et al. (1991) divided the SGB into 3 assemblages: the opposite-facing Greenwater and Burchell assemblages, and the younger overlapping Shebandowan assemblage (Shegelski 1980). Uranium–lead (U/Pb) geochronology (Corfu and Stott 1986, 1998) has shown that the Greenwater, Burchell and Saganagons assemblages are virtually the same age (*circa* 2720 Ma). Accordingly, these 3 assemblages were recombined as the "Greenwater" assemblage (Corfu and Stott 1998), which is associated with most, if not all, of the VMS-style mineralization described in the SGB (e.g., Farrow 1993, 1994; Osmani 1997a). Corfu and Stott (1998) also described the younger Kashabowie (2695 Ma) and Shebandowan (Timiskaming-type, 2685 to 2690 Ma) assemblages associated with D_1 and D_2 events, respectively.

Exploration and mining of base-metal deposits throughout the SGB have been ongoing since the early part of the 20th century. Past-producing base-metal mines in the region have questionable origins (North Coldstream copper-gold mine; e.g., Farrow 1995) or are associated with ultramafic sills and/or komatiitic flows (e.g., Shebandowan nickel-copper mine; Morton 1982). Despite relatively continuous exploration, the endowment of VMS-style mineralization for such a large belt is very small compared to

Summary of Field Work and Other Activities 2010,
Ontario Geological Survey, Open File Report 6260, p.16-1 to 16-22.

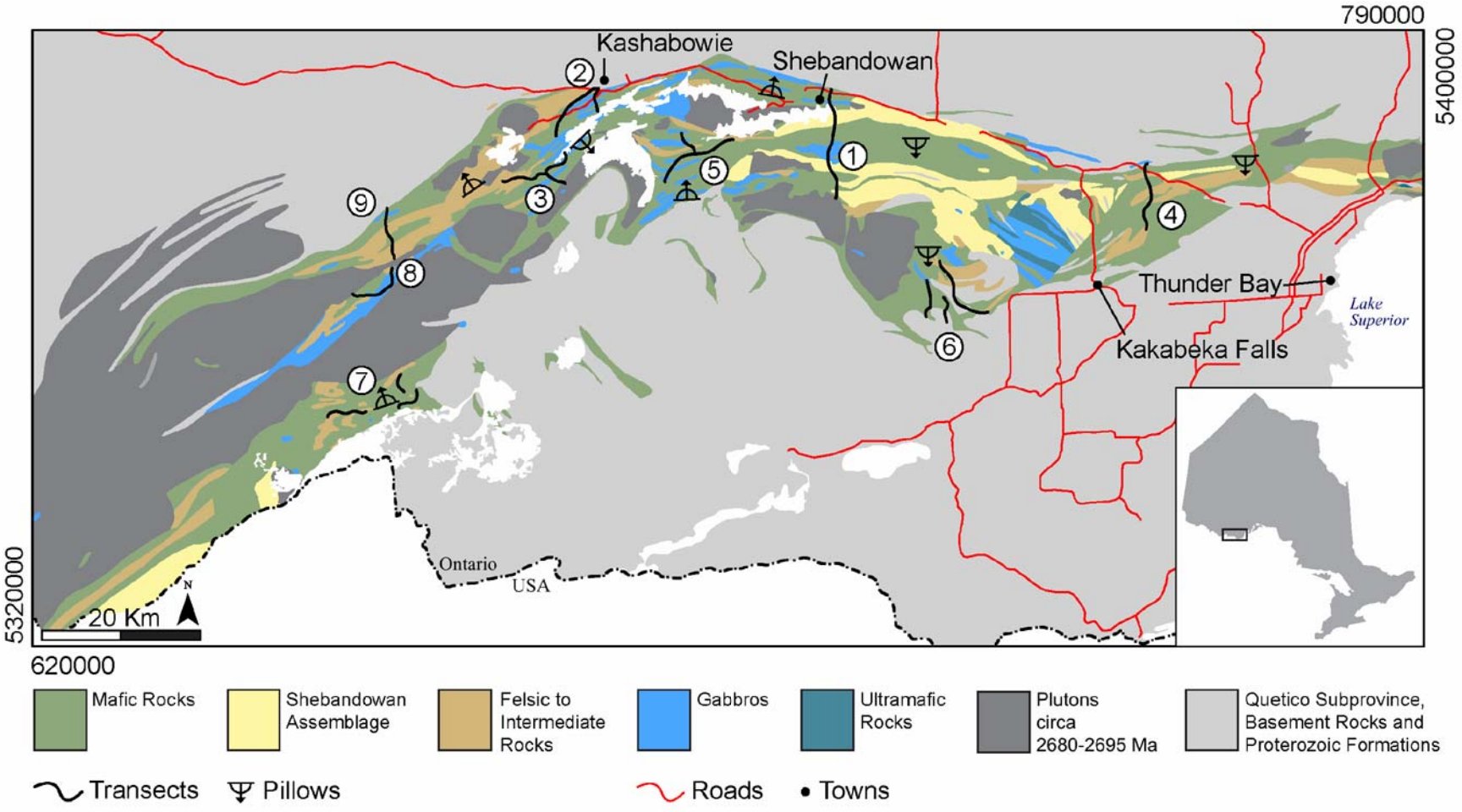

Figure 16.1. General geology of the Shebandowan greenstone belt showing location of mapped transects. Co-ordinates are in UTM Zone 15, NAD83.

time-equivalent successions at Winston Lake and Manitouwadge, and known deposits are noneconomic (total combined discovered VMS deposits <1.0 Mt: Farrow 1993, 1994; Hart and Trebilcock 2006; Osmani 1996). Rocks of the SGB are interpreted to have been deposited in a submarine island arc to rifted arc tectonic environment (e.g., Corfu and Stott 1998; Hart and Trebilcock 2006; Osmani 1996), a common volcanic environment associated with economic VMS deposits elsewhere in the Superior Province (e.g., Franklin et al. 2005; Galley, Hannington and Jonasson 2007). A better understanding of the regional stratigraphy and tectonic history of the Shebandowan greenstone belt will aid in future mineral exploration efforts.

ACCESS AND PREVIOUS WORK

The Shebandowan greenstone belt extends from Thunder Bay to the Quetico Provincial Park along Highway 11 to the village of Kashabowie, where the greenstone belt bends southward and is accessed through the logging road network from Route 802 South leading to the Greenwood Conservation Area. Eastern parts of the belt were accessed through residential roads that extend northward between the town of Kakabeka Falls and Highway 102. Southern transects were accessed through logging road networks off of the Boreal and Adrian Lake roads approximately 13 km west of the town of Kakabeka Falls on Route 590. Central parts of the belt were accessed by Gold Creek Road, which is approximately 5 km west of the village of Shebandowan on the Shebandowan Mine Road.

Most of the Shebandowan greenstone belt has been mapped by the Ontario Geological Survey within the last 20 years. However, some areas, such as the Saganagons greenstone belt, have not been mapped since the 1960s (e.g., Harris 1968). Field studies in the SGB have been regional, and township mapping projects (e.g., Brown 1995; Hart and Trebilcock 2006; Osmani 1997a; Rogers and Berger 1995) did not focus on detailed stratigraphic sections or regional variation in volcanic lithofacies. Studies that focussed on VMS mineralization at the property scale (e.g., Farrow 1994, 1995; Franklin 2003, 2005; Osmani 1996) are essentially isolated studies that did not discuss or compare the lithofacies, geochemistry and mineralization between adjacent properties, prospects or between greenstone belts.

MAPPING RESULTS

Nine transects (*see* Figure 16.1) were mapped and sampled at scales of 1:20 000 or in greater detail where outcrop coverage was extensive enough to allow for more detailed observations. Mapping was aimed at 1) defining and describing lithofacies and establishing a stratigraphy; 2) reconstructing the tectonic history; and 3) sampling for geochemical, isotopic and petrographic analyses that will be the framework for establishing the relationships between the SGB and time-stratigraphic equivalent greenstone belts. Numbers assigned to transects represent the order of which they were visited. In the description that follows, volcaniclastic nomenclature is based on the nongenetic granulometric classification originally proposed by Fisher (1966) and is based on variations in the percentage and size of clasts (>2 mm) relative to matrix (<2 mm).

Transect 1. Shebandowan–Duckworth

The Shebandowan–Duckworth transect is a predominantly north-to-south-oriented transect with mapping completed along Gold Creek Road through Duckworth Township and around the village of Shebandowan (*see* Figure 16.1). The section is dominated by near east-striking volcanic rocks, gabbroic intrusions and 2 Timiskaming-like sedimentary basins. The sedimentary basins divided the transect into 3 main components: the northernmost Shebandowan village area, the central Conacher–Duckworth

townships area, and the southernmost Gold Creek area in Duckworth Township. The transect terminated at the contact with the Quetico Subprovince to the north and with the granitic Kekekuab Lake pluton to the south. Late syenitic dikes are also present.

In the vicinity of the village of Shebandowan, rocks are predominantly fine-grained, aphyric to plagioclase-phyric massive mafic flows to flow breccias with fluidal fragments in a chloritic matrix. Near the contact with the Shebandowan pluton, the rocks were strongly cleaved with a schistose fabric and primary textures in the flows were destroyed. Although no younging indicators were identified, previous workers in the region have identified pillowed flows indicating a northward younging of strata (Morin 1970). At the boundary with the Quetico Subprovince, mafic rocks were isoclinally folded as indicated by tightly folded, narrow bands of plagioclase phenocrysts in an otherwise massive green coloured mafic flow. Sedimentary rocks, exposed amongst mafic flows near the contact, provide additional evidence for folding at the Shebandowan greenstone belt–Quetico Subprovince boundary. Medium- to coarse-grained, equigranular gabbroic intrusions, with locally developed weak cleavage, are present just north of Highway 11 along the main transmission line. Other intrusions include a pink-weathering, feldspar-rich monzonite dike.

The central region between the 2 Timiskaming-like basins in Conacher and Duckworth townships are also dominated by mafic flows, pillows, and flow breccias and an irregular gabbroic intrusion (*see* Figure 16.1). Mafic flows are fine grained, aphyric to coarsely plagioclase phyric (up to 3 cm crystals), and are massive to moderately cleaved. The coarsely plagioclase-phyric mafic flow is an important regional marker unit as it appears in several of the transects mapped this summer. Pillow shapes, mapped in this study and in previous work (Rogers 1995b), indicate that the succession youngs southward. Ultramafic flows or sills are common in the Shebandowan Mine–Greenwater Lake area to the west (*see* below) and, due to lack of primary structures, the exact level of emplacement of these ultramafic bodies remains uncertain (e.g., Morton 1982). However, 2 exposures of a mafic to ultramafic breccia with spinifex-textured ultramafic and pillow fragments (Photo 16.1A) were mapped during this study and comprise the only definitive evidence for ultramafic extrusive rocks in the Shebandowan Mine–Greenwater Lake area. Gabbros are mainly medium grained, massive and nondescript.

The southern part of the transect between the southern Timiskaming-like basin and the Kekekuab Lake pluton (*see* Figure 16.1) is composed of significantly different supracrustal assemblages than the northern parts of the transect. Grading in monolithic felsic tuff-breccia lithofacies suggest a southward-younging succession; however, regional map patterns and variation in cleavage are suggestive of folding (Rogers 1995b). The transect is predominantly underlain by interbedded intermediate to felsic tuffs, lapilli

Photo 16.1. Field photographs from the Shebandowan–Duckworth transect: A) spinifex-textured pillow breccia fragments; and B) rimmed lapilli in felsic tuffs associated with the Gold Creek occurrences.

tuffs, tuff breccias and minor flows. Intermediate rocks are characterized by feldspar-rich tuffs, lapilli tuffs and heterolithic tuff-breccia lithofacies interpreted to be debris flow units. Matrix to these tuffs was typically chloritic and likely is the result of alteration of more felsic protoliths since fragments are often felsic in appearance with up to 10 to 15% quartz crystals. A massive to autobrecciated feldspar-phyric intermediate flow was described near the southern end of the transect. Felsic rocks are white in colour and typically have quartz phenocrysts up 5 mm in size that compose up to 20% of the rock. Massive quartz-phyric flows to hypabyssal intrusions are present near the Gold Creek mineralized zone and near the northern contact with Timiskaming-type sedimentary rocks. Massive felsic rocks to the north are closely associated with a thickly bedded, monolithic tuff breccia to autobreccia suggestive of a collapsed felsic dome. Other felsic rocks include bedded lapilli tuffs, tuff breccias, and massive tuffs that are typically matrix-supported and are thickly bedded and locally graded. In the vicinity of the Gold Creek mineralization, patchy and fracture-associated yellow sericite alteration and pyrite mineralization is common in the felsic tuffs and lapilli tuffs. These altered and mineralized lapilli tuffs have fragments that are similar in composition to the matrix and the fragments have darkened rims (Photo 16.1B). Structurally, the intermediate and felsic rocks of this part of the transect are variously foliated throughout to locally highly fissile near the northern part of the transect. Clasts within lapilli tuffs and tuff breccias have been tectonically flattened and stretched. A single mafic unit was mapped at the “top” of the stratigraphic section where it is in contact with the Kekekuab Lake pluton. The mafic unit is fine to medium grained and massive, possibly due to recrystallization associated with contact metamorphism.

Transect 2. Vanguard–Coldstream

The Vanguard–Coldstream transect was largely oblique to regional strike and concentrated on exposures on Route 802 South and along logging roads that extend southeast toward Upper Shebandowan Lake (*see* Figure 16.1). The Vanguard East prospect and additional exposures are located on private residential roads near the village of Kashabowie on Highway 11. The transect terminates to the north at Highway 11 and is cut off to the south by the Haines gabbroic complex and the Upper Shebandowan Lake shear zone system (USSZ) approximately 10 km along Route 802 South (Osmani 1997c). As evidenced by the strong foliation, kink bands and the presence several shear zones as mapped by Osmani (1997c), determining the stratigraphy in this transect is not possible because of lack of outcrop and structural complexity resulting in multiple fault and/or fold repetitions. Shearing and faulting are common because of the close proximity of the transect to 2 major shear zones: the Crayfish Creek fault (Hodgkinson 1963) and the USSZ (Osmani 1997c). However, graded bedding in mafic volcaniclastic rocks described in this study and pillow shapes documented in previous work (Osmani 1997c) show a consistent younging direction to the north and northwest.

The Vanguard–Coldstream transect is underlain by a predominantly mafic succession that has been sheared, foliated and kinked at the north end near the intersection with 2 major shear and/or fault zones. The southernmost part of the transect is represented by a succession of fine-grained, moderately to strongly cleaved mafic flows with local carbonate-filled amygdules and flow-breccia units. Mafic flow breccias or debris flows contain fine-grained to aphanitic, aphyric fragments up to 0.5 to 1 m long (average 30 cm) that are fluidal in shape (Photo 16.2A). To the north (and stratigraphically above if the stratigraphic succession is intact) is a 0.5 km thick succession of foliated and laminated mafic tuff with millimetre-scale laminations noted by brown and dark green discontinuous layers that are likely boudinaged and deformed. Similar tuffaceous mafic rocks are associated with the massive sulphide mineralization at the Vanguard East and West prospects 7 km along regional strike. Tuffs are commonly siderite altered with patchy stretched pyrite clusters with trace amounts of sphalerite. Stratigraphically above the mafic tuffs is a 1 to 1.5 km thick succession of moderately to strongly foliated, massive mafic flows that are commonly variolitic (Photo 16.2B). Locally, the flows are more appropriately described as chlorite schists where shearing and deformation is intense and primary texture is destroyed. Flows are

locally silicified and contain 1 to 2% large, irregular and elliptical quartz-filled amygdules. There are a few exposures of pillows, or at least evidence for their selvages. At the base of these flows at the contact with a gabbro is a thin 50 to 100 m thick unit of a sericite-chlorite schist that is probably intermediate in composition. This rock has millimetre- to centimetre-scale light and dark grey bands that are caused by differences in sericite abundance. The mafic flows are capped by a 200 to 300 m thick chloritic schist zone with strong to intense foliation and little preserved primary textures. A 300 to 400 m thick unit of felsic to intermediate volcaniclastic rocks overlies the chloritic schist to the north. These rocks have cleaved and stretched quartz- and feldspar-phyric fragments averaging a few centimetres in size but as large as 30 cm. The matrix is aphanitic and contains small feldspar crystals. The stratigraphy in this transect is capped by an approximately 500 m thick succession of amygdaloidal to pillowed mafic flows with weak to strong foliation. Where cleaved, the mafic flows are more siliceous, chlorite altered, and mineralized with fine-grained, fracture-associated pyrite.

Intrusions in this transect are largely medium- to coarse-grained, massive, equigranular to plagioclase- and/or pyroxene-phyric gabbros. The gabbros that intrude the southern part of the transect tend to be massive and equigranular. Gabbroic intrusions that are in the middle and northern parts of the transect tend to be pyroxene and plagioclase phyric, respectively. Locally, the gabbros are rich in magnetite. In the East Coldstream gold prospect area, there are fine-grained felsic sills that are grey to white in colour, are sparsely quartz-phyric, and are siliceous to almost cherty and typically contain thin wispy chlorite clusters that are less than 1 to 3 cm in size. These have local weak siderite alteration. Minor syenite dikes are also present.

Transect 3. Grouse Lake–Hermia Road

The Grouse Lake–Hermia Road transect was mapped using several logging road networks that branch off of Route 802 South between 10 and 16 km south of Highway 11 (*see* Figure 16.1). These logging roads are generally perpendicular to oblique to regional strike. They cross a 5.5 km thick section of supracrustal rocks, between Greenwater Lake and the Burchell Lake pluton, and is bisected by the USSZ (Osmani 1997c). Exposure was enhanced by recent logging activity and many primary structures were visible. This transect can be subdivided into 2 sections: an upper part to the northeast of the USSZ, and a lower part located to the southwest of the shear zone. The shear zone itself is a 1 to 1.5 km thick zone comprised of several anastomosing shear zones through a predominantly mafic flow and tuff succession with minor gabbroic to ultramafic plug-like intrusions. There are minor thin units of strongly altered and foliated intermediate tuffaceous lithofacies that are very dark in colour and contain up to 30 to 40% garnet porphyroblasts up to 1.5 cm in size.

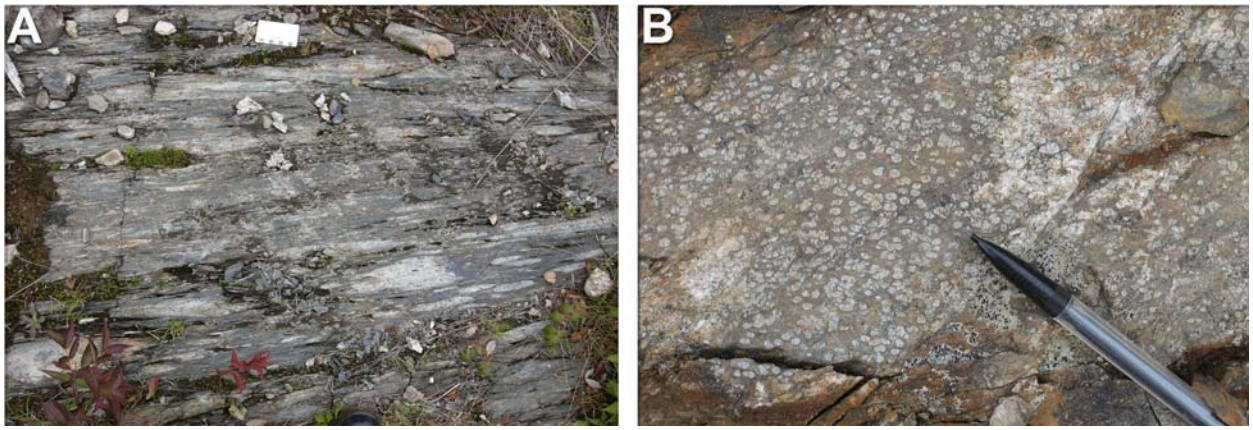

Photo 16.2. Field photographs from the Vanguard–Coldstream transect: A) mafic flow breccia; and B) variolitic mafic flow at stripped outcrop at the Vanguard East prospect.

The upper part of the Grouse Lake–Hermia Road transect is predominantly a sericitic, foliated and deformed felsic to intermediate volcanic succession composed of sericite-altered felsic flows to autobreccias, heterolithic lapilli tuffs to tuff breccias, and quartz-phyric felsic flows to flow breccias. Younging directions toward the northeast are inferred from pillows in mafic flows by Osmani (1997c); however, folding, shearing, and faulting within the adjacent felsic units suggest that there are multiple reversals in facing. Assuming the succession is northwest younging, the lower portion of this part of the transect is marked by a white-weathering quartz- and feldspar-rich felsic flow to autobreccia. Phenocrysts are up to 2 mm in size and locally compose up to 20 to 25% of the rock. In some areas, there are centimetre-scale quartz blobs that may be structural in origin, but also be could be vugs or clasts. Felsic flows are overlain by strongly foliated, felsic to intermediate, matrix-supported lapilli tuffs to tuff breccias that are fractured and quartz veined on fold axes resembling fold-thrust stacks, but with minimal displacement. Poorly sorted fragments are typically very fine grained to aphanitic, and are yellow-white, pink, green, and grey in colour, up to 3 cm in size, and compose 10 to 40% of rock. Locally, fragments are as large as 15 cm. To the northwest, overlying the heterolithic debris flows, are moderately to strongly sericite-altered felsic flows. There is frequently almost complete replacement of original rock with sericite and silica except for a few “fragments” separated by anastomosing yellow sericite. Locally, sericite alteration can be so intense that the rock has become yellow in colour, has a strongly kinked foliation and displays fluorite-filled fractures. Above the sericitic flows are bedded heterolithic lapilli tuffs defined by variation in lapilli size and composition. Sericitization is also prominent in these rocks. Matrix to the lapilli tuff is rusty coloured, and contains fragments of aphanitic felsic to intermediate volcanic rocks to minor cherty clasts. There are minor monolithic beds with predominately centimetre-scale intermediate volcanic fragments. The sericitic felsic units are capped by an epidote-altered mafic flow with trace pyrite mineralization and moderate epidote-quartz alteration in fractures and patches in the rock. There is also a possible synvolcanic, medium-grained, irregular finger-like tonalitic dike in the mafic flows.

The lower part of the Grouse Lake–Hermia Road is highlighted by a southward-younging, seemingly relatively intact, stratigraphic succession composed of a semi-conformable epidote-quartz alteration zone within pillowed mafic flows underlying a thick unit of finely bedded felsic tuff to lapilli tuff with local sericite alteration and local sulphide mineralization. This part of the transect has the regional characteristics of a VMS-producing environment (e.g., Galley, Hannington and Jonasson 2007) and the stratigraphic section is summarized graphically in Figure 16.2. The base of this succession is composed of massive to pillowed and locally flow brecciated mafic flows with minor massive intermediate flows. Foliation in these flows ranges in intensity and noted by stretched pillows and amygdules. Primary flow textures and structures were destroyed in strongly cleaved zones. The amount and degree of deformation and flattening seems to decrease to the southeast and stratigraphically upward. These flows are moderately to strongly epidote-quartz altered (Photo 16.3A) in patches, fractures and pillow cores over a strike length of approximately 4.5 km from Grouse Lake to Firefly Lake. Overlying the mafic and intermediate flows is an approximately 200 m thick unit of bedded intermediate tuff to lapilli tuffs with minor beds of heterolithic lapilli tuff or debris flows and magnetite-chert iron formation. Some of the fine tuffaceous layers and the debris flow are chlorite and garnet altered and have associated pyrite disseminations. A thin, discontinuous pillowed mafic flow partially separates the intermediate chloritic tuff from the overlying bedded felsic tuff and lapilli tuff. The felsic tuff is the most prominent and probably best exposed unit in this part of the transect. Beds range in size from less than 10 cm in tuff and sandy tuff layers to over 1 m thick in more lapilli-rich layers. Tuffs are predominantly feldspar rich with minor muddy fine-tuff beds and quartz-bearing tuff beds. Fine sandy tuff beds are often graded and fine southward. Lapilli tuff layers range from matrix to fragment supported, have centimetre-scale monolithic fragments that are typically aphanitic to fine grained, white-coloured and felsic in composition. Locally, fragments are bomb sized. Bedding in the tuff unit is remarkably planar in both tuff and lapilli layers and the contact between beds are sharp. Local zones of strong deformation in bedded units seem to be formed prior to lithification because foliation and cleavage intensity do not increase in these zones of strong internal folding. Rare bomb-sag structures are preserved in the tuff beds (Photo 16.3B). The felsic tuff

unit has local pyrite patches and disseminations with rare sphalerite. Alteration is typically sericitic and ranges in intensity from weak to moderate and locally strong in zones of mineralization. The felsic tuff succession is overlain by locally foliated and deformed mafic flows that have moderate to strong epidote alteration as boudinaged veins and patches.

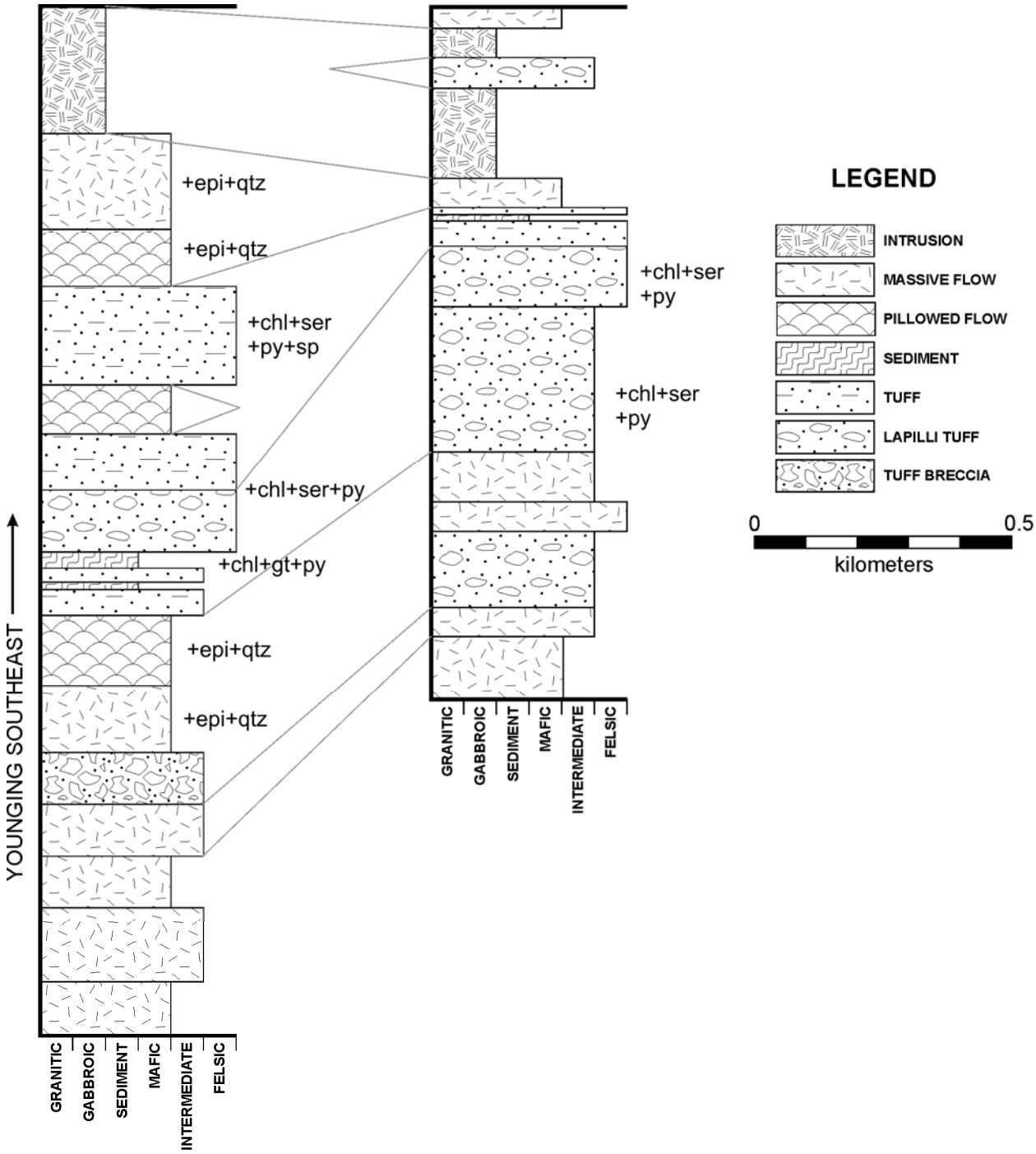

Figure 16.2. Graphic logs of mapped stratigraphy in surface exposures in the lower part of the Grouse Lake–Hermia Road transect. Younging direction is based on pillow shapes and graded bedding in tuffs. Abbreviations: chl = chlorite; epi = epidote; py = pyrite; qtz = quartz; ser = sericite; sp = sphalerite.

Gabbroic intrusions are common in both the footwall mafic to intermediate flows and in the hanging-wall flows. A layered gabbroic intrusion, noteworthy for variations in pyroxene phenocryst size and orientations, occurs in the lower part of the succession near the southwestern tip of Upper Shebandowan Lake. Gabbros near Grouse Lake are often "knobby" textured with 2 to 4 cm knobs of gabbro separated by 1 to 2 mm thick weak anastomosing cleavage interpreted to be the initial stages of foliation development. Biotite lamprophyre dikes trending north are present in this section. Some of these dikes are xenolith rich with abundant centimetre- to decimetre-scale, rounded actinolite nodules and blocky xenoliths of medium- to coarse-grained gabbroic and granitic intrusions.

Transect 4. Mud Lake Road

The Mud Lake Road transect was mapped in order to establish the stratigraphic setting that hosts the Mud Lake zinc occurrence (Farrow 1993) on Highway 102 in Oliver and Ware Townships (*see* Figure 16.1). Unfortunately, easily accessible outcrops were sparse and stratigraphy was difficult to determine based on this study's mapping alone. Therefore, to aid in stratigraphic reconstruction, regional maps were consulted (Brown and Fogal 1995a, 1995b) and will be checked in the field in 2011. No younging directions were found in this transect, but, regionally, are consistently northward based on pillows and graded bedding in tuffs (Brown 1995). The transect was accessed via residential and logging roads north of Oliver Road in Kakabeka Falls to Highway 102 and to the northern boundary of the SGB with the Quetico Subprovince in Ware Township.

Based on younging directions reported by Brown (1995), the youngest rocks in the transect are massive to pillowed mafic flows and pillow breccias. Minor massive pyroxene-phyric flows are observed also. Outcrops were generally of poor quality and primary textures were difficult to identify. Pillow breccias are composed of centimetre-scale fragments with thin fluidal glassy selvages or matrix. Stratigraphically above the mafic flows are mafic to intermediate lapilli tuffs to tuff breccias that appear to be andesitic in composition. Fragments are stretched, plagioclase-phyric and average 3 cm in size hosted in darker green-coloured matrix. Fragments may compose up to 50% of the rock. Locally, these are interpreted as flow breccias as blob-like flow fragments are hosted in matrix of hyaloclastite and carbonate. Overlying these intermediate lapilli tuffs and tuff breccias is an approximately 1.5 km thick succession of massive plagioclase-rich intermediate flows with minor interbedded mafic flows and flow breccias. The intermediate flows are fine grained, feldspar rich and contain few mafic minerals. Intermediate flows are overlain to the north by mafic to intermediate heterolithic, matrix-supported tuff breccias. Fragments compose up to 30 to 40% of the rock and range from medium-grained mafic, purple

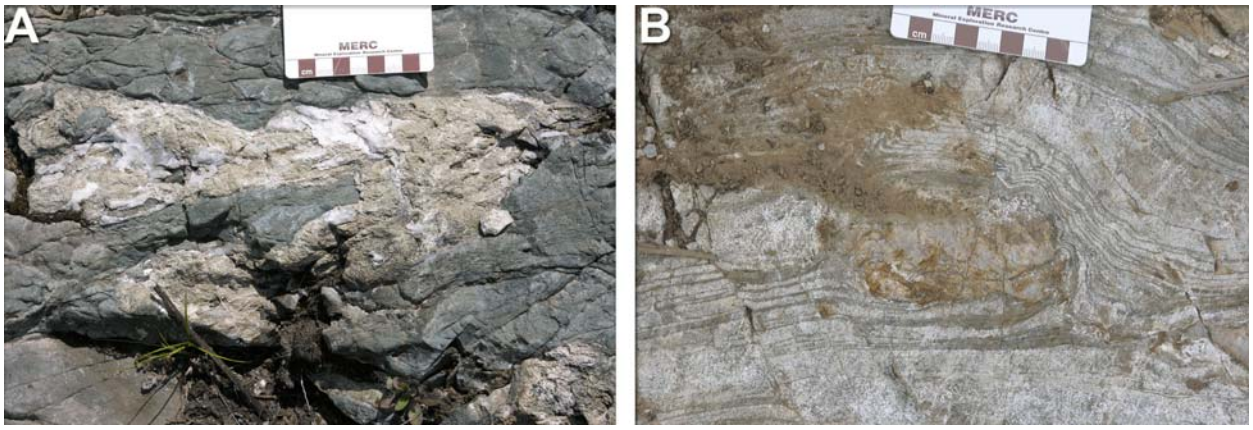

Photo 16.3. Field photographs from the Grouse Lake–Hermia Road transect: A) epidote-quartz altered mafic flows; and B) bomb-sag structure in bedded felsic tuff.

to white intermediate, and feldspar-phyric mafic clasts. The matrix is mafic in composition and has 1 to 2 mm feldspar crystals. Locally, more felsic to intermediate volcaniclastic units are present with primarily white to pink, feldspar-phyric fragments. These intermediate to mafic tuff breccias are overlain by the large and extensive felsic succession that hosts the Mud Lake zinc occurrence. This felsic unit is very extensive along the boundary between Oliver and Ware townships (Brown and Fogal 1995a, 1995b); however, limited outcrops were visited this summer and additional mapping is required to determine lithofacies variation within the unit. The Mud Lake zinc occurrence is a thinly bedded to brecciated chert, magnetite and sulphide (pyrite and sphalerite) horizon approximately 0.5 m thick at the contact between a dark grey quartz- and feldspar-phyric felsic dome (that is locally autobrecciated) and a massive to autobrecciated, feldspar-phyric felsic flow (Farrow 1993). The partly felsic unit that was visited west of the zinc occurrence along strike is also autobrecciated felsic flows and lapilli tuffs with 1 to 3 cm subangular to subrounded clast-supported fragments in a matrix of similar composition with coarse quartz and feldspar phenocrysts. From the Mud Lake top of the felsic succession to the Quetico Subprovince–Shebandowan greenstone belt boundary is a succession of weakly to strongly foliated, massive to pillowed mafic flows. Interlayered with the mafic flows are thin units of intermediate heterolithic tuff breccia to tuffaceous conglomerate with a fine lithic and crystal tuff matrix. Fragments are up to 20 cm in size and are composed of fine-grained mafic, coarse-grained gabbro, chert and massive sulphides (pyrite). Z-kinked, pink-weathering intermediate to felsic sandy tuffs with sparse medium-grained felsic fragments are also interlayered with the mafic flows. These felsic tuffs are massive to weakly laminated noted by colour differences.

Several mafic dikes, less than 1 m thick, intrude the intermediate lithofacies. Very thin, parallel aplitic dikes intrude the mafic to intermediate heterolithic lapilli tuffs and tuff breccias stratigraphically below the Mud Lake felsic succession. A single outcrop of a felsic to intermediate intrusion with long, acicular 3 to 4 cm amphibole needles was observed in the intermediate–mafic flow succession. Biotite-lamprophyre and mafic dikes are observed in the mafic flows near the Shebandowan greenstone belt–Quetico Subprovince boundary.

Structurally, the lithofacies of the Mud Lake Road transect were massive to weakly foliated, except near the northern margin of the greenstone belt, where rocks were moderately to strongly foliated and contained thin brittle faults with minimal displacement. Alteration is very weak to absent and consists of finely disseminated and patchy chlorite and sericite. Even the felsic lithofacies that host the Mud Lake zinc occurrence are very weakly altered, with only localized sericite alteration resulting in a faint lightening in colour compared to unaltered felsic lithofacies. This suggests that the hydrothermal system that resulting in the mineralization at Mud Lake was either short lived and localized or distal to the main hydrothermal vent.

Transect 5. Shebandowan Mine–Greenwater Lake

The Shebandowan Mine–Greenwater Lake transect was accessed via roads in the Shebandowan Mine property (owned by Vale, as of October 2010) and from logging roads accessible from the property that lead north to the margin of the Shebandowan pluton and south as far as Horseshoe Lake (*see* Figure 16.1). Additional outcrops were mapped in the Pinecone Lake area that is accessible by logging roads south of Greenwater Lake. The succession is folded and is likely thrusted repeatedly based on multiple reversals in younging directions documented in previous work (Morton 1982; Osmani 1997b). The northern margin of this transect is structurally influenced by the Crayfish Creek fault and related shear zones trending approximately east-southeast. Several fold axes and strike-parallel fault or shear zones are mapped throughout the area covered by this transect (Osmani 1997b); further mapping and structural analyses are required to determine the stratigraphy. Therefore, rocks will be described in terms of lithologic domains rather than in terms of stratigraphic units. The transect can be divided into 3 lithologic domains: a northern domain composed of mafic to felsic lithofacies, a “mine” domain in the middle of the transect composed of mafic to ultramafic flows and/or sills and chert-magnetite iron formation, and a southern domain composed of a succession of mafic to felsic lithofacies with minor iron formation.

The northern domain is defined as the part of the transect that extends north from the first appearance of intermediate to felsic rocks at near the boundary between Haines and Begin townships to the margin of the Shebandowan pluton (Osmani 1997b). The largest unit of intermediate to felsic rocks are intermediate lithic tuffs, pyroclastic breccias and flow breccias. Monolithic volcaniclastic layers contain subrounded to subangular fragments of intermediate volcanic rocks up to 10 to 15 cm in a clast-supported framework. Heterolithic volcaniclastic layers contain felsic to intermediate fragments and minor amygdaloidal, mafic-looking fragments with wispy margins. Additional intermediate lithofacies are exposed near the middle of the domain to the north. These are massive plagioclase-bearing intermediate tuffs or a flow with anastomosing cleavage and 1 to 5 mm plagioclase crystals composing 60 to 70% of rock. Locally, these are Z-folded and banded on millimetre scale with no obvious fragments. Mafic lithofacies in this domain are massive, pillowed and pillow brecciated flows that are typically aphyric and, locally, have spherulitic pillow margins and/or cores. Pillow selvages are typically thin and chloritic. Massive flows are weakly to strongly foliated with local sparsely amygdaloidal zones. Ultramafic lithofacies, although more commonly associated with the "mine" domain, are present as a thin layer of polygonally jointed and serpentinized flows and/or sills with minor amounts of talc resulting in a soapy feel on fracture surfaces. Intrusions are most commonly medium-grained, equigranular to plagioclase-phyric gabbros with minor tonalitic intrusions containing only 10 to 20% mafic minerals. Small syenitic and lamprophyric dikes are also present.

The "mine" domain is defined as part of the transect encompassing the Shebandowan Mine property and the region south of the northern domain to Horseshoe Lake. It is characterized by a lack of felsic to intermediate lithofacies and relative abundance of mafic to ultramafic extrusive and intrusive lithofacies. One pillowed mafic flow described within the mine property is characteristically coarsely plagioclase-phyric with phenocrysts up to 3 cm in size and composing up to 20% of flow (Photo 16.4A). This uniquely porphyritic flow was mapped in other transects during this study and may be a useful regional marker unit. Other mafic flows in this domain are massive, pillowed and brecciated and are typically fine grained and aphyric. Alteration is largely absent from the mafic flows with only local patchy chlorite and epidote alteration associated with sparse fine-grained pyrite mineralization. The "mine" ultramafic body, which is the host rock for the nickel-copper sulphides extracted from the Shebandowan Mine, is a strongly cleaved, dark green, fine-grained crystalline rock to a waxy dark green serpentinite where primary textures have been destroyed. Elsewhere in this domain, ultramafic lithofacies are brecciated, noted by resistant-weathering, stretched fragments in a rusty-looking talc-bearing matrix. Fragments on fresh surfaces were soapy feeling with serpentine and/or talc. Outside of the mine property, the ultramafic rocks are typically more massive, fine grained, and dark green in colour. Whether or not these ultramafic rocks are flows or sills remains debatable. The presence of talc-bearing breccias and strongly serpentinized polygonal jointing suggest an extrusive origin to at least some of the ultramafic bodies. In

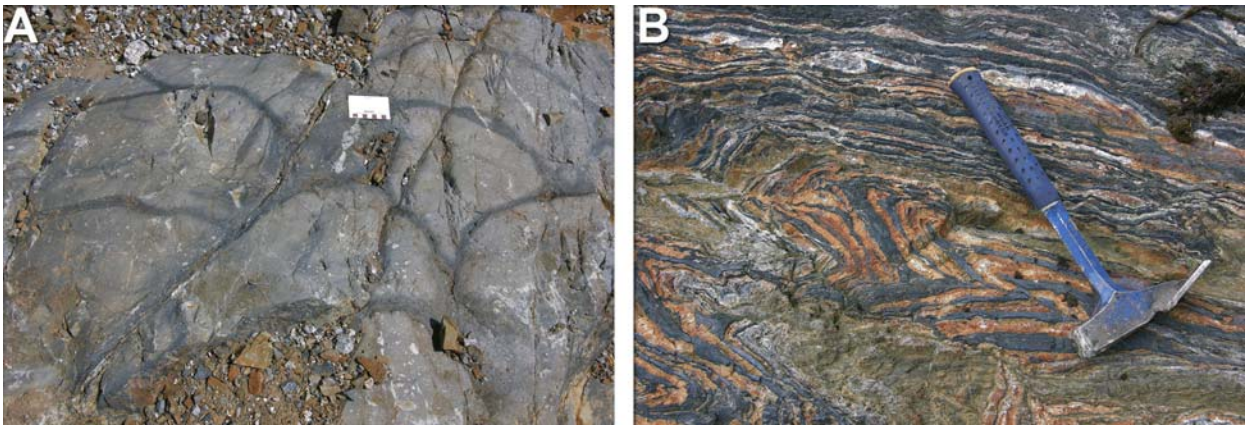

Photo 16.4. Field photographs from the Shebandowan Mine–Greenwater Lake transect: A) coarsely plagioclase-phyric pillowed mafic flows; and B) tightly folded chert-magnetite-sulphide iron formation interbedded with mafic flows.

other places, ultramafic rocks are on the same outcrop with gabbros and have no visible or recessive-weathering contact (poorly exposed due to heavy lichen cover) suggesting perhaps they are a product of differentiation of the gabbroic magma. Differentiation of the gabbro body into ultramafic and mafic components fits well with the interpretation that the coarsely plagioclase-phyric flows in the region would require eruption of plagioclase cumulates in order to produce such large phenocrysts in the mafic flows. Interbedded with mafic and ultramafic lithofacies in this domain are strongly folded and deformed, planar bedded chert-magnetite-jasper iron formations (Photo 16.4B) with minor sulphide-bearing beds. These are typically bedded on millimetre to centimetre scale and do not show much disruption of planar bedding even when strongly deformed. These iron formations are folded on a regional scale (Osmani 1997b) and their abundance in exposure may be a result of structural repetition. Intrusions are most commonly massive plagioclase- and/or pyroxene-phyric gabbro sills with minor syenitic and lamprophyric dikes.

The southern domain is defined as the mafic to felsic lithofacies south the main road access near Pinecone Lake. This domain was only briefly visited and additional mapping is planned for 2011. Lithofacies that were observed include weakly to moderately foliated, massive to pillowed mafic flows with local epidote alteration, “knobby”-textured medium-grained gabbros, and planar bedded chert-jasper-magnetite iron formation. Felsic lithofacies are white to grey coloured tuffs to lapilli tuffs, but were very poorly exposed.

Transect 6. Adrian–Aldina

The Adrian–Aldina transect, accessed from the Boreal and Adrian Lake roads (*see* Figure 16.1), was mapped to determine the stratigraphic setting associated with the Stares–Calvert property and massive sulphide occurrence documented by RJK Explorations Ltd. Outcrop coverage was relatively low because of thick boulder and sandy glacial outwash where larger boulders may have been misinterpreted as outcrops in some previous mapping (e.g., Berger 1995). Additional mapping is planned for next year to obtain both better mapping coverage and a better understanding on the structure and stratigraphy of this part of the SGB. Regional strike is primarily northwest with pillow shapes indicating that the succession youngs to the west (Berger 1995). This transect is also characterized by the presence of younger Timiskaming-like sedimentary successions that are intercalated with some of the volcanic lithofacies and may be structurally repeated.

Assuming a westward-younging succession, the youngest volcanic lithofacies of the Greenwater assemblage mapped in this transect were intermediate flows, monolithic tuff or flow breccias, and heterolithic tuff breccias in the Adrian Lake area. Monolithic lapilli tuffs and tuff breccias are medium grey with a medium-grained, feldspar-rich matrix. Light grey, matrix-supported fragments up to 15 cm in size are pyroxene-amphibole phyric in an aphanitic matrix. Intermediate heterolithic lapilli tuff to tuff breccias have a chloritic matrix and contain subrounded, matrix-supported mafic to intermediate fragments. Heterolithic tuffs are in sharp contact with bulbous, pyroxene- and plagioclase-phyric mafic pillow flows that contain pillows up to 1 m in size with 1 to 4 cm chloritic selvages. The transect is bisected by a shear zone that trends north-northwest along the Weigand River through the mafic flows. A fine- to medium-grained felsic dome or hypabyssal intrusion containing 10 to 15% quartz and feldspar phenocrysts up to 3 to 5 mm in size occurs at the shear zone. The flow is light grey, has weak mineral lineation shallowly plunging to the northwest, and has local, weak sericite alteration. To the west of the fault are massive mafic to intermediate flows and mafic to intermediate, matrix-supported heterolithic tuff breccias or tuffaceous conglomerates containing angular to subangular 10 to 20 cm fragments of mafic to intermediate volcanic rocks, minor gabbroic and feldspar-phyric granitic compositions. Fragments are moderate to poor sorted in a dark green chloritic matrix and the unit likely represents a debris flow unit.

There are other isolated outcrops of mafic flows that are difficult to place into the succession because of low outcrop coverage and apparent separation of these exposures from the main mass of volcanic

lithofacies by younger sedimentary strata (Berger 1995). Mafic flows to flow breccias are well exposed in Marks Township near the lower contact of the SGB with the granite-tonalite basement rocks to the south. Flow features include flow breccias and hyaloclastite. Calcite-filled, curvy fractures separate the flow breccias into centimetre- to decimetre-scale fluidal blocks with a preferred alignment. These are in close association with younger sandstones, greywackes and conglomerates (described below). Isolated exposures of mafic flows occur in Aldina Township where they are bulbous or pillowed flows with epidote alteration. No obvious pillow selvages were observed, but the surface is bumpy to hummocky. Because of the proximity to younger granitic intrusions, locally mafic flows are coarser grained amphibolites.

Sedimentary lithofacies seem to have a slightly more west to northwest orientation to their regional strike as previously mapped (Berger 1995) and are present as narrow, less than 100 m wide slivers in the western part of the transect or as thicker sections in large basins as in Adrian Township. Many exposures of the sedimentary lithofacies have been trenched because of associated pyrite mineralization in argillite and silicified sandstones that were likely geophysical anomalies. In Aldina Township, trenching exposed sphalerite-bearing massive sulphides hosted in a siliceous, and muscovite-rich, coarse-grained felsic-looking lithofacies that appears to have been recrystallized and appears volcanic in origin. However, close examination of the lithologies present in the trenches has revealed that sulphide mineralization is hosted in what appears to be a thickly bedded sequence of quartz-rich sediments with stratabound siderite alteration and pyrite mineralization. Some beds have boudinaged siderite layers (Photo 16.5A). Well-exposed outcrops of sedimentary lithofacies in a recent clearcut in Marks Township are in contact with mafic flows from the Greenwater assemblage. These sedimentary lithofacies are predominantly garnet-bearing, mafic tuffaceous greywackes with a strong bedded appearance and have sandy quartz-rich, garnet-poor layers. These beds are locally deformed and boudinaged with pronounced shear fabrics. At the contact with the mafic flows is a thin bed of intermediate to felsic heterolithic lapilli tuff in a plagioclase-rich matrix with crystals up to 3 mm in size. Fragments are white chert, fine-grained grey mafic and quartz-bearing intermediate lithofacies. In Adrian Township, trench and roadside exposures of the sedimentary lithofacies range from fine sandstone to greywacke and lesser gravel to pebble conglomeratic beds containing rounded to subangular fragments of mafic to intermediate volcanic rocks (Photo 16.5B). In Sackville Township, sedimentary lithofacies exposed in a trench are massive to thinly bedded, intermediate tuffaceous sandstones with minor magnetite-chert iron formation beds.

During a preliminary visit, a sample (RL-10-19) of a dark grey, thinly to thickly bedded fine sandstone to greywacke on Adrian Lake Road was collected to determine the maximum age of deposition the sedimentary lithofacies in this part of the SGB. Knowing the age of these sedimentary rocks is critical in interpreting the depositional and deformation history of this part of the belt. A total 170 detrital zircons

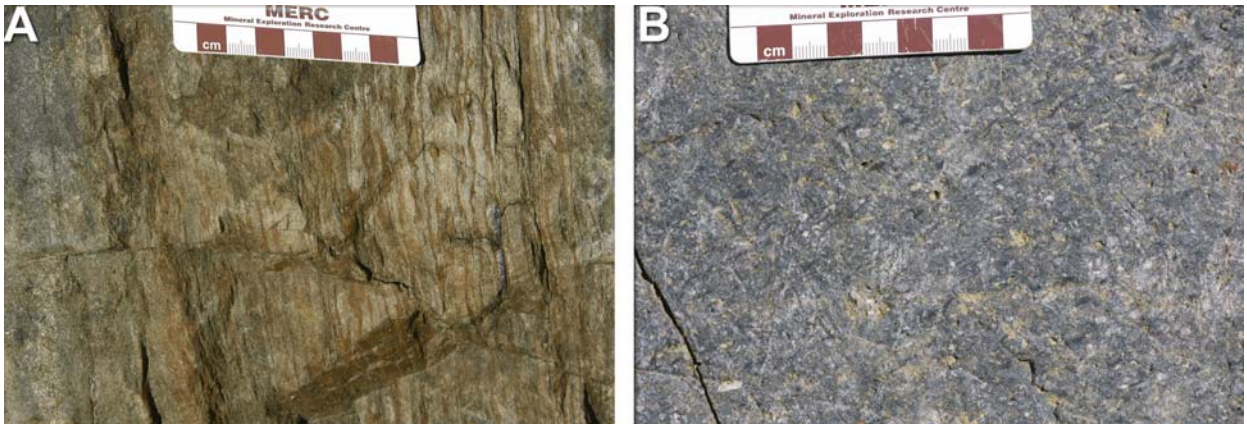

Photo 16.5. Field photographs from the Adrian–Aldina transect: A) siderite-bearing thinly bedded sandstone with boudinaged bedding; and B) gravelly sandstones in a trench dug by RJK Explorations.

were extracted and uranium-lead isotopes analyzed at the laser ablation inductively coupled plasma mass spectrometry (LA-ICP–MS) laboratory at Laurentian University to determine their age. Of the zircons analyzed, 77 grains were concordant, 54 grains were within 10% concordance, 16 grains required common lead correction and were within 10% concordance, whereas the remaining grains were greater than 10% discordant and were not used in the population analysis. The results of the analysis are summarized in Figure 16.3. The 3 main populations of zircons have ages of 2680 to 2690 Ma, 2720 Ma and 2750 Ma with ages as young as 2630 Ma and as old as 3300 Ma. This suggests a much younger maximum age of deposition and a older provenance than what was previously interpreted based on then-available U/Pb ages (Corfu and Stott 1998). Alternatively, older detrital zircons may represent inherited zircons in younger plutonic rocks.

Intrusions consist of mainly medium- to coarse-grained gabbros. Recent logging activity in the area has increased the amount of well-exposed outcrops and some areas that did not have previously mapped intrusions are now known to contain gabbro intrusions. In Aldina Township, some rocks previously mapped as mafic flows (Rogers 1995a) are actually gabbro intrusions that contain xenoliths of other gabbroic phases and coarse pegmatitic zones associated with shearing and fractures. The gabbros are locally heavily fractured into decimetre-scale blocks by white, recessive-weathering, 1 to 2 cm thick sheared fractures. Similarly in Sackville Township, rocks previously mapped as mafic flows (Rogers 1995c) are more appropriately classified as gabbro intrusions based on lack of flow textures and a medium- to coarse-grain size. Minor intrusive rocks include syenitic and lamprophyric dikes containing rounded actinolite nodules up to 10 cm in size.

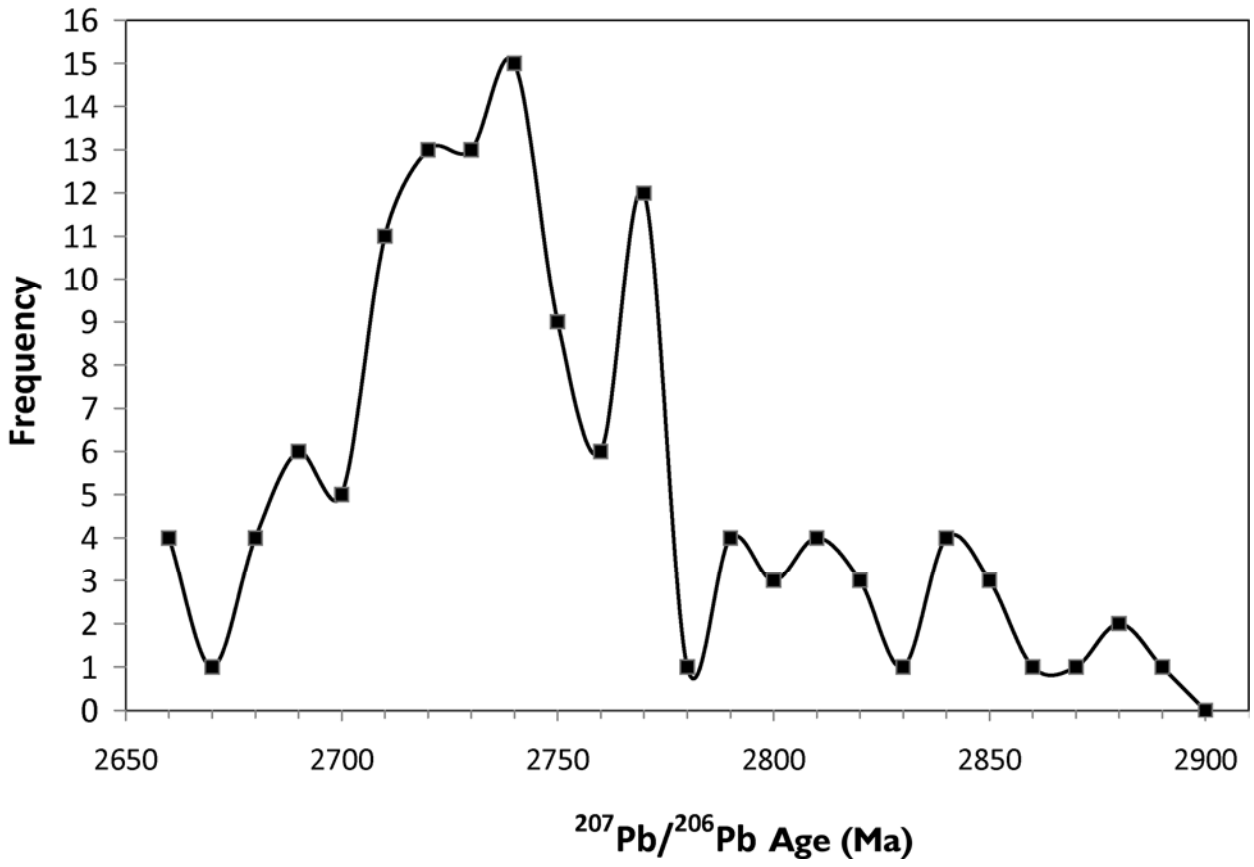

Figure 16.3. Histogram showing distribution of U/Pb ages of detrital zircons from sample RL-10-19.

Transect 7. Saganagons Greenstone Belt

The transect in the Saganagons greenstone belt was a series of north-south–oriented segments in the eastern part of the belt and included broadly spaced sampling traverses in the western part that was accessible by the logging road network that extends southward beyond the Greenwood Lake Conservation Area on Route 802 South (*see* Figure 16.1). Mapping in this part of the SGB was last completed by the Ontario Geological Survey in 1968 (Harris 1968). The succession is dominated by unaltered massive to pillowed mafic lavas intruded by white coloured quartz- and feldspar-phyric dikes with sharp margins (Photo 16.6A). These dikes are common in most locations and are likely related to the surrounding granitic intrusions at Mowe Lake and Saganaga Lake. The mafic flows are remarkably undeformed in the eastern part of the belt showing near perfectly preserved primary flow features such as intrapillow hyaloclastite (Photo 16.6B), pipe-like amygdules perpendicular to pillow margins and spherulitic pillow margins. Pillow shapes indicate that strata youngs to the north. Near the northern margin of the belt, rocks are strongly lineated, plagioclase-bearing amphibolites with no preserved primary structures. Small, medium-grained equigranular to pyroxene-phyric gabbroic intrusions are in the northeastern and south-central parts of the belt. Along the northern margin of the belt at the top of the stratigraphic section is a narrow massive to autobrecciated felsic flow and matrix-supported lapilli tuff. This was the only felsic lithofacies observed. Harris (1968) mapped and described several packages of supracrustal felsic lithofacies, but very few of these were intersected along the transects. One large previously mapped felsic unit was targetted for geochronologic sampling, but only dark green to medium grey pillowed and massive mafic flows were found at that locality. Further work is requires to confirm the existence and location of the other felsic lithofacies mapped by Harris (1968).

Transect 8. Wye Lake Area

The Wye Lake transect was conducted along logging road networks that branched to the southwest from the intersection of Hook Lake Road and Swamp Road and from the intersection northward along Swamp Road to the granitic intrusion that separates the northern and southern arms of the SGB (Hart and Metsaranta 2009) (*see* Figure 16.1). Few younging indicators were recognized and, based on grading within tuffs and pillow shapes, suggest a southeastward younging of the succession; however, deformation and faulting observed in the rocks suggest that the succession may be fault and/or fold repeated. The transect covered the entire width of the southern arm covering approximately 2.2 km of stratigraphic thickness. The results of this mapping are graphically summarized in Figure 16.4.

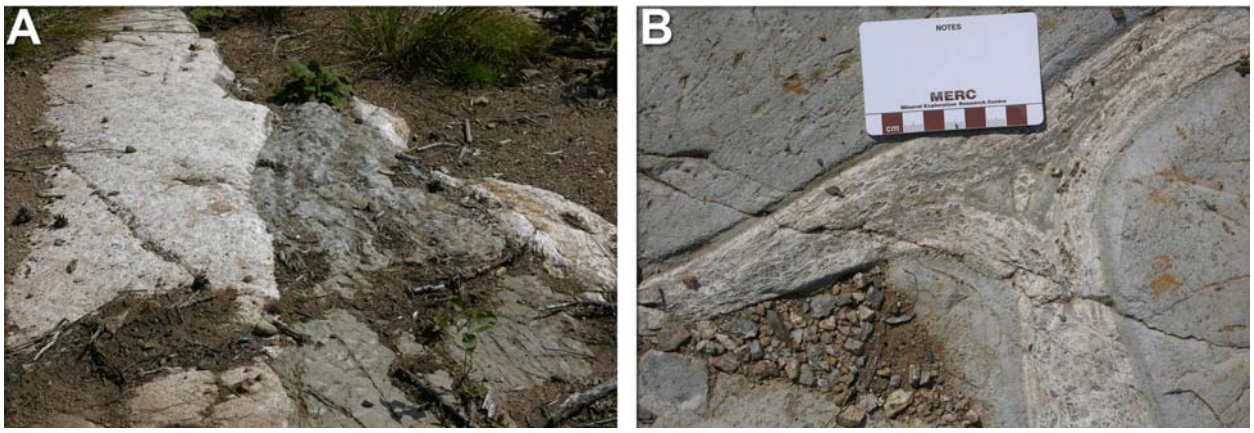

Photo 16.6. Field photographs from the Saganagons greenstone belt transect: A) contact between pillowed mafic flows (dark coloured) and a feldspar- and quartz-phyric granitic dike (light coloured); and B) thick hyaloclastite pillow selvages in mafic flow.

The lowermost strata on this transect, assuming a southeastward younging of the succession, is a massive to flow-brecciated and magnetite-rich mafic flow. Despite poor exposure, flow breccias were recognized based on weathering patterns on glacially polished and lichen-covered outcrop. Flow fragments are matrix supported and are up to 3 to 5 cm in size. Other mafic flows at the base of the succession are locally amygdaloidal (chlorite filled), pillowed and flow brecciated. There is weak to moderate hematite and chlorite alteration. Amygdules compose up to 10 to 15% of rock and are more abundant in pillowed flows. Deformation and flattening of the mafic flows is noted by stretched pillows to 5:1 length:width ratios. Interbedded with the pillowed flows are chert-magnetite-sulphide iron formations that range from 2 to 200 cm in thickness and are locally brecciated (Photo 16.7A). Overlying the mafic flows is a felsic to intermediate volcaniclastic unit that, in the easternmost part of mapped transect, is a thickly bedded, matrix-supported felsic tuff breccia to pyroclastic breccia with a chlorite-garnet altered matrix that is interpreted as a debris flow (*see* Figure 16.4). Fragments include quartz-phyric felsic, laminated felsic tuff and minor garnet-chlorite altered tuffs. Minor quartz- and feldspar-rich tuff and monolithic felsic autobreccia beds (Photo 16.7B) are interbedded with the altered tuff breccias. Approximately 150 m along strike with the altered tuff breccias is a felsic quartz-feldspar-phyric flow to

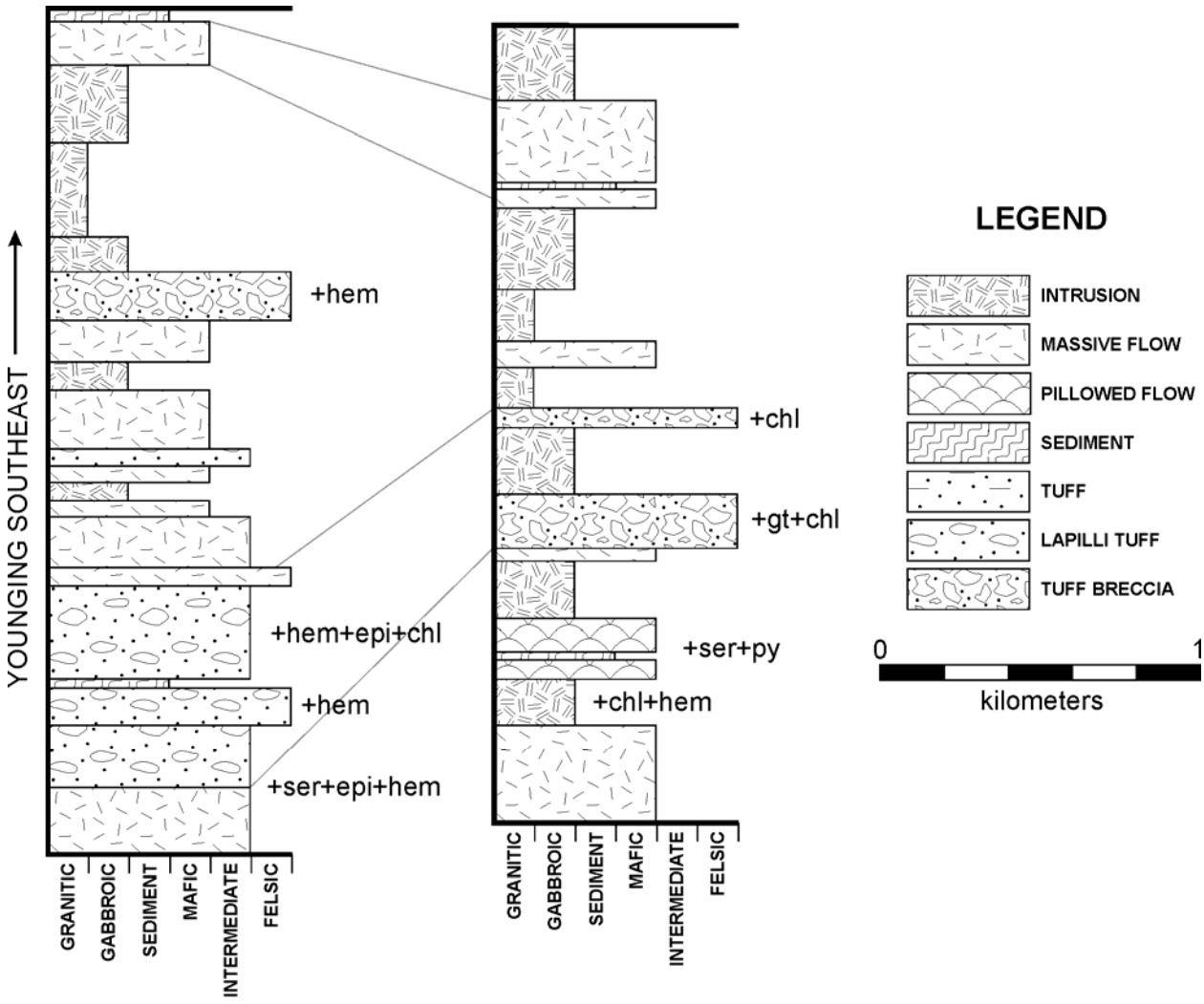

Figure 16.4. Graphic logs showing the mapped stratigraphy in the Wye Lake transect. Younging directions are based on pillow shapes and graded bedding in debris flows. Abbreviations: chl = chlorite; epi = epidote; gt = garnet; hem = hematite; py = pyrite; ser = sericite.

flow breccia with faint lapilli- and bomb-sized fragments up to 15 cm in size. Alteration is less intense with only local garnet-hematite alteration. Phenocrysts compose up to 20% of rock and are up to 3 mm in size. Four kilometres along strike in the southwestern part of the transect, and still within this unit (as mapped by Hart and Metsaranta 2009), are similar-looking bedded felsic tuff tuffs overlain by amygdaloidal intermediate flows and minor monolithic lapilli tuffs that locally contain centimetre-scale blocks noted by differences in amygdule concentrations and foliation patterns. The intermediate flows are overlain by an intermediate heterolithic lapilli tuff to tuffaceous conglomerate that is most likely a debris flow. Fragments are poorly to moderately sorted and are supported in a medium green fine sandy lithic tuff matrix. Fragments are 1 to 10 cm in size and range in composition from white aphanitic intermediate, chert, fine-grained rimmed mafic, to rare gabbro and granite. The intermediate heterolithic debris flow is overlain by quartz-feldspar porphyritic felsic flow breccias and pyroclastic breccias. Fragments are stretched to 1 to 50 cm in size, are monolithic and fine grained, poorly sorted and fragment supported. The matrix is composed of feldspar crystals and finer lithic fragments. This rock is pink in colour due to moderate pervasive hematite alteration. The succession of this transect is capped by a mafic flow to flow breccia that is very fine grained and aphyric, with local chlorite alteration and/or devitrification. Flows are interbedded with siliceous felsic tuff or cherty recrystallized sedimentary lithofacies where laminations are defined by light and dark layers. Cherty layers are finely laminated and layered with local sericite-altered felsic tuff. Sericite-altered layers contain stringers of pyrite comprising up to 10 to 15% of the rock with trace sphalerite.

Intrusions in the Wye Lake transect were primarily gabbro to leucogabbro that are medium grained and overall massive to weakly foliated. In the northern part of the transect, and presumably lower in the succession, the gabbros are massive and plagioclase phyric. Phenocrysts are subhedral, up to 8 mm in size, and compose 10% of rock. Higher in the succession, and to the southeast, are fine- to coarse-grained pyroxene-rich gabbros that locally contain up to 70% pyroxene crystals up to 4 cm long. Most gabbros in this transect have a weak, fracture-associated epidote-hematite alteration. Minor mafic and syenitic dikes are present throughout the rocks in the transect. Minor medium-grained, granitic intrusions were at the top of the section where they are associated with the contact between gabbros and supracrustal rocks.

Transect 9. Hamlin Lake–Moss Lake

The Hamlin Lake–Moss Lake transect is oriented slightly oblique to regional strike and mapping focusing on exposures along Swamp Road from the granitic intrusion that separates the north and south arms of the SGB (Hart and Metsaranta 2009) northward to the Shebandowan greenstone belt–Quetico

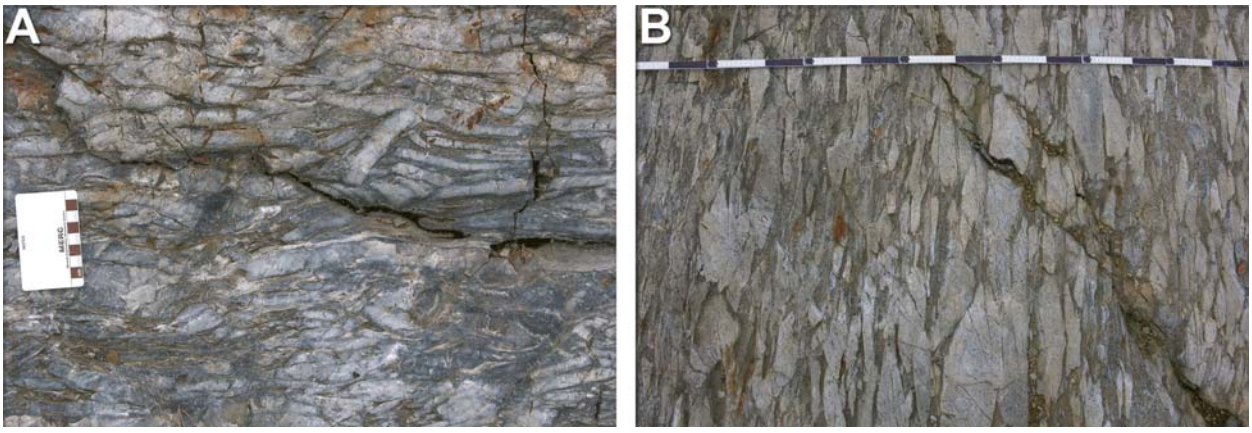

Photo 16.7. Field photographs from the Wye Lake Area transect: A) chert breccias interbedded with pillowed mafic flows and chert-magnetite iron formations; and B) felsic fragment-supported monolithic tuff breccia (autobreccia) in the immediate hanging wall to garnet-chlorite altered tuff breccias.

Subprovince boundary (Osmani 1997d) (*see* Figure 16.1). Possible grading in an intermediate tuff breccia in the southern part of the transect suggest a northwestern younging direction, which is in agreement with pillow shapes observed by Osmani (1997d). The succession seems to be relatively intact in the southern part of the transect as no major structures or zones of intense deformation were recognized. At the northern part of the transect, shearing and faulting were more prominent closer to the Shebandowan greenstone belt–Quetico Subprovince boundary.

The southern, and presumably the oldest, part of the transect includes strata that host the Hamlin Lake iron oxide-copper-gold (IOCG) deposit. The mineralization is hosted in a granitic breccia (Hart and Trebilcock 2006) with a chlorite-garnet–altered matrix near the contact with the granitic intrusion dividing the north and south arms of the belt. The base of the section is dominated by massive to pillowed mafic flows that are moderately epidote-hematite-chlorite altered and contain up to 10% disseminated pyrite locally. Alteration lightens the colour of the flows such that they resemble a more intermediate composition. Mafic flow breccias have up to 15 cm fluidal fragments and blebby epidote nodules forming pods and stretched veins. The mafic flows are overlain by intermediate to felsic lithofacies that include white-weathering, siliceous and quartz-phyric flows, autobreccias, and lapilli tuffs and tuff breccias. Flows and autobreccias contain quartz crystals up to 3 mm in size, composing up to 10% of the rock. Intermediate tuff breccias contain 1 to 30 cm predominantly mafic to intermediate amygdaloidal fragments with lesser chert fragments and green-grey fragments that are similar in composition to matrix. Fragments are matrix supported in a light grey-green lithic lapilli-rich matrix. A thin unit of medium-dark green chloritic mafic to intermediate flow breccias separates the felsic to intermediate lithofacies to the south from a massive, fresh-looking hematite- and potassic-altered, dark grey, quartz-phyric intermediate flow. Alteration is fracture associated, but, locally, gives the rock a fragmented appearance (Photo 16.8A). This flow is overlain by strongly foliated, chloritic and sericitic, quartz-phyric intermediate tuffaceous lithofacies containing stringers and disseminated pyrite. The thick intermediate succession is capped by a pillowed mafic flow that has very large 1 to 3 m pillows or lava tubes with thick chloritic and zoned selvages and epidote-quartz altered cores (Photo 16.8B). These large pillows grade northward into a cherty, matrix-supported flow breccia that is in contact with planar bedded chert breccia with centimetre-scale angular white chert fragments.

The northern part of the transect is composed of 2 major units: a thick mafic flow unit that hosts the shear-related Moss and Ardeen gold deposits, and an underlying massive white felsic flow to flow breccia unit. The massive felsic flow unit, that immediately overlies the pillowed mafic unit from the southern part of the transect, consists of fine-grained to aphanitic flows with moderate to strong foliation and

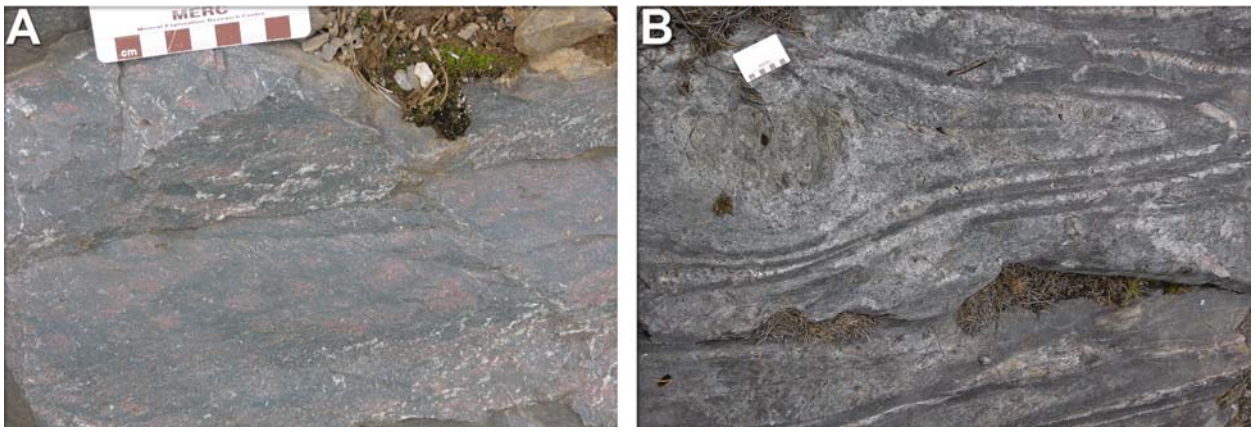

Photo 16.8. Field photographs from the Hamlin Lake–Moss Lake transect: A) patchy hematite and potassic alteration in dark grey felsic quartz-phyric flow resulting in fragmental-looking texture; and B) large epidote-quartz alteration in large metre-scale mafic pillows.

contain up to 20% 1 to 3 mm feldspar phenocrysts. Locally, the flows contain quartz-phenocrysts up to 3 mm in size. These rocks weather to a white colour, are pale grey-green on fresh surfaces and are relatively homogeneous over a thickness of approximately 1 km. There are local minor tuffaceous and tuff breccia layers within the felsic–intermediate flow succession. The overlying thick mafic flows are continuous to the Shebandowan greenstone belt–Quetico Subprovince boundary. These flows are massive flows that are relatively nondescript and, where sheared, are locally chloritic schists; some of the chloritic schists may be altered intermediate rocks. Thinly bedded magnetite-chert iron formation is associated with mafic flows.

The intrusions in this transect are typically pyroxene-phyric gabbros in the southern part of the transect to abundant sill-like bodies of feldspar-phyric syenitic to granitic composition in the northern part of the transect. These intrusions are medium grained and massive. Other minor intrusions are thin, fine-grained mafic and syenite dikes.

RECOMMENDATIONS FOR EXPLORATION

The transects were located in zones of known mineralization. Therefore, most of the alteration and mineralization mapped is associated with already discovered mineral showings. These include the Gold Creek gold prospect (transect 1), Vanguard East and West zinc-copper prospects (transect 2), Mud Lake zinc occurrence (transect 4), Shebandowan nickel-copper mine (transect 5), the Stares–Calvert zinc prospect (transect 6), Wye Lake zinc-copper prospect (transect 8), Hamlin Lake iron oxide-copper-gold prospect (transect 9), and the Moss and Ardeen gold prospects (transect 9).

However, an untested area that may have potential for VMS-type mineralization was recognized during mapping in the Grouse Lake area of the Grouse Lake–Hermia Lake transect (*see* Figure 16.1, transect 3). The quality and quantity of exposure was increased because of recent logging activity. Here, the lithofacies and their succession share similar characteristics to those hosting other Archean VMS deposits (e.g., Galley, Hannington and Jonasson 2007, and references therein) and are characterized by moderately to strongly epidote-altered pillow flows in the hanging wall to sericite- and chlorite-altered felsic tuffs and lapilli tuffs with stratabound pyrite and sphalerite mineralization (*see* Figure 16.2). Minor magnetite-chert iron formation may indicate the presence of hydrothermal venting. Quartz-phyric tonalitic intrusions and mafic sills intruding the felsic volcaniclastic lithofacies may indicate proximity to a potential heat source for the hydrothermal system driving alteration and mineralization. Based on these regional characteristics and their broad similarities to other Archean VMS-producing terranes, it is recommended that this area be further explored for VMS-type mineralization.

FUTURE WORK PLANNED

Lithogeochemical data (with major, trace and rare earth elemental analyses from the Geoscience Laboratories, Ontario Geological Survey) will be used to characterize lithofacies and construct a chemostratigraphic section that will aid stratigraphic correlation between transects and tectonic reconstruction of the Shebandowan greenstone belt. High-precision trace element data (to be analyzed in the laboratory of Dr. B. Kamber, Laurentian University) and radiogenic isotope data (Sm/Nd, $^{207}Pb/^{206}Pb$) will be used to characterize the petrogenesis and magmatic evolution of the SGB, and amount of crustal contamination. Isotopic and geochemical analyses will be necessary to fully establish linkages between adjacent greenstone belt segments. Geochronologic analyses (U/Pb; location of samples to be determined) will be used to better constrain the emplacement history of the SGB lithologies and to aid correlation with the adjacent Vermilion greenstone belt in northern Minnesota. Transmitted light and reflected light petrography will used to describe the lithofacies in greater detail including detailed mineralogy,

descriptions of primary and secondary textures, and clast composition and provenance. Petrographic analyses are an essential part of determining the temporal relationship between different alteration assemblages, and also in determining the timing of mineralization.

Samples were collected from the younger Timiskaming-like successor basins throughout the greenstone belt for detrital zircon age determinations at the LA-ICP–MS laboratory at Laurentian University. These samples were collected because the cost-effective and statistically significant results obtained by the analysis of more than 170 detrital zircons from a fine sandstone to wacke in Marks Township (*see* "Transect 6. Adrian–Aldina"; *see* Figure 16.3) yielded a much larger range of ages than previous geochronological analyses (Corfu and Stott 1998). A sample was collected from outcrops of a pebble to cobble polylithic conglomerate with clasts of mafic to felsic intrusive and extrusive rocks, jasper and sulphides on Shebandowan Mine Road. This sample is part of the most northerly regionally mapped successor sedimentary basin. Another sample was taken from thickly bedded massive sandstone to wacke in Duckworth Township representing the "middle" sedimentary basin in the SGB. The goal of this sampling and the analyses is to determine if a similar range of detrital zircon ages are present in each of the sedimentary basins to that of the southern basin in Marks and Adrian townships.

Mapping of the Vermilion, Winston Lake and Manitouwadge greenstone belts will commence in the summer of 2011. Similar transect-style mapping will be used to compare the stratigraphy, geodynamic setting and petrogenesis of the volcanic-plutonic rocks that host VMS-style mineralization and alteration. Additional mapping in the eastern and southern parts of the SGB is also planned for 2011 to fill gaps in the mapping coverage and to refine the stratigraphy.

ACKNOWLEDGMENTS

This is the first report of a four-year PhD thesis project supported by the Mineral Exploration Research Centre (MERC) at the Department of Earth Sciences, Laurentian University, and the Ontario Geological Survey and is co-supervised by Dr. Harold Gibson (LU) and Dr. Greg Stott (OGS). Additional members of the thesis committee are Dr. Doug Tinkham (LU) and Dr. Jim Franklin (Consultant). Additional funding is provided by the Natural Sciences and Engineering Research Council of Canada (NSERC) and the Society of Economic Geologists (SEG) Student Research Grant.

REFERENCES

Berger, B.R. 1995. Precambrian geology, Adrian Township; Ontario Geological Survey, Map 2617, scale 1:20 000.

Brown, G.H. 1995. Precambrian geology, Oliver and Ware townships; Ontario Geological Survey, Report 294, 48p.

Brown, G.H. and Fogal, R.I. 1995a. Precambrian geology, Oliver Township; Ontario Geological Survey, Map 2615, scale 1:20 000.

——— 1995b. Precambrian geology, Ware Township; Ontario Geological Survey, Map 2616, scale 1:20 000.

Corfu, F. and Stott, G.M. 1986. U–Pb ages for late magmatism and regional deformation in the Shebandowan Belt, Superior Province, Canada; Canadian Journal of Earth Sciences, v.23, p.1075-1082.

——— 1998. Shebandowan greenstone belt, western Superior Province: U-Pb ages, tectonic implications, and correlations; GSA Bulletin, v.110, p.1467-1484.

Davis, D.W., Schandl, E.S. and Wasteneys, H.A. 1994. U-Pb dating of minerals in alteration halos of Superior Province massive sulfide deposits; syngenesis versus metamorphism; Contributions to Mineralogy and Petrology, v.115, p.427-437.

Farrow, C.E.G. 1993. Base metal sulphide mineralization, Shebandowan greenstone belt; *in* Summary of Field Work and Other Activities 1993, Ontario Geological Survey, Miscellaneous Paper 162, p.4-8.

——— 1994. Base metal mineralization, Shebandowan greenstone belt, District of Thunder Bay, Ontario; *in* Summary of Field Work and Other Activities, 1994, Ontario Geological Survey, Miscellaneous Paper 163, p.97-104.

——— 1995. Alteration and sulphide mineralogy associated with base metal mineralization, Shebandowan greenstone belt, District of Thunder Bay, Ontario; *in* Summary of Field Work and Other Activities, 1995, Ontario Geological Survey, Miscellaneous Paper 164, p.82-86.

Fisher, R.V. 1966. Rocks composed of volcanic fragments; Earth Science Reviews, v.1, p.287-298.

Franklin, J.M. 2003. Review of the Canadian Golden Dragon base metal exploration program, Shebandowan Belt, NW Ontario; Franklin Geosciences Ltd. for Canadian Golden Dragon Resources Ltd., 18p.

——— 2005. Notes on the Sungold Property, Kashabowie area, Ontario, for Freewest Resources Canada Ltd.; Franklin Geosciences Ltd. for Freewest Resources Canada Ltd., 14p.

Franklin, J.M., Gibson, H.L., Jonasson, I.R. and Galley, A.G. 2005. Volcanogenic massive sulfide deposits; Economic Geology, 100th Anniversary Volume, p.523-560.

Galley, A.G., Hannington, M.D. and Jonasson, I.R. 2007. Volcanogenic massive sulphide deposits; *in* Mineral deposits of Canada: a synthesis of major deposit-types, district metallogeny, the evolution of geological provinces, and exploration methods, Geological Association of Canada, Mineral Deposits Division, Special Publication No. 5, p.141-161.

Harris, F.R. 1968. Saganagons Lake area, District of Thunder Bay; Ontario Geological Survey, Map 2149, scale 1:31 680.

Hart, T.M. and Metsaranta, D.-A. 2009. Precambrian geology of the Wye and Hamlin lakes area; Ontario Geological Survey, Preliminary Map P.2511, scale 1:20 000.

Hart, T.M. and Trebilcock, D.-A. 2006. Geology of the Hamlin and Wye lakes area, Shebandowan greenstone belt, Thunder Bay District; *in* Summary of Field Work and Other Activities, 2006, Ontario Geological Survey, Open File Report 6192, p.9-1 to 9-9.

Hodgkinson, J.M. 1963. Kashabowie sheet, Thunder Bay District; Ontario Geological Survey, Map 2128, scale 1:31 680.

Morin, J. 1970. Lower Shebandowan Lake, Thunder Bay District; Ontario Geological Survey, Map 2267, scale 1:31 680.

Morton, P. 1982. Archean volcanic stratigraphy, and petrology and chemistry of mafic and ultramafic rocks, chromite, and the Shebandowan Ni-Cu Mine, Shebandowan, northwestern Ontario; unpublished PhD thesis, Carleton University, Ottawa, Ontario, 346p.

Osmani, I.A. 1996. Geology and mineral potential of the upper and middle Shebandowan Lakes area, west-central Shebandowan greenstone belt; Ontario Geological Survey, Open File Report 5938, 82p.

——— 1997a. Geology and mineral potential: Greenwater Lake area, west-central Shebandowan greenstone belt; Ontario Geological Survey, Report 296, 135p.

——— 1997b. Precambrian geology, Begin, Lamport, and parts of Haines and Hagey townships—west half; Ontario Geological Survey, Map 2625, scale 1:20 000.

——— 1997c. Precambrian geology, Burchell–Greenwater lakes area—west half; Ontario Geological Survey, Map 2622, scale 1:20 000.

——— 1997d. Precambrian geology, Moss Township; Ontario Geological Survey, Map 2624, scale 1:20 000.

Peterson, D., Gallup, C., Jirsa, M. and Davis, D.W. 2001. Correlation of the Archean assemblages across the U.S.–Canadian border: Phase I geochronology; 47th Institute on Lake Superior Geology, Proceedings, v.47, pt.1, p.77-78.

Rogers, M.C. 1995a. Precambrian geology, Aldina Township; Ontario Geological Survey, Map 2620, scale 1:20 000.

——— 1995b. Precambrian geology, Duckworth Township; Ontario Geological Survey, Map 2621, scale 1:20 000.

——— 1995c. Precambrian geology, Sackville Township; Ontario Geological Survey, Map 2619, scale 1:20 000.

Rogers, M.C. and Berger, B.R. 1995. Precambrian geology, Adrian, Marks, Sackville, Aldina and Duckworth townships; Ontario Geological Survey, Report 295, 66p.

Shegelski, R.J. 1980. Archean cratonization, emergence and red bed development, Lake Shebandowan area, Canada; Precambrian Research, v.12, p.331-347.

Williams, H.R., Stott, G.M., Heather, K.B., Muir, T.L. and Sage, R.P. 1991. Wawa Subprovince; *in* Geology of Ontario, Ontario Geological Survey, Special Volume 4, Part 1, p.485-541.

APPENDIX J: OGS OPEN FILE REPORT 6282 (2012)

This appendix contains a report published by the Ontario Geological Survey that is a fieldtrip guidebook for volcanogenic massive sulphide (VMS) deposits of the Manitouwadge and Winston Lake greenstone belts. This field trip was run in conjunction with the Ontario Geological Survey, the Canadian Institute of Mining and Metallurgy Thunder Bay branch, and the Mineral Exploration Research Centre at Laurentian University. It contains summaries of the VMS history and detailed outcrop sketches that are unique to this guidebook and are not reproduced in the manuscripts presented in this thesis.

This report is available for free download from the website address stated below and is reproduced in this thesis with the permission of the Publication Sales and Services section of the Ontario Geological Survey.

Website

http://www.geologyontario.mndmf.gov.on.ca/mndmaccess/mndm_dir.asp?type=pub&id=OFR6282

Ontario

Ontario Geological Survey
Open File Report 6282

Winston Lake and Manitouwadge Revisited: Modern Views of Two Volcanogenic Massive Sulphide (VMS)-Endowed Greenstone Belts

A Field Trip Guidebook

2012

Ontario

ONTARIO GEOLOGICAL SURVEY

Open File Report 6282

Winston Lake and Manitouwadge Revisited: Modern Views of Two Volcanogenic Massive Sulphide (VMS)-Endowed Greenstone Belts. A Field Trip Guidebook.

by

R.W.D. Lodge

2012

Open File Reports of the Ontario Geological Survey are available for viewing at the John B. Gammon Geoscience Library in Sudbury and at the regional Mines and Minerals office whose district includes the area covered by the report (see below).

Copies can be purchased at Publication Sales and the office whose district includes the area covered by the report. Although a particular report may not be in stock at locations other than the Publication Sales office in Sudbury, they can generally be obtained within 3 working days. All telephone, fax, mail and e-mail orders should be directed to the Publication Sales office in Sudbury. Purchases may be made using cash, debit card, VISA, MasterCard, American Express, cheque or money order. Cheques or money orders should be made payable to the *Minister of Finance.*

John B. Gammon Geoscience Library
933 Ramsey Lake Road, Level A3
Sudbury, Ontario P3E 6B5

Tel: (705) 670-5615

Publication Sales
933 Ramsey Lake Rd., Level A3
Sudbury, Ontario P3E 6B5

Tel: (705) 670-5691 (local)
Toll-free: 1-888-415-9845 ext. 5691
Fax: (705) 670-5770
E-mail: pubsales.ndm@ontario.ca

Regional Mines and Minerals Offices:

Kenora - Suite 104, 810 Robertson St., Kenora P9N 4J2

Kirkland Lake - 10 Government Rd. E., Kirkland Lake P2N 1A8

Red Lake - Box 324, Ontario Government Building, Red Lake P0V 2M0

Sault Ste. Marie - 875 Queen St. E., Suite 6, Sault Ste. Marie P6A 6V8

Southern Ontario - P.O. Bag Service 43, 126 Old Troy Rd., Tweed K0K 3J0

Sudbury - 933 Ramsey Lake Rd., Level A3, Sudbury P3E 6B5

Thunder Bay - Suite B002, 435 James St. S., Thunder Bay P7E 6S7

Timmins - Ontario Government Complex, P.O. Bag 3060, Hwy. 101 East, South Porcupine P0N 1H0

Cette publication est disponible en anglais seulement.

Parts of this report may be quoted if credit is given. It is recommended that reference be made in the following form:

Lodge, R.W.D. 2012. Winston Lake and Manitouwadge revisited: modern views of two volcanogenic massive sulphide (VMS)-endowed greenstone belts. A field trip guidebook; Ontario Geological Survey, Open File Report 6282, 34p.

Contents

FIGURES

PHOTOS

TABLES

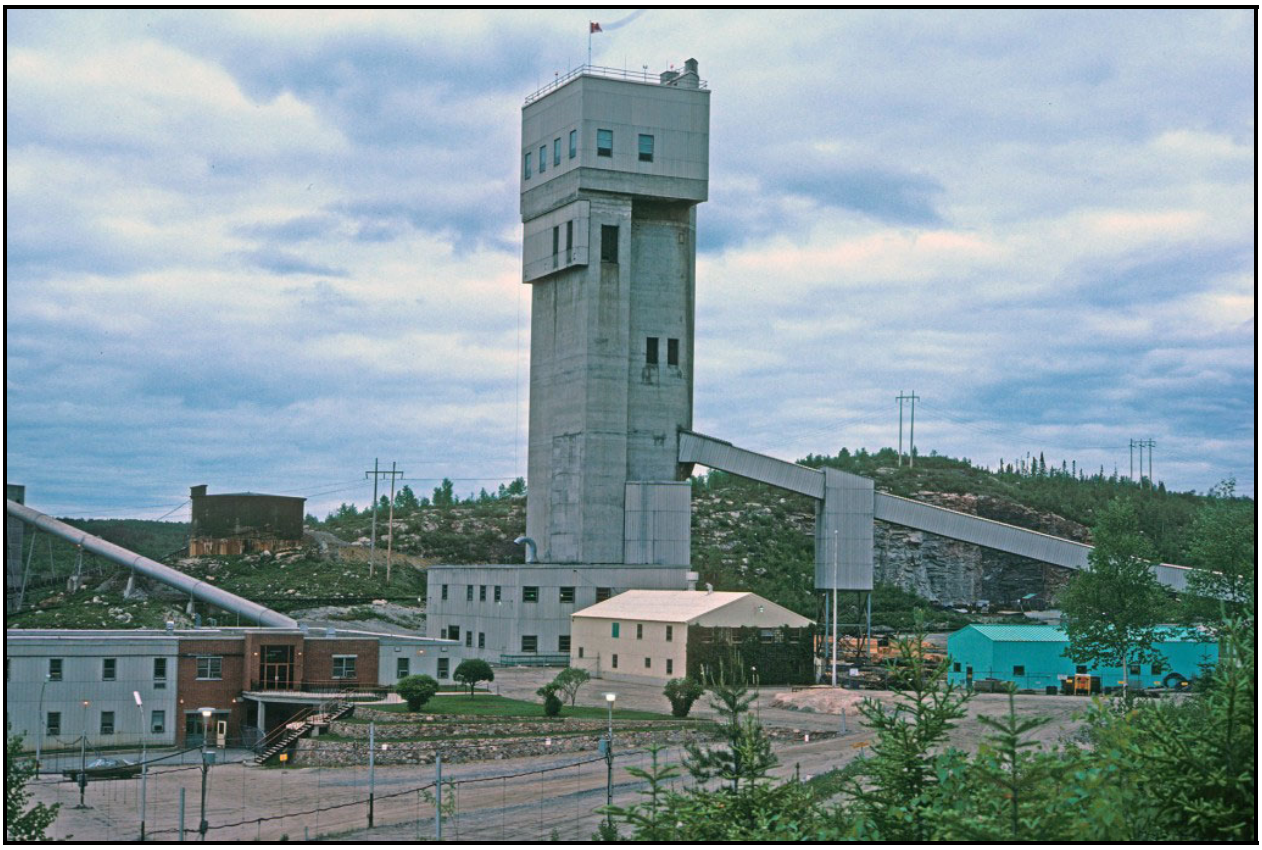

Image: Geco Mine main headframe in 1975. The image is reprinted with permission from photographer Rock Currier, Baldwin Park, California, and is available for viewing online at www.mindat.org.

ACKNOWLEDGMENTS

The author and colleagues would like to thank the staff and management of the mining and exploration companies that have permitted us to visit their properties during this field trip.

Winston Lake and Manitouwadge Revisited: Modern Views of Two Volcanogenic Massive Sulphide (VMS)-Endowed Greenstone Belts. A Field Trip Guidebook.

Robert W.D. Lodge[1]

Ontario Geological Survey
Open File Report 6282
2012

---

[1]**Department of Earth Sciences, Laurentian University, Sudbury, Ontario, Canada P3E 2C6**

Introduction

The Winston Lake and Manitouwadge greenstone belts are best known for hosting economic volcanogenic massive sulphide (VMS) deposits totalling almost 65 million tons of copper-zinc-lead ore (OGS 2011). These belts occur within the same tectonostratigraphic interval located along the northern margin of the Wawa Subprovince that is in contact with the Quetico Subprovince (Figure 1). Another noteworthy feature of these greenstone belts is the fact that they formed at the same time, *circa* 2720 Ma (Davis, Schandl and Wasteneys 1994; Zaleski, van Breemen and Peterson 1999). Other greenstone belts along the northern margin of the Wawa Subprovince, such as the Shebandowan and Vermilion greenstone belts, also formed *circa* 2720 Ma (Corfu and Stott 1998; Hart and Trebilcock 2006; Peterson et al. 2001), but have yet to yield an economic VMS deposit.

The Winston Lake and Manitouwadge greenstone belts and their VMS-hosting strata have received a fair amount of research at a property-scale (e.g., Osterberg 1993; Pan and Fleet 1995; Schandl, Gorton and Wasteneys 1995), a belt-scale (e.g., Zaleski and Peterson 1995; Zaleski, van Breemen and Peterson 1999), and a subprovince-scale (e.g., Kerrich, Polat and Xie 2008; Polat, Kerrich and Wyman 1999). There were also several field trips and published guidebooks (Severin, Balint and Sim 1991; Williams et al. 1991a; Zaleski et al. 1995). Previous research in these areas has been extremely valuable throughout the planning of this field trip and preparation of the guidebook.

The purpose of re-visiting the Winston Lake and Manitouwadge greenstone belts was to establish the geodymanic setting and petrogenesis of the greenstone belts at a regional scale to determine why the 2720 Ma greenstone belts of the Wawa Subprovince are so varied in their VMS endowment. This field trip will highlight some of the newly obtained data in the Winston Lake and Manitouwadge greenstone belts and will expose a new generation of geologists to these world-class VMS camps. This PhD project is funded by the Ontario Geological Survey (OGS) and the Mineral Exploration Research Centre (MERC) at Laurentian University (Sudbury, Ontario). Previously published reports for this project are available online from the Ontario Ministry of Northern Development and Mines publications portal, GeologyOntario, at www.ontario.ca/geology (Lodge 2010, 2011).

It should be noted that newly obtained geochemical data and U/Pb zircon ages presented in this guidebook are preliminary and their interpretation are subject to change pending future analyses. During field work more than 800 samples were collected. From these samples 400 geochemical analyses, 100 Nd and Pb isotopic analyses, and 13 for U/Pb geochronological analyses were completed. Some of this data is still forthcoming and will be made available online at GeologyOntario (www.ontario.ca/geology) in digital format as a Miscellaneous Release—Data (MRD) early in 2013.

Regional Geology

WINSTON LAKE GREENSTONE BELT

The Winston Lake Greenstone Belt (Figure 2) is a small belt located directly north of, and almost connected to the Schreiber–Hemlo greenstone belt (Williams et al. 1991b); however, the contact relationship of these belts is poorly constrained. Unlike the Manitouwadge greenstone belt, the Winston Lake greenstone belt is has not been mapped at a regional scale since the 1960s (Pye 1964). The belt is

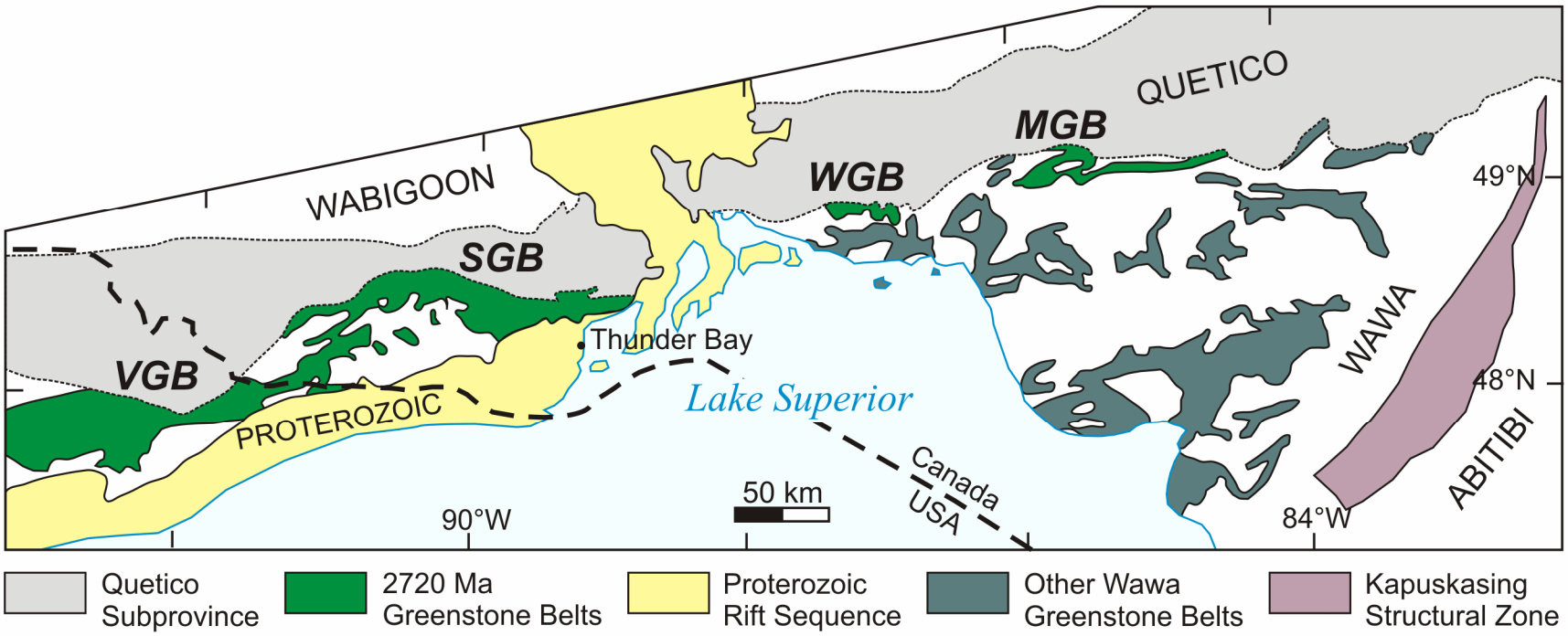

Figure 1. General geology of the Wawa Subprovince of the Superior Craton. Abbreviations: MGB, Manitouwadge greenstone belt; SGB, Shebandowan greenstone belt; VGB, Vermilion greenstone belt; WGB Winston Lake greenstone belt. Abitibi, Quetico, Wabigoon and Wawa labels refer to subprovinces of the Archean Superior Province. Figure *from* Lodge (2011).

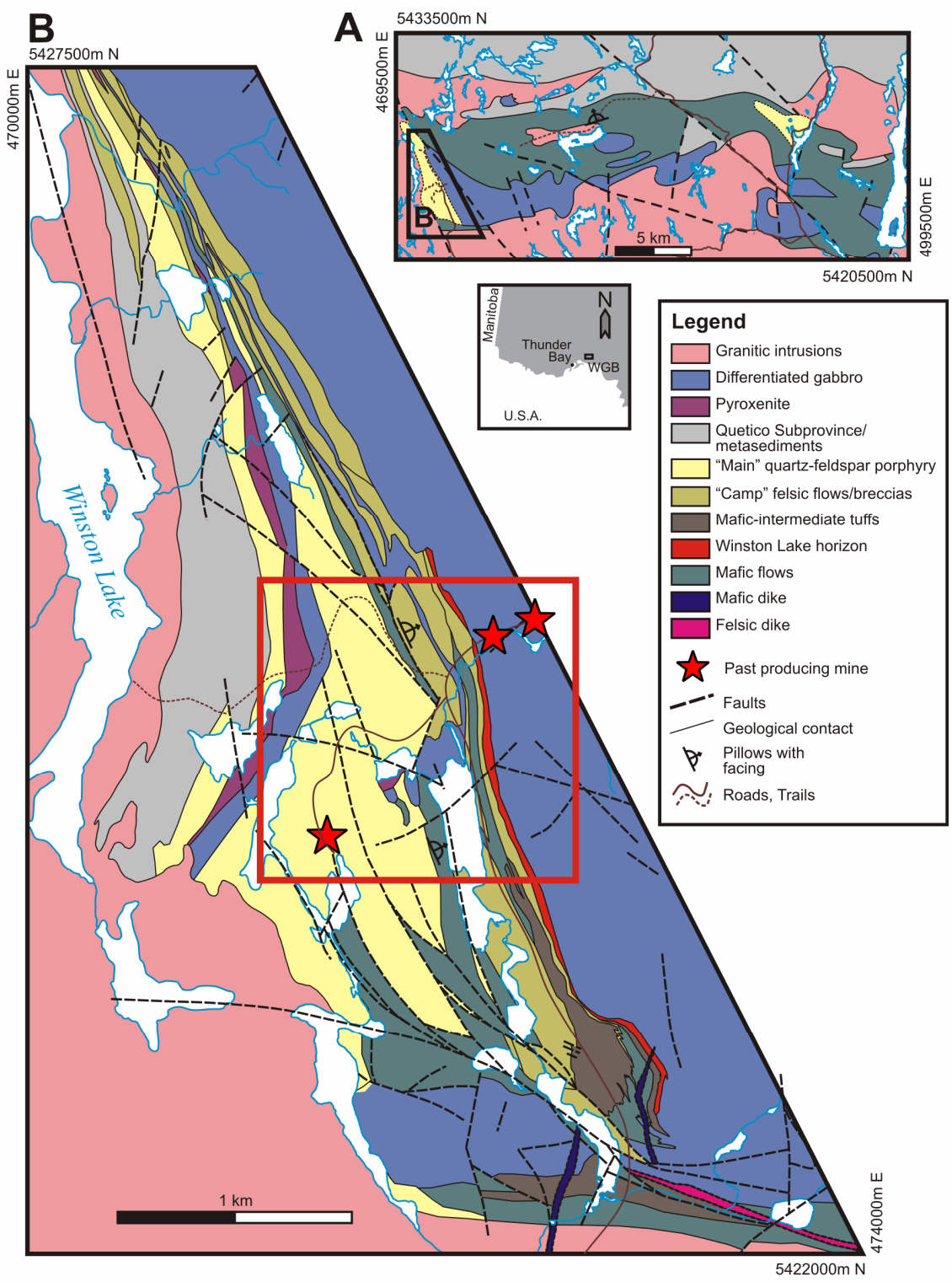

Figure 2. General geology of the Winston Lake greenstone belt (A) and the Winston Lake mine property (B). Geology *compiled from* Osterberg (1993), Pye (1964) and Bartley (1940). Figure is *modified from* Lodge (2011). Boxed area represent the region covered during this field trip and is illustrated in Figure 5.

bound to the north by the Quetico subprovince, to the west by the Winston Lake batholith, and to the south by the Crossman Lake batholith (Severin, Balint and Sim 1991). Regional metamorphic grade in the belt is lower amphibolite facies (Williams et al. 1991b). Metamorphosed hydrothermally altered rocks near the VMS deposits were initially interpreted as metasedimentary rocks because of the presence of aluminosilicate minerals (Pye 1964).

The belt has been informally subdivided into 2 main lithotectonic assemblages: the Winston Lake assemblage (Figure 2B) and the Big Duck Lake assemblage (a thick mafic unit composing most of the belt in Figure 2A) (Polat, Kerrich and Wyman 1999; Severin, Balint and Sim 1991). The Winston Lake assemblage is host to the VMS deposits and is composed of calc-alkalic, bimodal volcanic and siliciclastic rocks (Gorton and Schandl 1995). The Big Duck Lake assemblage consists of magnesium- to iron-tholeiitic basalts, quartz-feldspar porphyry dykes and sills, and their brecciated equivalents (Polat, Kerrich and Wyman 1999; Ritcey 1992). It has been assumed that the Big Duck Lake assemblage conformably overlies the Winston Lake assemblage and that the contact was intruded by a thick differentiated gabbro (Osterberg 1993). This field trip will not examine the Big Duck Lake assemblage and therefore it will not be discussed. Participants that are interested should consult the references cited above, in particular Ritcey (1992).

Prior to this research, only one U/Pb age of 2723±3 Ma was obtained from a felsic volcanic rock associated with the Winston Lake orebody (Davis, Schandl and Wasteneys 1994). Newly acquired and preliminary geochronological data suggest that the gabbro that separates the Winston and Big Duck Lake assemblages also has an age of 2720 Ma and that the age relationship between the two assemblages is relatively close. The structural history of the belt is also poorly constrained and two main structural events are interpreted: D_1 manifested as tilting of stratigraphy and a foliation development (north-northwest striking foliation in the Winston Lake assemblage; west-striking foliation in the Big Duck Lake assemblage), and D_2 represented by minor folds and faulting that offset contacts at the map scale (Osterberg 1993).

The Winston Lake assemblage is dominated by felsic volcanic and siliciclastic rocks. Despite the high degree of metamorphism and relatively high degree of deformation, many primary volcanic features are preserved in the volcanic rocks. Reliable younging directions obtained from pillowed flows and cross-bedding in volcaniclastic rocks suggest a westward-younging stratigraphy. The oldest supracrustal strata in this part of the belt are felsic volcaniclastic and siliciclastic rocks. These are conformably overlain by a quartz-feldspar porphyry flow (informally named the “Main” quartz-feldspar porphyry) that is associated with the Pick Lake VMS deposit. Altered mafic flows (informally named the ”Ladder” flow) separate the underlying quartz-feldspar porphyry from the overlying quartz- and feldspar-phyric felsic volcanic rocks (informally named the “Camp” felsic flow) that host the Winston Lake VMS deposit. These quartz- and feldspar-phyric felsic volcanic rocks were then presumably overlain by mafic flows of the Big Duck Lake assemblage, which was followed by the emplacement of a thick, synvolcanic differentiated gabbro at that contact; the gabbro sill hosts the zinc-rich Zenith orebody. The general stratigraphy of the Winston Lake assemblage is illustrated in Figure 3.

MANITOUWADGE GREENSTONE BELT

The Manitouwadge Greenstone Belt, MGB (Figure 4), is located north of the Schreiber–Hemlo greenstone belt and lies on the northern margin of the Wawa subprovince adjacent to the Quetico Subprovince (Williams et al. 1991b). The belt is composed of bimodal volcanic rocks, intrusions, and sedimentary rocks that have been metamorphosed to upper amphibolite facies. The metamorphic grade increases to granulite facies at the northern margin of the belt and into the adjacent Quetico subprovince.

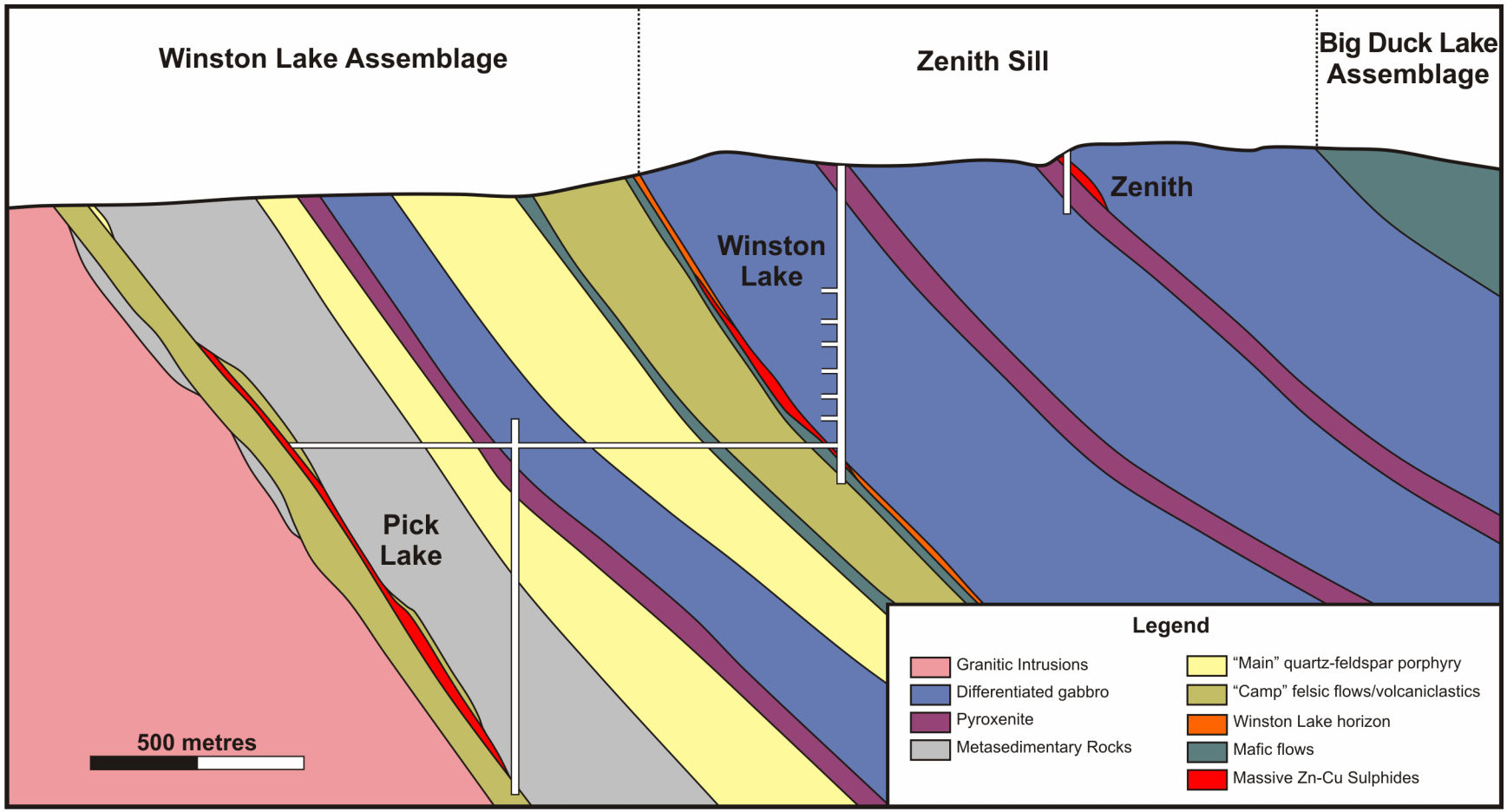

Figure 3. Schematic cross-section looking north-northwest through the strata hosting the VMS orebodies of the Winston Lake area. Figure *modified from* unpublished report, Inmet Mining Corporation (T. Anderson, personal communication, 2011).

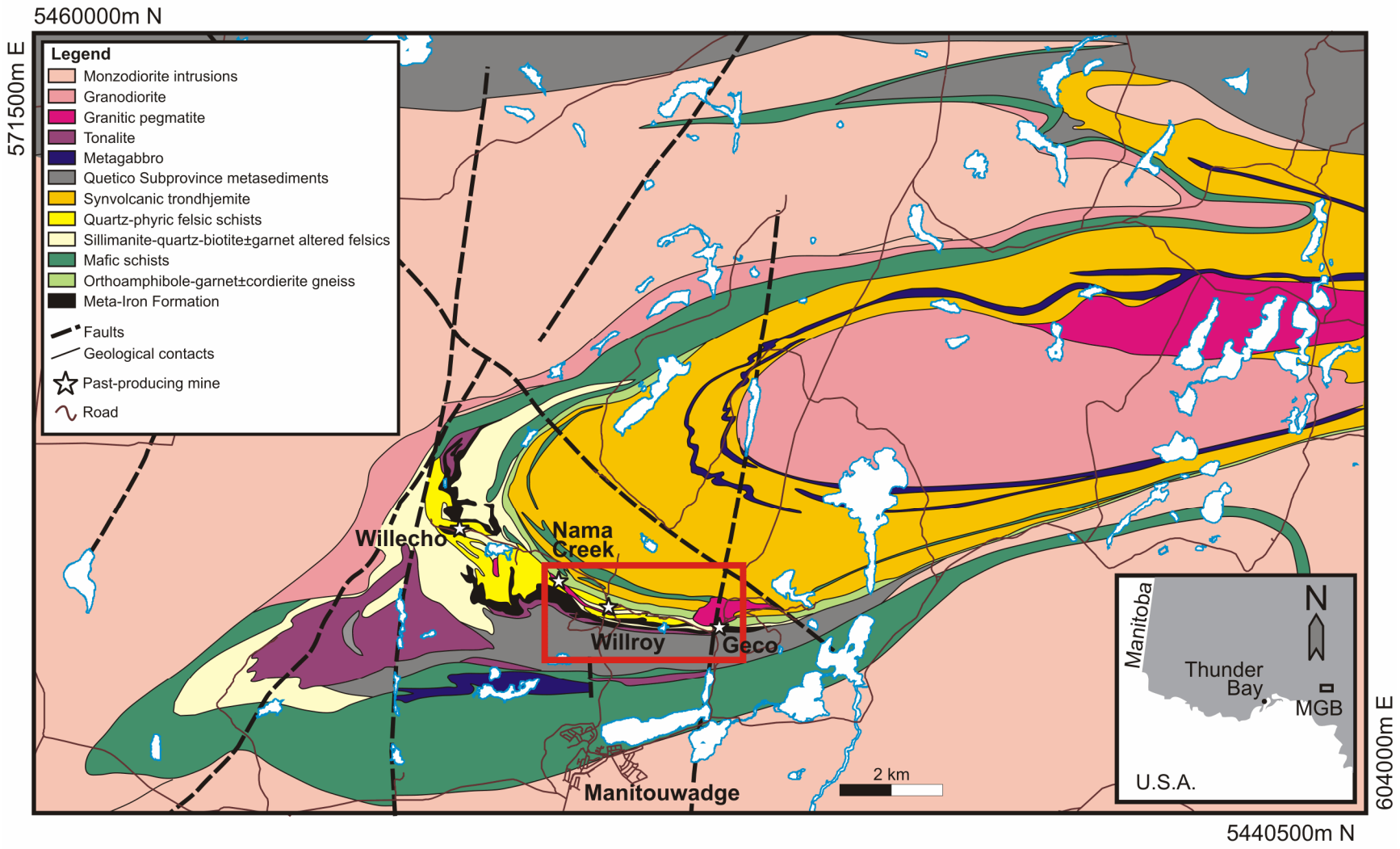

Figure 4. General geology of the Manitouwadge greenstone belt. Geology *from* Zaleski and Peterson (2001) and figure *modified from* Lodge (2011). Boxed area is the region visited in the field trip, also illustrated in Figure 7.

The supracrustal assemblages of the Manitouwadge greenstone belt are bound to the west and south by the Black Pic batholith.

Recent geochronological (Zaleski, van Breemen and Peterson 1999) and structural studies (Peterson and Zaleski 1999; Zaleski and Peterson 1995) have dramatically improved our understanding of the geological and structural history of the Manitouwadge greenstone belt. The supracrustal volcanic assemblages and a synvolcanic trondhjemite intrusion yielded U/Pb zircon ages of 2720 Ma. Most of the other granitic and alkalic intrusions in the belt are younger (<2690 Ma) and are syn- to late-deformation. Metasedimentary rocks in the southern part of the belt have a maximum depositional age of about 2693 Ma.

The most prominent map-scale structural feature of the belt is the large Manitouwadge synform that formed during D_3 deformation. The D_1 deformation is expressed as annealed mylonitic faults that are now zones of represented by "straight gneiss" in the vicinity of the Willroy and Geco mines (see stop M6) (Peterson and Zaleski 1999). The D_2 deformation is correlated with peak metamorphism and is represented by a map-scale repetition and sheath folding along the southern limb of the Manitouwadge synform. D_4 is represented as dextral shearing at the Wawa–Quetico boundary (Peterson and Zaleski 1999; Zaleski, van Breemen and Peterson 1999).

The supracrustal assemblages of the belt were subdivided into an inner and outer volcanic belt, separated by a band of metasedimentary rocks along the southern limb of the Manitowadge synform. The inner and outer volcanic belts are interpreted to be the same unit repeated by the D_2 Agam Lake syncline (Peterson and Zaleski 1999; Zaleski and Peterson 2001). The synvolcanic trondhjemite intrusion occurs within the core of the Manitouwadge synform. It is mantled by an orthoamphibole-cordierite-garnet gneiss. Outward from the core of the synform are a series of interlayered felsic volcanic rocks, their altered equivalents, and iron formation. All of the VMS deposits occur within the inner volcanic belt and therefore the field trip and guidebook descriptions will be limited to exposure of the inner volcanic belt. For additional descriptions of the outer volcanic belt please consult the references cited throughout this section.

History of VMS Deposits

Much of the mining and exploration history for the Winston Lake and Manitouwadge greenstone belts is published internally with the companies that have explored and mined these deposits. Most of these documents have not been published and therefore not available to the public. However, the Mineral Deposit Inventory (MDI) published by the Ontario Geological Survey (OGS 2011) has summarized current and historical information available for these deposits. Much of the historical information provided in this section is summarized from this database.

WINSTON LAKE CAMP

Massive zinc mineralization, now known as the Zenith deposit, in what is now interpreted to be a synvolcanic gabbroic sill was first discovered in 1879 by prospectors. Very little exploration was undertaken in the area until the grounds were claimed by Zenmac Metal Mines Ltd. in 1952. In the late 1960s, 165 000 tonnes of zinc-rich ore were mined from this deposit.

After the Zenith mine closed, the property was stagnant until 1978 when Corporation Faconbridge Copper (CFC) completed reconnaissance geological mapping and lithogeochemical sampling in the

region. Earlier interpretations of the "metasediments" (Bartley 1940; Pye 1964) were re-interpreted as metamorphosed felsic volcanic rocks. This was followed by more detailed property mapping, lithogeochemistry, and geophysical surveys, which defined the alteration zone located in the immediate footwall to the gabbro. Areas of Na_2O depletion and FeO, MgO, and Zn enrichment were outlined in the calc-alkalic volcanic rocks. CFC geologists also realized that the presence of massive sphalerite in the gabbro is unusual. The presence of VMS-like lithogeochemical signatures in the footwall to the gabbro led to the interpretation that the Zenith orebody was likely a large xenolith from a larger VMS orebody hosted at the top to the calc-alkalic felsic volcanic strata below the gabbro. With this newly recognized VMS potential, diamond drilling began in 1981 and targeted the felsic volcanic rocks at the base of the gabbro. In 1982, after drilling only 5 holes, CFC intersected 2.1 m of massive sulphides containing 1.1% Cu, 19.1% Zn, 22.2 g/t Ag and 0.73 g/t Au. Mining began in 1988 and continued until the mine was officially closed in 1998.

The surface expression of the Pick Lake orebody, the Anderson occurrence, was first reported by local prospectors in 1952. There was some shallow diamond drilling completed in the area but with no significant results. CFC picked up the claims following the discovery of the Winston Lake deposit in 1982. In 1983, a test diamond drill on the down-dip extension of the Anderson occurrence discovered the Pick Lake orebody. In 1993, Metall Mining (formerly Minnova and the operators of the mine at the time) began a 2200 m drift to mine the Pick Lake deposit through the mine workings at Winston Lake. The Pick Lake mine was abandoned when the Winston Lake mine shut down in 1998. The size and grade of the deposits in the Winston Lake area are summarized in Table 1.

Table 1. Summary of mining activity in the Winston Lake area. Summarized from unpublished Inmet Mining Corporation (T. Anderson, personal communication, 2011) and CFC company records. Also available from the Mineral Deposit Inventory (OGS 2011).

Orebody	Tonnage (Mt = million tonnes); Grade
Winston Lake Main	3.1 Mt; 16% Zn, 1% Cu, 30.1 g/t Ag, 1.0 g/t Au
Pick Lake	1.3 Mt; 16.5% Zn, 0.9% Cu
Zenith	0.16 Mt; 16.5% Zn

GECO AND WILLROY CAMPS

The Geco and Willroy VMS deposits were initially discovered by J.E. Thompson of the Ontario Department of Mines in 1931 when local natives shared their knowledge of rusty rocks near Manitouwadge Lake. In Thompson's report, the sulphide mineralization was described and the magnetic disturbance caused by the meta-iron formations was noted (Thompson 1932). The ground was first staked in 1943, but financing was not available because of the Second World War. In post-war years, interest in base metals again arose and the showings described by Thompson were staked in 1953 (Pye 1957). Drilling in the following year intersected the main orebody, which led to the incorporation of Geco Mines Limited. During the exploration rush that followed the initial discovery, the Willroy, Nama Creek, and Willecho deposits were discovered. Mining of the Willroy and Geco orebodies began in 1957. Mining of the Willroy, Nama Creek, and Willecho deposits ceased in 1977. The main ore body at Geco was continuously mined until the shut down in 1995.

The total tonnage and grade of the main deposits of the Manitouwadge area are summarized in Table 2. In addition to copper, zinc, and silver, minor amounts of gold, cadmium, and bismuth were recovered from the mines. The ore bodies had an average concentration of 0.3% Pb and it was extracted during milling until 1988 until it was no longer economically viable due to lower metal prices (Williams et al. 1991a).

Table 2. Summary of mining activity in the Manitouwadge area. Summarized by Zaleski and Peterson (2001) from unpublished Noranda Inc. company records. This information is also available in the Mineral Deposit Inventory (OGS 2011).

Mine Name	Orebody	Tonnage (Mt = million tonnes); Grade
Geco	Geco Main	52 Mt; 2.3% Cu, 8.2% Zn, 74 g/t Ag
	Geco 4/2 Cu	Approximately 3 Mt
	Geco 8/2 Zn	(cumulative)
Willory	Willroy 1	4.6 Mt; 1.3% Cu, 5.7% Zn, 48 g/t Ag (cumulative)
	Willroy 2	
	Willroy 3	
	Willroy 4	
	Willroy 5	
	Willroy 6	
Nama Creek	Nama Creek	0.3 Mt; 0.8% Cu, 3.9% Zn, 28 g/t Ag
Willecho	Willecho 1	3.8 Mt; 0.6% Cu, 3.9% Zn, 53 g/t Ag (cumulative)
	Willecho 2	
	Willecho 3	

Field Trip Stops

DAY 1 – WINSTON LAKE MINE AREA

The purpose of this portion of the field trip is to introduce the geological setting of strata hosting the VMS ore bodies at Winston Lake. Since most of the lithofacies of the greenstone belt are difficult to access, this part of the trip will focus on property-scale features and the role they played in the discovery of the orebodies. The stop locations will focus on the immediate footwall strata to the Winston Lake deposit and will highlight some of the recent geochronologic data obtained from this strata. The locations of the field stops are illustrated in Figure 5 and a brief description is provided below. All stops are also provided with UTM co-ordinates in NAD83 (Zone 16) reported as Easting (E) and Northing (N).

Note that in the descriptions of some of the units, the primary igneous names are used rather than their metamorphic names (e.g., gabbro versus amphibolite).

Stop W1 – Zenith Mine Open Pit

473182E 5424996N

This stop is located inside the main gate of the Winston Lake Mine. It is a short drive along mine property roads. From where we park, walk along the base of the cliff toward the lake. WARNING: The walk into the main pit area is on a narrow and steep-sided path. Walking to the exposures of sulphides in a large group is discouraged.

This stop represents the remnants of the original discovery in the Winston Lake area. The gabbro (now amphibolite) is massive with some low-angle shears cutting up the outcrop. The gabbro is differentiated and consist of phases ranging from leucocratic gabbro to pyroxenite (this is more apparent at Stop W2).

The Zenith orebody is mostly mined out but there are a few metre-scale slivers of massive sphalerite (Photo 1 (Right)) remaining. The ores are strictly zinc-rich and contain only minor amounts of pyrite, pyrrhotite, and chalcopyrite. The grain size of the sphalerite is generally coarse, most likely recrystallized during regional metamorphism.

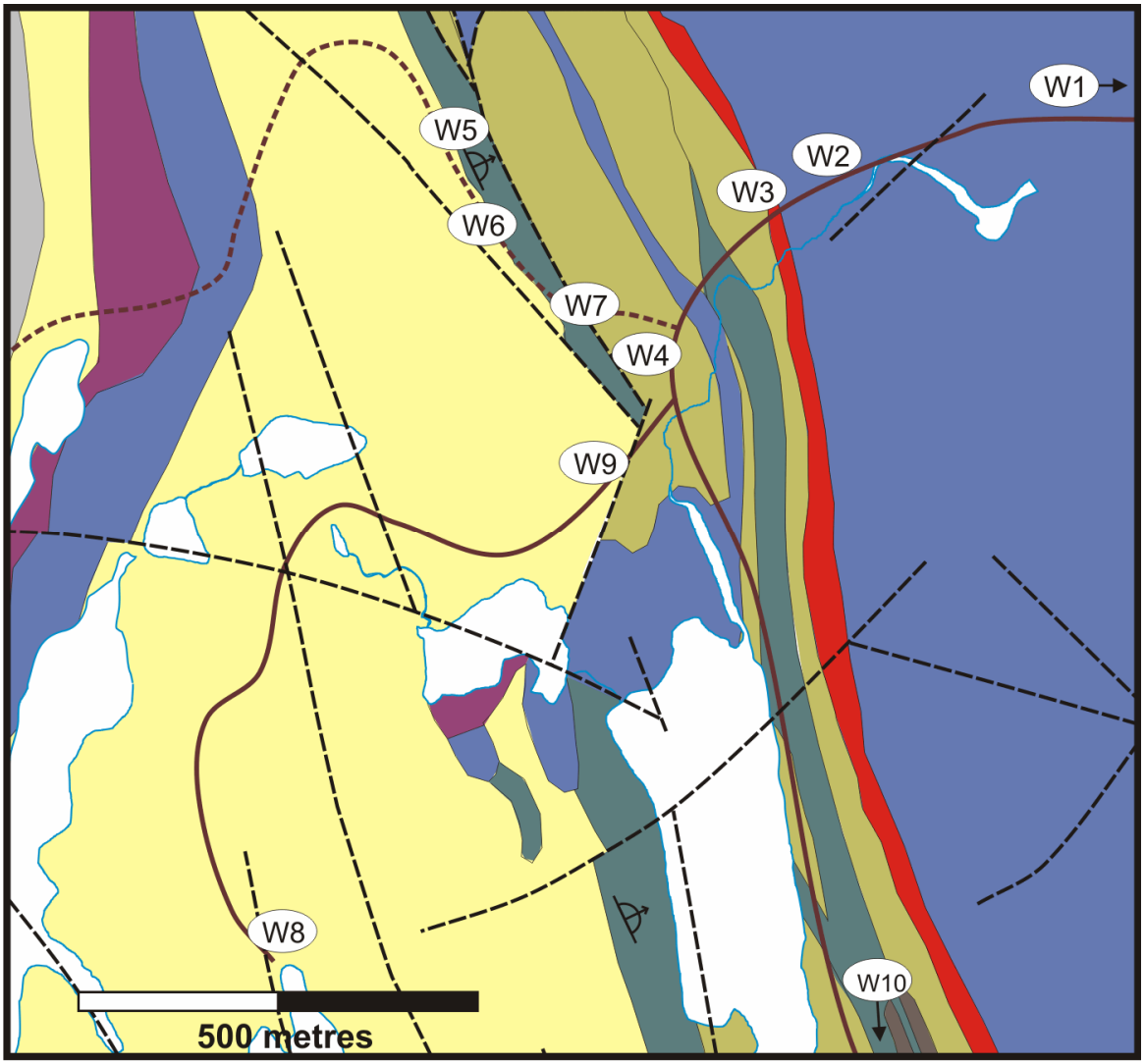

Figure 5. Geology of the Winston Lake mine area highlighting the location of field trip stops. Geology *summarized* and *modified from* Osterberg (1993). For location of figure and legend, refer to Figure 2.

Photo 1. (Left) Zenith mine open pit. (Right) Sphalerite-rich xenolith in gabbro.

Stop W2 – Differentiated Gabbro

472337E 5425082N

This stop is on the main road about 100 m back from the Winston Lake mine gate along the side of the road. The different phases of the gabbro intrusion are well exposed on either side of the road. This outcrop is very large and is dissected by a stream. We will not be crossing the stream.

Photo 2. Differentiated gabbro showing melanocratic and leucocratic layers.

This stop highlights the complexity and multiple phases of the gabbro. On either side of the road, near the gate to the Winston Lake mine site, are perfectly exposed road cuts and stripped exposures of the gabbro that hosts the Zenith orebody. At this stop, we are less than 100 m from the base of the intrusion.

In some locations, the gabbro has a layered appearance with layers of pyroxenite (now mostly hornblende) and more plagioclase-rich leucocratic layers (Photo 2). In other areas, there are pegmatitic patches with large centimetre-scale plagioclase crystals. The compositional layering in this intrusion ranges from centimetre-scale to metre-scale layers. Most of these variations are not mappable.

A leucocratic pegmatitic phase of the gabbro was sampled for U/Pb geochronology to determine the age of the gabbro. Zircons separated from the gabbro were low uranium, typical of gabbroic zircons, indicating that they were magmatic in origin rather than xenocrystic. These grains were analyzed using thermal ionization mass spectroscopy (TIMS) analysis at the University of Toronto, and yielded a U/Pb age of 2719.2±4.0 Ma. This age indicates that the gabbro that intruded and entrained the Winston Lake VMS body is synvolcanic, and the same age (or slightly younger) than the host rocks.

Stop W3 – Winston Lake Horizon

472200E 5425057N

This stop along the main road about 100 m west from the Stop W2. It is a large roadcut outcrop of the contact between the gabbro and the underlying felsic volcanic rocks.

Photo 3. Bedded felsic volcaniclastic unit known as the Winston Lake Horizon.

At this stop, the contact between the gabbro and the underlying calc-alkalic volcanic rock is exposed. Immediately below the contact with the gabbro is a layered siliceous tuff unit that is known as the Winston Lake Horizon (Photo 3). About 450 m down dip of this unit is the Winston Lake main orebody.

The finely laminated layers range in thickness from a few millimetres to 1 to 2 cm and range in composition from felsic tuff, chert and lesser mafic tuff. This unit is laterally extensive (*see* Figure 2) and continues almost the entire length of the Winston Lake assemblage. Trace element and rare earth element (REE) patterns suggest that this ash layer has an FII- to FIII-type felsic composition (Hart, Gibson and Lesher 2004). There is little variation in this volcaniclastic unit, both compositionally and texturally, although it is locally interlayered with mafic flows.

Stop W4 – Altered Felsic Volcanic Rocks in Footwall

472123E 5424987N

Continue south(west) along the road for about 150 m to the next stop. This stop is near the trail entrance to stops W5 to W7. There are about 100 m of roadcut outcrop of variably altered felsic volcanic rocks to examine.

This stop, and nearby outcrops typify the alteration facies (assemblages) found within the "Camp" felsic volcanic rocks. This unit is laterally extensive, but relatively thin (*see* Figure 2) and it is not known how many flows are represented within this unit. Unaltered equivalents of this rock are usually massive, coherent units that are quartz- and plagioclase-phyric, and locally contain flow banding. Minor felsic tuffs and tuff breccias have also been described in this unit elsewhere in the camp (Osterberg 1993). This unit has a U/Pb age of 2723±3 Ma (Davis, Schandl and Wasteneys 1994).

Altered versions of these quartz- and feldspar-phyric "Camp" flows contain variable amounts of biotite, muscovite, sillimanite, and cordierite (Photo 4). Phenocrysts may be locally preserved, but are more difficult to see. Lesser altered equivalents contain quartz-muscovite-biotite-feldspar assemblages. With increasing degree of alteration, the rocks contain cordierite, sillimanite knots, garnet and anthophyllite. Major element geochemistry shows extensive sodium depletion and local iron and/or

magnesium enrichment. Trace element and REE patterns indicate that this unit is an FIII-type felsic volcanic rock.

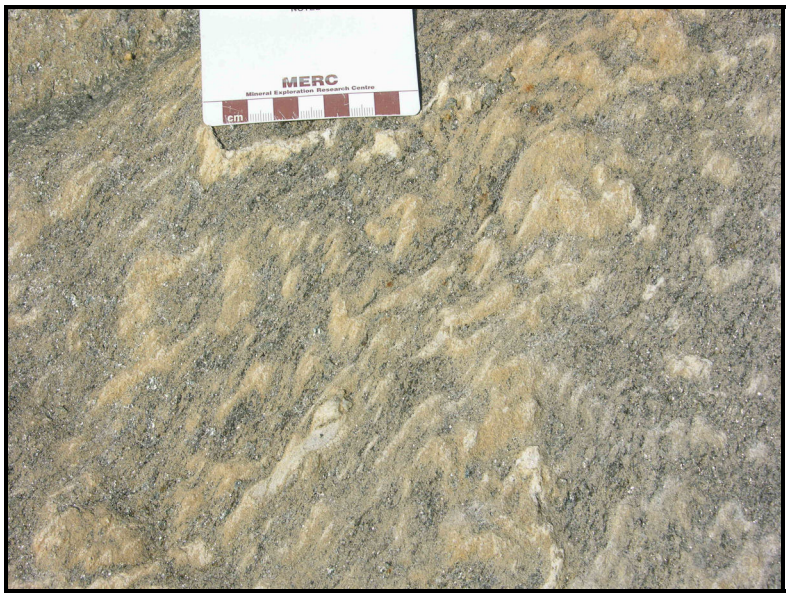

Photo 4. Altered felsic volcanic rock now a quartz-muscovite-sillimanite-biotite schist.

Stop W5 – Mafic "Ladder Flow"

471800E 5425200N

From the last stop, enter the trail that leads westward from the main road. The next stop is approximately 500 m along the trail. This is the furthest stop from the main road. We will return on the same trail and look at the lithofacies passed over on the return trip. WARNING: This is an ATV trail and there are many wet places and irregular surfaces. Please walk with caution and try and stay dry.

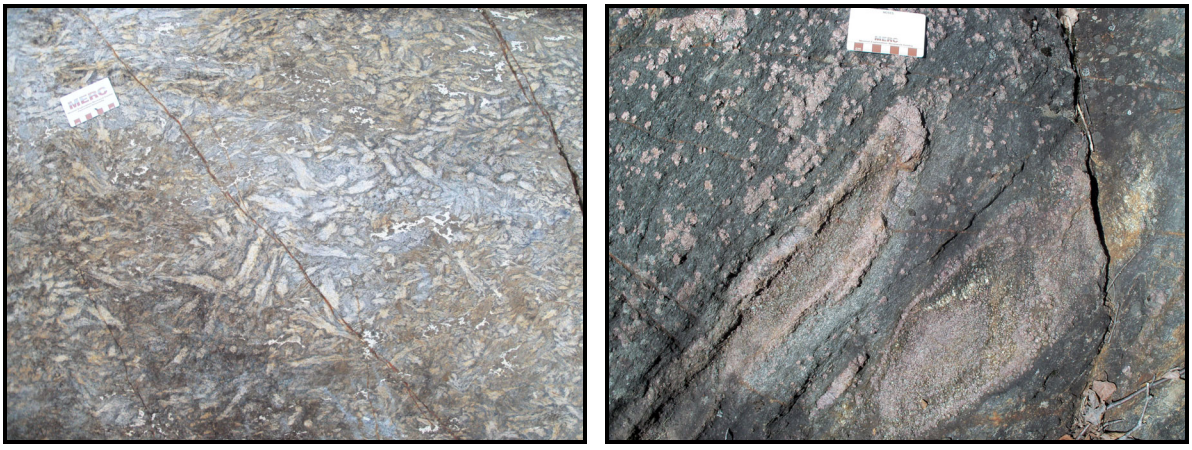

Photo 5. (Left) Coarse-grained orthoamphibole. (Right) Orthoamphibole-garnet-biotite schist.

The outcrop of the mafic "Ladder Flow" contains some of the most spectacular features that will be observed during this field trip. In addition to the coarse-grained mineral assemblages associated with metamorphosed hydrothermal alteration, the overall lack of significant deformation in this area has preserved the volcanic textures in the rock (Figure 6). Younging directions are still determinable in this

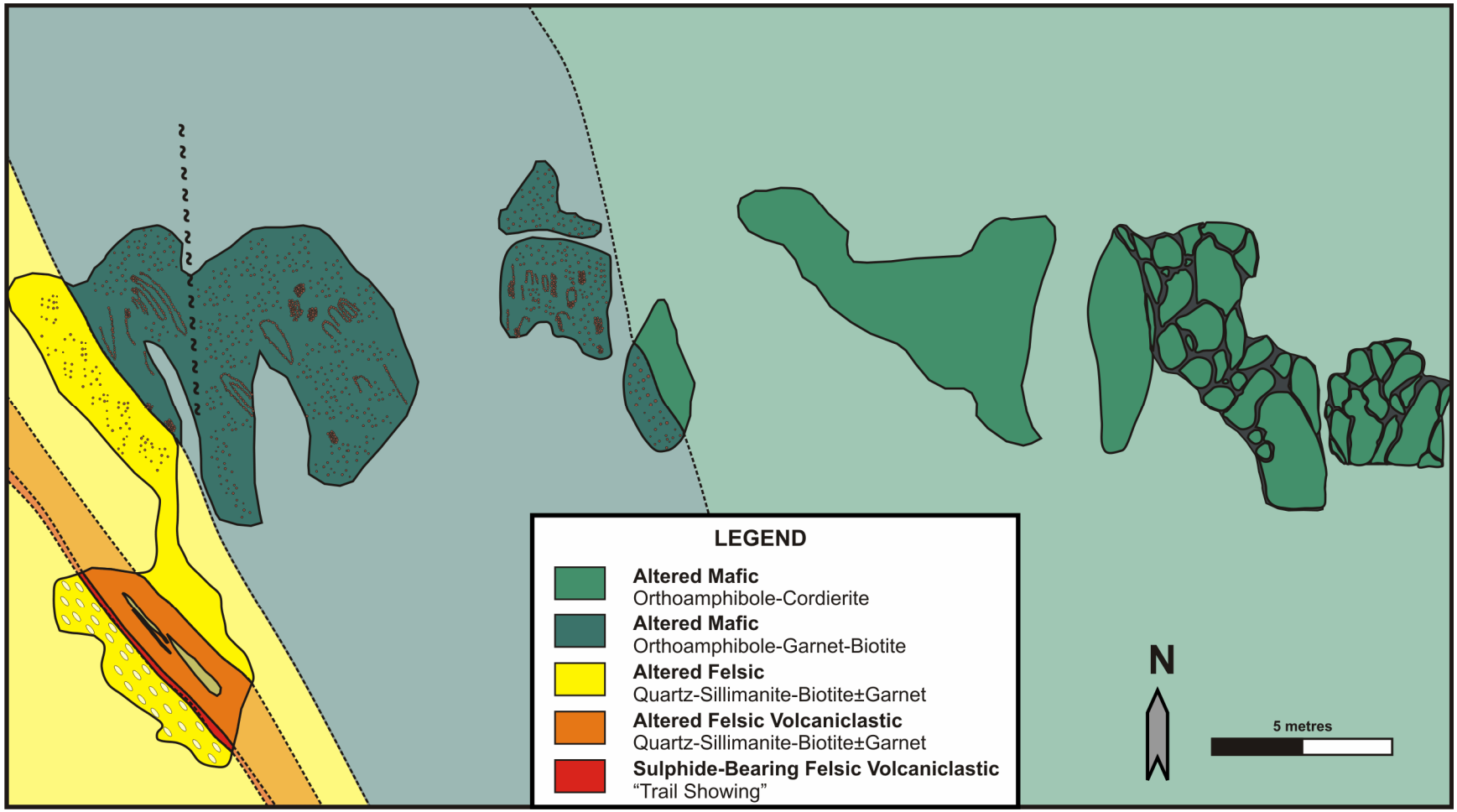

Figure 6. Outcrop sketch of the lower contact of the altered mafic "Ladder Flow" and the underlying altered felsic volcanics in the Winston Lake area. Sketch only incorporates areas that were cleaned and there are additional outcrops in the area.

unit and they indicate an eastward younging of the strata. As with most units in the Winston Lake assemblage, this unit is laterally extensive, but relatively thin. Unaltered equivalents of the “Ladder Flow" contain plagioclase phenocrysts.

At the eastern limit of this outcrop are spectacular exposures of an orthoamphibole-cordierite assemblage within the altered pillowed mafic flows. The pillows are metre-scale and their selvages are recessively weathered. There appears to be very little compositional difference between the pillow interior and the selvages, with the exception of slightly more biotite. Stratigraphically below the pillows is a 10 m thick massive basalt flow. This massive flow is very homogeneous and the only variations are the gradational changes in the size of the orthoamphibole crystals. These crystals can be up to 10 cm in size and are usually randomly oriented (Photo 5 (Left)). There is also a variable amount of cordierite and minor biotite in this massive lithofacies.

Near the lower contact with the altered felsic volcanic rocks, the “Ladder Flow” contains abundant clots, sheets, and veins of porphyroblastic garnet (Photo 5 (Right)). In addition to garnet-orthoamphibole-cordierite, there are also local concentrations of biotite and chlorite. This alteration style is interesting, but difficult to interpret. In some places it appears as if the garnet clots represent altered clasts in a breccia. In other locations, they may be altered pillow margins or deformed veins. Regardless, the sharp transition from massive orthoamphibole-cordierite altered flow into a more chaotic orthoamphibole-garnet-cordierite zone may indicate the transition from a massive to breccia facies of this unit. It may also represent a different chemical gradient within the alteration zone. Geochemically, the garnet-bearing rocks are still mafic in composition.

Stop W6 – Trail Showing

471867E 5425051N

From the previous stop, walk back towards the main road (east) for approximately 150 m. This stop is a flat, rusty outcrop that we walked over to get to the Ladder Flow.

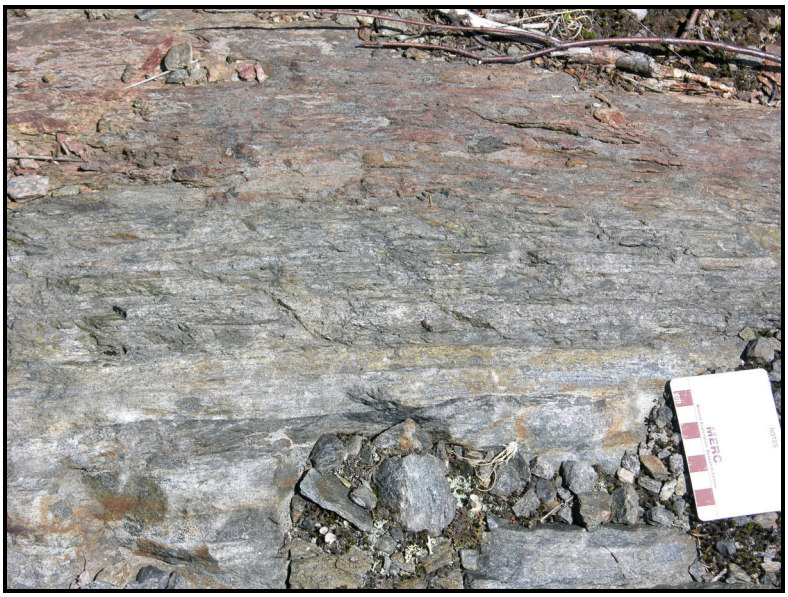

Photo 6. Felsic volcaniclastic rock hosting disseminated sulphides.

This stop represents one of the many smaller mineralized intervals in the Winston Lake camp. The mineralization in the "Trail Showing" is located near the contact between the "Ladder Flow" and underlying felsic volcanic rock and it is hosted within a siliceous, bedded volcaniclastic unit (Photo 6) that is up to 15 cm thick. It contains over 6000 ppm Cu and zinc-bearing metamorphic minerals such as gahnite are also present.

The bedded volcaniclastic unit is altered to a quartz-cordierite-biotite-garnet mineral assemblage containing variable amounts of orthoamphibole and sillimanite. The layering in the rock appears to be primary.

This unit is distinct and separates the mafic "Ladder Flow" and the underlying massive altered quartz- and feldspar-phyric "Main" felsic flow, which the trail crosses from there to the main road. The alteration assemblages in the massive flow are the same as those observed at Stop W4.

Stop W7 – Contact of "Ladder Flow" and Altered Felsic Volcanic Rocks

471918E 5424992N

Continuing back toward the main road along the trail, this stop is approximately 100 m from the previous stop. This is the last stop on the trail before returning to the main road.

Photo 7. Upper contact of altered mafic flow (Ladder Flow) and altered felsic volcanic.

This stop shows the contact between the "Ladder Flow" and the overlying "Camp" felsic volcanic rocks, which constitute the immediate footwall strata to the Winston Lake deposit. Prior to last summer, this outcrop was completely black with lichen and moss cover. Cleaning this otherwise black and featureless exposure resulted in a near-perfect exposure of an altered basaltic flow top breccia that is intermingled with the overlying felsic tuff (Photo 7). This is one of a few places where these flow features are exposed at surface. The variety of flow facies exhibited by the "Ladder Flow" indicates that this mafic unit is indeed a flow rather than a sill. Therefore, the contact at this stop is not a peperite caused by a sill mingling with overlying unconsolidated tuff. Rather, it is more likely that the felsic tuff settled on top of the basaltic flow top breccia.

At this location, the flow is altered to an orthoamphibole-garnet assemblage with retrograde chlorite and biotite. The garnet porphyroblasts are evenly distributed and occur in the felsic volcanic rock above the contact. This suggests some chemical exchange between the lithofacies at the contact during metamorphism, as previously suggested by Gorton and Schandl (1995). The overlying felsic tuff is altered to a quartz-muscovite-sillimanite-biotite mineral assemblage.

Stop W8 – Pick Lake Shaft Area

471579E 5424177N

About 150 m south of the trail entrance on the main road is the gate to the Pick Lake deposit. The Pick Lake mine shaft and the next stop are about 1.1 km from the gate. There are plenty of outcrops around the former shaft that show a variety of alteration facies. WARNING: Although the shaft has a concrete cap and is safe to walk on, please do not walk directly on old mine workings.

Photo 8. Quartz-muscovite-biotite-garnet schist near the Pick Lake mine shaft.

This stop is in the middle of the thickest part of the "Main" quartz-and feldspar-phyric felsic flow that forms the middle portion of the Winston Lake assemblage and the hanging wall to the Pick Lake orebody. The Pick Lake deposit is about 300 m directly below the former mine workings near this stop. The orebody is not associated with the rocks exposed here, rather is associated with felsic volcaniclastic and siliciclastic rocks that dip eastward underneath this unit (*see* Figure 3). We will not see the host rocks to the Pick Lake deposit on this trip because they are not easily accessible.

It is not clear based on the current or previous mapping whether the "Main" quartz- and feldspar-phyric flow is an intrusion or extrusion (e.g., Osterberg 1993). There appears to be very little textural variation in the unit throughout the area. Despite being quite thick in this area, the unit is massive and the only variations are in the degree of alteration and mineral assemblages. These mineralogical changes, which include varying amount of biotite and garnet (Photo 8), are gradational and do not appear to represent primary compositional layering. If it is an extrusive unit, it is a very massive one with only a thin brecciated carapace (*see* Stop W9). Phenocryst sizes in unaltered parts of this unit are much larger (3 to 4 mm) compared to the "Camp" felsic volcanic rocks in the footwall to the Winston Lake orebody.

A sample of this unit was submitted for U/Pb dating by TIMS analysis at the University of Toronto. The sample yielded a homogeneous population of zircon that produced an age of 2721±1 Ma. This confirms that the unit is the same age as the host rocks to the Winston Lake orebody. There is some variation in the trace element geochemistry of this unit as it ranges from an FI- to FIII-type felsic volcanic rocks. This indicates that despite its homogeneous appearance it consists of more than one felsic unit.

Stop W9 – Pick Lake Felsic Breccias

473182E 5424996N

This stop is a roadside outcrop on the Pick Lake road approximately 100 m away from the gate. This is the last stop inside the Pick Lake gated road.

Photo 9. Matrix-supported quartz-phyric felsic volcanic breccia.

At this stop, the monolithic breccia phase of the quartz-and feldspar-phyric felsic flow (Photo 9) is well exposed on the roadside. It is not certain if this breccia is a volcanic or structural texture. Given that the main part of this body is thick, massive and homogeneous, and that it has been confirmed to be the same age as the surrounding volcanic rocks, it is possible that this may represent the synvolcanic intrusion that was the feeder for the overlying felsic flows and volcaniclastic units. It is common for hypabyssal synvolcanic intrusions to be brecciated at their margins. Alternatively, it could represent the breccia margin of a flow.

The fragments are lenticular and stretched defining a pronounced stretching lineation. They contain quartz and plagioclase phenocrysts that make up to 15% of the fragment. The anastomosing matrix is composed of quartz-biotite-muscovite mineral assemblages and composes up to 25% of the rock. There is no obvious layering in the rock but there are some variation in the abundance and size of the clasts that may represent crude bedding.

Stop W10 – Tuffaceous Metasedimentary Rocks

472699E 5423145N

This stop is on the main road 1.8 km south of the Pick Lake gate and is adjacent to the power lines. There are several roadcut outcrops that are worth examining. This is the last stop of this portion of the field trip.

This is the final stop of the Winston Lake portion of the field trip. The tuffaceous metasedimentary rocks are along strike and south of the orebodies, and do not contain mineral assemblages that indicate significant hydrothermal alteration. They were classified as "intermediate volcaniclastics" by Osterberg (1993). There are many sedimentary structures in this unit, such as cross-bedding (Photo 10), that suggest it is a reworked volcaniclastic deposit. The composition of the rock suggests that the provenance is mostly mafic with only a minor felsic component.

Photo 10. Low-angle cross-bedded mafic-intermediate tuffaceous metasedimentary rock.

At this stop, mineral assemblages range from biotite-quartz-garnet to biotite-quartz-hornblende and even local concentrations of lapilli-sized clasts of mafic composition. These compositional variations are on the metre- to outcrop-scale.

A sample of this unit within the finer grained, cross-bedded part of the exposure was sent for detrital zircon analysis at the laser ablation inductively coupled plasma mass spectrometry LA-ICP–MS at Laurentian University, Sudbury (Ontario). The results show a single peak centered around 2720 Ma, suggesting that the source of detritus was local and from volcanic units dated 2720 Ma. The composite, mafic-felsic composition of these rocks suggests that they are not primary volcanic deposits. They may represent distal, reworked facies of slump fans deposited during rifting that originated from bimodal volcanic units within the Winston Lake assemblage.

DAY 2 – GECO AND WILLROY MINE AREA

This portion of the field trip is an introduction to the mineralization and alteration of the Geco and Willroy mining camp. The trip is organized to show the variation in the geological setting of the various ore bodies within the mine property, by taking a regional-scale transect through the VMS-hosting strata of the Manitouwadge greenstone belt. Finally, the trip will examine the deposit-scale stratigraphy and variation in the alteration facies associated with these ore zones. The stop locations are illustrated in Figure 7.

Note in descriptions of some of the units primary igneous names are used rather than their metamorphic names (e.g., felsic volcanic versus quartz-feldspar-muscovite schist).

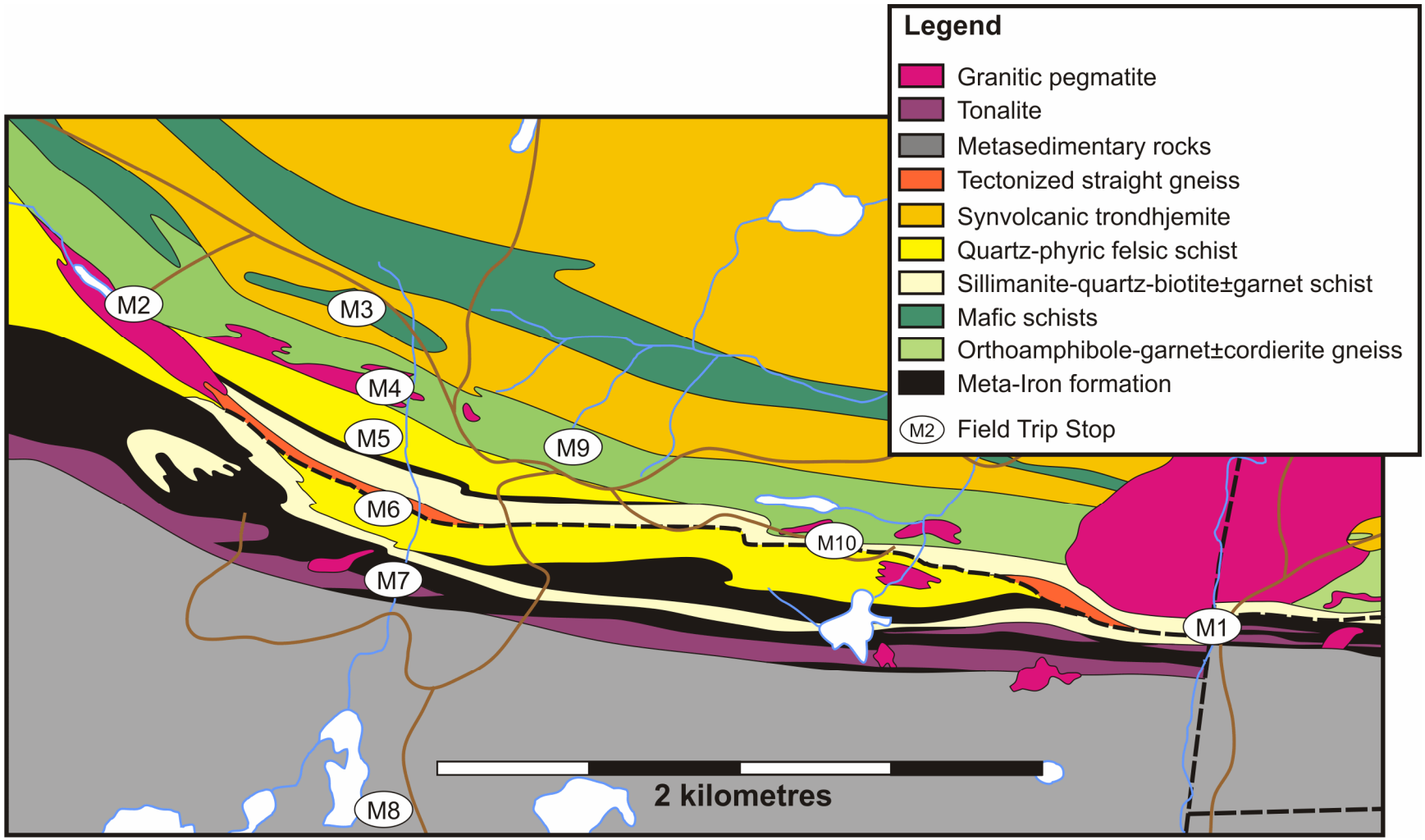

Figure 7. Geology of the Geco and Willroy mine areas showing the location of field trip stops. Geology *modified from* Zaleski and Peterson (2001).

Stop M1 – Geco Main Pits

587952E 5445211N

After checking into the mine site, drive approximately 2 km back along the main road and park on the side of the road adjacent to the Geco Main pit. From there you can see what remains of the head frame and reclaimed open pit operations. This is a good place to find ore samples in the overburden near the fence at the smaller piton the east side of the road. Please do not attempt to cross containment fencing.

Photo 11. Geco main open pit.

These pits represent the main ore body of the Geco mine. These filled pits represent the surface expression of the ore bodies below. Fifty-five million tons of copper-zinc-lead-silver ore was mined from this open pit and underground workings. Unfortunately, we cannot get up to the rocks adjacent to the pit and accessible outcrop is limited in the immediate vicinity of the main ore body.

Most of the geology and stratigraphy was defined during the underground mining activities. The main orebody is enveloped by a sillimanite-muscovite-quartz schist (similar to the Willroy 1 orebody at stop M10) and quartzite. The main ore is consists of massive zinc-copper-lead sulphides that have been recrystallized during metamorphism. There is a halo of stringer chalcopyrite mineralization around the main ore body hosted in sillimanite-muscovite-quartz schist (Zaleski et al. 1995). The sillimanite-muscovite-quartz schist has been dated at 2720±2Ma (Davis, Schandl and Wasteneys 1994).

This stop is located at the easternmost extension of the main orebody where it grades and thins into zinc-rich massive sulphides in association with meta-iron formation. The previously mapped stratigraphic relationship of the main ore zone and iron formation-associated ore body at this location suggests that the main ore body cross-cuts the strata at a low angle (Zaleski et al. 1995).

Stop M2 – Nama Creek Open Pit

584200E 5446331N

Drive back northward and turn left onto the road that travels behind the Geco headframe. This road will take you to the former rail bed that connected the Willroy and Geco camps. Travel on this road for approximately 4.7 km and turn left into the access road for the Nama Creek Open Pit. WARNING: This open pit is now filled with water but is not fenced. Please use extreme caution when navigating the outcrops adjacent to the pond.

Photo 12. (Left) Nama Creek open pit. (Right) Zinc-rich iron formation at edge of pit.

The Nama Creek deposit (Photo 12 (Left)) is an example of the zinc-rich mineralization that is associated with iron formation (Photo 12 (Right)). The small size and low grade zinc mineralization made this operation marginally profitable. Most of the strata to the west are intruded by a granitic pegmatite. There is not much left exposed here now, but at the eastern limit of the pit there is some exposure of the rocks that host and are associated with the mineralization.

The Nama Creek orebody is near the contact between orthoamphibole-garnet-cordierite gneiss and sillimanite-muscovite-quartz schist. The orthoamphibole-garnet-cordierite gneiss is exposed at the northern margin of the pit before it is cross-cut by a granitic pegmatite further west. The sillmanite-muscovite-quartz schist is locally exposed to the south of the open pit. The orebody is composed of coarse-grained pyrite, pyrrhotite, sphalerite and galena in iron formation.

The general strata of the ore body is best visible at the eastern limit of the pit where the gneiss, schist, and magnetite-quartz iron formation are all exposed. This outcrop represents the easternmost extension of the orebody along strike. Zinc mineralization is present in some of the host rocks as gahnite, a pale green Zn-bearing spinel.

Stop M3 – Synvolcanic Trondhjemite

587952E 5445211N

From the Nama Creek access road, continue approximately 600 m eastward on the main road back toward the Willroy and Geco mines. Stops M3 to M8 are along the containment dam on the west side of the creek and represent a regional-scale transect through the strata of the greenstone belt. WARNING: The dam is single-lane and steep sided without guard rails. Please drive slowly and carefully on the dam. It will be a one-way trip until we reach the southern end of the dam where it intersects another road.

This is the first stop on the regional-scale transect through the Manitouwadge greenstone belt. This stop is located at the contact region of the synvolcanic trondhjemite in the core of the Manitouwadge synform and variably altered mafic to felsic volcanic rocks.

Despite the high degree of deformation and upper amphibolite metamorphism, at this particular stop there are what appear to be mafic to intermediate xenoliths in the trondhjemite (Photo 13). North of this location, the intrusion is much more massive and does not contain such fragments. The presence of such xenoliths near the contact with the supracrustal assemblages suggests a brittle, hypabyssal regime. In addition, there is an increase in the amount of biotite and garnet in the trondhjemite near the contact with the orthoamphibole-garnet-cordierite gneiss . This has been interpreted to be a pre-metamorphic

hydrothermal alteration (Zaleski et al. 1995). Further evidence for a synvolcanic trondhjemite is that the intrusion has a U/Pb age of 2720±2 Ma (Zaleski, van Breemen and Peterson 1999) which is the same age as the volcanic rocks at the Geco main orebody.

Photo 13. Trondhjemite with fragments (xenoliths?) of intermediate volcanic rocks.

Stop M4 – Orthoamphibole-Garnet-Cordierite Gneiss

585129E 5446034N

Drive southward along the containment dam for about 300 m to the next stop. Participants are welcome to walk the entire length of exposures along the dam. The guidebook will highlight the different facies, but there are many interesting small-scale variations in the rocks that may be worthwhile examining.

The orthoamphibole-cordierite-garnet±biotite gneiss unit (Photo 14) is regional in extent and appears to mantle the synvolcanic trondhjemite (Zaleski and Peterson 2001). We will see additional, and perhaps better exposures of this unit at stops M9 and M10. This metamorphosed alteration facies is interlayered with a variety of other alteration facies noted by variation in mineralogy, grain-size and textures.

This unit appears to be in the footwall to most of the orebodies in the Manitouwadge area, assuming a generally southward younging stratigraphy. Although no primary textures or minerals remain after hydrothermal alteration and metamorphism, the geochemistry of these rocks suggest that the protolith was an alkali-depleted, iron- and magnesium-altered tholeiitic mafic rock (see Figure 8 for Stop W10). This probably represents the chlorite zone of VMS-type alteration. There is some evidence these altered mafic rocks were locally interlayered with felsic lithofacies based on a bimodal distribution of TiO_2 (Zaleski et al. 1995) and enriched high field strength elements (HFSE) relative to mafic lithofacies (Pan and Fleet 1995). It is not uncommon to have similar chlorite-type alteration facies in both mafic and felsic protoliths in a VMS system.

Photo 14. Very coarse grained orthoamphibole-cordierite gneiss.

Stop M5 – Quartz-phyric Felsic Volcanic Rocks

585110E 5445878N

Continue southward along the containment dam for approximately 200 m to the next stop.

The quartz-phyric felsic volcanic rock (Photo 15 (Left)) is spatially associated with the Willroy and Geco orebodies and is interlayered with the iron formation. This unit is characterized by the prominent 1 to 3 mm quartz phenocrysts composing up to 20% of the rock. Geochemically, at this location, there is an obvious depletion of Na_2O in the massive part of the unit suggesting it was also part of the VMS alteration system. The variation in muscovite abundance in the rocks suggests zones of potassic alteration.

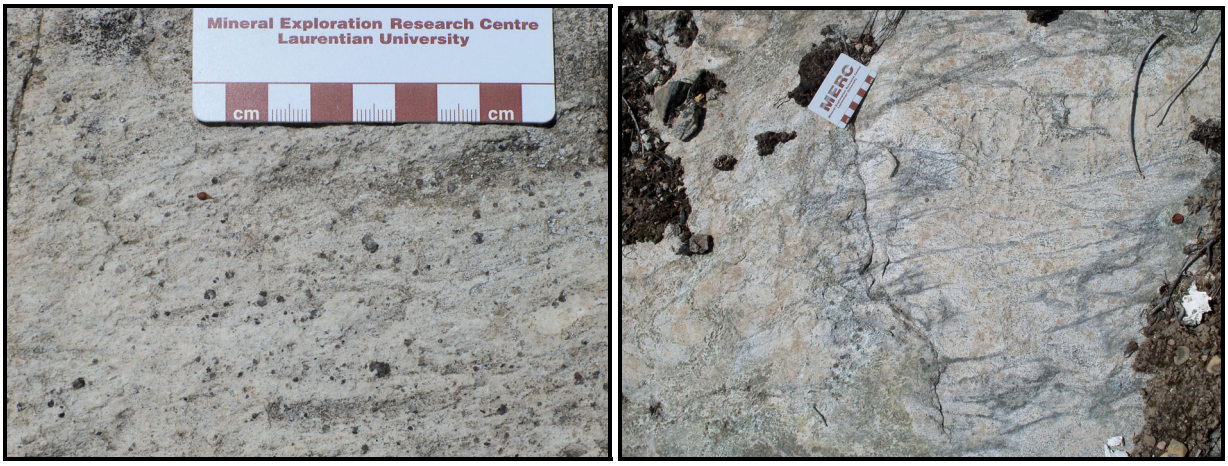

Photo 15. (Left) Massive quartz-phyric felsic volcanic (schist). (Right) In-situ breccia of felsic volcanic rock (schist).

Towards the margin of this unit, there are what appear to be in-situ breccias (Photo 15 (Right)). These breccias are monolithic and are composed of a similar lithofacies to the more massive parts of the quartz-phyric unit. The matrix has quartz phenocrysts and is composed of muscovite, biotite, and garnet. These breccias are interpreted to be primary volcanic features and therefore represent a proximal volcaniclastic deposit or flow breccia (Zaleski et al. 1995).

Near the contacts with iron formation, this unit grades into a calc-silicate breccia. These rocks are composed of diffuse quartz-phyric to aphyric felsic fragments in a matrix composed of calc-silicate minerals such as plagioclase, clinopyroxene, Ca-amphibole, garnet, epidote, and titanite. This calc-silicate rock is interpreted to be a metasomatically-altered felsic volcanic rock (Zaleski et al. 1995).

Stop M6 – "Tectonic Straight Gneiss"

587952E 5445211N
Continue southward along the containment dam for approximately 300 m to the next stop.

Despite the high degree of deformation in the Manitouwadge greenstone belt as a whole, these rocks appear notably strained with a strong penetrative planar fabric. The mineralogy of these rocks appears to be similar to that of felsic volcanic rocks and felsic altered equivalents; however, much more strongly strained. Coarser grained beds form boudinage textures (Photo 16) and there is an apparent overall reduction of grain size.

Zaleski and Peterson (1995) interpreted these rocks as annealed mylonites and evidence for an early D1 deformation event resulting in thrust repetition of the felsic units and iron formation. They are also associated with map-scale truncations of iron formation (Zaleski and Peterson, 1995; Zaleski and Peterson 2001).

Photo 16. Tectonized altered felsic volcanic with boudinaged layers.

Stop M7 – Meta-Iron Formation

585138E 5445404N
Continue southward along the containment dam for approximately 200 m to the next stop. This is the last stop along the containment dam.

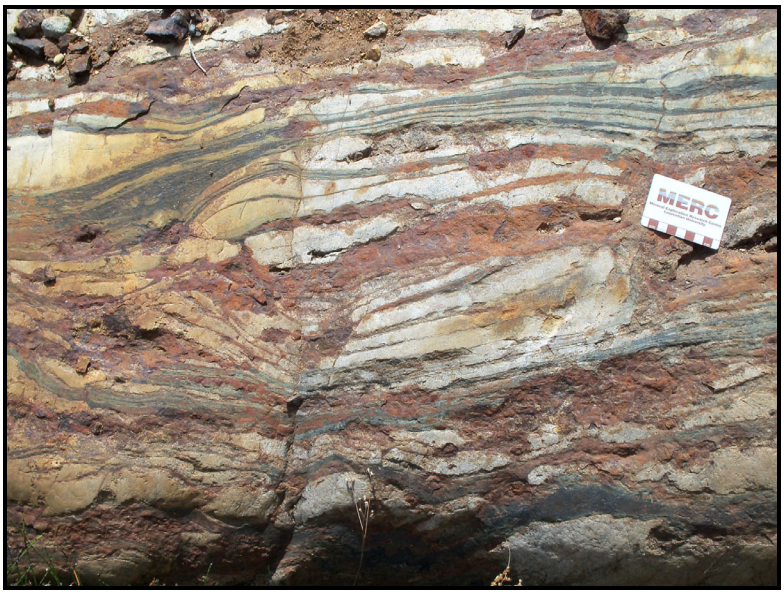

Photo 17. Quartz-magnetite iron formation.

This is just one of many exposures of metamorphosed iron formation (Photo 17) in the Manitouwadge area, with more to the north along the containment dam. The iron formation is closely associated with the ore zones in this mining camp and is likely an expression of the hydrothermal activity that deposited the orebodies. The geochemistry of the iron formation shows low Al_2O_3, Na_2O and K_2O, suggesting there is very little detrital or volcanic component (Zaleski et al. 1995). This outcrop is the southernmost iron formation and is along strike from the Geco open pit at Stop M1.

The iron formation at this stop consists mostly of alternating layers of white to grey quartz and magnetite. Near the contacts with felsic units, there are other iron-bearing minerals present such as grunerite, actinolite, garnet, and/or clinopyroxene. Some of these layers are possibly altered volcanic rocks that were interlayered with the iron formation.

The iron formation appears to grade into sulphide-facies iron formation and eventually massive sulphides at the Geco and Willroy ore bodies (Friesen, Pierce and Weeks 1982). This explains why the iron formation at this stop has relatively minor sulphide content, being distal from Geco but more sulphides closer to stops M4 and M5 which are more proximal to Willroy.

Stop M8 – Metagreywacke

585019E 5444550N

Turn left onto the road that intersects the containment dam and drive southward toward the Willroy tailings pond for approximately 700 m. Turn right into the access road for the tailings dam building and park near the edge of the pond. The outcrop is located near the boulder dam at the southern tip of the tailings pond.

This stop is intended to show metasedimentary rocks typical of the Manitouwadge greenstone belt, and to resolve discussions regarding the question of the volcanic or sedimentary origin of the rocks observed so far. They have nothing to do with the VMS mineralization in the camp and have a maximum age of deposition of 2693 Ma based on detrital zircon analysis (Zaleski, van Breemen and Peterson 1999).

At this stop, the metagreywackes (Photo 18) are planar bedded at the centimetre-scale. They are fine-grained and composed of biotite, quartz, feldspar, and varying amounts of hornblende and muscovite.

Elsewhere in the belt, there are chaotic folds between planar layers that are interpreted to be soft sediment deformation features (Zaleski et al. 1995; Zaleski, van Breemen and Peterson 1999).

Photo 18. Planar bedded metagreywacke.

Stop M9 – Willroy Mill Site

585743E 5445822N

From the Willroy tailings pond building access road, turn left and drive northward on the main road for about 400 m to an intersection. Keep right at the fork to avoid going back to the containment dam. From the intersection, continue northward 1.2 km to the next stop. The large cleared area on top of the hill is the former mill site for the Willroy mines. The field trip stop is at the former rail bed.

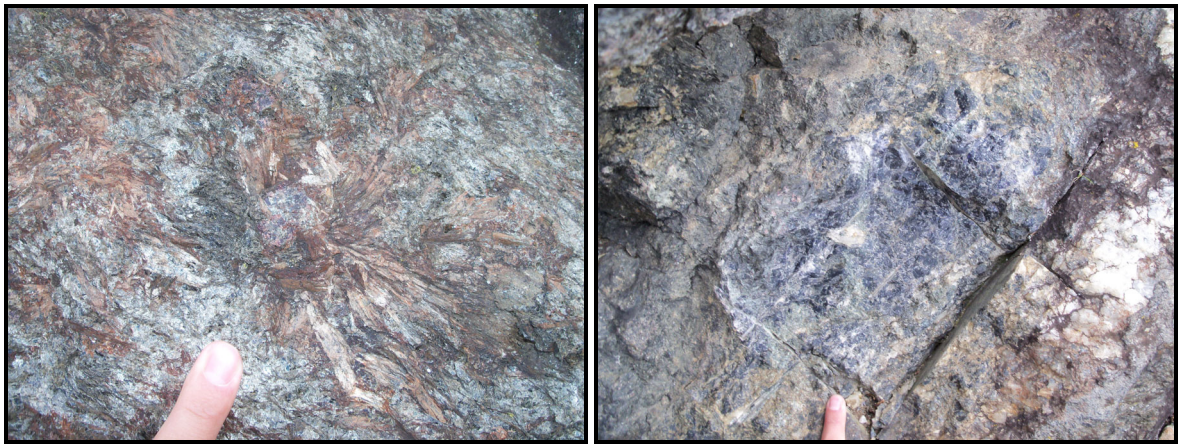

Photo 19. (Left) Coarse garnet with radiating orthoamphibole. (Right) Large, 40 cm cordierite crystal.

The unit that is exposed has been seen at previous stops and will also be exposed at the last stop. The purpose of this stop is to see the orthoamphibole-garnet-cordierite gneiss and the extraordinary grain sizes that can develop in this unit. Please no hammering on these rocks. There are a few exposures where these coarse grain sizes can be found.

The orthoamphibole-garnet-cordierite gneiss has variable amounts of biotite, plagioclase, and staurolite and is interlayered on the metre-scale with garnet-biotite-sillimanite±cordierite gneiss/schist. The orthoamphibole crystals (Photo 19 (Left)) are often as large as 5 cm and occur as aligned or radiating prisms. Cordierite crystals (Photo 19 (Right)) can be very large and are up to 40 cm in size.

Stop M10 – Willroy 1 Open Pit

586606E 5445517N

Drive eastward from the former Willroy mill site about 200 m and turn right onto a narrow road that leads to the Willroy 1 open pit. The pit is about 800 m off the main road. WARNING: The open pit is fenced off but is still very dangerous. Please stay away from the fence and under no circumstances attempt to go inside the fenced area. This is the last stop of the field trip.

The purpose of this stop is to show the deposit-scale variation in the alteration facies present in most of the orebodies in the Manitouwadge mining camp. The Willroy 1 deposit (Photo 20 (Left)) was a stringer-to-disseminated copper sulphide orebody hosted in altered felsic volcanic rocks near the contact between the orthoamphibole-cordierite-garnet gneiss and sillimanite-muscovite-quartz schists (Figure 8). New trace element data of these rocks reveals the pre-alteration bimodal composition of the volcanic rocks (according to the revised Winchester and Floyd (1977) plot by Pearce (1996)) and F-III classification (Hart, Gibson and Lesher 2004) of the felsic lithofacies (Figure 9).

Photo 20. (Left) Willroy 1 open pit. (Right) Sillimanite-clotted altered felsic volcanic rock.

A short walk south along the access road from the fence reveals an exposure of the quartz-phyric felsic volcanic unit that was observed at Stop M5. There is considerably more deformation at this location as evidenced by a stronger foliation with kink folds. There are also some tonalitic and aplitic dikes that intrude this unit. The rocks are relatively unaltered but have a very similar primitive mantle-normalized trace element patterns (normalizing values from Sun and McDonough 1989) to the altered facies that occurs closer to the open pit (Figure 9).

The sillimanite-muscovite-quartz±garnet schist is exposed just south of the fence. Walking east along the fence, the schist becomes increasingly sillimanite knotted (Photo 20 (Right)). These knobs are more resistant to weathering and are 1 to 2 cm in size. There are also pegmatite and tonalite dykes intruding these layers. Geochemically, these rocks are FIII-type felsic volcanic rocks (*see* Figure 9).

Directly along strike from the open pit (and therefore the Willroy 1 orebody) is a muscovite-schist that is similar in appearance to the schists that envelope some of the Geco orebodies. The muscovite is fairly coarse grained and feels silky to the touch. Sillimanite is present as pinkish rosettes on the foliation

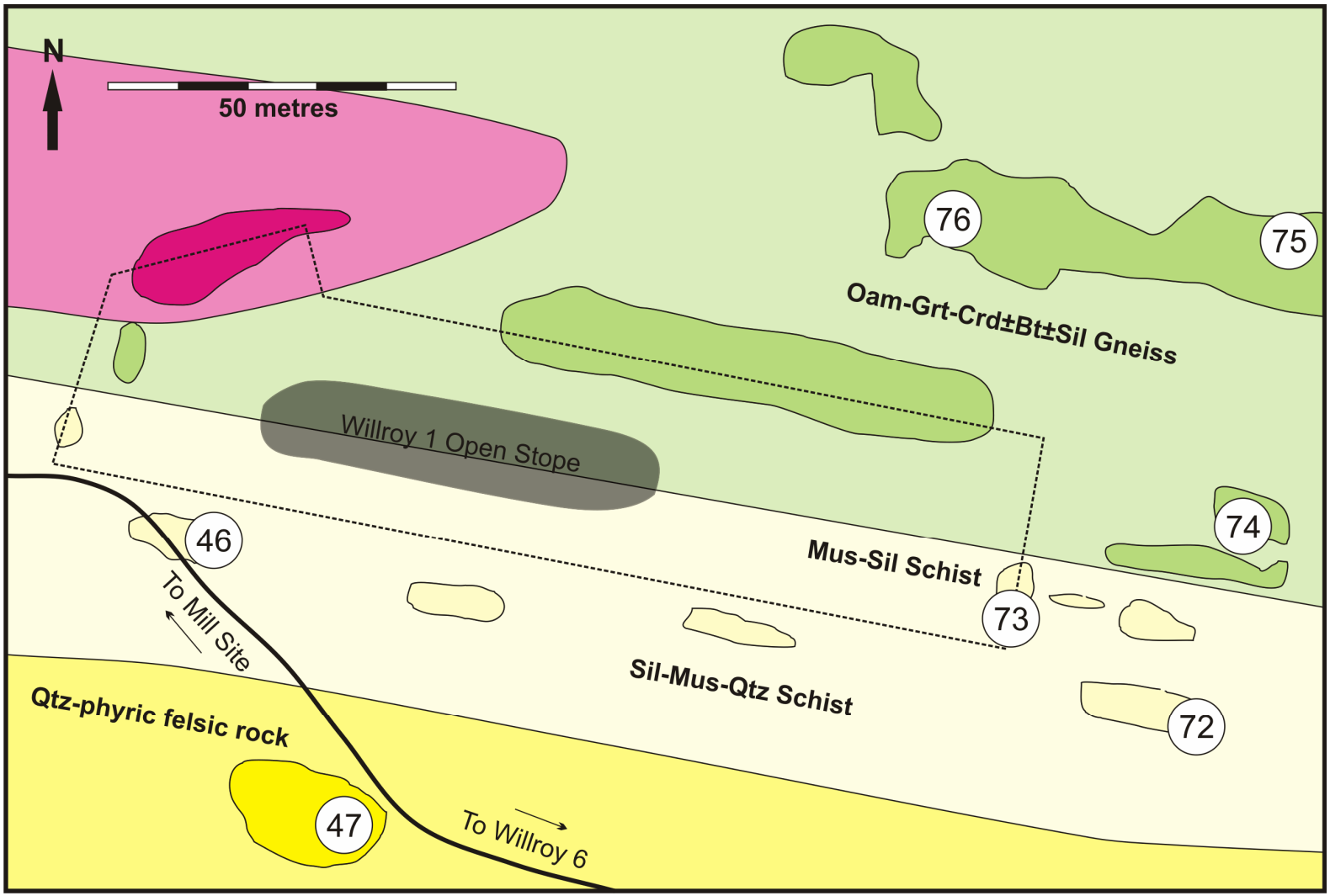

Figure 8. Detailed geology of the area around the Willroy 1 open pit. Figure *modified from* Zaleski et al. (1995). Unit colors are the same as in the legend for Figure 4 and 7. Circles indicate sample numbers and correlate with geochemistry diagrams in Figure 9.

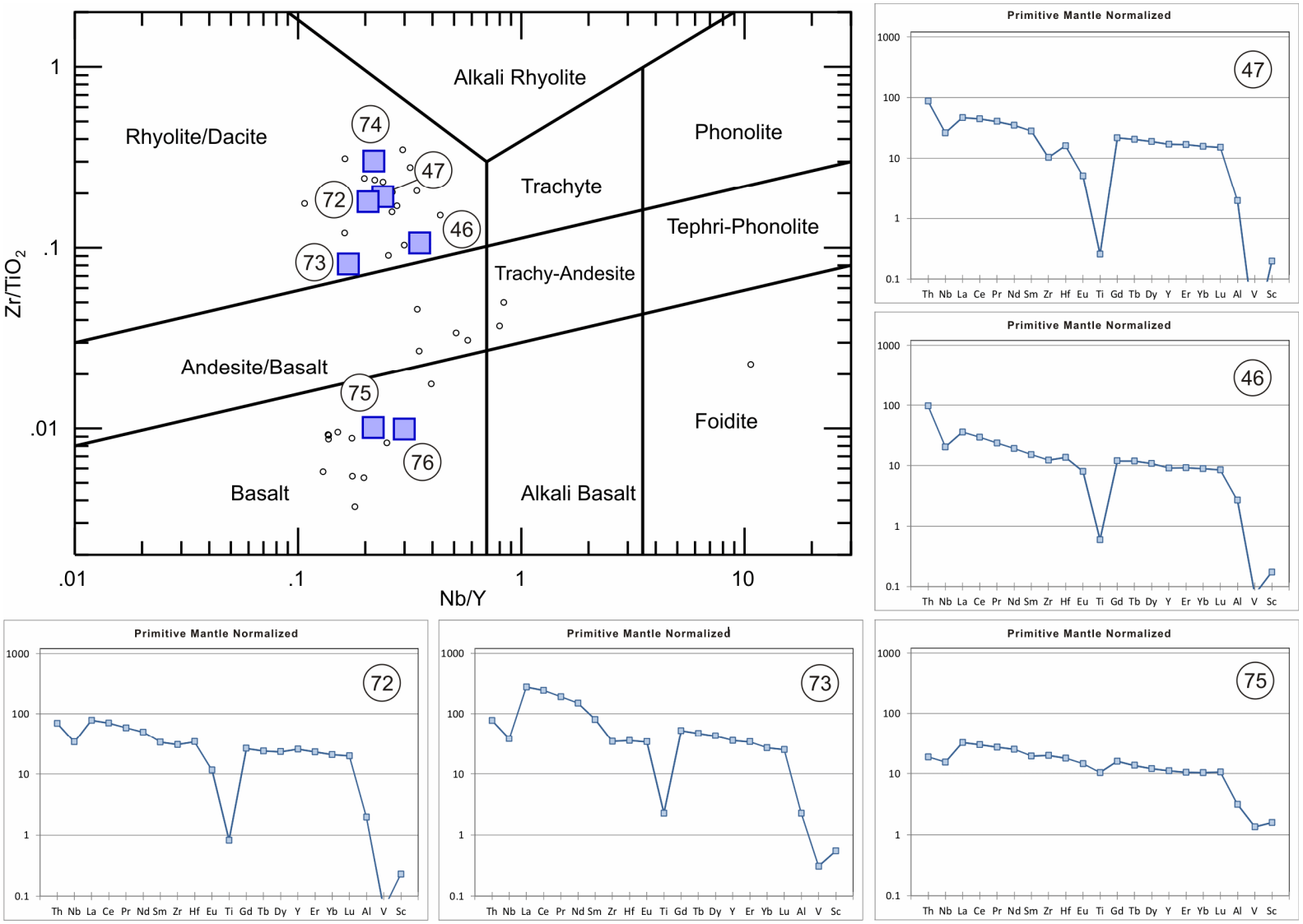

Figure 9. Trace element diagrams for samples collected from the strata hosting the Willroy 1 copper stringer ore body. Classification diagram *from* Winchester and Floyd (1977) as *modified by* Pearce (1996). The trace element spider diagrams are normalized using values for primitive mantle from Sun and McDonough (1989).

surface. Closer to the contact with the orthoamphibole-cordierite-garnet gneiss, the muscovite-sillimanite schist is increasingly quartz rich and very strongly foliated.

Continuing northward on the eastern edge of the fence are exposures of the orthoamphibole-cordierite-garnet gneiss. There are some exposures of large 10 to 15 cm cordierite crystals. Ortho-amphiboles often display a blue iridescence caused by the presence of exsolution lamellae. Garnets are 1 to 4 cm in size and commonly show a dextral sense of rotation based on quartz inclusions and trails. On larger outcrops, metre-scale layering within this unit is defined by variation in mineral abundances and grain sizes. The cause of the layering could either be because of compositional variation in the alteration facies or pre-alteration lithofacies.

References

Bartley, M.W. 1940. Geology of the Big Duck-Aquasabon Lakes area; Ontario Geological Survey, Map 49k, scale 1:31 680.

Corfu, F. and Stott, G.M. 1998. Shebandowan greenstone belt, western Superior Province: U-Pb ages, tectonic implications, and correlations; Geological Society of America Bulletin, v.110, p.1467-1484.

Davis, D.W., Schandl, E.S. and Wasteneys, H.A. 1994. U-Pb dating of minerals in alteration halos of Superior Province massive sulfide deposits; syngenesis versus metamorphism; Contributions to Mineralogy and Petrology, v.115, p.427-437.

Friesen, R.G., Pierce, G.A. and Weeks, R.M. 1982. Geology of the Geco base metal deposit; Geological Association of Canada, Special Paper 25, 343p.

Gorton, M.P. and Schandl, E.S. 1995. An unusual sink for rare earth elements: The rhyolite-basalt contact of the Archean Winson Lake volcanogenic massive sulphide deposit, Superior Province, Canada; Economic Geology v.90, p.2065-2072.

Hart, T.M., Gibson, H.L. and Lesher, C.M. 2004. Trace element geochemistry and petrogenesis of felsic volcanic rocks associated with volcanogenic massive Cu-Zn-Pb sulphide deposits; Economic Geology v.99, p.1003-1013.

Hart, T.M. and Trebilcock, D.-A. 2006. Geology of the Hamlin and Wye lakes area, Shebandowan greenstone belt, Thunder Bay District; *in* Summary of Field Work and Other Activities 2006, Ontario Geological Survey, Open File Report 6192, p.9-1 to 9-9.

Kerrich, R., Polat, A. and Xie, Q. 2008. Geochemical systematics of a 2.7 Ga Kinojevis Group (Abitibi), and Manitouwadge and Winston Lake (Wawa) Fe-rich basalt-rhyolite associations: Backarc rift oceanic crust? Lithos, v.101, p.1-23.

Lodge, R.W.D. 2010. Volcanology and lithofacies of the Shebandowan greenstone belt, Wawa Subprovince; *in* Summary of Field Work and Other Activities 2010, Ontario Geological Survey, Open File Report 6260, p.16-11 to 16-22.

———2011. A progress report on the volcanology, stratigraphy and geodynamic setting of greenstone belts of age 2720 Ma near the Wawa–Quetico subprovincial boundary; *in* Summary of Field Work and Other Activities 2011, Ontario Geological Survey, Open File Report 6270, p.11-11 to 11-13.

Ontario Geological Survey 2011. Mineral Deposit Inventory—2011; Ontario Geological Survey.

Osterberg, S.A. 1993. Stratigraphy, physical volcanology, and hydrothermal alteration of the footwall rocks to the Winston Lake massive sulfide deposits, northwestern Ontario; unpublished PhD thesis, University of Minnesota, Minneapolis, Minnesota, 351p.

Pan, Y. and Fleet, M.E. 1995. Geochemistry and origin of cordierite-orthoamphibole gneiss and associated rocks at an Archean volcanogenic massive sulphide camp: Manitouwadge, Ontario,Canada; Precambrian Research, v.74, p.73-89.

Pearce, J.A. 1996. A user's guide to basalt discrimination diagrams *in* Trace Element Geochemistry of Volcanic Rocks: Applications for Massive Sulphide Exploration, Geological Association of Canada, Short Course Notes 12, p.79-133.

Peterson, D., Gallup, C., Jirsa, M., and Davis, D.W. 2001. Correlation of the Archean assemblages across the U.S.–Canadian border: Phase I geochronology; *in* Part 1 - Programs and Abstracts, 47th Annual Meeting, Institute on Lake Superior Geology, Proceedings Volume 47, p.77-78.

Peterson, V.L. and Zaleski, E. 1999. Structural history of the Manitouwadge greenstone belt and its volcanogenic Cu-Zn massive sulphide deposits, Wawa Subprovince, south-central Superior Province; Canadian Journal of Earth Sciences, v.36, p.605-625.

Polat, A., Kerrich, R. and Wyman, D.A. 1999. Geochemical diversity in oceanic komatiites and basalts from the late Archean Wawa greenstone belts, Superior Province, Canada: Trace element and Nd isotope evidence for a heterogeneous mantle; Precambrian Research, v.94, 139-173.

Pye, E.G. 1957. Geology of the Manitouwadge area; Ontario Department of Mines Annual Report 66, p.144.

———1964. Mineral deposits of the Big Duck Lake area, District of Thunder Bay, Ontario Department of Mines Geological Report 27, p.58.

Ritcey, D.J. 1992. Geology and mineralization in the vicinity of Big Duck Lake, Ontario; unpublished MSc thesis, University of Ottawa, Ottawa, Ontario, p.235

Schandl, E.S., Gorton, M.P., and Wasteneys, H.A. 1995. Rare earth element geochemistry of the metamorphosed volcanogenic massive sulfide deposits of the Manitouwadge mining camp, Superior Province, Canada; A potential exploration tool? Economic Geology and the Bulletin of the Society of Economic Geologists, v.90, p.1217-1236.

Severin, P.W.A., Balint, F., and Sim, R. 1991. Geological setting of the Winston Lake massive sulphide deposit, Mineral Deposits in the Western Superior Province, Ontario; Geological Survey of Canada Open File 2164, p.58-73.

Sun, S-S. and McDonough, W.F. 1989. Chemical and isotopic systematics of oceanic basalts: Implications for mantle composition and processes, *in* Magmatism in the Ocean Basins, The Geological Society, Special Publication 42, p.313-345.

Thompson, J.E. 1932. Geology of the Heron Bay–White Lake area; Ontario Department of Mines, Annual Report 1933, v.41, pt.6, p.34-47.

Williams, H.R., Breaks, F.W., Schnieders, B.R., Smyk, M.C., Charlton, S.G. and Lockwood, H.C. 1991a. Field guide to the Manitouwadge area; *in* 8th IAGOD Symposium, Field Trip Guidebook, Mineral Deposits in the western Superior Province, Ontario, Field Trip 9, Geological Survey of Canada, Open File 2164, p.7-25.

Williams, H.R., Stott, G.M., Heather, K.B., Muir, T.L. and Sage, R.P. 1991b. Wawa Subprovince; *in* Geology of Ontario, Ontario Geological Survey, Special Volume 4, Part 1, p.485-541.

Winchester, J.A. and Floyd, P.A. 1977. Geochemical discrimination of different magma series and their differentiation products using immobile elements; Chemical Geology, v.20, p.325-343.

Zaleski, E. and Peterson, V.L. 1995. Depositional setting and deformation of massive sulfide deposits, iron-formation, and associated alteration in the Manitouwadge greenstone belt, Superior Province, Ontario; Economic Geology and the Bulletin of the Society of Economic Geologists v.90, 2244-2261.

———2001. Geology of the Manitouwadge greenstone belt and the Wawa–Quetico subprovince boundary, Ontario. Geological Survey of Canada, Map 1917A.

Zaleski, E., Peterson, V.L., Lockwood, H.C., and van Breemen, O. 1995. Geology, structure and age relationships of the Manitouwadge greenstone belt and the Wawa subprovince boundary, northwestern Ontario, Field Trip Guidebook; Institute on Lake Superior Geology, 41st annual meeting, Proceedings v.41, Part 2B, p.77.

Zaleski, E., van Breemen, O., and Peterson, V.L. 1999. Geological evolution of the Manitouwadge greenstone belt and Wawa–Quetico subprovince boundary, Superior Province, Ontario, constrained by U-Pb zircon dates of supracrustal and plutonic rocks; Canadian Journal of Earth Science v.36, p.945-966.

Metric Conversion Table

Conversion from SI to Imperial			Conversion from Imperial to SI		
SI Unit	*Multiplied by*	*Gives*	*Imperial Unit*	*Multiplied by*	*Gives*
		LENGTH			
1 mm	0.039 37	inches	1 inch	**25.4**	mm
1 cm	0.393 70	inches	1 inch	**2.54**	cm
1 m	3.280 84	feet	1 foot	**0.304 8**	m
1 m	0.049 709	chains	1 chain	20.116 8	m
1 km	0.621 371	miles (statute)	1 mile (statute)	**1.609 344**	km
		AREA			
1 cm^2	0.155 0	square inches	1 square inch	**6.451 6**	cm^2
1 m^2	10.763 9	square feet	1 square foot	**0.092 903 04**	m^2
1 km^2	0.386 10	square miles	1 square mile	2.589 988	km^2
1 ha	2.471 054	acres	1 acre	0.404 685 6	ha
		VOLUME			
1 cm^3	0.061 023	cubic inches	1 cubic inch	**16.387 064**	cm^3
1 m^3	35.314 7	cubic feet	1 cubic foot	0.028 316 85	m^3
1 m^3	1.307 951	cubic yards	1 cubic yard	0.764 554 86	m^3
		CAPACITY			
1 L	1.759 755	pints	1 pint	0.568 261	L
1 L	0.879 877	quarts	1 quart	1.136 522	L
1 L	0.219 969	gallons	1 gallon	**4.546 090**	L
		MASS			
1 g	0.035 273 962	ounces (avdp)	1 ounce (avdp)	28.349 523	g
1 g	0.032 150 747	ounces (troy)	1 ounce (troy)	**31.103 476 8**	g
1 kg	2.204 622 6	pounds (avdp)	1 pound (avdp)	**0.453 592 37**	kg
1 kg	0.001 102 3	tons (short)	1 ton(short)	**907.184 74**	kg
1 t	1.102 311 3	tons (short)	1 ton (short)	**0.907 184 74**	t
1 kg	0.000 984 21	tons (long)	1 ton (long)	**1016.046 908 8**	kg
1 t	0.984 206 5	tons (long)	1 ton (long)	**1.016 046 9**	t
		CONCENTRATION			
1 g/t	0.029 166 6	ounce (troy) / ton (short)	1 ounce (troy) / ton (short)	34.285 714 2	g/t
1 g/t	0.583 333 33	pennyweights / ton (short)	1 pennyweight / ton (short)	1.714 285 7	g/t

OTHER USEFUL CONVERSION FACTORS

	Multiplied by	
1 ounce (troy) per ton (short)	31.103 477	grams per ton (short)
1 gram per ton (short)	0.032 151	ounces (troy) per ton (short)
1 ounce (troy) per ton (short)	20.0	pennyweights per ton (short)
1 pennyweight per ton (short)	0.05	ounces (troy) per ton (short)

*Note: Conversion factors in **bold** type are exact. The conversion factors have been taken from or have been derived from factors given in the* Metric Practice Guide for the Canadian Mining and Metallurgical Industries*, published by the Mining Association of Canada in co-operation with the Coal Association of Canada.*

ISSN 0826-9580 (Print)
ISBN 978-1-4606-0610-0 (Print)

ISSN 1916-6117 (online)
ISBN 978-1-4606-0611-7 (PDF)